Contributions to the Mathematical Systems Medicine of Antimicrobial Therapy and Genotype-Phenotype Inference.

Habilitationsschrift

zur Lehrbefähigung am Fachbereich Mathematik und Informatik der Freien Univeristät, Berlin
eingereicht am 26. Juni 2019 von

Max von Kleist, PhD
Robert-Koch Institut, Nordufer 20, 13353 Berlin
Tel.: +49 30 187544458
Email: kleistM@rki.de; vkleist@zedat.fu-berlin.de

Tag des öffentlich-wissenschaflichen Vortrags: 8. Dezember 2020

Contributions to the Mathematical Systems Medicine of Antimicrobial Therapy and Genotype-Phenotype Inference.

Summary of Publications for Habilitation

Introduction

The following summary of my publications describes the main ideas in the corresponding research articles and clarifies my contribution in multi-author publications. I decided to apply for habilitation according to §2.I.1.(c) of the Habilitationsordnung (this path is usually referred as "Kumulative Habilitation").

I selected 13 first- or last author publications for this habilitation that concern contributions to the mathematical systems medicine of antiviral therapy [tMH10, tMS$^+$11, FtK$^+$11, tMMS12, DSt12, DWSt15, Dt16, DSt16, DDKt18, DSD$^+$19, DDKt19], as well as inference of genotype-phenotype associations [SDH$^+$15, SSJ$^+$18]. The selected publications represent my major contributions in this research field since submitting my doctoral thesis [1] in September 2009.

Own contribution: All indicated publications follow author ordering procedures common to the natural sciences. My contributions will be further exemplified below. In summary, three publications are single first author publications [tMH10, tMS$^+$11, tMMS12]. In these publications, I was involved in the drafting and execution of research ideas, as well as in the research design, the communication between the project members and I wrote the bulk of the manuscripts. One publications [FtK$^+$11] is a shared first-author, shared corresponding-author publication. This is a multi-disciplinary publication, where I was involved in the drafting and execution of the stochastic modelling and simulation part, except for the pharmacokinetic modelling and analysis (justifying the shared first-authorship). I also contributed to the research design and the communication between the project members (justifying the shared corresponding-authorship). I contributed to writing most parts of the manuscript, except the pharmacokinetic modelling. In the remaining publications, I am either sole last (corresponding) author [DSt12, DWSt15, Dt16, DSt16, DDKt18, DSD$^+$19, DDKt19], or shared corresponding/last author [SDH$^+$15, SSJ$^+$18]. With regards to the publications where I am sole last author, my main contribution is in the design of the research project, the drafting of the ideas and supervision. Moreover, I wrote the bulk of these manuscripts with input from the other authors. The two shared last author publications [SDH$^+$15, SSJ$^+$18] are again multi-disciplinary publications. In publication [SDH$^+$15], I designed and implemented the biostatistical methods that allow to analyse- and interpret the data generated by my experimental collaboration partners. I contributed to writing the manuscript and wrote all supplementary texts. In [SSJ$^+$18], I designed the biostatistical methods that allow to analyse- and interpret the data generated by my experimental collaboration partners and supervised their implementation. I contributed to writing the manuscript and supplementary texts.

Scientific area: *Scientific Research* sets itself apart from other human endeavours by its requisite to generate *testable* explanations and *reproducible* predictions. However, when considering research on human subjects, large (ethical and practical) restrictions are imposed on the testability and reproducibility of interventions. For example, it is not possible to directly analyse a drugs' effect at an arbitrary resolution within a living being (e.g. at the level of drug-protein interaction) and it is often very difficult to control experimental conditions in humans (diet, sleep-wake cycles, stress conditions, etc...). As with other disciplines, *testability* can still be achieved by breaking down the process of interest into its individual, directly testable, subprocesses and by building a chain of arguments that explain a clinical response in terms of these individual parts. For example, the research goal could be to elucidate the relationship between drug administration and liver damage to determine the safety of a drug. At the molecular level, the drug interacts with a cellular protein. This interaction affects particular subsets of cellular pathways, which, all together, change the cellular phenotype. Multiple cells within an organ interact with one another, triggering a change at the organ level, which may lead to a change in a measurable biomarker for e.g. liver damage.

A major challenge in this area of research is to correctly interpret and mathematically integrate the *testable* sub-processes. The process of testing- and assembling testable sub-processes to explain clinical outcomes quantitatively is called *Systems Medicine* or *Translational Medicine*. Noteworthy, mathematics and computer science are absolutely essential to enabling *Systems Medicine* due to their ability to analyse, integrate and test vast amounts of potential explanations/models. Major theoretical challenges are currently met in (i) multi-scale modelling and -simulation and the inference of unknown mathematical models and -functions that describe- and integrate the testable biological sub-processes.

Besides theoretical challenges in multi-scale modelling and simulation, another important aspect is the integration of lab- and clinical data into the process. In the last years, large progress has been made in RNA and DNA sequencing technologies through the introduction of next- and third-generation sequencing techniques. These technologies can generate gigabytes of data in a single run and are nowadays routinely used in clinical settings. However, unlike with traditional methods, the *direct* interpretation of the data is no longer feasible, as it requires multiple steps of computer-based processing and analysis. Furthermore, the sheer amount of simultaneously testable hypotheses and the high error rates of these techniques bears great risk for false positive "discovery". Major challenges are therefore to develop methods allowing to (ii) mechanistically and phenotypically interpret the data and to (iii) develop robust statistical methods to avoid misleading interpretations.

Apart from technical challenges, the work described here are truly interdisciplinary projects carried out in close cooperation with wet-lab scientist and clinicians. While I describe my contributions in detail, I want to gratefully acknowledge the contribution of my experimental partners, without whom many projects would not have been sucessful. In the following two sections, the selected thirteen projects are introduced, shortly sumarized and my contributions are clarified. The projects are categorised into two inter-connected areas, based on the kind of underlying data and mathematical approaches taken. The first section describes my contributions to mathematical systems medicine of antiviral therapy, whereas the second section describes my contribution to the inference of genotype-phenotype associations.

Mathematical Systems Medicine of Antimicrobial Therapy

In the selected publications, I concentrated on modelling, simulation and optimal control applied to antiviral treatment, -prophylaxis, virus evolution and infection dynamics.

Modelling. I focussed on *kinetic* modelling approaches, and with regards to the modelling philosophy, I followed both a minimal, data-driven, approach whenever a dynamical description or input was sufficient and parameter estimation would in-justify more complex models. To the contrary, mechanistic models were developed when biological pre-knowledge and parameters were readily available and when the intention was to explore/predict scenarios beyond the scope of the data. Often mixed strategies were used, for example a data-driven, minimal approach to model drug concentrations (i.e. pharmacokinetic inputs) and a mechanistic approach to model viral dynamics, which are affected by the pharmacokinetic input [FtK$^+$11, DSt12, DSt16, DDKt18, DSD$^+$19]. Also, the two approaches were used to validate- and add interpretability to one another [Dt16]. A major focus was on biological systems which, at least partially, display stochastic behaviour. Applications include the emergence of drug resistance during treatment, the modelling of the mechanisms of action of antiviral drugs or the modelling of infection dynamics, which are inherently stochastic (since not every exposure leads to infection).

Simulation. Simulation of intrinsically stochastic systems in biology requires solving the chemical master equation (CME), or to sample from its solution via Monte-Carlo techniques. Directly solving-, or even sampling from the solution of the chemical master equation quickly becomes infeasible as its complexity grows exponentially with the number of biological- or chemical species considered. To overcome this dilemma, hybrid approaches can be used. Their basic underlying assumption is that some chemical- or biological species can be accurately approximated using a (stochastic) differential equation (ODE/SDE) based approach, while the remaining species are modelled using the CME approach. The resulting coupled system is then either solved directly or Monte-Carlo techniques are used to sample from its solution.

In the selected publications different approaches were used: In [DWSt15], a coarse-grained (dimension-reduced) CME was directly solved as part of an *optimal control problem*. In [tMMS12], analytical solutions were derived to compute *mean first passage times* of the underlying CME. In [DSt16] hybrid formulations (ODE-CME) were derived and subsequently a finite state projection (FSP) was applied to the CME part, which allowed to solve the coupled system numerically using ODE integration schemes. In [DDKt19] branching techniques were used to compute analytical solutions of the CME for $t \to \infty$. In the remaining publications, hybrid Monte-Carlo techniques were implemented and used to study the stochastic viral response to drug treatment and prophylaxis: In [tMH10, tMS$^+$11, FtK$^+$11] and [DSt12], an (adaptive) integral-method was used and an adaptive FSP scheme was developed for the EXTRANDE algorithm and used in [DDKt18, DSD$^+$19].

Many of these projects required novel algorithmic developments [DWSt15, DDKt18, DSD$^+$19] and efficient implementations that could be parallelized and run on a high-performance computing cluster [tMH10, tMS$^+$11, FtK$^+$11, DSt12, DDKt18, DSD$^+$19].

HIV transduction model

The first contribution [tMH10] was concerned with the development of a stochastic "transduction model" that relates drug treatment to HIV replication, quasi-species- and resistance dynamics. The "transduction model" essentially allows to link predictive markers of (time-varying) drug efficacy at different levels (molecular target, cellular level) to clinical endpoints (virus load measurements). The "transduction model" constitutes a versatile modelling platform that can be extended based on specific research questions to be addressed. In HIV infection, different measures, such as cellular single-round replication assays and clinical viral load decay, are used to assess drug efficacy *in vitro* and *in vivo*. For the newly introduced class of integrase inhibitors, a huge discrepancy between these two measures of efficacy was observed. Hence, a thorough understanding of the relation between these two measures of drug efficacy was warranted.
My contribution in [tMH10] concerns the development of a novel virus dynamics model, which allows for a mechanistic integration of the mode of action of all approved drugs and which, based on hybrid-stochastic simulation, allowed to predict viral dynamics (the clinical endpoint) and resistance evolution on arbitrary fitness landscapes. Notably, the model was derived from first principles and coarse-grained such that available (*in vitro*/*clinical*) parameters could be used for its parameterisation. A new measure, the reproductive capacity, was developed that allowed a fair comparison of efficacy between the different drug classes. Using this measure, we could show that the drug-target half life is a key characteristic that affects both the emergence of resistance, as well as the *in vitro-in vivo* correlation of efficacy measures in HIV treatment. We found that protease inhibitors, due to the short half-life of their target, decrease the total amount of viral replication and the emergence of resistance most efficiently.
The project started towards my final year at the Hamilton Institute Ireland and was completed during my Post-Doc at the FU Berlin. I conceived and designed the project. The model- and the adaptive hybrid Monte-Carlo simulation scheme was implemented by myself and Stefan Menz. Data interpretation was carried out by myself with input from Stefan Menz and Wilhelm Huisinga. I wrote the paper with contributions from Stefan Menz and Wilhelm Huisinga.

Application to resistance-mitigating therapy

Next, we wanted to apply the developed framework to investigate whether HIV treatment schemes can be designed that mitigate drug resistance development and preserve future treatment options. Currently, it is recommended to change treatment only after treatment- or virological failure. However, when virological failure is detected, a viral rebound with resistant viruses has already occurred and these resistant viruses are then likely to be "archived" in long-lived/latently infected cells, which could remove future treatment options permanently.
The probability of *de novo* resistance emergence is a function of the selection pressure exerted by the drug treatment and, at the same time, the total amount of replication. The total amount of replication is, in turn, a function of the population size. The idea presented in [tMS$^+$11] is to use an initial treatment regimen that decreases the viral population size and to pro-actively switch to a treatment regimen with orthogonal resistance profile before the outgrowth and archiving of viruses that are resistant to the first treatment line. To determine the time to switch treatment

we utilised the reproductive capacity, which was introduced in [tMH10]. This measure summarises both the abundance and the instantaneous replication potential of each quasi-species for each possible treatment line. Based on this measure, an ideal time to switch treatment is given when the derivative of the reproductive capacity changes its sign (from negative to positive). The interpretation of this measure is that the total number of treatment-susceptible strains are less effectively cleared than the resistant viruses grow (the treatment does "more harm than good").

Based on massively parallel hybrid stochastic simulations we estimated that an optimal trade-off is achieved when treatment is pro-actively switched at about 80 days after the therapy initiation. Interestingly, a randomized trial indicated that continuous pro-active treatment alternation can improve clinical outcome. Our results indicate that a similar improvement might also be reached after a single pro-active treatment switch.

The approach taken in [tMS$^+$11] can be considered to follow some ideas of model-predictive control. However, there is no guarantee that the treatment scheme is also mathematically *optimal*. However, due to the complexity of the underlying dynamical system considered in [tMS$^+$11] (essentially a CME with about $(M \cdot 7)^{10^{10}}$ states; M= number of viral quasi-species), an optimal control approach was not feasible using the model in [tMS$^+$11]. We therefore developed a coarse-grained Markov state model of viral dynamics and resistance development in [DWSt15] that was fitted to available clinical data. Next, we developed algorithms to solve the optimal control problem for this reduced-state CME.

Optimal control is an active field of research when applied to stochastic dynamical systems [2], as imposed by our field of study. In our work we investigate switched systems, which are particularly challenging to solve as the cost function cannot be differentiated with respect to the control (i.e. as in the forward-backward sweep algorithm). Solving the control problem therefore boils down to solving a combinatorial problem for which we adapted dynamical programming techniques. In [DWSt15], we investigate two approaches: (i) a feedback-control strategy (closed-loop control) and (ii) a pro-active strategy (open-loop control). Mathematically, the problem is to find the optimal actions for each possible state of the infection that minimise the time-discounted costs of the illness, the treatment and the diagnostics.

Ad (i): In [3], we had developed the theory of 'Markov control processes with rare state observations'. The theory is an extension to classical Markov Control by introducing costly diagnostics into the control function. Applied to the HIV-resistance mitigating therapy, it allows for a diagnostic-guided treatment strategy, based on infrequent and patient-specific diagnostic schedules. An optimal policy (which treatment to take and when to take the next diagnostic) can be computed based on an adapted policy iteration scheme applied to the corresponding *Bellmann* equation.

Ad (ii): The pro-active strategy does not consider diagnostics (and thus no diagnostic costs). Here, we consider a Bolza-type cost function, that was parameterised in analogy to (i). To compute the *optimal* pro-active strategy, we apply linear programming techniques to the corresponding performance criterion (forward solution) and the Hamiltonian (backward solution) to prune the space of possible controls, akin to a branch-and-cut algorithm.

Our mathematical modelling suggested that both optimal strategies (i)-(ii) perform better than the current clinical protocols in terms of economic means, life prolongation and reduction of

onwards HIV-transmission and that the two strategies perform similarly to one another.
In [tMS$^+$11] I conceived and designed the project. Programming was conducted by myself and Stefan Menz and codes were uploaded as a supplementary material. I enabled and performed large-scale simulations on the HPC at the National University Ireland using the portable batch systems. Data interpretation was carried out by myself, Stefan Menz, Wilhelm Huisinga and Christof Schütte. Clinical input was given by Hartmut Stocker and Kaikawus Arasteh. I wrote the paper with inputs from Hartmut Stocker, Kaikawus Arasteh, Stefan Menz, Wilhelm Huisinga and Christof Schütte and I managed the communication between project members at FU, Uni Potsdam and the AVK.
In [DWSt15] I conceived the idea for the paper and supervised Sulav Duwal, who implemented all algorithms to compute the *pro-active* treatment strategy and the algorithms for solving the feedback control, based on work by Stefanie Winkelmann. Codes and software (treatment optimizer, "TOP") are available through my webpage. I developed and implemented the coarse-grained CME model. Simulations were performed by Sulav Duwal with input and supervision from me. Interpretation and analysis of simulation data was carried by myself and Sulav Duwal with inputs from Stefanie Winkelmann and Christof Schütte. I wrote the paper together with Sulav Duwal.

The molecular mechanism of action of NRTIs

In the preceding works antiviral treatment was considered as a categorial "on" and "off" variable. Next, we wanted to capture the precise relation between drug concentration and the drugs' effect. Most frequently, this relation is modelled by the so-called $E_{\max}$ equation, whose parameters are fittet to the available (molecular-, cellular- or clinical-) data.
At the molecular level, the $E_{\max}$ equation can, in some cases, be mechanistically derived from first principles [1]. In these cases, it describes the relative reduction in the targeted reactions' velocity. However, it is not clear whether it is an accurate description of the drugs effect at higher levels of resolution, i.e. to describe the drugs' effect on cellular phenotypes, or clinical endpoints. We set out to explore this relation in more detail for the antiviral class of nucleoside reverse transcriptase inhibitors (NRTIs). NRTIs are so-called 'prodrugs', i.e. the chemical entity that is administered is not pharmacologically active. Rather, NRTIs get chemically modified after absorption by HIV target-cells to form the active moiety, the NRTI-triphosphate (TP). Noteworthy, the concentrations of the pharmacologically active NRTI-TP within cells and the pro-drug in the blood plasma are usually non-linearly related and temporally asynchronous [4]. Thus, applying the $E_{\max}$ equation to plasma prodrug concentrations to describe clinical efficacy will most certainly provide incorrect predictions.
In [tMMS12], we set out to build the first mechanistic model of the molecular mechanisms of action (MMOA) of NRTIs: The pharmacologically active NRTI-TP competes with endogenous deoxynucleoside triphosphates (dATP, dCTP, dGTP or dTTP) for incorporation into nascent viral DNA during reverse transcription (RT), i.e. shortly after a virus has fused with a target cell (typically a CD4$^+$ T cell) and before proviral integration into host cells. When the inhibitor gets incorporated into the nascent viral DNA, it essentially halts further polymerisation until excised from the DNA, because the necessary chemical group for attaching the next incoming

nucleotide is missing in the NRTI. I modelled the process of viral DNA polymerisation by reverse transcriptase as a Markov process and derived analytical solutions for the *mean first passage time* (time to finalise the DNA polymerisation). The drugs' direct effect was then assessed as the relative increase in the *mean first passage time*, compared to the absence of drug. *In vitro* kinetic parameters for the model were gathered from a large body of published literature and allowed to predict the relation between NRTI-TP intracellular concentrations and residual reverse transcription for all ≈10 NRTIs, their combinations and various viral genotypes. Furthermore, it allowed to quantify viral fitness and epistasis from micro-kinetic measurements.
But are these predictions correct, and have all important molecular processes been modelled? Amongst other things, the MMOA model allows to predict antiviral potency (50% inhibitory concentration, IC_{50}) of any antiviral from *in vitro* data. To assess the validity of these predictions, we implemented an entirely independent approach (a typical top-down approach) using only clinical data to predict the very same parameter, the antivirals' IC_{50} in [Dt16]. While the top-down approach is limited in its scope (may not be extrapolatable), it certainly represents the relevant, clinical efficacy endpoint and consequently allows to assess whether the MMOA model can be extrapolated to the clinical condition. In the top-down approach, we combined models of the plasma- and intracellular pharmacokinetics and viral dynamics, leaving the IC_{50} as the only 'free' parameter. For all drugs tested (where clinical data was available), the top-down- and MMOA predicted IC_{50} were in excellent agreement, giving us confidence in the relevance and validity of the MMOA model. Subsequently, we used the MMOA model to assess scenarios for which clinical data is not available or cannot be derived, for example the clinical potency of antivirals against *resistant* viral strains.
In [tMMS12] I conceived, designed, managed and implemented the project with biological input from Roland Marquet. I conducted all simulations. Philipp Metzner provided mathematical input regarding the computation of the *mean first passage times*. Data interpretation was carried out by myself, Roland Marquet and Christof Schütte. I wrote the paper with inputs from Roland Marquet. Codes are available as supplementary material in [DSt16].
In [Dt16] I conceived the idea for the paper and supervised Sulav Duwal, who implemented everything and conducted the simulations. Interpretation and analysis of simulation data was carried by myself and Sulav Duwal. I wrote the paper together with Sulav Duwal. Codes for the MMOA model were provided as supplementary material in [DSt16].

HIV prophylaxis

Using the HIV transduction model [tMH10], the MMOA model [tMMS12] and various models of antiviral pharmacokinetics, we had laid the foundation for exploring novel clinical applications. One such promising applications is HIV chemo-prophylaxis. HIV prophylaxis has nowadays become an integral tool to control the spread of HIV, because neither a cure, nor a vaccine exist despite over 30 years of intense research. The core idea of HIV prophylaxis is to provide antivirals to uninfected individuals that are at risk of becoming infected. The administered antiviral can then lower the risk- or entirely prevent HIV infection. Prophylaxis thus works in a similar way to a vaccination, only that the prophylactic protection is a direct function of the antivirals' concentration at the moment of pathogen exposure.

We started working on the topic of pre-exposure prophylaxis (PrEP) before the approval of the first PrEP regimen in 2012 [DSt12]. Since then we have made a few contributions which I will shortly summarise in a thematic (not chronological) order:

Based on the HIV transduction model [tMH10], we derived a branching process formulation for the infection probability in [DDKt19]. We analytically solved the branching process, which allowed us to compute the probability of infection for any (fixed) drug concentration, for any drug, based on its molecular mechanisms of action. This (i) enabled to assess the drug-class specific utility of antivirals and to (ii) assess the prophylactic potential of each drug by considering clinical concentrations ranges typically achieved during treatment. We found that protease inhibitors displayed an atypical switch-like concentration-prophylaxis profile. This profile would likely make them unsuitable as prophylactic efficacy may alternate between zero and complete protection if, e.g. an individual misses a drug dose. Secondly, based on clinical concentrations, we found several candidates out of the ≈ 30 treatment-approved drugs may offer complete HIV protection. These were nevirapine, dolutegravir, efavirenz, darunavir, rilpivirine and etravirine.

In [DSt16] we wanted to incorporate varying drug concentrations that change due to drug dosing and drug-specific pharmacokinetics. This would allow to assess different dosing schemes and the effects of e.g. adherence which is currently considered the main barrier to prophylactic efficacy. We utilised the previously developed MMOA model [tMMS12] to compute the potency of all treatment-approved NRTIs in a 'bottom-up' sense. Furthermore, we utilised various 'top-down' pharmacokinetic models that we had previously developed [DSt12, Dt16]. We then developed a hybrid CME-finite state projection approach that we solved directly. Pharmacokinetics (PK) were therein regarded deterministically and according to the mechanisms of action of the considered drug, the pharmacokinetics would affect a specific parameter of the virus dynamics in a time-dependent fashion. We then set up an infinitesimal generator that modelled the intrinsically stochastic dynamics of HIV during its first replication cycle, subjected to the (time-varying) drug effects with a 'sink' state that denoted the probability to survive the first replication cycle and produce viral progeny. The probability of reaching this state for $t \to \infty$ was used to approximate the infection risk. This coupled PK- finite state CME was co-evolved numerically using standard ODE integration schemes. Within this framework, we could also model infection after exposure to multiple viruses, by assuming statistical independence.

While the developed numerical approach is quite powerful, its central underlying assumption is that 'if the virus isn't cleared in the first replication cycle, it cannot be cleared any time after'. Biologically, if the virus survives the first replication cycle, it will produce on average 1000 progeny viruses (eliminating all progeny will thus be $p(D)^{999}$ less likely; $p(D) < 1$ being the probability to eliminate one virus during one replication cycle in the presence of drug D). Therefore, our underlying assumption is quite realistic, if the drugs' potency is weak-to-moderate (which applied for all drugs analysed in [DSt16]). However, if the drug is very potent ($p(D)$ very close to 1), or if the drug directly affects the production of viral progeny (as in the case of protease inhibitors), the numerical approach developed in [DSt16] may under-predict prophylactic efficacy.

In [FtK$^+$11] and [DSt12] we therefore used a different numerical approach: Here, we massively sampled viral trajectories using the hybrid stochastic-deterministic integral method (an exact method). I.e., pharmacokinetics were again treated deterministically and reactions affecting the

viral dynamics were adaptively assigned to a stochastic vs. a deterministic regimen. We applied this approach to (i) assess the prophylactic efficacy of nevirapine in preventing the transmission of HIV from an HIV-infected mother to her child [FtK$^+$11] and (ii) to assess the prophylactic efficacy of tenofovir against sexual transmission of HIV [DSt12]. Regarding (i) we found that when nevirapine is given to an HIV infected mother during labor, it protects the child because it is trans-placentally delivered to the child before it is exposed to maternal (HIV-infected) blood during birth. Regarding (ii), we found that tenofovir (which was approved as part of PrEP in 2012) insufficiently ($\leq 80\%$) protects against HIV infection and that its protective levels only build up very slowly, i.e. after several dosing events.

Numerically, we classified hydrid stochastic trajectories as infection events, whenever the virus population outgrew a particular threshold. However, this threshold was arbitrarily chosen. We chose a large threshold, which increased the compute-time of our simulations. By contrast, a small threshold may under-predict the prophylactic efficacy.

To prevent any biases from manually choosing thresholds to classify viral trajectories as infection events, we developed a numerically accurate (error-controlled) technique in [DDKt18, DSD$^+$19]. Again, we used a hybrid sampling strategy. We treated pharmacokinetics deterministically and viral dynamics as intrinsically stochastic. We then adapted the numerically exact EXTRANDE algorithm to our needs. Specifically, using results from [DDKt19], we were able to compute an 'extinction simplex'. The extinction simplex denotes the part of the viral state space where the probability of viral extinction exceeds a particular threshold $\varepsilon > 0$. The user-defined threshold ε is then directly related to the probability of misclassifying a viral trajectory as an infection event. Generally, this threshold can be set to the inverse of the number of stochastic samples, which guarantees that the misclassification error is smaller than the sampling error. The extinction simplex is then adapted in such way that it takes the maximum achievable drug concentration (= largest simplex) for any future times into account. Our algorithms therefore allows for the exact and computationally efficient computation of prophylactic efficacy for any arbitrary prophylactic dosing- and adherence regimen. Using population pharmacokinetic models for efavirenz [DSD$^+$19] and dolutegravir [DDKt18] we then predicted their respective prophylactic efficacy for PrEP, 'PrEP on demand' and post-exposure prophylaxis using different levels of adherence and viral exposures. We found that reduced dose (300mg) efavirenz may be a superior and cost-effective alternative to currently approved Truvada (tenofovir + emtricitabine) providing almost 100% protection, whereas dolutegravir may be non-inferior to Truvada.

I conceptualised and designed the project in [DDKt19] together with Sulav Duwal as part of his PhD work, which I supervised. I managed the communication between all project members. Sulav Duwal and I developed the methods and Sulav Duwal implemented everything. Data interpretation was carried out by myself and Sulav Duwal with inputs from Saye Khoo. I wrote the paper with Sulav Duwal and input on clinical aspects was provided by Laura Dickinson and Saye Khoo. A software is provided through my webpage (PrEP-Predictor).

The project [DSt16] was conceptualized by me and Sulav Duwal as part of his PhD work. Codes were written by Sulav Duwal and myself and are available as supplementary material in [DSt16]. Vikram Sunkara contributed the FSP idea and Sulav Duwal and I wrote the manuscript.

The idea for the inter-disciplinary project [FtK$^+$11] emerged through discussions between myself and Monika Frank during my Post-Doc with Christof Schütte and her PhD with Charlotte

Kloft. I implemented and wrote all parts concerning the viral- and pharmacodynamic modelling, whereas Monika Frank performed and documented the pharmacokinetic modelling with data provided by Andrea Kunz and Gundula Harms. I also largely managed the communication between the project members at the Charité, the pharmacy department at FU and myself/Christof Schütte.
In [DSt12], I developed the idea for the project and contributed the initial code for the integral method, which Sulav Duwal then used as part of his overall implementation. The pharmacokinetic modelling part was developed by Sulav Duwal during his Bachelor's thesis, which I supervised. I wrote the paper with input from Sulav Duwal and Christof Schütte.
The idea for the inter-disciplinary project [DDKt18] emerged from discussions between myself, Sulav Duwal, Laura Dickinson and Saye Khoo. I managed the project and the communication between project members. Sulav Duwal and I developed the methods and Sulav Duwal implemented everything. Data interpretation was carried out by myself and Sulav Duwal with inputs from Saye Khoo and Laura Dickinson who provided the pharmacokinetic modelling. I wrote the paper with Sulav Duwal and Laura Dickinson and with inputs by Saye Khoo.
The idea for the inter-disciplinary project [DSD$^+$19] emerged from discussions between myself, Sulav Duwal, Laura Dickinson and Saye Khoo. I managed the project and the communication between project members. I supervised Daniel Seeler who implemented everything and performed simulations as part of his Master's thesis based on previous work by Sulav Duwal. Data interpretation was carried out by myself and Daniel Seeler with inputs from Laura Dickinson who provided the pharmacokinetic modelling. I wrote the paper with Daniel Seeler and with inputs by Laura Dickinson and Saye Khoo.

Inference of Genotype-Phenotype Associations

The second set of publications [SDH$^+$15, SSJ$^+$18] is related to the analysis and interpretation of data arising from next-generation sequencing (NGS) experiments, specifically genotype-phenotype mapping. The broader context and its association with *translational systems medicine* is that NGS, and more recently nanopore sequencing, are now routinely used in diagnostics and it is envisaged to use them for treatment personalisation. Standard bioinformatics pipelines (e.g. assembly, alignment, quality control), may inform about the existence and abundance of particular mutations in a sample. But in most cases it is unclear how to use this information for treatment personalisation. E.g., what is the level of drug resistance conferred by the detected viral quasi-species and what is its propensity to develop resistance? Genotype-phenotype mapping can fill this gap by relating the genomic sequence to phenotypic endpoints, such as drug resistance or fitness.
Standard methods for genotype-phenotype mapping involve the laborious generation and testing of each genotype in a phenotypic assay, or to measure its selection and outgrowth in an evolutionary experiment [5]. The latter can also be performed based on massive amounts of patient data, if genotyping has been performed and sufficient information on the treatment history (=information on selection pressure) is available. However, the precise treatment conditions (co-medication, adherence, pharmacokinetics) are usually not available or -controllable in human subjects as there are many confounding factors. To fill this gap, we developed a novel

quantitative high-throughput genotype-phenotype mapping method, the Mutational Interference Mapping Experiment (MIME). Our method [SDH$^+$15] was published in *Nature Methods* and featured on the cover of the September issue in 2015.

Biological domain. Although not confined to a specific biological domain, we focussed in our work on non-coding RNA (ncRNA). NcRNA denotes a large class of RNA molecules (tRNA, snoRNA, lncRNA, etc...) that are not translated to protein and that continue to be discovered and annotated. To date, we already know that they regulate virtually all cellular processes. Consequently, many recent discoveries associate ncRNA with various, poorly understood, diseases. Currently, despite their important role, ncRNAs are not systematically exploited as drug targets, mainly because the functional mechanisms are often insufficiently understood. As in the case of proteins, it is believed that their three dimensional structure allows to create chemical micro-milieus that can determine their function. However, RNAs are structurally flexible and the mechanisms and dynamics governing ncRNA structure are not well described. Notably, through genotype-phenotype mapping as outlined below, the MIME method can significantly contribute to understanding RNA function & structure to a level of detail that would be sufficient to guide pharmacophore design.

Disease. In our work described herein, we focus on studying the function of ncRNA in RNA viruses (viruses who's genome is an RNA; Examples: HIV, Influenza, Hepatitis C, Ebolavirus, ...). May viruses have extremely compact genomes with many overlapping regulatory functions. I.e. they code for proteins, as well as many non-coding RNAs that help to reprogram an infected human cell to produce viral progeny. The HIV genome, for example, codes for only 9 proteins. The number of ncRNAs that it codes for is currently unknown.

The 5' untranslated region (5' UTR) of the HIV genome is a non-coding RNA that is highly conserved between distinct patient-derived viruses. It is thus a prime suspect for a functional ncRNA. In our publications, we specifically studied the various functions of this ncRNA in HIV replication. Our work may thus create valuable insights to pharmacologically target the 5' UTR of HIV to prevent HIV replication.

The Mutational Interference Mapping Experiment

The method was initially applied to study the function of the HIV 5' UTR *in vitro* [SDH$^+$15], and subsequently extended to the *in cellulo* situation [SSJ$^+$18]. The method is related to "*in vitro* evolution" for which Francis Arnold received the Nobel price in chemistry in 2018. The core idea is to (i) create a pool (library) of all possible genotypes through random mutation, to (ii) subject this pool to a specific selection pressure, e.g. the binding to a protein and (iii) to physically separate the genotypes according to functionality (e.g. into bound- and unbound RNA) and to (iv) sequence both the functionally selected- and deselected genotypes using NGS, which provides information regarding their abundance.

My contributions are the development of mathematical and statistical methods that allow interpretation and analysis of the generated NGS data: (A) Through mathematical modelling, I could show that the frequency of a mutation in the deselected pool, divided by the frequency in the selected pool equals the change in function that the respective mutation confers (=the phenotype; e.g. binding affinity). Since NGS provides all mutational frequencies in a single

run, our method thus allows to predict the phenotype of $N \cdot 3$ mutations from a single experiment (N being the length of the considered molecule, 3 is the number of possible mutations per residue). However, NGS is error-prone and thus many detected "mutations" may actually be sequencing errors, which could lead to false positive "discoveries". (B) My second contribution is to develop a robust statistical method that allows to ascertain whether predicted phenotypes are significant and whether the signal (mutation frequency) exceeds the sequencing error. The core idea is based on re-sampling techniques: To re-sample the phenotype, pairs of residues are considered, with only one residue mutated. Since only a subset of NGS reads cover both residues, the method is related to cross-validation and the jack-knife procedure. Assessing all pairs of residues then allow to empirically construct a probability density function for each of the $N \cdot 3$ phenotypic estimates and assess whether they are significantly different from the wild type. This process runs in $\mathcal{O}(N^2)$. Contributions (A) and (B) allow to analyse the phenotypic contribution of all single-mutations. Moreover, they allow to characterise functional domains in the molecule: i.e. all positions where mutations significantly decrease function constitute the *functional domain*. However, at this point it is not clear how they affect the function. For example, is the residue directly interacting with another molecule (as in RNA-protein interactions)? Or does it contribute to the folding of the RNA, such that the protein-RNA interaction can take place? (C) The third contribution resolves this ambiguity: Through combinatorics, I developed a method that identifies residues within the RNA that directly interact with one another to form a *functional structure*. The method identifies residue pairs, where structure-altering mutations at only one residue negatively affect the molecule's function and where structure reconstituting mutations at both residues restore function, i.e. we look at pairs of mutated residues that confer a particular form of *positive epistasis*.

In [SDH+15] the MIME method was introduced to study RNA-protein binding *in vitro*, and applied to HIV genomic RNA capturing by the *gag* protein. In [6] we introduced a GUI-software that perform all analysis steps. In [SSJ+18] we adopted the method to *in cellulo* experiments to study the intracellular regulation of viral genome production and viral genome packaging by the 5'UTR of HIV. Interestingly, the ratio of mutation frequencies in the deselected vs. selected pools was again directly related to the phenotypic endpoint.

In [SDH+15] I developed and implemented all mathematical-/statistical tools to allow genotype-phenotype mapping and to infer function-associated ncRNA structure directly from next-generation sequencing data, while Redmond P Smyth and Roland Marquet developed the idea for-, and conducted all experiments. Bioinformatic processing of the raw data (alignment, trimming, quality control) was performed by Redmond P Smyth. All authors contributed to analysing the data. I contributed to writing the main manuscript and wrote all supplementary texts. In [SSJ+18] I developed the mathematical/statistical tools and closely supervised my student (Maureen R Smith) who implemented everything. Redmond P Smyth and Roland Marquet developed the idea for the experiments and Redmond P Smyth performed all experiments and the primary bioinformatic processing. Data was jointly analysed. I contributed to writing the manuscript and wrote all supplementary texts.

Further Publications

The thirteen selected publications describe my major research after completing my doctoral thesis. I addition, I co-authored another 29 publications (+ 1 patent) which I did not include in the selection of manuscripts for the habilitation procedure. Publications [7, 8, 9, 10, 11, 12] could have been added to the list based on my contributions, but I chose not to include them because they focus on other topics than the ones presented herein. I did not include [6] as it concerned a software development based on existing ideas presented in [SDH$^+$15]. Publications [3, 2, 13] are mathematical papers, where the main mathematical ideas were largely contributed by Stefanie Winkelmann and Wei Zhang respectively. Publication [5] involved crucial methods development by me and my PhD student at the time, Kaveh Pouran Yousef, to infer genotype-phenotype associations, as well as the writing of the manuscript. However, our contribution was not gratified with appropriate authorship and thus this publication is not included in the list. Publication [14] was written during an internship as part of my Bachelor studies. Research in [15, 16, 17] was largely based on ideas from my PhD supervisor. Publication [4] was based on my own ideas, but largely part of my PhD research [1]. Publications [18, 19, 20, 21, 22, 23, 24, 25] mainly involved clinical data analysis where I contributed some methods development and ideas, however where I was not the lead researcher or PI. Publications [26, 27] study HIV evolution from surveillance data. I did not include the former because I am not the first- or corresponding author, whereas the latter was not included in the list because I consider my contribution was not significant enough to justify this inclusion. Publications [28, 29] involve some intellectual contributions from my side, but insufficient to be included here.

Thirteen Publications Selected for Habilitation Procedure

DDKt18. Sulav Duwal, Laura Dickinson, Saye Khoo, and **von Kleist, Max**. Hybrid stochastic framework predicts efficacy of prophylaxis against HIV: An example with different dolutegravir prophylaxis schemes. *PLoS Comput Biol*, 14(6):e1006155, 2018.

DDKt19. Sulav Duwal, Laura Dickinson, Saye Khoo, and **von Kleist, Max**. Mechanistic framework predicts drug-class specific utility of antiretrovirals for HIV prophylaxis. *PLoS Comput Biol*, 15(1):e1006740, 2019.

DSD$^+$19. Sulav Duwal, Daniel Seeler, Laura Dickinson, Saye Khoo, and **von Kleist, Max**. The utility of efavirenz-based prophylaxis against HIV infection. a systems pharmacological analysis. *Front Pharmacol*, 10:199, 2019.

DSt12. Sulav Duwal, Christof Schütte, and **von Kleist, Max**. Pharmacokinetics and pharmacodynamics of the reverse transcriptase inhibitor tenofovir and prophylactic efficacy against HIV-1 infection. *PloS one*, 7:e40382, 2012.

DSt16. Sulav Duwal, Vikram Sunkara, and **von Kleist, Max**. Multiscale systems-pharmacology pipeline to assess the prophylactic efficacy of nrtis against HIV-1. *CPT: pharmacometrics & systems pharmacology*, 5:377–387, 2016.

Dt16. Sulav Duwal and **von Kleist, Max**. Top-down and bottom-up modeling in system pharmacology to understand clinical efficacy: An example with NRTIs of HIV-1. *European journal of pharmaceutical sciences*, 94:72–83, 2016.

DWSt15. Sulav Duwal, Stefanie Winkelmann, Christof Schütte, and **von Kleist, Max**. Optimal treatment strategies in the context of 'treatment for prevention' against HIV-1 in resource-poor settings. *PLoS computational biology*, 11:e1004200, 2015.

FtK$^+$11. Monica Frank*, **von Kleist*$^+$, Max**, Andrea Kunz, Gundel Harms, Christof Schütte, and Charlotte Kloft$^+$. Quantifying the impact of nevirapine-based prophylaxis strategies to prevent mother-to-child transmission of HIV-1: a combined pharmacokinetic, pharmacodynamic, and viral dynamic analysis to predict clinical outcomes. *Antimicrobial agents and chemotherapy*, 55:5529–5540 (*equal contribution, $^+$ co–corresponding), 2011.

SDH$^+$15. Redmond P Smyth*, Redmond P, Laurence Despons, Gong Huili, Serena Bernacchi, Marcel Hijnen, Johnson Mak, Fabrice Jossinet, Li Weixi, Jean-Christophe Paillart, **von Kleist*, Max**, and Roland Marquet*. Mutational interference mapping experiment (MIME) for studying RNA structure and function. *Nature methods*, 12:866–872 (*shared corr. authorship), 2015.

SSJ$^+$18. Redmond P Smyth*, Maureen R Smith, Anne-Caroline Jousset, Laurence Despons, Géraldine Laumond, Thomas Decoville, Pierre Cattenoz, Christiane Moog, Fabrice Jossinet, Marylène Mougel, Jean-Christophe Paillart, **von Kleist*, Max**, and Roland Marquet*. In cell mutational interference mapping experiment (in cell MIME) identifies the 5' polyadenylation signal as a dual regulator of HIV-1 genomic rna production and packaging. *Nucleic Acids Res*, 46(9):e57 (*shared corr. authorship), 2018.

tMH10. **von Kleist, Max**, Stephan Menz, and Wilhelm Huisinga. Drug-class specific impact of antivirals on the reproductive capacity of HIV. *PLoS computational biology*, 6:e1000720, 2010.

tMMS12. **von Kleist, Max**, Philipp Metzner, Roland Marquet, and Christof Schütte. HIV-1 polymerase inhibition by nucleoside analogs: cellular- and kinetic parameters of efficacy, susceptibility and resistance selection. *PLoS computational biology*, 8:e1002359, 2012.

tMS$^+$11. **von Kleist, Max**, Stephan Menz, Hartmut Stocker, Keikawus Arasteh, Christof Schütte, and Wilhelm Huisinga. HIV quasispecies dynamics during pro-active treatment switching: impact on multi-drug resistance and resistance archiving in latent reservoirs. *PloS one*, 6:e18204, 2011.

Other Publications

1. M von Kleist. *Combining Pharmacology and Mutational Dynamics to Understand and Combat Drug Resistance in HIV*. PhD thesis, Hamilton Institute/NUIM, `https://www.hamilton.ie/publications/MaxvonKleist_2009_PhDThesis.pdf`, September 2009.

2. W Zhang, C Hartmann, and M von Kleist. Optimal control of markov jump processes: Asymptotic analysis, algorithms and application to modelling of chemical reaction systems. *Communications in Mathematical Sciences*, 16(2):293–331, 2018.

3. S Winkelmann, C Schütte, and M von Kleist. Markov control processes with rare state observation: theory and application to treatment scheduling in HIV-1. *Communications in Mathematical Sciences*, 12(5):859–877, 2014.

4. M von Kleist and W Huisinga. Pharmacokinetic-pharmacodynamic relationship of NRTIs and its connection to viral escape: an example based on zidovudine. *European journal of pharmaceutical sciences*, 36:532–543, March 2009.

5. B A Rath, K P Yousef, D K Katzenstein, R W Shafer, C Schütte, M von Kleist, and T C Merigan. In vitro HIV-1 evolution in response to triple reverse transcriptase inhibitors & in silico phenotypic analysis. *PloS one*, 8:e61102, 2013.

6. M R Smith, R P Smyth, R Marquet, and M von Kleist. MIMEAnTo: profiling functional RNA in mutational interference mapping experiments. *Bioinformatics*, 32:3369–3370, 2016.

7. K P Yousef, A Streck, C Schütte, H Siebert, R Hengge, and M von Kleist. Logical-continuous modelling of post-translationally regulated bistability of curli fiber expression in Escherichia coli. *BMC systems biology*, 9:39, July 2015.

8. K Pouran Yousef, K Meixenberger, M R Smith, S Somogyi, S Gromöller, D Schmidt, B Gunsenheimer-Bartmeyer, O Hamouda, C Kücherer, and M von Kleist. Inferring HIV-1 transmission dynamics in germany from recently transmitted viruses. *Journal of acquired immune deficiency syndromes*, 73:356–363, 2016.

9. Vikram S and M von Kleist. Coupling cellular phenotype and mechanics to understand extracellular matrix formation and homeostasis in osteoarthritis. *IFAC-PapersOnLine*, 49(26):38–43, 2016.

10. T Haase, V Sunkara, B Kohl, C Meier, P Bußmann, J Becker, M Jagielski, M von Kleist*, and W Ertel*. Discerning the spatio-temporal disease patterns of surgically induced OA mouse models. *PLoS One*, 14(4):e0213734 (*corresponding authors), 2019.

11. M.N. Ozel, A. Kulkarni, A. Hasan, J. Brummer, M. Moldenhauer, I.-M. Daumann, H. Wolfenberg, V. Dercksen, F.R. Kiral, M. Weiser, S. Prohaska, M. von Kleist*, and P.R. Hiesinger*. Serial synapse formation through filopodial competition for synaptic seeding factors. *Developmental Cell (in press) *corresponding authors*, 2019.

12. P Gupta, A Gramatke, R Einspanier, C Schütte, M von Kleist*, and J Sharbati*. In silico cytotoxicity assessment on cultured rat intestinal cells deduced from cellular impedance measurements. *Toxicol In Vitro*, 41:179–188, 2017 (*corresponding authors).

13. M von Kleist, C Schütte, and W Zhang. Statistical Analysis of the First Passage Path Ensemble of Jump Processes. *Journal of Statistical Physics*, 170(4):809–843, 2018.

14. D. Franke, J. Pavlovic, T. S. Utesch, M. von Kleist, J. Schultz, G. Dollenmaier, and K. Moelling. *Novel Vaccination Strategies*, chapter 14: Update on Antiviral DNA Vaccine Research (2000–2003). Wiley, 2004.

15. R Telgmann, M von Kleist, and W Huisinga. Software supported modelling in pharmacokinetics. In *CompLife*, volume 4216 of *Lecture Notes in Computer Science*, pages 216–225. Springer, 2006.

16. M. von Kleist, C. Kloft, and W. Huisinga. Combining systems biology with physiologically-based pharmacokinetics to support the understanding of drug effects. In *Proceedings of Foundations of Systems Biology in Engeneering (FOSBE), Stuttgart*, pages 231–236, 2007.

17. M von Kleist and W Huisinga. Physiologically based pharmacokinetic modelling: a sub-compartmentalized model of tissue distribution. *Journal of pharmacokinetics and pharmacodynamics*, 34:789–806, 2007.

18. B Rath, M von Kleist, F Tief, K Karsch, E Tuerk, S Muehlhans, F Louis, H Skopnik, B Schweiger, and S Duwe. Virus load kinetics and resistance development during oseltamivir treatment in infants and children infected with Influenza A(H1N1) 2009 and Influenza B viruses. *The Pediatric infectious disease journal*, 31:899–905, 2012.

19. B A Rath, M von Kleist, M E Castillo, L Kolevic, P Caballero, G Soto-Castellares, A M Amedee, J E Robinson, D K Katzenstein, R B Van Dyke, and R A Oberhelman. Antiviral resistance and correlates of virologic failure in the first cohort of HIV-infected children gaining access to structured antiretroviral therapy in Lima, Peru: a cross-sectional analysis. *BMC Infect Dis*, 13:1, 2013.

20. B Rath, F Tief, K Karsch, S Muehlhans, P Obermeier, E Adamou, X Chen, L Seeber, C Peiser, C Hoppe, M von Kleist, T Conrad, and B Schweiger. Towards a personalised approach to managing influenza infections in infants and children - food for thought and a note on oseltamivir. *Infect Disord Drug Targets*, 13(1):25–33, 2013.

21. X Chen, K Pouran Yousef, S Duwe, K Karsch, S Grover, S Wählisch, P Obermeier, F Tief, S Mühlhans, L Seeber, M von Kleist, B Schweiger, and B Rath. Quantitative influenza follow-up testing (QIFT)–a novel biomarker for the monitoring of disease activity at the point-of-care. *PLoS One*, 9(3):e92500, 2014.

22. J Katchanov, M von Kleist, K Arasteh, and H Stocker. 'Time-to-amphotericin B' in cryptococcal meningitis in a European low-prevalence setting: analysis of diagnostic delays. *QJM : monthly journal of the Association of Physicians*, 107:799–803, 2014.

23. K Meixenberger, A Hauser, K Jansen, K P Yousef, S Fiedler, M von Kleist, S Norley, S Somogyi, O Hamouda, N Bannert, B Bartmeyer, and C Kücherer. Assessment of ambiguous base calls in HIV-1 pol population sequences as a biomarker for identification of recent infections in HIV-1 incidence studies. *J Clin Microbiol*, 52(8):2977–83, 2014.

24. K Meixenberger, K P Yousef, S Somogyi, S Fiedler, B Bartmeyer, M von Kleist, and C K´ucherer. Characterization of natural polymorphic sites of the HIV-1 integrase before the introduction of HIV-1 integrase inhibitors in Germany. *J Int AIDS Soc*, 17(4 Suppl 3):19746, 2014.

25. S Muehlhans, M von Kleist, T Gretchukha, M Terhardt, U Fegeler, W Maurer, L Namazova-Baranova, G Gaedicke, A Baranov, and B Rath. Awareness and utilization of reporting pathways for adverse events following immunization: online survey among pediatricians in Russia and Germany. *Paediatr Drugs*, 16(4):321–30, 2014.

26. K Meixenberger, K P Yousef, M R Smith, S Somogyi, S Fiedler, B Bartmeyer, O Hamouda, N Bannert, M von Kleist, and C K´ucherer. Molecular evolution of HIV-1 integrase during the 20 years prior to the first approval of integrase inhibitors. *Virology journal*, 14:223, November 2017.

27. K Hanke, N R Faria, D Kühnert, KP Yousef, A Hauser, K Meixenberger, A Hofmann, V Bremer, B Bartmeyer, O Pybus, C Kücherer, M von Kleist, and N Bannert. Reconstruction of the genetic history and the current spread of HIV-1 subtype A in Germany. *J Virol*, 93(12), Jun 2019.

28. P Gupta, S Peter, M Jung, A Lewin, G Hemmrich-Stanisak, A Franke, M von Kleist, C Schütte, R Einspanier, S Sharbati, and J Zur Bruegge. Analysis of long non-coding RNA and mRNA expression in bovine macrophages brings up novel aspects of mycobacterium avium subspecies paratuberculosis infections. *Sci Rep*, 9(1):1571, 2019.

29. A. Rittig, T. Haase, A. Pletnyov, B. Kohl, W. Ertel, M. von Kleist, and V. Sunkara. SLCV -A supervised learning-computer vision combined strategy for automated muscle fibre detection in cross sectional images. *PeerJ*, 7:e7053, 2019.

Patents

30. M von Kleist and C Schütte. Reduction technique for pharmacological models to support planning, execution and analysis of clinical studies. German patent office (DPMA). Pat.Nr.: 10 2010 060 311, 2010.

PLOS COMPUTATIONAL BIOLOGY

RESEARCH ARTICLE

Hybrid stochastic framework predicts efficacy of prophylaxis against HIV: An example with different dolutegravir prophylaxis schemes

Sulav Duwal[1]*, Laura Dickinson[2], Saye Khoo[2], Max von Kleist[1]*

1 Department of Mathematics & Computer Science, Freie Universität Berlin, Berlin, Germany, **2** Institute of Translational Medicine, University of Liverpool, Liverpool, United Kingdom

* sulav@zedat.fu-berlin.de (SD); max.kleist@fu-berlin.de (MvK)

OPEN ACCESS

Citation: Duwal S, Dickinson L, Khoo S, von Kleist M (2018) Hybrid stochastic framework predicts efficacy of prophylaxis against HIV: An example with different dolutegravir prophylaxis schemes. PLoS Comput Biol 14(6): e1006155. https://doi.org/10.1371/journal.pcbi.1006155

Editor: Katia Koelle, Duke University, UNITED STATES

Received: December 22, 2017

Accepted: April 21, 2018

Published: June 14, 2018

Data Availability Statement: All relevant data are within the paper and its Supporting Information files.

Funding: MvK and SD acknowledge financial support from the BMBF e:Bio junior research group 'Systems Pharmacology & Disease Control', grant number 031A307. SK has received funding from Gilead, ViiV Healthcare, Merck and Janssen for the HIV Drug Interactions website, and for research grants. The funders had no role in study design,

Abstract

To achieve the 90-90-90 goals set by UNAIDS, the number of new HIV infections needs to decrease to approximately 500,000 by 2020. One of the 'five pillars' to achieve this goal is pre-exposure prophylaxis (PrEP). Truvada (emtricitabine-tenofovir) is currently the only medication approved for PrEP. Despite its advantages, Truvada is costly and requires individuals to adhere to the once-daily regimen. To improve PrEP, many next-generation regimen, including long-acting formulations, are currently investigated. However, pre-clinical testing may not guide candidate selection, since it often fails to translate into clinical efficacy. On the other hand, quantifying prophylactic efficacy in the clinic is ethically problematic and requires to conduct long (years) and large (N>1000 individuals) trials, precluding systematic evaluation of candidates and deployment strategies. To prioritize- and help design PrEP regimen, tools are urgently needed that integrate pharmacological-, viral- and host factors determining prophylactic efficacy. Integrating the aforementioned factors, we developed an efficient and exact stochastic simulation approach to predict prophylactic efficacy, as an example for dolutegravir (DTG). Combining the population pharmacokinetics of DTG with the stochastic framework, we predicted that plasma concentrations of 145.18 and 722.23nM prevent 50- and 90% sexual transmissions respectively. We then predicted the reduction in HIV infection when DTG was used in PrEP, PrEP 'on demand' and post-exposure prophylaxis (PEP) before/after virus exposure. Once daily PrEP with 50mg oral DTG prevented 99–100% infections, and 85% of infections when 50% of dosing events were missed. PrEP 'on demand' prevented 79–84% infections and PEP >80% when initiated within 6 hours after virus exposure and continued for as long as possible. While the simulation framework can easily be adapted to other PrEP candidates, our simulations indicated that oral 50mg DTG is non-inferior to Truvada. Moreover, the predicted 90% preventive concentrations can guide release kinetics of currently developed DTG nano-formulations.

data collection and analysis, decision to publish, or preparation of the manuscript.

Competing interests: The authors have declared that no competing interests exist.

Author summary

In 2012, pre-exposure prophylaxis (PrEP) with Truvada was approved. It is considered one of the 'five pillars' by UNAIDS to drastically reduce HIV transmission. However, Truvada provides imperfect protection, is costly and individuals often fail to adhere to the once-daily regimen. Next-generation PrEP compounds, including long-acting formulations, are currently developed to improve PrEP. However, clinical trials using next-PrEP often fail. Since they involve many (>1000) individuals and long durations this incurs unacceptable costs, apart from individual tragedies. While animal- and *ex vivo*/*in vitro* experiments poorly translate into human efficacy, predictive tools are urgently needed that allow for PrEP candidate prioritisation. We developed an efficient simulation tool to predict the prophylactic utility of arbitrary dosing regimen. After developing population pharmacokinetic models for dolutegravir (DTG), we set out to predict its prophylactic utility in PrEP, PrEP 'on demand' and post-exposure prophylaxis. We found that 50mg DTG is non-inferior to Truvada in all aforementioned prophylaxis schemes. Moreover, we determined concentrations-prophylaxis profiles, which can guide release kinetics of currently developed DTG nano-formulations.

Introduction

HIV-1 continues to be one of the greatest public health challenges. While it is possible to suppress virus replication with antiretroviral combination treatment, the virus can persist in cellular and anatomical reservoirs for decades, precluding a cure [1–3]. Because of the inability to cure HIV, preventing its transmission is of utmost importance. The 90-90-90 target formulated by UNAIDS aim to end AIDS by 2030. An intermittent goal will be a drastic reduction of new HIV infections: While approximately 2.1 million individuals became infected with HIV in 2015 [4], the intention is to reduce this number to 500,000 cases by 2020 and to fewer than 200,000 by 2030.

Currently, pre-exposure prophylaxis (PrEP) for high-risk individuals is one of the five 'pillars' set by UNAIDS to achieve a drastic reduction in HIV infections. Of the available agents, tenofovir and emtricitabine (Truvada) have been extensively studied and were approved by the FDA and EMEA in 2012 and 2016 respectively. Most studies agree that Truvada can potently prevent HIV infection, if individuals adhere to the once-daily regimen [5, 6]. However, major shortcomings of Truvada-based PrEP are its costs [7], the fact that it imperfectly protects from infection, and the necessity for daily drug intake, which often leads to inadequate adherence. These deficits of Truvada-based PrEP may be overcome by next-generation PrEP regimen, including more cost-efficient drugs, and drug formulations that require antiviral injections only every few month (see [8] for an overview of the PrEP pipeline).

Quantifying prophylactic efficacy in the clinic is ethically problematic and extremely expensive, since it requires to conduct large ($N > 1000$ individuals) trials over very long time spans (years) to obtain statistically evaluable results. On the other hand, *pre-clinical* PrEP experiments only allow to study certain aspects in isolation. While PrEP efficacy is the result of a multivariate interplay of viral- and host factors there is a lack of translational tools to integrate available knowledge and to rationalize which agents and dosing regimen to test clinically. Having predictive models at hand that allow to rule out-, or prioritize certain regimen can avoid putting individuals at harm and greatly reduce clinical failure rates and associated costs.

Our intention was to develop a method that integrates pharmacokinetic and pharmacodynamic (PK/PD), as well as viral characteristics to *a priori* assess the *per contact* prophylactic efficacy of arbitrary PrEP strategies against HIV.

Recently, modelling approaches have been developed to predict the per-contact PrEP efficacy [9, 10] by integrating various host and viral factors. Despite their advantages, these approaches conventionally neglect the pharmacokinetic–pharmacodynamic characteristics of HIV drugs and are therefore unable to simulate drug dosing, and dose frequency in order to ascertain how PrEP can most effectively be deployed. We recently developed a novel approach which fully integrates the pharmacology of nucleotide reverse transcriptase inhibitors (NRTIs) [11]. This approach, however, approximates virus extinction by its elimination probability during the first replication cycle. While this assumption is reasonable for moderately potent prophylactic compounds (like all investigated NRTIs), it underestimates the prophylactic efficacy of highly potent drugs and fails to predict efficacy in post-exposure prophylaxis (PEP). We overcome the aforementioned limitations by building on recent developments for the simulation of stochastic processes [12], implementing a numerically exact simulation approach to assess PrEP/PEP efficacy for time-varying drug concentrations (pharmacokinetics). The benefit of such integrative framework is to elucidate the relative importance of the distinct pharmacological and viral factors, such as the on- and offset of prophylactic protection, sensitivity to missed dosing events, -virus inoculum size and -timing of virus exposure. In the current work, we combine population pharmacokinetics with the novel stochastic simulation method to analyze different PrEP/PEP schedules with the second-generation integrase inhibitor dolutegravir.

Methods

The initial replication events after exposure to HIV are highly stochastic. Typically, a low number of founder viruses is responsible for establishing infection [13–16] and the transmission probability per *sexual* exposure [17, 18] is very low. While two types of stochastic noise are typically considered in biology, roughly categorized as internal- vs. external noise [19, 20], we herein focused on the former. This assumes that the stochastic outcome of viral exposure (infection/non-infection) can be explained by the order in which reaction occur. For example, when a single virus comes into proximity of target cells, it may either be cleared or it may infect the target cell which can trigger a systemic infection. Prophylactic drugs shift the balance between these two events in favor of virus clearance. Stochastic dynamics of this type are defined by a multivariate Poisson process. The evolution of the state probabilities given the initial state x_0 is then described by the chemical master equation (CME). For each possible state x_i we have

$$\begin{aligned}\frac{d}{dt}\mathbb{P}(X_t = x_i|X_0 = x_0) \quad &= \quad \sum_{k=1}^{K} a_k(x_i - v_k)\cdot\mathbb{P}(X_t = x_i - v_k|X_0 = x_0) \\ &\quad -a_k(x_i)\cdot\mathbb{P}(X_t = x_i|X_0 = x_0),\end{aligned}$$

for time $t \geq 0$, with $X_t \in \mathbb{N}^s$ denoting the state of the system (the combination of the number of viruses, infected cells and drug particles), where s denotes the overall number of variables ('species'). In the equation above, the index k runs over all reactions and a_k, v_k denote the reaction propensity of the k^{th} reaction and its stoichiometric change vector respectively. A practical problem with the CME is that even for moderately sized systems (s small) the *curse of dimensionality* is encountered and consequently the CME is intractable [21].

Hybrid formulation

It has been shown that intrinsic stochastic fluctuations may be negligible in the so-called large copy number regimen (when $X_t >> 1$) and consequently, an ODE approach that models concentrations of molecules X_t/Ω, suffices [22]. In the current work, we re-formulate the above stated CME into a hybrid stochastic-deterministic (discrete-continuous) system $X_t = (Y_t; Z_t)$, where Y_t denotes the discrete-stochastic and Z_t denotes the continuous-deterministic part. In our application, we view the antiviral pharmacokinetics (concentration time profile) as the external dynamical environment Z_t, which we will model in terms of a low-dimensional set of ODEs (exemplified below). This is common practice in the pharmacometrics/systems pharmacology field and is supported by the fact that typically large quantities of drug molecules reach the target site. The target site concentrations $D_t \subseteq Z_t$ affect reaction propensities of our internal stochastic system, which models the stochastic events after exposure (viral replication and clearance reactions). The internal system Y_t represents the state of the viral compartments represented by the number of free viruses V, early stage infected T cells T_1 and late infected T cells T_2, i.e $Y_t = [V, \mathrm{T}_1, \mathrm{T}_2,]^T$, exemplified below.

While this reduces the dimensionality, propensity functions of the stochastic sub-system are subsequently time-dependent, i.e. the continuous-deterministic drug concentration-time profile may affect reaction rates of the discrete-stochastic subsystem Y_t on an infinitesimally small time scale. We will tackle this problem algorithmically, enabling the numerically exact estimation of prophylactic efficacy.

Prophylactic efficacy of a drug regimen

Our goal is to estimate the prophylactic efficacy φ of particular medication regimen S_D. The prophylactic efficacy denotes the reduction in infection probability *per contact*,

$$\varphi(Y_0, S_D) = 1 - \frac{1 - P_{\mathrm{E}}(Y_0|S_D)}{1 - P_{\mathrm{E}}(Y_0|\varnothing)} \quad (\text{prophylactic efficacy}), \tag{1}$$

where $P_{\mathrm{E}}(Y_0|S_D)$ and $P_{\mathrm{E}}(Y_0|\varnothing)$ denote the virus extinction probabilities for a particular prophylactic regimen S_D and in the absence of prophylactic drugs $\varnothing$ respectively. The extinction probability is defined as

$$P_{\mathrm{E}}(Y_0) \coloneqq \mathbb{P}\left(Y_t = \begin{bmatrix} 0 \\ 0 \\ 0 \end{bmatrix} \,\middle|\, Y_0 = \begin{bmatrix} \mathrm{V} \\ \mathrm{T}_1 \\ \mathrm{T}_2 \end{bmatrix} \right) \tag{2}$$

for $t \to \infty$ and where Y_0 denotes the initial state of the stochastic viral dynamics subsystem. In other words, the extinction probability is the probability that a stochastic trajectory eventually reaches the absorbing state $[0, 0, 0]^T$ of the viral subsystem Y. Naturally, the infection probability is the complement of the extinction probability, $P_{\mathrm{I}}(Y_0) = 1 - P_{\mathrm{E}}(Y_0)$. The terms $P_{\mathrm{E}}(Y_0|S_D)$, $P_{\mathrm{E}}(Y_0|\varnothing)$ will be computed using a mathematical model of the viral dynamics that mechanistically considers the direct effects of antivirals on their respective target processes (outlined in a related article [23]), as well as individual drug pharmacokinetics following particular prophylaxis regimen.

Viral dynamics (stochastic part)

We adopted the viral dynamics model described in [24, 25]. Long-lived and latently infected cells are only implicitly considered (outlined at the end of the section), motivated by the

Table 1. Parameters used for the viral dynamics model. Excerpt from [24], except for CL(naive), which assumed that virus clearance is smaller in virus-naive individuals compared to infected individuals, in line with [55, 87]. All parameters refer to the absence of drug treatment ∅. All parameters in units [1/day]).

Parameter	Value	Reference
λ_T	$2{\cdot}10^9$	[82]
δ_T, δ_{T_1}	0.02	[83]
δ_{T_2}	1	[84]
δ_{PIC}	0.35	[35, 85]
k	0.35	[35]
β	$8{\cdot}10^{-12}$	[86]
N_T	670	[24, 83]
CL(naive)	2.3	[10, 28]

https://doi.org/10.1371/journal.pcbi.1006155.t001

observation that transmitted viruses are not macrophage-tropic [26, 27] and in line with related modelling approaches [9, 10, 28–30]. Although this model is a coarse representation of the molecular events happening during virus replication, it allows to accurately and mechanistically describe the effect of all existing antiretroviral drug classes on viral replication, as demonstrated in e.g. [31], and can be parameterized by *in vitro* and *clinical* data, Table 1. The modelled viral replication cycle consists of free infectious viruses V, uninfected T-cells, early infected T-cells (T_1) and productively infected T-cells (T_2). Early infected T-cells (T_1) and productively infected T-cells (T_2) denote T-cells prior- and after proviral integration respectively, where the latter produces virus progeny. During the onset of infection the number of viruses is relatively low and the number of uninfected T-cells T_u is fairly unaffected by virus dynamics [28, 32, 33]. We thus consider $T_u = \lambda_T/\delta_T$ to be constant over the course of simulations. The dynamics of the stochastic viral replication model after virus exposure are then defined by six reactions (the model is depicted in S1 Fig):

$$a_1 = \quad (\mathrm{CL} + \mathrm{CL_T} \cdot \mathrm{T_u}) \cdot V_t \quad \text{(clearance of free virus; } V \rightarrow *) \tag{3}$$

$$a_2 = \quad (\delta_{\mathrm{PIC}} + \delta_{\mathrm{T_1}}) \cdot \mathrm{T}_{1,t} \quad \text{(clearance of early infected cell; } \mathrm{T_1} \rightarrow *) \tag{4}$$

$$a_3 = \quad \delta_{\mathrm{T_2}} \cdot \mathrm{T}_{2,t} \quad \text{(clearance of late infected cell; } \mathrm{T_2} \rightarrow *) \tag{5}$$

$$a_4 = \quad \beta \cdot \mathrm{T_u} \cdot V_t \quad \text{(infection of a susceptible cell; } V \rightarrow \mathrm{T_1}) \tag{6}$$

$$a_5(D_t) = \quad (1 - \eta_D(t)) \cdot k \cdot \mathrm{T}_{1,t} \quad \text{(proviral integration; } \mathrm{T_1} \rightarrow \mathrm{T_2}) \tag{7}$$

$$a_6 = \quad \mathrm{N_T} \cdot \mathrm{T}_{2,t} \quad \text{(production of virus; } \mathrm{T_2} \rightarrow \mathrm{V} + \mathrm{T_2}), \tag{8}$$

with $\mathrm{CL_T} = \left(\frac{1}{\rho_{\mathrm{rev}}} - 1\right) \cdot \beta$ in eq (3), as outlined in [24] where $\rho_{rev} = 0.5$ denotes the probability to successfully complete reverse transcription in the absence of inhibitors [34, 35]. Free viruses are cleared by the immune system with a rate constant CL. Further, free viruses can be also cleared during unsuccessful T-cell infection $\mathrm{CL_T}$ through the destruction of essential viral components of the reverse transcription-, or pre-integration complex [34, 35]. The term β represents the lumped rate of infection of T-cells, including the processes of virus attachment to the cell, fusion and reverse transcription, leading to an early infected cell T_1, before proviral integration. The term k denotes the rate by which early infected T_1 cells are transformed into

productively infected T_2 cells, involving proviral integration and cellular reprogramming. The term N_T denotes the rate of production of infectious virus progeny by productively infected T_2 cells. The terms $\delta_{T_1} < \delta_{T_2}$ denote the rates of clearance of T_1 and T_2 cells respectively and δ_{PIC} denotes the rate of intracellular destruction of the pre-integration complex. Parameters for the viral model are summarized in Table 1 and a mechanistic derivation of the dynamics from first principles is given in [24] (Supplementary Text therein). In this article, we study distinct prophylactic schemes with the second-generation integrase inhibitor dolutegravir (DTG). Integrase inhibitors act intracellularly by preventing proviral integration. In our virus dynamics model (eqs (3)–(8)), this translates into a decrease in propensity function a_5 by a factor $(1 - \eta_D)$. Notably, DTG is active in its adminstered form (does not require biotransformation) and has physicochemical attributes that allow the unbound drug to rapidly cross the cellular membrane. We modelled the *direct* effect of dolutegravir using the Emax-equation [36]

$$\eta_D(t) = \frac{D_t^m}{IC_{50}^m + D_t^m}, \tag{9}$$

where D_t is the target site concentration of the drug at time t and the term IC_{50} and m denote the drug concentration at which the targeted process is inhibited by 50% and a hill coefficient [37] respectively. Note that the equation above couples the stochastic viral dynamics subsystem Y_t to the deterministic subsystem Z_t, where the latter propagates the drug concentrations $D_t \subseteq Z_t$.

Pharmacodynamic parameters. The hill coefficient m and 50% inhibitory concentration IC_{50} have been measured *ex vivo* using single-round infection assays in primary human peripheral blood mononuclear cells, supplemented with 50% human serum [38]. However, the measured IC_{50} has to be corrected for protein binding, since dolutegravir is highly protein bound in human plasma (98.9%) which will be underestimated by the assay (which utilizes 50% human serum). This correction is in line with the widely accepted 'free drug hypothesis' [39] that states that the available concentrations at the target site (intracellular space) correspond to the *unbound* moieties [40, 41]. Dolutegravir obeys physico-chemical characteristics to enable the *unbound* drug to rapidly cross cellular membranes, generating an equilibrium between the *unbound* drug on either side of the cellular membrane [42]. However, since the *unbound* fraction $f_{u,\text{assay}}$ in the assay is different to the physiological *unbound* fraction $f_{u,\text{plasma}}$, the measured IC_{50} value needs to be adjusted/scaled. After protein adjustment, we obtain $IC_{50} = 89 (CV = 25.3\%)$ [nM] and $m = 1.3 (CV = 15.3\%)$, see related article [23].

Dolutegravir pharmacokinetics (deterministic part)

We used non-linear mixed effects modelling techniques [43] to derive a *descriptive* pharmacokinetic model that accurately captures the observed pharmacokinetic variability within- and across different patients. In this framework, both a minimal structural model $f(\theta_i, \cdot)$ is fitted to clinical data, alongside with statistical models describing the distribution of pharmacokinetic parameters θ within the population, as well as the measurement- or unexplained noise.

Let $\mathcal{D}_{i,t}$ be the measured plasma concentration of a drug in the i^{th} individual at time point t. The likelihood of that measurement is defined through

$$\mathcal{D}_{i,t} = f(\theta_i, t) \cdot (1 + \epsilon_{i,t}) + \tilde{\epsilon}_{i,t} \tag{10}$$

where f denotes the solution of the structural model (a low dimensional set of ordinary differential equations; see below) that corresponds to the measurement. The vector θ_i contains the pharmacokinetic parameters for the i^{th} individual. The variables $\epsilon_{i,t}$ and $\tilde{\epsilon}_{i,t}$ denote proportional and additive error terms (measurement- or unexplained noise), which are typically

assumed to be normal distributed, i.e. $\epsilon_{i,t} \sim \mathcal{N}(0, \sigma^2)$ and $\tilde{\epsilon}_{i,t} \sim \mathcal{N}(0, \tilde{\sigma}^2)$. The *prior* probability is typically assumed to be a multivariate log-normal distribution with

$$\log \theta_i = \log \theta + r_i, \tag{11}$$

where θ denotes the vector of mean population parameters (fixed effects) and r_i is normal distributed, i.e. $r_i \sim \mathcal{N}(0, \Psi)$.

Parameter and model inference. We used dolutegravir concentration-time data from two clinical studies. One study assessed 50mg once daily dolutegravir administered to 17 healthy volunteers for 10 days and serial blood sampling performed up to 216 hours after the final dose [44] (n = 12 female, n = 8 Caucasian). The second study was performed in 39 HIV-infected patients (n = 2 female, n = 27 Caucasian) stable on efavirenz-based therapy (viral load <40 copies/mL), switched to dolutegravir (50mg once daily). Random, single blood samples were drawn over the 24 hour dosing interval 1, 2, 3 and 4 weeks post-switch [45]. Median (range) age, weight and BMI of all individuals were 47 years (26-68), 76 kg (51-105) and 26 kg/m^2. All data were modelled simultaneously and the first-order estimation (FOCE-I) method of NONMEM (v.7.3, ICON plc, Dublin, Ireland), interfaced with Pirana (v.2.9.0; www.pirana-software.com) was used for parameter inference. One- and two compartment models were explored with differences between hierarchical models assessed by statistical and graphical methods. The minimal objective function value (OFV; equal to -2 log likelihood) was used as a goodness-of-fit diagnostic with a decrease of at least 3.84 units corresponding to a statistically significant difference between nested models (p = 0.05, χ^2 distribution, 1 degree of freedom). Standard errors of the estimates were determined with the COVARIANCE option of NONMEM and individual Bayesian parameter and concentration estimates by the POSTHOC option. Random effects (inter-individual, inter-occasion variability) in model parameters were included if model fit was improved (i.e. ΔOFV $\geq$-3.84 points). To describe residual variability, proportional, additive and a combined proportional-additive error models were evaluated and the best fitting were carried forward. The effect of residual efavirenz concentrations on dolutegravir clearance was determined by estimating 5 separate fixed effects (CL/F values) for dolutegravir alone in healthy volunteers (study 1) and for weeks, 1, 2, 3, 4, post-switch from efavirenz in HIV-infected patients (study 2). Other covariates assessed in the model included weight, age, body mass index (BMI), sex, ethnicity, HIV status, and food consumption within 3 hours of drug intake. A forwards inclusion-backwards elimination method [46] was used to determine whether there were any important associations between parameter estimates and covariates. Each covariate was introduced separately and only retained in the model if inclusion produced a statistically significant decrease in OFV of at least 3.84 units ($p \leq 0.05$, χ^2 distribution, 1 degree of freedom) and was biologically plausible. A backwards elimination step was carried out once all relevant covariates were incorporated and covariates retained if removal from the model produced a significant increase in OFV (> 10.83 points; $p \leq 0.001$, χ^2 distribution, 1 degree of freedom).

Final PK model. The final model was a two-compartment model with oral absorption:

$$\frac{d}{dt} Z_1 = -k_a \cdot Z_1 \tag{12}$$

$$\frac{d}{dt} D = \frac{d}{dt} Z_2 = \frac{k_a \cdot Z_1}{V_c/F_{\text{bio}}} - \frac{\text{CL}/F_{\text{bio}}}{V_c/F_{\text{bio}}} \cdot Z_2 - \frac{Q/F_{\text{bio}}}{V_c/F_{\text{bio}}} \cdot Z_2 + \frac{Q/F_{\text{bio}}}{V_p/F_{\text{bio}}} \cdot Z_3 \tag{13}$$

$$\frac{d}{dt} Z_3 = \frac{Q/F_{\text{bio}}}{V_c/F_{\text{bio}}} \cdot Z_2 - \frac{Q/F_{\text{bio}}}{V_p/F_{\text{bio}}} \cdot Z_3, \tag{14}$$

whereby Z_1 and Z_3 denote the amount of drug in the dosing compartment and the concentration of dolutegravir in the peripheral compartment respectively. The variable of interest is the concentration in the blood plasma (central compartment), i.e. $D = Z_2$. Dosing events were modelled as impulse inputs, with

$$Z_{1,t} = Z_{1,t} + \text{dose}_k, \tag{15}$$

whenever the current simulation time t coincided with a dosing event τ_k. In the equations above, k_a and CL/F_{bio} denote the uptake and bioavailability-adjusted drug clearance respectively. The term V_c/F_{bio} and V_p/F_{bio} are the bioavailability-adjusted volume of the central and peripheral compartment. The term Q/F_{bio} is the intercompartmental clearance rate adjusted for bioavailability.

Numerical simulation of hybrid model

As mentioned before, direct computation of the extinction probabilities in eq (1) may not be possible as Y_t still contains a prohibitively large number of states. In the following, we will utilize the results from a related article [23] in combination with the novel EXTRANDE algorithm [12] to compute the extinction probabilities for *time-varying* drug effects, i.e. taking drug pharmacokinetics into account.

We consider $a_0(Y_t, D_t) = \sum_k a_k(Y_t, D_t)$ to be the sum of the K reaction propensities changing the internal stochastic system. Note that in the exact SSA [47], no external input exists and therefore the propensities stay constant in between two reaction firings. In this case, the time to the next reaction event is exponentially distributed with parameter a_0. In our case $a_0(t)$ changes between two stochastic reaction firings because of pharmacokinetic inputs. Solving this problem requires to compute $a_0(t)$ by numerical integration each time after a stochastic reaction has fired, which can be computationally expensive. Instead, in EXTRANDE, an upper bound B for $a_0(t)$ is estimated and thinning techniques (rejection steps) are employed. For a look-ahead time horizon L, the upper bound B_{t+L} is chosen, such that

$$B_{t+L} \geq a_0(Y_{t+u}, D_{t+u}) \tag{16}$$

holds for all $u \leq L$ and assuming no stochastic reaction fires within the time interval $t + L$. When L is fixed, it is possible to solve for D_{t+L}, since it is assumed that stochastic reactions do not affect D. E.g. if the dynamics of $D \subseteq Z$ are determined by a set of ordinary differential equations, numerical integration from t to $t + L$ enables to predict D_{t+L}, which in turn allows to compute $a_0(Y_{t+u}, D_{t+u})$.

The internal stochastic system is then augmented with an extra reaction (a K+1th reaction), whose firing does not change the state of the stochastic subsystem Y. The probability of firing this extra reaction at time $t + L$ is proportional to the ratio $\frac{B_{t+L} - a_0(Y_{t+u}, D_{t+u})}{B_{t+L}}$.

Obviously, it has to be guaranteed that eq (16) is true for the entire look-ahead time horizon L. On the other hand when B_{t+L} is chosen to be too large, many extra reactions will be fired (rejection/thinning step) and the algorithm becomes inefficient. A key to efficient simulation with EXTRANDE is therefore a good choice of B_{t+L}, which in turn depends on the look-ahead time horizon L.

Upper bound *B* and look-ahead horizon *L*. From equation eq (9) it is clear that $(1 - \eta_D) \in [0, 1]$ and consequently

$$a_0(Y_{t+u}, D_{t+u}) \leq a_0(Y_t, \varnothing), \tag{17}$$

for any time interval $0 \leq u \leq \tau$ *before* a stochastic reaction has fired where parameter $\varnothing$ denotes

the absence of drugs. Consequently, we used $B = a_0(Y_t, \varnothing)$ throughout the article as an upper bound to meet condition $a_0(Y_{t+u}, D_{t+u}) \leq B$ without the requirement to select a look-ahead time horizon L.

Classification of trajectories. When using EXTRANDE to assess the PrEP/PEP efficacy, we are particularly interested in classifying stochastic trajectories as *extinction* or *infection* events. The virus dynamics model has an absorbing state $Y_t = [0, 0, 0]^T$ corresponding to virus extinction. Whenever trajectories hit this state we can stop the simulation. To stop the simulation when trajectories move away from the extinction state is not a straightforward choice.

Given a user-defined threshold $\varepsilon << 1$ we only consider stochastic states within an *extinction simplex*, e.g. states Y for which

$$P_{\mathrm{E}}(Y_t, D_{\max}(t)) \geq \varepsilon \tag{18}$$

is true, i.e. extinction can occur with a probability greater ε. Simulations are consequently stopped whenever $P_{\mathrm{E}}(Y_t, D_{\max}(t)) < \varepsilon$, where $D_{\max}(t) = \max_{u\in[t,\,\infty]} D_u$ denotes the maximum achievable drug concentration in $[t, \infty]$ to be pre-computed from a pharmacokinetic trajectory. This criterium guarantees that the numerical error in classifying trajectories as infection events stays below the user defined criteria $\varepsilon << 1$.

In a related article [23], we derived analytical solutions for computing the extinction probability for any particular state of the virus dynamics system, under the assumption that the drug concentrations D were constant (for computing the *extinction simplex*, we use $D = D_{\max}(t)$):

$$\log_{10}(P_{\mathrm{E}}(Y, D)) \quad = \quad \mathrm{V} \cdot \log_{10}(P_{\mathrm{E}}(\hat{\mathrm{V}}, D)) + \mathrm{T}_1 \cdot \log_{10}(P_{\mathrm{E}}(\hat{\mathrm{T}}_1, D)) + \mathrm{T}_2 \cdot \log_{10}(P_{\mathrm{E}}(\hat{\mathrm{T}}_2, D)).$$

where $P_{\mathrm{E}}(Y_0 = \hat{\mathrm{V}})$, $P_{\mathrm{E}}(Y_0 = \hat{\mathrm{T}}_1)$ and $P_{\mathrm{E}}(Y_0 = \hat{\mathrm{T}}_2)$ denote the extinction probabilities when only one virus, one early- or one productively infected cell was present, and V, T_1 and T_2 denote the number of viruses, early- and late infected cells. These terms can be further decomposed (see related article [23]) into

$$P_{\mathrm{E}}(Y_0 = \hat{\mathrm{V}}) = \min\left(1, 1 - \frac{a_4}{a_1 + a_4} \cdot \frac{a_5(D)}{a_2 + a_5(D)} \cdot \left(1 - \frac{1}{R_0(V, D)}\right)\right) \tag{19}$$

$$P_{\mathrm{E}}(Y_0 = \hat{\mathrm{T}}_1) = \min\left(1, 1 - \frac{a_5(D)}{a_2 + a_5(D)} \cdot \left(1 - \frac{1}{R_0(V, D)}\right)\right) \tag{20}$$

$$P_{\mathrm{E}}(Y_0 = \hat{\mathrm{T}}_2) = \min\left(1, \frac{1}{R_0(V, D)}\right), \tag{21}$$

where $R_0(V, D) = \frac{a_4}{a_1 + a_4} \cdot \frac{a_5(D)}{a_2 + a_5(D)} \cdot \frac{a_6}{a_3}$ is the reproductive number in the presence of drug D, i.e. the expected number of viruses emerging from a single parent virus in one replication cycle.

The *extinction simplex* (eq (18)) then divides the entire state space of $Y \in \mathbb{N}^3$ into two sets: one where the extinction is possible (the probability of extinction exceeds ε) and one where irreversible infection occurred. Consequently, we can stop simulating and classify a trajectory as an 'infection event' whenever the trajectory leaves the *extinction simplex*. Moreover, the *extinction simplex* is dynamically adapted through the simulations by adaptation of $D_{\max}(t)$. The effects of changing drug concentrations on the *extinction simplex* are illustrated in Fig 1 for a short course PrEP ('PrEP on demand') with dolutegravir in a virtual patient. The green triangle highlights the *extinction simplex* without drugs. Obviously, the *extinction simplex* in the absence of drugs is enclosed by the *extinction simplices* in presence of antivirals (i.e. viral

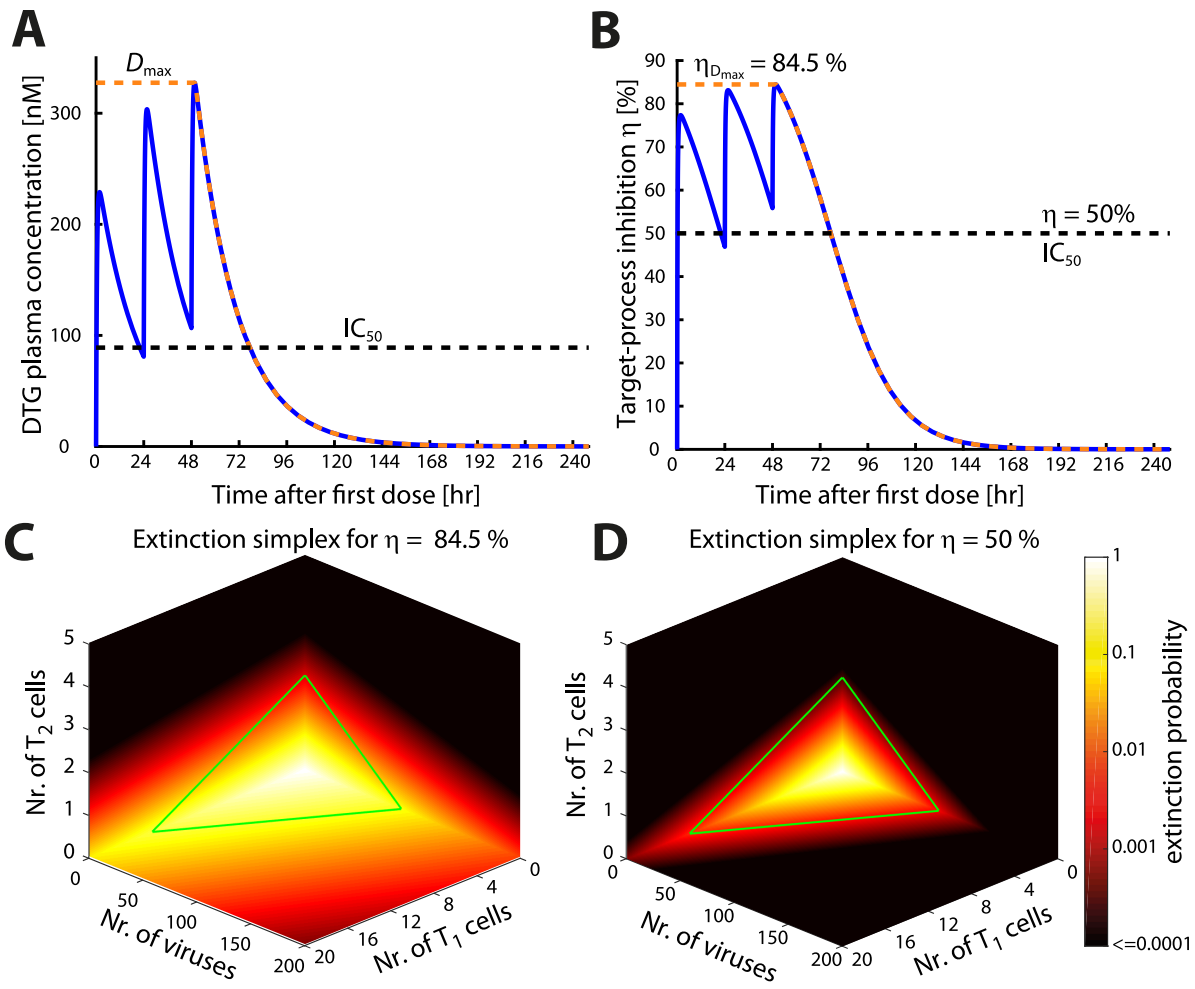

Fig 1. Adaptation of extinction simplex for pharmacokinetics. A: Exemplary DTG pharmacokinetics for 3days of 2mg oral DTG once daily. The blue line represents DTG plasma concentrations. The dashed orange line represents the function $D_{max}(t)$, which for a particular t returns the maximum DTG concentration achieved in any future time i.e $D_{max}(t) = \max(D(u))$ where $u \in [t, \infty)$. The black horizontal dashed line marks the IC_{50} for DTG [38]. **B**: Instantaneous target-process inhibition (blue line) corresponding to the concentration-time profile in **A**. The orange line is the target-process efficacy profile for $D_{max}(t)$. The black horizontal dashed line marks $\eta = 50\%$. **C**: Extinction simplex (viral infection state where the probability of viral extinction is greater than ε) corresponding to $\eta_{D_{max}} = 84.5\%$. **D**: The extinction simplex corresponding to $\eta = 50\%$. Panels **C&D** show the state space with three dimensions corresponding to number of free viruses, early-infected T cells (T_1) and late-stage infected T cells (T_2). The color varies from bright yellow denoting certain extinction, to black denoting an extinction probability less than 0.0001. The region enclosed by green lines is the extinction simplex in absence of antivirals.

https://doi.org/10.1371/journal.pcbi.1006155.g001

extinction may still be possible in the presence of drugs when the viral population is substantial as in post-exposure prophylaxis PEP). Fig 2 shows two exemplary trajectories for the coupled pharmacokinetic-viral dynamic system, in case of low (5%) adherence to a 2mg oral dolutegravir regimen. Panels A & B show the instantaneous drug efficacy η (panel A) and the corresponding viral trajectory which is classified as an 'infection event' (panel B), whereas panels C & D show an exemplary trajectory where virus elimination occurs.

Infection of long-lived cells. It has been proposed that long lived- and latently infected cells denote a major barrier to the elimination of HIV and that they may be established early in infection [48–50]. Thus, if any of these compartments become infected after viral exposure, infection may be considered irreversible. During simulations we considered two parameters,

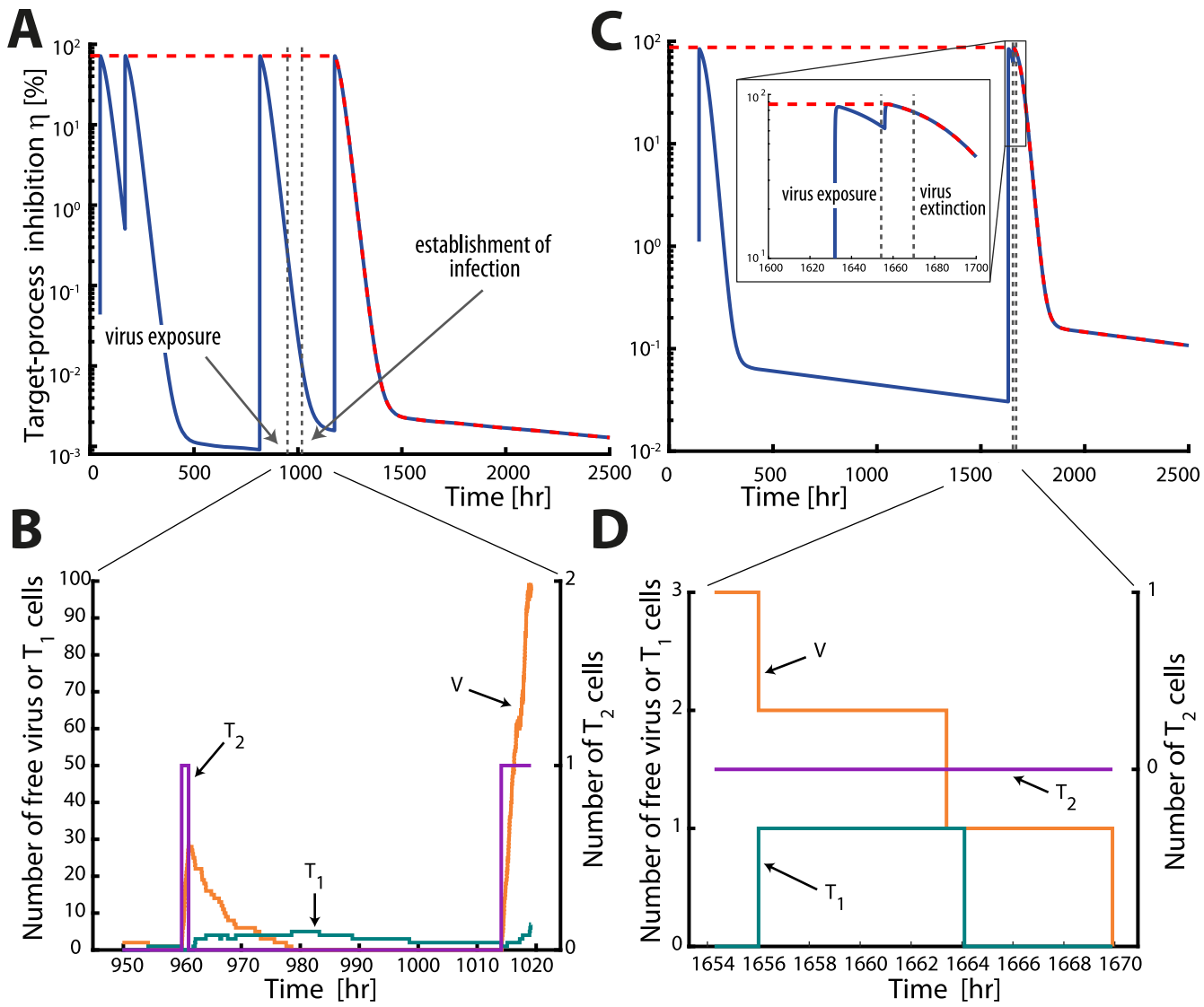

Fig 2. Examplary trajectories for time-varying drug effects. The left panels show an example of an infection event, whereas the right panels show an example of viral extinction for chronic PrEP with 2mg DTG and 5% adherence. Panels **A** and **C** depict the instantaneous target-process inhibition profiles and panels **B** and **D** depict the corresponding viral trajectories using the adapted EXTRANDE algorithm. Viral exposure occurs randomly during a 3 month period and is sampled from the distribution parameterized in [11] (Figure 2 therein). **A&C:** The blue lines depict the instantaneous target-process inhibition profiles $\eta_D(t)$. The dashed red line denotes the maximum target-process inhibition $\eta_{D_{max}}(t)$. The leftmost grey vertical dashed lines mark the time of viral exposure, whereas the rightmost lines marks the time point of either establishment of infection (panel **A**) or virus extinction (panel **C**). **B&D:** Stochastic trajectories of viral compartments (orange: free viruses, green: early-infected cells T_1, purple: late-infected T_2 cells) for the time after virus exposure and before virus infection/extinction. Stochastic simulations are stopped in panel **B** when the trajectories leave the extinction simplex and because of virus extinction in panel **D**.

https://doi.org/10.1371/journal.pcbi.1006155.g002

$p_{M|a_4} = 1.25 \cdot 10^{-4}$ and $p_{L|a_5} = 8 \cdot 10^{-6}$ to assess whether a long-lived cell (e.g. macrophage) had been infected or whether a latently infected cell emerged. These parameter choices accurately reproduce viral decay kinetics during antiretroviral combination therapy, as shown in [24, 25] and recapture estimated reservoir sizes during chronic infection [2, 48]. I.e., during simulations, whenever reaction R4, or R5 fires, it is assessed whether a long lived- or latently infected cell emerged.

The complete pseudo-code of the adapted EXTRANDE algorithm is presented S1 Text.

Simulation of pre- and post-exposure prophylaxis

Codes were written in MatLab R2016b (MathWorks, Natick, MA; v. 9.1, including optimization, parallel computing and statistics toolboxes). Individual pharmacokinetic model parameters for healthy individuals were drawn from the distributions defined by the parameter estimates from the final dolutegravir population pharmacokinetic model (Table 2; NONMEM $SIMULATION, n = 1000 individuals; eqs (12)–(14)). We then simulated individual pharmacokinetic profiles for the prophylactic schedule S_D under consideration using ode15s in MatLab. To simulate different adherence levels, a sequence of uniformly distributed random numbers with $r_i \sim \mathcal{U}(0,1)$ was drawn and the ith dose was missed if $r_i >$ adherence level. The number of viruses to be inoculated were drawn from a previously parameterized distribution that accurately resembles the relation between transmitter virus loads and recipient infection probabilities [11]. In brief, we used a two-stage process: First, we sampled the viral load VL in a potential transmitter. Earlier work [11] (Supplementary Note 4 therein) showed that the virus load distribution in potential transmitter populations [51] follows a log-normal distribution, i.e. $\mathrm{VL} \sim \log\mathcal{N}(\mu,\sigma)$ with $\mu = 4.51$ and $\sigma = 0.98$. Secondly, we used the virus load in the transmitter to determine the number of viruses V_0 entering a replication-competent compartment in the virus-exposed individual using a binomial model: $V_0 \sim \mathcal{B}(f(\mathrm{VL}), r_{\mathrm{homo}})$ with $r_{\mathrm{homo}} = 3.71 \times 10^{-3}$ for homosexual exposure [11], $f(\mathrm{VL}) = ||\mathrm{VL}^c||$, where $||\cdot||$ is the next integer function, and $c = 0.389$ [52, 53]. For PrEP simulations with different adherence levels, a time of virus exposure was randomly drawn within a 3 month interval. The corresponding drug concentrations at this time and the number of transmitted viruses reaching a target cell compartment were used as the initial states for EXTRANDE and simulated until stopping criteria were satisfied, illustrated in Fig 2 for virus infection (panels A & B) and -elimination (panels C & D). For 'PrEP on demand' simulations, the time of virus exposure was fixed as indicated in the corresponding graphics. In case of PEP, virus was inoculated as stated above and the stochastic viral dynamics were simulated in the absence of drugs until the time of PEP initiation to determine the initial condition of the system and henceforth simulated until a stopping criterium was reached.

In total, for each prophylactic strategy, 5000 simulations were run.

Results

Pharmacokinetics of oral dolutegravir

A total of 354 plasma concentration measurements from 56 individuals were used to build the population pharmacokinetic (PK) model for dolutegravir (DTG). Healthy volunteers (N = 17)

Table 2. Pharmacokinetic parameter estimates. The table displays the estimated pharmacokinetic parameter estimates for healthy individuals. Interindiviual variability (random effects) was included on drug clearance $\mathrm{CL}/F_{\mathrm{bio}}$ and the volume of distribution V_c/F_{bio}. These parameters were log-normal distributed as outlined in the *Methods* section, eq (11), with coefficient of variation [%] $CV = 100 \cdot \sqrt{e^{\sigma^2} - 1}$, where σ^2 is the variance of the associated normal distribution. A covariance of $11.3\% = 100 \cdot \sqrt{e^{\sigma^2_{x,y}} - 1}$ between $x = \mathrm{CL}/F_{\mathrm{bio}}$ and $y = V_c/F_{\mathrm{bio}}$ was estimated. The absorption rate constant was fixed [88] to $2.24\mathrm{h}^{-1}$. Residual variability (eq (10)) was described by a combined proportional-additive model for healthy volunteers [$\sigma = 0.213$ (37.2%) and $\tilde{\sigma} = 0.0019$ mg/L (40.9%), respectively] and a proportional error model for HIV-infected patients [$\sigma = 0.402$ (24.2%)].

parameter	value	unit	*CV* [%]
V_p/F_{bio}	0.73	L	-
Q/F_{bio}	0.0082	L/h	-
$\mathrm{CL}/F_{\mathrm{bio}}$	0.85	L/h	16.9
V_c/F_{bio}	17.7	L	16.4

https://doi.org/10.1371/journal.pcbi.1006155.t002

contributed rich PK profiles with a total of 270 samples taken between 0 hours (pre-dose) and 216 hours after a final DTG dose. In addition, eighty-four measurements, randomly drawn between 1-25.75 hours post-dose were available from HIV patients week 1, 2, 3 and 4 weeks post-efavirenz switch. A two-compartment pharmacokinetic model best described the data (Fig 1A) and was fitted in a Bayesian context to fully capture inter-individual pharmacokinetic variability. Following multivariate analysis, allometric scaling (centered on 70kg) of weight was considered as a fixed effect in the model. Different values of apparent oral clearance (CL/F_{bio}) were estimated for DTG alone in healthy volunteers and in patients following 1, 2, 3 and 4 weeks post-treatment switch. Residual variability was described by a combined proportional-additive model for healthy volunteers and a proportional error model for HIV-infected patients. All parameter estimates for healthy volunteers are displayed in Table 2. The model was used to generate PK parameters of virtual patients populations, whose PK-profiles are summarized in Fig 3B–3D alongside observed DTG concentrations, Fig 3C and 3D.

As can be seen in Fig 3B, dolutegravir is rapidly absorbed after oral administration and maximal concentrations are achieved after t_{max} = 1.58 hours (population 5–95% range 1.53–1.63). Pharmacokinetics reach a steady state after about 4 doses. During steady state, minimum- (pre-dose) and maximum concentrations were C_{min} = 2918nM (1916–4336) and C_{max} = 8471nM (6353–11331) for 50mg oral DTG and the half life of the drug was 14.5h (5–95% range 13.5–15.9).

Prophylactic utility of oral dolutegravir

Fig 4A shows the relation between the plasma concentration of DTG and its prophylactic efficacy after homosexual virus exposure. For these simulations, the number of viruses reaching a replication-competent compartment after homosexual contact were sampled from a previously parameterized virus exposure model [11] (Fig.2 and Supplementary Note 4 therein). The estimated concentration ranges achieved at steady state for 2-, 10- and 50mg oral DTG once daily were 117–339, 583–1694 and 2918–8471nM respectively as indicated on the y-axis of Fig 4A. Within this concentration range, the median prophylactic efficacy for once daily 2mg ranged from 43.6 to 75.7%. For 10mg, efficacies ranged from 87.1 to 97.5%, and for 50mg almost complete (99.5 to 100%) protection was achieved. The estimated concentrations to prevent 50- and 90% infections, $EC_{50}(\hat{V})$ and $EC_{90}(\hat{V})$, were 145.18 and 722.23nM respectively.

Sensitivity to incomplete medication adherence

During pre-exposure prophylaxis, medication adherence may be incomplete. Fig 4B displays the prophylactic efficacy of once daily 50mg, 10mg and 2mg oral dolutegravir, considering varying levels of adherence (25-, 50-, 75-, 95- and 100% of doses taken). Viral challenges were simulated to randomly take place during a 3 month interval with inoculum sizes drawn from a previously parameterized distribution [11], see Fig 2 for two examples. The mean predicted prophylactic efficacies for 50mg with 25-, 50-, 75-, 95- and 100% adherence were 60% (95% confidence bounds: 55.15–64.84), 85.54% (82.58–88.50), 96.63% (95.19–98.07), 98.88% (98.04–99.71) and 99.36% (98.73–99.99), respectively. Notably, the prophylactic efficacy of 50mg oral DTG becomes saturated, and exceeds 95%, if at least 75% of the pills were taken. Conversely, 2mg and 10mg oral dolutegravir allow for considerable residual infection events and 2mg oral dolutegravir efficacy increases almost linear with increasing adherence levels.

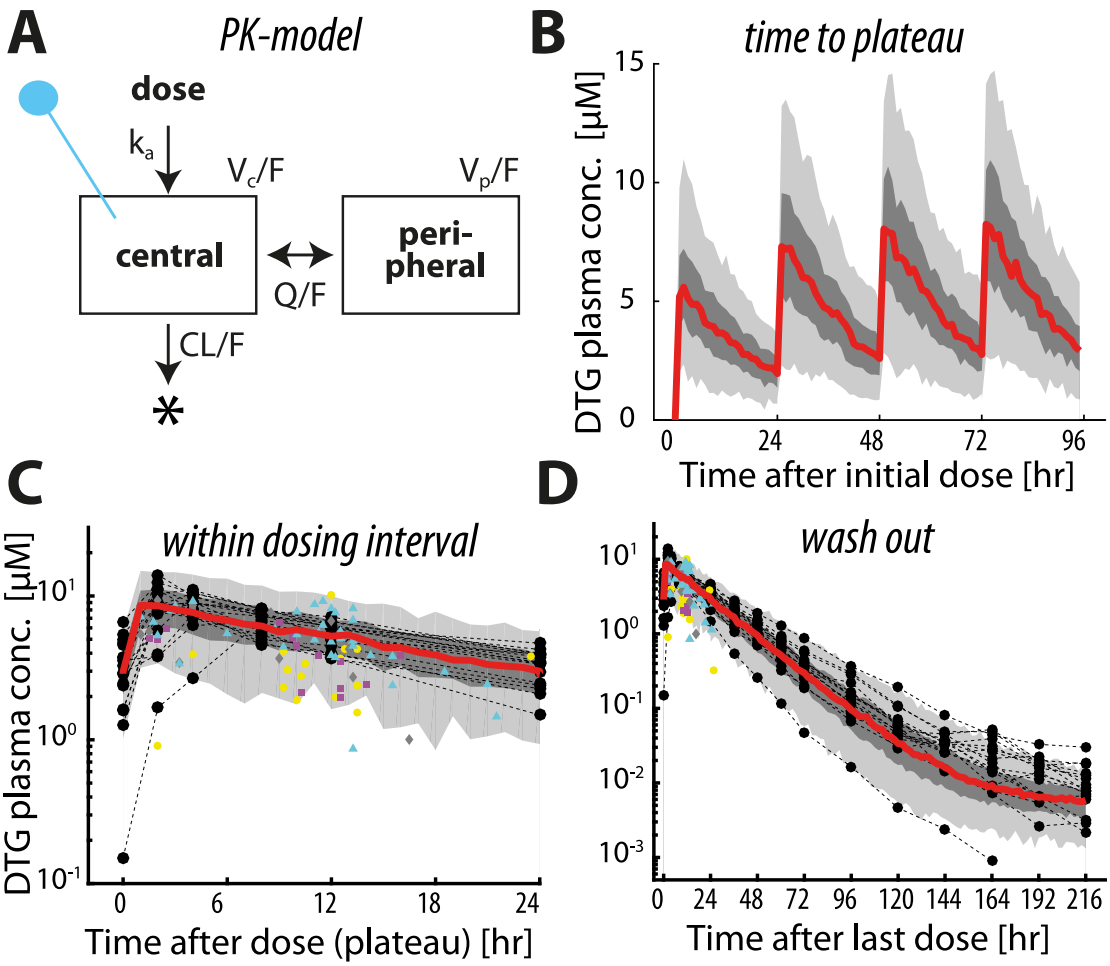

Fig 3. Population pharmacokinetics of dolutegravir (DTG). A: Pharmacokinetic model. Concentrations within the central compartment with bioavailability-adjusted volume V_c/F correspond to measured plasma concentrations of DTG (indicated by the blue pin). Parameters k_a, Q/F_{bio} and CL/F_{bio} denote the uptake and bioavailability-adjusted inter-compartimental and drug clearance rate respectively and V_p/F_{bio} denotes the bioavailability adjusted volume of the peripheral compartment (which summarizes all 'deep' compartments, which are not in rapid exchange with the plasma). **B:** Predicted plasma concentration time profiles of dolutegravir (DTG) for the first four days after initiation of a once daily 50mg oral regimen ($N = 300$ virtual patients). The red line depicts the median predicted concentrations, whereas the dark- and light grey areas present the quartile range and 5–95% range respectively. Predicted (red line, grey areas) and measured plasma concentrations during 24h after drug intake in steady state (panel **C**) and after cessation of drug intake (panel **D**). Black circles and thin dashed lines represent DTG plasma concentration profiles in healthy volunteers (n = 17 concentration time profiles, 270 data points in total), whereas yellow circles, purple squares, grey diamonds and cyan triangles are DTG plasma concentration measurements in HIV patients (n = 39) observed 1, 2, 3 and 4 weeks after switching from efavirenz-based therapy to dolutegravir. Altogether, 354 plasma concentration measurements from 56 individuals are depicted.

https://doi.org/10.1371/journal.pcbi.1006155.g003

PrEP on demand/event-based dosing

'PrEP on demand' denotes a short-term pre-exposure prophylaxis, initiated only a few hours before a potential viral exposure. This strategy has recently been evaluated in the IPERGAY study using Truvada [54]. We simulated a dosing scheme similar to the IPERGAY protocol [54]: An individual at risk initiates PrEP only a few hours before a potential viral exposure and takes two consecutive doses 24 and 48hours after the first dose. Fig 4C depicts the predicted prophylactic efficacy of DTG when taken 'on demand'. Population pharmacokinetic profiles for 'PrEP on demand' using 50mg are depicted in Fig 3A. The mean prophylactic efficacies for

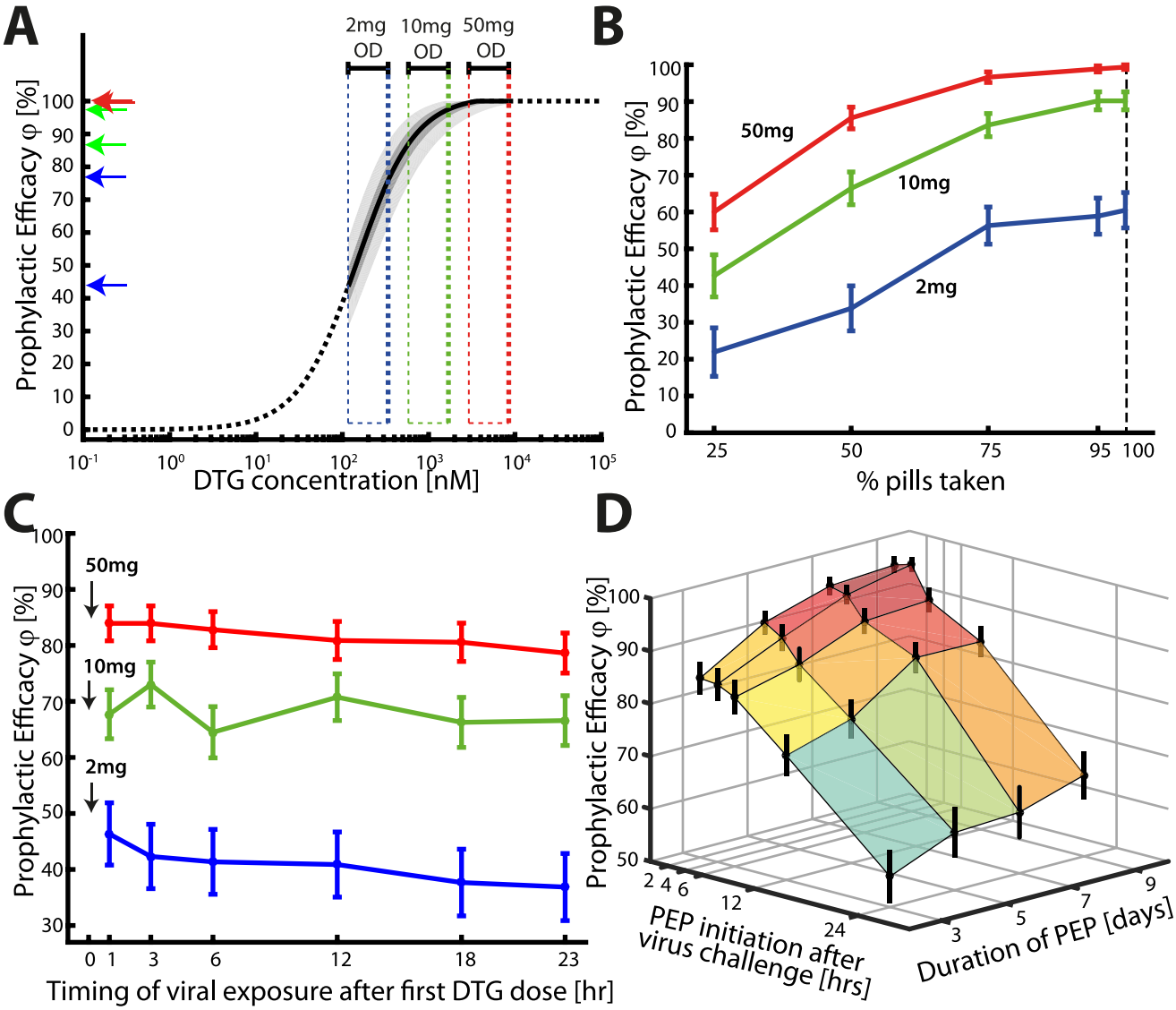

Fig 4. Efficacy of different DTG prophylactic regimen. A: Prophylactic utility of chronically administered oral DTG regimen (homosexual contact [11]). The red-, green and blue dashed boxes mark the considered concentration ranges of DTG [C_{min} (pre-dose), C_{max}] achieved with 50, 10 and 2mg once daily (OD) oral dosing. The left pointing arrows at the y-axis mark the respective prophylactic efficacy ranges. **B:** Prophylactic efficacy of chronically adminstered oral DTG regimen with varying adherence levels. The red-, green- and blue lines denote mean prophylactic efficacy for a 50mg, 10mg and 2mg oral DTG regimen. Errorbars depict the 95% confidence bounds for the ensemble estimate, computed using Greenwoods formula. **C:** Prophylactic efficacy of DTG for 'PrEP on demand'. Only three doses of oral DTG were ingested at 0, 24 and 48 hours. Homosexual viral exposure occurred within the first dosing interval at either 1, 3, 6, 12, 18 or 23 hours after initiating 'PrEP on demand'. The red, green and blue lines represent the mean prophylactic efficacy for 'PrEP on demand' using 50-, 10 or 2mg respectively, where error bars denote the 95% confidence bounds for the ensemble estimate, computed using Greenwoods formula. **D:** Prophylactic efficacy for 'post exposure prophylaxis' (PEP) with 50mg DTG for various durations of PEP (y-axis; 3, 5, 7 and 9 days) and delayed initiation of PEP after homosexual viral exposure (x-axis; 2, 4, 6, 12 and 24 hours). Error bars mark the 95% confidence bounds computed using Greenwoods formula.

https://doi.org/10.1371/journal.pcbi.1006155.g004

50mg varied, depending on the timing of the first dose with respect to viral exposure, between 78.63–83.93% (95% confidence bounds: 75.05–87.05), for 10mg between 64.49–73.01% (59.92–77.02) and for 2mg it was 36.86–46.34% (30.87–51.90). The prophylactic efficacy decreased with decreasing dose and also with increasing time difference between the initiation of 'PrEP on demand' and viral exposure, clearly visible for 50 and 10mg. This trend is opposite to the trend for 'PrEP on demand' with Truvada [11]. A reason for this is the fast uptake of

systemic DTG (compare Fig 4B), whereas the Truvada's active components tenofovir diphosphate (TFV-DP) and emtricitabine triphosphate (FTC-TP) require intracellular phosphorylation after cellular uptake of the parent compound, which delays the time until maximal concentrations are achieved at the target site [31, 55]. Since DTG does not need to undergo any chemical modification, and according to 'free drug hypothesis' the unbound intracellular concentration largely reflects the unbound plasma concentration, implying that the drug rapidly reaches the target site.

Post-exposure prophylaxis (PEP)

Lastly, we wanted to assess the efficacy of 50mg oral DTG in preventing infection when taken as post-exposure prophylaxis (PEP). We assessed the prophylactic efficacy with regard to different durations of PEP and with regard to the timing of initiation after virus exposure in Fig 4D. Fig 4D indicates that 50mg oral DTG can effectively prevent infection ($> 80\%$) when initiated shortly (within 6 hours) after exposure and when continued for as long as possible. The graphics indicate that the efficacy starts to drop when PEP is initiated later than 6 hours and when it is taken shorter than 7 days. Also, our simulations suggest that initiating the prophylaxis earlier has a more pronounced effect than prolonging PEP, arguing for the immediate start of PEP in case of known- or suspected HIV exposure.

Comparison with Truvada

We previously estimated that once daily PrEP with Truvada provides $\approx 96\%$ protection in fully adherent individuals [11]. While it is difficult to quantify PrEP adherence clinically [56], a surrogate measure is often calculated based on the percentage of individuals with detectable drug. Corresponding clinical efficacy estimates in apparently highly adherent individuals were 86-100% in the IPERGAY study [57], 58-96% in the PROUD study [6] and 96% in the Partners PrEP OLE study. In comparison, we predicted almost complete (99-100%) protection when 50mg DTG was taken once daily for prophylaxis. The VOICE [58] and FEM-PrEP [59] studies indicated that Truvada may not prevent infection in poorly adherent individuals, i.e. if $\approx 30\%$ of individuals had detectable drug. In comparison, with 25% adherence to once daily 50mg DTG, we estimated about 60% protection and over 85% protection if at least half the drugs were taken. For 'PrEP on demand' with Truvada, we recently estimated [11] that about 74–92% infections can be averted, depending on the time of viral exposure relative to the initiation of Truvada dosing. The corresponding efficacy estimate in the IPERGAY trial was 86% [54], in line with our previous work. Herein, we predicted that 'on demand' PrEP with 50mg DTG is non-inferior to Truvada, providing 78.63–83.93% protection. Lastly, while PEP with Truvada is not recommended due to the slow intracellular accumulation of pharmacologically active NRTI-triphosphates, PEP with 50mg DTG can prevent about 80% infections when initiated no later than 6hours post exposure. In summary, our simulations indicate that prophylaxis with 50mg DTG is non-inferior to Truvada and that it may outperform Truvada when individuals' medication adherence substantially deviates from a once daily PrEP protocol, as in the case of poor adherence and post-exposure prophylaxis.

Discussion

While pre-exposure prophylaxis with Truvada can prevent sexual HIV-1 transmission, it has severe limitations that are to be overcome by next-generation PrEP regimen [8]. However, drug candidate selection for next-generation PrEP and selection of administration schemes in clinical trials are prone to high failure rates. One reason is the poor translatability of animal- and ex vivo/in vitro experiments, whereas the statistical requirement of large sample sizes

(N > 1000 individuals) and long trial durations to detect prophylactic efficacy *clinically* leads to exorbitant costs. Thus, there is an unmet need for tools to *a priori* assess the utility-, select and prioritise next generation PrEP candidates for human trials.

Our intent was to develop a method that integrates pharmacokinetic and pharmacodynamic (PK/PD), as well as viral characteristics (inoculum size, timing of exposure) to *a priori* assess prophylactic strategies against HIV. Such integrative framework allows for the intelligent design of once-daily, episodic PrEP, as well as simulating the on- and offset of event-driven PrEP [54] or long-acting injectable PrEP formulations [60–62]. Moreover, it allows to assess how stable a prophylaxis is when individuals poorly adhere to the planned prophylaxis scheme, i.e. when individuals miss dosing events or start to take the drugs shortly before- or only after exposure to HIV. The use of population pharmacokinetic models allows for an accurate description of the observed pharmacokinetic variability within- and across patients, which can be used to assess the effectiveness of PrEP coverage in metabolically diverse population (Figs 3 and 4). While the attributes which make any compound favourable *in the clinic* extend beyond PK/PD, our approach is particularly useful to rule out- or prioritize PrEP candidates and/or strategies for further *clinical* investigation.

To enable this ambitious goal we had to develop the theoretical basis that would enable us to accurately predict infection/extinction events for any arbitrary prophylaxis dosing regimen. The theoretical context is to compute solutions of the chemical master equation (CME), which is intractable due to the *curse of dimension*. Most naturally, instead of directly solving the CME, it is possible to sample trajectories using Monte Carlo techniques such as the stochastic simulation algorithm (SSA) [47] and to empirically reconstruct $\mathbb{P}(X_t = x_i)$ from the trajectories. However, it is not clear when to classify a trajectory as an infection event. Moreover, stochastic simulations become inefficient when reaction propensities are high, which is typically encountered in a large copy number regimen, e.g. when $X_t >> 1$. To solve the latter issue (large copy number regimen), a number of hybrid methods have been proposed that partition a system $X = (Y, Z)$ into species Y that are represented by a discrete-stochastic (CME) model and species Z that are approximated by their concentrations [63, 64]. Since Z then evolves on an infinitesimally small time scale, a natural consequence of this partitioning is that stochastic propensity functions $a(Y_t, Z_t)$ evolve between two *stochastic* reaction firings $(t, t + \tau)$. Thus, numerically exact computation requires to solve an integration problem to compute $a(Y_t, Z_{t+u})$. In sampling-based methods, i.e. the integral-based methods employed in [25, 55], frequent initialization of numerical integrators can become a major computational burden (i.e. τ small). Direct hybrid methods [65–67] overcome this problem, however these methods still require to directly solve the CME part, which can be prohibitively large (involving thousands of states), limiting their applicability. In S2 Fig we show a comparison of simulations results obtained by integral-based (e.g. as used in [25, 55]) sampling methods vs. the EXTRANDE method, as well as their respective run times. As expected, the results are identical, while the simulation time is lower for EXTRANDE.

The method we are using is the recently developed EXTRANDE (extra reaction algorithm for networks in dynamic environment) method [12]. The EXTRANDE approach is based on a rejection, or thinning and allows for the numerically exact simulation of intrinsically stochastic kinetics embedded in a dynamical environment, i.e. the stochastic sub-system Y may constitute time-dependent propensities that are affected by the dynamic environment Z. We adapted EXTRANDE to allow the numerically exact prediction of infection/virus clearance in the context of time-varying drug inhibition. The key adaptation was to define proper stopping criteria that classify trajectories as infection events. To this end, utilizing results from a related article [23], we were able to compute and dynamically update an *extinction simplex* (eq (18)), i.e. a

part of the state space in which extinction can occur, see Fig 1. Whenever a trajectory leaves the *extinction simplex*, it is safe to classify it as an infection event and to stop the simulation.

Classifying trajectories as infection events is not a straightforward choice: Using arbitrary thresholds $Y_{\mathrm{tr}} = [V_t = c_0, T_{1,t} = c_1, T_{2,t} = c_2]^T$ can significantly distort predictions (e.g. 'PrEP efficacy') or increase computational run-time: While too small thresholds overestimate the number of infection events, large thresholds increase the computational run-time unnecessarily, since stochastic simulations become very inefficient when $Y >> 1$. Furthermore, there is no control- or knowledge of the numerical error made (the probability to falsely classify a trajectory as an infection event). Using the *extinction simplex* method proposed herein, it is guaranteed that the probability to falsely classify a trajectory stays below a user-defined threshold $\varepsilon << 1$. Moreover, the algorithmic run-time is optimal for providing this user-defined precision.

Particularly during 'PrEP on demand' or 'PEP' simulations, dynamic adaptation of the *extinction simplex* can be algorithmically harnessed: Note that there is a positive relation between the size of the *extinction simplex* and the drug concentration D (compare Fig 1). After the last dosing events in 'PrEP on demand' or 'PEP' simulations the size of the extinction simplex shrinks as the drug concentration tapers, making it more likely that stopping criteria are met, which minimizes runtime.

We used our framework to assess the utility of dolutegravir (DTG), which may be suitable for prophylaxis, since it has a good safety profile [68], a high resistance barrier [69] and a long half life in the blood plasma. Foremost, utilizing *in vitro* and *in vivo* parameters in our mathematical framework, we estimated that concentrations of $\mathrm{EC}_{50}(\hat{\mathrm{V}}) = 145.18$ and $\mathrm{EC}_{90}(\hat{\mathrm{V}}) = 722.23$nM prevent 50- and 90% infections respectively. These concentrations can guide dosing and release kinetics of nanoformulated long-acting dolutegravir, which is currently in preclinical development [62]. Moreover, as soon as human pharmacokinetic data is available, our framework can easily be adapted to predict the PrEP utility of the long-acting formulation (by updating the pharmacokinetic model). As an example, we focussed on *oral* DTG herein, for which we had sufficient pharmacokinetic data to build a population PK model. Combining this model with the EXTRANDE framework, allowed to assess different prophylactic strategies: Overall, our simulations suggested that oral 50mg OD DTG may have a potential for PrEP with an estimated efficacy of 99 to 100% (perfect adherence). For comparison, we previously estimated that Truvada may prevent 96% of infections when taken once daily (perfect adherence) [11]. Our model suggests that DTG's protective efficacy remains high ($> 80\%$) even at adherence levels as low as 50%. This apparent forgiveness to poor adherence is due to DTG's prophylactic potency rather than its halflife: I.e. if most DTG doses are taken, concentrations ranges are achieved where the concentration-prophylaxis profile is saturating (compare Fig 4A). Consequently, concentration changes do not proportionally translate into changes in prophylactic efficacy. In event-driven PrEP, we predicted that prophylactic efficacy reflects the drug profile in the blood plasma (compare Fig 3), which is characterized by a rapid absorption ($t_{\max} \approx 1.58$ [h]) and slow elimination. This is in contrast to tenofovir-emtricitabine (Truvada) whose activity is not reflected by their plasma levels, since these drugs require conversion to intracellular diphosphates [31, 55] to exert their antiviral activity, delaying the overall onset of activity. The main advantage of DTG over Truvada is in the context of post-exposure prophylaxis (PEP), where we predicted that it can potently prevent infection if initiated no later than 6hours post-exposure and taken for at least 5 days. We do not suggest to use single drug PEP with DTG; the sole purpose was to determine whether DTG would be effective, if individuals fail to take it *before* virus exposure. This kind of assessment allows to quantify the risks of prophylaxis in

situations where the regimen is not taken as intended and moreover provides a scientific basis to include it in PEP multi-drug combinations.

Our model has several limitations, but also a number of important advantages. Our simulations do not take into account drug concentrations at the site of mucosal exposure (e.g. cervix, rectum) [60, 70]. These concentrations have, however, not been validated as targets for successful prevention or treatment, whereas data exist (albeit limited) for plasma drug concentrations. Instead, we modelled based on *unbound* concentrations, in line with the widely accepted 'free drug hypothesis', stating that unbound concentrations at the target site are responsible for pharmacological action. For drugs highly bound to plasma protein ($> 90\%$), naturally since plasma protein concentrations are lower in tissues other than plasma, their *total* concentrations at sites other than the plasma are magnitudes lower [70]. Strikingly, however, the unbound plasma concentrations coincide with the unbound tissue concentrations [71], strongly arguing for the validity of the 'free drug hypothesis' [40, 41]. Therefore, throughout the work, we assumed, according to the 'free drug hypothesis' [39] that the unbound concentrations in plasma and at the target site coincide. Note that dolutegravir is highly lipophilic ($\log P \approx 2$), enabling the *unbound* drug to rapidly cross cellular membranes, generating an equilibrium between the *unbound* drug on either side of the cellular membrane [42].

We estimated the probability of virus clearance (and the prophylactic efficacy φ) as a function of the number of viruses ultimately reaching a target cell environment after sexual exposure, and not as a function of mucosal exposure. The utilized virus exposure model [11] is calibrated to reflect the per-contact infection risks for typical transmitter virus loads and different routes of sexual exposure exposure. However, it should be noted that in an accompanying article [23], we also observed that increasing the inoculum size decreases the prophylactic efficacy, i.e. estimates of prophylactic efficacy depend on the route of transmission: For example, if exposure to HIV occurs via blood transfusion (large inoculum size), most prophylactic drugs may fail to offer protection.

Our framework can be adapted or developed in a number of ways. The separate impact of treatment as prevention [72] (reduction of donor virus load to decrease contagiousness) versus prophylactic efficacy in the recipient individual can be simulated by calibrating the virus inoculum distribution [11]. The effect of PrEP on *resistance transmission* from a donor to a recipient can be incorporated in the framework by increasing IC_{50} in eq (9) (fold resistance) and possibly reducing certain reaction constants (fitness deficits). Likewise, the effects of PrEP on *resistance emergence* can be considered. However, during the *early* events after virus exposure (when infection can still be averted), the population size may be too small for resistance to appear *de novo* in the exposed individual. For example, a particular point mutation appears with probability $1 - (1 - \mu)^n$, where $\mu \approx 2.2 \cdot 10^{-5}$ [73] is the per base mutation rate of HIV per cell infection (= reverse transcription event) and n the number of cell infection events. According to these numbers, it requires ≈ 30000 cells to be infected for resistance to arise with 50% probability. Considering these numbers, a likely scenario for *de novo* resistance to appear is when PrEP had not been taken at the time of exposure, such that the infection expanded exponentially and a resistant mutant may have been generated at random. When PrEP is (re-)initiated at some later time it could provide the necessary pressure to select out the resistant type from the quasispecies population. Modelling these events is out of the scope of the recent work, as it requires distinct (and more coarse) simulation approaches, e.g. [25, 74].

It is well known that the establishment of a latent reservoir is the major barrier to viral extinction during treatment [49] and this reservoir may be established as early as 3 days post infection [48, 50]. We considered infection of long lived cells during our simulations, as outlined in the *Methods* section. I.e., whenever long-lived cells became infected during simulations, viral extinction was considered infeasible. Notably, there are two sources: one with a half

life of ≈ 14 days is responsible for the second phase of viral decay that can be observed in infected patients on combination treatment [75, 76]. This reservoir has been attributed to infected macrophages [75, 77]. Based on the mentioned half life of this reservoir, it would require $T(x) = -\frac{\ln(1-x)}{\ln(2)/t_{1/2}}$ days to eliminate a single cell with probability x under complete virus inhibition, e.g. ≈ 45 days to eliminate a single infected macrophage with 90% probability ($x = 0.9$) and over 90 days to eliminate this reservoir with 99% probability. Latent infected T cells decline even slower, with a half life of ≈ 6-44 month [78–80]. This reservoir is partly responsible for the third phase of 'decay' and is assumed to prevent HIV cure during effective combination treatment.

In summary, we have developed an innovative modelling approach to *a priori* assess prophylactic roll-out strategies by fully integrating individual PK/PD profiles and viral dynamics into a hybrid stochastic-deterministic framework. We used this framework to assess the prophylactic efficacy of the second-generation integrase inhibitor dolutegravir with respect to poor adherence, in event-driven prophylaxis and post-exposure prophylaxis. Overall our simulations showed that oral prophylaxis with 50mg DTG is non-inferior to Truvada and has profound advantages with respect to post-exposure prophylaxis. Moreover, we predicted that concentrations above $EC_{90} = 722.23nM$ can prevent > 90% infections after sexual exposure. These target concentrations can guide loading doses for novel long-acting nanoformulations of DTG [62]. By adapting the pharmacokinetics model, the framework can easily be used to predict the prophylactic utility of other candidate drugs currently under development, such as oral maraviroc (MVC) [81], and raltegravir (RAL) long-acting injectable rilpivirine [60] or cabotegravir [61], or it may be adapted to predict vaccine efficacy.

Supporting information

S1 Fig. Schematic of the HIV replication cycle and mechanism of interference by dolutegravir. The viral dynamics model (adapted from [24, 25]) consists of free infectious viruses V, early infected T-cells (T_1), productively infected T-cells (T_2) and uninfected T-cells $T_u = const.$. Early infected T-cells (T_1) and productively infected T-cells (T_2) denote T-cells prior- and after proviral integration respectively, where the latter produces virus progeny. Free viruses are cleared by the immune system with a rate constant CL. Further, free viruses can be also cleared during unsuccessful T-cell infection CL_T through the destruction of essential viral components of the reverse transcription-, or pre-integration complex [34, 35]. The term β represents the lumped rate of infection of T-cells, including the processes of virus attachment to the cell, fusion and reverse transcription, leading to an early infected cell T_1, before proviral integration. The term k denotes the rate by which early infected T_1 cells are transformed into productively infected T_2 cells, involving proviral integration and cellular reprogramming. The term N_T denotes the rate of production of infectious virus progeny by productively infected T_2 cells. The terms $\delta_{T_1} < \delta_{T_2}$ denote the rates of clearance of T_1 and T_2 cells respectively and δ_{PIC} denotes the rate of intracellular destruction of the pre-integration complex. Parameters are summarized in Table 1. The second-generation integrase inhibitor dolutegravir (DTG) prevents proviral integration and consequently decreases k by a factor $(1 - \eta_D)$. Long-lived and latently infected cells are implicitly considered in the model, i.e. the parameters $p_{M|a_4}$ and $p_{L|a_5}$ denote the conditional probabilities that a long lived- or a latent cell, which are a barrier to viral eradication, become infected. These rare events define algorithmic stopping criteria (irreversible infection) when modelling complex prophylactic regimen, e.g. long-term pre-exposure prophylaxis with inadequate adherence. DTG: dolutegravir.
(EPS)

S2 Fig. Comparison of EXTRANDE (green) and integral-based hybrid stochastic-deterministic simulation (red). A: Prophylactic efficacy for 'post exposure prophylaxis' (PEP) with 50mg DTG for various durations of PEP (x-axis; 3, 5, 7 and 9 days) and when initiated 24 hours after homosexual viral exposure. Error bars mark the 5-95% range computed using Greenwoods formula. **B:** Corresponding simulation run times on an intel i7 core with 2.5Ghz and 16 GB RAM. **C:** Simulation run times for the subset of simulations where infection occurred. Median (25-75 quartile ranges) runtime (sec) for 3 days PEP: 8.524 (2.4–20.5) vs. 10.548 (2.4–26.1); 5 days PEP: 10.0 (2.8–25.9) vs. 23.0 (6.8–48.1); 7 days PEP: 17.4 (5.3–35.4) vs. 25.5 (10.1–57.4) and 9 days PEP: 26.1 (7.6–57.3) vs. 34.1 (12.0–82.3).
(EPS)

S1 Text. The supplementary text contains a complete pseudo-code for the adapted EXTRANDE algorithm used for simulating initial viral dynamics during prophylaxis.
(PDF)

Acknowledgments

S.D, M.v.K and L.D. acknowledge fruitful communications with Akil Jackson.

Author Contributions

Conceptualization: Sulav Duwal, Max von Kleist.

Formal analysis: Sulav Duwal, Laura Dickinson, Saye Khoo, Max von Kleist.

Funding acquisition: Max von Kleist.

Investigation: Sulav Duwal, Laura Dickinson, Max von Kleist.

Methodology: Sulav Duwal, Laura Dickinson, Max von Kleist.

Project administration: Max von Kleist.

Supervision: Saye Khoo, Max von Kleist.

Visualization: Sulav Duwal.

Writing – original draft: Sulav Duwal, Laura Dickinson, Saye Khoo, Max von Kleist.

References

1. Trono D, Van Lint C, Rouzioux C, Verdin E, Barré-Sinoussi F, Chun TW, et al. HIV persistence and the prospect of long-term drug-free remissions for HIV-infected individuals. Science. 2010; 329(5988):174–180. https://doi.org/10.1126/science.1191047 PMID: 20616270
2. Ho YC, Shan L, Hosmane NN, Wang J, Laskey SB, Rosenbloom DIS, et al. Replication-competent noninduced proviruses in the latent reservoir increase barrier to HIV-1 cure. Cell. 2013; 155:540–551. https://doi.org/10.1016/j.cell.2013.09.020 PMID: 24243014
3. Archin NM, Sung JM, Garrido C, Soriano-Sarabia N, Margolis DM. Eradicating HIV-1 infection: seeking to clear a persistent pathogen. Nature Reviews Microbiology. 2014; 12(11):750–764. https://doi.org/10.1038/nrmicro3352 PMID: 25402363
4. UNAIDS. AIDS by the numbers. (http://www.unaids.org/sites/default/files/media_asset/AIDS-by-the-numbers-2016_en.pdf), accessed 18-Dec-2017; 2016.
5. Grant RM, Lama JR, Anderson PL, McMahan V, Liu AY, Vargas L, et al. Preexposure chemoprophylaxis for HIV prevention in men who have sex with men. N Engl J Med. 2010; 363(27):2587–2599. https://doi.org/10.1056/NEJMoa1011205 PMID: 21091279
6. McCormack S, Dunn DT, Desai M, Dolling DI, Gafos M, Gilson R, et al. Pre-exposure prophylaxis to prevent the acquisition of HIV-1 infection (PROUD): effectiveness results from the pilot phase of a pragmatic open-label randomised trial. Lancet. 2016; 387(10013):53–60. https://doi.org/10.1016/S0140-6736(15)00056-2 PMID: 26364263

7. Keller SB, Smith DM. The price of tenofovir-emtricitabine undermines the cost-effectiveness and advancement of pre-exposure prophylaxis. AIDS. 2011; 25(18):2308–2310. https://doi.org/10.1097/QAD.0b013e32834d3cab PMID: 22067201
8. AIDS Vaccine Advocacy Coalition. Pre-Exposure Prophylaxis (PrEP) by the Numbers, (available at http://www.avac.org/sites/default/files/resource-files/prep_BTN_aug2016.pdf, accessed 22-Oct-2017.).
9. Conway JM, Konrad BP, Coombs D. Stochastic analysis of pre- and postexposure prophylaxis against HIV infection. SIAM J Appl Math. 2013; 73(2):904–28. https://doi.org/10.1137/120876800
10. Tuckwell HC, Shipman PD, Perelson AS. The probability of HIV infection in a new host and its reduction with microbicides. Math Biosci. 2008; 214(1-2):81–86. https://doi.org/10.1016/j.mbs.2008.03.005 PMID: 18445499
11. Duwal S, Sunkara V, von Kleist M. Multiscale Systems-Pharmacology Pipeline to Assess the Prophylactic Efficacy of NRTIs Against HIV-1. CPT Pharmacometrics Syst Pharmacol. 2016; 5(7):377–387. https://doi.org/10.1002/psp4.12095 PMID: 27439573
12. Voliotis M, Thomas P, Grima R, Bowsher CG. Stochastic simulation of biomolecular networks in dynamic environments. PLoS Comput Biol. 2016; 12(6):e1004923. https://doi.org/10.1371/journal.pcbi.1004923 PMID: 27248512
13. Keele BF, Giorgi EE, Salazar-Gonzalez JF, Decker JM, Pham KT, Salazar MG, et al. Identification and characterization of transmitted and early founder virus envelopes in primary HIV-1 infection. PNAS. 2008; 105(21):7552–7557. https://doi.org/10.1073/pnas.0802203105 PMID: 18490657
14. Abrahams MR, Anderson JA, Giorgi EE, Seoighe C, Mlisana K, Ping LH, et al. Quantitating the multiplicity of infection with human immunodeficiency virus type 1 subtype C reveals a non-poisson distribution of transmitted variants. J Virol. 2009; 83(8):3556–3567. https://doi.org/10.1128/JVI.02132-08 PMID: 19193811
15. Fischer W, Ganusov VV, Giorgi EE, Hraber PT, Keele BF, Leitner T, et al. Transmission of single HIV-1 genomes and dynamics of early immune escape revealed by ultra-deep sequencing. PloS one. 2010; 5(8):e12303. https://doi.org/10.1371/journal.pone.0012303 PMID: 20808830
16. Li H, Bar KJ, Wang S, Decker JM, Chen Y, Sun C, et al. High Multiplicity Infection by HIV-1 in Men Who Have Sex with Men. PLoS Pathog. 2010; 6(5):e1000890. https://doi.org/10.1371/journal.ppat.1000890 PMID: 20485520
17. Royce RA, Seña A, Cates W Jr, Cohen MS. Sexual transmission of HIV. N Engl J Med. 1997; 336(15):1072–1078. https://doi.org/10.1056/NEJM199704103361507 PMID: 9091805
18. Boily MC, Baggaley RF, Wang L, Masse B, White RG, Hayes RJ, et al. Heterosexual risk of HIV-1 infection per sexual act: systematic review and meta-analysis of observational studies. Lancet Infect Dis. 2009; 9(2):118–129. https://doi.org/10.1016/S1473-3099(09)70021-0 PMID: 19179227
19. Schnoerr D, Sanguinetti G, Grima R. Approximation and inference methods for stochastic biochemical kinetics—a tutorial review. Journal of Physics A Mathematical and Theoretical. 2017; 50(9):093001, 60. https://doi.org/10.1088/1751-8121/aa54d9
20. Tsimring LS. Noise in biology. Reports on progress in physics Physical Society. 2014; 77:026601. https://doi.org/10.1088/0034-4885/77/2/026601
21. Gillespie DT. Stochastic Simulation of Chemical Kinetics. Annu Rev Phys Chem. 2007; 58(1):35–55. https://doi.org/10.1146/annurev.physchem.58.032806.104637 PMID: 17037977
22. Kurtz TG. Approximation of population processes. vol. 36. CBMS-NSF Regional Conference Series in Applied Mathematics ed. SIAM; 1981.
23. Duwal S, Dickinson L, Khoo SH, von Kleist M. Mechanistic framework predicts utility of antiretroviral drugs for HIV prophylaxis. submitted for publication 2017.
24. von Kleist M, Menz S, Huisinga W. Drug-class specific impact of antivirals on the reproductive capacity of HIV. PLoS Comput Biol. 2010; 6(3):e1000720. https://doi.org/10.1371/journal.pcbi.1000720 PMID: 20361047
25. von Kleist M, Menz S, Stocker H, Arasteh K, Schütte C, Huisinga W. HIV Quasispecies Dynamics during Pro-active Treatment Switching: Impact on Multi-Drug Resistance and Resistance Archiving in Latent Reservoirs. PLoS One. 2011; 6(3):e18204. https://doi.org/10.1371/journal.pone.0018204 PMID: 21455303
26. Isaacman-Beck J, Hermann EA, Yi Y, Ratcliffe SJ, Mulenga J, Allen S, et al. Heterosexual transmission of human immunodeficiency virus type 1 subtype C: Macrophage tropism, alternative coreceptor use, and the molecular anatomy of CCR5 utilization. J Virol. 2009; 83(16):8208–8220. https://doi.org/10.1128/JVI.00296-09 PMID: 19515785
27. Ping LH, Joseph SB, Anderson JA, Abrahams MR, Salazar-Gonzalez JF, Kincer LP, et al. Comparison of viral Env proteins from acute and chronic infections with subtype C human immunodeficiency virus

type 1 identifies differences in glycosylation and CCR5 utilization and suggests a new strategy for immunogen design. J Virol. 2013; 87(13):7218–7233. https://doi.org/10.1128/JVI.03577-12 PMID: 23616655

28. Tan WY, Wu H. Stochastic modeling of the dynamics of CD4+ T-cell infection by HIV and some Monte Carlo studies. Math Biosci. 1998; 147(2):173–205. https://doi.org/10.1016/S0025-5564(97)00094-1 PMID: 9433062

29. Stafford MA, Corey L, Cao Y, Daar ES, Ho DD, Perelson AS. Modeling plasma virus concentration during primary HIV infection. J Theor Biol. 2000; 203(3):285–301. https://doi.org/10.1006/jtbi.2000.1076 PMID: 10716909

30. Perelson AS. Modelling viral and immune system dynamics. Nat Rev Immunol. 2002; 2(1):28–36. https://doi.org/10.1038/nri700 PMID: 11905835

31. Duwal S, von Kleist M. Top-down and bottom-up modeling in system pharmacology to understand clinical efficacy: An example with NRTIs of HIV-1. Eur J Pharm Sci. 2016; 94:72–83. https://doi.org/10.1016/j.ejps.2016.01.016 PMID: 26796142

32. Perelson AS, Kirschner DE, De Boer R. Dynamics of HIV infection of CD4+ T cells. Math Biosci. 1993; 114(1):81–125. https://doi.org/10.1016/0025-5564(93)90043-A PMID: 8096155

33. Pearson JE, Krapivsky P, Perelson AS. Stochastic theory of early viral infection: continuous versus burst production of virions. PLoS Comput Biol. 2011; 7(2):e1001058. https://doi.org/10.1371/journal.pcbi.1001058 PMID: 21304934

34. Pierson TC, Zhou Y, Kieffer TL, Ruff CT, Buck C, Siliciano RF. Molecular characterization of preintegration latency in human immunodeficiency virus type 1 infection. J Virol. 2002; 76(17):8518–8531. PMID: 12163571

35. Zhou Y, Zhang H, Siliciano JD, Siliciano RF. Kinetics of human immunodeficiency virus type 1 decay following entry into resting CD4+ T cells. J Virol. 2005; 79(4):2199–2210. https://doi.org/10.1128/JVI.79.4.2199-2210.2005 PMID: 15681422

36. Chou TC. Theoretical basis, experimental design, and computerized simulation of synergism and antagonism in drug combination studies. Pharmacolog Rev. 2006; 58(3):621–681. https://doi.org/10.1124/pr.58.3.10

37. Shen L, Peterson S, Sedaghat AR, McMahon MA, Callender M, Zhang H, et al. Dose-response curve slope sets class-specific limits on inhibitory potential of anti-HIV drugs. Nat Med. 2008; 14(7):762–766. https://doi.org/10.1038/nm1777 PMID: 18552857

38. Laskey SB, Siliciano RF. Quantitative evaluation of the antiretroviral efficacy of dolutegravir. JCI Insight. 2016; 1(19):e90033. https://doi.org/10.1172/jci.insight.90033 PMID: 27882352

39. Smith DA, Di L, Kerns EH. The effect of plasma protein binding on in vivo efficacy: misconceptions in drug discovery. Nat Rev Drug Discov. 2010; 9(12):929–939. https://doi.org/10.1038/nrd3287 PMID: 21119731

40. Watkins WJ, Desai MC. HCV versus HIV drug discovery: Déjà vu all over again? Bioorg Med Chem Lett. 2013; 23(8):2281–2287. https://doi.org/10.1016/j.bmcl.2013.02.070 PMID: 23489621

41. Boffito M, Back DJ, Blaschke TF, Rowland M, Bertz RJ, Gerber JG, et al. Protein binding in antiretroviral therapies. AIDS Res Hum Retroviruses. 2003; 19(9):825–835. https://doi.org/10.1089/088922203769232629 PMID: 14585213

42. von Kleist M, Huisinga W. Physiologically based pharmacokinetic modelling: a sub-compartmentalized model of tissue distribution. J Pharmacokinet Pharmacodyn. 2007; 34:789–806. https://doi.org/10.1007/s10928-007-9071-3 PMID: 17899329

43. Pinheiro JC, Bates DM. Mixed-effects model in S and S-Plus. Springer; 2009.

44. Elliot E, Amara A, Jackson A, Moyle G, Else L, Khoo S, et al. Dolutegravir and elvitegravir plasma concentrations following cessation of drug intake. J Antimicrob Chemother. 2016; 71:1031–1036. https://doi.org/10.1093/jac/dkv425 PMID: 26679246

45. Bracchi M, Pagani N, Clarke A, Adams T, Waters L, Bolton M, et al. Multicentre open-label pilot study of switching from efavirenz to dolutegravir for central nervous system (CNS) toxicity. In: International Congress of Drug Therapy in HIV Infection, Glasgow, UK, Abstract P209; 2016.

46. Bonate PL, Steimer JL. Pharmacokinetic-pharmacodynamic modeling and simulation. Springer, New York; 2011.

47. Gillespie DT. Exact stochastic simulation of coupled chemical reactions. J Phys Chem. 1977; 81:2340–61. https://doi.org/10.1021/j100540a008

48. Chun TW, Engel D, Berrey MM, Shea T, Corey L, Fauci AS. Early establishment of a pool of latently infected, resting CD4(+) T cells during primary HIV-1 infection. PNAS. 1998; 95:8869–8873. https://doi.org/10.1073/pnas.95.15.8869 PMID: 9671771

49. Chun TW, Moir S, Fauci AS. HIV reservoirs as obstacles and opportunities for an HIV cure. Nat Immunol. 2015; 16(6):584–589. https://doi.org/10.1038/ni.3152 PMID: 25990814

50. Whitney JB, Hill AL, Sanisetty S, Penaloza-MacMaster P, Liu J, Shetty M, et al. Rapid seeding of the viral reservoir prior to SIV viraemia in rhesus monkeys. Nature. 2014; 512:74–77. https://doi.org/10.1038/nature13594 PMID: 25042999

51. Yousef KP, Meixenberger K, Smith MR, Somogyi S, Gromöller S, Schmidt D, et al. Inferring HIV-1 Transmission Dynamics in Germany From Recently Transmitted Viruses. JAIDS Journal of Acquired Immune Deficiency Syndromes. 2016; 73(3):356–363. https://doi.org/10.1097/QAI.0000000000001122

52. Wilson DP, Law MG, Grulich AE, Cooper DA, Kaldor JM. Relation between HIV viral load and infectiousness: a model-based analysis. Lancet. 2008; 372(9635):314–320. https://doi.org/10.1016/S0140-6736(08)61115-0 PMID: 18657710

53. Quinn TC, Wawer MJ, Sewankambo N, Serwadda D, Li C, Wabwire-Mangen F, et al. Viral load and heterosexual transmission of human immunodeficiency virus type 1. Rakai Project Study Group. N Engl J Med. 2000; 342(13):921–929. https://doi.org/10.1056/NEJM200003303421303 PMID: 10738050

54. Molina JM, Capitant C, Spire B, Pialoux G, Cotte L, Charreau I, et al. On-Demand Preexposure Prophylaxis in Men at High Risk for HIV-1 Infection. N Engl J Med. 2015; 373(23):2237–2246. https://doi.org/10.1056/NEJMoa1506273 PMID: 26624850

55. Duwal S, Schütte C, von Kleist M. Pharmacokinetics and pharmacodynamics of the reverse transcriptase inhibitor tenofovir and prophylactic efficacy against HIV-1 infection. PLoS One. 2012; 7(7):e40382. https://doi.org/10.1371/journal.pone.0040382 PMID: 22808148

56. Haberer JE, Bangsberg DR, Baeten JM, Curran K, Koechlin F, Amico KR, et al. Defining success with HIV pre-exposure prophylaxis: a prevention-effective adherence paradigm. AIDS. 2015; 29:1277–1285. PMID: 26103095

57. Grant R, Anderson P, McMahan V, Liu A, Amico K, Mehrotra M, et al. Results of the iPrEx open-label extension (iPrEx OLE) in men and transgender women who have sex with men: PrEP uptake, sexual practices, and HIV incidence. AIDS. 2014; p. 20–25.

58. Marrazzo JM, Ramjee G, Richardson BA, Gomez K, Mgodi N, Nair G, et al. Tenofovir-based preexposure prophylaxis for HIV infection among African women. N Engl J Med. 2015; 372:509–518. https://doi.org/10.1056/NEJMoa1402269 PMID: 25651245

59. Van Damme L, Corneli A, Ahmed K, Agot K, Lombaard J, Kapiga S, et al. Preexposure prophylaxis for HIV infection among African women. The New England journal of medicine. 2012; 367:411–422. https://doi.org/10.1056/NEJMoa1202614 PMID: 22784040

60. McGowan I, Dezzutti CS, Siegel A, Engstrom J, Nikiforov A, Duffill K, et al. Long-acting rilpivirine as potential pre-exposure prophylaxis for HIV-1 prevention (the MWRI-01 study): an open-label, phase 1, compartmental, pharmacokinetic and pharmacodynamic assessment. Lancet HIV. 2016; 3:e569–e578. https://doi.org/10.1016/S2352-3018(16)30113-8 PMID: 27658864

61. Markowitz M, Frank I, Grant RM, Mayer KH, Elion R, Goldstein D, et al. Safety and tolerability of long-acting cabotegravir injections in HIV-uninfected men (ECLAIR): a multicentre, double-blind, randomised, placebo-controlled, phase 2a trial. Lancet HIV. 2017; 4:e331–e340. https://doi.org/10.1016/S2352-3018(17)30068-1 PMID: 28546090

62. McMillan J, Szlachetka A, Slack L, Sillman B, Lamberty B, Morsey B, et al. Pharmacokinetics of a long-acting nanoformulated dolutegravir prodrug in rhesus macaques. Antimicrobial agents and chemotherapy. 2017; p. AAC–01316.

63. Pahle J. Biochemical simulations: stochastic, approximate stochastic and hybrid approaches. Brief Bioinform. 2009; 10(1):53–64. https://doi.org/10.1093/bib/bbn050 PMID: 19151097

64. Szúkely T, Burrage K. Stochastic simulation in systems biology. Comput Struct Biotechnol J. 2014; 12:14–25. https://doi.org/10.1016/j.csbj.2014.10.003

65. Menz S, Latorre J, Schütte C, Huisinga W. Hybrid stochastic-deterministic solution of the chemical master equation. Multiscale Modeling & Simulation. 2012; 10:1232–62. https://doi.org/10.1137/110825716

66. Jahnke T. On reduced models for the chemical master equation. Multiscale Modeling & Simulation. 2011; 9(4):1646–1676. https://doi.org/10.1137/110821500

67. Hasenauer J, Wolf V, Kazeroonian A, Theis FJ. Method of conditional moments (MCM) for the Chemical Master Equation: A unified framework for the method of moments and hybrid stochastic-deterministic models. J Math Biol. 2013. https://doi.org/10.1007/s00285-013-0711-5 PMID: 23918091

68. Keeshin SW, Feinberg J. Evaluation of dolutegravir safety for the treatment of HIV-1. Expert Opin Drug Saf. 2015; 14:141–147. https://doi.org/10.1517/14740338.2015.973845 PMID: 25347230

69. Eron JJ, Clotet B, Durant J, Katlama C, Kumar P, Lazzarin A, et al. Safety and efficacy of dolutegravir in treatment-experienced subjects with raltegravir-resistant HIV type 1 infection: 24-week results of the VIKING Study. J Infect Dis. 2013; 207:740–748. https://doi.org/10.1093/infdis/jis750 PMID: 23225901

70. Else LJ, Taylor S, Back DJ, Khoo SH. Pharmacokinetics of antiretroviral drugs in anatomical sanctuary sites: the male and female genital tract. Antivir Ther. 2011; 16:1149–1167. https://doi.org/10.3851/IMP1919 PMID: 22155899

71. Avery LB, Bakshi RP, Cao YJ, Hendrix CW. The male genital tract is not a pharmacological sanctuary from efavirenz. Clin Pharmacol Ther. 2011; 90:151–156. https://doi.org/10.1038/clpt.2011.99 PMID: 21633344

72. Cohen MS, Chen YQ, McCauley M, Gamble T, Hosseinipour MC, Kumarasamy N, et al. Prevention of HIV-1 infection with early antiretroviral therapy. N Engl J Med. 2011; 365(6):493–505. https://doi.org/10.1056/NEJMoa1105243 PMID: 21767103

73. Mansky LM, Temin HM. Lower in vivo mutation rate of human immunodeficiency virus type 1 than that predicted from the fidelity of purified reverse transcriptase. J Virol. 1995; 69:5087–5094. PMID: 7541846

74. Rosenbloom DIS, Hill AL, Rabi SA, Siliciano RF, Nowak MA. Antiretroviral dynamics determines HIV evolution and predicts therapy outcome. Nat Med. 2012; 18:1378–1385. https://doi.org/10.1038/nm.2892 PMID: 22941277

75. Perelson AS, Essunger P, Cao Y, Vesanen M, Hurley A, Saksela K, et al. Decay characteristics of HIV-1-infected compartments during combination therapy. Nature. 1997; 387:188–191. https://doi.org/10.1038/387188a0 PMID: 9144290

76. Simon V, Ho DD. HIV-1 dynamics in vivo: implications for therapy. Nat Rev Microbiol. 2003; 1:181–190. https://doi.org/10.1038/nrmicro772 PMID: 15035022

77. Stevenson M. HIV-1 pathogenesis. Nat Med. 2003; 9:853–860. https://doi.org/10.1038/nm0703-853 PMID: 12835705

78. Finzi D, Blankson J, Siliciano JD, Margolick JB, Chadwick K, Pierson T, et al. Latent infection of CD4+ T cells provides a mechanism for lifelong persistence of HIV-1, even in patients on effective combination therapy. Nat Med. 1999; 5(5):512–517. https://doi.org/10.1038/8394 PMID: 10229227

79. Zhang L, Ramratnam B, Tenner-Racz K, He Y, Vesanen M, Lewin S, et al. Quantifying residual HIV-1 replication in patients receiving combination antiretroviral therapy. N Engl J Med. 1999; 340:1605–1613. https://doi.org/10.1056/NEJM199905273402101 PMID: 10341272

80. Chun TW, Justement JS, Moir S, Hallahan CW, Maenza J, Mullins JI, et al. Decay of the HIV reservoir in patients receiving antiretroviral therapy for extended periods: implications for eradication of virus. J Infect Dis. 2007; 195:1762–1764. https://doi.org/10.1086/518250 PMID: 17492591

81. Gulick RM, Wilkin TJ, Chen YQ, Landovitz RJ, Amico KR, Young AM, et al. Phase 2 Study of the Safety and Tolerability of Maraviroc-Containing Regimens to Prevent HIV Infection in Men Who Have Sex With Men (HPTN 069/ACTG A5305). Journal Infect Dis. 2017; 215:238–246.

82. Wei X, Ghosh SK, Taylor ME, Johnson VA, Emini EA, Deutsch P, et al. Viral dynamics in human immunodeficiency virus type 1 infection. Nature. 1995; 373(6510):117–122. https://doi.org/10.1038/373117a0 PMID: 7529365

83. Sedaghat AR, Siliciano RF, Wilke CO. Constraints on the dominant mechanism for HIV viral dynamics in patients on raltegravir. Antivir Ther. 2009; 14(2):263–271. PMID: 19430101

84. Markowitz M, Louie M, Hurley A, Sun E, Mascio MD, Perelson AS, et al. A novel antiviral intervention results in more accurate assessment of human immunodeficiency virus type 1 replication dynamics and T-cell decay in vivo. J Virol. 2003; 77:5037–5038. https://doi.org/10.1128/JVI.77.8.5037-5038.2003 PMID: 12663814

85. Koelsch KK, Liu L, Haubrich R, May S, Havlir D, Günthard HF, et al. Dynamics of total, linear nonintegrated, and integrated HIV-1 DNA in vivo and in vitro. J Infect Dis. 2008; 197(3):411–419. https://doi.org/10.1086/525283 PMID: 18248304

86. Sedaghat AR, Dinoso JB, Shen L, Wilke CO, Siliciano RF. Decay dynamics of HIV-1 depend on the inhibited stages of the viral life cycle. PNAS. 2008; 105(12):4832–4837. https://doi.org/10.1073/pnas.0711372105 PMID: 18362342

87. Frank M, von Kleist M, Kunz A, Harms G, Schütte C, Kloft C. Quantifying the impact of nevirapine-based prophylaxis strategies to prevent mother-to-child transmission of HIV-1: a combined pharmacokinetic, pharmacodynamic, and viral dynamic analysis to predict clinical outcomes. Antimicrob Agents Chemother. 2011; 55(12):5529–5540. https://doi.org/10.1128/AAC.00741-11 PMID: 21947390

88. Zhang J, Hayes S, Sadler BM, Minto I, Brandt J, Piscitelli S, et al. Population pharmacokinetics of dolutegravir in HIV-infected treatment-naive patients. Br J Clin Pharmacol. 2015; 80(3):502–514. https://doi.org/10.1111/bcp.12639 PMID: 25819132

PLOS COMPUTATIONAL BIOLOGY

RESEARCH ARTICLE

Mechanistic framework predicts drug-class specific utility of antiretrovirals for HIV prophylaxis

Sulav Duwal[1]*, **Laura Dickinson**[2], **Saye Khoo**[2], **Max von Kleist**[1]*

1 Department of Mathematics & Computer Science, Freie Universität Berlin, Germany, **2** Institute of Translational Medicine, University of Liverpool, United Kingdom

* sulav@zedat.fu-berlin.de (SD); max.kleist@fu-berlin.de (MvK)

Citation: Duwal S, Dickinson L, Khoo S, von Kleist M (2019) Mechanistic framework predicts drug-class specific utility of antiretrovirals for HIV prophylaxis. PLoS Comput Biol 15(1): e1006740. https://doi.org/10.1371/journal.pcbi.1006740

Editor: Sebastian Bonhoeffer, ETH Zürich, SWITZERLAND

Received: December 22, 2017

Accepted: December 20, 2018

Published: January 30, 2019

Data Availability Statement: All relevant data are within the paper and its Supporting Information files.

Funding: MvK. and SD acknowledge financial support from the BMBF e:Bio junior research group 'Systems Pharmacology & Disease Control', grant number 031A307. SK has received funding from Gilead, ViiV Healthcare, Merck and Janssen for the HIV Drug Interactions website, and for research grants. The funders had no role in study design, data collection and analysis, decision to publish, or preparation of the manuscript.

Abstract

Currently, there is no effective vaccine to halt HIV transmission. However, pre-exposure prophylaxis (PrEP) with the drug combination Truvada can substantially decrease HIV transmission in individuals at risk. Despite its benefits, Truvada-based PrEP is expensive and needs to be taken once-daily, which often leads to inadequate adherence and incomplete protection. These deficits may be overcome by next-generation PrEP regimen, including currently investigated long-acting formulations, or patent-expired drugs. However, poor translatability of animal- and *ex vivo*/*in vitro* experiments, and the necessity to conduct long-term (several years) human trials involving considerable sample sizes (N>1000 individuals) are major obstacles to rationalize drug-candidate selection. We developed a prophylaxis modelling tool that mechanistically considers the mode-of-action of all available drugs. We used the tool to screen antivirals for their prophylactic utility and identify lower bound effective concentrations that can guide dose selection in PrEP trials. While *in vitro* measurable drug potency usually guides PrEP trial design, we found that it may over-predict PrEP potency for all drug classes except reverse transcriptase inhibitors. While most drugs displayed graded concentration-prophylaxis profiles, protease inhibitors tended to switch between none- and complete protection. While several treatment-approved drugs could be ruled out as PrEP candidates based on lack-of-prophylactic efficacy, darunavir, efavirenz, nevirapine, etravirine and rilpivirine could more potently prevent infection than existing PrEP regimen (Truvada). Notably, some drugs from this candidate set are patent-expired and currently neglected for PrEP repurposing. A next step is to further trim this candidate set by ruling out compounds with ominous safety profiles, to assess different administration schemes in silico and to test the remaining candidates in human trials.

Author summary

Pre-exposure prophylaxis (PrEP) is a novel, promising strategy to halt HIV transmission. PrEP with Truvada can substantially decrease the risk of infection. However, individuals often inadequately adhere to the once-daily regimen and the drug is expensive. These

Competing interests: The authors have declared that no competing interests exist.

shortcomings may be overcome by next-generation PrEP compounds, including long-acting formulations. However, poor translatability of animal- and *ex vivo*/*in vitro* experiments, and difficulties in conducting long-term trials involving considerable sample sizes ($N > 1000$ individuals) make drug-candidate selection and optimization of administration schemes costly and often infeasible. We developed a simulation tool that mechanistically considers the mode-of-action of all antivirals. We used the tool to screen all available antivirals for their prophylactic utility and identified lower bound effective concentrations for designing PrEP dosing regimen in clinical trials. We found that *in vitro* measured drug potency may over-predict PrEP potency, for all antiviral classes except reverse transcriptase inhibitors. We could rule out a number of antivirals for PrEP repurposing and predicted that darunavir, efavirenz, nevirapine, etravirine and rilpivirine provide complete protection at clinically relevant concentrations. Further trimming of this candidate set by compound-safety and by assessing different implementation schemes is envisaged.

Introduction

Pre-exposure prophylaxis (PrEP) to prevent HIV infection (using drugs which are licensed for its treatment) has been assessed in people at high risk of sexual transmission. Of the available agents, once-daily tenofovir and emtricitabine (Truvada) have been extensively studied, and demonstrate protective efficacy (59–100% [1, 2]) in individuals who are adherent to the medication; conversely poor medication adherence explains the lack of protection observed in some trials [3]. However, major shortcomings of Truvada-based PrEP are its costs [4], a residual infection risk and the necessity for daily drug intake (which often leads to inadequate adherence). These deficits may be overcome by next-generation PrEP regimen, including patent-expired antivirals and long-acting formulations.

Studies assessing next-generation PrEP regimen are underway [5], but rational selection of which agents to advance into PrEP trials based on their intrinsic pharmacology and mode of action has not been comprehensively or systematically undertaken. Moreover, studies have focussed on patent-protected compounds [6], which are likely unaffordable in resource-constrained settings [4] hit hardest by the epidemic.

The considerable sample sizes ($N > 1000$ individuals) and clinical trial duration required (years) to test any new candidate against tenofovir-emtricitabine, and the need to assess regimens with forgiveness for missed dosing or episodic, event-driven PrEP make the current strategy of empirical drug selection costly and prone to failure. We chose to explore an alternative strategy by developing a mathematical modelling tool to assess the per-contact efficacy of anti-HIV drugs. This approach allows prediction of prophylactic utility by integrating drug specific factors (pharmacokinetic/pharmacodynamic (PK/PD) attributes) and attributes of the targeted risk group in order to probe and discard candidates, accelerate drug development and markedly reduce costs. In this work, we are particularly interested in agents where existing patents had already, or are about to expire, in order to maximise the potential impact for low and middle income countries.

Various epidemiological modelling approaches have been used to predict the public health benefits of PrEP [7] and the risk of emergent drug resistance [8–10]. These approaches are highly dependent on *ad hoc* parameter assumptions [11] (specifically the per-contact PrEP efficacy), which may explain the different and contradictory predictions which have emerged.

Knowledge of the per-contact PrEP efficacy, ideally concentration-prophylaxis relationships, are currently lacking and parameters derived from animal models poorly translate into

human efficacy. Concentration-prophylaxis relationships are particularly critical to define lower concentrations in human trials that can attain e.g. > 90% protection: I.e., ideally a PrEP candidate should be dosed such that the concentrations stay above this target (e.g. 90% protection) and at the same time avoid adverse effects in all individuals. For prophylaxis, there is a general void of information regarding drug-specific and drug-class specific concentration-prophylaxis relationships. While the potency of drugs to inhibit HIV replication can readily be measured *in vitro*, researchers are often unaware that this measure of drug potency may not coincide with the potency to prevent HIV infection (prophylactic potency) and consequently PrEP trial design may be flawed, incurring costs and putting individuals at risk.

In a top-down approach, Hendrix et al. [12] analyzed available clinical data for Truvada to define concentration-prophylaxis relationships. However, this approach is naturally limited to PrEP candidates where sufficient clinical data already exists and is not able to disentangle the potency of the administered drugs from confounding factors. More mechanistic, bottom-up approaches integrate various host- and viral factors [13–18] to predict the probability of viral extinction. Despite their advantages, these approaches conventionally do not establish concentration-prophylaxis relations, or they are specific to particular drugs [17] or drug classes [18].

In this work, we will first analyze the drug-class specific relation between *in vitro* potency and PrEP efficacy and its dependency on the amount- and type of transmitted virus. Utilizing pharmacokinetic and pharmacodynamic data for all treatment-approved drugs, and simulating typical viral exposures during sexual contact, we will then screen all treatment-approved drugs for their PrEP utility and assess the sensitivity of the prophylactic endpoint with regard to uncertainties in viral dynamics parameters and with regard to variabilities in drug concentration, which can typically result from inter-individual metabolic differences or differences in medication adherence. Our central aim is to provide a tool to screen out drug candidates with a lack of- or uncertain prophylactic efficacy.

Methods

Before HIV infection is irreversibly established, viral replication is highly stochastic [19], corroborated by the observation of a low transmission probability per exposure [20, 21] and a low number of founder viruses responsible for establishing infection [22–25]. The stochasticity can be explained by the order in which viral dynamics reactions occur: For example, when a single virus comes into proximity of target cells, it may either be cleared or it may infect the target cell which can eventually lead to systemic infection. In the current work, we will make use of branching process theory [26] to derive analytical solutions for the probability of viral extinction [13, 15], i.e. the probability to hit the absorbing state where all viral compartments go extinct. These solutions can be used directly to benchmark antivirals for their potential to prevent infection as exemplified in the current work, or they can be used to design efficient algorithms for the numerically *exact* simulation of complex prophylactic dosing regimen as proposed in a related article [27].

Prophylactic efficacy

The infection probability $P_I(Y_0)$ for some initial state Y_0 is the complement of the extinction probability $P_E(Y_0)$

$$P_I(Y_0) = 1 - P_E(Y_0), \tag{1}$$

where Y_0 denotes the initial viral population in a replication enabling (target-cell) environment. Throughout the article we will use $Y = [V, T_1, T_2]^T$, i.e. the state of the viral dynamics is defined by infectious viruses, early- and productively infected cells as outlined below. The

extinction probability is defined by

$$P_{\mathrm{E}}(Y_0) \coloneqq \mathbb{P}\left(Y_t = \begin{bmatrix} 0 \\ 0 \\ 0 \end{bmatrix} \middle| \; Y_0 = \begin{bmatrix} \mathrm{V} \\ \mathrm{T}_1 \\ \mathrm{T}_2 \end{bmatrix} \right) \tag{2}$$

for $t \to \infty$. In words, the probability that all viral compartments will eventually go extinct. The prophylactic efficacy φ then denotes the reduction in infection probability *per contact*,

$$\varphi = 1 - \frac{P_{\mathrm{I}}(Y_0|D)}{P_{\mathrm{I}}(Y_0|\varnothing)} \quad (\text{prophylactic efficacy}), \tag{3}$$

where $P_{\mathrm{I}}(Y_0|D)$ and $P_{\mathrm{I}}(Y_0|\varnothing)$ denote the infection probabilities in the presence- and absence of prophylactic drugs D respectively. The term $P_{\mathrm{I}}(Y_0|D)$ was computed using a mathematical model of the viral dynamics (below) and by mechanistically considering the *direct* effects of the distinct antivirals on viral replication whereas $P_{\mathrm{I}}(Y_0|\varnothing)$ is computed analogously, assuming the absence of drug $D = 0$.

Drug-class specific *direct* effects on virus replication

Virus replication dynamics. We adopted the viral dynamics model described in [28, 29]. Although this model is a coarse representation of the molecular events happening during virus replication, it allows to accurately and mechanistically describe the effect of all existing antiretroviral drug classes on viral replication, as demonstrated in e.g. [30], and can be parameterized by available *in vitro* and *clinical* data. Unlike the original model [28, 29] we do not consider macrophages, motivated by the observation that transmitted viruses are not macrophage-tropic [31, 32] and in line with related modelling approaches [13, 14, 33–35]. The model is schematically depicted in Fig 1. The modelled viral replication cycle consists of free infectious viruses, uninfected T-cells, early infected T-cells (T_1) and productively infected T-cells (T_2). Early infected T-cells (T_1) and productively infected T-cells (T_2) denote T-cells prior- and after proviral integration respectively, where the latter produces virus progeny. The term $\mathrm{T}_{\mathrm{u}} = \lambda_{\mathrm{T}}/\delta_{\mathrm{T}}$ denotes the steady state level of uninfected T-cells prior to virus challenge, where λ_{T} denotes the birth and δ_{T} the death rate of uninfected T-cells. During the onset of infection the number viruses are relatively low and the number of uninfected T-cells is fairly unaffected by virus dynamics [33, 36]. Thus, for all computations, we consider the number of uninfected T-cells to be constant, in line with related approaches [14, 15]. The dynamics of the stochastic viral replication model after virus exposure are then defined by six reactions. In absence of antivirals $\varnothing$ we have

$$a_1(\varnothing) = \quad (\mathrm{CL} + \mathrm{CL}_{\mathrm{T}} \cdot \mathrm{T}_{\mathrm{u}}) \cdot V \quad (\text{clearance of free virus; } V \to *) \tag{4}$$

$$a_2(\varnothing) = \quad (\delta_{\mathrm{PIC}} + \delta_{\mathrm{T}_1}) \cdot \mathrm{T}_1 \quad (\text{clearance of early infected cell; } \mathrm{T}_1 \to *) \tag{5}$$

$$a_3(\varnothing) = \quad \delta_{\mathrm{T}_2} \cdot \mathrm{T}_2 \quad (\text{clearance of late infected cell; } \mathrm{T}_2 \to *) \tag{6}$$

$$a_4(\varnothing) = \quad \beta \cdot \mathrm{T}_{\mathrm{u}} \cdot \mathrm{V} \quad (\text{successful infection of a suscept. cell; } V \to \mathrm{T}_1) \tag{7}$$

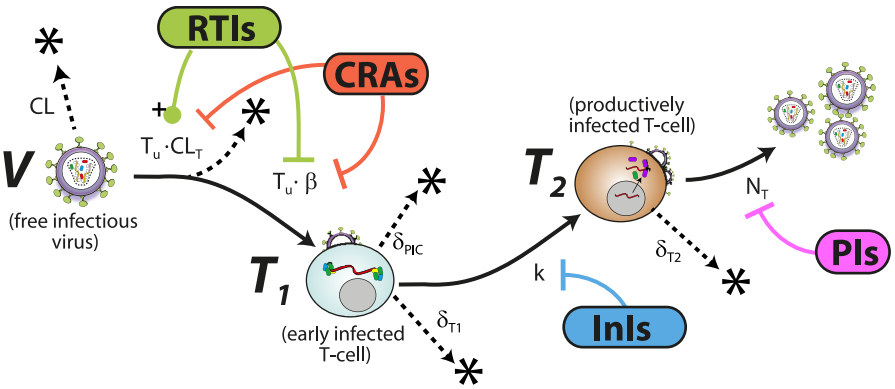

Fig 1. Schematic of the HIV replication cycle and mechanism of interference by treatment-approved drug classes. Free viruses are cleared by the immune system with a rate constant CL. Further, free viruses can be also cleared during unsuccessful T-cell infection CL_T through the destruction of essential viral components of the reverse transcription-, or pre-integration complex [37, 38]. The term β represents the lumped rate of infection of T-cells, including the processes of virus attachment to the cell, fusion and reverse transcription, leading to an early infected cell T_1, before proviral integration. Similarly, the term k denotes the rate by which early infected T_1 cells are transformed into productively infected T_2 cells, involving proviral integration and cellular reprogramming. The term N_T denotes the rate of production of infectious virus progeny by productively infected T_2 cells. The rates β, CL_T, k and N_T may be modified by different antiretrovirals as indicated by bars (inhibition) and pointers with plus sign (drug-dependent increase). The terms $\delta_{T_1} < \delta_{T_2}$ denote the rates of clearance of T_1 and T_2 cells respectively and δ_{PIC} denotes the rate of intracellular destruction of the pre-integration complex. CRA: Co-receptor antagonists, RTIs: reverse transcriptase inhibitors, InIs: Integrase inhibitors, PIs: Protease inhibitors.

https://doi.org/10.1371/journal.pcbi.1006740.g001

$$a_5(\varnothing) = \quad k \cdot T_1 \quad \text{(proviral integration; } T_1 \rightarrow T_2\text{)} \tag{8}$$

$$a_6(\varnothing) = \quad N_T \cdot T_2 \quad \text{(production of infectious virus; } T_2 \rightarrow V + T_2\text{)}, \tag{9}$$

with $CL_T = \left(\frac{1}{\rho_{rev,\varnothing}} - 1\right) \cdot \beta$ in Eq (4) as outlined in [28] where $\rho_{rev,\varnothing} = 0.5$ denotes the probability to successfully complete reverse transcription in the absence of inhibitors [37, 38]. Free viruses are cleared by the immune system with a rate constant CL. Further, free viruses can be also cleared during unsuccessful T-cell infection CL_T through the destruction of essential viral components of the reverse transcription-, or pre-integration complex intracellularly after the virus entered the cell [37, 38]. The term β represents the lumped rate of infection of T-cells, including the processes of virus attachment to the cell, fusion and reverse transcription, leading to an early infected cell T_1, before proviral integration. Similarly, the term k denotes the rate by which early infected T_1 cells are transformed into productively infected T_2 cells, involving proviral integration and cellular reprogramming. The term N_T denotes the rate of production of infectious virus progeny by productively infected T_2 cells (*infectious burst size)*. The terms $\delta_{T_1} < \delta_{T_2}$ denote the rates of clearance of T_1 and T_2 cells respectively and δ_{PIC} denotes the rate of intracellular destruction of the pre-integration complex. Parameters for the viral model are summarized in Table 1 and a mechanistic derivation of the dynamics from first principles is given in [28] (Supplementary Text therein).

Class-specific *direct* drug effects. The *direct* effect of drugs $D \in \{\text{RTI, CRA, InI, PI}\}$ on their target process is typically modelled using the Emax-equation [39]

$$\eta_D(t) = \frac{D_t^m}{IC_{50}^m + D_t^m}, \tag{10}$$

where D_t is the target site concentration of the drug and the term IC_{50} and m denote the drug

concentration at which the targeted process is inhibited by 50% and a hill coefficient [40] respectively. In the current article we will assume that drug concentrations stay constant over the course of infection, which allows to study drug- and drug class specific properties with regard to prophylaxis. This assumption is overcome in related article [27], where pharmacokinetic inputs are explicitly considered to evaluate particular prophylactic dosing regimen.

Reverse transcriptase inhibitors. In the presence of reverse transcriptase inhibitors RTI the reaction propensities a_1 and a_4 are affected [28], i.e.

$$a_1(\mathrm{RTI}) = \left(\mathrm{CL} + \left(\frac{1}{\rho_{rev,\varnothing}} - (1-\eta_{\mathrm{RTI}})\right)\cdot\beta\cdot \mathrm{T_u}\right)\cdot V \tag{11}$$

$$a_4(\mathrm{RTI}) = (1-\eta_{\mathrm{RTI}})\cdot\beta\cdot \mathrm{T_u}\cdot V \tag{12}$$

where $\eta_{\mathrm{RTI}} \in [0, 1]$ follows from Eq (10). Eq (11) results from the specific action of reverse transcriptase inhibitors: they act only after irreversible fusion of viral particles and release of viral contents has occurred by halting reverse transcription, which increases the probability that essential viral constituents get cleared intracellularly preventing viral replication to progress. Thus, inhibition by RTIs can lead to an increase of cell-dependent clearance of viral particles as modelled in Eq (11) (see Supplementary Information of [28] for an explicit derivation). From the equations it becomes evident that the increase in cell-dependent clearance (effect on a_1) matches the reduction in successful infection (effect on a_4). The validity of this model has been assessed in [30].

Other inhibitor classes. Co-receptor antagonists (CRA) decrease the infection propensity a_4 and a_1, whereas integrase inhibitors InI decrease a_5 and protease inhibitors PI reduce a_6 respectively by a factor $(1 - \eta_D)$ [28]:

$$a_1(\mathrm{CRA}) = \left(\mathrm{CL} + (1-\eta_{\mathrm{CRA}})\cdot\left(\frac{1}{\rho_{\mathrm{rev},\varnothing}} - 1\right)\cdot\beta\cdot \mathrm{T_u}\right)\cdot V \tag{13}$$

$$a_4(\mathrm{CRA}) = (1-\eta_{\mathrm{CRA}})\cdot\beta\cdot \mathrm{T_u}\cdot V \tag{14}$$

$$a_5(\mathrm{InI}) = (1-\eta_{\mathrm{InI}})\cdot k\cdot \mathrm{T_1} \tag{15}$$

$$a_6(\mathrm{PI}) = (1-\eta_{\mathrm{PI}})\cdot \mathrm{N_T}\cdot \mathrm{T_2} \tag{16}$$

Note that unlike RTIs, CRAs decrease the adsorption of viral particles by cells, which does not *per se* lead to a cell-dependent clearance of viral particles as in the case of RTIs. InIs block proviral integration, affecting a_5 and PIs prevent maturation, which lowers the amount of *infectious* viruses produced.

Probability of virus extinction

For the ease of notation we introduce the unit vectors $\widehat{\mathrm{V}}$, $\widehat{\mathrm{T}}_1$ and $\widehat{\mathrm{T}}_2$ which represent the states where only one infected compartment is present (either virus, early- or late infected cells)

$$\widehat{\mathrm{V}} = \begin{bmatrix}1\\0\\0\end{bmatrix},\ \widehat{\mathrm{T}}_1 = \begin{bmatrix}0\\1\\0\end{bmatrix},\ \widehat{\mathrm{T}}_2 = \begin{bmatrix}0\\0\\1\end{bmatrix} \tag{17}$$

Table 1. Parameters generally used for the viral dynamics model. Excerpt from [28], except for CL(naive), which assumed that virus clearance is smaller in virus-naive individuals compared to infected individuals, in line with [17, 72]. All parameters refer to the absence of drug treatment ∅. All parameters in units [1/day], except for λ [cells/day] and β [1/day/virus]. Parameter sensitivity was assessed in S2 Text.

Parameter	Value	Reference	Parameter	Value	Reference
λ_T	$2{\cdot}10^9$	[78]	k	0.35	[38]
δ_T, δ_{T_1}	0.02	[79]	β	$8{\cdot}10^{-12}$	[80]
δ_{T_2}	1	[81]	N_T	670	[28, 79]
δ_{PIC}	0.35	[38, 82]	CL(naive)	2.3	[14, 33]

https://doi.org/10.1371/journal.pcbi.1006740.t001

While free virus is typically transmitted, our framework also allows to study prophylactic efficacy for arbitrary initial states. Using the notation above, any state of the system can be expressed as a linear combination of the unit vectors above. For example, $5 \cdot \widehat{V} \oplus 3 \cdot \widehat{T}_1 \oplus 12 \cdot \widehat{T}_2$ denotes the state where we have 5 viruses, 3 early infected cells and 12 late infected cells. In S1 Text we provide a detailed derivation of infection/extinction probabilities after viral exposure. Herein, we will provide a sketch of the central idea.

Starting from a single virus $Y_0 = \widehat{V}$, we can write the Chapman-Kolmogorov equation:

$$P_E(Y_0 = \widehat{V}) \quad = \quad \sum_{n=0}^{\infty} \mathbb{P}(Y_r = n \cdot \widehat{V} | Y_0 = \widehat{V}) \cdot P_E(Y_r = \widehat{V})^n. \tag{18}$$

In words, the extinction probability $P_E(Y_0 = \widehat{V})$ is given by the probability that n viruses are produced in a single replication cycle r, $\mathbb{P}(Y_r = n \cdot \widehat{V} | Y_0 = \widehat{V})$, and that all of these viruses *eventually* go extinct, considering all possible values of n. Herein we assumed *statistical independence*, i.e. $P_E(Y_r = n \cdot \widehat{V}) = P_E(Y_r = \widehat{V})^n$. Furthermore, the extinction probabilities for parent- and progeny virus are identical when the inhibitor efficacy is constant, i.e. $P_E(Y_0 = \widehat{V}) = P_E(Y_r = \widehat{V})$. Next, we construct the embedded Markov chain [26] corresponding from the continuous-time Markov jump model depicted in Fig 1 with parameters in Table 1 (details in S1 Text). This allows to derive algebraic formulas for $\mathbb{P}(Y_r = n \cdot \widehat{V} | Y_0 = \widehat{V}),\ n = 0 \ldots \infty$. Substituting these into Eq (18), rearranging and solving for $P_E(Y_0 = \widehat{V})$ yields a quadratic formula. Solving the quadratic formula, and using $P_E(\cdot) = 1 - P_I(\cdot)$ we derive analytical solutions for the infection probabilities after exposure to a single virus $\widehat{V}$, early- $\widehat{T}_1$ and late infected cell $\widehat{T}_2$:

$$P_I(Y_0 = \widehat{V}) = \max\left(0, \frac{a_4(D)}{a_1(D) + a_4(D)} \cdot \frac{a_5(D)}{a_2 + a_5(D)} \left(1 - \frac{1}{R_0(D)}\right)\right) \tag{19}$$

$$P_I(Y_0 = \widehat{T}_1) = \max\left(0, \frac{a_5(D)}{a_2 + a_5(D)} \cdot \left(1 - \frac{1}{R_0(D)}\right)\right) \tag{20}$$

$$P_I(Y_0 = \widehat{T}_2) = \max\left(0, 1 - \frac{1}{R_0(D)}\right). \tag{21}$$

where $R_0(D)$ denotes the basic reproductive number, i.e. the average number of viruses produced from a single founder virus [41] in a single replication cycle under the action of drug D. Using our model we have $R_0(D) = \frac{a_4(D)}{a_1(D)+a_4(D)} \cdot \frac{a_5(D)}{a_2+a_5(D)} \cdot \frac{a_6(D)}{a_3}$. The first solution $P_I(\cdot) = 0$ of

Eqs (19)–(21) are valid in the regimen where $R_0(D) \leq 1$, i.e. in the regimen where extinction is certain. The second solution describes the case where infection may occur, i.e. $R_0(D) > 1$. The pre-terms in the second solution of Eqs (19) and (20) denote the bottlenecking probabilities that a late-infected, virus producing cell is reached, starting from a free virus (Eq (19)) or starting from an early infected cell (Eq (20)) respectively.

We can assume *statistical independence* during the onset of infection (i.e. competition for target cells is negligible) as noted before. Hence, for any given combination of free virus, early-stage infected cell and late-stage infected cell the extinction probability is given by

$$P_{\mathrm{E}}\left(Y_0 = \begin{bmatrix} \mathrm{V} \\ \mathrm{T}_1 \\ \mathrm{T}_2 \end{bmatrix}\right) = \left(P_{\mathrm{E}}(Y_0 = \widehat{\mathrm{V}})\right)^{\mathrm{V}} \cdot \left(P_{\mathrm{E}}(Y_0 = \widehat{\mathrm{T}}_1)\right)^{\mathrm{T}_1} \cdot \left(P_{\mathrm{E}}(Y_0 = \widehat{\mathrm{T}}_2)\right)^{\mathrm{T}_2}, \quad (22)$$

where the exponents V, T_1 and T_2 denote the number of free virus, early- and late-stage infected cells present and where we notice that $P_{\mathrm{E}}(\cdot) = 1 - P_{\mathrm{I}}(\cdot)$.

Virus exposure model

Initial viral exposure after sexual intercourse occurs at tissue sites typically not receptive for establishing and shedding HIV infection (e.g. mucosal tissues). Hence, the virus needs to pass several bottlenecks and physiological barriers to reach a replication enabling (target-cell) environment where infection can be established and from where it can shed systemically [42]. To determine realistic inoculum sizes after sexual exposure to HIV, we previously developed a data-driven statistical model linking plasma viremia in a transmitter to the initial viral population Y_0 in a replication-enabling environment [18] (Supplementary Note 4 therein for details). Herein, we used the 'exposure model' to compute drug efficacy estimates after homosexual exposure presented in section *Prophylactic efficacy of treatment-approved antivirals*. In brief, this 'exposure model' was developed to capture key clinical observations: (i) the average HIV transmission probabilities per exposure as reported in [20, 21, 43]. (ii) the fact that viral loads in the untreated transmitter population are approximately log-normal distributed [18, 44–46] ($\mu = 4.51$, $\sigma = 0.98$) and (iii) the observation that the plasma viremia in the transmitter is the most dominant factor determining HIV transmission [44, 47–49]. More specifically, it was reported that each 10-fold increase in the transmitter's viral load increases the transmission probability per coitus by approximately 2.45-fold [47] (similar values confirmed in [49]). The aforementioned clinical observations can be summarised in the formula below:

$$\bar{P}_{\mathrm{trans}} = \int_{v=0}^{\infty} P(\mathrm{VL} = v) \cdot \left(\sum_{n=0}^{\infty} P(Y_0 = n \cdot \widehat{\mathrm{V}} | \mathrm{VL} = v) \cdot P_{\mathrm{I}}(Y_0 = n \cdot \widehat{\mathrm{V}})\right) \quad (23)$$

where $\bar{P}_{\mathrm{trans}}$ is the average transmission probability per exposure/coitus (given in (i)), $P(\mathrm{VL} = v)$ is the probability density of viral load in the donor (log-normal distributed, given in (ii)), $P_{\mathrm{I}}(Y_0 = n \cdot \widehat{\mathrm{V}})$ is the infection probability when n viruses reach a replication enabling site (computed from the virus dynamics model above with $P_{\mathrm{I}}(Y_0 = \widehat{\mathrm{V}}) \approx 0.0996$) and $P(Y_0 = n \cdot \widehat{\mathrm{V}} | \mathrm{VL} = v)$ denotes the 'exposure model' (the probability that n viruses reach a replication-enabling compartment after viral exposure from a transmitter with virus load v). For the 'exposure model', we assumed a binomial distribution

$$P(Y_0 = n \cdot \widehat{\mathrm{V}} | \mathrm{VL} = v) = \binom{\lceil v^m \rceil}{n} \cdot r^n \cdot (1 - r)^{\lceil v^m \rceil - n)} \quad (24)$$

where $m = \log_{10}(2.45)$ is given by (iii) [47] and the *success probability r* was estimated in a previous work [18] (Supplementary Note 4 therein), e.g. $r_{\text{homo}} = 3.71 \cdot 10^{-3}$ for homosexual exposure. However, the model can be adapted to the different exposure types (e.g. heterosexual, needle-stick, etc . . .). In this model, the *success probability r* summarises both the extent of local exposure, as well as the probability of passing all bottlenecking physiological barriers and reaching a replication enabling target cell compartment. Lastly, in line with Keele et al. [22], we observed that if infection occurs in our model it is established by a very low number of viruses after homosexual contact and usually by a single founder virus after heterosexual contact.

Results

Relation between direct effects and prophylactic efficacy

Drug-specific inhibition of viral replication can be studied *in vitro*, for example in single-round turnover experiments [40] or even more mechanistically using enzymatic assays in conjunction with appropriate mathematical models [50]. Since the infection risk per exposure is already low in untreated individuals [20, 21], exploring the prophylactic efficacy (reduction in infection risk) in the clinic is difficult, requiring very long (several years) clinical trials with many individuals ($N > 1000$) to achieve statistically evaluable results. Systematic evaluation of concentration-effect relations is not feasible in this context, notwithstanding ethical concerns.

We wanted to gain a deeper insight how *in vitro* measurable direct drug efficacy η translates into prophylactic efficacy φ (reduction in infection probability per exposure) in a drug-class specific manner. Particularly, since different antiviral drug classes inhibit distinct stages in the HIV replication cycle, we wanted to elucidate how these different mechanisms of action affect prophylaxis. We combined Eqs (11)–(16) with Eqs (19)–(21) into Eq (3) to predict prophylactic efficacy. When relating *direct* drug effects η to prophylactic efficacy φ we observed striking drug-class specific differences as illustrated in Fig 2. Using parameters from Table 1 we found that the prophylactic efficacy φ may be less than predicted by *in vitro* measurable direct drug effects η. The sole exception are reverse transcriptase inhibitors (RTI) in case of exposure to a single virus particle $Y_0 = \widehat{V}$ where the two measures of drug efficacy coincide. While the prophylactic efficacy after exposure to a single virus are moderately less than the direct effects of co-receptor antagonists CRA and integrase inhibitors InI respectively (Fig 2A), there is a profound difference for protease inhibitors, which do not seem to reduce HIV transmission unless their direct efficacy η exceeds $\approx 95\%$. Interestingly, a similar observation using a different mathematical model and only distinguishing RTIs and PIs has been made by Conway et al. [13].

While HIV-transmission typically occurs after exposure to free virus, it is still useful to study the prophylactic efficacy of distinct drug classes in the hypothetical case when infected cells were present in the exposed individual. A realistic example for this scenario is post-exposure prophylaxis (PEP): During PEP, drugs are taken shortly *after* virus exposure and initial viral replication steps may have taken place generating early- or late infected cells. As can be seen in Fig 2B and 2C, the prophylactic efficacy of all drugs profoundly deteriorates compared to their direct effects, i.e. only very effective (in terms of η) drugs may prevent systemic infection once cells become infected in the exposed individual. An exception are integrase inhibitors: their prophylactic efficacy φ is moderately less than their direct effect η (panel B) if only early infected cells T_1 (before proviral integration) were present. Thus, while the prophylactic efficacy of all other drug classes is profoundly less than their direct effects once infected cells emerged, integrase inhibitors may still potently prevent infection. An intuitive explanation for the deterioriation of prophylactic efficacy can be made in terms

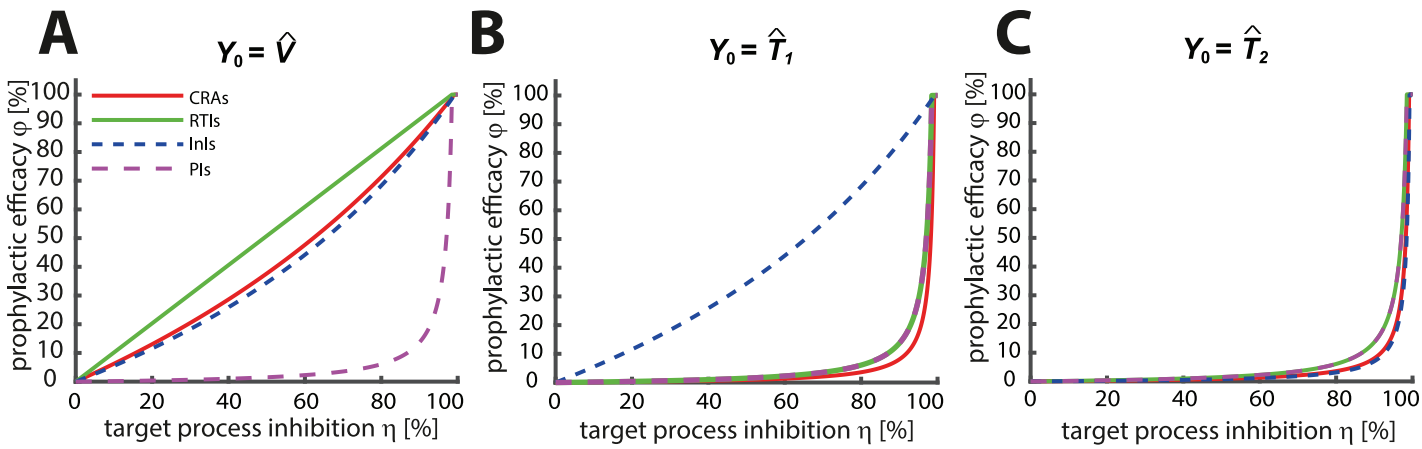

Fig 2. Relation between direct drug effect and prophylactic efficacy. The relation between direct drug effect η and prophylactic efficacy φ (reduction in infection) is shown for different drug classes utilizing the viral model depicted in Fig 1 with parameters stated in Table 1. Panel **A**: Relation between η and φ when a single virus $Y_0 = \hat{V}$ reached a replication-enabling compartment in the virus-exposed individual. Panel **B**: Relation between η and φ when a single early infected cell $Y_0 = \hat{T}_1$ or (panel **C**) a late infected T-cell $Y_0 = \hat{T}_2$ reached a replication-enabling compartment. Solid red lines: CRAs, solid green line: RTIs, dashed blue line: InI, dashed purple line: PIs.

https://doi.org/10.1371/journal.pcbi.1006740.g002

of changes in drug-target stoichiometry: For example, after exposure to a single virus $\hat{V}$, drugs from the classes of CRAs, RTIs and InIs need to block a single reaction to foster viral extinction. For PIs however, the same is only achieved if maturation of the entire viral progeny is inhibited (possibly hundreds of particles). Similarly, when considering a single early infected cell $\hat{T}_1$, CRAs and RTIs can only prevent further viral expansion *after* viral progeny has emerged. Subsequently, for each viral particle (possibly hundreds) the respective target processes (receptor binding, reverse transcription) need to be blocked by the inhibitors. Along the same lines of argumentation it is also evident that prophylactic efficacy is generally more favourable in the case of PrEP, compared to post-exposure prophylaxis (PEP), where initial viral replication may have occurred.

In vitro drug potency may overestimate PrEP potency

In vitro measured drug potency IC_{50}, IC_{90} usually guides the design of PrEP trials [51]. In particular, dosing regimen are designed so that the majority of individuals achieve drug levels just above the 90% inhibitory concentrations IC_{90}. However, it has never been rigorously investigated whether these 'target concentrations' are sufficient to provide 90% protection against HIV infection. Integrating Eq (10) into Eqs (11)–(16), (19) and (3) allows to predict the concentration-prophylaxis profile for different HIV-1 inhibitor classes. Rearranging this composite equation reveals how *in vitro* measured drug potency IC_{50}, IC_{90} can be translated into prophylactic potency (50% and 90% reduction in infection risk, EC_{50} and EC_{90}, respectively), guiding clinical trial design. The derived analytical expressions for the prophylactic efficacy (reduction in infection risk) indicate that the shape of the concentration-prophylaxis profile varies considerably for different HIV-1 inhibitor classes with important consequences for their prophylactic endpoints (% reduction in HIV transmissibility).

After exposure to a single virion $Y_0 = \hat{V}$, the overall shape of the concentration-prophylaxis profile for co-receptor antagonists (CRAs), reverse transcriptase inhibitors (RTIs) and integrase inhibitors (InIs) is a classical Emax equation (the equation of choice for evaluating

concentration-effect relations), see S1 Text for derivation.

$$\varphi(\widehat{\mathrm{V}}) = \tfrac{R_0(\varnothing)}{R_0(\varnothing)-1} \cdot \frac{D^m}{\mathrm{IC}_{50}^m\left(\frac{1}{\upsilon}\right) + D^m} \overset{R_0(\varnothing)\gg 1}{\approx} \frac{D^m}{\mathrm{EC}_{50}^m + D^m} \qquad \text{(CRA)} \tag{25}$$

$$\varphi(\widehat{\mathrm{V}}) = \tfrac{R_0(\varnothing)}{R_0(\varnothing)-1} \cdot \frac{D^m}{\mathrm{IC}_{50}^m + D^m} \overset{R_0(\varnothing)\gg 1}{\approx} \frac{D^m}{\mathrm{EC}_{50}^m + D^m} \qquad \text{(RTI)} \tag{26}$$

$$\varphi(\widehat{\mathrm{V}}) = \tfrac{R_0(\varnothing)}{R_0(\varnothing)-1} \cdot \frac{D^m}{\mathrm{IC}_{50}^m\left(\frac{1}{\vartheta}\right) + D^m} \overset{R_0(\varnothing)\gg 1}{\approx} \frac{D^m}{\mathrm{EC}_{50}^m + D^m} \qquad \text{(InI)} \tag{27}$$

where D denotes the concentration of the drug in the blood plasma, m is a slope parameter and IC_{50} denotes the plasma concentration of the drug that inhibits the targeted process (co-receptor binding, reverse transcription or proviral integration) by 50 percent. This parameter can typically be measured *in vitro*, e.g. using single-round turnover experiments [40] and is stated in Table 2 for various drugs. Parameters $\upsilon = \frac{\mathrm{CL}\cdot\rho_{\mathrm{rev},\varnothing}}{\mathrm{CL}\cdot\rho_{\mathrm{rev},\varnothing}+\beta\cdot\mathrm{T_u}} < 1$ and $\vartheta = \frac{\delta_{\mathrm{PIC}}+\delta_{\mathrm{T_1}}}{\delta_{\mathrm{PIC}}+\delta_{\mathrm{T_1}}+k} < 1$ denote the respective probabilities, in the absence of drugs, that the virus is eliminated before entering a host cell, and that essential virus compartments get cleared intracellularly after reverse transcription and before provirus integration. The parameter EC_{50} denotes the plasma concentration of the drug that decreases the probability of infection by 50%, i.e. the *prophylactic potency* of the drug. $R_0(\varnothing)$ denotes the basic reproductive number in the absence of drugs, i.e. the average number of viruses produced from a single founder virus [41] in a single replication cycle when no antivirals were present ($R_0(\varnothing) \approx 67$ according to the utilized model). When the target cell density is sufficiently high (herein considered as a target cell environment), we have $R_0(\varnothing) \gg 1$ and hence the left-side scaling factor in Eqs (25)–(27) will be close to one, $R_0(\varnothing)/(R_0(\varnothing) - 1) \approx 1$. An analysis with low target cell densities is provided in S2 Text.

In case of exposure to a single virus particle $\widehat{\mathrm{V}}$, the slope parameters in the right-most equations coincide with the slope parameter for the respective drug-targeted process m (Eq (10)), stated in Table 2. Notably, for RTIs, we have $\mathrm{EC}_{50} \approx \mathrm{IC}_{50}$, i.e. the drugs potency measured *in vitro* in single-round turnover experiments [40] directly translates into its potency to prevent infection. Using parameters from Table 1 we observe $\mathrm{EC}_{50} > \mathrm{IC}_{50}$ for CRAs and InIs, i.e. compared to their *in vitro* potency, they are less potent in preventing infection. This is largely due to the respective factors ϑ^{-1}, $\upsilon^{-1} > 1$, compare Fig 3A–3C. For InIs this observation is robust across a broad range of parameter values, as shown in S2 Text. Consequently, for InIs, higher concentrations are required to prevent infection than suggested after conducting the respective *in vitro* experiments. For CRAs, predictions are parameter dependent, S2 Text. Rearranging Eqs (25)–(27) allows to directly compute the drug concentration that prevents infection with x percent probability (the EC_x) from the corresponding *in vitro* 50% inhibitory concentration IC_{50} (derivations in S3 Text): In case of exposure *to a single virus particle* we get

$$\mathrm{EC}_x = \mathrm{IC}_{50} \cdot \left(F \cdot \frac{x}{100 \cdot C - x}\right)^{1/m}, \tag{28}$$

where EC_x is the drug concentration that achieves x percent of prophylactic efficacy and the

Table 2. Pharmacodynamic and pharmacokinetic parameters. IC_{50} [nM] and m [unit less] values are available from single turnover experiments in primary peripheral blood mononuclear cells supplemented with 50% human serum from Shen et al. [40], Laskey et al. [92] (DTG) and Jilek at al. [93] (MVC). Because some compounds are highly protein bound, IC_{50} values had to be adjusted for protein binding as outlined in the S5 Text. Indicated values are after protein adjustment. IC_{50} values are reported to be log normal distributed and m values to be normal distributed [40, 93] with respective coefficients of variation $CV = 100 \cdot \sigma/\mu$ [%]. Parameters C_{min} and C_{max} refer to the minimum and maximum concentrations in [nM] during chronic administration using the standard dosing regimen, taken from Shen et al. [40] except those for DTG [94], RPV [95] and MVC [96] (150mg twice daily). $t_{1/2}$—half life of the drug in [hr], f_b—fraction of the drug bound to plasma proteins in [%]. $^{+}$These values were fixed to the typical parameter distributions observed for all other compounds. $^{\diamond}$Parameters were taken from Drug Bank when available https://www.drugbank.ca/, accession numbers: DB04835, DB00625, DB00238, DB00705, DB08864, DB06817, DB09101, DB08930, DB01072, DB00701, DB01264, DB00224, DB00220, DB00932 or $^{\flat}$PubChem https://pubchem.ncbi.nlm.nih.gov, id: 92727. When parameters were not readily available in these databases, parameters were obtained from the indicated literature source. MVC -maraviroc, EFV -efavirenz, NVP -nevirapine, DLV -delavirine, ETR -etravirine, RPV -rilpivirine, RAL -raltegravir, EVG -elvitegravir, DTG -dolutegravir, ATV -atazanavir, APV -amprenavir, DRV -darunavir, IDV -indinavir, LPV -lopinavir, NFV -nelfinavir, SQV -saquinavir, TPV -tipranavir.

Class	Name	IC_{50}	(CV)	m	(CV)	C_{min}	C_{max}	f_b	$t_{1/2}$
CRA	MVC	5.06	(290)	0.61	(27.9)	45	557	76$^{\diamond}$	14$^{\diamond}$
RTI	EFV	10.7	(16.7)	1.69	(4.73)	5630	12968	99.4 [83]	40$^{\diamond}$
RTI	NVP	116	(31.2)	1.55	(9.68)	10883	25153	60$^{\diamond}$	45$^{\diamond}$
RTI	DLV	336	(44.7)	1.56	(11.5)	10672	27134	98 [84]	5.8$^{\diamond}$
RTI	ETR	8.59	(16.3)	1.81	(12.7)	688	1617	99.9 [85]	35 [86]
RTI	RPV	7.73	(17.9)	1.92	(10.4)	177	470	99.1$^{\diamond}$	44.5$^{\diamond}$
InI	RAL	25.5	(12.1)	1.1	(4.55)	203	3996	83$^{\diamond}$	9$^{\diamond}$
InI	EVG	55.6	(43.8)	0.95	(4.21)	301	1661	99$^{\diamond}$	8.7$^{\diamond}$
InI	DTG	89.0	(25.3^{+})	1.3	(15.4^{+})	2918	8471	98.9$^{\diamond}$	14.5 [87]
PI	ATV	23.9	(11.8)	2.69	(10.4)	899	6264	86 [88]	7$^{\diamond}$
PI	APV	262	(12.6)	2.09	(6.70)	2870	14319	90$^{\diamond}$	7.1$^{\diamond}$
PI	DRV	45.0	(21.6)	3.61	(8.86)	5081	14783	95 [85]	15$^{\diamond}$
PI	IDV	130	(11.0)	4.53	(7.94)	1827	12508	60 [89]	1.8$^{\diamond}$
PI	LPV	70.9	(20.1)	2.05	(5.85)	8757	15602	99 [60]	2.5$^{\flat}$
PI	NFV	327	(26.8)	1.81	(12.7)	2285	5104	98$^{\diamond}$	3.5$^{\diamond}$
PI	SQV	88.0	(9.7)	3.68	(6.25)	897	13282	97 [90]	3.9 [91]
PI	TPV	483	(18.0)	2.51	(14.3)	35598	77585	99.9$^{\diamond}$	5$^{\diamond}$

https://doi.org/10.1371/journal.pcbi.1006740.t002

term $F \geq 1$ is a drug class specific factor

$$F = \begin{cases} \left(\mathrm{CL} + \frac{\beta \cdot \mathrm{T_u}}{\rho}\right)/\mathrm{CL}, & \text{for CRA} \\ 1, & \text{for RTI} \\ 1/\vartheta, & \text{for InI.} \end{cases} \tag{29}$$

and

$$C \coloneqq \frac{R_0(\varnothing)}{R_0(\varnothing) - 1} \approx 1, \tag{30}$$

if $R_0(\varnothing) \gg 1$. Importantly, when exposure to multiple viruses occurs, the concentration-prophylaxis profile is no longer an Emax equation for any inhibitor class, Fig 3A–3C. Furthermore, the slope parameter increases and the EC_{50} may exceed the *in vitro* measurable IC_{50} value. At large inoculum, the corresponding profiles become switch-like. For protease inhibitors (PIs), we derive a power function to describe their prophylactic efficacy (mechanistic derivation in S1 Text):

$$\varphi(\widehat{\mathrm{V}}) = \frac{1}{R_0(\varnothing) - 1} \cdot \frac{D^m}{\mathrm{IC}_{50}^m} = C \cdot \frac{D^m}{\mathrm{IC}_{50}^m} \quad \text{(PI)} \qquad \text{for } 0 \leq \varphi \leq 1, \tag{31}$$

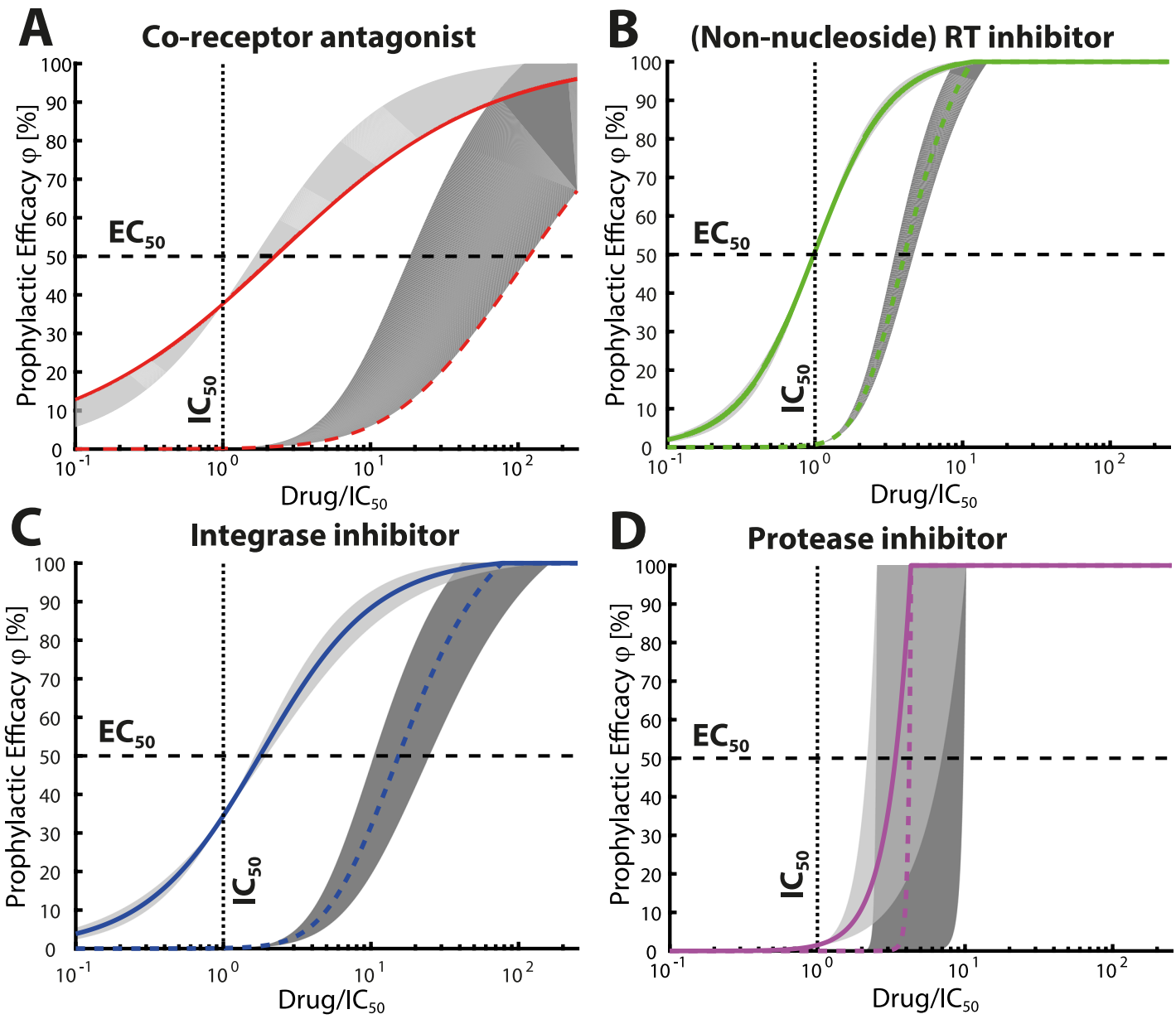

Fig 3. Shape of the concentration-prophylaxis profile. Colored lines depict the concentration-prophylaxis profile for an average drug class-specific slope parameter $\bar{m}$ in Eq (10). Solid colored line for an inoculum of one virus $Y_0 = \widehat{V}$ and dashed colored line for an inoculum of $Y_0 = 100 \cdot \widehat{V}$. Shaded areas indicate the concentration-prophylaxis profile for the smallest m_{min} and largest class-specific slope parameter m_{max} for the respective drug class as indicated in Table 2. **A**: Co-receptor antagonists. Currently only one co-receptor antagonist, maraviroc, is approved. We use $\bar{m} = m_{min} = 0.61$ and also plot $m_{max} = 1$ as a reference. **B**: Non-nucleoside reverse transcriptase inhibitors (NNRTIs); $\bar{m} = 1.71$, $m_{min} = 1.55$ and $m_{max} = 1.92$. Nucleoside reverse transcriptase inhibitors (NRTI) have been analyzed in [18]. **C**: Integrase inhibitors, $\bar{m} = 1.12$, $m_{min} = 0.95$ and $m_{max} = 1.3$. **D**: Protease inhibitors; $\bar{m} = 2.87$, $m_{min} = 1.81$ and $m_{max} = 4.53$. Utilized virus dynamics parameters are stated in Table 1.

https://doi.org/10.1371/journal.pcbi.1006740.g003

where $C << 1$ is a constant. Moreover, for realistic (large) $R_0(\varnothing) \gg 3$ their plasma concentration has to exceed their IC_{50} to decrease the probability of infection by at least 50%, Fig 3D. Similarly, we can rearrange the equation above and obtain

$$EC_x = IC_{50} \cdot \left(G \cdot \frac{x}{100}\right)^{1/m}, \tag{32}$$

for the exposure to a *to a single virus*, where $G := R_0(\varnothing) - 1$. Again, in case of exposure to multiple viruses, the slope parameter and EC_{50} increase, making the prophylactic efficacy of PIs exhibiting a switch-like behaviour as can be seen in Fig 3D. This switch-like behaviour makes the prophylactic use of PIs vulnerable to non-adherence, as well as general variations in concentrations (e.g. pharmacokinetics, inter-individual variability), and the prophylactic efficacy with these inhibitors may alternate between zero- or complete protection.

Prophylactic efficacy of treatment-approved antivirals

The combination of the nucleoside reverse transcriptase inhibitors (NRTIs) emtricitabine and tenofovir (Truvada) is the only intervention approved for pre-exposure prophylaxis (PrEP). According to our previous estimates [18], Truvada provides 96% protection in fully adherent individuals, which is in line with clinical estimates of 86-100% protection in the IPERGAY study [1], 58-96% in the PROUD study [2] and 96% in the Partners PrEP OLE study in apparently highly adherent individuals. The VOICE [3] and FEM-PrEP [52] studies indicated that Truvada may not prevent infection in poorly adherent individuals.

Currently, a number of drugs are under investigation for PrEP repurposing [6]. Notably, all currently investigated compounds are patent-protected and may not be affordable in resource-constrained countries hit hardest by the epidemic. In this work, we wanted to unselectively assess the utility of treatment-approved antivirals for prophylaxis and to assess whether currently neglected (patent-expired) compounds may be cost-efficient alternatives to be further explored in non-profit prophylaxis programmes.

We utilized comprehensive sets of drug-specific pharmacodynamic- and pharmacokinetic parameters (Table 2) to parameterize Eq (10) and to predict the prophylactic efficacy of treatment approved CRAs, non-nucleoside reverse transcriptase inhibitors (NNRTIs), InIs and PIs at clinically relevant concentration ranges (the class of NRTIs have been analyzed in earlier work [18]). Moreover, we sampled the extent of viral exposure (number of viruses transmitted and reaching a replication-enabling compartment; Eq (22)) from a previously parameterized distribution [18] that accurately reflects transmitter virus loads and drug-free infection probabilities after sexual contact. The resultant benchmark is depicted in Fig 4. Fig 4 allows for an initial screen of the utility of the various drugs for oral PrEP. Most analyzed drugs, except for maraviroc (MVC), raltegravir (RAL), elvitegravir (EVG) and nelfinavir (NFV), potently prevent infection at concentrations ranges typically encountered in fully adherent individuals during treatment (range between minimum- to maximum concentration, $[C_{min}; C_{max}]$). During prophylaxis, adherence to the dosing regimen is a major problem and we thus consider a lower bound concentration that would arise if the drug had not been taken for three days prior to exposure C_{low} (thin dashed vertical line in Fig 4) to emphasise a 'pharmacokinetic safety margin' in case of poor adherence. Numerical values for the computed maximum prophylactic efficacy and the efficacy at the lower bound concentrations are reported in Table 3 alongside with estimated EC_{50} and EC_{90} values. While in Table 3 we report the EC_{50} and EC_{90} values after challenge with a single virus $\widehat{V}$, the corresponding values after virus challenges sampled from the distribution for homosexual exposure Eq (24) were almost identical, see S4 Text for a comparison. Our simulations indicate a residual risk of infection for most analyzed drugs. Notably, most protease inhibitors may confer anything from none- to absolute protection within relevant concentration ranges, $[C_{low}; C_{max}]$, which highlights a severe limitation to their PrEP use in the context of poor adherence or pharmacokinetic (intra-/inter individual) variability. An exception among this rule is darunavir (DRV), which is predicted to be almost fully protective for the entire concentration range.

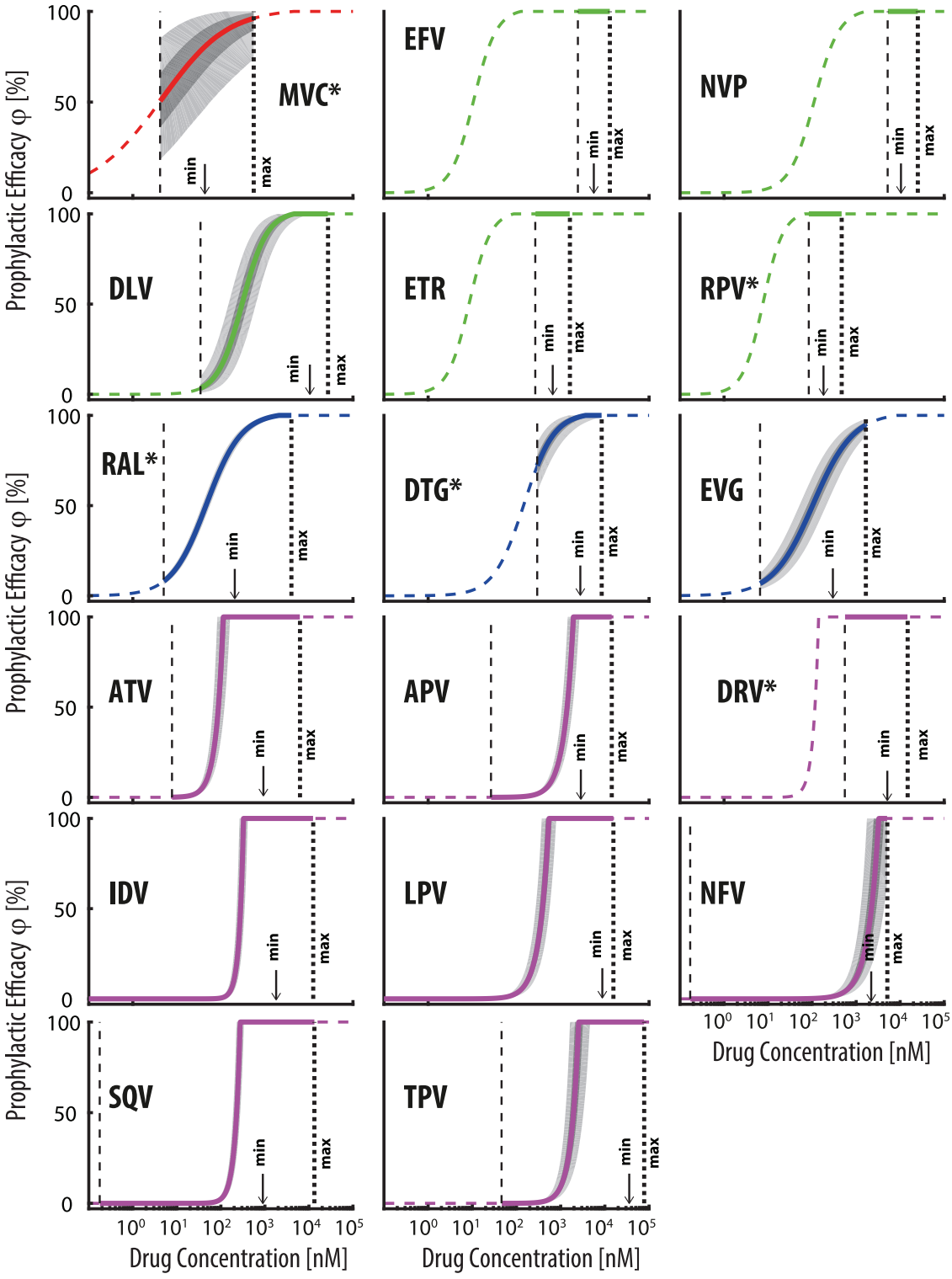

Fig 4. Drug specific prophylactic efficacy. Solid and dashed colored lines depict the concentration-prophylaxis profile for the individual drugs. The solid lines represent the concentration-prophylaxis profiles and light and dark grey areas indicate the quartile ranges and 5-95% ranges of the concentration-prophylaxis profile, considering uncertainty in pharmacodynamic parameters (Table 2) and the distribution of viral inoculum sizes after homosexual exposure to HIV using the virus exposure model' (Methods section and [18]). Maximum clinically achievable concentrations C_{max} for chronic oral administration of the standard dosing regimen and a lower bound concentration C_{low} that would be achieved if the last dose had been taken three days prior to virus

exposure are marked by thick and thin vertical black dashed lines respectively. For IDV, LPV, NFV and SQV C_{low} falls below the range of the x-axis. Downward pointing arrows indicate minimum (pre-dose) concentrations achieved for standard regimen in *adherent* individuals as reported in [40], [96] and [95]. MVC -maraviroc, EFV -efavirenz, NVP -nevirapine, DLV -delavirdine, ETR -etravirine, RPV -rilpivirine, RAL -raltegravir, EVG -elvitegravir, DTG -dolutegravir, ATV -atazanavir, APV -amprenavir, DRV -darunavir, IDV -indinavir, LPV -lopinavir, NFV -nelfinavir, SQV -saquinavir, TPV -tipranavir. *recently or currently tested for PrEP.

https://doi.org/10.1371/journal.pcbi.1006740.g004

Of the analyzed non-PI drugs, the NNRTIs efavirenz (EFV), nevirapine (NVP), etravirine (ETR) and rilpivirine (RPV) are extremely potent with regard to prophylaxis: These drugs prevent infection, even when the drug had not been taken for three consecutive days, Table 3. Notably, NVP and EFV are patent-expired and may represent suitable candidates for use in resource-constrained settings (price per day ≈ 0.1US$). The co-receptor antagonist maraviroc (MVC) and the integrase inhibitor dolutegravir (DTG) retain some prophylactic efficacy (50 and 72% respectively) at lower bound concentrations C_{low}. The CRA maraviroc (MVC), the NNRTI rilpivirine (RPV) and the InI raltegravir (RAL) are currently investigated for use as PrEP compounds (long-acting injections of RPV and RAL; oral- or topical application of MVC). In our simulations the predicted PrEP efficacy of these drugs would drop to 8% (RAL) and 50% (MVC) when the drug had not been taken for three consecutive days prior to virus exposure. Notably, RPV remained 100% effective.

Lastly, we want to note that our predictions are based on viral dynamics parameters that may under-predict prophylactic efficacy, as indicated in S2 Text. The main purpose of this modelling study was to rule out drug candidates, based on lack-off- or uncertain- prophylactic

Table 3. Prophylactic efficacy and sensitivity to incomplete adherence. The table shows the prophylactic efficacy (% reduction in infection probability) of all investigated drugs at their respective maximum achievable drug concentrations after chronic oral administration of the standard regimen and its efficacy at a concentration level that would be reached if the last dose had been taken least three days prior to virus exposure $C_{low} = C_{min} \cdot e^{-2.24 \cdot k_e}$, with $k_e = \ln(2)/t_{1/2}$ and halflifes $t_{1/2}$ reported in Table 2. The 5-95% range of these estimates are shown in brackets and consider uncertainty in pharmacodynamic parameters IC_{50}, m and variability in virus exposure after homosexual contact, according to the 'virus exposure model' (Methods section and Duwal et al. [18]. The last two columns show the EC_{50} and EC_{90} in the case when an individual was exposed to a single virus $\widehat{V}$. MVC -maraviroc, EFV -efavirenz, NVP -nevirapine, DLV -delavirdine, ETR -etravirine, RPV -rilpivirine, RAL -raltegravir, EVG -elvitegravir, DTG -dolutegravir, ATV -atazanavir, APV -amprenavir, DRV -darunavir, IDV -indinavir, LPV -lopinavir, NFV -nelfinavir, SQV -saquinavir, TPV -tipranavir. *currently investigated for PrEP.

	prophylactic efficacy φ [%]				$EC_{50}(\widehat{V})$	$EC_{90}(\widehat{V})$
drug	$\varphi(C_{max})$		$\varphi(C_{low})$		**[nM]**	**[nM]**
MVC*	96.10	(74.11;100)	50.12	(18.63;85.42)	11.45	349.63
EFV	100	(100;100)	100	(100;100)	10.55	36.23
NVP	100	(100;100)	100	(100;100)	114.06	438.06
DLV	100	(100;100)	3.38	(0.88;10.19)	329.50	1254.58
ETR	100	(100;100)	100	(100;100)	8.45	26.75
RPV*	100	(100;100)	100	(99.02;100)	7.61	22.55
RAL*	100	(100;100)	8.15	(6.32;10.23)	45.40	302.36
DTG*	100	(99.03;100)	72.12	(57.77;84.85)	145.18	722.23
EVG	94.61	(89.02;97.97)	6.96	(3.66;12.49)	108.66	976.25
ATV	100	(100;100)	0.08	(0.04;0.15)	87.44	108.79
APV	100	(100;100)	0.01	(0.01;0.03)	1394.96	1848
DRV*	100	(100;100)	100	(100;100)	118.32	139.24
IDV	100	(100;100)	0	(0;0)	280.80	319.71
LPV	100	(100;100)	0	(0;0)	389.69	519.09
NFV	100	(64.01;100)	0	(0;0)	2253.66	3118.34
SQV	100	(100;100)	0	(0;0)	227.29	266.66
TPV	100	(100;100)	0	(0;0.02)	1944.89	2458.09

https://doi.org/10.1371/journal.pcbi.1006740.t003

efficacy. While some drugs' prophylactic efficacy might be under-predicted, this *conservative* choice of parameters provides a more solid scientific basis for the remaining candidates that are predicted to be potent.

Discussion

Our intent was to develop a tool to screen out unsuitable candidates for PrEP based on unfavourable pharmacokinetic and pharmacodynamic characteristics. Clearly, the attributes which make any compound favourable extend beyond PK/PD, and critically also depend on tolerability, ease of dosing, cost and acceptability. Nevertheless, screening antiretroviral agents based on their intrinsic antiviral activity, mode of action, duration of efficacy beyond the dosing interval, and tolerance for missed dosing is a logical starting point when assessing potential candidates for PrEP.

Strikingly, we observed that *in vitro* measured drug potency may over-estimate PrEP potency in a drug-class specific manner. For all non-RTI drugs dosing schedules in clinical trials may have to be adjusted accordingly to reach the desired prophylaxis endpoints (% protection). We provide an easy-to-use software tool to determine the corresponding target concentrations (www.systems-pharmacology.org/prep-predictor).

For non-PI drugs, we observed a more graded relationship between their prophylactic efficacy and drug concentrations. At low virus inoculum sizes, the slope of their concentration-prophylaxis profile is largely determined by the slope coefficient that describes their direct effects [40]. Notably, for PIs we observed a very steep concentration prophylaxis profile, suggesting that within clinically relevant ranges for oral PrEP (Fig 4) their efficacy is likely to switch between zero- and complete protection, in an 'either-or' scenario. This characteristic renders PIs particularly vulnerable to poor adherence and drug-drug interactions. An intuitive explanation for this steep concentration-prophylaxis profile of PIs (power function in Eq (31)) is based on its unfortunate drug-to-target stoichiometry: A single late infected cell T_2 produces hundreds of infectious viruses on average (using parameters from Table 1 $a_6/a_3 = 670$) and a PI needs to prevent all of them from becoming infectious to fully prevent infection. By contrast, all other compounds only need to prevent a single viral entity from progressing, explaining the proportionality to the EMAX equation seen in Eqs (25)–(27).

By screening all treatment-approved antivirals for their PrEP utility, we predicted that efavirenz (EFV), nevirapine (NVP), etravirine (ETR), rilpivirine (RPV) and darunavir (DRV) may fully prevent infection after oral application and in case of poor adherence (Table 3 and Fig 4). Notably, these compounds have favourable inhibitory quotients (clinically achieved concentrations vastly exceed their EC_{50}) and their long elimination half-lives guarantees that inhibitory quotients stay in that favourable range. The drugs maraviroc (MVC) and dolutegravir (DTG) potently prevent infection but may allow for HIV transmission when individuals poorly adhere to the medication. Notably, the NNRTIs EFV, NVP, RPV and ETR exhibit long elimination half-lives (30-40h) and achieve concentrations required for PrEP to act quickly, and durably. However, there are some safety concerns with liver toxicity, which contraindicate e.g. the use of NVP in uninfected individuals. Liver toxicity to ETR remains to be elucidated in the context of prophylaxis. Skin reactions (ETR and EFV) and neuropsychiatric effects (EFV) have been reported in the context of HIV treatment that need to be evaluated in the context of potential PrEP applications. Likewise, skin reactions and rare liver toxicities with DRV need careful assessment in the context of PrEP repurposing. Moreover, the particular concentration-prophylaxis profile, as depicted in Fig 4, argues for a form of DRV administration that is not dependent on daily dosing for maintaining drug levels (e.g. slow release or nanoparticle formulations). For rilpivirine (RPV), our simulations suggest that near complete protection

can be achieved when concentrations exceed EC_{90}, Fig 4. RPV is currently investigated as a long-acting formulation in HPTN076 using 1200mg injections every 2 month which yields tough concentrations (median 186 nM) well in excess of this target. However, significant variability is still observed related to gender, and between injections on different occasions [51] which could be incorporated into future model generations. Besides rilpivirine, maraviroc (MVC; 300mg once daily), and raltegravir (RAL) are currently clinically investigated for oral PrEP. Our simulations suggest MVC may incompletely prevent infection even at maximum concentrations and that its efficacy steadily drops with declining levels down to 50% when the drug had not been taken for three days prior to exposure. Results from the NEXT-PrEP (HPTN 069) phase II study observed that MVC may not be potent enough on its own and that among those acquiring HIV infection, MVC concentrations were low, absent or variable [53]. Our model prediction is consistent with the reported lack of efficacy of MVC as PrEP in animals and human explant samples [54] and suggests that the potency of MVC, against infection may be less than its potency in preventing HIV replication ($EC_{50} > IC_{50}$, $EC_{90} > IC_{90}$). However, EC_{50}, EC_{90} estimates for co-receptor antagonists are highly parameter sensitive (S2 Text) warranting further research into elucidating the early infection dynamics. Using the parameters presented in Table 1, we estimate that the EC_{90} may be around 350nM, which is approximately 70 times larger than its IC_{50} (conversion formula provided in the results section). Notably, during the dose finding for MVC an IC_{90} of only 3.9nM (2ng/ml) was considered and this estimate was taken directly to determine target concentrations providing 90% prophylactic efficacy. Other compounds currently under investigation (HPTN-083) [55], but not evaluated in our study are the novel long-acting integrase inhibitor cabotegravir.

Our model has several limitations, but also a number of important advantages. Our simulations do not take into account drug concentrations at the site of mucosal exposure (e.g. cervix, rectum) [51, 56]. These concentrations have, however, not been validated as targets for successful prevention or treatment, whereas data exist (albeit limited) for plasma drug concentrations. Instead, we modelled based on *unbound* concentrations, in line with the broadly accepted 'free drug hypothesis'. Under the 'free drug hypothesis', the unbound concentrations are assumed to be available at the target site to exert pharmacological effects. For drugs highly bound to plasma protein (> 90%), naturally, their *total* concentrations at sites other than the plasma are magnitudes lower [56]. Strikingly, however, the unbound concentrations are identical [57]. Therefore, throughout the work, we assumed, according to the 'free drug hypothesis' [58] that the unbound concentrations in plasma and at the target site coincide, where the latter exerts the antiviral effect [59, 60]. All analyzed NNRTIs, InIs and PIs, except for raltegravir (RAL), are highly lipophilic, enabling the *unbound* drug to rapidly cross cellular membranes, generating an equilibrium between the *unbound* drug on either side of the cellular membrane [61]. Even for the weakly lipophilic compound raltegravir, intracellular concentrations are proportional to plasma concentrations by a factor precisely resembling their unbound moiety [62, 63], strongly arguing for the validity of the 'free drug hypothesis' for all analyzed drugs. However, ultimate proof in terms of local measurements in humans are lacking currently and may be difficult to obtain experimentally. On the contrary, nucleoside reverse transcriptase inhibitors (NRTIs), which we analysed in a previous work [18] are not expected to obey the 'free drug hypothesis' [17, 30, 64]. These compounds need to be actively taken up by cells and converted intracellularly into pharmacologically active triphosphates (NRTI-TP). Since the expression of transporters and intracellular enzymes is likely cell-specific, different cell types may contain vastly different concentrations of pharmacologically active compound. It is therefore entirely unclear what relevance concentration measurements of NRTI-TPs in tissue homogenates [65] (containing HIV target- and non-target cells) from sites of viral exposure (e.g. cervix, rectum) have in terms of prophylaxis.

Utilising the virus exposure model Eqs (23) and (24), we estimated the probability of virus clearance (and the prophylactic efficacy φ) as a function of the number of viruses ultimately reaching a target cell environment, and not as a function of mucosal exposure. The quantitative role of a number of physiological processes underlying primary infection is currently not fully resolved and impossible to measure in humans (e.g. the cells involved at the local site of exposure, their abundance, locations, their capabilities to transduce virus through physiological barriers and the respective R_0s). It is known however, that the virus has to overcome a number of physiological bottlenecks/barriers to reach a compartment that permits viral expansion. Despite the mucosal barrier, the sub-mucosal target cell density might initially be low [66], such that only a tiny fraction of viruses find a target cell before being cleared. It has also been reported [66–68], that target cells are subsequently recruited to the site of initial exposure due to inflammation and seminal exposure, mitigating the 'low target cell bottleneck' subsequently. If the low target-cell bottleneck is only prevalent during the first replication cycle it can also be modelled by simply considering a smaller virus inoculum that reaches a target-cell environment. In our approach, to obviate model- and parameter uncertainties, we chose a minimal/parsimoneous, data-driven approach that treats all physiological barriers as a single bottleneck lumped in terms of the 'success probability' r in Eq (24).

The target cell environment herein is a compartment that is decisive for establishing- and shedding infection (this compartment requires $R_0 > 1$). We also assumed that this compartment is well-perfused at the time scale of interest. Under this assumption, viral kinetic parameters measured in plasma coincide with kinetic parameters at the target cell environment, after converting the deterministic reaction parameters to their respective stochastic counterparts (Table 1).

Notably, the model (see Methods section) is calibrated [18] to reflect the per-contact infection risks for typical transmitter virus loads and different modes of sexual exposure (homo- and heterosexual), but can also be adapted to model intravenous exposure by e.g. injection. The calibrated virus exposure model [18] (see Methods section) predicts that either none- or a single infectious virus enter a replication enabling compartment in the majority of hetero-/homosexual contacts. Thus, we suggest that $EC_{50}(\widehat{V})$, $EC_{90}(\widehat{V})$ values stated in Table 3 provide a good proxy for the drug-specific prophylactic potency after sexual exposure to HIV (see also S4 Text for a comparison). Importantly, we also observed that increasing the inoculum size decreases the prophylactic efficacy of all drug classes considered (as suggested by increasing EC_{50} and EC_{90}) and increases the steepness of the concentration prophylaxis profile, Fig 3. PIs in particular displayed an almost switch-like prophylactic profile in the case of large inoculum sizes. These observations strikingly indicate that preventive target concentrations can depend on the route of transmission. I.e., intravenous exposure to HIV (larger inoculum sizes compared to sexual exposure) may require higher concentrations for HIV prevention.

When $R_0(\varnothing)$ is relatively large, we find that our predictions of prophylactic efficacy and -potency for or CRAs, RTIs and InIs are relatively invariant to parameter changes (compare Eqs (25)–(30)). However, we find that when considering an extremely broad range of $1.7 < R_0(\varnothing) < 112$ values, as in S2 Text, that the parameters used are rather *conservative* in the sense that they disfavour the drugs and may under-predict prophylactic efficacy. With regard to our work's aim (screen out candidates based on lack-off-, or uncertain potency) such a *conservative* parameter choice should be preferred. For PIs, although highly sensitive to changes R_0 (compare Eqs (31) and (32)) the qualitative statements made (the prophylactic potency is less than suggested by IC50, as well as the steep shape of the concentration-prophylaxis profile) are unaffected for arbitrary, yet realistic parameters, as analysed in S2 Text. However, in the provided software tool (www.systems-pharmacology.org/prep-predictor) it is possible to freely

change all virus dynamics parameters. Notably, Ribero et al. [69] have recently estimated $R_0 \approx 8$ during *acute* infection (≤ 10 days after exposure, virus is detectable), which is much lower than the value used by us $R_0 \approx 67$, which considers viral replication immediately after exposure, in the so-called *eclipse phase* before virus becomes detectable. Our R_0 value is relatively high because we assume a lower CL (clearance of free virus) during this early phase of infection, in line with other modelling approaches [14, 33] and in line with the observation that adaptive immune responses develop only after about 14 days post exposure [70]. However, if we utilise CL = 23 (1/day), as in Ribero et al. [69], we obtain similar values of R_0.

The knowledge of concentration-prophylaxis relationships between drug classes, and for each component of a particular drug class allows for the intelligent design of PrEP regimens, including how quickly protection can be achieved after a loading dose and how forgiving the regimen is towards missed dosing events. In related article [27] we develop a sophisticated simulation framework that allows to make use of population pharmacokinetic models, to fully explore inter-individual pharmacokinetics and to assess sensitivity towards dosing, individual pharmacokinetic variability and timing of viral challenges.

Our model can be adapted or developed in a number of ways. On a technical side, the analytical solutions provided in the article can be neatly integrated into hybrid stochastic-deterministic algorithms that consider time-varying drug concentrations (pharmacokinetics), as outlined in an accompanying article [27]. In brief, therein we utilize analytic solutions for the extinction probability, Eq (22), to define a set of states where extinction is feasible (*extinction simplex*). Whenever trajectories leave the *extinction simplex*, simulations can be stopped and a hybrid stochastic-deterministic trajectory can be safely classified as an *infection event*. Regarding applications, the separate impact of treatment as prevention [71] (in the case of the donor) versus prophylactic efficacy in the exposed individual can be readily simulated by calibrating the virus load distribution in potential transmitter populations (see 'exposure model' in the Methods section). The effect of PrEP on the transmission of resistance can be estimated by altering $R_0(\varnothing)$ (the fitness cost of resistance) and by simultaneously increasing IC_{50} in Eq (10) (extent of resistance). The fitness cost of resistance translates into a decreased transmissibility of resistance in the absence of drugs (Eqs (19)–(21)), while the extent of resistance translates into an increased transmissibility relative to the wildtype at increasing drug concentrations, as e.g. illustrated in [18] (Figure 3 therein). Consequently, provided any transmitted resistance confers some fitness defect, prophylaxis may increase the frequency of transmitted resistance relative to the wildtype, but not its absolute occurrence [18, 72]. Since resistance to HIV drugs generally develops in a stepwise manner, the change in EC_{50} following acquisition of a resistance mutation can be introduced into this model, to identify a zone of selective pressure for the *de novo* evolution or spread of resistance under PrEP. However, during the early events when the virus infection can still be averted, the population size is too small for resistance to appear *de novo*: A single point mutation appears with probability $1 - (1 - \mu)^k$ at a particular base, where $\mu \approx 2.2 \cdot 10^{-5}$ is the per base mutation rate of HIV during reverse transcription [73] and k is the number of reverse transcription (= cell infection) events. Thus, *de novo* resistance can be assumed to appear, if e.g. PrEP had not been taken at the time of exposure, such that the infection expanded exponentially, and when PrEP is (re-)initiated some time after this early infection has been established. *De novo* resistance development in the context of poor adherence can be modelled in analogy to the work conducted by Rosenbloom et al. [74].

It is well known that the establishment of a latent reservoir is the major barrier to viral extinction during treatment [75] and this reservoir may be established as early as 3 days post infection [76, 77]. In the current framework, we computed viral extinction when $t \to \infty$, assuming drug concentrations stayed constant. Thus, extinction estimates are not affected by the inclusion of a long lived cellular compartment. In an accompanying article [27] we

overcome this assumption, explicitly considering drug pharmacokinetics and e.g. short-course prophylaxis. In the accompanying article infection of long lived cells are considered as an algorithmic stopping criterium: I.e., whenever long lived cells become infected, viral extinction is considered infeasible.

In summary, we have developed a mechanistic modelling tool to *a priori* screen antivirals for their prophylactic utility. Our approach revealed that *in vitro* measured drug potency (IC_{50}, IC_{90}) should not be used directly to identify lower bound effective concentrations in PrEP trials: With the exception of reverse transcriptase inhibitors, PrEP potency may be less than *in vitro* drug potency, i.e. higher concentrations of drug are required for prophylaxis than suggested by their *in vitro* potency. Consequently, when clinical trial design is guided by *in vitro* drug potency, prophylactic dosing regimen may be selected that attain insufficient concentrations to adequately prevent HIV infection.

Instead, we recommend to use the tool provided (www.systems-pharmacology.org/prep-predictor) to translate *in vitro* drug potency into prophylactic efficacy. We used the developed methods to assess the prophylactic utility of all treatment approved antivirals, allowing to rule out particular candidates by lack-of-, or uncertain prophylactic efficacy. To this end, we presented results using viral dynamics parameters that may under-predict prophylactic efficacy (S2 Text). These preliminary screens indicated that darunavir (DRV), efavirenz (EFV), nevirapine (NVP), etravirine (ETR) and rilpivirine (RPV) may fully prevent infection at concentrations typically achieved during treatment and with an adequate 'pharmacokinetic margin'. Notably, this prediction is robust across a wide range of (uncertain) parameters (S2 Text). Moreover, we predicted that maraviroc (MVC) and dolutegravir (DTG) can potently prevent infection, but that these drugs do not provide a comparable 'pharmacokinetic margin'. Furthermore, predictions for MVC are uncertain with respect to viral dynamics parameters (efficacy may both be over- or underpredicted). A next logical step is to further trim this candidate set by ruling out compounds with ominous safety profiles, followed by an assessment of different dosing (roll-out) schemes.

Supporting information

S1 Text. The Supplementary Text contains a step-by-step derivation of the equations for the extinction/infection probability presented in the main article.
(PDF)

S2 Text. The Supplementary Text contains a sensitivity analysis with respect to viral dynamics parameters.
(PDF)

S3 Text. The Supplementary Text contains details of the IC_{50}-to-EC_{50} conversion.
(PDF)

S4 Text. The Supplementary Text compares the EC_{50} and EC_{90} (antiviral concentrations that provide 50- and 90% protection) after viral challenge with (i) a single virus $\widehat{V}$, and after virus challenges (ii) sampled from the distribution for homosexual exposure, Eq (24).
(PDF)

S5 Text. The Supplementary Text contains details of the protein-binding adjustment for pharmacodynamic parameters.
(PDF)

Author Contributions

Conceptualization: Sulav Duwal, Max von Kleist.

Formal analysis: Sulav Duwal, Laura Dickinson, Saye Khoo, Max von Kleist.

Investigation: Sulav Duwal, Laura Dickinson, Max von Kleist.

Methodology: Sulav Duwal, Max von Kleist.

Project administration: Saye Khoo, Max von Kleist.

Software: Sulav Duwal.

Supervision: Saye Khoo, Max von Kleist.

Writing – original draft: Sulav Duwal, Max von Kleist.

Writing – review & editing: Laura Dickinson, Saye Khoo.

References

1. Grant R, Anderson P, McMahan V, Liu A, Amico K, Mehrotra M, et al. Results of the iPrEx open-label extension (iPrEx OLE) in men and transgender women who have sex with men: PrEP uptake, sexual practices, and HIV incidence. AIDS. 2014; p. 20–25.
2. McCormack S, Dunn DT, Desai M, Dolling DI, Gafos M, Gilson R, et al. Pre-exposure prophylaxis to prevent the acquisition of HIV-1 infection (PROUD): effectiveness results from the pilot phase of a pragmatic open-label randomised trial. Lancet. 2016; 387(10013):53–60. https://doi.org/10.1016/S0140-6736(15)00056-2 PMID: 26364263
3. Tenofovir-based preexposure prophylaxis for HIV infection among African women. N Engl J Med. 2015; 372:509–518. https://doi.org/10.1056/NEJMoa1402269 PMID: 25651245
4. Keller SB, Smith DM. The price of tenofovir-emtricitabine undermines the cost-effectiveness and advancement of pre-exposure prophylaxis. AIDS. 2011; 25(18):2308–2310. https://doi.org/10.1097/QAD.0b013e32834d3cab PMID: 22067201
5. Boffito M, Jackson A, Asboe D. Pharmacology lessons from chemoprophylaxis studies. Clin Infect Dis. 2014; 59 Suppl 1:S52–S54. https://doi.org/10.1093/cid/ciu250 PMID: 24926035
6. AIDS Vaccine Advocacy Coalition. Pre-Exposure Prophylaxis (PrEP) by the Numbers, (available at http://www.avac.org/sites/default/files/resource-files/prep_BTN_aug2016.pdf, accessed 22-Oct-2017.).
7. Gomez GB, Borquez A, Case KK, Wheelock A, Vassall A, Hankins C. The cost and impact of scaling up pre-exposure prophylaxis for HIV prevention: a systematic review of cost-effectiveness modelling studies. PLoS Med. 2013; 10:e1001401. https://doi.org/10.1371/journal.pmed.1001401 PMID: 23554579
8. Abbas UL, Glaubius R, Mubayi A, Hood G, Mellors JW. Antiretroviral therapy and pre-exposure prophylaxis: combined impact on HIV transmission and drug resistance in South Africa. J Infect Dis. 2013; 208:224–234. https://doi.org/10.1093/infdis/jit150 PMID: 23570850
9. Supervie V, Barrett M, Kahn JS, Musuka G, Moeti TL, Busang L, et al. Modeling dynamic interactions between pre-exposure prophylaxis interventions & treatment programs: predicting HIV transmission & resistance. Sci Rep. 2011; 1:185. https://doi.org/10.1038/srep00185 PMID: 22355700
10. Supervie V, Garcia-Lerma JG, Heneine W, Blower S. HIV, transmitted drug resistance, and the paradox of preexposure prophylaxis. PNAS. 2010; 107:12381–12386. https://doi.org/10.1073/pnas.1006061107 PMID: 20616092
11. Dimitrov D, Boily MC, Brown ER, Hallett TB. Analytic review of modeling studies of ARV Based PrEP interventions reveals strong influence of drug-resistance assumptions on the population-level effectiveness. PloS one. 2013; 8:e80927. https://doi.org/10.1371/journal.pone.0080927 PMID: 24282559
12. Hendrix CW. Exploring concentration response in HIV pre-exposure prophylaxis to optimize clinical care and trial design. Cell. 2013; 155(3):515–518. https://doi.org/10.1016/j.cell.2013.09.030 PMID: 24243011
13. Conway JM, Konrad BP, Coombs D. Stochastic analysis of pre- and postexposure prophylaxis against HIV infection. SIAM J Appl Math. 2013; 73(2):904–28. https://doi.org/10.1137/120876800
14. Tuckwell HC, Shipman PD, Perelson AS. The probability of HIV infection in a new host and its reduction with microbicides. Math Biosci. 2008; 214(1-2):81–86. https://doi.org/10.1016/j.mbs.2008.03.005 PMID: 18445499

15. Pearson JE, Krapivsky P, Perelson AS. Stochastic theory of early viral infection: continuous versus burst production of virions. PLoS Comput Biol. 2011; 7(2):e1001058. https://doi.org/10.1371/journal.pcbi.1001058 PMID: 21304934

16. Yan AWC, Cao P, McCaw JM. On the extinction probability in models of within-host infection: the role of latency and immunity. J Math Biol. 2016; 73:787–813. https://doi.org/10.1007/s00285-015-0961-5 PMID: 26748917

17. Duwal S, Schütte C, von Kleist M. Pharmacokinetics and pharmacodynamics of the reverse transcriptase inhibitor tenofovir and prophylactic efficacy against HIV-1 infection. PLoS One. 2012; 7(7):e40382. https://doi.org/10.1371/journal.pone.0040382 PMID: 22808148

18. Duwal S, Sunkara V, von Kleist M. Multiscale Systems-Pharmacology Pipeline to Assess the Prophylactic Efficacy of NRTIs Against HIV-1. CPT Pharmacometrics Syst Pharmacol. 2016; 5(7):377–387. https://doi.org/10.1002/psp4.12095 PMID: 27439573

19. Carlson JM, Schaefer M, Monaco DC, Batorsky R, Claiborne DT, Prince J, et al. HIV transmission. Selection bias at the heterosexual HIV-1 transmission bottleneck. Science. 2014; 345(6193):1254031. https://doi.org/10.1126/science.1254031 PMID: 25013080

20. Royce RA, Seña A, Cates W Jr, Cohen MS. Sexual transmission of HIV. N Engl J Med. 1997; 336 (15):1072–1078. https://doi.org/10.1056/NEJM199704103361507 PMID: 9091805

21. Boily MC, Baggaley RF, Wang L, Masse B, White RG, Hayes RJ, et al. Heterosexual risk of HIV-1 infection per sexual act: systematic review and meta-analysis of observational studies. Lancet Infect Dis. 2009; 9(2):118–129. https://doi.org/10.1016/S1473-3099(09)70021-0 PMID: 19179227

22. Keele BF, Giorgi EE, Salazar-Gonzalez JF, Decker JM, Pham KT, Salazar MG, et al. Identification and characterization of transmitted and early founder virus envelopes in primary HIV-1 infection. PNAS. 2008; 105(21):7552–7557. https://doi.org/10.1073/pnas.0802203105 PMID: 18490657

23. Abrahams MR, Anderson JA, Giorgi EE, Seoighe C, Mlisana K, Ping LH, et al. Quantitating the multiplicity of infection with human immunodeficiency virus type 1 subtype C reveals a non-poisson distribution of transmitted variants. J Virol. 2009; 83(8):3556–3567. https://doi.org/10.1128/JVI.02132-08 PMID: 19193811

24. Fischer W, Ganusov VV, Giorgi EE, Hraber PT, Keele BF, Leitner T, et al. Transmission of single HIV-1 genomes and dynamics of early immune escape revealed by ultra-deep sequencing. PloS one. 2010; 5 (8):e12303. https://doi.org/10.1371/journal.pone.0012303 PMID: 20808830

25. Li H, Bar KJ, Wang S, Decker JM, Chen Y, Sun C, et al. High Multiplicity Infection by HIV-1 in Men Who Have Sex with Men. PLoS Pathog. 2010; 6(5):e1000890. https://doi.org/10.1371/journal.ppat.1000890 PMID: 20485520

26. Allen LJS. An Introduction to Stochastic Processes with Applications to Biology. Chapman & Hall/CR; 2011.

27. Duwal S, Dickinson L, Khoo S, von Kleist M. Hybrid stochastic framework predicts efficacy of prophylaxis against HIV: An example with different dolutegravir prophylaxis schemes. PLoS Comput. Biol. 2018, 14(6):e1006155. https://doi.org/10.1371/journal.pcbi.1006155 PMID: 29902179

28. von Kleist M, Menz S, Huisinga W. Drug-class specific impact of antivirals on the reproductive capacity of HIV. PLoS Comput Biol. 2010; 6(3):e1000720. https://doi.org/10.1371/journal.pcbi.1000720 PMID: 20361047

29. von Kleist M, Menz S, Stocker H, Arasteh K, Schütte C, Huisinga W. HIV Quasispecies Dynamics during Pro-active Treatment Switching: Impact on Multi-Drug Resistance and Resistance Archiving in Latent Reservoirs. PLoS One. 2011; 6(3):e18204. https://doi.org/10.1371/journal.pone.0018204 PMID: 21455303

30. Duwal S, von Kleist M. Top-down and bottom-up modeling in system pharmacology to understand clinical efficacy: An example with NRTIs of HIV-1. Eur J Pharm Sci. 2016; 94:72–83. https://doi.org/10.1016/j.ejps.2016.01.016 PMID: 26796142

31. Isaacman-Beck J, Hermann EA, Yi Y, Ratcliffe SJ, Mulenga J, Allen S, et al. Heterosexual transmission of human immunodeficiency virus type 1 subtype C: Macrophage tropism, alternative coreceptor use, and the molecular anatomy of CCR5 utilization. J Virol. 2009; 83(16):8208–8220. https://doi.org/10.1128/JVI.00296-09 PMID: 19515785

32. Ping LH, Joseph SB, Anderson JA, Abrahams MR, Salazar-Gonzalez JF, Kincer LP, et al. Comparison of viral Env proteins from acute and chronic infections with subtype C human immunodeficiency virus type 1 identifies differences in glycosylation and CCR5 utilization and suggests a new strategy for immunogen design. J Virol. 2013; 87(13):7218–7233. https://doi.org/10.1128/JVI.03577-12 PMID: 23616655

33. Tan WY, Wu H. Stochastic modeling of the dynamics of CD4+ T-cell infection by HIV and some Monte Carlo studies. Math Biosci. 1998; 147(2):173–205. https://doi.org/10.1016/S0025-5564(97)00094-1 PMID: 9433062

34. Stafford MA, Corey L, Cao Y, Daar ES, Ho DD, Perelson AS. Modeling plasma virus concentration during primary HIV infection. J Theor Biol. 2000; 203(3):285–301. https://doi.org/10.1006/jtbi.2000.1076 PMID: 10716909

35. Perelson AS. Modelling viral and immune system dynamics. Nat Rev Immunol. 2002; 2(1):28–36. https://doi.org/10.1038/nri700 PMID: 11905835

36. Perelson AS, Kirschner DE, De Boer R. Dynamics of HIV infection of CD4+ T cells. Math Biosci. 1993; 114(1):81–125. https://doi.org/10.1016/0025-5564(93)90043-A PMID: 8096155

37. Pierson TC, Zhou Y, Kieffer TL, Ruff CT, Buck C, Siliciano RF. Molecular characterization of preintegration latency in human immunodeficiency virus type 1 infection. J Virol. 2002; 76(17):8518–8531. PMID: 12163571

38. Zhou Y, Zhang H, Siliciano JD, Siliciano RF. Kinetics of human immunodeficiency virus type 1 decay following entry into resting CD4+ T cells. J Virol. 2005; 79(4):2199–2210. https://doi.org/10.1128/JVI.79.4.2199-2210.2005 PMID: 15681422

39. Chou TC. Theoretical basis, experimental design, and computerized simulation of synergism and antagonism in drug combination studies. Pharmacolog Rev. 2006; 58(3):621–681. https://doi.org/10.1124/pr.58.3.10

40. Shen L, Peterson S, Sedaghat AR, McMahon MA, Callender M, Zhang H, et al. Dose-response curve slope sets class-specific limits on inhibitory potential of anti-HIV drugs. Nat Med. 2008; 14(7):762–766. https://doi.org/10.1038/nm1777 PMID: 18552857

41. Heffernan JM, Smith RJ, Wahl LM. Perspectives on the basic reproductive ratio. J R Soc Interface. 2005; 2:281–293. https://doi.org/10.1098/rsif.2005.0042 PMID: 16849186

42. Joseph SB, Swanstrom R, Kashuba ADM, Cohen MS. Bottlenecks in HIV-1 transmission: insights from the study of founder viruses. Nat Rev Microbiol. 2015; 13(7):414–25. https://doi.org/10.1038/nrmicro3471 PMID: 26052661

43. Powers KA, Poole C, Pettifor AE, Cohen MS. Rethinking the heterosexual infectivity of HIV-1: a systematic review and meta-analysis. Lancet Infect Dis. 2008; 8(9):553–563. https://doi.org/10.1016/S1473-3099(08)70156-7 PMID: 18684670

44. Quinn TC, Wawer MJ, Sewankambo N, Serwadda D, Li C, Wabwire-Mangen F, et al. Viral load and heterosexual transmission of human immunodeficiency virus type 1. Rakai Project Study Group. N Engl J Med. 2000; 342(13):921–929. https://doi.org/10.1056/NEJM200003303421303 PMID: 10738050

45. Mellors JW, Rinaldo C Jr, Gupta P, White RM, Todd JA, Kingsley LA. Prognosis in HIV-1 infection predicted by the quantity of virus in plasma. Science. 1996; 272(5265):1167–1170. https://doi.org/10.1126/science.272.5265.1167 PMID: 8638160

46. Yousef KP, Meixenberger K, Smith MR, Somogyi S, Gromöller S, Schmidt D, et al. Inferring HIV-1 Transmission Dynamics in Germany From Recently Transmitted Viruses. JAIDS Journal of Acquired Immune Deficiency Syndromes. 2016; 73(3):356–363. https://doi.org/10.1097/QAI.0000000000001122

47. Wilson DP, Law MG, Grulich AE, Cooper DA, Kaldor JM. Relation between HIV viral load and infectiousness: a model-based analysis. Lancet. 2008; 372(9635):314–320. https://doi.org/10.1016/S0140-6736(08)61115-0 PMID: 18657710

48. Attia S, Egger M, Müller M, Zwahlen M, Low N. Sexual transmission of HIV according to viral load and antiretroviral therapy: systematic review and meta-analysis. AIDS. 2009; 23(11):1397–1404. https://doi.org/10.1097/QAD.0b013e32832b7dca PMID: 19381076

49. Hughes JP, Baeten JM, Lingappa JR, Magaret AS, Wald A, de Bruyn G, et al. Determinants of per-coital-act HIV-1 infectivity among African HIV-1-serodiscordant couples. J Infect Dis. 2012; 205(3):358–365. https://doi.org/10.1093/infdis/jir747 PMID: 22241800

50. von Kleist M, Metzner P, Marquet R, Schütte C. HIV-1 polymerase inhibition by nucleoside analogs: cellular- and kinetic parameters of efficacy, susceptibility and resistance selection. PLoS Comput Biol. 2012; 8(1):e1002359. https://doi.org/10.1371/journal.pcbi.1002359 PMID: 22275860

51. McGowan I, Dezzutti CS, Siegel A, Engstrom J, Nikiforov A, Duffill K, et al. Long-acting rilpivirine as potential pre-exposure prophylaxis for HIV-1 prevention (the MWRI-01 study): an open-label, phase 1, compartmental, pharmacokinetic and pharmacodynamic assessment. Lancet HIV. 2016; 3:e569–e578. https://doi.org/10.1016/S2352-3018(16)30113-8 PMID: 27658864

52. Van Damme L, Corneli A, Ahmed K, Agot K, Lombaard J, Kapiga S, et al. Preexposure prophylaxis for HIV infection among African women. The New England journal of medicine. 2012; 367:411–422. https://doi.org/10.1056/NEJMoa1202614 PMID: 22784040

53. Gulick RM, Wilkin TJ, Chen YQ, Landovitz RJ, Amico KR, Young AM, et al. Phase 2 Study of the Safety and Tolerability of Maraviroc-Containing Regimens to Prevent HIV Infection in Men Who Have Sex With

Men (HPTN 069/ACTG A5305). Journal Infect Dis. 2017; 215:238–246. https://doi.org/10.1093/infdis/jiw525 PMID: 27811319

54. McGowan I, Nikiforov A, Young A, Cranston R, Landovitz RJ, Bakshi R, et al. PrEP Impact on T-Cell Activation and Explant Infection: HPTN 069/ACTG 5305 Substudy. In: CROI2016, Boston. Oral presentation 104; 2016.

55. Markowitz M, Frank I, Grant RM, Mayer KH, Elion R, Goldstein D, et al. Safety and tolerability of long-acting cabotegravir injections in HIV-uninfected men (ECLAIR): a multicentre, double-blind, randomised, placebo-controlled, phase 2a trial. Lancet HIV. 2017; 4:e331–e340. https://doi.org/10.1016/S2352-3018(17)30068-1 PMID: 28546090

56. Else LJ, Taylor S, Back DJ, Khoo SH. Pharmacokinetics of antiretroviral drugs in anatomical sanctuary sites: the male and female genital tract. Antivir Ther. 2011; 16:1149–1167. https://doi.org/10.3851/IMP1919 PMID: 22155899

57. Avery LB, Bakshi RP, Cao YJ, Hendrix CW. The male genital tract is not a pharmacological sanctuary from efavirenz. Clin Pharmacol Ther. 2011; 90:151–156. https://doi.org/10.1038/clpt.2011.99 PMID: 21633344

58. Smith DA, Di L, Kerns EH. The effect of plasma protein binding on in vivo efficacy: misconceptions in drug discovery. Nat Rev Drug Discov. 2010; 9(12):929–939. https://doi.org/10.1038/nrd3287 PMID: 21119731

59. Watkins WJ, Desai MC. HCV versus HIV drug discovery: Déjà vu all over again? Bioorg Med Chem Lett. 2013; 23(8):2281–2287. https://doi.org/10.1016/j.bmcl.2013.02.070 PMID: 23489621

60. Boffito M, Back DJ, Blaschke TF, Rowland M, Bertz RJ, Gerber JG, et al. Protein binding in antiretroviral therapies. AIDS Res Hum Retroviruses. 2003; 19(9):825–835. https://doi.org/10.1089/088922203769232629 PMID: 14585213

61. von Kleist M, Huisinga W. Physiologically based pharmacokinetic modelling: a sub-compartmentalized model of tissue distribution. J Pharmacokinet Pharmacodyn. 2007; 34:789–806. https://doi.org/10.1007/s10928-007-9071-3 PMID: 17899329

62. Sandkovsky U, Swindells S, Robbins BL, Nelson SR, Acosta EP, Fletcher CV. Measurement of plasma and intracellular concentrations of raltegravir in patients with HIV infection. AIDS. 2012; 26:2257–2259. https://doi.org/10.1097/QAD.0b013e328359a978 PMID: 22948265

63. Wang L, Soon GH, Seng KY, Li J, Lee E, Yong EL, et al. Pharmacokinetic modeling of plasma and intracellular concentrations of raltegravir in healthy volunteers. Antimicrob Agents Chemother. 2011; 55:4090–4095. https://doi.org/10.1128/AAC.00593-11 PMID: 21746959

64. von Kleist M, Huisinga W. Pharmacokinetic-pharmacodynamic relationship of NRTIs and its connection to viral escape: an example based on zidovudine. Eur J Pharm Sci. 2009; 36(4-5):532–543. https://doi.org/10.1016/j.ejps.2008.12.010 PMID: 19150497

65. Cottrell ML, Yang KH, Prince HMA, Sykes C, White N, Malone S, et al. A Translational Pharmacology Approach to Predicting HIV Pre-Exposure Prophylaxis Outcomes in Men and Women Using Tenofovir Disoproxil Fumarate +/- Emtricitabine. J Infect Dis. 2016.

66. Haase AT. Targeting early infection to prevent HIV-1 mucosal transmission. Nature. 2010; 464(7286):217–23. https://doi.org/10.1038/nature08757 PMID: 20220840

67. Li Q, Estes JD, Schlievert PM, Duan L, Brosnahan AJ, Southern PJ, et al. Glycerol monolaurate prevents mucosal SIV transmission. Nature. 2009; 458(7241):1034–8. https://doi.org/10.1038/nature07831 PMID: 19262509

68. Haaland RE, Hawkins PA, Salazar-Gonzalez J, Johnson A, Tichacek A, Karita E, et al. Inflammatory genital infections mitigate a severe genetic bottleneck in heterosexual transmission of subtype A and C HIV-1. PLoS Pathog. 2009; 5(1):e1000274. https://doi.org/10.1371/journal.ppat.1000274 PMID: 19165325

69. Ribeiro RM, Qin L, Chavez LL, Li D, Self SG, Perelson AS. Estimation of the initial viral growth rate and basic reproductive number during acute HIV-1 infection. J Virol. 2010; 84(12):6096–102. https://doi.org/10.1128/JVI.00127-10 PMID: 20357090

70. McMichael AJ, Borrow P, Tomaras GD, Goonetilleke N, Haynes BF. The immune response during acute HIV-1 infection: clues for vaccine development. Nat Rev Immunol. 2010; 10(1):11–23. https://doi.org/10.1038/nri2674 PMID: 20010788

71. Cohen MS, Chen YQ, McCauley M, Gamble T, Hosseinipour MC, Kumarasamy N, et al. Prevention of HIV-1 infection with early antiretroviral therapy. N Engl J Med. 2011; 365(6):493–505. https://doi.org/10.1056/NEJMoa1105243 PMID: 21767103

72. Frank M, von Kleist M, Kunz A, Harms G, Schütte C, Kloft C. Quantifying the impact of nevirapine-based prophylaxis strategies to prevent mother-to-child transmission of HIV-1: a combined pharmacokinetic, pharmacodynamic, and viral dynamic analysis to predict clinical outcomes. Antimicrob

Agents Chemother. 2011; 55(12):5529–5540. https://doi.org/10.1128/AAC.00741-11 PMID: 21947390

73. Mansky LM, Temin HM. Lower in vivo mutation rate of human immunodeficiency virus type 1 than that predicted from the fidelity of purified reverse transcriptase. J Virol. 1995; 69:5087–5094. PMID: 7541846

74. Rosenbloom DIS, Hill AL, Rabi SA, Siliciano RF, Nowak MA. Antiretroviral dynamics determines HIV evolution and predicts therapy outcome. Nat Med. 2012; 18:1378–1385. https://doi.org/10.1038/nm.2892 PMID: 22941277

75. Chun TW, Moir S, Fauci AS. HIV reservoirs as obstacles and opportunities for an HIV cure. Nat Immunol. 2015; 16(6):584–589. https://doi.org/10.1038/ni.3152 PMID: 25990814

76. Whitney JB, Hill AL, Sanisetty S, Penaloza-MacMaster P, Liu J, Shetty M, et al. Rapid seeding of the viral reservoir prior to SIV viraemia in rhesus monkeys. Nature. 2014; 512:74–77. https://doi.org/10.1038/nature13594 PMID: 25042999

77. Chun TW, Engel D, Berrey MM, Shea T, Corey L, Fauci AS. Early establishment of a pool of latently infected, resting CD4(+) T cells during primary HIV-1 infection. PNAS. 1998; 95:8869–8873. https://doi.org/10.1073/pnas.95.15.8869 PMID: 9671771

78. Wei X, Ghosh SK, Taylor ME, Johnson VA, Emini EA, Deutsch P, et al. Viral dynamics in human immunodeficiency virus type 1 infection. Nature. 1995; 373(6510):117–122. https://doi.org/10.1038/373117a0 PMID: 7529365

79. Sedaghat AR, Siliciano RF, Wilke CO. Constraints on the dominant mechanism for HIV viral dynamics in patients on raltegravir. Antivir Ther. 2009; 14(2):263–271. PMID: 19430101

80. Sedaghat AR, Dinoso JB, Shen L, Wilke CO, Siliciano RF. Decay dynamics of HIV-1 depend on the inhibited stages of the viral life cycle. PNAS. 2008; 105(12):4832–4837. https://doi.org/10.1073/pnas.0711372105 PMID: 18362342

81. Markowitz M, Louie M, Hurley A, Sun E, Mascio MD, Perelson AS, et al. A novel antiviral intervention results in more accurate assessment of human immunodeficiency virus type 1 replication dynamics and T-cell decay in vivo. J Virol. 2003; 77:5037–5038. https://doi.org/10.1128/JVI.77.8.5037-5038.2003 PMID: 12663814

82. Koelsch KK, Liu L, Haubrich R, May S, Havlir D, Günthard HF, et al. Dynamics of total, linear nonintegrated, and integrated HIV-1 DNA in vivo and in vitro. J Infect Dis. 2008; 197(3):411–419. https://doi.org/10.1086/525283 PMID: 18248304

83. Almond LM, Hoggard PG, Edirisinghe D, Khoo SH, Back DJ. Intracellular and plasma pharmacokinetics of efavirenz in HIV-infected individuals. J Antimicrob Chemother. 2005; 56(4):738–744. https://doi.org/10.1093/jac/dki308 PMID: 16141277

84. Cheng CL, Smith DE, Carver PL, Cox SR, Watkins PB, Blake DS, et al. Steady-state pharmacokinetics of delavirdine in HIV-positive patients: Effect on erythromycin breath test. Clin Pharmacol Ther. 1997; 61(5):531–543. https://doi.org/10.1016/S0009-9236(97)90133-8 PMID: 9164415

85. Brown KC, Patterson KB, Jennings SH, Malone SA, Shaheen NJ, Prince HMA, et al. Single and multiple dose pharmacokinetics of darunavir plus ritonavir and etravirine in semen and rectal tissue of HIV-negative men. J Acquir Immune Defic Syndr. 2012; 61(2):138. https://doi.org/10.1097/QAI.0b013e31825cb645 PMID: 22614898

86. Schöller-Gyüre M, Kakuda TN, Raoof A, De Smedt G, Hoetelmans RM. Clinical pharmacokinetics and pharmacodynamics of etravirine. Clinical pharmacokinetics. 2009; 48(9):561–574. https://doi.org/10.2165/10895940-000000000-00000 PMID: 19725591

87. Dickinson L, Bracchi M, Elliot E, Else L, Khoo S, Back D, et al. Population pharmacokinetics (PK) of dolutegravir (DTG) alone and following treatment switch. In: Journal of the International AIDS Society. vol. 19. INT AIDS SOCIETY AVENUE DE FRANCE 23, GENEVA, 1202, SWITZERLAND; 2016.

88. Delille CA, Pruett ST, Marconi VC, Lennox JL, Armstrong WS, Arrendale RF, et al. Effect of protein binding on unbound atazanavir and darunavir cerebrospinal fluid concentrations. J Clin Pharmacol. 2014; 54(9):1063–1071. https://doi.org/10.1002/jcph.298 PMID: 24691856

89. Letendre SL, Capparelli EV, Ellis RJ, McCutchan JA, Group HNRC, et al. Indinavir population pharmacokinetics in plasma and cerebrospinal fluid. Antimicrobial agents and chemotherapy. 2000; 44(8):2173–2175. https://doi.org/10.1128/AAC.44.8.2173-2175.2000 PMID: 10898694

90. Holladay JW, Dewey MJ, Michniak BB, Wiltshire H, Halberg DL, Weigl P, et al. Elevated alpha-1-acid glycoprotein reduces the volume of distribution and systemic clearance of saquinavir. Drug Metab Dispos. 2001; 29(3):299–303. PMID: 11181499

91. Veldkamp AI, van Heeswijk RP, Mulder JW, Meenhorst PL, Schreij G, van der Geest S, et al. Steady-state pharmacokinetics of twice-daily dosing of saquinavir plus ritonavir in HIV-1-infected individuals. JAIDS. 2001; 27(4):344–349. PMID: 11468422

92. Laskey SB, Siliciano RF. Quantitative evaluation of the antiretroviral efficacy of dolutegravir. JCI Insight. 2016; 1(19):e90033. https://doi.org/10.1172/jci.insight.90033 PMID: 27882352

93. Jilek BL, Zarr M, Sampah ME, Rabi SA, Bullen CK, Lai J, et al. A quantitative basis for antiretroviral therapy for HIV-1 infection. Nat Med. 2012; 18(3):446–451. https://doi.org/10.1038/nm.2649 PMID: 22344296

94. Dickinson L, Bracchi M, Elliot E, Else L, Khoo S, Back D, et al. Population pharmacokinetics (PK) of dolutegravir (DTG) alone and following treatment switch. In: International Congress of Drug Therapy in HIV Infection, Glasgow, UK. Abstract P094; 2016.

95. Crauwels HM, van Heeswijk RP, Vandevoorde A, Buelens A, Stevens M, Hoetelmans RM. The effect of rilpivirine on the pharmacokinetics of methadone in HIV-negative volunteers. J Clin Pharmacol. 2014; 54(2):133–140. https://doi.org/10.1002/jcph.222 PMID: 24203510

96. Kakuda TN, Abel S, Davis J, Hamlin J, Schöller-Gyüre M, Mack R, et al. Pharmacokinetic interactions of maraviroc with darunavir/ritonavir, maraviroc with etravirine, and maraviroc with etravirine/darunavir/ritonavir in healthy volunteers: results of two drug interaction trials. Antimicrob Agents Chemother. 2011; 55:2290–6. https://doi.org/10.1128/AAC.01046-10 PMID: 21383098

frontiers in Pharmacology

ORIGINAL RESEARCH
published: 13 March 2019
doi: 10.3389/fphar.2019.00199

https://doi.org/10.3389/fphar.2019.00199

The Utility of Efavirenz-based Prophylaxis Against HIV Infection. A Systems Pharmacological Analysis

Sulav Duwal[1†], *Daniel Seeler*[1†], *Laura Dickinson*[2], *Saye Khoo*[2] *and Max von Kleist*[1*]

[1] *Department of Mathematics and Computer Science, Systems Pharmacology and Disease Control, Institute of Bioinformatics, Freie Universität Berlin, Berlin, Germany,* [2] *Department of Molecular and Clinical Pharmacology, University of Liverpool, Liverpool, United Kingdom*

Pre-exposure prophylaxis (PrEP) is considered one of the five "pillars" by UNAIDS to reduce HIV transmission. Moreover, it is a tool for female self-protection against HIV, making it highly relevant to sub-Saharan regions, where women have the highest infection burden. To date, Truvada is the only medication for PrEP. However, the cost of Truvada limits its uptake in resource-constrained countries. Similarly, several currently investigated, patent-protected compounds may be unaffordable in these regions. We set out to explore the potential of the patent-expired antiviral efavirenz (EFV) as a cost-efficient PrEP alternative. A population pharmacokinetic model utilizing data from the ENCORE1 study was developed. The model was refined for metabolic autoinduction. We then explored EFV cellular uptake mechanisms, finding that it is largely determined by plasma protein binding. Next, we predicted the prophylactic efficacy of various EFV dosing schemes after exposure to HIV using a stochastic simulation framework. We predicted that plasma concentrations of 11, 36, 1287 and 1486ng/mL prevent 90% sexual transmissions with wild type and Y181C, K103N and G190S mutants, respectively. Trough concentrations achieved after 600 mg once daily dosing (median: 2017 ng/mL, 95% CI:445–9830) and after reduced dose (400 mg) efavirenz (median: 1349ng/mL, 95% CI: 297–6553) provided complete protection against wild-type virus and the Y181C mutant, and median trough concentrations provided about 90% protection against the K103N and G190S mutants. As reduced dose EFV has a lower toxicity profile, we predicted the reduction in HIV infection when 400 mg EFV-PrEP was poorly adhered to, when it was taken "on demand" and as post-exposure prophylaxis (PEP). Once daily EFV-PrEP provided 99% protection against wild-type virus, if ≥50% of doses were taken. PrEP "on demand" provided complete protection against wild-type virus and prevented ≥81% infections in the mutants. PEP could prevent >98% infection with susceptible virus when initiated within 24 h after virus exposure and continued for at least 9 days. We predict that 400 mg oral EFV may provide superior protection against wild-type HIV. However, further studies are warranted to evaluate EFV as a cost-efficient alternative to Truvada. Predicted prophylactic concentrations may guide release kinetics of EFV long-acting formulations for clinical trial design.

Keywords: PrEP, modeling, PK-PD, translation, repurposing, resource-constrained, cost-efficient, PEP

OPEN ACCESS

Edited by:
Lei Xi,
VCU School of Medicine, Virginia Commonwealth University, United States

Reviewed by:
Collet Dandara,
University of Cape Town, South Africa
Ayyappa Chaturvedula,
University of North Texas Health Science Center, United States

***Correspondence:**
Max von Kleist
max.kleist@fu-berlin.de

[†]These authors share first authorship

Specialty section:
This article was submitted to Translational Pharmacology, a section of the journal Frontiers in Pharmacology

Received: *14 December 2018*
Accepted: *18 February 2019*
Published: *13 March 2019*

Citation:
Duwal S, Seeler D, Dickinson L, Khoo S and von Kleist M (2019) The Utility of Efavirenz-based Prophylaxis Against HIV Infection. A Systems Pharmacological Analysis. Front. Pharmacol. 10:199. doi: 10.3389/fphar.2019.00199

1. INTRODUCTION

The ambitious goals formulated by UNAIDS are to end AIDS by 2030 (UNAIDS, 2017). However, unlike many other infections, no cure is available to clear HIV infection. Ending AIDS therefore heavily relies on strategies to reduce the number of new HIV infections from an estimated 2.1 million in 2014 (UNAIDS, 2015) to 500,000 cases by 2020 and to fewer than 200,000 by 2030 (UNAIDS, 2016). While a vaccine would be the ideal tool for the purpose, intrinsic difficulties have so far precluded the development of an effective vaccine against HIV. Despite these setbacks, the development of about 30 antiviral compounds to stop HIV replication has been an overwhelming success (Gulick, 2018) in HIV research.

In light of the current situation, recent years have seen an increasing interest in utilizing antivirals not only for treatment, but also to prevent HIV transmission. Two general strategies are currently investigated for this purpose:

(i) Treatment-as-prevention (TasP) intends to put individuals with an HIV diagnosis immediately on treatment, which essentially makes them non-contagious (Cohen et al., 2011). However, a major limitation of this approach is that HIV is typically transmitted early after infection (Brenner et al., 2007; Yousef et al., 2016), when the recently infected individual is unaware of his/her HIV status and has consequently not initiated TasP. Thus, maximizing the epidemiological impact of TasP also requires to improve HIV diagnosis, which is a central component of the 90-90-90 strategy (UNAIDS, 2017).

(ii) Pre-exposure prophylaxis (PrEP) acts on the viral dynamics in the virologically challenged individual immediately after virus exposure. Akin to a vaccination, PrEP increases the probability that transmitted virus gets cleared, protecting individuals from becoming irreversibly infected. However, unlike vaccination, PrEP protection is a direct function of the concentration of prophylactic drugs at the target site.

Once-daily oral PrEP with the drug combination Truvada (tenofovir disoproxil fumarate-emtricitabine) has been approved since 2012 in the US and since 2016 in the EU. Initial clinical studies with Truvada demonstrated its utility as a PrEP agent (Grant et al., 2010), while subsequent studies indicated that the efficacy of Truvada-based PrEP was highly dependent on the individual's adherence to the once daily regimen. While it is difficult to quantify PrEP adherence clinically (Haberer et al., 2015), efficacy estimates in apparently highly adherent individuals were 86–100% in the IPrEx OLE study, 58–96% in the PROUD study and 96% in the Partners PrEP OLE study (Grant et al., 2014; McCormack et al., 2016). The VOICE and FEM-PrEP studies indicated that Truvada may not prevent infection in poorly adherent individuals, i.e., if 30% of individuals had detectable drug in their blood plasma (Van Damme et al., 2012; Marrazzo et al., 2015). Mathematical modeling of Truvada-based PrEP (Duwal et al., 2016) established the precise relationship between drug pharmacokinetics and prophylactic efficacy confirming many clinical observations (i.e., quantifying the prophylactic efficacy to be $\approx$ 96% in fully adherent individuals).

While adherence is a major current concern that motivates the identification of novel long-acting drug candidates and optimized deployment strategies (AVAC, 2019), a currently neglected factor is the cost of PrEP, with the majority of HIV infections occurring in resource-constrained countries (UNAIDS, 2016). Keller and Smith (2011) noted that the price of Truvada currently undermines the advancement of pre-exposure prophylaxis, particular in resource-constrained settings. Yet regrettably, current PrEP research focusses entirely on patent-protected compounds (AVAC, 2019). This makes it unlikely that a current, or next-generation PrEP regimen will become broadly implemented in resource-constrained regions where they could benefit most. Moreover, PrEP is the only strategy by which women can protect themselves against HIV infection, making PrEP highly relevant in regions like sub-Saharan Africa, where young women are the most relevant target group to halt the ongoing spread of HIV (Dellar et al., 2015; Maxmen, 2016), accounting for $\approx$ 7000 infections per week (Mathur et al., 2016).

A natural progression would therefore be whether currently neglected, patent-expired compounds might make good candidates for PrEP repurposing. Based on an initial computational assessment of potential candidates (Duwal et al., 2019), we focus herein on the patent-expired non-nucleoside reverse transcriptase inhibitor (NNRTI) efavirenz (EFV), which is successfully used in HIV treatment, particularly in resource-constrained settings, where it costs as little as 0.1US$ per day. To this end, we assess efavirenz pharmacokinetics, consider its mode of action and establish the relationship between pharmacokinetics and prophylactic efficacy. Since reduced-dose (400 mg) efavirenz has a considerably improved safety profile, we assess the prophylactic efficacy of 400 mg oral EFV when used in chronic PrEP, PrEP on demand and post-exposure prophylaxis (PEP).

2. PATIENTS

A previously developed population pharmacokinetic (PK) model, constructed using data collected as part of ENCORE 1 was used. ENCORE 1 was a multi-center, double-blind, placebo-controlled trial designed to compare standard dose efavirenz (600 mg once daily) to a reduced dose (400 mg once daily) in HIV-infected, treatment-naive adults. Patients recruited at sites across Africa, Asian, South America, Europe and Oceania were randomized (1:1) to receive efavirenz 600 or 400 mg once daily in combination with tenofovir disoproxil fumarate/emtricitabine (Truvada, 300/200 mg once daily) (ENCORE1 Study Group, 2014; ENCORE1 Study Group et al., 2015).

At weeks 4 and 12 of therapy, single random blood samples were drawn between 8-16 hours post-dose, additionally intensive sampling was undertaken in a subgroup of patients between weeks 4 and 8 [pre-dose (0 h), 2, 4, 8, 12, 16 and 24 h post-dose]. Plasma efavirenz was quantified using a validated HPLC-MS/MS method (Amara et al., 2011). Overall, 606 patients (n=131, 32% female) randomized to efavirenz 600 mg (n = 311) and 400 mg once daily (n = 295) contributed 1491 samples for model development [median (range) 2 (1–9) per patient].

Median (range) age and weight were 35 years (18–69) and 65kg (39–148) and baseline viral load ranged between 162 and 10,000,000 copies/mL. The majority of patients were of African and Asian ethnicity (37 and 33%, respectively) with the remainder identifying as Hispanic (17%), Caucasian (13%) and Aboriginal and Torres Strait Islander (0.2%).

3. METHODS

3.1. Efavirenz Pharmacokinetics

Efavirenz (EFV) is a non-nucleoside reverse transcriptase inhibitor that is frequently used in first-line therapy in resource-constrained regions in combination with emtricitabine (FTC) and tenofovir disoproxil fumerate (TDF) for treatment of HIV infection. EFV is a small (molecular mass: 315.6 g/mol) lipophilic (LogP ≈ 4) compound that is highly bound to plasma proteins (human serum albumin and α-1-acid glycoprotein). The unbound fraction of the drug in human plasma (f_u) is $<$ 1% (Almond et al., 2005; Fayet et al., 2008; Burhenne et al., 2010; Avery et al., 2011, 2013a). Efavirenz is a known inducer of various CYP-P450 enzymes (Fichtenbaum and Gerber, 2002), including *CYP2B6*, which is the main enzyme mediating its own metabolism (Ward et al., 2003; Ogburn et al., 2010). Moreover, it is known that CYP-P450 polymorphisms, in particular *CYP2B6* can lead to large inter-individual variations in EFV concentrations (Orrell et al., 2016). We derived statistical models for the inter-individual variability in plasma pharmacokinetic profiles, particularly taking CYP P450 polymorphisms (*CYP2B6* and *CYP2A6*) in a representative population (ENCORE 1) into account. Furthermore, we modeled metabolic autoinduction and established the relationship between plasma- and target-site concentrations.

3.1.1. Pharmacokinetic Model Building

The population pharmacokinetic analysis of ENCORE 1 has previously been reported (Dickinson et al., 2015, 2016). Briefly, nonlinear mixed effects modeling using NONMEM (v. 7.2; ICON Development Solutions, Ellicott City, MD, USA) was applied to the efavirenz concentration-time data using FOCE-I. The impact of the following covariates on efavirenz apparent oral clearance (CL/F_{bio}) was investigated: age, weight, fat-free mass (FFM), body mass index (BMI), sex, ethnicity and CYP P450 genotypes *CYP2B6* 516G>T, *CYP2B6* 983T>C, *CYP2B6* 15582C>T, *CYP2A6**9B, *CYP2A6**17, *CYP3A4**22, *NR1I3* 540C>T and *NR1I3* 1089T>C. Specifically, of the 606 patients with PK data, 95% had a blood sample for genotyping (n=574), although amplification failed for a small number of individuals (*CYP2B6* 15582C>T and *CYP3A4**22, n=1; *CYP2A6**17, n=2; *CYP2A6**9B, n=4). To drive the PrEP simulations, the final model was used to simulate PK parameters of 1000 virtual patients receiving efavirenz using the same distribution of significant covariates as the original dataset. PK parameters of all virtual patients are summarized in **Supplementary Table 1**.

Efavirenz concentrations over time were best described by a 1 compartment model parameterized by apparent oral clearance [population value of CL/F_{bio}; estimate (RSE%): 11.9L/h (2.4%) for the reference (wild-type) CYP genotype for all four SNPs; *CYP2B6*: 516G>T/983T>C/*CYP2A6**9B/*17 of a 70kg weighing individual], apparent volume of distribution [population mean V/F_{bio}; 282 L (5.2%)] and absorption rate constant k_a fixed to a value of $0.6h^{-1}$ (Arab-Alameddine et al., 2009):

$$\frac{d}{dt}Z_1 = -k_a \cdot Z_1 \tag{1}$$

$$\frac{d}{dt}D_{i,j} = \frac{k_a \cdot Z_1}{V_i/F_{bio}} - \frac{CL_{i,j}(t)/F_{bio}}{V_i/F_{bio}} \cdot D_{i,j} \tag{2}$$

whereby Z_1 denotes the amount of drug in the dosing compartment. The variable of interest is the concentration in the blood plasma (central compartment), i.e., D. Dosing events were modeled as impulse inputs, with

$$Z_{1,t} = Z_{1,t} + dose_k, \tag{3}$$

whenever the current simulation time t coincided with a dosing event τ_k. In the equations above, $CL_{i,j}(t)/F_{bio}$ denotes the bioavailability-adjusted, individual drug clearance at occasion j and k_a denotes the rate of drug uptake. The term V_i/F_{bio} is the bioavailability-adjusted volume of distribution of individual i. Interindividual and interoccasion variability was supported on CL/F_{bio} [36.6% (10.8%) and 21.0 (27.7%), respectively] and residual error was defined by a proportional model [20% (8.6%)]. CL/F_{bio} and V/F_{bio} were allometrically scaled by weight (centered on 70 kg) and *CYP2B6* 516G>T/983T>C/*CYP2A6**9B/*17 composite genotype significantly reduced efavirenz CL/F_{bio} between 4.5-82% , depending on allele combinations, compared to the reference genotype. Pharmacokinetic parameters for a 70 kg individual with reference genotype are summarized in **Table 1.** Overall, there were 16 genotype subgroups (**Supplementary Table 2**). Grouping of patients as extensive, intermediate or slow metabolisers (see below) as part of the modelling process (or after the final model was obtained) did not impact individual parameter estimates. The reduced genotype groups were defined as follows: (i) extensive metabolisers, (ii) intermediate metabolisers and (iii) slow metabolisers as detailed in Dickinson et al. (2015).

For initial model building clearance was assumed to reflect values *after* metabolic autoinduction since pharmacokinetic data was collected at weeks 4 and 12 of therapy. In the following, we consider the autoinduction explicitly, since it affects PrEP efficacy shortly after its initiation (e.g., "PrEP on demand").

3.1.2. Metabolic Autoinduction

In our work, we modeled metabolic autoinduction similarly to the model proposed by Zhu et al. (2009). We defined the term α as the ratio of the mean clearance on day 1 to the mean clearance at steady state (after autoinduction). The clearance ratio α is then computed as $\alpha = \frac{\mathbb{E}_i(CL_{i,t_0})}{\mathbb{E}_i(CL_{i,SS})}$ where the *average* clearance on the first day $\mathbb{E}_i(CL_{i,t_0}) = 5.76$L/h was taken from Zhu et al. (2009) and the *average* clearance at steady state $\mathbb{E}(CL_{i,SS}) = 9.86$L/h was computed from the virtual patient population (**Supplementary Table 1**), deriving $\alpha = 0.58$. For each virtual patient generated from the population pharmacokinetic model,

TABLE 1 | Pharmacokinetic parameters.

Parameter	Value	Unit	Parameter	Value	Unit
CL_{ss}/F_{bio}	11.9	L/h	V/F_{bio}	282	L
α	0.58	–	σ	0.20	–
$CV_{IIV}(CL_{ss}/F_{bio})$	36.6	%	$CV_{IOV}(CL_{ss}/F_{bio})$	21.0	%

*The table displays the pharmacokinetic parameter estimates for a 70 kg individual with reference genotype (reference: CYP2B6, pos. 516:GG, pos. 516:TT and for CYP2A *9B and *17: CC/CC or CC/CT or CC/TT or CA/CC or CA/CT or AA/CC or AA/CT Dickinson et al., 2015). Inter-individual variability (IIV), as well as inter-occasional variability (IOV) was included on drug clearance CL/F_{bio}. These parameters were log-normal distributed with coefficient of variation [%] $CV = 100 \cdot \sqrt{e^{\sigma^2} - 1}$, where σ^2 is the variance of the associated normal distribution. Weight was considered to affect $CL_{ss}(i)/F_{bio} = CL_{ss}/F_{bio} \cdot (\text{weight}(i)/70)^{0.75}$ and the volume of distribution $V(i)/F_{bio} = V/F_{bio} \cdot (\text{weight}(i)/70)$ through allometric scaling. Residual variability was described by a proportional error model ($\sigma = 0.2$).*

the individual clearance at steady state was available and the clearance at day 1 was computed using $CL_{i,t_0} = \alpha \cdot CL_{i,SS}$. Zhu et al. (2009) proposed a model for time-dependent autoinduction that we used herein

$$CL_i(t) = CL_{i,t_0} + \left(CL_{i,SS} - CL_{i,t_0}\right) \cdot \frac{t - t_0}{(t - t_0) + T_{50}} \qquad (4)$$

where $CL_i(t)$ is the individual clearance rate at the time t and t_0 is the time of the first EFV dose. $CL_i(0)$ and $CL_{i,SS}$ represent the clearance rates at day 1 and at steady state. The term $T_{50} = 245$h (Zhu et al., 2009) is the time where the clearance rate reaches half of its steady-state value.

3.1.3. Target-site Concentrations

The general perception is that only the free/unbound intracellular concentration at the site of action (intracellular space) is available to exert an antiviral effect (Smith et al., 2010). For highly lipophilic drugs like EFV, passive diffusion may be the dominating transport mechanisms and therefore the *unbound/free* drug concentrations are identical on both sides of biomembranes, whereas the relation between the *total* concentrations can be computed by considering unspecific drug retention by e.g. binding to plasma proteins or lipids. These assumptions are implemented in so called partition coefficient models commonly used in physiologically based pharmacokinetic modeling, see von Kleist and Huisinga (2007) for an overview. To test whether EFV is dominantly transported into cells by passive diffusion/equilibrating transport we implemented partition coefficient models and compared the predictions with intracellular concentration measurements in **Supplementary Text 1**. We found overwhelming evidence for passive diffusion/equilibrating transport as the dominating mechanism of cellular drug uptake. Moreover, under passive diffusion and unspecific drug retention, there is a direct proportionality between plasma concentrations and concentrations at the site of action. This proportionality implies that we can model the effect of EFV based on plasma drug concentrations (derivations in **Supplementary Text 1**).

3.2. Direct Effects

We modeled the *direct* effect of efavirenz using the sigmoidal Emax-equation (Chou, 2006)

$$\eta_D(t) = \frac{D_t^m}{IC_{50}^m + D_t^m}, \qquad (5)$$

TABLE 2 | Pharmacodynamic parameters.

Strain	IC_{50} (± sd)	m (± sd)	*f*
wild type	5.4 (± 0.9)	1.69 (±0.08)	1
Y181C	$2.8 \cdot IC_{50}$(wt)	$0.9 \cdot m$(wt)	0.78
K103N	$89.1 \cdot IC_{50}$(wt)	$0.83 \cdot m$(wt)	0.74
G190S	$72.1 \cdot IC_{50}$(wt)	$0.6 \cdot m$(wt)	0.24

*The table displays the pharmacodynamic parameters for wild type (Shen et al., 2008) and different viral mutants (Sampah et al., 2011). The hill coefficient m (unit less) was assumed to be normal distributed and IC_{50} values (nmol/L) were assumed to be log-normal distributed (Jilek et al., 2012). Parameters were corrected for protein binding as outlined in **Supplementary Text 1**. Parameter f (unit less) denotes the fitness of the respective strains. The respective parameter distributions for the mutants (IC_{50}, m) were computed by assuming an identical coefficient of variation as compared to the wild type.*

where D_t is the plasma concentration of the drug at time t, which is directly proportional to the target-site concentration (previous section and **Supplementary Text 1**) and the term IC_{50} and m denote the plasma concentration at which the targeted process is inhibited by 50% and a hill coefficient (Shen et al., 2008), respectively. Parameters are displayed in **Table 2** for wild type, K103N, Y181C and G190S mutants together with their standard deviation. Note that the equation above couples the stochastic viral dynamics (below) to the deterministic pharmacokinetics (above). The hill coefficient m and 50% inhibitory concentration IC_{50} have been measured *ex vivo* using single-round infection assays in primary human peripheral blood mononuclear cells, supplemented with 50% human serum for *wild-type* HIV and various resistance mutations (K103N, Y181C and G190S) (Shen et al., 2008; Sampah et al., 2011). Since the *ex vivo* assay was performed with 50% human serum, the measured IC_{50} has to be corrected for protein content, since the drugs' potency might otherwise be overestimated, particularly for highly protein bound drugs like EFV. The IC_{50} correction is demonstrated in **Supplementary Text 1**, together with a sensitivity analysis with regard to uncertainties in measuring the unbound fraction of EFV in human blood plasma.

3.3. Viral dynamics.

We adopted the viral dynamics model described in von Kleist et al. (2010) and von Kleist et al. (2011). Long-lived and latently infected cells are only implicitly considered (outlined at the end of the section), motivated by the observation that

transmitted viruses are not macrophage-tropic (Isaacman-Beck et al., 2009; Ping et al., 2013) and in line with related modeling approaches (Tan and Wu, 1998; Stafford et al., 2000; Perelson, 2002; Tuckwell et al., 2008; Conway et al., 2013). Although this model is a simplified representation of the molecular events happening during virus replication, it allows to accurately and mechanistically describe the effect of all existing antiretroviral drug classes on viral replication, as previously reported in (e.g., Duwal and von Kleist, 2016), and can be parameterized by *in vitro* and *clinical* data, **Table 3**. The modeled viral replication cycle consists of free infectious viruses V, uninfected T-cells (T_u), early infected T-cells (T_1) and productively infected T-cells (T_2). Early infected T-cells (T_1) and productively infected T-cells (T_2) denote T-cells prior- and after proviral integration, respectively, where the latter produces virus progeny. During the onset of infection the number of viruses is relatively low and the number of uninfected T-cells T_u is fairly unaffected by viral dynamics (Perelson et al., 1993; Tan and Wu, 1998; Pearson et al., 2011). We thus consider $T_u = \lambda_T/\delta_T$ to be constant over the course of simulations. The stochastic dynamics of viral replication after virus exposure are then defined by six reactions:

$$
\begin{aligned}
a_1(D_t) &= \left(\mathrm{CL_V} + \mathrm{CL_T}(D_t, \mathrm{mut}) \cdot \mathrm{T_u}\right) \cdot V_t && \text{(clearance of free virus; } V \to *) && (6)\\
a_2 &= \left(\delta_{\mathrm{PIC}} + \delta_{\mathrm{T_1}}\right) \cdot \mathrm{T}_{1,t} && \text{(clearance of early infected cell; } \mathrm{T_1} \to *) && (7)\\
a_3 &= \delta_{\mathrm{T_2}} \cdot \mathrm{T}_{2,t} && \text{(clearance of late infected cell; } \mathrm{T_2} \to *) && (8)\\
a_4(D_t) &= (1 - \eta_D(t)) \cdot \beta \cdot f(\mathrm{mut}) \cdot \mathrm{T_u} \cdot V_t && \text{(infection of a susceptible cell; } V \to \mathrm{T_1}) && (9)\\
a_5 &= k \cdot \mathrm{T}_{1,t} && \text{(proviral integration; } \mathrm{T_1} \to \mathrm{T_2}) && (10)\\
a_6 &= \mathrm{N_T} \cdot \mathrm{T}_{2,t} && \text{(production of virus; } \mathrm{T_2} \to \mathrm{V} + \mathrm{T_2}), && (11)
\end{aligned}
$$

with $\mathrm{CL_T}(D_t, \mathrm{mut}) = \left(\frac{1}{\rho_{\mathrm{rev}}} - (1 - \eta_D(t))\right) \cdot \beta \cdot f(\mathrm{mut})$ in Equation (6), as outlined in von Kleist et al. (2010) where $\rho_{rev} = 0.5$ denotes the probability to successfully complete reverse transcription in the absence of inhibitors (Pierson et al., 2002; Zhou et al., 2005) and $f(\mathrm{mut})$ denotes the fitness of the mutant. Free viruses can be cleared within T-cells during unsuccessful infection with rate $\mathrm{CL_T}$ by destruction of essential viral components of the reverse transcription-, or pre-integration complex (Pierson et al., 2002; Zhou et al., 2005) or it may get cleared by the immune system with a rate constant $\mathrm{CL_V}$. Further, the term β represents the lumped rate of infection of T-cells, including the processes of virus attachment to the cell, fusion and reverse transcription, leading to an early infected cell T_1, before proviral integration. The term k denotes the rate by which early infected T_1 cells are transformed into productively infected T_2 cells, involving proviral integration and cellular reprogramming. The term $\mathrm{N_T}$ denotes the rate of production of infectious virus progeny by productively infected T_2 cells. The terms $\delta_{\mathrm{T_1}} < \delta_{\mathrm{T_2}}$ denote the rates of clearance of T_1 and T_2 cells, respectively, and δ_{PIC} denotes the rate of intracellular destruction of the pre-integration complex. Parameters for the viral model are summarized in **Table 3**. In this article, we study distinct prophylactic schemes with the non-nucleoside reverse transcriptase inhibitor efavirenz. Reverse transcriptase inhibitors act intracellularly on reverse transcription. In our viral dynamics model this translates into an increase of propensity function a_1 and a proportional decrease in propensity function a_4. Derivations and motivation of this mechanisms of action from first principles are given in von Kleist et al. (2010) (Supplementary Methods therein).

3.4. Virus Exposure

Initial viral exposure after sexual intercourse occurs at tissue sites typically not receptive for establishing and shedding HIV infection (e.g., mucosal tissues). Hence, the virus needs to pass several physiological barriers to reach a replication enabling (target-cell) environment where infection can be established and from where it can shed systemically (Joseph et al., 2015).

To determine realistic inoculum sizes after sexual exposure to HIV (initial states for hybrid stochastic simulations), we previously developed a data-driven statistical model linking plasma viremia in a transmitter (VL) to the initial viral population Y_0 in a replication-enabling environment (Duwal et al., 2016) (Supplementary Note 4 therein for details) precisely capturing average per contact transmission rates for various types of exposure. In brief, we assume a binomial model

$$P(Y_0 = V | \mathrm{VL} = \nu) = \binom{[\nu^m]}{n} \cdot r^n \cdot (1 - r)^{[\nu^m] - n} \qquad (12)$$

where $[\cdot]$ is the nearest integer function, $m = \log_{10}(2.45)$ is given by Wilson et al. (2008) and the *success probability* r was estimated in a previous work (Duwal et al., 2016) (Supplementary Note 4 therein), e.g., $r_{\mathrm{homo}} = 3.71 \cdot 10^{-3}$ for homosexual- and $r_{\mathrm{hetero}} = 3.63 \cdot 10^{-4}$ for heterosexual exposure. The parameter

TABLE 3 | Parameters used for the viral dynamics model.

Parameter	Value	References	Parameter	Value	References
λ_T	$2{\cdot}10^9$	Wei et al., 1995	k	0.35	Zhou et al., 2005
δ_T, δ_{T_1}	0.02	Sedaghat et al., 2009	β	$8{\cdot}10^{-12}$	Sedaghat et al., 2008
δ_{T_2}	1	Markowitz et al., 2003	N_T	670	Sedaghat et al., 2009; von Kleist et al., 2010
δ_{PIC}	0.35	Zhou et al., 2005; Koelsch et al., 2008	CL_V	2.3	Tan and Wu, 1998; Tuckwell et al., 2008

Excerpt from von Kleist et al. (2010), except for CL_V*, which assumed that virus clearance is smaller in virus-naive individuals compared to infected individuals, in line with Frank et al., 2011; Duwal et al., 2012. All parameters refer to the absence of drug treatment ∅. All parameters in units (1/day), except for λ (cells/day) and β (1/(day · virus)).*

VL denotes the viral load in a potential transmitter (assumed to be log-normal distributed with $\mu = 4.51, \sigma = 0.98$ (Duwal et al., 2016)). In this model, the *success probability r* summarizes both the extent of local exposure, as well as the probability of passing all bottlenecking physiological barriers and reaching a replication enabling target cell compartment. Herein, we used the "exposure model" to compute drug efficacy estimates after sexual exposure presented in **Figures 3**, **4**.

3.5. Numerical Simulation

We use the exact numerical simulation scheme proposed in Duwal et al. (2018). Briefly, the modeled system is split into stochastic reactions describing viral dynamics and a set of ordinary differential equations describing individual EFV pharmacokinetics after drug administration, including covariates (e.g., CYP2B6 polymorphisms), autoinduction and the relationship between plasma- and target-site concentrations outlined above. In our approach EFV pharmacokinetics affect certain stochastic reaction propensities as outlined in Equations (6), (9). This hybrid system is then simulated using the numerically exact EXTRANDE algorithm (Voliotis et al., 2016) and hybrid trajectories are classified as extinction events when all viral compartments are cleared. On the other hand, trajectories were considered infections if (i) either long-lived- or latently infected cells emerged, or if (ii) the trajectories left an *extinction simplex* ($\epsilon = 0.0001$), meaning that it becomes unlikely (probability $\leq \epsilon$) that the virus will eventually be cleared (details provided in Duwal et al., 2018).

3.6. Prophylactic Efficacy of a Drug Regimen

Our goal is to estimate the prophylactic efficacy φ of a particular medication regimen S_D. The prophylactic efficacy denotes the reduction in infection risk *per contact*, with φ =100% indicating complete protection and φ =0% indicating no change in infection risk.

$$\varphi(Y_0, S_D) = 1 - \frac{P_{\mathrm{I}}(Y_0|S_D)}{P_{\mathrm{I}}(Y_0|\varnothing)} \quad \text{(prophylactic efficacy)}, \qquad (13)$$

where $P_{\mathrm{I}}(Y_0|S_D)$ and $P_{\mathrm{I}}(Y_0|\varnothing)$ denote the virus infection probabilities for a particular prophylactic scheme S_D and in the absence of prophylactic drugs ($\varnothing$), respectively, for initial state $Y_0 = [V, \mathrm{T}_1, \mathrm{T}_2]^T$ (number of viral particles, early- and late infected cells in a replication-enabling compartment). The probabilities $P_{\mathrm{I}}(Y_0|S_D)$ are approximated by the number of simulations that were classified as *infection events* divided by the *total* number of hybrid stochastic simulation runs for each particular prophylaxis scheme S_D during PrEP, PrEP "on demand" and PEP simulations. $P_{\mathrm{I}}(Y_0|\varnothing)$ can be computed using the analytical formulas derived in Duwal et al. (2019).

Simulation of Pre- and Post-Exposure Prophylaxis

Codes were written in MATLAB R2018b (MathWorks, Natick, MA; v. 9.5, including the statistics toolbox). Individual pharmacokinetic model parameters were drawn from the distributions defined by the parameter estimates from the final efavirenz population pharmacokinetic model (**Table 2**), generating 1000 virtual patients (**Supplementary Table 1**). We then simulated individual pharmacokinetic profiles for the prophylactic schedule S_D under consideration using ode113 in MATLAB. To simulate different adherence levels, a sequence of uniformly distributed random numbers with $r_i \sim \mathcal{U}(0, 1)$ was drawn and the ith dose was missed if $r_i >$ adherence level.

The number of viruses to be inoculated was drawn from the virus exposure model, where we first sampled the viral load in a potential transmitter ($\log_{10}\mathrm{VL} \sim \mathcal{N}(4.51, 0.98)$) and then used the virus load in the transmitter to determine the number of viruses V_0 entering a replication-competent compartment in the virus-exposed individual using Equation. (12). Samples with $V_0 = 0$ were rejected (they do not contribute to the infection risk). For once-daily PrEP simulations with different adherence levels, a time of virus exposure was randomly drawn within a 3 month interval starting at day 31 after PrEP initiation. The corresponding drug concentrations at this time and the number of transmitted viruses reaching a target cell compartment were used as the initial states for EXTRANDE and simulated until stopping criteria were satisfied (either virus clearance or infection). For "PrEP on demand" simulations, the time of virus exposure was fixed as indicated in the corresponding graphics. In the case of PEP, virus was inoculated as stated above and the stochastic viral dynamics were simulated in the absence of drugs until the time of PEP initiation (to determine the initial condition of the system), and henceforth simulated until a stopping criterium was reached.

In total, for each prophylactic scenario, 10000 simulations were run and $P_{\mathrm{I}}(Y_0|S_D)$ was computed as the fraction of simulations that resulted in infection.

4. RESULTS

4.1. Pharmacokinetics

The standard EFV dose used in treatment is 600 mg once daily taken orally. However, this dose is associated with neurotoxic effects (Rakhmanina and van den Anker, 2010; Apostolova et al., 2015), which could be prohibitive when using EFV as prophylaxis. Notably, neurotoxicity is associated with EFV plasma concentrations (and CYP2B6 polymorphism) (Rakhmanina and van den Anker, 2010). Therefore, a reduced, 400 mg dose has recently been explored, significantly reducing the risk of neurotoxicity while maintaining sufficient antiviral effects (ENCORE1 Study Group, 2014; ENCORE1 Study Group et al., 2015).

In **Figures 1A,B** we depict simulated pharmacokinetics of once daily oral EFV with 400 and 600 mg. EFV was quickly absorbed with a median $t_{\max} \approx$ 5.90h (95% CI: 4.56–7.88) and has a long median half life $t_{1/2} \approx$ 35.57h (CI: 14.28–125.26) at day 1 and a median half life $t_{1/2} \approx$ 20.77h (CI: 8.34–73.15) after metabolic autoinduction, in agreement with the literature (Avery et al., 2011, 2013a; Dickinson et al., 2015). Due to its linear pharmacokinetics, the dose reduction 600 $\rightarrow$ 400 mg resulted in a concentration reduction of $\approx 2/3$ for the 400mg dosing regime. In **Figures 1C,D**, we show the long-term pharmacokinetics after

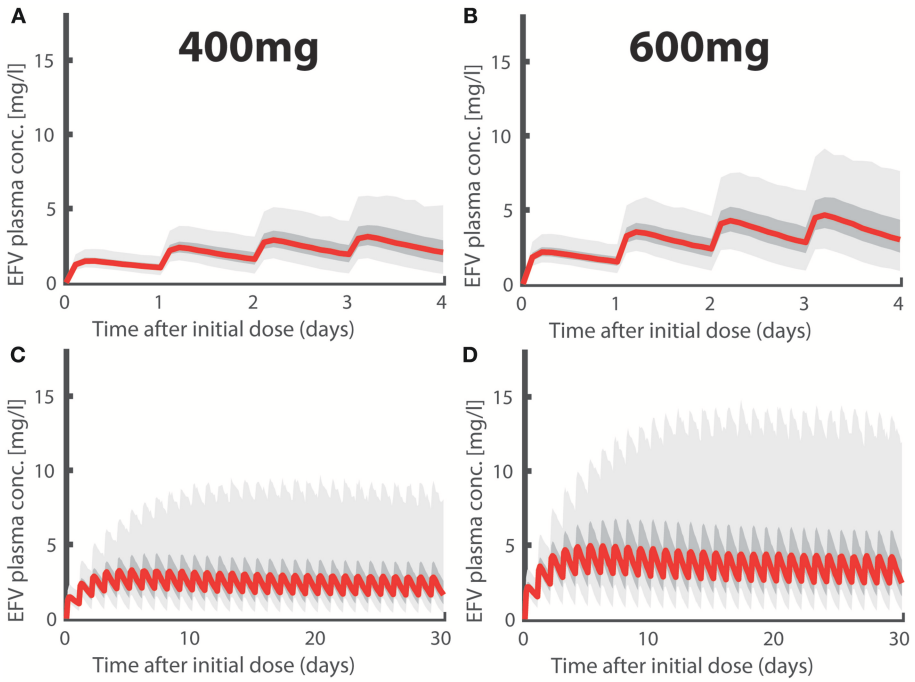

FIGURE 1 | Efavirenz Pharmacokinetics. Population plasma pharmacokinetics for the first four days after intake of **(A)** 400- and **(B)** 600-mg daily oral EFV. Long-term pharmacokinetics of **(C)** 400- and **(D)** 600-mg daily oral EFV due to metabolic autoinduction. Light gray regions encompass 95% of individual PK predictions, whereas dark gray areas encompass 50% of the predictions (quartiles). The thick red line marks the median pharmacokinetic profiles.

multiple dosing. Two things come to mind: (i) after an initial plateau phase (4–5 doses), concentrations tend to decrease, due to metabolic autoinduction, reaching median trough levels of $\approx$ 1.35 and $\approx$ 2.02 mg/L (95% CI: 0.30–6.55 and 0.45–9.83mg/L) in the 400- and 600mg dosing regime, respectively. (ii) The variability in the predicted pharmacokinetic profiles increases after multiple dosing with some individuals achieving concentrations $>$ 10 (mg/L) (light grey area indicating the 95% range). This observation is attributable to genetic polymorphisms affecting some individuals of our virtual patient cohort that slowly metabolize EFV. Interestingly, there is clinical evidence that some individuals, particularly slow metabolisers, achieve concentrations $>$ 10 (mg/L), and that the proportion of these individuals is much higher for the 600 mg regimen (Dickinson et al., 2015). In our simulations, 11.3% in the 600 mg group eventually exceed concentration of 10 mg/L, whereas it is only 2.5% in the 400 mg group. If EFV toxicity is proportional to exposure, as suggested by Rakhmanina and van den Anker (2010), this may indicate that dose reduction could significantly reduce the risk of adverse effects. But is it also protective against infection?

4.2. Concentration-prophylaxis Profile

We used the analytical solutions presented in Duwal et al. (2019) to compute concentration-prophylaxis profiles $\varphi(Y_0, S_D)$ assuming a single virus particle enters a replication-enabling compartment ($Y_0 = [1, 0, 0]^T$), see **Figure 2A**. The reason is that the virus exposure model (Methods section) predicts that in most cases only a single virus enters a replication-competent compartment after (homo-/hetero-)sexual exposure, if a virus manages at all to pass the various bottlenecking physiological barriers after sexual exposure. Besides the *wild-type* virus, we also show the prophylaxis profile against transmitted drug resistance with viruses carrying EFV resistance mutations G190S, K103N and Y181C (Rhee et al., 2003). As a visual guide, the shaded areas mark the 95% trough (pre-dose) concentration ranges achieved at plateau and after metabolic autoinduction for once daily 400 mg efavirenz (computed using the POP-PK model).

Figure 2A suggests that once daily EFV (with 400 mg) provides complete protection against HIV infection after exposure to *wild-type* virus and resistant viruses carrying the Y181C mutation. After exposure to the G190S and K103N mutants, $>>$50% protection is provided by once daily 400 mg EFV and $>>$60% protection by the 600 mg regime. Since selection of drug resistant variants is a major concern, we evaluated the relative transmissibility of mutant viruses when compared with *wild-type* virus as $\varphi_{\text{wt}} - \varphi_{\text{mut}}$ in **Figure 2B**. The figure can be interpreted as follows: At low concentrations there is no reduction in infection if an individual was exposed to *wild-type* and/or mutant virus. At an intermediate concentration range (between 0.001 and 0.1 for Y181C and between 0.001 and 1 mg/L for K103N, G190S, respectively), infections with the *wild type* would be prevented, while the prophylaxis cannot, or only partially reduce the infection risk after exposure to mutant virus. The maximum corresponds to the maximal difference in risk reduction, meaning that resistant virus is more likely

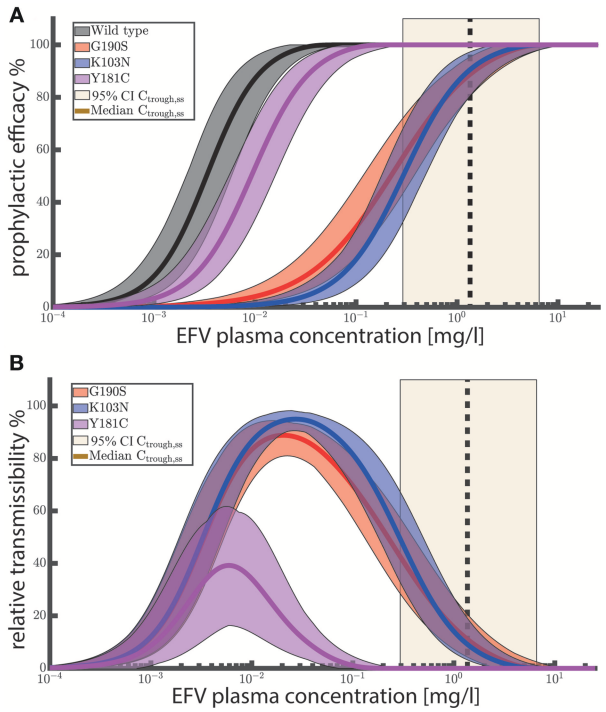

FIGURE 2 | (A) Prophylactic efficacy against different viral genotypes. Predicted efficacy ranges are depicted as colored shaded areas, with superimposed mean efficacy estimates as solid lines. Ninety-five percent confidence intervals of steady-state EFV trough (pre-dose) concentrations $C_{trough,ss}$ for 400 mg EFV after once daily dosing are depicted as light yellow areas with the vertical black dashed line marking the median trough concentration. **(B)** Relative transmissibility $\varphi_{wt} - \varphi_{mut}$ of mutant viruses. Colored areas depict the ranges of relative transmissibility and solid lines indicate the mean relative transmissibility.Yellow shaded areas depict the 95% CI of EFV trough (pre-dose) concentrations after 400 mg once daily at steady state. Black dashed vertical lines indicate the corresponding median trough concentrations. The prophylactic efficacy against a single virus was computed using the analytical solutions provided in Duwal et al. (2018) (Equation 19–21 therein) for 1000 logarithmically spaced concentrations between 10^{-4} and 25 mg/L using 1000 sampled values for IC_{50} and m per viral genotype (**Table 2**). For each viral genotype, $IC_{50_{assay}}$ and m were sampled from a log-normal and normal distribution respectively as stated in the caption of **Table 2**. $IC_{50_{assay}}$ were corrected for plasma binding using $f_{u,plasma} = 0.2\%$ to obtain $IC_{50_{plasma}}$, as outlined in **Supplementary Text 1**. Changes in drug sensitivity for the mutants considered the fold changes stated in **Table 2**. Fitness defects of the mutants were considered using $\beta(\text{mut}) = f(\text{mut}) \cdot \beta(\text{wt})$.

transmitted than the *wild type*. At very high EFV concentrations, the infection risk with both *wild type* and mutant is reduced. Importantly, when inspecting (population) *median* EFV trough (pre-dose) concentrations after 400 mg once daily dosing (dashed vertical black line in **Figure 2B**) , we can see that the relative transmissibility of the Y181C mutant is zero, while the relative transmissibilities of the G190S and K103N mutants are less than 20%. The analysis suggests that the typical concentration ranges achieved after once daily EFV do not, or just slightly, favor resistance transmission over *wild type* for the considered single-substitution mutants. Note that these mutations decrease EFV susceptibility by ≈ 90 fold, **Table 2**. However, clinically derived isolates may contain multiple substitutions and confer even higher levels of EFV resistance.

Since poor drug adherence may give rise to lower EFV concentrations and since it is a major factor confounding the clinical efficacy of Truvada (Haberer et al., 2015), we next set out to test whether similar issues are to be expected for 400 mg oral EFV for pre-exposure prophylaxis, or when EFV is used "on demand" and post-exposure.

4.3. Once-daily PrEP With 400 mg EFV

The predicted prophylactic efficacy of once daily PrEP with 400 mg is shown in **Figure 3A** as a function of adherence after exposure to either *wild-type* virus or after exposure to drug resistant mutants. As can be seen, if at least 75% of doses were taken, complete protection against the *wild-type* virus and against the Y181C mutant was achieved. Notably, for these viral genotypes protection was > 95% if 50% of the pills were taken and ≈ 90% when ≈25% of the pills were taken. In contrast, after exposure to resistant viruses carrying the G190S or K103N mutation, protection was >82% when at least 75% of the once daily 400 mg EFV pills were taken, gradually dropping to ≈ 50% protection when every fourth pill was taken.

We next wanted to assess how quickly the prophylactic protection vanishes, when consecutive EFV doses were missed (illustratively depicted in **Supplementary Figure 1**). In order to do so, we simulated 400 mg EFV-based once daily PrEP with 100% adherence. Subsequently, we computed how long it will take for the concentrations to drop below the respective 50%, or 90% protective levels (EC_{50}, EC_{90}). We computed that a median of 7 (CI: 2–32) consecutive doses need to be missed in order to provide less than 50% protection against *wild-type* virus. Correspondingly, 5 (CI: 1–26) consecutive doses need to be missed to provide less than 90% protection against *wild-type* virus.

4.4. "PrEP on Demand" With 400 mg EFV

Next, we evaluated whether 400 mg EFV "on demand" would protect against HIV infection. We tested an "on demand" dosing scheme similar to the one recently tested for Truvada-based PrEP (Molina et al. , 2015): The first EFV dose was taken within a time window of 1–23 h *prior* to virus exposure and followed by two more doses, 24- and 48- hours after the initial dose. Our predictions indicate that EFV-based "PrEP on demand" provides complete protection against *wild-type* virus and against the Y181C single mutant, when initiated 1–23 h prior to virus exposure. Protection against the single mutants G190S and K103N was still > 81% for 400 mg "PrEP on demand." This surprisingly superior prophylactic efficacy of EFV "on demand" can be attributed to its rapid uptake and slow elimination. Particularly the latter ensures that virus gets eliminated when EFV is taken as "PrEP on demand." The comparatively higher efficacy of "PrEP on demand," when compared to once daily PrEP with low adherence can be explained as follows: In the case of once-daily PrEP, several *consecutive* dose intakes may be missed, which allows the EFV concentrations to fall below their respective EC_{50}, EC_{90}. If virus exposure occurs during

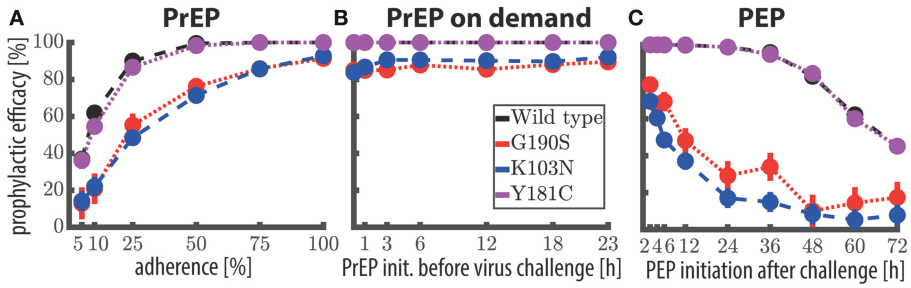

FIGURE 3 | Prophylactic efficacy of EFV against the *wild-type* and resistant virus using different prophylaxis schemes. **(A)** Predicted prophylactic efficacies for once daily 400 mg oral EFV PrEP with different levels of adherence. For example in the 25% adherence scheme, each dosing event was randomly missed with 75% chance. Colored dots mark the median predicted prophylactic efficacy and error bars mark the 95% confidence interval (computed using Greenwood's formula), considering variabilities in pharmacokinetic, as well as pharmacodynamic parameters. **(B)** Predicted prophylactic efficacy of 400 mg oral EFV during "PrEP on demand" (3 doses) depending on the time of PrEP initiation with respect to viral encounter, respectively. **(C)** Predicted prophylactic efficacy of post-exposure prophylaxis (9 doses) with 400 mg oral EFV as a function of the time of PEP initiation after viral challenge. Simulations were conducted using the hybrid EXTRANDE method outlined in the Methods section. In total, 10,000 stochastic simulations were performed to estimate prophylactic efficacy for each condition (e.g., viral challenge with K103N during chronic PrEP with 5% adherence is one condition).

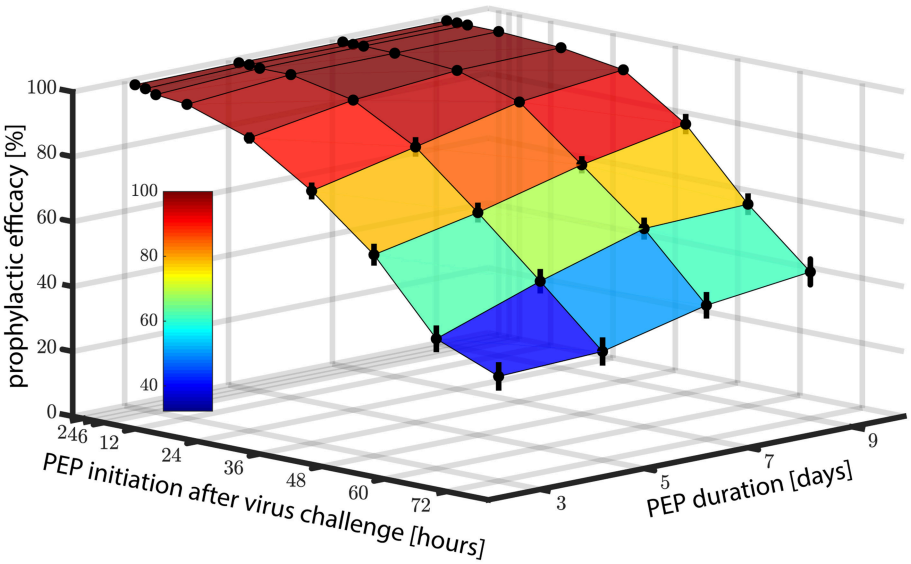

FIGURE 4 | Prophylactic efficacy of *PEP* against *wild type* virus depending on both the time of PEP initiation and the number of subsequent 400 mg EFV doses taken. Error bars denote the 95% confidence intervals, computed using Greenwood's formula. Prophylactic efficacy was estimated for each condition based on 10,000 hybrid EXTRANDE simulations as outlined in the Methods section.

these time windows of low EFV concentrations, infection may occur (illustrated in **Supplementary Figure 1**). In contrast, if all "PrEP on demand" pills are taken, concentrations will be above the EC_{90} at the time of exposure, and, due to the long half life of EFV remain above this value, until the virus is eliminated (which typically would happen $\leq$ 1 week post exposure Konrad et al., 2017).

4.5. Post-Exposure Prophylaxis With 400 mg EFV

Motivated by the promising predictions regarding the use of EFV in pre-exposure prophylaxis, we also wanted to investigate whether EFV could prevent infection, if taken as post-exposure prophylaxis (PEP). In **Figure 4**, we show the predicted prophylactic efficacy of 400 mg oral EFV as a function of both the delay in PEP initiation and the duration of PEP after challenge with *wild-type* virus. In **Figure 4** it becomes evident that it is more critical to initiate PEP early after exposure, than to prolong PEP duration. For example, when PEP is initiated as late as 72 h post virus exposure and the duration of PEP is three days (3 consecutive doses), the prophylactic efficacy was estimated to be ≈20%. If the duration of PEP was increased to 9 days, the prophylactic efficacy increases to only ≈40%. However, if PEP was initiated shortly after virus exposure (e.g., within 2 h), the prophylactic efficacy increases to 100%, even if the PEP duration was only 3 days.

As a midpoint, taking the first PEP dose within 24 h post-exposure resulted in prophylactic efficacies of $>$ 88, $>$ 94, $>$

97 and > 98% against the *wild type* for 3, 5, 7, and 9 dose intakes, respectively.

Next, we wanted to investigate in more detail the sensitivity of PEP efficacy towards the timing of PEP initiation in the *wild type* and drug resistant mutants. To simplify interpretation, we assumed a PEP duration of 9 days (9 doses). Predictions are shown in **Figure 3C**. PEP provided > 98% protection against the *wild type* and the Y181C mutant when started within 12 h after virus exposure. Protection against viruses containing the G190S mutation was > 21% using the same parameters, and > 11% for the K103N mutant. These simulations indicate that EFV may potently protect against infection with *wild type* and the weakly resistant Y181C virus, when initiated within 24 h post expose. The prophylactic efficacy against transmitted, highly resistant viruses carrying the G190S or K103N mutation is insufficient for post-exposure prophylaxis.

5. DISCUSSION

Truvada-based PrEP is being implemented in a number of countries (AVAC, 2019), however, there are two major limitations to its optimal use: (i) its costs (Keller and Smith, 2011), and (ii) its sensitivity to poor medication adherence (Haberer et al., 2015).

Current PrEP research focusses on overcoming adherence-related concerns, either in terms of promoting drug adherence, or through the development of novel long-acting drugs/drug formulations for HIV prophylaxis, that only require monthly drug administration (McGowan et al., 2016; Markowitz et al., 2017; McMillan et al., 2017). However, little has been done to investigate cost-efficient Truvada alternatives that may be affordable in low- and middle-income countries hit hardest by the epidemic.

A recent computational screen of the prophylactic potential of treatment-approved compounds for PrEP repurposing suggested that darunavir, efavirenz, nevirapine, etravirine and rilpivirine may more potently prevent HIV infection than Truvada at clinically relevant concentration ranges (Duwal et al., 2019). Of these candidates we set out to investigate efavirenz in more detail, since it is both inexpensive and readily available in most resource-constrained settings.

However, 600 mg EFV has been associated with neurotoxicity (Rakhmanina and van den Anker, 2010; Apostolova et al., 2015). Decloedt and Maartens (2013) and Siccardi et al. (2012) have previously suggested a connection between EFV metabolism and toxicity, indicating that slow metabolisers, who have higher plasma concentrations, also have a higher tendency to experience adverse effects (associations have been made between the major EFV metabolite and neurotoxicity). The direct association between plasma concentrations and CNS side effects has also been reported in Marzolini et al. (2001). Motivated by these studies, we explicitly considered genetic polymorphisms affecting EFV metabolism. Moreover, since EFV pharmacokinetics are linear, dose reductions would naturally lead to decreased EFV exposure (and consequently toxicity) as investigated in the ENCORE 1 trial (ENCORE1 Study Group, 2014; ENCORE1 Study Group et al., 2015), which suggested non-inferiority of the 400 mg EFV regimen with regard to treatment. Motivated by these results, we set out to investigate the prophylactic potential of 400 mg EFV.

Our simulations strongly suggest that 400 mg efavirenz can potently prevent infection with drug susceptible HIV, when used as once daily PrEP, during "PrEP on demand" and even as PEP, if initiated early enough after exposure (**Figures 3**, **4**). Overall, these simulations suggest that EFV provides a good efficacy margin with respect to incomplete adherence and various event-driven dosing scenarios. Notably, if the association between EFV toxicity and metabolism is evident, it could also be envisioned that individuals that experience adverse effects may even further reduce EFV dosing. For example, using the POP-PK model, we predicted that the number of patients experiencing plasma concentrations of > 10 mg/L following a 200mg once daily dosing regimen is only 0.1%.

However, our simulations also suggested that EFV-based post-exposure prophylaxis (PEP) may insufficiently protect against transmitted, highly resistant strains (K103N, G190S), as depicted in **Figure 3C**. We should also note that circulating resistant viruses may have multiple compensatory mutations that increase fitness and resistance through epistatic effects (Rath et al., 2013). Thus, their phenotypic attributes may deviate from laboratory strains with single point mutations that were evaluated in the present analysis and by Sampah et al. (2011). A recent study (Zazzi et al., 2018) highlighted high levels of NNRTI resistance particularly in South Africa, but it is unclear whether the analyzed NNRTI resistance mutations also confer high level resistance against EFV. Regarding high level resistance mutations, the Stanford database currently reports a prevalence $\pi_{\text{untreated}} << 5\%$ [1] in the *untreated* population in South Africa, mainly conferred by K103N. The prevalence of resistance mutations in *treated* individuals π_{treated} is much higher: K103N $\approx$ 30%, Y181C $\approx$ 20% and G190A/S $\approx$ 15% [2], but comparable to Truvada resistance mutations (M184V: 48–60%; K65R: 4–15%) in *treated* individuals. Notably, the overall risk of exposure to resistant strains would be much smaller than these numbers, as it is both determined by prevalence, as well as the probability of resistance-associated treatment failure in the donor at the moment of virus transmission, e.g., mathematically **Prob.**{exposure to res.} = **Prob.**{untreated.}$\cdot\pi_{\text{untreated}}$ + **Prob.**{treated.}$\cdot$ **Prob.**{failing due to resistance} $\cdot\pi_{\text{treated}}$. The calculations state that resistance exposure from *treated* individuals may only originate from those *treated* individuals that fail on the treatment at the time of exposure, due to resistance emergence (if they are successfully treated at the time of exposure, they are non-contagious Cohen et al., 2011).

Another important aspect that is quantified in **Supplementary Text 2** is resistance emergence in the exposed individual *prior* to PEP initiation. As can be seen in **Supplementary Text 2**, the probability of resistance emergence increases with the delay between virus exposure and PEP initiation. For example, we calculated that if PEP is initiated 3 days after exposure (72 h), the virus had either gone extinct

[1] https://hivdb.stanford.edu/page/surveillance-map/
[2] https://hivdb.stanford.edu/cgi-bin/MutPrevBySubtypeRx.cgi

or developed resistance with 38% probability. This *de novo* resistance may subsequently be selected by EFV, limiting future treatment options. On the other hand, if PEP is initiated within 12 hours, the probability of resistance emergence in the exposed individual *prior* to PEP is <0.01%. Thus, both in terms of lack of efficacy (**Figure 4**), as well as in terms of resistance (**Supplementary Text 2**), the window of opportunity with regards to PEP is short. Based on our simulations, PEP should be initiated as early as possible and is contraindicated if the suspected virus exposure occurred more than 3 days ago. The same considerations also apply for Truvada-based prophylaxis.

Our predictions regarding EFV prophylactic efficacy depend on (i) parameters of EFV potency (IC_{50}) and (ii) the concentrations of EFV at the target site.

Regarding EFV potency, one limitation of our work is that we used parameters determined *ex vivo* (Shen et al., 2008; Sampah et al., 2011) using primary human peripheral blood mononuclear cells (PBMCs). These cell mixtures are commonly used as surrogate markers to determine drug efficacy, since they contain a large proportion of $CD4^+$ T-cells (the primary HIV target cell type). Moreover, utilised parameters are generally in agreement with published values from other sources (Smith et al., 2001; Parkin et al., 2004; Avery et al., 2013b; Hu and Kuritzkes, 2014; Schauer et al., 2014) (after correction for protein binding; **Supplementary Text 1**).

Regarding the *relevant* target-site concentrations of EFV, there has been some debate since the *total* (protein bound and unbound) EFV concentrations in tissues have been reported to be highly heterogeneous (Thompson et al., 2015) and some studies have suggested associations between drug heterogeneity and incomplete HIV suppression (Fletcher et al., 2014), whereas others report high concentrations in tissues related to HIV exposure (Thompson et al., 2015). There are two main mechanisms that could explain heterogeneous drug distribution, which we discuss in detail:

a) Active transport (e.g. P-glycoprotein): In this case, the expression of transporters in particular cell types may cause concentration differences between distinct tissues. Notably, active transport would cause a difference in the *unbound* concentrations, which are available to exert an antiviral effect. As a consequence of active efflux, lower amounts of EFV may be available in some relevant target cells, giving rise to pharmacological sanctuaries relevant to EFV prophylaxis. A detailed analysis of EFV active transport (Burhenne et al., 2010) however revealed that it does not affect EFV intracellular concentrations. Moreover, EFV is a small (molecular mass: 315.6 g/mol) and highly lipophilic (LogP $\approx$ 4) compound that could rapidly cross biomembranes by passive diffusion. Thus, even if EFV was a substrate of cellular transporters, the *dominating* (i.e. fastest) mechanism mediating cellular uptake and efflux is probably passive diffusion. Furthermore, passive diffusion does not imply that the *total* (protein bound and -unbound) concentrations on either side of a biomembrane are equal, but rather implies that the *unbound* concentrations are equal. I.e. at each side of a biomembrane, EFV may be (un-)specifically retained by binding to biomolecules (lipids, proteins, see von Kleist and Huisinga, 2007 for an overview). However, since only the *unbound* concentration is available for drug-target interaction, EFV concentrations exerting antiviral effects would be identical in different cell types under passive diffusion.

b) Protein binding: EFV is highly (> 99%) bound to plasma proteins (Boffito et al., 2003), mainly albumin and $\alpha-1$-acid glycoprotein. Naturally, the concentrations of these proteins are magnitudes lower in tissues, which affects the amount of protein-bound EFV (and consequently the *total* concentrations). Studies that measure *unbound* drug concentrations lend strong support to this hypothesis. Avery et al. reported that the *unbound* EFV concentrations in plasma and semen (Avery et al., 2011) and in plasma and cerebrospinal fluid are nearly identical (Avery et al., 2013a). Importantly, considering albumin concentrations (calculations in **Supplementary Text 1**) in proposed sanctuary sites, we can precisely recover differences in *total* EFV concentrations reported, e.g., semen-to-plasma ratio: 3.4–5 % (Reddy et al., 2002; Avery et al., 2011) and cervical fluid-to-plasma ratio: 0.4% (Dumond et al., 2007). The fact that *unbound* plasma-, cerebrospinal fluid- cervical fluid and semen concentrations are nearly identical also suggests that EFV can cross the blood-brain, blood-testis and blood-uterine barrier.

In summary, these combined observations strongly argue that the distribution of EFV in tissues is governed by passive diffusion and (un-)specific binding to plasma proteins. In terms of PK-PD modeling, this implies that the *unbound* concentration in plasma are representative for the *unbound* concentration within target cells ($CD4^+$ immune cells/T-cells; derivations in **Supplementary Text 1**). When *unbound* concentrations are proportionally related to the *total* concentrations, it also implies that EFV *total* plasma concentrations can be used as a marker of drug efficacy (Marzolini et al., 2001). As a cautionary note we want to add that there could still be additional unaccounted, specific barriers lowering EFV *unbound* concentrations in physiological sites relevant for establishing the initial infection upon sexual exposure to HIV-1 (male genital compartment, female genital compartment and rectum), which warrant further verification. However, based on the discussions above, we would strongly disagree with the statement by Dumond et al., that "agents such as efavirenz that achieve *total* genital tract exposures less than 10% of blood plasma are less attractive PrEP/PEP candidates" (Dumond et al., 2007). This simplistic criterium of selecting drug candidates ignores the drug's individual pharmacology, might only select drugs that are not extensively protein bound, or select highly protein-bound candidates merely as a function of genital albumin concentrations. Our simulations are however in line with a later study from the same group (Dumond et al., 2012), which find that the concentrations at the site of virus exposure (in Dumond et al., 2012 the female genital tract) are proportional to unbound plasma concentrations during *chronic dosing*. However, it is unclear after how many dosing events this equilibrium between plasma and target site concentrations is achieved. While plasma concentrations rapidly peak at a t_{max} of about 5.9 h, there could be a time-delay in building up concentrations at the site of infection, which could impair the efficacy of "PrEP on demand" and PEP (compare **Figures 3B,C**), in the sense that it becomes more important to initiate the respective protocols as early as possible.

Notably, genital tract concentrations measured after the first dose in Dumond et al. (2007) are in line with our predictions, arguing for our modeling approach and for the presumed fast kinetics of cellular uptake by passive diffusion (see also **Supplementary Text 1**).

Another limitation of our study is that the parametrization of the PK model is based on data from HIV-infected individuals, while prophylaxis is intended for healthy individuals. In fact, it is unclear whether there are significant differences with respect to e.g., drug metabolism as a consequence of the infection status. For example, measured EFV plasma concentrations (400 mg once daily) in healthy individuals from Burhenne et al. (2010) are similar to those predicted herein. However, our model predicts large inter-individual variabilities due to pharmacogenomics (CYP 450 C2B6 polymorphisms). This hints toward the fact, that the pharmacokinetic differences between healthy vs. infected individuals could be small in comparison to the variability due to CYP polymorphisms. On the other hand, a study in healthy Ugandan individuals reports EFV concentrations (Mukonzo et al., 2009) that are considerably larger than predicted by our model. At the moment it is unclear whether differences are due to the infection status, or contributed to differences in ethnicity, weight, or co-medications: I.e. ethnicity ("black") has been associated with lower EFV clearance (Barrett et al., 2002). However, it is unclear whether concentration differences are due to a higher proportion of poor metabolisers in Ugandans, as suggested by Mukonzo et al. (2009), or other factors. It is interesting to note here that "gender" was a significant co-variate in the Ugandan study whereas it was not associated with changes in EFV PK in the ENCORE 1 study (Dickinson et al., 2015). While the drug's half life is similar for ENCORE 1 patients (35.57h; CI: 14.28–125.26) and healthy men in the Ugandan study (Mukonzo et al., 2009) (37.3h in wild type and 54.7h in slow metabolisers), the drug's terminal half life in females in the Ugandan study (Mukonzo et al., 2009) was twice as large as that for men. For comparison, a meta-analysis of 16 phase I studies reports a difference of only 10% (Barrett et al., 2002), warranting further research to clarify the mechanistic sources of the discrepancy between the results from the phase I studies (Barrett et al., 2002), the Ugandan study (Mukonzo et al., 2009) and the data from ENCORE 1 (Dickinson et al., 2015).

Regarding possible co-medications, it is worth mentioning that efavirenz has a large drug interaction potential. For example, it has been shown in Fan et al. (2009) that certain herbal medicines might compete for CYP2B6 metabolisms raising plasma levels, potentially up to toxic ranges. In any case, toxicity in the context of EFV-PrEP remains to be elucidated clinically and it remains to be elucidated if even further dose reductions would be suitable for PrEP in particular populations. The present work provides a good starting point to support these decisions, e.g., based on the concentration-prophylaxis profiles presented in **Figure 2**.

Moreover, EFV is an inducer of many CYP enzymes (Fichtenbaum and Gerber, 2002), possibly altering the pharmacology of co-medications. Thus, co-medication with EFV-based PrEP might require careful monitoring. The Liverpool drug-interaction database provides an excellent overview over known effects of EFV on various co-medications (https://www.hiv-druginteractions.org/).

Overall, this mathematical modelling study argues for the experimental investigation of EFV as a cost-efficient alternative PrEP candidate based on its superior prophylactic efficacy and forgiveness to incomplete adherence and event-driven usage. However, further analysis emphasising on the safety of EFV in the context of PrEP/PEP is warranted.

DATA AVAILABILITY

All data is contained in the manuscript.

AUTHOR CONTRIBUTIONS

SD and MvK conceptualized and designed the study. SD and DS performed the analysis on modeling prophylactic efficacy. LD performed the PK analysis. MvK wrote the manuscript with inputs from SD, DS, LD, and SK. All authors contributed to the analysis of the results.

FUNDING

MvK acknowledges financial support from the BMBF e:Bio junior research group Systems Pharmacology & Disease Control, grant number 031A307.

SUPPLEMENTARY MATERIAL

The Supplementary Material for this article can be found online at: https://www.frontiersin.org/articles/10.3389/fphar.2019.00199/full#supplementary-material

Supplementary Figure 1 | The figure shows an example of a concentration-time profile for chronic PrEP with 400 mg oral EFV and 25% adherence, where a temporal window for infection arises and EFV concentrations are insufficient for protection.

Supplementary Text 1 | The supplementary text contains an in-depth analysis of EFV cellular uptake, providing support for the free drug hypothesis and for equilibrative transport or passive diffusion as the main cellular uptake mechanisms of EFV. Furthermore, it analyses whether the drug potency is sensitive to uncertainty in drug binding.

Supplementary Text 2 | This supplementary text quantifies the probability of EFV resistance emergence prior to PEP initiation. We derive the probability of resistance emergence as a function of the time between virus exposure and start of post-exposure prophylaxis. The aim is to provide decision support on whether to start PEP after suspected exposure or not.

Supplementary Table 1 | The table shows the individual pharmacokinetic parameters (CL_{ss}/F_{bio}, V/F_{bio} and k_a) of all virtual patients.

Supplementary Table 2 | The table shows the considered single nucleotide polymorphisms associated with EFV metabolism and how they were modeled to affect efavirenz apparent oral clearance in the population pharmacokinetic model.

REFERENCES

AIDS Vaccine Advocacy Coalition. (2019) *Pre-Exposure Prophylaxis (PrEP).* Available online at: http://www.avac.org/sites/default/files/resource-files/prep_BTN_aug.pdf (Accessed dec 14, 2019).

Almond, L. M., Hoggard, P. G., Edirisinghe, D., Khoo, S. H., and Back, D. J. (2005). Intracellular and plasma pharmacokinetics of efavirenz in HIV-infected individuals. *J. Antimicrob. Chemother* 56, 738–744. doi: 10.1093/jac/dki308

Amara, A., Tjia, J., Dutton, J., Else, L., Back, D., and Khoo, S. (2011). "Development and validation of a hplc-ms/ms assay to quantify the antiretroviral (arv) drug, efavirenz and its major metabolites in plasma," in *British Mass Spectrometry Society Meeting, Abstract BMS S11-1240* (Cardiff).

Apostolova, N., Funes, H. A., Blas-Garcia, A., Galindo, M. J., Alvarez, A., and Esplugues, J. V. (2015). Efavirenz and the cns: what we already know and questions that need to be answered. *J. Antimicrob. Chemother* 70, 2693–708. doi: 10.1093/jac/dkv183

Arab-Alameddine, M., Di Iulio, J., Buclin, T., Rotger, M., Lubomirov, R., Cavassini, M., et al. (2009). Pharmacogenetics-based population pharmacokinetic analysis of efavirenz in HIV-1-infected individuals. *Clin. Pharmacol. Ther.* 85, 485–94. doi: 10.1038/clpt.2008.271

Avery, L. B., Bakshi, R. P., Cao, Y. J., and Hendrix, C. W. (2011). The male genital tract is not a pharmacological sanctuary from efavirenz. *Clin. Pharmacol. Ther.* 90, 151–156. doi: 10.1038/clpt.2011.99

Avery, L. B., Sacktor, N., McArthur, J. C., and Hendrix, C. W. (2013a). Protein-free efavirenz concentrations in cerebrospinal fluid and blood plasma are equivalent: applying the law of mass action to predict protein-free drug concentration. *Antimicrob. Agents Chemother* 57, 1409–14. doi: 10.1128/AAC.02329-12

Avery, L. B., Zarr, M. A., Bakshi, R. P., Siliciano, R. F., and Hendrix, C. W. (2013b). Increasing extracellular protein concentration reduces intracellular antiretroviral drug concentration and antiviral effect. *AIDS Res. Hum. Retrovirus.* 29, 1434–1442. doi: 10.1089/aid.2013.0031

Barrett, J. S., Joshi, A. S., Chai, M., Ludden, T. M., Fiske, W. D., and Pieniaszek Jr, H. J. (2002). Population pharmacokinetic meta-analysis with efavirenz. *Int. J. Clin. Pharmacol. Ther.* 40, 507–519. doi: 10.5414/CPP40507

Boffito, M., Back, D. J., Blaschke, T. F., Rowland, M., Bertz, R. J., Gerber, J. G., et al. (2003). Protein binding in antiretroviral therapies. *AIDS Res. Hum. Retrovirus.* 19, 825–835. doi: 10.1089/088922203769232629

Brenner, B. G., Roger, M., Routy, J.-P., Moisi, D., Ntemgwa, M., Matte, C., et al. (2007). High rates of forward transmission events after acute/early HIV-1 infection. *J. Infect. Dis.* 195, 951–959. doi: 10.1086/512088

Burhenne, J., Matthée, A.-K., Pasáková, I., Röder, C., Heinrich, T., Haefeli, W. E., et al. (2010). No evidence for induction of ABC transporters in peripheral blood mononuclear cells in humans after 14 days of efavirenz treatment. *Antimicrob. Agents Chemother.* 54, 4185–4191. doi: 10.1128/AAC.00283-10

Chou, T.-C. (2006). Theoretical basis, experimental design, and computerized simulation of synergism and antagonism in drug combination studies. *Pharmacolog. Rev.* 58, 621–681. doi: 10.1124/pr.58.3.10

Cohen, M. S., Chen, Y. Q., McCauley, M., Gamble, T., Hosseinipour, M. C., Kumarasamy, N., et al. (2011). Prevention of HIV-1 infection with early antiretroviral therapy. *N. Engl. J. Med.* 365, 493–505. doi: 10.1056/NEJMoa1105243

Conway, J. M., Konrad, B. P., and Coombs, D. (2013). Stochastic analysis of pre- and postexposure prophylaxis against HIV infection. *SIAM J. Appl. Math.* 73, 904–928. doi: 10.1137/120876800

Decloedt, E. H., and Maartens, G. (2013). Neuronal toxicity of efavirenz: a systematic review. *Expert Opin. Drug Saf.* 12, 841–846. doi: 10.1517/14740338.2013.823396

Dellar, R. C., Dlamini, S., and Karim, Q. A. (2015). Adolescent girls and young women: key populations for HIV epidemic control. *J. Int. AIDS Soc.* 18(2 Suppl. 1):19408. doi: 10.7448/IAS.18.2.19408

Dickinson, L., Amin, J., Else, L., Boffito, M., Egan, D., Owen, A., et al. (2015). Pharmacokinetic and pharmacodynamic comparison of once-daily efavirenz (400 mg vs. 600 mg) in treatment-naïve HIV-infected patients: results of the ENCORE1 study. *Clin. Pharmacol. Ther.* 98, 406–416. doi: 10.1002/cpt.156

Dickinson, L., Amin, J., Else, L., Boffito, M., Egan, D., Owen, A., et al. (2016). Comprehensive pharmacokinetic, pharmacodynamic and pharmacogenetic evaluation of once-daily efavirenz 400 and 600 mg in treatment-naïve HIV-infected patients at 96 weeks: Results of the encore1 study. *Clin. Pharmacokinet.* 55, 861–873. doi: 10.1007/s40262-015-0360-5

Dumond, J. B., Nicol, M. R., Kendrick, R. N., Garonzik, S. M., Patterson, K. B., Cohen, M. S., et al. (2012). Pharmacokinetic modelling of efavirenz, atazanavir, lamivudine and tenofovir in the female genital tract of HIV-infected pre-menopausal women. *Clin. Pharmacokinet.* 51, 809–822. doi: 10.1007/s40262-012-0012-y

Dumond, J. B., Yeh, R. F., Patterson, K. B., Corbett, A. H., Jung, B. H., Rezk, N. L., et al. (2007). Antiretroviral drug exposure in the female genital tract: implications for oral pre- and post-exposure prophylaxis. *AIDS* 21, 1899–1907. doi: 10.1097/QAD.0b013e328270385a

Duwal, S., Dickinson, L., Khoo, S., and von Kleist, M. (2018). Hybrid stochastic framework predicts efficacy of prophylaxis against HIV: an example with different dolutegravir prophylaxis schemes. *PLoS Comput. Biol.* 14:e1006155. doi: 10.1371/journal.pcbi.1006155

Duwal, S., Dickinson, L., Khoo, S., and von Kleist, M. (2019). Mechanistic framework predicts drug-class specific utility of antiretrovirals for hiv prophylaxis. *PLoS Comput. Biol.* 15:e1006740. doi: 10.1371/journal.pcbi.1006740

Duwal, S., Schütte, C., and von Kleist, M. (2012). Pharmacokinetics and pharmacodynamics of the reverse transcriptase inhibitor tenofovir and prophylactic efficacy against HIV-1 infection. *PLoS ONE* 7:e40382. doi: 10.1371/journal.pone.0040382

Duwal, S., Sunkara, V., and von Kleist, M. (2016). Multiscale systems-pharmacology pipeline to assess the prophylactic efficacy of NRTIs against HIV-1. *CPT Pharmacometr. Syst. Pharmacol.* 5, 377–387. doi: 10.1002/psp4.12095

Duwal, S., and von Kleist, M. (2016). Top-down and bottom-up modeling in system pharmacology to understand clinical efficacy: an example with NRTIs of HIV-1. *Eur. J. Pharm. Sci.* 94, 72–83. doi: 10.1016/j.ejps.2016.01.016

ENCORE1 Study Group (2014). Efficacy of 400 mg efavirenz versus standard 600 mg dose in HIV-infected, antiretroviral-naive adults (ENCORE1): a randomised, double-blind, placebo-controlled, non-inferiority trial. *Lancet* 383, 1474–1482. doi: 10.1016/S0140-6736(13)62187-X

ENCORE1 Study Group, Carey, D., Puls, R., Amin, J., Losso, M., Phanupak, P., et al. (2015). Efficacy and safety of efavirenz 400 mg daily versus 600 mg daily: 96-week data from the randomised, double-blind, placebo-controlled, non-inferiority ENCORE1 study. *Lancet Infect Dis.* 15, 793–802. doi: 10.1016/S1473-3099(15)70060-5

Fan, L., Wang, J.-C., Jiang, F., Tan, Z.-R., Chen, Y., Li, Q., et al. (2009). Induction of cytochrome p450 2b6 activity by the herbal medicine baicalin as measured by bupropion hydroxylation. *Eur. J. Clin. Pharmacol.* 65, 403–409. doi: 10.1007/s00228-008-0594-3

Fayet, A., Béguin, A., de Tejada, B. M., Colombo, S., Cavassini, M., Gerber, S., et al. (2008). Determination of unbound antiretroviral drug concentrations by a modified ultrafiltration method reveals high variability in the free fraction. *Ther. Drug Monit.* 30, 511–522. doi: 10.1097/FTD.0b013e3181817318

Fichtenbaum, C. J., and Gerber, J. G. (2002). Interactions between antiretroviral drugs and drugs used for the therapy of the metabolic complications encountered during HIV infection. *Clin. Pharmacokinet.* 41, 1195–211. doi: 10.2165/00003088-200241140-00004

Fletcher, C. V., Staskus, K., Wietgrefe, S. W., Rothenberger, M., Reilly, C., Chipman, J. G., et al. (2014). Persistent HIV-1 replication is associated with lower antiretroviral drug concentrations in lymphatic tissues. *Proc. Natl. Acad. Sci. U.S.A.* 111, 2307–2312. doi: 10.1073/pnas.1318249111

Frank, M., von Kleist, M., Kunz, A., Harms, G., Schütte, C., and Kloft, C. (2011). Quantifying the impact of nevirapine-based prophylaxis strategies to prevent mother-to-child transmission of HIV-1: a combined pharmacokinetic, pharmacodynamic, and viral dynamic analysis to predict clinical outcomes. *Antimicrob. Agents Chemother.* 55, 5529–5540. doi: 10.1128/AAC.00741-11

Grant, R. M., Anderson, P. L., McMahan, V., Liu, A., Amico, K. R., Mehrotra, M., et al. (2014) Uptake of pre-exposure prophylaxis, sexual practices, and HIV incidence in men and transgender women who have sex with men: a cohort study. *Lancet Infect Dis.* 14, 820–829. doi: 10.1016/S1473-3099(14)70847-3

Grant, R. M., Lama, J. R., Anderson, P. L., McMahan, V., Liu, A. Y., Vargas, L., et al. (2010). Preexposure chemoprophylaxis for HIV prevention in men who have sex with men. *N. Engl. J. Med.* 363, 2587–2599. doi: 10.1056/NEJMoa1011205

Gulick, R. M. (2018). Investigational antiretroviral drugs: What is coming down the pipeline. *Top Antivir. Med.* 25, 127–132.

Haberer, J. E., Bangsberg, D. R., Baeten, J. M., Curran, K., Koechlin, F., Amico, K. R., et al. (2015). Defining success with HIV pre-exposure prophylaxis: a prevention-effective adherence paradigm. *AIDS* 29, 1277–1285. doi: 10.1097/QAD.0000000000000647

Hu, Z., and Kuritzkes, D. R. (2014). Altered viral fitness and drug susceptibility in HIV-1 carrying mutations that confer resistance to nonnucleoside reverse transcriptase and integrase strand transfer inhibitors. *J. Virol.* 88, 9268–9276. doi: 10.1128/JVI.00695-14

Isaacman-Beck, J., Hermann, E. A., Yi, Y., Ratcliffe, S. J., Mulenga, J., Allen, S., et al. (2009). Heterosexual transmission of human immunodeficiency virus type 1 subtype C: macrophage tropism, alternative coreceptor use, and the molecular anatomy of CCR5 utilization. *J. Virol.* 83, 8208–8220. doi: 10.1128/JVI.00296-09

Jilek, B. L., Zarr, M., Sampah, M. E., Rabi, S. A., Bullen, C. K., Lai, J., et al. (2012). A quantitative basis for antiretroviral therapy for HIV-1 infection. *Nat. Med.* 18, 446–451. doi: 10.1038/nm.2649

Joseph, S. B., Swanstrom, R., Kashuba, A. D. M., and Cohen, M. S. (2015). Bottlenecks in HIV-1 transmission: insights from the study of founder viruses. *Nat. Rev. Microbiol.* 13, 414–425. doi: 10.1038/nrmicro3471

Keller, S. B., and Smith, D. M. (2011). The price of tenofovir-emtricitabine undermines the cost-effectiveness and advancement of pre-exposure prophylaxis. *AIDS* 25, 2308–2310. doi: 10.1097/QAD.0b013e32834d3cab

Koelsch, K. K., Liu, L., Haubrich, R., May, S., Havlir, D., Günthard, H. F., et al. (2008). Dynamics of total, linear nonintegrated, and integrated HIV-1 DNA *in vivo* and *in vitro*. *J. Infect. Dis.* 197, 411–419. doi: 10.1086/525283

Konrad, B. P., Taylor, D., Conway, J. M., Ogilvie, G. S., and Coombs, D. (2017). On the duration of the period between exposure to HIV and detectable infection. *Epidemics* 20, 73–83. doi: 10.1016/j.epidem.2017.03.002

Markowitz, M., Frank, I., Grant, R. M., Mayer, K. H., Elion, R., Goldstein, D., et al. (2017). Safety and tolerability of long-acting cabotegravir injections in HIV-uninfected men (ECLAIR): a multicentre, double-blind, randomised, placebo-controlled, phase 2a trial. *Lancet HIV* 4, e331–e340. doi: 10.1016/S2352-3018(17)30068-1

Markowitz, M., Louie, M., Hurley, A., Sun, E., Mascio, M. D., Perelson, A. S., et al. (2003). A novel antiviral intervention results in more accurate assessment of human immunodeficiency virus type 1 replication dynamics and T-cell decay *in vivo*. *J. Virol.* 77, 5037–5038. doi: 10.1128/JVI.77.8.5037-5038.2003

Marrazzo, J. M., Ramjee, G., Richardson, B. A., Gomez, K., Mgodi, N., Nair, G., et al. (2015). Tenofovir-based preexposure prophylaxis for HIV infection among african women. *N. Engl. J. Med.* 372, 509–518. doi: 10.1056/NEJMoa1402269

Marzolini, C., Telenti, A., Decosterd, L. A., Greub, G., Biollaz, J., and Buclin, T. (2001). Efavirenz plasma levels can predict treatment failure and central nervous system side effects in HIV-1-infected patients. *AIDS* 15, 71–75. doi: 10.1097/00002030-200101050-00011

Mathur, S., Pilgrim, N., and Pulerwitz, J. (2016). PrEP introduction for adolescent girls and young women. *Lancet HIV* 3, e406–e408. doi: 10.1016/S2352-3018(16)30115-1

Maxmen, A. (2016). Older men and young women drive south african HIV epidemic. *Nature* 535, 335–335. doi: 10.1038/nature.2016.20273

McCormack, S., Dunn, D. T., Desai, M., Dolling, D. I., Gafos, M., Gilson, R., et al. (2016). Pre-exposure prophylaxis to prevent the acquisition of HIV-1 infection (PROUD): effectiveness results from the pilot phase of a pragmatic open-label randomised trial. *Lancet* 387, 53–60. doi: 10.1016/S0140-6736(15)00056-2

McGowan, I., Dezzutti, C. S., Siegel, A., Engstrom, J., Nikiforov, A., Duffill, K., et al. (2016). Long-acting rilpivirine as potential pre-exposure prophylaxis for HIV-1 prevention (the MWRI-01 study): an open-label, phase 1, compartmental, pharmacokinetic and pharmacodynamic assessment. *Lancet HIV* 3, e569–e578. doi: 10.1016/S2352-3018(16)30113-8

McMillan, J., Szlachetka, A., Slack, L., Sillman, B., Lamberty, B., Morsey, B., et al. (2017). Pharmacokinetics of a long-acting nanoformulated dolutegravir prodrug in rhesus macaques. *Antimicrob. Agents Chemother.* 62, e01316-17. doi: 10.1128/AAC.01316-17

Molina, J. M., Capitant, C., Spire, B., Pialoux, G., Cotte, L., Charreau, I., et al. (2015). On-demand preexposure prophylaxis in men at high risk for HIV-1 infection. *N. Engl. J. Med.* 373, 2237–2246. doi: 10.1056/NEJMoa1506273

Mukonzo, J. K., Röshammar, D., Waako, P., Andersson, M., Fukasawa, T., Milani, L., et al. (2009). A novel polymorphism in abcb1 gene, cyp2b6*6 and sex predict single-dose efavirenz population pharmacokinetics in ugandans. *Br. J. Clin. Pharmacol.* 68, 690–699. doi: 10.1111/j.1365-2125.2009.03516.x

Ogburn, E. T., Jones, D. R., Masters, A. R., Xu, C., Guo, Y., and Desta, Z. (2010). Efavirenz primary and secondary metabolism *in vitro* and *in vivo*: identification of novel metabolic pathways and cytochrome p450 2a6 as the principal catalyst of efavirenz 7-hydroxylation. *Drug Metab. Dispos.* 38, 1218–1229. doi: 10.1124/dmd.109.031393

Orrell, C., Bienczak, A., Cohen, K., Bangsberg, D., Wood, R., Maartens, G., et al. (2016). Effect of mid-dose efavirenz concentrations and CYP2B6 genotype on viral suppression in patients on first-line antiretroviral therapy. *Int. J. Antimicrob. Agents* 47, 466–472. doi: 10.1016/j.ijantimicag.2016.03.017

Parkin, N. T., Hellmann, N. S., Whitcomb, J. M., Kiss, L., Chappey, C., and Petropoulos, C. J. (2004). Natural variation of drug susceptibility in wild-type human immunodeficiency virus type 1. *Antimicrob. Agents Chemother* 48, 437–443. doi: 10.1128/AAC.48.2.437-443.2004

Pearson, J. E., Krapivsky, P., and Perelson, A. S. (2011). Stochastic theory of early viral infection: continuous versus burst production of virions. *PLoS Comput. Biol.* 7:e1001058. doi: 10.1371/journal.pcbi.1001058

Perelson, A. S. (2002). Modelling viral and immune system dynamics. *Nat. Rev. Immunol.* 2, 28–36. doi: 10.1038/nri700

Perelson, A. S., Kirschner, D. E., and De Boer, R. (1993). Dynamics of HIV infection of CD4+ T cells. *Math. Biosci.* 114, 81–125. doi: 10.1016/0025-5564(93)90043-A

Pierson, T. C., Zhou, Y., Kieffer, T. L., Ruff, C. T., Buck, C., and Siliciano, R. F. (2002). Molecular characterization of preintegration latency in human immunodeficiency virus type 1 infection. *J. Virol.* 76, 8518–8531. doi: 10.1128/JVI.76.17.8518-8513.2002

Ping, L.-H., Joseph, S. B., Anderson, J. A., Abrahams, M.-R., Salazar-Gonzalez, J. F., Kincer, L. P., et al. (2013). Comparison of viral Env proteins from acute and chronic infections with subtype c human immunodeficiency virus type 1 identifies differences in glycosylation and CCR5 utilization and suggests a new strategy for immunogen design. *J. Virol.* 87, 7218–7233. doi: 10.1128/JVI.03577-12

Rakhmanina, N. Y., and van den Anker, J. N. (2010). Efavirenz in the therapy of HIV infection. *Expert. Opin. Drug Metab. Toxicol.* 6, 95–103. doi: 10.1517/17425250903483207

Rath, B. A., Yousef, K. P., Katzenstein, D. K., Shafer, R. W., Schütte, C., von Kleist, M., et al. (2013). *In vitro* HIV-1 evolution in response to triple reverse transcriptase inhibitors & in silico phenotypic analysis. *PLoS ONE* 8:e61102. doi: 10.1371/journal.pone.0061102

Reddy, Y. S., Gotzkowsky, S. K., Eron, J. J., Kim, J. Y., Fiske, W. D., Fiscus, S. A., et al. (2002). Pharmacokinetic and pharmacodynamic investigation of efavirenz in the semen and blood of human immunodeficiency virus type 1-infected men. *J. Infect Dis.* 186, 1339–1343. doi: 10.1086/344311

Rhee, S.-Y., Gonzales, M. J., Kantor, R., Betts, B. J., Ravela, J., and Shafer, R. W. (2003). Human immunodeficiency virus reverse transcriptase and protease sequence database. *Nucleic Acids Res.* 31, 298–303. doi: 10.1093/nar/gkg100

Sampah, M. E. S., Shen, L., Jilek, B. L., and Siliciano, R. F. (2011). Dose-response curve slope is a missing dimension in the analysis of HIV-1 drug resistance. *Proc. Natl. Acad. Sci. U.S.A.* 108, 7613–7618. doi: 10.1073/pnas.1018360108

Schauer, G. D., Huber, K. D., Leuba, S. H., and Sluis-Cremer, N. (2014). Mechanism of allosteric inhibition of HIV-1 reverse transcriptase revealed by single-molecule and ensemble fluorescence. *Nucleic Acids Res.* 42, 11687–11696. doi: 10.1093/nar/gku819

Sedaghat, A. R., Dinoso, J. B., Shen, L., Wilke, C. O., and Siliciano, R. F. (2008). Decay dynamics of HIV-1 depend on the inhibited stages of the viral life cycle. *Proc. Natl. Acad. Sci. U.S.A.* 105, 4832–4837. doi: 10.1073/pnas.0711372105

Sedaghat, A. R., Siliciano, R. F., and Wilke, C. O. (2009). Constraints on the dominant mechanism for HIV viral dynamics in patients on raltegravir. *Antivir. Ther.* 14, 263–271.

Shen, L., Peterson, S., Sedaghat, A. R., McMahon, M. A., Callender, M., Zhang, H., et al. (2008). Dose-response curve slope sets class-specific limits on inhibitory potential of anti-HIV drugs. *Nat. Med.* 14, 762–766. doi: 10.1038/nm1777

Siccardi, M., Almond, L., Schipani, A., Csajka, C., Marzolini, C., Wyen, C., et al. (2012). Pharmacokinetic and pharmacodynamic analysis of efavirenz dose

reduction using an *in vitro-in vivo* extrapolation model. *Clin. Pharmacol. Ther.* 92, 494–502. doi: 10.1038/clpt.2012.61

Smith, D. A., Di, L., and Kerns, E. H. (2010). The effect of plasma protein binding on *in vivo* efficacy: misconceptions in drug discovery. *Nat. Rev. Drug Discov.* 9, 929–939. doi: 10.1038/nrd3287

Smith, P. F., DiCenzo, R., and Morse, G. D. (2001). Clinical pharmacokinetics of non-nucleoside reverse transcriptase inhibitors. *Clin. Pharmacokinet.* 40, 893–905. doi: 10.2165/00003088-200140120-00002

Stafford, M. A., Corey, L., Cao, Y., Daar, E. S., Ho, D. D., and Perelson, A. S. (2000). Modeling plasma virus concentration during primary HIV infection. *J. Theor. Biol.* 203, 285–301. doi: 10.1006/jtbi.2000.1076

Tan, W. Y., and Wu, H. (1998). Stochastic modeling of the dynamics of CD4+ T-cell infection by HIV and some Monte Carlo studies. *Math. Biosci.* 147, 173–205. doi: 10.1016/S0025-5564(97)00094-1

Thompson, C. G., Bokhart, M. T., Sykes, C., Adamson, L., Fedoriw, Y., Luciw, P. A., et al. (2015). Mass spectrometry imaging reveals heterogeneous efavirenz distribution within putative HIV reservoirs. *Antimicrob. Agents Chemother* 59, 2944–2948. doi: 10.1128/AAC.04952-14

Tuckwell, H. C., Shipman, P. D., and Perelson, A. S. (2008). The probability of HIV infection in a new host and its reduction with microbicides. *Math. Biosci.* 214, 81–86. doi: 10.1016/j.mbs.2008.03.005

UNAIDS (2015). *AIDS by the Numbers 2015*. Technical report. Available online at: http://www.unaids.org/en/resources/documents/2015/AIDS_by_the_numbers_2015 (Accessed Dec 14, 2018).

UNAIDS (2016). *AIDS by the Numbers.* Available online at: (http://www.unaids.org/sites/default/files/media_asset/AIDS-by-the-numbers-2016_en.pdf), (Accessed Dec 14, 2018).

UNAIDS (2017). *Ending Aids: progress Towards the 90-90-90 Targets*. Available online at: (http://www.unaids.org/sites/default/files/media_asset/Global_AIDS_update_2017_en.pdf) (Accessed dec 14, 2018).

Van Damme, L., Corneli, A., Ahmed, K., Agot, K., Lombaard, J., Kapiga, S., et al. (2012). Preexposure prophylaxis for HIV infection among African women. *N Engl. J. Med.* 367, 411–422. doi: 10.1056/NEJMoa1202614

Voliotis, M., Thomas, P., Grima, R., and Bowsher, C. G. (2016). Stochastic simulation of biomolecular networks in dynamic environments. *PLoS Comput. Biol.* 12:e1004923. doi: 10.1371/journal.pcbi.1004923

von Kleist, M., and Huisinga, W. (2007). Physiologically based pharmacokinetic modelling: a sub-compartmentalized model of tissue distribution. *J. Pharmacokinet Pharmacodyn.* 34, 789–806. doi: 10.1007/s10928-007-9071-3

von Kleist, M., Menz, S., and Huisinga, W. (2010). Drug-class specific impact of antivirals on the reproductive capacity of HIV. *PLoS Comput. Biol.* 6:e1000720. doi: 10.1371/journal.pcbi.1000720

von Kleist, M., Menz, S., Stocker, H., Arasteh, K., Schütte, C., and Huisinga, W. (2011). HIV quasispecies dynamics during pro-active treatment switching: impact on multi-drug resistance and resistance archiving in latent reservoirs. *PLoS ONE* 6:e18204. doi: 10.1371/journal.pone.0018204

Ward, B. A., Gorski, J. C., Jones, D. R., Hall, S. D., Flockhart, D. A., and Desta, Z. (2003). The cytochrome P450 2B6 (CYP2B6) is the main catalyst of efavirenz primary and secondary metabolism: implication for HIV/AIDS therapy and utility of efavirenz as a substrate marker of CYP2B6 catalytic activity. *J. Pharmacol. Exp. Ther.* 306, 287–300. doi: 10.1124/jpet.103.049601

Wei, X., Ghosh, S. K., Taylor, M. E., Johnson, V. A., Emini, E. A., Deutsch, P., et al. (1995). Viral dynamics in human immunodeficiency virus type 1 infection. *Nature* 373, 117–122. doi: 10.1038/373117a0

Wilson, D. P., Law, M. G., Grulich, A. E., Cooper, D. A., and Kaldor, J. M. (2008). Relation between HIV viral load and infectiousness: a model-based analysis. *Lancet* 372, 314–320. doi: 10.1016/S0140-6736(08)61115-0

Yousef, K. P., Meixenberger, K., Smith, M. R., Somogyi, S., Gromöller, S., Schmidt, D., et al. (2016). Inferring HIV-1 Transmission dynamics in Germany from recently transmitted viruses. *J. Acq. Immune Defic. Syndr.* 73, 356–363. doi: 10.1097/QAI.0000000000001122

Zazzi, M., Hu, H., and Prosperi, M. (2018). The global burden of HIV-1 drug resistance in the past 20 years. *PeerJ* 6:e4848. doi: 10.7717/peerj.4848

Zhou, Y., Zhang, H., Siliciano, J. D., and Siliciano, R. F. (2005). Kinetics of human immunodeficiency virus type 1 decay following entry into resting CD4+ T cells. *J. Virol.* 79, 2199–2210. doi: 10.1128/JVI.79.4.2199-2210.2005

Zhu, M., Kaul, S., Nandy, P., Grasela, D. M., and Pfister, M. (2009). Model-based approach to characterize efavirenz autoinduction and concurrent enzyme induction with carbamazepine. *Antimicrob. Agents Chemother.* 53, 2346–2353. doi: 10.1128/AAC.01120-08

Conflict of Interest Statement: The authors declare that the research was conducted in the absence of any commercial or financial relationships that could be construed as a potential conflict of interest.

OPEN ACCESS Freely available online

PLoS one

Pharmacokinetics and Pharmacodynamics of the Reverse Transcriptase Inhibitor Tenofovir and Prophylactic Efficacy against HIV-1 Infection

Sulav Duwal, Christof Schütte, Max von Kleist*

Department of Mathematics and Computer Science, Free University Berlin, Berlin, Germany

Abstract

Antiviral pre-exposure prophylaxis (PrEP) through daily drug administration can protect healthy individuals from HIV-1 infection. While PrEP was recently approved by the FDA, the potential long-term consequences of PrEP implementation remain entirely unclear. The aim of this study is to predict the efficacy of different prophylactic strategies with the pro-drug tenofovir-disoproxil-fumarate (TDF) and to assess the sensitivity towards timing- and mode of TDF administration (daily- vs. single dose), adherence and the number of transmitted viruses. We developed a pharmacokinetic model for TDF and its active anabolite tenofovir-diphosphate (TFV-DP) and validated it with data from 4 different trials, including 4 distinct dosing regimes. Pharmacokinetics were coupled to an HIV model and viral decay following TDF mono-therapy was predicted, consistent with available data. Subsequently, a stochastic approach was used to estimate the % infections prevented by (i) daily TDF-based PrEP, (ii) one week TDF started either shortly before, or -after viral exposure and (iii) a single dose oral TDF before viral challenge (sd-PrEP). Analytical solutions were derived to assess the relation between intracellular TFV-DP concentrations and prophylactic efficacy. The predicted efficacy of TDF was limited by a slow accumulation of active compound (TFV-DP) and variable TFV-DP half-life and decreased with increasing numbers of transmitted viruses. Once daily TDF-based PrEP yielded $\leq$80% protection, if at least 40% of pills were taken. Sd-PrEP with 300 mg or 600 mg TDF could prevent $\leq$50% infections, when given at least before virus exposure. The efficacy dropped to $\leq$10%, when given 1 h before 24 h exposure. Efficacy could not be increased with increasing dosage or prolonged administration. Post-exposure prophylaxis poorly prevented infection. The use of drugs that accumulate more rapidly, or local application of tenofovir gel may overcome the need for drug administration long before virus exposure.

Citation: Duwal S, Schütte C, von Kleist M (2012) Pharmacokinetics and Pharmacodynamics of the Reverse Transcriptase Inhibitor Tenofovir and Prophylactic Efficacy against HIV-1 Infection. PLoS ONE 7(7): e40382. doi:10.1371/journal.pone.0040382

Editor: Jianming Tang, University of Alabama at Birmingham, United States of America

Received March 2, 2012; **Accepted** June 5, 2012; **Published** July 11, 2012

Funding: SD and MvK acknowledge funding from the DFG research center MATHEON provided through project A21 "Modeling, Simulation and Therapy Optimization for Infectious Diseases." The funders had no role in study design, data collection and analysis, decision to publish, or preparation of the manuscript.

Competing Interests: The authors have declared that no competing interests exist.

* E-mail: vkleist@zedat.fu-berlin.de

Introduction

Tenofovir disoproxil fumerate (TDF) is an antiviral pro-drug, belonging to the class of nucleoside reverse transcriptase inhibitors (NRTIs) used for the treatment of the human immunodeficiency virus 1 (HIV-1) [1] and hepatitis B. For HIV-1 treatment, it is currently recommended as a backbone component in first-line highly active antiretroviral therapy (HAART) [2]. TDF is administered orally. After first pass of TDF through the liver, tenofovir (TFV), an analogue of the endogeneous deoxyadenosine monophosphate (dAMP) [3], is formed. TFV is also the predominant circulating form [4,5]. After uptake into HIV target cells, TFV can become sequentially phosphorylated to form tenofovir diphosphate (TFV-DP), the active form, which is an analog of endogeneous deoxyadenosine triphosphate (dATP). TFV-DP subsequently competes with dATP for incorporation into nascent viral DNA during HIV-1 reverse transcription (RT), where it prevents further DNA polymerization during RT, once it becomes incorporated [6]. TFV-DP thus prevents the production of pro-viral DNA, which is required for stable host cell infection and viral replication.

While most studies characterize the pharmacokinetics of TFV in the blood plasma e.g. [7–10] only a few studies [11,12] focus on the intracellular pharmacokinetics of the active anabolite, TFV-DP, or establish a link between the pharmacokinetics of TFV in plasma and TFV-DP in the intracellular space [13,14], which is particularly important, since the plasma pharmacokinetics of NRTIs and the pharmacokinetics of their active intracellular anabolites are often nonlinearly related and temporally asynchronous e.g. [15,16]. Thus, for establishing the link between dose and response, the link between plasma- and intracellular pharmacokinetics is essential, and can subsequently be used to predict the effect of drug administration on virus dynamics. This complete PK-PD link for NRTIs has only rarely been achieved [17]. For TDF, no *in silico* model exists to the authors' knowledge, which integrates dosing, pharmacokinetics and antiviral response.

While TDF is an important drug for HIV treatment, it is also being evaluated as a core component of pre-exposure prophylaxis regimens (PrEP) to prevent HIV infection [18]. Interim reports indicate variable outcomes for PrEP strategies: Whereas some trials report no benefit of PrEP regimens (FEM-PrEP) [19], others report 44 % to 73 % reduced HIV acquisition [20–22]. While the

efficacy of TDF-based PrEP may depend on the mode of transmission (hetero- vs. homosexual, or by needle-stick infection), it is often argued that prophylactic success could be affected by how strictly patients adhere to their (TDF-based) regimen [23]. Based on the average half life of TFV-DP in peripheral blood mononuclear cells (PBMCs) it has been previously stated that TDF is pharmacologically "forgiving" in the context of poor adherence [3]. However, TFV-DP pharmacokinetics indicate a large inter-patient variability [11,14], potentially leading to heterogeneous protection in patients that equally adhere to their TDF-based regimen. Also, adherence in some patients in clinical trials may have been even lower than the pharmacological "forgiveness" of the drug [24].

The goal of the present study is to provide an *in silico* model that consistently predicts intracellular TFV-DP pharmacokinetics based on different TDF dosing schemes. Subsequently, we use previously published direct pharmacodynamic models to ultimately link the pharmacokinetics of oral TDF to its clinical response. Once this link is established, we use stochastic simulation to predict the relative infection risk, when TDF-based PrEP or mixed PrEP/PEP strategies are applied with different levels of adherence and timing of TDF administration and we point out factors that may impair TDF-based PrEP. In view of the recent approval of truvada (300 mg TDF + 200 mg emitricitabine (FTC)) for PrEP by the FDA, this may raise awareness, encourage experimental assessment and help to avoid the misuse of TDF-based PrEP.

Materials and Methods

Pharmacokinetic & Pharmacodynamic Data

TFV concentrations in blood plasma following either doses of 75, 150, 300 or 600 mg oral TDF were taken from three independent clinical trials [7,9,12] and used to verify pharmacokinetic model selection and evaluation (see Table S1). Individual intracellular elimination of TFV-DP was assessed using the data from [11], which observe the decline of TFV-DP in PBMCs after discontinuation of TDF treatment (see Table S2). After successful development of the pharmacokinetic model, it was coupled to a model of viral dynamics and used to predict antiviral efficacy of 28 days TDF monotherapy in asymptotically infected individuals following 75, 150, 300 or 600 mg oral TDF dosing, simultaneously estimating the PK-PD coupling parameter IC_{50} (fifty percent inhibitory concentration) and testing different alternative models for intracellular uptake and anabolism of TFV. Predicted viral load kinetics were compared to viral load data from [12] (pharmacodynamic endpoint) and used for model selection (see Text S1). The final coupled pharmacokinetic-pharmacodynamic model was used to predict the prophylactic efficacy of TDF for a wide range of parameter sets using stochastic simulation techniques.

Assessment of Alternative Pharmacokinetic Models

We assessed different pharmacokinetic models for TFV in plasma after 75-, 150- 300- and 600 mg dosing in line with available trial data [7,9,12] and followed a stepwise model-building process, in which the following reasonable assumption was made: We neglected the impact of intracellular TFV-DP pharmacokinetics on the plasma pharmacokinetics of TFV, since it can be assumed to marginally influence the overall pharmacokinetics of TFV (total mass of TFV-DP in PBMCs is extremely small: $C_{cell} \cdot V_{PBMC} \leq 0.0008\text{mg}$; total volume of PBMCs: $\leq 1 \cdot 10^{-6}\text{L}$ [25,26]; plasma volume $\approx 3.5\text{L}$). This assumption allowed us to independently develop the plasma pharmacokinetics model and then subsequently model the influx and conversion of TFV to intracellular TFV-DP, depending on the actual TFV concentration in blood plasma.

The pharmacokinetic model building process was guided by goodness-of-fit and comparative model assessment in terms of Akaike information. Pharmacokinetic parameters were estimated by minimizing the weighted residual sum of squared errors WRSE(j) of the *j*th model according to.

$$\text{WRSE(j)} = \arg\min_{P_j} \sum_{i=1}^{n_t} \left(\frac{\tilde{Y}_j(t_i,P_j) - Y(t_i)}{Y(t_i)} \right)^2 \quad (1)$$

were P_j is a vector of pharmacokinetic parameters for candidate model j, $\tilde{Y}_j(t_i,P_j)$ are model-predicted TFV or TFV-DP concentrations for parameter set P_j at time t_i and $Y(t_i)$ are the corresponding observed concentrations. Candidate models j were then comparatively assessed using Akaike's information criteria (AIC), where the AIC-value of the *j*th model has been computed according to [27]:

$$\text{AIC(j)} = n_t \cdot \log(\text{WRSE(j)}) + 2 \cdot n_P(j) \quad (2)$$

where n_t denotes the number of observations and $n_P(j)$ denotes the number of parameters required for the *j*th model. Subsequently, the model with the best (the lowest) AIC was selected and further used.

Final Pharmacokinetic Model

Based on predictive performance and Akaike information (see Table 3) we found that two compartments (plus a dosing compartment) best described TFV plasma pharmacokinetics, in line with previous studies [13,14,28]. A third compartment was used to model the pharmacokinetics of intracellular TFV-DP [13,14]. Intracellular pharmacokinetics of TFV-DP were linked to the plasma concentration via saturable uptake and anabolism ($V_{max}(i)$ and K_m) with individual maximum velocity of uptake and anabolism and individual first order elimination kinetics $k_{out}(i)$ (see Table S2), which best described the available data (see Text S1). The final model for the TFV plasma- and intracellular TFV-DP pharmacokinetics is illustrated in Figure 1A. The TFV/TFV-DP pharmacokinetic model constitutes four compartments: $D(t)$ represents the mass of tenofovir in the dosing reservoir. C_1 is the central compartment, which represents the plasma concentration of TFV. The second compartment C_2 represents the poorly perfused (peripheral) tissues and the cellular compartment C_{cell} resembles the concentrations of TFV-DP in peripheral blood mononuclear cells (PBMCs). Parameters k_{12} and k_{21} are the rate constants for influx and outflux to-/from the peripheral compartment C_2 and k_a and k_e are the rates of TFV uptake and elimination into/out of C_1 respectively. All final parameters are represented in Table 1. The value for k_a and the bioavailability F_{bio} were fixed to $1\ \text{h}^{-1}$ [28] and 0.32 [12] respectively, while all other parameters were estimated.

The ordinary differential equations for the final model are displayed below:

$$\frac{\text{d}}{\text{d}t} C_1(t) = \frac{F_{bio} \cdot k_a \cdot D(t)}{V_1} - C_1(t) \cdot k_e - k_{12} \cdot C_1(t) + k_{21} \cdot C_2(t) \quad (3)$$

$$\frac{\text{d}}{\text{d}t} C_2(t) = k_{12} \cdot C_1(t) - k_{21} \cdot C_2(t) \quad (4)$$

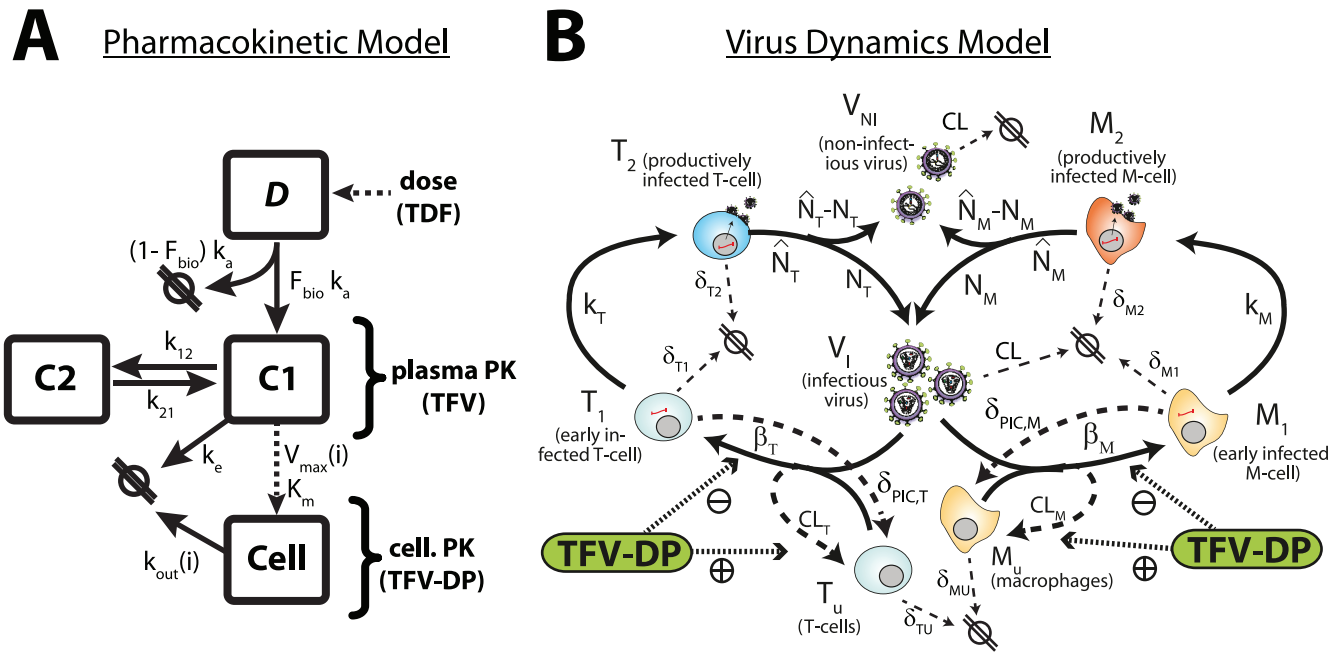

Figure 1. Pharmacokinetic model of TFV and intracellular TFV-DP and model of viral kinetics. A: Pharmacokinetic model. Parameters k_a and k_e are the absorption and elimination rate constants of the central compartment **C1** (which resembles plasma pharmacokinetics of TFV) respectively. The parameters k_{12} and k_{21} denote the influx and outflux rate constant to-/from the peripheral compartment **C2** respectively. Both compartments (central-/peripheral-) have the same volume of distribution V_1. The dotted line from the central compartment to the intracellular compartment **C3** represents subsumed processes, namely the cellular uptake of TFV and subsequent phosphorylation to TFV-DP, which were related to the plasma concentration of TFV (**C1**) by Michaelis-Menten kinetics, with parameters K_m and individual parameter $V_{max}(i)$. The parameter $k_{out}(i)$ is the individual, cellular elimination rate constant of TFV-DP. B: Virus dynamics model. T-cell and macrophage target cells (T_U, M_U) can become successfully infected by infective virus V_I with lumped infection rate constants β_T and β_M, respectively, creating early infected cells T_1 and M_1. Infection can also be unsuccessful after the irreversible step of fusion (rate constant CL_T and CL_M, dashed lines), eliminating the virus and rendering the cell uninfected. Early infected cells T_1 and M_1 can destroy essential viral proteins or DNA prior to integration with rate constants $\delta_{PIC,T}$ and $\delta_{PIC,M}$ (dashed lines) returning the cell to an uninfected stage. The genomic viral DNA can become integrated with rate constants k_T and k_M creating late infected cells T_2 and M_2, which can release new infectious- and non infectious virus V_I and V_{NI} with rate constants $N_T, \left(\widehat{N_T} - N_T\right)$ and $N_M, \left(\widehat{N_M} - N_M\right)$, respectively. All cellular compartments x can get destroyed by the immune system with respective rate constants δ_x and the free virus gets cleared with rate constant CL (thin dashed lines). The pharmacologically active form of tenofovir (tenofovir-diphosphate, TFV-DP, green box) inhibits successful cell-infection (parameter $\beta_{T/M}$) and increases the rate of unsuccessful infection (parameter $CL_{T/M}$).

$$\frac{d}{dt}C_{cell}(t,i) = \frac{V_{max}(i)\cdot C_1(t)}{K_m + C_1(t)} - C_{cell}(t,i)\cdot k_{out}(i) \qquad (5)$$

where V_1 represents the volume of the central compartment. The parameters $V_{max}(i)$ and K_m describe the (saturable) processes of TFV-uptake and conversion to TFV-DP within PBMCs, while $k_{out}(i)$ denotes the rate of elimination of TFV-DP from the PBMCs, which was found to vary between distinct patients (see Table S2 and model comparison in Text S1). The concentration in the dosing compartment $D(t)$ was estimated according to:

$$D(t) = D(\tau_{i-1})\cdot e^{-k_a\cdot t} + \delta(t)\cdot \mathrm{dose}(\tau_i) \qquad (6)$$

where $D(\tau_{i-1})$ denotes the mass of TDF in the dosing compartment at the last dosing event τ_{i-1}. The parameter $\delta(t)$ denotes a delta dirac function which takes the value 1 at the discrete dosing events $t = \tau_i$ and is otherwise zero.

Viral Dynamics

In order to predict (i) viral load kinetics following TDF treatment in HIV-infected patients and (ii) the infection probability for uninfected individuals, we adopted the virus dynamics model from [29,30], which is depicted in Figure 1B. For predicting viral load kinetics in infected individuals, we used the deterministic infected (drug-free) fix-point of the model as a starting condition and then monitored viral dynamics following TDF monotherapy. For assessing the infection probability, we used the uninfected fix-point of the model as starting condition and inoculated the respective number of infectious viruses to simulate viral challenges.

In brief, the virus dynamics model comprises T-cells, macrophages, free non-infectious virus (T_U,M_U,V_{NI}, respectively), free infectious virus V_I, and four types of infected cells: infected T-cells and macrophages *prior* to proviral genomic integration (T_1 and M_1, respectively) and infected T-cells and macrophages *after* proviral genomic integration (T_2 and M_2, respectively). The average rates of change of the different species are given by the following system of ODEs:

$$\frac{d}{dt}T_U = \lambda_T + \delta_{PIC,T}\cdot T_1 - \delta_T\cdot T_U - \beta_T(t)\cdot V_I\cdot T_U$$

$$\frac{d}{dt}M_U = \lambda_M + \delta_{PIC,M}\cdot M_1 - \delta_M\cdot M_U - \beta_M(t)\cdot V_I\cdot M_U$$

Table 1. Pharmacokinetic and pharmacodynamic parameters.

param.	value	param.	value
k_e	$^{-1}$0.12 h	V_1	244 L
k_{12}	$^{-1}$0.2926 h	$\widetilde{k_{\text{out}}}$	$^{-1}$0.006$^{*,\#}$ [0.002;0.026] h
k_{21}	$^{-1}$0.1537 h	k_a	$^{+}$1
IC_{50}	$^{-1}$75.7 µg. L	$_{\text{bio}}$F	‡0.32
K_{m}	$^{-1}$29.3 µg. L	$\widetilde{V_{\text{max}}}$	$^{-1}$1.44*§ [0.5;24] µg. L^{-1}. h

*median parameter and range. $^{\#}$ see Table 4 for individual values. $^{+}$ value set to 1 [28]. ‡ parameter from [12]. § computed using eq. (S2), Text S1.
doi:10.1371/journal.pone.0040382.t001

$$\frac{\mathrm{d}}{\mathrm{d}t}\mathrm{T}_1 = \beta_{\mathrm{T}}(t)\cdot V_{\mathrm{I}}\cdot\mathrm{T}_{\mathrm{U}} - (\delta_{\mathrm{T}_1} + \delta_{\mathrm{PIC,T}} + k_{\mathrm{T}})\cdot\mathrm{T}_1$$

$$\frac{\mathrm{d}}{\mathrm{d}t}\mathrm{M}_1 = \beta_{\mathrm{M}}(t)\cdot V_{\mathrm{I}}\cdot\mathrm{M}_{\mathrm{U}} - (\delta_{\mathrm{M}_1} + \delta_{\mathrm{PIC,M}} + k_{\mathrm{M}})\cdot\mathrm{M}_1 \qquad (7)$$

$$\frac{\mathrm{d}}{\mathrm{d}t}\mathrm{T}_2 = k_{\mathrm{T}}\cdot\mathrm{T}_1 - \delta_{\mathrm{T}_2}\cdot\mathrm{T}_2$$

$$\frac{\mathrm{d}}{\mathrm{d}t}\mathrm{M}_2 = k_{\mathrm{M}}\cdot\mathrm{M}_1 - \delta_{\mathrm{M}_2}\cdot\mathrm{M}_2$$

$$\frac{\mathrm{d}}{\mathrm{d}t}V_{\mathrm{I}} = \mathrm{N}_{\mathrm{M}}\cdot\mathrm{M}_2 + \mathrm{N}_{\mathrm{T}}\cdot\mathrm{T}_2$$

$$- V_{\mathrm{I}}\cdot[\mathrm{CL} + (\mathrm{CL}_{\mathrm{T}}(t) + \beta_{\mathrm{T}}(t))\cdot\mathrm{T}_{\mathrm{U}} + (\mathrm{CL}_{\mathrm{M}}(t) + \beta_{\mathrm{M}}(t))\cdot\mathrm{M}_{\mathrm{U}}]$$

$$\frac{\mathrm{d}}{\mathrm{d}t}V_{\mathrm{NI}} = [(\widehat{\mathrm{N_T}} - \mathrm{N}_{\mathrm{T}})\mathrm{T}_2 + (\widehat{\mathrm{N_M}} - \mathrm{N}_{\mathrm{M}})\mathrm{M}_2] - \mathrm{CL}\cdot V_{\mathrm{NI}},$$

where λ_{T} and λ_{M} are the birth rates of uninfected T-cells and macrophages, and δ_{T} and δ_{M} denote their death rate constants. The parameters $\delta_{\mathrm{PIC,T}}$ and $\delta_{\mathrm{PIC,M}}$ refer to the intracellular degradation of essential components of the pre-integration complex, e.g., by the host cell proteasome, which return early infected T-cells and macrophages to an uninfected stage, respectively. Parameters $\beta_{\mathrm{T}}(t)$ and $\beta_{\mathrm{M}}(t)$ denote the rate of successful virus infection of T-cells and macrophages in the presence of TFV-DP, respectively, while the parameters $\mathrm{CL}_{\mathrm{T}}(t)$ and $\mathrm{CL}_{\mathrm{M}}(t)$ denote the clearance of virus through unsuccessful infection of T-cells and macrophages [29] in the presence of TFV-DP at the respective time t. Parameters k_{T} and k_{M} are the rate constants of proviral integration into the host cell's genome and $\widehat{\mathrm{N_T}}$ and $\widehat{\mathrm{N_M}}$ denote the total number of released infectious and non-infectious virus from late infected T-cells and macrophages and N_{T} and N_{M} are the rates of release of infectious virus. The parameters δ_{T_1},δ_{T_2},δ_{M_1} and δ_{M_2} are the death rate constants of T_1,T_2,M_1 and M_2 cells, respectively. The free virus (infectious and non-infectious) gets cleared by the immune system with rate constant CL.

Pharmacokinetic-Pharmacodynamic Coupling

We have previously shown that the antiviral effect of NRTIs (like TDF) can be regarded by an inhibition of the rate of successful cell infection $\beta_{\mathrm{T/M}}$ and a proportional increase in the number of unsuccessful infection events $\mathrm{CL}_{\mathrm{T/M}}$ [29]. We can thus write:

$$\beta_{\mathrm{T/M}}(t) = \beta_{\mathrm{T/M}}(\phi)\cdot(1-\eta(t)) \qquad (8)$$

$$\mathrm{CL}_{\mathrm{T/M}}(t) = \left(\frac{1}{\rho_{\mathrm{rev}}} - (1-\eta(t))\right)\cdot\beta_{\mathrm{T/M}}(\phi), \qquad (9)$$

where $(1-\eta(t))$ denotes the residual infection, when TFV is applied and $\rho_{\mathrm{rev}} \approx 0.5$ [31] is the probability that infection is successful in the absence of treatment. The efficacy of TFV-DP at time t was implemented using the standard Emax-model with slope parameter 1 [32].

$$1-\eta(t) = \frac{\mathrm{IC}_{50}}{\mathrm{IC}_{50} + C_{\mathrm{cell}}(t)} \qquad (10)$$

where IC_{50} denotes the intracellular TFV-DP concentration (compartment C_{cell} in Fig. 2A), which reduces cell infection by 50%.

Prediction of Relative Infection Risk in the Presence of TDF

Although per-contact infection probabilities have previously been estimated for different routes of HIV transmission [33,34] (e.g. $\approx$0.5–4% for homosexual receptive contact), it is not known how much infectious virus actually reaches a cellular environment that facilitates its reproduction (further on referred to as 'inoculum size'). Moreover, several (unknown) co-factors may alter this number. It could be possible that virus does not reach a cellular environment that facilitates its reproduction during the majority of sexual contacts, as indicated by low per-contact-transmission probabilities [34]. During those sexual contacts where infection occurs, the data from [35,36] indicate that a small number of founder particles (estimated to be of the order 1–5 in the majority of infections) establish the viral population within the newly infected individual. However, due to the inherent uncertainties about the co-factors that potentially alter the number of transmitted viruses, we will not compute relative per-contact-infection probabilities under TDF administration, but rather compute the percentage of infections prevented for distinct inoculum sizes, relative to the absence of drug. The relative infection probability is typically assessed in clinical trials from a cohort of patients, without detailed knowledge of the viral inoculum sizes and the circumstances of transmission.

In the simulations, infection was irreversible by the time that the predicted number of viruses exceeded 1 million particles (because the system behaves deterministically and approaches its infection fix-point). Therefore, we recorded an infection event during our simulations, whenever the viral population crossed this threshold in a previously uninfected 'virtual patient' at risk. The percentage infections prevented, when TDF is taken prophylactically was then calculated using the following formula:

$$\%\text{infections prevented} = 100\cdot\left(1 - \frac{P(\text{inf.}|V_{t_0},S)}{P(\text{inf.}|V_{t_0},\phi)}\right) \qquad (11)$$

where $P(\text{inf.}|V_{t_0},\phi)$ is the probability of infection in the absence of drugs ϕ, when $V_{t_0} \in \{1,5,20,100\}$ infectious viruses come into

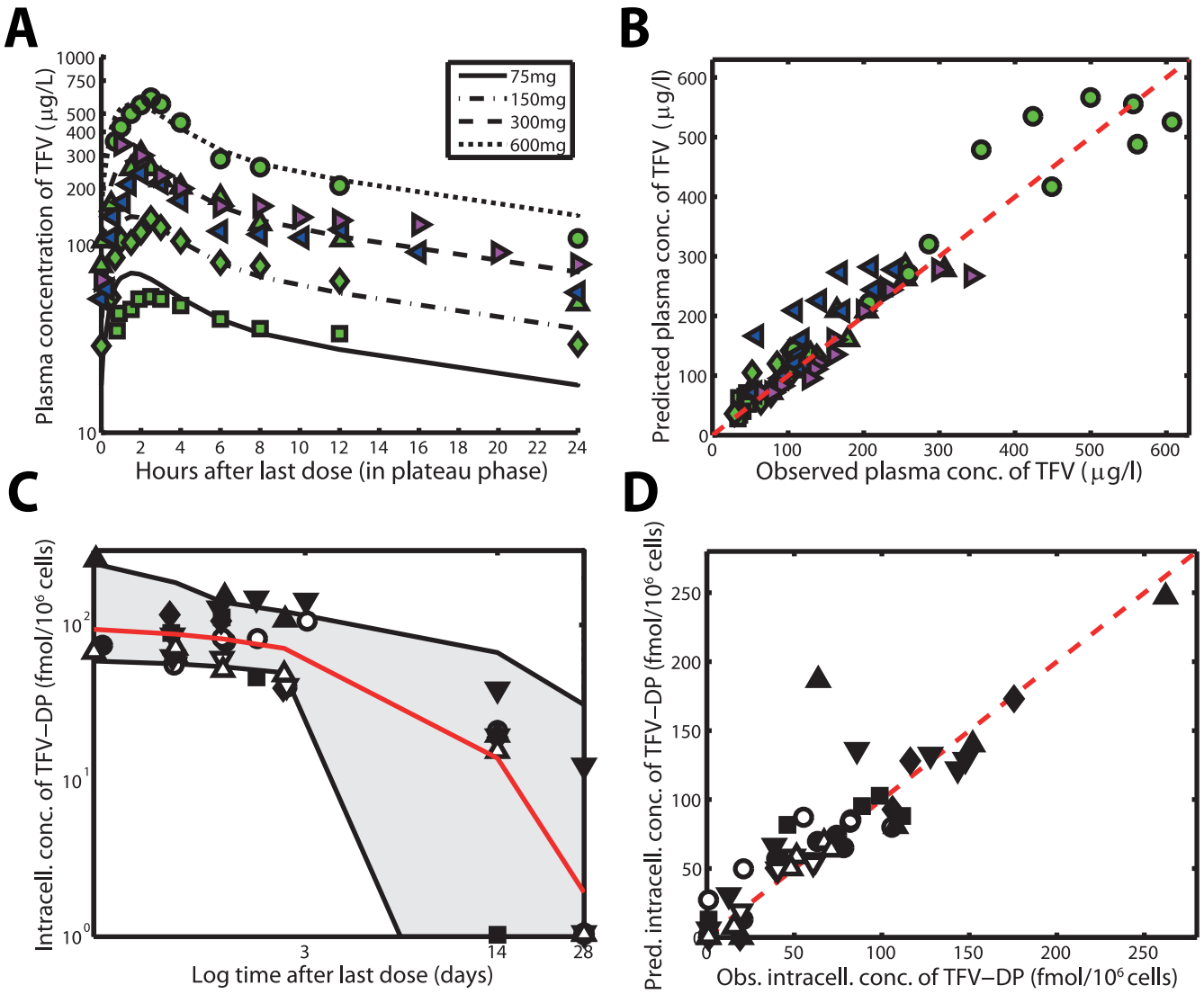

Figure 2. Pharmacokinetics of TFV for different doses of oral TDF at plateau and intracellular TFV-DP concentrations after treatment cessation. A: Predicted pharmacokinetics of TFV after once daily 75-, 150-, 300- and 600 mg oral TDF (lines) together with data from [7,9,12] (markers). B: Goodness-of-fit plot for the plasma pharmacokinetics of TFV with data from 3 clinical studies and 4 different dosing schemes [7,9,12]. The dashed red line indicates the line of unity, whereas the green squares, -diamonds, triangles and filled dots represent the observed TFV concentrations in [12] following 75-, 150-, 300- or 600 mg once daily administration of TDF. The blue left-pointing triangles and the magenta right-pointing triangles represent observed TFV concentrations after 300 mg once daily oral administration from [9] and [7] respectively. C: Predicted pharmacokinetics of intracellular TFV-DP after stopping of 300 mg once daily oral TDF dosing (lines) together with data from [11] (markers). D: Goodness-of-fit plot for intracellular TFV-DP. The up- and downward pointing filled and open triangles, open- and filled circles, filled squares and filled diamonds indicate intracellular TFV-DP pharmacokinetics after stopping 300 mg once daily oral TDF dosing in 8 different individuals from [11].
doi:10.1371/journal.pone.0040382.g002

contact with a cellular environment that facilitates their reproduction within the susceptible individual. The predicted probability of infection in the absence of drugs $P(\text{inf.}|V_{t_0},\phi)$ was $10\pm1.3\%$, $40\pm2.1\%$, $87\pm1.5\%$ and $100\pm0\%$, respectively, when $V_{t_0}=1$, 5, 20 or 100 viruses were inoculated. $P(\text{inf.}|V_{t_0},S)$ is the corresponding probability of infection when prophylactic strategy S is used. We evaluated the following TDF-based prophylactic strategies: a) 300 mg oral TDF taken once daily when 20, 40, 60, 80 or 100% of pills are ingested, b) TDF is taken around the time of viral exposure (6, 1 h before exposure or 1, 6, or 48 h after exposure) and continued for 7 days (1w-PrEP/PEP) or c/d) a single oral dose of 300 or 600 mg TDF is taken at either 1, 6, 12, 24 or 48 hours before exposure to virus (sd-PrEP).

During strategy a) (once daily oral TDF) adherence was implemented using a "roulette-wheel selection" technique: A uniformly distributed random number r on the open interval (0,1) is drawn at each potential dosing time (each 24 hours of simulated time). If this random number r is less than or equal to the adherence level (e.g. $r\leq0.4$ for adherence level 40%), then a dose is given to the virtual patient; otherwise not.

Modeling the infection probability requires to regard the intrinsic stochasticity and discreteness of the infection event: Either the transmitted virus becomes entirely cleared by the immune system before establishing stable infection, or the infection expands and disseminates throughout the body [18]. Reverse transcriptase inhibitors like TDF decrease the probability of cell infection and therefore increase the probability that HIV

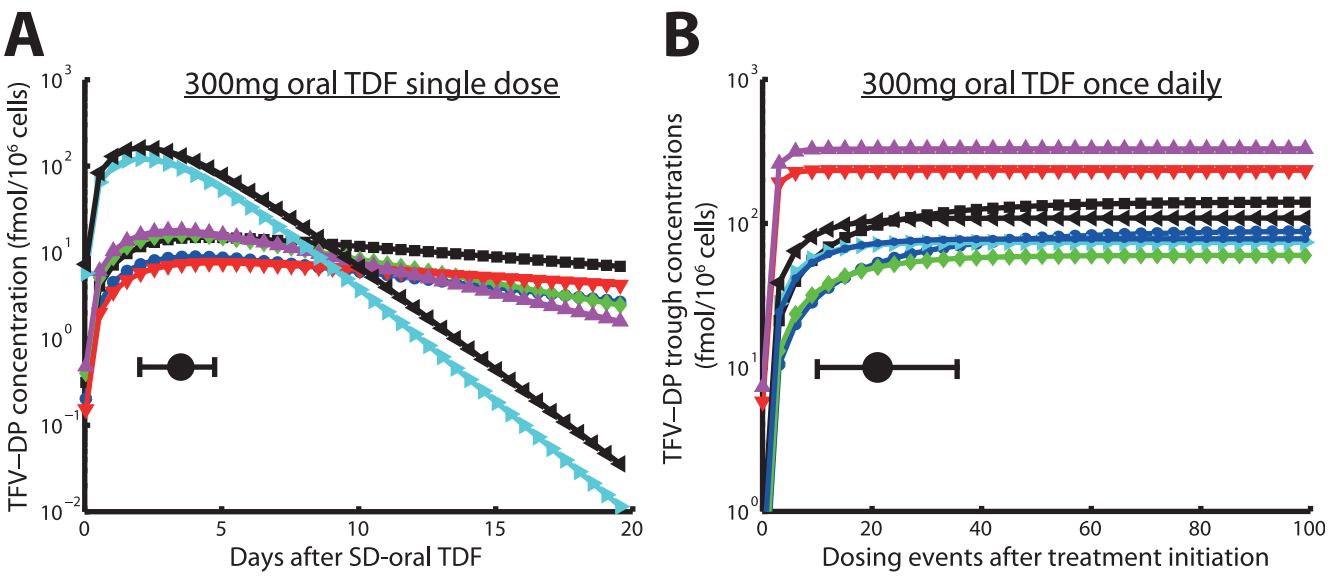

Figure 3. Predicted TFV-DP intracellular pharmacokinetics following a single dose oral 300 mg TDF and accumulation of TFV-DP after daily 300 mg oral TDF. A: Predicted intracellular pharmacokinetics of TFV-DP in PBMCs after a single 300 mg oral TDF dose. Solid black circle and horizontal error bar indicate the t_{max} value and its range. B: Trough levels of TFV-DP in PBMCs following 300 mg oral TDF every 24hours, indicating the accumulation of active compound. The solid black circle and the horizontal error bar indicate the time until plateau concentrations are reached and the range for this parameter. Blue cirles, black squares, green diamonds, red downward pointing triangles, magenta upward-pointing triangles, cyan right-ward pointing triangles, black left-pointing triangles and blue asterisks indicate individual predictions for 8 patients.
doi:10.1371/journal.pone.0040382.g003

can become entirely cleared before establishing stable infection [37]. In order to fully regard the intrinsic stochasticity of rare events in the utilized model and to predict the impact of PrEP on HIV transmission, we use the stochastic-deterministic simulation algorithm presented in [30]. Unless otherwise stated, we ran 2000 stochastic-deterministic simulations for each parameter set to estimate the infection probabilities with sufficient statistical confidence.

Results

Plasma & Intracellular Pharmacokinetics

Predicted concentration-time profiles of TFV after 75-, 150-, 300- and 600 mg once daily dosing of TDF using the final pharmacokinetic model (eqs. (3)-(6)) are shown in Fig. 2A (lines) together with available data from 3 clinical trials [7,9,12] (markers). It can be seen that TFV rapidly appears in the plasma ($t_{max} \approx 2$ h) and decays in a bi-phasic manner for all analyzed dosing schemes. The estimated terminal half life of plasma TFV was ≈ 19 hours, in line with previous estimates [3]. TFV concentrations increase proportionally with increasing dose, indicating dose-linear pharmacokinetics. A goodness-of-fit plot with regard to plasma concentrations is shown in Fig. 2B. The plot indicates an overall spread around the line of unity, supporting the predictive power of the model. The predicted decay behavior of TFV-DP in PBMCs after stopping TDF dosing is shown in Fig. 2C together with available data [11]. The grey area therein indicates the predicted range of kinetic behavior, whereas the solid red line indicates the estimated median TFV-DP decay. Note that the variation (grey range) is quite large, which is however in line with other studies [14]. A goodness-of-fit plot with regard to individual predicted vs. observed intracellular TFV-DP concentrations is shown in Fig. 2D for the data coming from the distinct patients (markers). The predicted average half life of TFV-DP was very large $(125\text{h} \approx \widetilde{t_{1/2}} = \ln(2)/\widetilde{k_{out}})$. Overall, the plot indicates a spread around the line of unity (dashed red line in Fig. 2D), supporting the approach chosen for estimating individual decay kinetics of TFV-DP in peripheral blood mononuclear cells (PMBCs) rather than using an average value for all patients (see also model comparison in Text S1).

The predicted concentration time profile of TFV-DP after a single dose of 300 mg oral TDF is shown in Fig. 3A. It can be seen that TFV-DP reaches its maximal concentrations after a median time of 85 h (range: 49–113 h) following a single dose of TDF. The maximally achievable concentrations vary between individuals and are within the range of 7.6 to 163 fmol/10^6 cells (median value: 16 fmol/10^6 cells) in case of a single dosing event.

The accumulation of intracellular TFV-DP in the case of daily 300 mg oral TDF is shown in Fig. 3B. TFV-DP trough concentrations (concentrations immediately before the next dose) reach their plateau levels after a median of 21 once daily dosing events (range 10–36). On the contrary, plateau levels of the parent compound TFV are reached within 7 dosing events in blood plasma already (data not shown).

Antiviral Efficacy During Mono-therapy in HIV-infected Individuals

For further model evaluation and estimation of the remaining parameters IC_{50} and K_m, we coupled the pharmacokinetics of intracellular TFV-DP to an established model of the HIV-life cycle [28,30] (see *Methods* section) and subsequently predicted the 56 days viral dynamics in asymptomatically HIV infected individuals following a 28 days mono-therapy (day 0–28) with either 75-, 150-, 300- and 600 mg TDF. Our predictions are shown in Fig. 4A, B, C, D together with data from the corresponding dose escalation study [12]. The dashed lines and open circles in Fig. 4A, B, C, D indicate clinically observed median $\log_{10}$ viral load decay from [12], whereas the solid lines and filled circles indicate the predicted median $\log_{10}$ viral decay using our model. The respective weighted residual sum of squared errors WRSE (see eq. (1)), denoting the

absolute deviation between experimental and predicted viral load decay is shown in Text S1 (the Table therein) and indicates an overall good predictive power of the coupled PK-PD model. Notably, the experimental median viral decay profile for the 300 mg dose group indicated maximally achievable viral decay, as the 600 mg dosing could not produce steeper viral decay than the 300 mg scheme.

Efficacy of Daily TDF for the Prevention of HIV-1 Infection

The predicted percent infections prevented by continuous once daily 300 mg TDF PrEP are shown in Fig. 5A. It can be seen that continuous PrEP can avert $\approx$80% infections, under 100% adherence and with small inoculum sizes (1 infectious virus). Under a fivefold increase in inoculum size, TDF is still efficacious, preventing $\approx$75% of infections. However, if the inoculum size is further increased (100 infectious viruses come into contact with target cells), the efficacy drastically drops to levels of $\approx$20% protection. On the other hand, imperfect adherence above the level of 40% has only a small impact on the predicted efficaciousness of TDF, confirming previous pharmacologic considerations about the pharmacokinetic forgiveness of the drug [3]. We statistically tested whether adherence and inoculum size impact on the efficacy of TDF-based PrEP, based on our simulation results. We found that decreasing adherence has a small impact of the efficacy of TDF-based PrEP (infection probabilities are not significantly altered if adherence is as low as 60%). However, if adherence is below 40%, TDF-based protection is significantly altered ($p < 0.05$). Furthermore, when large numbers of viruses become transmitted, we observe a stronger impact of adherence (see Fig. 5A). The inoculum size determined the efficacy of TDF-based PrEP for all conditions tested ($p < 0.01$, see Table S3).

In summary, the protective effect of TDF appears to be much less sensitive to poor adherence (as long as adherence is above 40%), but is dependent on the actual mode of transmission, i.e. how many viruses become transmitted. Notably, in a substudy of Partners PrEP (serodiscordant couples in Kenya/Uganda) using TDF only, an overall efficacy of 62% (confidence interval: 34%;78%) was reported, which corresponds to our predictions for the case when small numbers of viruses become transmitted (inoculum size 1–20 in Fig. 5A). The number of distinct founder viruses was estimated to be rather low (of the order 1–5 for heterosexual- and homosexual transmission) [35,36], which stresses the importance of PrEP efficacy at low inoculum sizes for the prevention of HIV-1 transmission and supports the predictive power of our model.

Efficacy of One Week extended TDF prophylaxis during Viral Exposure

We predicted the efficiency of TDF when started either 6 or 1 h before exposure or 1, 6, or 48 h after exposure and continued for 7 days (1w-PrEdP/PEP). The results (see Fig. 5B) indicate a maximally achievable efficacy of 1w-PrEP/PEP of $\approx$30% when started 6h before viral challenge for small inoculum sizes. The maximum achievable efficacy was similar to the sd-PrEP regimen. The efficacy of 1w-PrEP/PEP was influenced by inoculum size ($p < 0.01$, for all tested conditions, see Table 6) and dropped drastically as the inoculum size increased. 1w-PrEP/PEP efficacy was also affected by the timing of TDF initiation, particularly for large inoculum sizes ($p < 0.05$, see Fig. 5B), with earlier times of regimen initiation resulting in higher efficacy. Overall, our predictions indicate that extended (one week) prophylaxis with TDF initiated shortly before viral exposure offers little benefit compared to sd-PrEP (Figure 5C, D). If TDF is initiated after viral exposure, its efficacy is rather limited.

A recent investigation showed that 28 days of a post-exposure prophylactic triple drug regimen containing TDF [38–40] is safe, but data indicating the efficiency is missing for TDF alone or TDF containing regimen in humans. Efficacy of PEP using tenofovir has to date only been demonstrated in non-human studies, e.g. [41,42]. The conducted experiments, however, indicate that the prophylactic efficacy of post-exposure TDF may depend on the type of virus used [43] and on particular pharmacokinetics, possibly limiting the translation of these results to TDF-based PEP in human.

Efficacy of Single Dose TDF Prophylaxis Shortly before Exposure (sd-PrEP)

We tested the efficacy of single dose 300- and 600 mg oral TDF given either 1, 6, 12, 24 or 48 h before viral exposure in Fig. 5C, D respectively. Notably, sd-PrEP could reach a maximum efficacy of $\approx$50% with small inoculum sizes, when given 24 hours prior to exposure. The efficacy dropped gradually when the inoculum size increased. In particular, sd-PrEP was completely inefficient when large inoculum sizes were encountered (if $\geq$ 100 infectious viruses come into contact with target cells). The dependency of sd-PrEP efficacy on inoculum size was significant for all tested conditions at the $p < 0.01$ level (Table S5, S6). Despite a dependency on the inoculum size, sd-PrEP efficacy was also significantly altered by the timing of drug administration, see Figure 5C, D. Generally speaking, sd-PrEP efficacy was highest if TDF was taken 12–48 h before viral exposure and almost completely inefficient when taken only 1 h before exposure, which limits it's practical use as a single-dose prevention drug. The poor efficacy of sd-PrEP, as well as the dependency on the timing of TDF administration is based on its pharmacokinetics: TFV-DP, the active moiety, requires approximately 21 (range: 10–36, see Fig. 3B) dosing events to reach plateau levels and to exert its maximum effect. During single dose administration, TFV-DP still requires about 85 h hours (range: 49–113, see Fig. 3A) to reach maximum concentrations C_{max}. Therefore, TDF needs to be taken early enough ($\geq$ 48 hours) to allow for intracellular TFV-DP levels to build up. Once TFV-DP levels have been achieved, they persist in most patients, owing to the long half life of intracellular TFV-DP.

We also tested whether the effect of single dose TDF PrEP could be potentiated, if the standard dose was doubled (see Figure 5D). The prophylactic efficacy was, however, not markedly different for most conditions tested, see Fig. 5C&D and Table S7 for a statistical evaluation.

Relation between Intracellular TFV-DP Concentrations and Prevention of HIV-1 Infection

We have derived an analytical formula in Text S2 to assess the relation between intracellular TFV-DP concentrations and the % HIV-1 infections prevented. The percent infections prevented by distinct intracellular TFV-DP concentrations is shown in Fig. 6 (based on the analytic solution). It can be seen that the EC_{50} value (concentrations of intracellular TFV-DP necessary to prevent 50% of HIV-1 infections) is increasing for larger virus inoculum sizes. The computed EC_{50} values were 29, 40, 77 fmol/10^6 cells for inoculum size 1, 5 and 20 respectively, which is below the concentration range achieved when 300 mg TDF is given once daily in an adherent patient (dark grey area in Fig. 6). On the contrary, the EC_{50} for a viral inoculum size of 100 is above the concentration range typically achieved during once daily PrEP with 300 mg TDF (EC_{50} = 411 fmol/10^6 cells). TFV-DP concen-

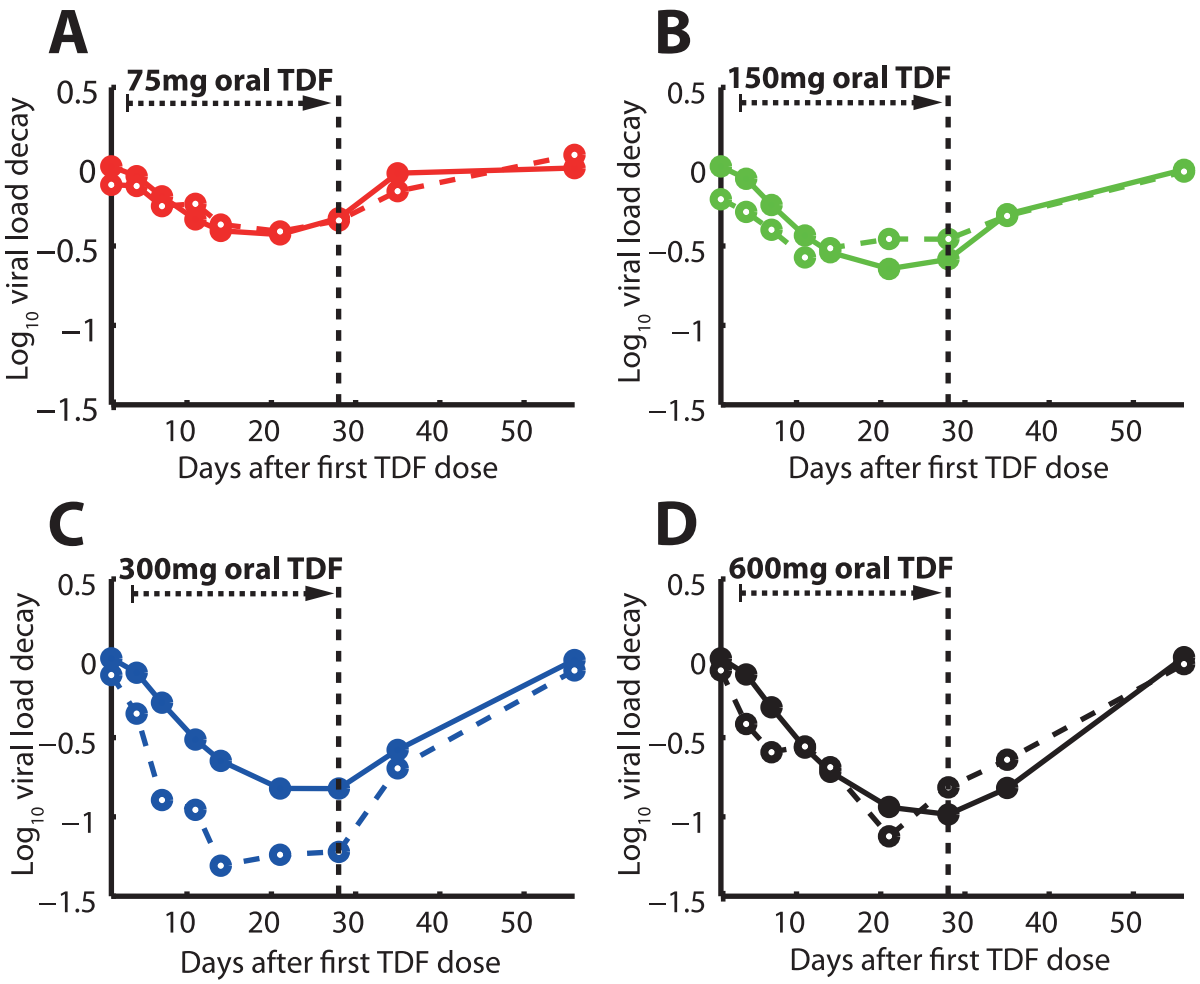

Figure 4. Viral load $\log_{10}$ kinetics during- and after 28 days of TDF mono-therapy. Black dashed vertical lines indicate the withdrawal of TDF dosing. Solid lines represent predicted median viral kinetics using the coupled PK-PD model, whereas dashed lines represent the observed viral kinetics [12]. Once daily 75mg TDF dosing. B: Once daily 150 mg TDF dosing. C: Once daily 300 mg TDF dosing. D: Once daily 600 mg TDF dosing.
doi:10.1371/journal.pone.0040382.g004

trations to prevent 90% infections EC_{90} were 267, 348, 640 and 2866 fmol/10^6 cells for virus inoculum size 1, 5, 20 and 100 respectively (see Fig. 6).

Discussion

The plasma pharmacokinetics of TFV were best described by a two compartment model (compartments C_1 and C_2) with first order absorption and elimination, based on statistical model comparison. Similar models were also used by most other groups to describe the pharmacokinetics of TFV in blood plasma [14,28,44,45]. Pharmacokinetic parameter estimates (Table 1) agree well with previous studies [14], indicating a large volume of distribution, bi-phasic decay with a particularly slow terminal half life of $\approx$19 h, in line with previous estimates [3]. Inter-individual variations in parameter values characterizing plasma pharmacokinetics were estimated to be small in related studies [14,28,44] (coefficient of variation less than 50%). We therefore decided to ignore inter-individual variations in parameters describing the plasma pharmacokinetics of TFV. To the contrary, parameters describing the intracellular pharmacokinetics of TFV-DP display a large inter-individual variability (in our model this affects parameters k_{out} and V_{max}).

NRTIs like tenofovir exert their effects through their intracellular phosphorylated moieties, which are often non-linearly related to plasma pro-drug concentrations [15,17,46]. As a consequence, plasma pro-drug concentrations may poorly predict pharmacological activity [47,48]. For NRTIs it is therefore necessary to model the pharmacokinetics of the active intracellular form explicitly. Here, we followed a step-wise model building process to establish the link between plasma pro-drug and intracellular TFV-DP pharmacokinetics, where we first independently estimated intracellular TFV-DP elimination. Statistic model evaluation using typical- vs. individual estimates of the elimination rate constant k_{out} indicated that taking intracellular pharmacokinetic variations into account does not only improve the prediction of intracellular TFV-DP concentrations (see Fig. 2D), but also improves the prediction of viral decay following TDF mono-therapy with different doses (see Text S1). Notably, we predicted a large variation for the k_{out} parameter (range: 0.002–0.026 h^{-1}), which is, however, within the confidence interval of previous estimates (confidence interval: 0.0007–0.0372 h^{-1}) [14]. The typical half life of TFV-DP was very large ($\widetilde{t_{1/2}} = \ln(2)/\widetilde{k_{out}} \approx 125$h; range: 26–386h), which is in good agreement with other studies [14,49,50]. Due to the lack of intracellular TFV-DP pharmacokinetic data illuminating the

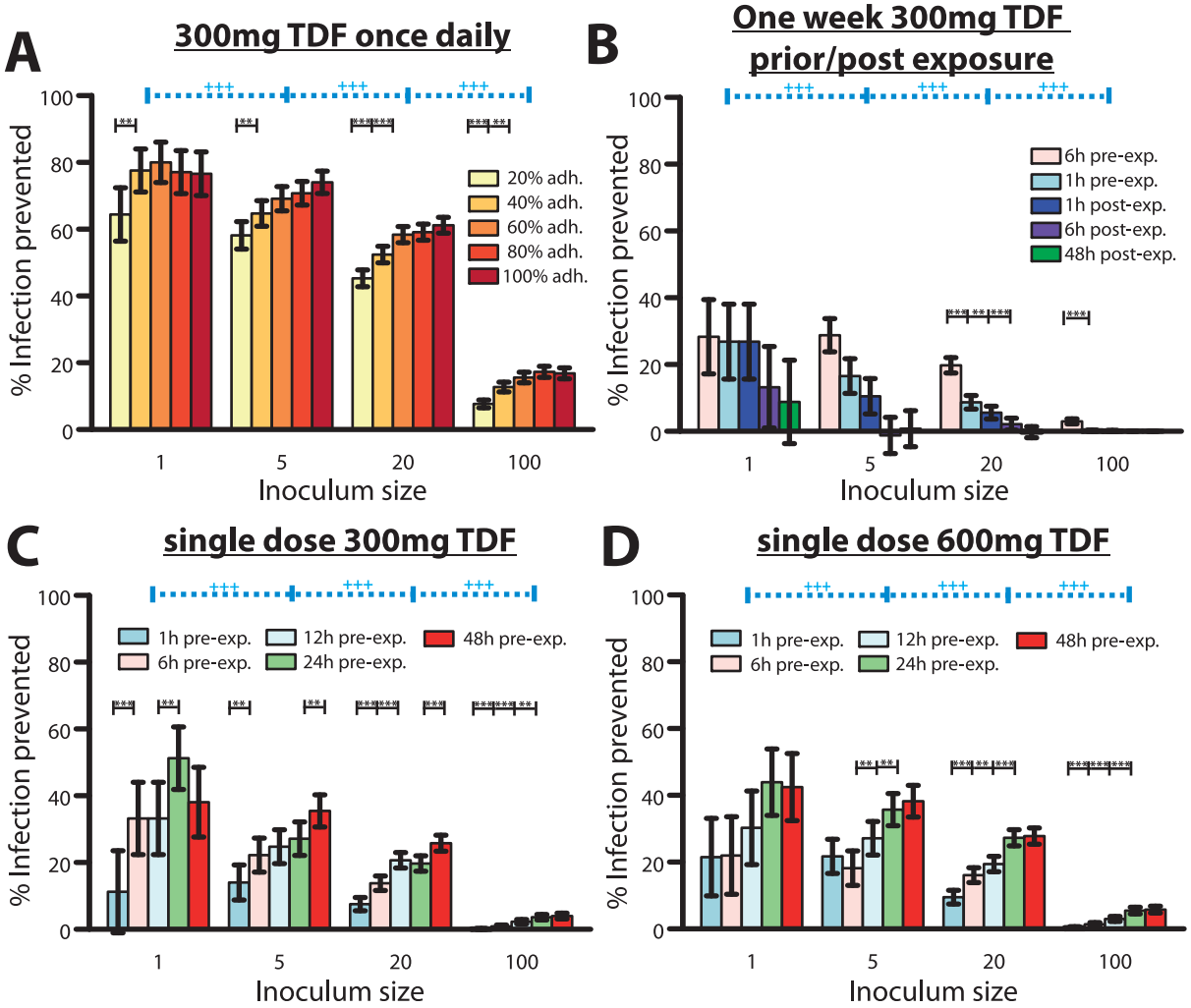

Figure 5. Predicted % infections prevented by distinct TDF-based prophylactic strategies for various parameter sets. A: Predicted % infections prevented by once daily 300 mg TDF taken at different levels of adherence and with distinct virus inoculum sizes. **,*** prophylactic efficacy depends on adherence at the $p < 0.05$ or $p < 0.01$ level respectively. B: Predicted % infections prevented by a one week 300 mg TDF (1w-PrEP/PEP) when started at distinct times before/after exposure with distinct numbers of viruses. **,*** prophylactic efficacy depends on the timing of start of TDF administration at the $p < 0.05$ or $p < 0.01$ level respectively. C: Predicted % infections prevented by a single dose 300 mg TDF (sd-PrEP) when taken at distinct times before exposure with distinct virus inoculum sizes. **,*** prophylactic efficacy depends on the timing of TDF single dose administration at the $p < 0.05$ or $p < 0.01$ level respectively. D: Predicted % infections prevented by a single dose 600 mg TDF (sd-PrEP) when taken at distinct times before exposure with distinct virus inoculum sizes. Error bars represent confidence bounds calculated using Greenwood's formula. $^{+++}$ prophylactic efficacy depends on the inoculum size. The predicted probability of infection in the absence of drugs $P(\text{inf.}|V_{t_0},\phi)$ was $10\pm1.3\%$, $40\pm2.1\%$, $87\pm1.5\%$ and $100\pm0\%$ when $V_{t_0}=1$, 5, 20 or 100, respectively, viruses were inoculated.
doi:10.1371/journal.pone.0040382.g005

uptake of this specimen, we estimated the kinetics of influx/anablism of intracellular TFV-DP (and the IC_{50} value) by comparing viral decay kinetics following 28 days of TDF monotherapy with different doses. Based on model comparison, we found that a saturable influx with individual (maximally achievable) influx rates would best describe the pharmacodynamic data. Notably, others [13,14] also found a saturable uptake based on pharmacokinetic data alone (without taking viral decay into account) and found a large variation in the uptake rate [14], consistent with our findings. The saturable uptake kinetics translate into maximally achievable TFV-DP concentrations, which results in maximally achievable viral decay upon increasing doses of TDF. As can be seen in Fig. 4C & D (dashed lines) clinically measured viral decay from [12] appears to be greater for 300- vs. 600 mg TDF, which was not reproduced by our model predictions (solid lines in Fig. 4C & D). The authors of the clinical report [12] however stated that the difference in viral decay between the two doses was not significant and may be attributed to noise and the small size of the population tested (8 individuals for each dose respectively in [12]) rather than having a mechanistic reason.

In previous studies, average plateau TFV-DP concentrations from different studies were in the range 80 to 160 fmol/10^6cells [3,14], whereas the individual TFV-DP concentrations varied between 10.6 to 441 fmol/10^6cells [14] when 300 mg oral TDF was administered once daily. Our model predicted average plateau levels were 130 fmol/10^6cells (range: 52–327 fmol/10^6cells; see Fig. 3B), which is consistent with previous findings. TFV-DP accumulates very slowly, owing to its long half life. We estimated that plateau concentrations will be achieved after 21 dosing events (range: 10–36), which is in the range of previous pharmacologic considerations [3] (23 once daily dosing events). The slow

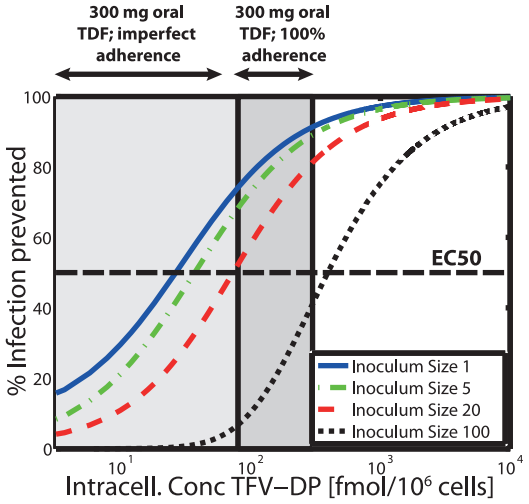

Figure 6. Predicted % infections prevented vs. intracellular TFV-DP concentrations for distinct virus inoculum sizes. The solid blue-, dash-dotted green, dashed red and dotted black lines show the concentration-response profile for virus inoculum size 1, 5, 20 and 100 respectively. The thick dashed horizontal black line indicates the TFV-DP concentration, which prevents 50% of infections (EC_{50}). The dark grey area indicates the TFV-DP concentration range achieved during once daily 300 mg oral TDF dosing with 100% adherence, whereas the light grey extension to the left indicates the range of concentrations resulting from imperfect adherence. Predictions are based on the approximate analytic solution derived in Text S2.
doi:10.1371/journal.pone.0040382.g006

accumulation of TFV-DP limits its prophylactic use as a single dose drug, although prophylactically effective concentrations may already be achieved $\geq$ 24h after a single dosing event in some patients (see Fig. 3A). In the absence of data reporting TFV-DP concentrations in PBMCs after a single 300 mg oral TDF dose we are, however, not able to directly verify these predictions. Notably, very similar TFV-DP concentrations in rectal tissue biopsies after a single 300 mg oral TDF dosing event were observed by Patterson et al. in a very recent study [51] (discussed later on).

As suggested by Piliero et al. [47], the intracellular half life of phosphorylated NRTIs is a key determinant of their clinical efficacy. Often, however, the typical half life from different individuals is taken as a reference and inter-individual differences in the pharmacokinetics of activated NRTI anabolites are neglected. In the case of TDF, large variations in the intracellular pharmacokinetics may exist, which warrant further investigation in order to optimize its efficacy both for prophylaxis and treatment.

We predicted that the long half life of intracellular TFV-DP translates into desirable properties in the case of continuous PrEP, which is pharmacologically 'forgiving' in the case of poor adherence, if at least 40% of the pills are ingested (see Fig. 5A). While these pharmacologic considerations have been previously discussed [3], we are presenting a quantification of these effects by combining pharmacokinetics, viral dynamics and stochastic simulation in a single integrated *in silico* model.

It was recently suggested that the willingness to take pills may be a major obstacle for the implementation of PrEP strategies in practice [24]. In line with this statement, Donnel et al. [52] found a significant difference in HIV infection between individuals with detectable vs. undetectable TFV in blood. Of note, for the levels to drop from 70 ng/mL (median concentrations in [52]) to $<$0.1 ng/mL (limit of detection in [52]), patients require to take less than 14% of their drugs (one out of seven doses), as TFV exhibits a long terminal half life in plasma ($\approx$19 h). This indicates that the willingness to take daily medication for HIV prevention may be extremely low in some individuals with undetectable drug (adherence $<$14%). It also raises concern that willingness to take PrEP may in fact be a major obstacle for the implementation of PrEP in practice as considered by Van Damme et al. [24]. The results by Donnel et al. [52] and Van Damme et al. [24] also indicate and that the estimates of PrEP efficacy may have been contaminated by extremely poor adherence of some individuals in the trials. In agreement with this assumption, clinical outcomes with TDF-based continuous PrEP indicate highly variable outcomes: from either being inefficient (FEM-PrEP) [19] to 44–73% reduced HIV acquisition [20–22]. A sub-study of Partners PrEP assessed the efficacy of continuous 300 mg daily TDF administered to the healthy partner in sero-discordant couples in Kenya and Uganda. The overall efficacy was 62% (confidence interval: 34%;78%) and may be higher in adherent patients [24]. We predicted a prophylactic efficacy of 65%–80% for inoculum size 1–5 in patients that take at least 40% of their drugs, see Fig. 5A. In view of the possible contamination of Partner PrEP trials results by extremely poor adherence in some individuals, our slight overprediction of TDF efficacy may be anticipated. Further analysis is required in order to assess the proportion of individuals with *sufficient* adherence.

In the case of short-course pre-exposure TDF, or post-exposure TDF, prophylactic success is limited by a slow accumulation of the intracellular active component TFV-DP (only $\approx$20% infections are prevented if TDF is taken 1h before exposure, see Fig. 5B, C, D and Table S4, S5, S6. Note also that intracellular TFV-DP may require 21 dosing events on average to reach plateau levels, see Fig. 0B. In view of the recent approval of Truvada (300 mg TDF +200 mg emtricitabine) for pre-exposure prophylaxis by the FDA, prescribers should inform their patients about these potential shortcomings, in order to avoid HIV-1 infection by inadequate use of prophylaxis in combination with risk compensation [53]. HIV-infection in combination with the inadequate use of PrEP may also select drug resistance, which could limit treatment perspectives for infected individuals. In terms of short-course pre-exposure prophylaxis other drugs may be more suitable that accumulate rapidly, such as nevirapine [37], which is successfully used for prevention of mother-to-child infection.

Based on the model parameters, the duration of action required to ensure that virus particles are eliminated with e.g. 99% probability, $T_{\mathrm{elim}}(99\%)$ may be computed according to

$$T_{\mathrm{elim}}(99\%) = -\left(\frac{\ln\left(1-(0.99)^{1/V_{t_0}}\right)}{\mathrm{cl_V}}\right), \quad \text{with}$$

$\mathrm{cl_v} = \mathrm{CL} + \beta_{\mathrm{T}}(t)\cdot \mathrm{T_U} + \beta_{\mathrm{M}}(t)\cdot \mathrm{M_U}$. For the parameters used $T_{\mathrm{elim}}(99\%) < 3$ days would suffice for inoculum sizes $V_{t_0} \in \{1,5,20,100\}$. Taken together, this may indicate that, *pharmacologically*, single dose PrEP drugs taken shortly before potential viral exposure are required to accumulate rapidly in target cells, but may not have to persist for more than 3 days, in line with the pharmacological attributes of most NNRTIs.

In contrast to our predictions (Fig. 5B), some non-human studies found that TDF-based post-exposure prophylaxis may be highly efficient: Tsai et al. [42] treated macaques for variable durations after exposure with SIVmne and tested viral markers. In their non-human model of TDF-based PEP, viral titers remained undetectable in some monkeys until week 48 post-exposure, indicating that some protection was achieved, in particular for longer durations of PEP (28 days) and timely start of prophylaxis (within 24 hours post-exposure) [42]. It was however argued [54] that TDF-PEP

may enhance immune controlled viral replication down to undetectable levels, rather than actually preventing infection. Furthermore, the efficacy in the primate model were depending on the type of virus used [43] (which are SIV strains, not HIV-1) and may also depend on the particular pharmacokinetics in the primate model, which may be different to the human. Altogether, the non-human studies with TDF-based PrEP may not translate into human.

It is not precisely known how much virus is being transmitted from an infected to an uninfected individual during e.g. sexual contact. Moreover, it is not known how many transmitted viruses actually reach a target cellular environment that allows their reproduction, and what types of cells are relevant for the initial infection. Also, the number of transmitted viruses, the availability of target cells and the subset of viruses that reach a cellular environment that facilitates their reproduction may be altered by the circumstances of HIV-1 transmission and several unknown co-factors. While the earliest stages of mucosal transmission of HIV-1 have not been directly observed in human and are not fully understood, animal experiments suggest that $CD4^+$ T-cells are probably the principal cell type infected at the portal of entry and throughout the earliest stages of infection [55]. These cells are mainly located in the sub-mucosa [56]. Although exposure at the mucosal surface may be substantial, only a fraction of HIV-particles may penetrate the intact epithelial layer and reach target cells [57–59] (denoted as inoculum size throughout the manuscript). Low per-contact infection probabilities further indicate that infectious virus may not reach a cellular environment that facilitates their reproduction during most sexual contacts [33,34] (per-contact infection probabilities $\ll 5\%$), in contrast to other routes of transmission such as blood transfusion [34] (per-contact infection probabilities $>95\%$). Recent studies further showed, based on genotyping, that most infections ($\geq 75\%$) resulting from sexual HIV-1 transmission can be traced back to a single founder virus, or small populations of founder viruses [35,36]. Since the majority of new infections result from sexual HIV-1 transmission, PrEP intervention strategies may already effectively curb sexual HIV-1 transmission by preventing infection with small virus inoculum sizes. However, in the presence of co-existing infections, the integrity of the mucosal barrier may be compromised, which increases inoculum size [60]. Furthermore, co-existing infections may increase HIV-1 acquisition by increasing the availability of target cells in the sub-mucosa [60]. While we did not take co-infections into account, future research is warranted to elucidate the role of co-infections in the context of PrEP-strategies.

Our predictions revealed that the prophylactic efficacy of TDF decreases with an increasing number of inoculated viruses (see Fig. 5A, B, C, D), making TDF more efficient when only a few viruses reach a target cell environment and less efficient for large numbers of viruses. This observation can be explained as follows: a) At clinically relevant concentrations, TDF may only inhibit a certain proportion of potential target cell infections P. b) Some minimum number of infectious viruses $V_{\min}$ may already result in infection with almost 100% probability. When only a proportion of potential target cell infections are prevented, some inoculum size V_{t_0} exists where $P \cdot V_{t_0} > V_{\min}$. Therefore, TDF becomes inefficient above a certain inoculum size. The effect of TDF is particularly limiting, if P cannot be decreased by increasing TDF dosage (TFV uptake & anabolism become saturated, see eq. (5) and grey range in Fig. 6).

While it has recently been suggested to combine antiviral strategies for HIV-1 prevention [61], in this work, we predict a dependency of PrEP efficacy on inoculum size, which could make combined HIV prevention efforts synergistic: 'test and treat'/'treatment as prevention' strategies [62] aim to reduce the infectiousness of seropositive individuals by initiating HAART immediately after diagnosis, which effectively down-sizes their viral load and therefore the number of viruses transmitted to an uninfected individual. We predict that PrEP is highly efficient in the scenario where only few viral particles become transmitted, which possibly makes the two HIV-prevention efforts synergistic. This assumption, however, warrants further experimental confirmation.

The developed model is based on several assumptions, which we outline in the following:

a) We used intracellular TFV-DP concentrations in PBMCs as a marker of efficacy. PBMCs are surrogate markers, which consist of different cell types of which the majority, however, is susceptible to HIV-1 infection [26]. Different cell types may differentially phosphorylate TFV, depending on the expression of transporters and enzymes relevant to the intracellular phosphorylation of this drug. In line with this argument, Patterson et al. [51] recently found higher levels of TFV-DP in tissue biopsies from the rectum as compared to cervix and vagina after a single dose of Truvada (300 mg TDF and 200 mg emtricitabine). Remarkably, the median concentrations of TFV-DP in the rectal biopsies (displayed in units fmol/g tissue in [51]) are within the same range as those concentrations predicted in Figure 3A after unit conversion (1 fmol/10^6 cells $\approx 10^6/180$ fmol/mL tissue; 1 mg tissue ≈ 1 mL tissue). However, it is not entirely clear, what implications the distinct TFV-DP levels detected by Patterson et al. [51] may have in terms of HIV-1 prophylaxis: Only a subset of cells in the genital/rectal biopsies may be relevant for HIV-1 infection (e.g. $CD4^+$ lymphocytes [55]). Thus, it is not entirely clear if e.g. lower TFV-DP concentrations in these biopsies imply lower concentrations in cells *relevant* to HIV-1 infection or only in those *not relevant* to infection. Human studies, which analyze TFV-DP levels in purified $CD4^+$ cells, are missing. Purified $CD4^+$ cells derived from rectal biopsies in macaques indicate identical TFV-DP levels when compared to PBMC levels, which suggests that the PBMC surrogate marker is a good indicator for TFV-DP levels in cells relevant to HIV-1 infection.

b) Recent work suggests that the efficacy of NRTIs like TDF is affected by the levels of endogenous competing nucleotides dNTP (specifically: dATP for TFV-DP) [6,63]. Although this is likely to contribute to the efficacy of TFV-DP to prevent particular routes of infection, we could not take this information into account, because information concerning dNTP levels in target cells in different physiologic locations is lacking for humans. However, once these levels become available, their impact on the (cell-specific) susceptibility may be probed by sophisticated models, such as [6].

c) Vaginal TFV gel has been used successfully to prevent heterosexual HIV-1 infection [64]. Vaginal TFV gel exhibits entirely different pharmacokinetics compared to oral TDF dosing. TFV-DP levels in vaginal lymphocytes may be significantly higher in relation to the systemic levels (TFV-DP in PBMCs) after local exposure [65,66]. Most importantly, local exposure may mitigate the need for dosing long before exposure, which may be the greatest obstacle for the sucess of oral PrEP in practice. While the current model is useful in predicting the effects of oral TDF administration on HIV-1 infection, sophisticated pharmacokinetic modelling of vaginal TFV gel [67] in combination with stochastic

Table 2. Parameters used for the viral model.

Param.	Value	Ref.	Param.	Value	Ref.
λ_T	$2{\cdot}10^9$	[73]	λ_M	$6.9{\cdot}10^7$	[74]
δ_T, δ_{T_1}	0.02	[74]	δ_M, δ_{M_1}	0.0069	[74]
δ_{T_2}	1	[69]	δ_{M_2}	0.09	[29]
$b{\cdot}q{\cdot}\rho_{PR}$	0.67	[29]	ρ_{rev}	0.5	[31]
$\delta_{PIC,T}$	0.35	[21,75]	$\delta_{PIC,M}$	0.0035	[29]
k_T	0.35	[31]	k_M	0.07	[29]
$\beta_T(\phi)$	$8{\cdot}10^{-12}$	[76]	$\beta_M(\phi)$	10^{-14}	[29]
$\widehat{N}_T$	1000	[74]	$\widehat{N}_M$	100	[74]
CL(infected)	23	[70]	CL(naive)	2.3	[71,72]

All parameters refer to the absence of drug treatment ϕ. All parameters in units [1/day], except ρ_{rev} and $b{\cdot}q{\cdot}\rho_{PR}$ (unit less). $N_{T/M} = b{\cdot}q{\cdot}\rho_{PR}{\cdot}\widehat{N}_{T/M}$ [29].
doi:10.1371/journal.pone.0040382.t002

modelling may enable to assess its prophylactic efficacy *in silico* in the future.

d) In the absence of data elucidating the levels of TFV-DP in uninfected individuals, we assumed that TFV-DP levels in PBMCs from infected individuals vs. uninfected individuals are similar. Since TFV pharmacokinetics (parent compound) have been reported to be similar in healthy- and HIV-infected individuals [5], we found it reasonable to assume that TFV-DP levels are also similar.

e) It has recently been reported that TFV may become phosphorylated within red blood cells (RBCs) [68]. While standard procedures for the preparation of PBMC samples may not prevent their contamination with RBCs, this may hamper the accuracy of determination of TFV-DP in PBMC samples. Therefore, differences in RBC contamination may in part contribute to the variability of TFV-DP levels in PBMC measurements. The relevance and impact of RBC contamination on TFV-DP levels is not yet fully understood and further research is warranted to assess its role.

f) In individuals with established infection, the rates of viral elimination CL(infected) have been determined in a number of clinical studies, see e.g. [69,70]. Because of ethical reasons, the elimination of HIV in uninfected/newly infected individuals CL(naive) has never been directly observed. We assumed that viral elimination CL(naive) is lower in uninfected than in infected individuals, because the immune system may not recognize HIV readily in the naive patient. In line with other studies [71,72], we therefore set the parameter CL(naive) = 2.3 [1/day] (see Table 2), which reproduced clinical infection probabilities in previous work [37].

The presented modeling approach may be extended to e.g. assess the consequences of TDF-based PrEP intervention on drug resistance emergence, or TDF-based PrEP efficacy in the case when resistant virus becomes transmitted. Also, the combined effects of emtricitabine (FTC) and TDF remain to be elucidated, but can be studied by extending the presented model with the pharmacokinetics of FTC, once data on intracellular FTC-triphosphate becomes available.

Supporting Information

Table S1 Assessment of alternative models for plasma TFV pharmacokinetics. Goodness-of-fit in terms of the weighted residual sum of squared errors (WRSE) of model predicted vs. experimental data following either doses of 75, 150, 300 or 600 mg oral TDF from three independent clinical trials [7,9,12] for a one compartment- vs. a two compartment model. The models were compared by computing the Akaike information (AIC) and the model with the lowest AIC value was used subsequently (the two compartment model). Goodness-of-fit plots are shown in Fig. 2A-B (main article).
(PDF)

Table S2 Predicted individual TFV-DP elimination kinetics. Estimated individual plateau concentrations $C_0(i)$ and elimination rates $k_{out}(i)$ of TFV-DP from PBMCs (after treatment cessation). Parameters were estimated assuming first-order decay kinetics according to: $C_{cell}(i,t) = C_0(i){\cdot}e^{-t{\cdot}k_{out}(i)}$ using the data from [11].
(PDF)

Table S3 Contingency table for infection events during once daily PrEP with 300 mg TDF. Predictions are based on 2000 'virtual patients' simulations respectively. The first number in the brackets in columns 2–6 indicates the number of 'virtual patients' that remained uninfected after viral challenge, whereas the second number indicates the number of patients that became infected. For example, when 20% of once daily 300 mg TDF pills are ingested and patients are challenged with inoculum size one (one virus reaches a target cell environment), 1927 'virtual patients' remain uninfected, whereas 73 became infected.
(PDF)

Table S4 Contingency table of infection events for one week of TDF-based PrEP with 300 mg started around the time of exposure (1w-PrEP/PEP). Predictions are based on 2000 'virtual patients' simulations respectively. The first number in the brackets in columns 2–6 indicates the number of 'virtual patients' that remained uninfected after viral challenge, whereas the second number indicates the number of patients that became infected. For example, when 300 mg TDF is taken 6 hours before viral challenge, continued for one week and patients are challenged with inoculum size one (one virus reaches a target cell environment), 1866 'virtual patients' remain uninfected, whereas 134 became infected.
(PDF)

Table S5 Contingency table of infection events for a single oral TDF dose 300 mg (sd-PrEP). Predictions are based on 2000 'virtual patients' simulations respectively. The first number in the brackets in columns 2–6 indicates the number of 'virtual patients' that remained uninfected after viral challenge, whereas the second number indicates the number of patients that became infected. For example, when 300 mg TDF are taken 1 hour before viral challenge and patients are challenged with inoculum size one (one virus reaches a target cell environment), 1818 virtual patients remain uninfected, whereas 182 became infected.
(PDF)

Table S6 Contingency table of infection events for a single oral TDF dose 600mg (sd-PrEP). Predictions are based on 2000 'virtual patients' simulations respectively. The first number in the brackets in columns 2–6 indicates the number of 'virtual patients' that remained uninfected after viral challenge, whereas the second number indicates the number of patients that became infected. For example, when 600mg TDF are taken 1hour before viral challenge and patients are challenged with inoculum size one (one virus reaches a target cell environment), 1839 virtual patients remain uninfected, whereas 161 became infected. $^{+++}$

Inoculum size has a significant impact on the number of infections at the $p < 0.01$ level (χ^2-test).
(PDF)

Table S7 Statistical test of difference of prophylactic efficacy between 300 mg sd-PrEP and 600 mg sd-PrEP with TDF. The distinct fields show the p-value for a χ^2-test between the prophylactic efficacy between 300 mg and 600 mg sd-PrEP with TDF. The predicted outcome was significantly different between the two distinct dosing regimens, if the p-value is $p < 0.05$, or $p < 0.01$ respectively (yellow- and red-shaded fields).
(PDF)

Text S1 The supplementary text contains the derivation of the model for intracellular TFV-DP uptake and anabolism as well as a model evaluation.
(PDF)

Text S2 The supplementary text contains the derivation of an approximate analytical formula for the computation of the probability of infection with distinct virus inoculum sizes in relation to the concentration of TFV-DP present.
(PDF)

Acknowledgments

M.v.K acknowledges fruitful discussions with M. an der Heiden, C. Kücherer and B. Bartmeyer at the Robert-Koch-Institut Berlin.

Author Contributions

Conceived and designed the experiments: SD MvK. Performed the experiments: SD MvK. Analyzed the data: SD CS MvK. Wrote the paper: MvK.

References

1. Chapman T, McGavin J, Noble S (2003) Tenofovir disoproxil fumarate. Drugs 63: 1597–1608.
2. National Institute of Health (NIH). Current HIV treatment guidelines: Available: http://www.aidsinfo.nih.gov/guidelines/. Accessed: 27 Feb 2012).
3. Anderson PL, Kiser JJ, Gardner EM, Rower JE, Meditz A, et al. (2011) Pharmacological considerations for tenofovir and emtricitabine to prevent HIV infection. J Antimicrob Chemother 66: 240–250.
4. Naesens L, Balzarini J, Bischofberger N, Clercq ED (1996) Antiretroviral activity and pharmacokinetics in mice of oral bis(pivaloyloxymethyl)-9-(2- phosphonylmethoxyethyl)adenine, the bis(pivaloyloxymethyl) ester prodrug of 9-(2-phosphonylmethoxyethyl)adenine. Antimicrob Agents Chemother 40: 22–28.
5. Kearney BP, Flaherty JF, Shah J (2004) Tenofovir disoproxil fumarate: clinical pharmacology and pharmacokinetics. Clin Pharmacokinet 43: 595–612.
6. von Kleist M, Metzner P, Marquet R, Schütte C (2012) Polymerase inhibition by nucleoside analogs: Cellular- and kinetic parameters of efficacy, susceptibility and resistance selection. Plos Comput Biol 8: e1002359.
7. Droste JAH, van Wissen CPWGMV, Kearney BP, Buffels R, Vanhorssen PJ, et al. (2005) Pharmacokinetic study of tenofovir disoproxil fumarate combined with rifampin in healthy volunteers. Antimicrob Agents Chemother 49: 680–684.
8. Blum MR, Chittick GE, Begley JA, Zong J (2007) Steady-state pharmacokinetics of emtricitabine and tenofovir disoproxil fumarate administered alone and in combination in healthy volunteers. J Clin Pharmacol 47: 751–759.
9. Chittick GE, Zong J, Blum MR, Sorbel JJ, Begley JA, et al. (2006) Pharmacokinetics of tenofovir disoproxil fumarate and ritonavir-boosted saquinavir mesylate administered alone or in combination at steady state. Antimicrob Agents Chemother 50: 1304–1310.
10. Jullien V, Téluyer JM, Rey E, Jaffray P, Krivine A, et al. (2005) Population pharmacokinetics of tenofovir in human immunodeficiency virus-infected patients taking highly active antiretroviral therapy. Antimicrob Agents Chemother 49: 3361–3366.
11. Hawkins T, Veikley W, Claire RLS, Guyer B, Clark N, et al. (2005) Intracellular pharmacokinetics of tenofovir diphosphate, carbovir triphosphate, and lamivudine triphosphate in patients receiving triple-nucleoside regimens. J Acquir Immune Defic Syndr 39: 406–411.
12. Barditch-Crovo P, Deeks SG, Collier A, Safrin S, Coakley DF, et al. (2001) Phase I/II trial of the pharmacokinetics, safety, and antiretroviral activity of tenofovir disoproxil fumarate in human immunodeficiency virus-infected adults. Antimicrob Agents Chemother 45: 2733–2739.
13. Hirt D, Ekouvi DK, Pruvost A, Urien S, Arriv E, et al. (2011) Plasma and intracellular tenofovir pharmacokinetics in the neonate (anrs 12109 trial, step 2). Antimicrob Agents Chemother 55: 2961–2967.
14. Baheti G, Kiser JJ, Havens PL, Fletcher CV (2011) Plasma and intracellular population pharmacokinetic analysis of tenofovir in HIV-1 infected patients. Antimicrob Agents Chemother.
15. von Kleist M, Huisinga W (2009) Pharmacokinetic-pharmacodynamic relationship of NRTIs and its connection to viral escape: an example based on zidovudine. Eur J Pharm Sci 36: 532–543.
16. Sharma PL, Nurpeisov V, Hernandez-Santiago B, Beltran T, Schinazi RF (2004) Nucleoside inhibitors of human immunodeficiency virus type 1 reverse transcriptase. Curr Top Med Chem 4: 895–919.
17. Hurwitz SJ, Asif G, Schinazi RF (2007) Development of a population simulation model for HIV monotherapy virological outcomes using lamivudine. Antivir Chem Chemother 18: 329–341.
18. Garca-Lerma JG, Paxton L, Kilmarx PH, Heneine W (2010) Oral pre-exposure prophylaxis for HIV prevention. Trends Pharmacol Sci 31: 74–81.
19. [No authors listed] (2011) Early end for FEM-PrEP HIV prevention trial. AIDS Patient Care STDS 25: 383.
20. Grant RM, Lama JR, Anderson PL, McMahan V, Liu AY, et al. (2010) Pre-exposure chemoprophylaxis for HIV prevention in men who have sex with men. N Engl J Med 363: 2587–2599.
21. University of Washington (2011). Pivotal study finds that HIV medications are highly effective as prophylaxis against HIV infection in men and women in africa.
22. Centers for Disease Control and Prevention (CDC) (2011). CDC trial and another major study find PrEP can reduce risk of HIV infection among heterosexuals.
23. Hayden EC (2011) HIV drug-prevention strategy carries risks. Nature 476: 260–261.
24. Van Damme L, Corneli A, Ahmed K, Agot K, Lombaard J, et al. (2012) The FEMPrEP trial of emtricitabine/tenofovir disoproxil fumarate (truvada) among African women. In: The 19th Conference on Retroviruses and Oportunistic Infections, Abstract 32LB, March 5–8.
25. Chapman EH, Kurec AS, Davey FR (1981) Cell volumes of normal and malignant mononuclear cells. J Clin Pathol 34: 1083–1090.
26. Bisset LR, Lung TL, Kaelin M, Ludwig E, Dubs RW (2004) Reference values for peripheral blood lymphocyte phenotypes applicable to the healthy adult population in switzerland. Eur J Haematol 72: 203–212.
27. Bonate PL (2006) Pharmacokinetic-Pharmacodynamic Modeling and Simulation. Springer.
28. Gagnieu MC, Barkil ME, Livrozet JM, Cotte L, Miailhes P, et al. (2008) Population pharmacokinetics of tenofovir in AIDS patients. J Clin Pharmacol 48: 1282–1288.
29. von Kleist M, Menz S, Huisinga W (2010) Drug-class specific impact of antivirals on the reproductive capacity of HIV. PLoS Comput Biol 6: e1000720.
30. von Kleist M, Menz S, Stocker H, Arasteh K, Schütte C, et al. (2011) HIV quasispecies dynamics during pro-active treatment switching: impact on multi-drug resistance and resistance archiving in latent reservoirs. PLoS One 6: e18204.
31. Zhou Y, Zhang H, Siliciano JD, Siliciano RF (2005) Kinetics of human immunodeficiency virus type 1 decay following entry into resting CD4+ T cells. J Virol 79: 2199–2210.
32. Shen L, Peterson S, Sedaghat AR, McMahon MA, Callender M, et al. (2008) Doseresponse curve slope sets class-specific limits on inhibitory potential of anti-HIV drugs. Nat Med 14: 762–766.
33. Baggaley RF, White RG, Boily MC (2010) Infectiousness of HIV-infected homosexual men in the era of highly active antiretroviral therapy. AIDS 24: 2418–2420.
34. Royce RA, Sea A, Cates W, Cohen MS (1997) Sexual transmission of HIV. N Engl J Med 336: 1072–1078.
35. Keele BF, Giorgi EE, Salazar-Gonzalez JF, Decker JM, Pham KT, et al. (2008) Identification and characterization of transmitted and early founder virus envelopes in primary HIV-1 infection. Proc Natl Acad Sci U S A 105: 7552–7557.
36. Salazar-Gonzalez JF, Bailes E, Pham KT, Salazar MG, Guffey MB, et al. (2008) Deciphering human immunodeficiency virus type 1 transmission and early envelope diversification by single-genome amplification and sequencing. J Virol 82: 3952–3970.
37. Frank M, von Kleist M, Kunz A, Harms G, Schütte C, et al. (2011) Quantifying the impact of nevirapine-based prophylaxis strategies to prevent mother-to-child transmission of HIV-1: a combined pharmacokinetic, pharmacodynamic, and viral dynamic analysis to predict clinical outcomes. Antimicrob Agents Chemother 55: 5529–5540.
38. Mayer KH, Mimiaga MJ, Gelman M, Grasso C (2012) Raltegravir, tenofovir df, and emtricitabine for post-exposure prophylaxis to prevent the sexual transmission of HIV: Safety, tolerability and adherence. J Acquir Immune Defic Syndr .

39. Tosini W, Muller P, Prazuck T, Benabdelmoumen G, Peyrouse E, et al. (2010) Tolerability of HIV postexposure prophylaxis with tenofovir/emtricitabine and lopinavir/ritonavir tablet formulation. AIDS 24: 2375–2380.
40. Winston A, McAllister J, Amin J, Cooper DA, Carr A (2005) The use of a triple nucleoside-nucleotide regimen for nonoccupational HIV post-exposure prophylaxis. HIV Med 6: 191–197.
41. Otten RA, Smith DK, Adams DR, Pullium JK, Jackson E, et al. (2000) Efficacy of postexposure prophylaxis after intravaginal exposure of pig-tailed macaques to a human-derived retrovirus (human immunodeficiency virus type 2). J Virol 74: 9771–9775.
42. Tsai CC, Emau P, Follis KE, Beck TW, Benveniste RE, et al. (1998) Effectiveness of postinoculation (r)-9-(2-phosphonylmethoxypropyl) adenine treatment for prevention of persistent simian immunodeficiency virus sivmne infection depends critically on timing of initiation and duration of treatment. J Virol 72: 4265–4273.
43. Lifson JD, Piatak M, Cline AN, Rossio JL, Purcell J, et al. (2003) Transient early post-inoculation anti-retroviral treatment facilitates controlled infection with sparing of CD4+ T cells in gut-associated lymphoid tissues in SIVmac239-infected rhesus macaques, but not resistance to rechallenge. J Med Primatol 32: 201–210.
44. Benaboud S, Hirt D, Launay O, Pannier E, Firtion G, et al. (2012) Pregnancy-related effects on tenofovir pharmacokinetics: a population study with 186 women. Antimicrob Agents Chemother 56: 857–862.
45. Bouazza N, Urien S, Hirt D, Frange P, Rey E, et al. (2011) Population pharmacokinetics of tenofovir in HIV-1-infected pediatric patients. J Acquir Immune Defic Syndr 58: 283–288.
46. Hurwitz SJ, Asif G, Kivel NM, Schinazi RF (2008) Development of an optimized dose for coformulation of zidovudine with drugs that select for the K65R mutation using a population pharmacokinetic and enzyme kinetic simulation model. Antimicrob Agents Chemother 52: 4241–4250.
47. Piliero PJ (2004) Pharmacokinetic properties of nucleoside/nucleotide reverse transcriptase inhibitors. J Acquir Immune Defic Syndr 37 Suppl 1: S2–S12.
48. Peter K, Gambertoglio JG (1998) Intracellular phosphorylation of zidovudine (ZDV) and other nucleoside reverse transcriptase inhibitors (RTI) used for human immunodeficiency virus (HIV) infection. Pharm Res 15: 819–825.
49. Pruvost A, Negredo E, Benech H, Theodoro F, Puig J, et al. (2005) Measurement of intracellular didanosine and tenofovir phosphorylated metabolites and possible interaction of the two drugs in human immunodeficiency virus-infected patients. Antimicrob Agents Chemother 49: 1907–1914.
50. Pruvost A, Negredo E, Théodoro F, Puig J, Levi M, et al. (2009) Pilot pharmacokinetic study of human immunodeficiency virus-infected patients receiving tenofovir disoproxil fumarate (TDF): investigation of systemic and intracellular interactions between TDF and abacavir, lamivudine, or lopinavir-ritonavir. Antimicrob Agents Chemother 53: 1937–1943.
51. Patterson KB, Prince HA, Kraft E, Jenkins AJ, Shaheen NJ, et al. (2011) Penetration of tenofovir and emtricitabine in mucosal tissues: implications for prevention of hiv-1 transmission. Sci Transl Med 3: 112re4.
52. Donnell D, Baeten J, Hendrix C, Bumpus N, Bangsberg D, et al. (2012) Tenofovir disoproxil fumarate drug levels indicate PrEP use is strongly correlated with HIV-1 protective effects: Kenya and uganda. In: The 19th Conference on Retroviruses and Oportunistic Infections, Abstract 30, March 5–8.
53. Cohen J (2012) Aids research. FDA panel recommends anti-hiv drug for prevention. Science 336: 792.
54. Emau P, Jiang Y, Agy MB, Tian B, Bekele G, et al. (2006) Post-exposure prophylaxis for SIV revisited: animal model for HIV prevention. AIDS Res Ther 3: 29.
55. Haase AT (2010) Targeting early infection to prevent HIV-1 mucosal transmission. Nature 464: 217–223.
56. Pudney J, Quayle AJ, Anderson DJ (2005) Immunological microenvironments in the human vagina and cervix: mediators of cellular immunity are concentrated in the cervical transformation zone. Biol Reprod 73: 1253–1263.
57. Bobardt MD, Chatterji U, Selvarajah S, der Schueren BV, David G, et al. (2007) Cell-free human immunodeficiency virus type 1 transcytosis through primary genital epithelial cells. J Virol 81: 395–405.
58. Wu L (2008) Biology of HIV mucosal transmission. Curr Opin HIV AIDS 3: 534–540.
59. Morrow G, Vachot L, Vagenas P, Robbiani M (2008) Current concepts of HIV transmission. Curr Infect Dis Rep 10: 133–139.
60. Galvin SR, Cohen MS (2004) The role of sexually transmitted diseases in HIV transmission. Nat Rev Microbiol 2: 33–42.
61. Hallett TB, Baeten JM, Heffron R, Barnabas R, de Bruyn G, et al. (2011) Optimal uses of antiretrovirals for prevention in HIV-1 serodiscordant heterosexual couples in south africa: a modelling study. PLoS Med 8: e1001123.
62. Cohen MS, Chen YQ, McCauley M, Gamble T, Hosseinipour MC, et al. (2011) Prevention of HIV-1 infection with early antiretroviral therapy. N Engl J Med 365: 493–505.
63. Garca-Lerma JG, Aung W, er Cong M, Zheng Q, Youngpairoj AS, et al. (2011) Natural substrate concentrations can modulate the prophylactic efficacy of nucleotide HIV reverse transcriptase inhibitors. J Virol 85: 6610–6617.
64. Karim QA, Karim SSA, Frohlich JA, Grobler AC, Baxter C, et al. (2010) Effectiveness and safety of tenofovir gel, an antiretroviral microbicide, for the prevention of HIV infection in women. Science 329: 1168–1174.
65. Dobard C, Sharma S, Martin A, Pau CP, Holder A, et al. (2012) Durable protection from vaginal simian-human immunodeficiency virus infection in macaques by tenofovir gel and its relationship to drug levels in tissue. J Virol 86: 718–725.
66. Schwartz JL, Rountree W, Kashuba ADM, Brache V, Creinin MD, et al. (2011) A multi-compartment, single and multiple dose pharmacokinetic study of the vaginal candidate microbicide 1% tenofovir gel. PLoS One 6: e25974.
67. Katz DF, Gao Y, Kang M (2011) Using modeling to help understand vaginal microbicide functionality and create better products. Drug Deliv Transl Res 1: 256–276.
68. Durand-Gasselin L, Silva DD, Benech H, Pruvost A, Grassi J (2007) Evidence and possible consequences of the phosphorylation of nucleoside reverse transcriptase inhibitors in human red blood cells. Antimicrob Agents Chemother 51: 2105–2111.
69. Markowitz M, Louie M, Hurley A, Sun E, Mascio MD, et al. (2003) A novel antiviral intervention results in more accurate assessment of human immunodeficiency virus type 1 replication dynamics and T-cell decay in vivo. J Virol 77: 5037–5038.
70. Ramratnam B, Bonhoeffer S, Binley J, Hurley A, Zhang L, et al. (1999) Rapid production and clearance of HIV-1 and hepatitis C virus assessed by large volume plasma apheresis. Lancet 354: 1782–1785.
71. Tan WY, Wu H (1998) Stochastic modeling of the dynamics of CD4+ T-cell infection by HIV and some monte carlo studies. Math Biosci 147: 173–205.
72. Tuckwell HC, Shipman PD, Perelson AS (2008) The probability of HIV infection in a new host and its reduction with microbicides. Math Biosci 214: 81–86.
73. Wei X, Ghosh SK, Taylor ME, Johnson VA, Emini EA, et al. (1995) Viral dynamics in human immunodeficiency virus type 1 infection. Nature 373: 117–122.
74. Sedaghat AR, Siliciano RF, Wilke CO (2009) Constraints on the dominant mechanism for HIV viral dynamics in patients on raltegravir. Antivir Ther 14: 263–271.
75. Koelsch KK, Liu L, Haubrich R, May S, Havlir D, et al. (2008) Dynamics of total, linear nonintegrated, and integrated HIV-1 DNA in vivo and in vitro. J Infect Dis 197: 411–419.
76. Sedaghat AR, Dinoso JB, Shen L, Wilke CO, Siliciano RF (2008) Decay dynamics of HIV-1 depend on the inhibited stages of the viral life cycle. Proc Natl Acad Sci U S A 105: 4832–4837.

Citation: CPT Pharmacometrics Syst. Pharmacol. (2016) 5, 377–387; doi:10.1002/psp4.12095

https://doi.org/10.1002/psp4.12095

ORIGINAL ARTICLE

Multiscale Systems-Pharmacology Pipeline to Assess the Prophylactic Efficacy of NRTIs Against HIV-1

S Duwal[1]*, V Sunkara[1,2] and M von Kleist[1]*

While HIV-1 continues to spread, the use of antivirals in preexposure prophylaxis (PrEP) has recently been suggested. Here we present a modular systems pharmacology modeling pipeline, predicting PrEP efficacy of nucleotide reverse transcriptase inhibitors (NRTIs) at the scale of reverse transcription, target-cell, and systemic infection and after repeated viral exposures, akin to clinical trials. We use this pipeline to benchmark the prophylactic efficacy of all currently approved NRTIs in wildtype and mutant viruses. By integrating pharmacokinetic models, we find that intracellular tenofovir-diphosphate builds up too slowly to halt infection when taken "on demand" and that lamivudine may substitute emtricitabine in PrEP combinations. Lastly, we delineate factors confounding clinical PrEP efficacy estimates and provide a method to overcome these. The presented framework is useful to screen and optimize PrEP candidates and strategies and to understand their clinical efficacy by integrating the diverse scales which determine PrEP efficacy.

CPT Pharmacometrics Syst. Pharmacol. (2016) **5**, 377–387; doi:10.1002/psp4.12095; published online 21 July 2016.

Study Highlights

WHAT IS THE CURRENT KNOWLEDGE ON THE TOPIC?

☑ Preexposure prophylaxis using tenofovir, with or without emtricitabine, may reduce HIV infection.

• WHAT QUESTION DID THIS STUDY ADDRESS?

☑ How do molecular parameters, pharmacokinetics, virus dynamics, mode of transmission, transmitter virus loads, and risk behavior influence PrEP-efficacy endpoints against wildtype and resistant viruses? Are other NRTIs suitable?

• WHAT THIS STUDY ADDS TO OUR KNOWLEDGE

☑ We present a modular systems pharmacology modeling pipeline for NRTIs, predicting their effect at the scale of reverse transcription ε, target-cell infection η, and PrEP efficacy after a single ψ and repeated viral exposure ω_T. Novel aspects include the mechanistic multiscale integration of these efficacy endpoints, novel infection, and exposure models (modules III–IV) and the ability to simulate clinical trials (module V).

• HOW MIGHT THIS CHANGE DRUG DISCOVERY, DEVELOPMENT, AND/OR THERAPEUTICS

☑ PK-PD studies for PrEP are unethical, leaving a knowledge gap when designing phase III studies. Our framework provides guidance by identifying pharmacological requirements for PrEP candidates and strategies and may help planning and evaluating clinical trials.

Despite intensive research, HIV cannot be cured to date,[1] necessitating life-long treatment of infected individuals to contain the virus and prevent immunodeficiency. At the same time the HIV epidemic continues to spread, with ~2.1 million new infections in 2014.[2] While an effective vaccine remains to be developed[3] a current way forward lies in the repurposing of existing antiviral drugs to prevent transmission, or to develop novel compounds for that purpose.[4] Two strategies have been proposed in this context:

1. Treatment-as-prevention (TasP) involves therapy initiation shortly after infection.[5] As a consequence, the treated individuals' virus load decreases, which also decreases the contagiousness originating from this individual.[6,7] A recent study,[8] however, indicates that onwards transmission may occur very soon after infection, when individuals are unaware of their serologic status and consequently have not yet initiated TasP, which potentially limits its epidemiologic impact.
2. Preexposure prophylaxis (PrEP) involves antiviral drug administration to uninfected individuals at risk of acquiring HIV infection.[9] Early studies have investigated chronic administration of the nucleoside reverse transcriptase inhibitors (NRTI) tenofovir disoproxil fumarate (TDF) alone or in combination with emtricitabine (FTC), with variable outcomes.[10] Recent studies also investigated PrEP "on demand," i.e., PrEP administered shortly before or around viral exposure.[23]

The goal of this work is to develop an integrated mechanistic modeling pipeline to determine PrEP efficacy of NRTIs, integrating pharmacokinetics (PK) and pharmacodynamics (PD), as well as parameters related to the mode and timing of viral challenge. The pipeline has a building block structure and different parts can be used to assess the PrEP efficacy of other drug classes as well.

NRTIs are administered as prodrugs, which are taken up by target cells and successively phosphorylated by cellular kinases. Their tri-phosphorylated moieties compete with endogenous nucleotides for incorporation into nascent proviral DNA during reverse transcription,[12] effectively halting the process and thus preventing target cell infection. The

[1]Department of Mathematics & Computer Science, Freie Universität Berlin, Berlin, Germany; [2]Konrad-Zuse-Institut für Informationstechnik, Berlin, Germany. *Correspondence to: S Duwal (sulav@zedat.fu-berlin.de) or M von Kleist (max.kleist@fu-berlin.de)
Received 29 April 2016; accepted 20 June 2016; published online on 21 July 2016. doi:10.1002/psp4.12095

uptake and intracellular activation of these compounds causes an asynchrony between plasma prodrug concentrations and the concentrations of the active (triphosphorylated) moiety at the target-site, so that prodrug plasma pharmacokinetics poorly predicts their efficacy.[13] Moreover, due to the competitive mode of inhibition, NRTI efficacy can be target-cell-dependent.[14,15] While only some of these issues are addressed by most modeling efforts,[11,16] we have recently developed and validated a molecular mechanism of action (MMOA) model[17] for this inhibitor class, allowing to determine the compounds' effect on reverse transcription ε and target cell infection η. Moreover, we developed pharmacokinetic models linking prodrug administration with effect-site concentrations for the NRTIs TDF,[18] FTC and 3TC.[17] In this work, we link the MMOA model with pharmacokinetic models, which allows exploring the impact of pharmacokinetic attributes, as well as pharmacodynamic parameters, including drug resistance, on drug efficacy. We will then take this approach one step further, by extending the framework to assess the inhibitors' potential for repurposing as PrEP compounds, estimating the compounds' effect on preventing systemic infection ψ after a single exposure with n viruses. The latter allows assessing different PrEP schemes (e.g., chronic administration vs. "on demand"). In a last step, to assess the epidemiologic impact of these compounds, we derive a statistical model linking transmitter virology with virus exposure in the individual at risk for different modes of transmission. We then estimate the long-term efficacy of PrEP ω_T after repeated viral challenges, akin to a clinical study. The final framework is readily integrable into epidemiologic models aiming to assess PrEP or TasP or both. All intermediate steps of this pipeline have been validated with available data.

METHODS

Pharmacokinetics

We will use previously developed models for TDF, FTC, and 3TC, which link oral prodrug application with intracellular tri-phosphate pharmacokinetics.[17,18] In brief, the plasma pharmacokinetics of their dominant circulating forms (tenofovir (TFV), FTC, and 3TC) are best described by a two-compartment model with first-order absorption. Intracellular uptake and phosphorylation was described by Michaelis-Menten-type saturable kinetics and elimination was modeled by first-order kinetics. Details and parameterizations can be found in **Supplementary Note 1**.

We chose to predict average patients' pharmacokinetic profiles, but extensions to virtual patient populations from Pop-PK models are straightforward. For the modeled NRTI combinations, we assume no pharmacokinetic interaction at the level of intracellularly active NRTI-triphosphates (NRTI-TP), but extensions are possible.[19]

Molecular mechanism of action

We will utilize a previously developed[15] and validated[17] MMOA model for NRTIs, which explicitly considers reverse transcriptase (RT)-mediated polymerization of nascent viral DNA. NRTI-TPs interfere with polymerization by competing with endogenous nucleotides for incorporation into viral DNA. For as long as they are integrated in the primer, they halt the RT process, which allows the cell to eliminate crucial viral components intracellularly, reducing the virus' chance to infect the cell by integrating its proviral DNA. The MMOA model takes *in vitro* measurable microkinetic parameters as input (binding affinity, maximum catalytic rate, excision efficacy) and computes the inhibition of reverse transcription ε. This measure is subsequently converted into inhibition of target-cell infection η following a challenge by a single virus, with corresponding IC_{50}. The MMOA model, including its parametrization is exemplified in **Supplementary Note 2**.

For NRTI combinations, we assume that the presence of one NRTIs does not affect the microkinetic parameters of the respective other NRTI. The MMOA model readily allows assessing combinatorial effects and this is outlined in **Supplementary Note 2**.

Probability of infection after challenge with *n* viruses

After virus exposure during, e.g., intercourse, viruses need to overcome several physiological barriers to reach a target-cell environment. Assuming n viruses reach an immediate target-cell environment, the probability of infection is given by:

$$P(\text{inf}|V_0=n)=1-(1-P(\text{inf}|V_0=1))^n, \text{ (assuming statistical independence)} \quad (1)$$

where $P(\text{inf}|V_0=1)$ and $P(\text{inf}|V_0=n)$ are the probabilities of establishing infection if 1 or $n=0,\ldots,\infty$ virus(es) reach a target-cell environment, respectively. Thus, 1) the number of viruses reaching a target-cell environment n (next section) and 2) the infection probability given a single virus (this section) need to be appropriately modeled.

Typically, HIV produces $\approx$1,000 daughter viruses for each virus completing its replication cycle, making its subsequent extinction unlikely. Consequently, for all cases considered here the probability of the virus completing its first replication cycle provides a good approximation for the probability of establishing infection (see Discussion for limitation). To compute the infection probability, we used two different mathematical approaches, based on the chemical master equation (CME), and a branching process, which delivers an analytical solution of the CME for $t \to \infty$.

The CME can be directly derived from an established viral dynamics model[25] and is detailed in **Supplementary Note 3**. The probability of target-cell infection in the presence of NRTIs η is an integral part of this CME, providing a link to the MMOA model.

We used the CME, whenever the effect of NRTIs change on the time-scale of interest, i.e., to simulate the effect of NRTIs shortly after initiation of prophylaxis ("PrEP on demand"). When the concentrations of NRTI-TPs are almost constant over time (e.g., "chronic administration") the branching process is sufficient.

PrEP efficacy

The efficacy of PrEP φ, defined as the reduction of infection *per challenge* with $i=1,\cdots,\infty$ viruses (e.g., after coitus with an infected individual) is then readily computed by:

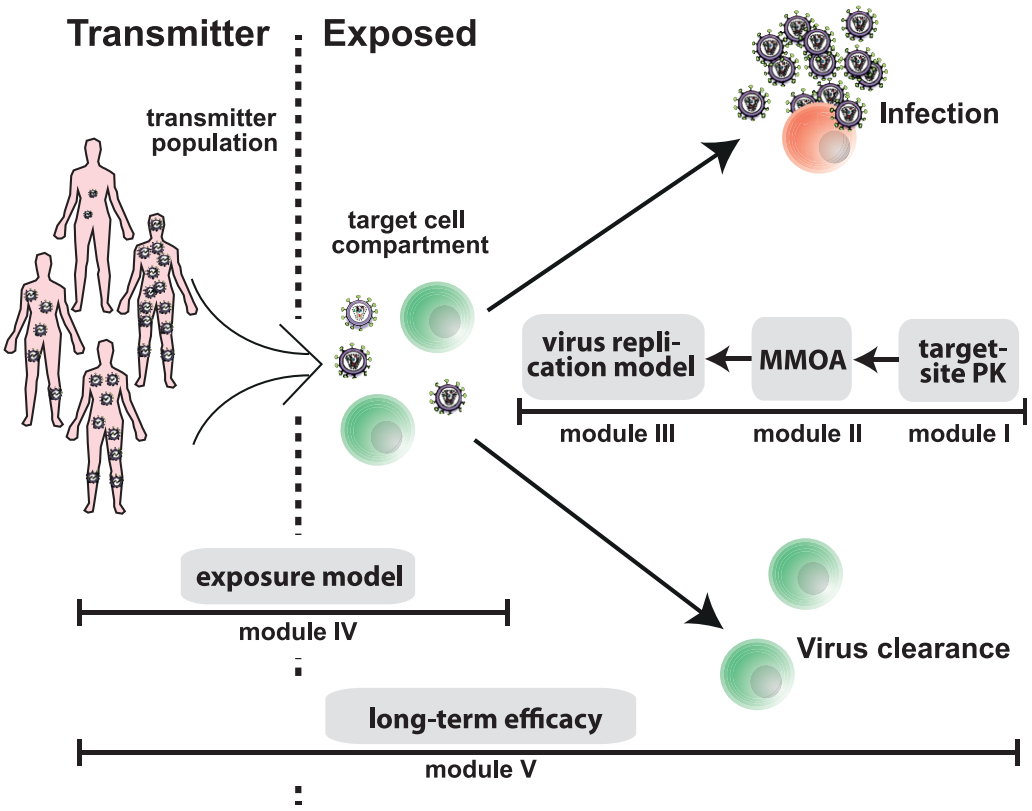

Figure 1 Modular modeling framework. The virus replication model (module III) can be used to compute the probability of infection of an exposed person after viral challenge, given a particular drug inhibition (input from module II) and viral exposure (input from module IV). Model details are elaborated in **Supplementary Note 3**. Module IV represents a statistical model of the relation between the viral load in a transmitter, the mode of transmission (e.g., homosexual contact) and the number of viruses entering a target cell compartment in the exposed person. It is derived in **Supplementary Note 4**, where the parametrization is also given. The mechanisms of action model (MMOA) provides the link between intracellular NRTI-TP concentrations, target process inhibition ε (reverse transcriptase-mediated polymerization), and inhibition of target cell infection η. It can be used to quantify effects of all currently approved NRTIs and NRTI combinations, including inhibition of mutant viruses; see **Supplementary Note 2** for details and model parameters. Pharmacokinetic models (module I), which establish the link between prodrug administration and intracellularly active NRTI-TPs have been developed for TDF, FTC, and 3TC and allow to evaluate different PrEP strategies (e.g., dosing regimen), related to these compounds (summarized in **Supplementary Note 1**). Finally, module V can be used to assess the efficacy of PrEP strategies in preventing infection after multiple viral challenges ω_T, akin to clinical trials (see **Supplementary Note 5** for derivations).

$$\varphi = 1 - \frac{P_S(\text{inf}|V_0 = i)}{P_\varnothing(\text{inf}|V_0 = i)} \quad . \tag{2}$$

Here, $P_S(\text{inf}|V_0 = i)$ and $P_\varnothing(\text{inf}|V_0 = i)$ denote the infection probabilities after exposure to $i = 1, \ldots, \infty$ viruses when a PrEP strategy S was applied vs. PrEP was not applied $\varnothing$. The PrEP efficacy per typical exposure ψ is then defined by:

$$\psi = 1 - \sum_{i=1}^{\infty} P(V_0 = i|n > 0)(1 - \varphi) \tag{3}$$

which is $\approx (1 - \bar{P}_S(\text{inf})/\bar{P}_\varnothing(\text{inf}))$, where $\bar{P}_{S/\varnothing}(\text{inf})$ denote the infection probabilities for a *typical* exposure during coitus. In the equation above, $P(V_0 = i|n > 0) = P(V_0 = i)/(1 - P(V_0 = 0))$ is the conditional probability that $i = 1, \ldots, \infty$ viruses reach a target-site compartment after exposure (e.g., coitus) among all cases where there was an actual exposure that could have led to infection ($n > 0$ viruses reach a replication-relevant compartment). The exposure probabilities are detailed next and in **Supplementary Note 4**.

Viral exposure module

The infection probability after coitus is strongly correlated with the donor viral load.[6] This correlation is likely attributed to an increased number of transmitted viruses in high viral load donors. While there is strong evidence that only very few founder viruses establish infection,[21] the distribution of the number of transmitted viruses and its dependence on the donor viral load is unclear. Here, we propose a model to bridge the donor viral load with the distribution of transmitted viruses in the recipient.

We assume that the number of viruses transmitted and reaching a target-cell environment n is a binomially distributed random variable, parameterized by the donor viral load. The probability of transmitting exactly n viruses to the recipient when the viral load in the donor is k is then given by:

$$P(V_0 = n|\text{VL} = k) = \binom{||k^m||}{n} \cdot r^n \cdot (1 - r)^{(||k^m|| - n)} \tag{4}$$

where m is an exponent of the viral load k, $||\cdot||$ is the next integer function, and r is the success probability.

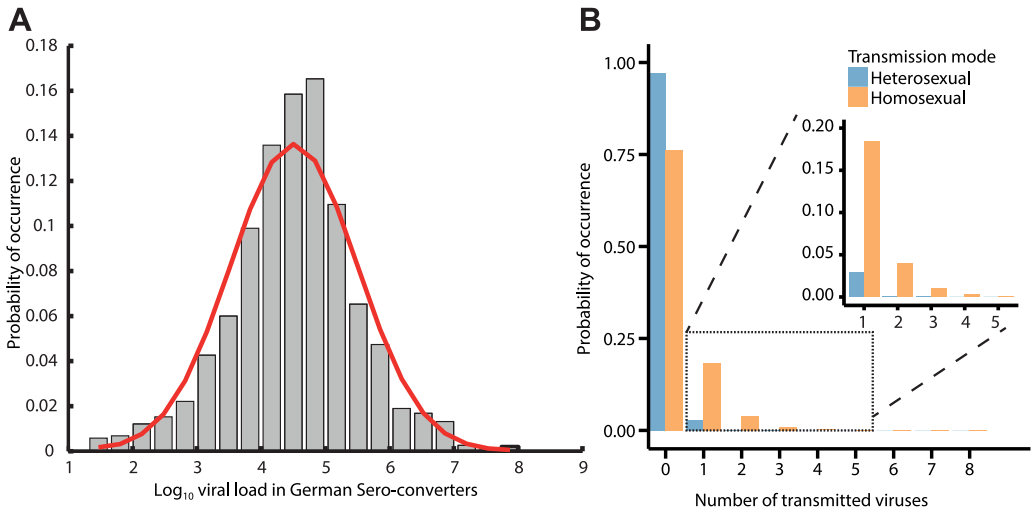

Figure 2 Virus exposure model (module IV). **a**: Virus load distribution ($\log_{10}$ scale) in a representative transmitter population (German Sero-converter study[8,27]). **b**: Estimated distribution of virus exposure in a target cell environment n following unprotected hetero- and homosexual intercourse (blue and orange bars) with an infected individual. Inset: Probability that ≥ 1 virus enters a replication-relevant compartment. Derivations are provided in **Supplementary Note 4**.

The parametrization and model derivations are outlined in **Supplementary Note 4**. From here, $P(V_0{=}n)$, can be computed (it is needed in Eq. 3), i.e., $P(V_0{=}n){=}\int_{k=0}^{\infty} P(\mathrm{VL}{=}k)\cdot P(V_0{=}n|\mathrm{VL}{=}k)$, as shown in **Figure 2**.

Efficacy against repeated viral challenges

Up to now, we assessed PrEP efficacy per exposure ψ. However, clinical trials report the ratio of incidence rates in the treated and placebo arms as a measure of efficacy[5,22–24] (see also **Supplementary Note 5** for derivations). The latter may be a consequence of an individual being repeatedly exposed, and subject to, e.g., risk behavior and trial follow-up duration making this estimate poorly comparable between trials. The relation between *average* PrEP efficacy (per challenge) ψ and clinical trial efficacy ω_T is given by:

$$(1-\omega_T)=\frac{1-\left(1-\bar{P}_{\varnothing}(\mathrm{inf})\cdot(1-\psi)\right)^{T\cdot \mathrm{N}_S}}{1-\left(1-\bar{P}_{\varnothing}(\mathrm{inf})\right)^{T\cdot \mathrm{N}_{\varnothing}}}, \qquad (5)$$

where N_S and $\mathrm{N}_{\varnothing}$ denote the number of unprotected sex acts with an infected individual in the PrEP arm S and the placebo arm $\varnothing$ per person per month, respectively, and T denotes the trial duration in months. $\bar{P}_{\varnothing}(\mathrm{inf})$ denotes the probability (frequency) of infection in the placebo arm per challenge and ω_T denotes the estimated PrEP efficacy from the incidence rates in a clinical trial of duration T.

Software

We used MatLab R2015a (MathWorks, Natick, MA; v. 8.5, including optimization and bioinformatics toolbox) and R (v. 3.1.2, Vienna, Austria) for modeling and simulation. Sample codes are provided as Online Supplementary Materials.

RESULTS

Modular modeling framework

We have constructed a modular pipeline to assess the efficacy of different NRTIs in prophylactic regimen. The pipeline (**Figure 1**) consists of five modules that can be combined, depending on the scientific question. Pharmacokinetic models (module I) for the NRTIs TDF, FTC, and 3TC, linking oral drug administration with the pharmacokinetics of the active intracellular moiety (TFV-DP, FTC-TP, and 3TC-TP), have been developed previously,[17,18] allowing to assess different dosing schedules, adherence, etc. The intracellular concentrations can be coupled to an MMOA model[15] (module II), which enables quantifying the effect of NRTIs, alone and in combination, on target cell infection η, for wildtype and mutant viruses, after exposure to a single virion as exemplified in **Supplementary Note 2**. A previously developed viral replication model[25] (module III), that has also been shown to be predictive in[17,18,26] can then be used to predict the infection probability, given an exposure to n viruses during, e.g., coitus with an infected person. The latter can be used to assess PrEP efficacy ψ *per coitus* (see Eq. 3). Module IV simulates viral exposure, depending on the transmitter viral load. The derivation of module IV and its parametrization are elaborated in **Supplementary Note 4** and the next section. Module V assesses the long-term efficacy of PrEP. That is, after repeated viral challenges, akin to a clinical trial.

Mode of transmission and viral exposure

We analyzed virus load data from the German Sero-converter cohort, which is a nationwide, multicenter, open, prospective long-term observational cohort initiated in 1997.[8,27] We restricted the analysis to untreated individuals with a known seroconversion-date and risk group ($N = 1{,}213$). We found this data source particularly relevant, since viral load data from both early as well as chronic infection is included

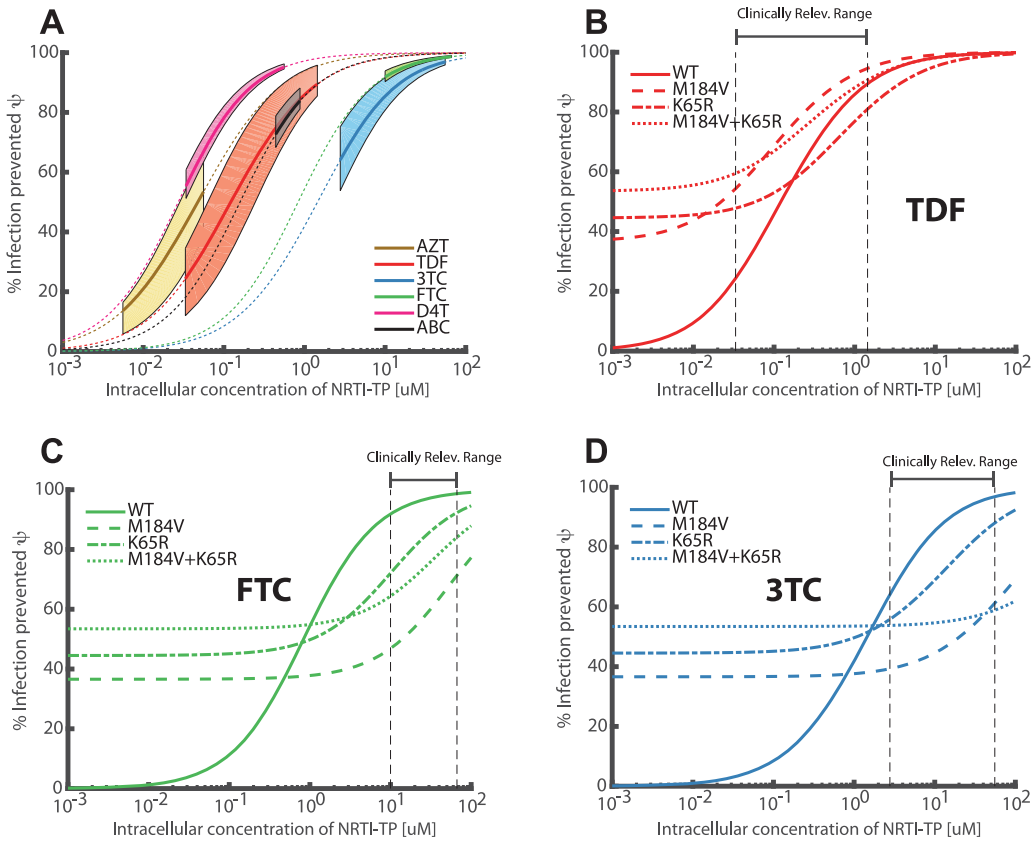

Figure 3 Target-cell NRTI-TP concentration vs. risk reduction in wildtype and mutant viruses (modules II-IV) ψ. **a**: Mean efficacies (% infections prevented) following viral exposure during a single unprotected homosexual intercourse (Eq. 3) are illustrated by the dotted lines. Solid thick lines mark the risk reduction profile at clinically relevant ranges for the respective drugs (indicated ranges only provide a rough guidance as outlined in **Supplementary Note 3**). Shaded areas indicate the corresponding IQR of the efficacy estimate, taking variability in microscopic parameters (module II) and virus exposure (module IV, **Figure 2b**) into account. **b**–**d**: Mean efficacies ψ of TDF, FTC, and 3TC against the wildtype virus are highlighted by solid lines. Efficacies against mutant viruses combine both drug effects and inherent fitness defects of the mutants. The relative reduction in infection with the mutant virus in the presence of drug vs. the wildtype virus in the absence of drugs is evaluated (dashed line: M184V, dash-dotted line: K65R, dotted line M184V/K65R double mutant), see section "Concentration vs. risk reduction in wildtype and mutant viruses" for details. Vertical black dashed lines indicate the clinically relevant drug concentrations range after chronic therapy.

(median duration of infection: 18 weeks, IQR: 3–42 weeks), acknowledging that HIV-1 onwards transmission may preferentially occur rather shortly after infection.[8] The viral load in this cohort was log-normal distributed, with mean $\mu_{\log_{10}\mathrm{VL}}=4.51$ and $\sigma=0.98$ (see **Figure 2a**), in agreement with other studies.[28]

Figure 2b shows the probability distribution of viral exposure following hetero- and homosexual intercourse, which was computed by combining data depicted in **Figure 2a** with Eq. 4. Note that in the majority of cases no virus enters a replication compartment and subsequently infection will not occur, whereas a few viruses (one to five) may be transmitted occasionally and may subsequently establish infection. This result is in line with Keele *et al.*,[21] who report that only very few founder viruses establish infection. Overall, our results indicate that viral exposure is stronger during homosexual than during heterosexual intercourse (compare blue and orange bars in **Figure 2b**).

Concentration vs. risk reduction in wildtype and mutant viruses

The MMOA model allows assessing the inhibition of target cell infection η by different NRTIs. We used this information as part of our modeling pipeline (see Methods and **Supplementary Note 3**) to assess the concentration–response (percentage of systemic infections prevented ψ, Eq. 3) for zidovudine (AZT), TDF, 3TC, FTC, stavudine (D4T), and abacavir (ABC). The profiles are shown in **Figure 3a** and allow for the first assessment of the suitability of these drugs for repurposing as PrEP compounds. For further assessment, toxicity needs to be included. Note that the solid lines and the background shading in **Figure 3a** show the expected efficacy and interquartile range at clinically relevant concentrations (see **Supplementary Note 3**). We predict that AZT can prevent 14–53% of infections at clinically relevant concentrations, followed by TDF (24–89%), D4T (55–95%), ABC (73–84%), 3TC (64–96%), and FTC (92–99%), with

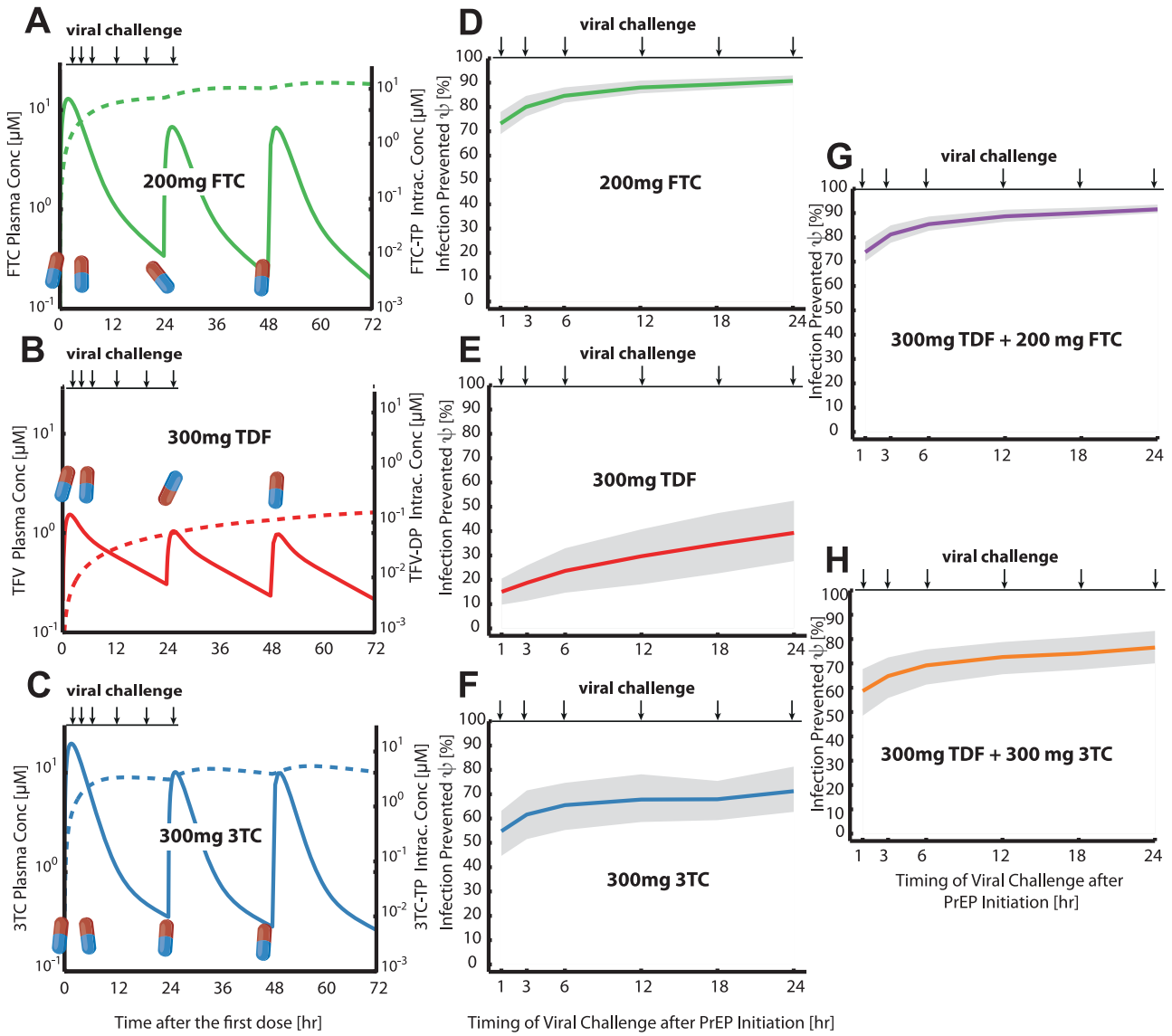

Figure 4 Efficacy ψ of PrEP "on demand" against infection following unprotected homosexual intercourse within 24hours after PrEP initiation (modules I-IV). **a–c**: Pharmacokinetic profiles during PrEP "on demand" for the circulating NRTI prodrug (solid lines) and the intracellular, active NRTI-TP moiety (dashed lines). FTC oral dose was 400 mg at 0 hours, followed by 200 mg at 24 and 48 hours (**a**), while TDF or 3TC dosage was 600 mg at 0 hours, followed by 300 mg at 24 and 48 hours, respectively. **d–e**: Infections averted for PrEP "on demand" when viral challenge occurred either 1, 3, 6, 12, 18, or 24 hours after PrEP initiation with either FTC (**d**), TDF (**e**), or 3TC (**f**). Solid lines indicate the mean % infections averted (see Eq. 3), while shaded areas indicate interquartile ranges of this estimate, taking variability in microscopic parameters (module II) and virus exposure during homosexual intercourse (module IV, **Figure 2b**) into account. **g,h**: Infections averted for combinations of TDF+FTC (**g**) and TDF+3TC (**h**), taken "on demand" (double doses at day 0, followed by single doses at days 1, 2). Combination predictions assumed that no significant pharmacokinetic interactions occur, pharmacodynamic interactions were modeled as outlined in **Supplementary Note 2**.

corresponding IC_{50} values of 0.046, 0.1, 0.025, 0.15, 1.72, and 0.82 [μM] (NRTI-TP concentrations with respect to preventing target-cell infection following exposure with a single virion (η)). We further assessed the efficacy of TDF, FTC, and 3TC in preventing infection due to transmitted drug resistance.[29] Resistance to FTC and 3TC is associated with the M184V mutation, whereas resistance to TDF is associated with the K65R mutation.[30,31] Note that inhibition of the mutant viruses can readily be assessed in the MMOA model (see **Supplementary Note 2**). Furthermore, the MMOA model allows to assess the fitness costs associated with these mutations. In line with *ex vivo* experiments,[32,33] both the M184V and K65R mutant conferred a fitness disadvantage predicted by the MMOA model. (f(mut)= 63, 55 and 46% of the wildtype fitness for M184V, K65R, and the M184V/K65R double mutant). The predicted PrEP efficacy of TDF, FTC, and 3TC against wildtype (WT) and mutant viruses (M184V, K65R, and M184V/K65R) is shown in **Figure 3b–d**. We assessed the percentage of infections prevented by

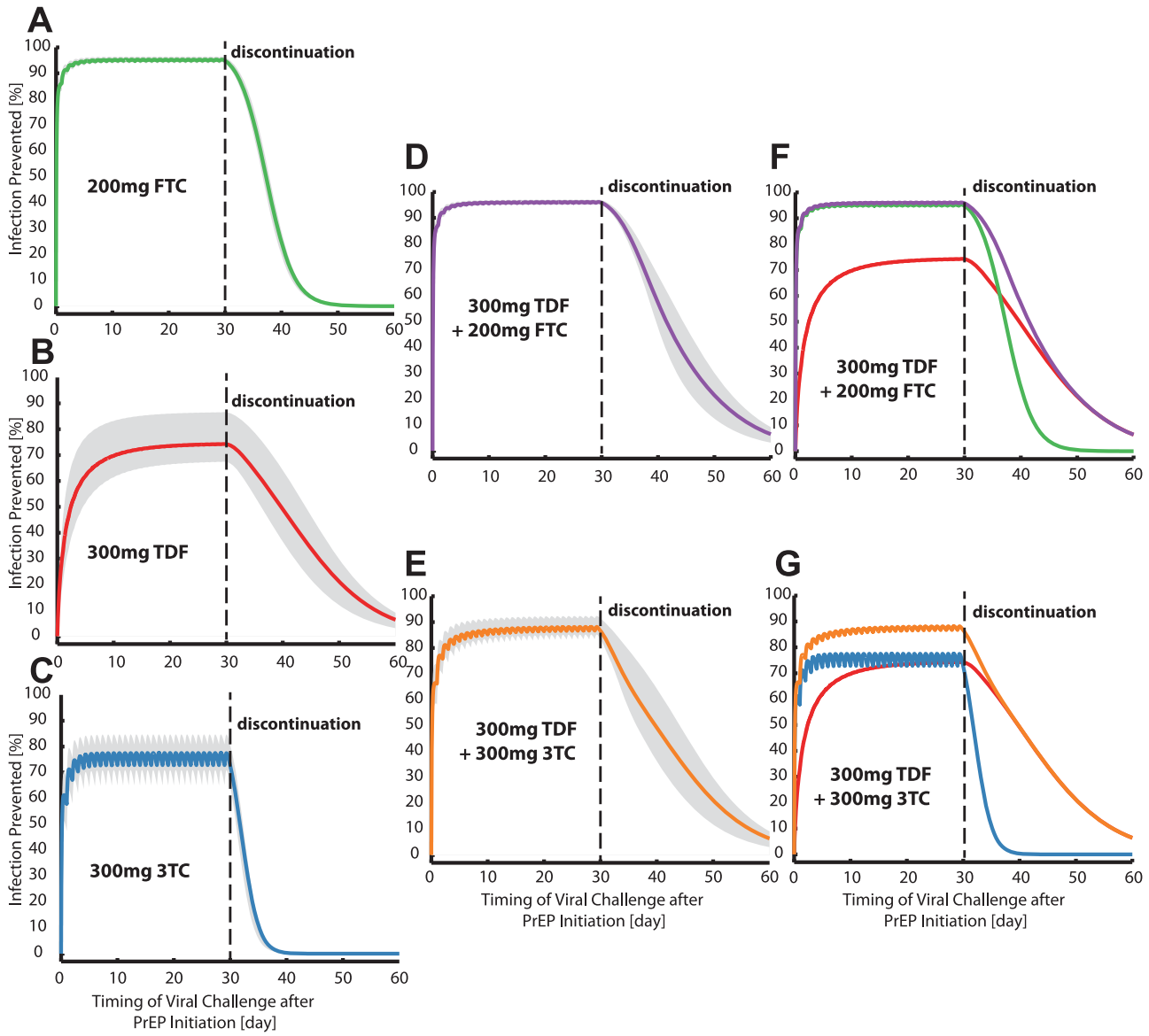

Figure 5 Risk reduction profile ψ for an unprotected homosexual intercourse occurring within 30 days of PrEP or after its discontinuation (modules I-IV). **a**–**e**: Mean risk reduction profiles (see Eq. 3) when either oral doses of 200 mg FTC (**a**), 300 mg TDF (**b**), 300 mg 3TC (**c**), 300 mg TDF+200 mg FTC (**d**), 300 mg TDF+300 mg 3TC (**e**) were administered daily for 30 days and discontinued thereafter are illustrated by solid lines. Shaded areas indicate interquartile ranges of this estimate, taking variability in microscopic parameters (module II) and virus exposure during homosexual intercourse (module IV, **Figure 2b**) into account. **f**: The mean risk reduction profile for the combination 300 mg TDF + 200 mg FTC (violet solid line) is shown together with the mean risk reduction profiles for the single drugs FTC (green) and TDF (red). **g**: The mean risk reduction profile for the combination 300 mg TDF + 300 mg 3TC (orange solid line) is shown together with the mean risk reduction profiles for the single drugs 3TC (blue) and TDF (red). Combination predictions assumed that no significant pharmacokinetic interactions occur, pharmacodynamic interactions were modeled as outlined in **Supplementary Note 2**.

prophylaxis after exposure to the mutant virus relative to the wildtype virus in the absence of drugs, i.e.:

$$\left(1-\int_{k=0}^{\infty} P(\mathrm{VL}=k)\cdot\left(\sum_{n=0}^{\infty} P(V_0=n|\mathrm{VL}=k)\cdot\frac{P_{S,\mathrm{mut}}(\mathrm{inf}\,|\,V_0=n)}{P_{\varnothing,\mathrm{wt}}(\mathrm{inf}\,|\,V_0=n)}\right)\right), \tag{6}$$

where "mut" denotes the mutant virus (M184V, K65R or M184V/K65R) and "wt" denotes the wildtype virus. Thus, both the effect of the drugs, as well as inherent fitness costs, are simultaneously evaluated, allowing to assess whether PrEP fosters the transmission of resistant viruses (this is the case whenever mutant transmission is more effective; i.e., whenever the dashed line is below the solid line in **Figure 3b–d**). The simulations show that the K65R mutation may decrease the PrEP efficacy of TDF, while the M184V-containing virus is hyper-susceptible to TDF. The M184V/K65R double mutant is almost as susceptible as

Table 1 Bias of clinical-trial efficacy estimates ω_T through risk compensation and follow-up duration

	Trial-based PrEP efficacy estimates ω_T								
	ψ = 70%			ψ = 80%			ψ = 90%		
Follow-up durations in months T	Risk compensation			Risk compensation			Risk compensation		
	0%	10%	20%	0%	10%	20%	0%	10%	20%
6	68.01	64.93	61.86	78.48	76.38	74.28	89.14	88.06	86.99
12	65.66	62.46	59.30	76.65	74.42	72.21	88.09	86.93	85.77
18	63.26	59.96	56.73	74.76	72.41	70.09	86.99	85.73	84.49
24	60.83	57.44	54.14	72.82	70.35	67.92	85.84	84.49	83.15
36	55.93	52.39	48.99	68.81	66.11	63.48	83.42	81.88	80.36

Trial-based PrEP efficacy estimates ω_T (after repeated viral challenges) for different levels of risk compensation (reported as $100 \cdot ((N_S - N_\varnothing)/N_\varnothing)$ and trial durations T were estimated using Eq. 5 (with verifications provided in **Supplementary Note 5**). The number of unprotected sex acts per month with an infected individual $N_\varnothing$ in the untreated arm was set to 1.19. The infection risk per coitus $\bar{P}(\text{inf})$ was set to 3% and the prophylactic efficacy *per coitus* ψ was set to 70, 80, and 90%, respectively.

the wildtype, but has a profound fitness deficit. In the case of FTC, both the M184V and K65R mutation, as well as the double mutant, diminish its PrEP efficacy from 92–99% (wildtype) to 72–92% (K65R) and 47–71% (M184V). In the case of 3TC, mutations K65R, M184V, and the double mutant gradually diminish its efficacy down to complete resistance (in case of the double mutant). At low drug concentrations, the fitness defect of the resistant viruses leads their reduced transmissibility (≈37–54% less likely to be transmitted than the wildtype in the absence of drugs).

Efficacy shortly after PrEP initiation

Next, we assessed the prophylactic efficacy of TDF, FTC and 3TC alone, or in combination, when initiated shortly before exposure ("on demand"), akin to the IPERGAY protocol.[23] In this protocol, individuals initiate PrEP up to 24 hours before viral exposure with a double-dose and then take two more pills on days 1 and 2. Evaluated pill sizes were 200 mg (FTC) or 300 mg (3TC or TDF). Based on previously developed PK models,[17,18] we simulated the (population-average) plasma and intracellular pharmacokinetics for TFV, FTC, and 3TC, respectively TFV-DP, FTC-TP, and 3TC-TP. As can be seen in **Figure 4a–c**, intracellular concentrations (dashed lines) quickly increase to almost steady state levels for FTC-TP and 3TC-TP after ≈6–12 hours, but not for TFV-DP, arguing that TFV-DP may not reach protective levels when applied "on demand." For an exposure occurring either 1, 3, 6, 12, 18, or 24 hours after PrEP initiation, **Figure 4d–f** shows the prophylactic efficacy ψ of the different drugs used in isolation. All tested drugs are more efficiently preventing infection, if the viral challenge occurs late with respect to PrEP initiation. Emtricitabine seems to be most efficacious, preventing 73–90% of potential infections, followed by 3TC (55–71%). Tenofovir seems to poorly prevent infection when taken "on demand," only preventing 15–40% of potential infections after virus exposure. The latter corroborates the hypothesis that protective TFV-DP levels may build up too slowly in the intracellular compartment to provide sufficient protection.[34] The efficacy of the combination 3TC+TDF was 59–77%, whereas the efficacy of the combination FTC+TDF mirrored the efficacy profile of FTC alone (74–92%, see **Figure 4g**). The observed clinical trial efficacy estimate for FTC+TDF in IPERGAY was 86%.[23] Technical details of the drug combination model are elaborated in **Supplementary Note 2**.

Efficacy after PrEP discontinuation

The prophylactic efficacy of TDF, FTC, and 3TC, alone or in combination, during chronic PrEP and after its discontinuation is assessed in **Figure 5a–e**, based on (population-average) pharmacokinetics after oral administration of 200 mg FTC or 300 mg TDF or 300 mg 3TC daily, or combinations thereof. Daily administration of FTC, TDF, and 3TC for 30 days prior to viral exposure lead to a prophylactic efficacy ψ of ≈95, 74, and 75%, respectively. After discontinuation, FTC, TDF, and 3TC remain $\geq$ 50% effective for about 7, 10, and 2 days, respectively, with the PrEP efficacy of 3TC declining most rapidly. The combination FTC+TDF and 3TC+TDF prevent ≈96% and 87% of infections, respectively, after 30 days of daily administration. Corresponding observed clinical trial estimates for high-level adherence FTC+TDF PrEP are $\omega_T = 86-100\%$[35] and 58−96%.[24] We predict that both combinations remain $\geq$ 50% effective for about 10 days after discontinuation. **Figure 5f,g** shows the efficacy of the combination, with the efficacy of the single drugs superimposed (note that the combinatorial effects are not independent, **Supplementary Note 2**). The graphic indicates that tenofovir preserves the prophylactic efficacy after discontinuation of the combination and thus makes the regimen robust to poor adherence.

Long-term efficacy (against repeated virus challenges)

Table 1 depicts the results of a simulated clinical trial with untreated/placebo and PrEP-treated arms in men who have sex with men (MSM) for different levels of risk compensation and follow-up durations (T = 6, 12, 18, 24, and 36 months). The infection probability per unprotected sex act with an uninfected individual $\bar{P}_\varnothing(\text{inf})$ was fixed to 3%.[36,37] We considered the PrEP strategy to prevent infections per challenge with probability ψ=70, 80, and 90%, respectively. For each efficacy, 0, 10, and 20% risk compensation (additional percentage of risky sex acts in the treated arm compared to the untreated/placebo arm) were assessed. The number of risky sex act per month and individual $N_\varnothing$ was set to 1.19, based on a reported value of seven risky acts[38] and assuming a prevalence of ≈17% in MSM.[39] For all cases, the clinical trial

estimated efficacy ω_T is lower than the PrEP efficacy per challenge ψ and it decreases with increasing follow-up time. The decrease is more pronounced when the PrEP efficacy per challenge ψ is low. At 36 months of follow-up, without risk compensation, the clinical trial efficacy estimate ω_T underestimated the actual PrEP efficacy per challenge ψ by 14, 11, and 7%, respectively, for $\psi = 70$, 80, and 90%. This underestimation becomes even more pronounced when risk compensation occurs.

Taken together, our simulations point to a profound limitation in estimating and comparing PrEP efficacy from incidence rates in clinical trials (as currently done): On the one hand, a clinical trial has to be long enough to provide a statistically reasonable estimate of the incidence rate (a considerable number of individuals have to become infected). On the other hand, the longer the trial, the more confounded will the efficacy estimate ω_T be in relation to the actual PrEP efficacy ψ (see **Table 1**). For this reason we provide the following formula, allowing to convert clinical efficacy estimates ω_T into unbiased PrEP efficacies per challenge ψ, which can be compared between different studies (see **Supplementary Note 5**).

$$(1-\psi) = \frac{1 - \sqrt[T\cdot NS]{\left(1-\bar{P}_{\varnothing}(\text{inf})\right)^{N_{\varnothing}\cdot T} + \omega_T - \omega_T \cdot \left(1-\bar{P}_{\varnothing}(\text{inf})\right)^{N_{\varnothing}\cdot T}}}{\bar{P}_{\varnothing}(\text{inf})}, \tag{7}$$

where the subscript S, $\varnothing$ denote the PrEP and untreated/placebo arms, respectively.

DISCUSSION

In this work, we presented a modular multiscale systems pharmacology modeling pipeline that can be assembled in a building block manner to assess the PrEP efficacy of NRTIs at various levels, ranging from target process inhibition ε, inhibition of target-cell infection η, and systemic infection ψ, and finally long-term efficacy after multiple viral challenges ω_T. The model allows a flexible integration of processes occurring on different scales: We integrated the microscale interaction between intracellularly active NRTI-TPs with RT-mediated viral DNA polymerization, with meso-, macro-, and population-scale processes, such as the pharmacokinetics, replication dynamics, viral transfer, up to the long-term infection probability after repeated virus exposure, akin to a clinical trial.

Module I (pharmacokinetics) is obviously drug-specific. We utilized previously developed models[17,18] for 3TC, FTC, and TDF. The module was used to assess the efficacy ψ of PrEP "on demand" and after its discontinuation (see **Figures 4** and **5**). We observed that TFV-DP accumulation may be too slow for PrEP "on demand," in agreement with Ref. 40, who put forward similar concerns. Our analysis also showed, in contrast to dominating views, that FTC is more effective than TDF for PrEP, owing to the fact that higher concentrations may be achieved in target cells and that effective concentrations build up faster than for TDF. On the other hand, TDF seems to be less susceptible to imperfect adherence owing to its long terminal half-life.[18] Moreover, FTC's efficacy is more profoundly reduced by drug-resistant strains.[29] The latter highlights the complementary roles of the two drugs. The Partner PrEP study[41] compared the efficacy of TDF alone vs. TDF+FTC, which is partly motivated by cost-effectiveness considerations. As previously mentioned, our analysis discourages the use of TDF alone for PrEP. In addition, we showed that the drug combination 3TC+TDF may be a cost-effective alternative to TDF+FTC.

In a previous study[42,43] PrEP efficacy was analyzed in a TDF+FTC combination and an EC_{90}=16 fmol/10^6cells ($\approx$ 0.09 μM) for TFV-DP was estimated ($EC_{50} \approx 0.01\mu$M). This estimate, however, discarded the role of FTC-TP in the analyzed PrEP combination. In the light of FTC's efficacy (see **Figures 3–5**) the previous estimate may vastly underpredict TFV-DP's actual EC_{90}. We predicted actual single-drug potencies (IC_{50}s) of 0.1 and 0.82 μM for TFV-DP and FTC-TP, respectively.

Module II (molecular mechanism of effect) allows to translate *in vitro* measurable microparameters into measures of *ex vivo* efficacy (prevention of target cell infection η). The model is applicable to all currently approved NRTIs and furthermore allows studying drug efficacy against mutant viruses and mutation-associated fitness deficits. The latter is particularly useful, since it is unethical to test PrEP in individuals exposed to drug-resistant viruses. Furthermore, coupled to modules III–V and embedded into epidemiologic models, this allows studying the effect of PrEP on drug resistance spread. We used module II in conjunction with modules III–IV to benchmark the PrEP suitability of various NRTIs. Similar approaches may be used to benchmark PrEP compounds currently under development,[4,44] i.e., nonnucleoside reverse transcriptase inhibitors (NNRTI) or integrase inhibitors, or approved drugs for repurposing, with NNRTIs possibly being cost-effective alternatives. Obviously, toxicity endpoints have to be included. Note that the MMOA model can in principle predict inhibition of mitochondrial polymerase-γ, which is frequently associated with toxicity after NRTI administration.[45] However, since uptake and anabolism of NRTI is cell-type-specific, NRTI-TP concentrations need to be determined in toxicity-relevant compartments.[46]

Motivated by the fact that NRTIs are competitive inhibitors,[14] a recent work[11] aimed to predict PrEP efficacy solely from the relation of intracellular active TDF and FTC moieties vs. endogenous nucleotide concentrations dNTP in different tissue homogenates. Because they found higher TFV-DP:dATP ratios in rectal vs. female genital tissue homogenates, they concluded that TDF is more effective in males. The inverse relation was observed for FTC, which was taken as evidence for higher efficacy in females. However, serious drawbacks of this work are the use of tissue homogenates, which may not represent HIV-1 target cells (more below) and the application of an incomplete and incorrect translational model: The assumption therein[11] is that the ratio of NRTI-TP vs. dNTP determines its effect and may thus explain different PrEP efficacy observed in males and females in clinical trials. This translation of a molecular marker to clinical efficacy lacks substantiation, given that a mechanistic model that assesses the potency at each step from its molecular effect

to its clinical efficacy is missing. Moreover, it is evidently wrong at the molecular level: Cottrell *et al.*'s interpretation would permit that two different active agent concentrations $[\text{NRTI-TP}]_1$ and $[\text{NRTI-TP}]_2$ exert the same effect as long as the ratio NRTI-TP:dNTP remains fixed. This assumption is incorrect and misleading, since the interactions of NRTIs and dNTPs with the RT-mediated polymerization process are inherently nonlinear and saturable. We strongly recommend the use of an MMOA model instead (i.e., module II) to capture all involved processes and to translate the considerations mechanistically into clinical effects. In a previous work[15] (the basis of module II), we derived a simple formula, which allows to roughly assess how the efficacy of NRTI-TPs against reverse transcription changes with dNTP concentrations

$$\tilde{\text{IC}}_{50} \approx \frac{r_{\text{exc}}}{k_{\text{term}} + r_{\text{exc}}} \cdot K_{\text{D},I}\left(1 + \frac{[\text{dNTP}]}{K_{\text{D,dNTP}}}\right). \tag{8}$$

where r_{exc} denotes the (potentially cell-specific) rate of NRTI excision, $K_{\text{D},I}$ and $K_{\text{D,dNTP}}$ denote the dissociation constants of the inhibitor and the competing endogenous substrate to their target, respectively, and k_{term} denotes the incorporation/polymerization constant for the considered NRTI-TP. When substituting realistic dNTP concentrations from HIV-1 target cells[47] and $K_{\text{D,dNTP}}$ values from **Table SN2.1** (**Supplementary Note 2**), one can easily see that the ratio $\frac{[\text{dNTP}]}{K_{\text{D,dNTP}}} \ll 1$ for deoxycytosine-triphosphate (dCTP). Thus, FTC efficacy is not increased by decreasing dCTP concentrations, in contrast to Cottrell *et al.*'s interpretations.[11] For TDF, decreasing deoxyadenosine-triphosphate (dATP) concentrations may increase its potency up to two-fold. However, differences may also arise through cell-dependent rates of excision (different amounts of excision substrates: ATP, PPi), or cell-dependent differences in NRTI-TP concentrations, all of which warrant further investigation once the cellular compartments responsible for the early steps of infection for the various routes of transmission are identified. Besides these molecular factors, different clinical PrEP outcomes in the group of women and men can arise through the magnitude of virus exposure after contact (inoculum size; compare **Figure 2b**) or through differences in adherence, trial duration, and risk compensation (compare Eq. 7). Note that the interplay between these putative factors can be assessed within the presented framework once the corresponding data are available.

Module III allows computing infection probabilities and drug efficacies ψ following viral exposure and is based on a validated model of the viral replication cycle.[25] The module assumes a "boom or bust" process (see **Supplementary Note 3**), where successful completion of the first viral replication cycle approximates the probability of infection. The latter assumption is violated whenever subsequent replication cycles cannot be neglected. Examples include prophylaxis with protease inhibitors, which reduce the number of viral progeny *after* one replication cycle. Furthermore, if very large inoculum sizes (>1,000 viruses) coincide with the application of highly efficient prophylaxis (>99%), the model assumptions may be violated.

Module IV, which estimates from the transmitter's viral load the distribution of viruses entering a target-cell compartment, is obviously not drug-specific. A noteworthy feature is that the stochastic nature of HIV-1 transmission is explicitly taken into account. To our knowledge there is currently no model making this connection and thus there is currently no model linking TasP in the transmitter population with PrEP in the exposed population at risk. To this end, the model is readily integrable into epidemiological models.

We generally assumed, akin to other studies,[42] that the concentrations of NRTI-TP in peripheral mononuclear blood cells (PBMC) serve as a good surrogate measurement for HIV target cells after different modes of transmission. While some authors state concentrations of NRTI-TP in rectal/mucosal cell homogenates,[48] these samples usually contain a large fraction of HIV insusceptible cells over which the concentrations are averaged, in contrast to PBMC consisting mainly of HIV-1 susceptible cells.[49] It is important to acknowledge that NRTI-TP concentrations are likely different in different cell types, since they are taken up by active transport and require intracellular phosphorylation. Due to experimental difficulties, only few studies have extracted actual target cells ($CD4^+$) from relevant anatomic sites and subsequently measured NRTI-TP concentrations. These studies[40] indicate that PBMC cells, $CD4^+$ cells from relevant anatomical sites and from the peripheral blood contain similar concentrations of NRTI-TP after oral administration, arguing that the use of the PBMC surrogate measurement is justifiable. However, more research is needed to quantify NRTI-TP concentrations in target cells derived from anatomical target sites. Note also that NRTI-TP measurements may depend on the sampling design and sample processing,[50] strongly arguing for standardization in NRTI-TP quantification.

The success of PrEP with TDF+FTC has delivered a proof of concept and motivated the exploration of other PrEP candidates.[4] Suitable PrEP compounds require an excellent safety profile, efficaciousness, and cost-effectiveness. Moreover, they should not contribute to the spread of drug resistance and be robust to imperfect adherence. The latter point is currently addressed by the development of long-acting injectable compounds and PrEP "on demand." The presented modular system pharmacology pipeline is a useful tool to screen and optimize suitable PrEP candidates and PrEP strategies by integrating the diverse scales which determine PrEP efficacy.

Acknowledgments. M.v.K. and S.D. acknowledge financial support from the BMBF e:Bio junior research group "Systems Pharmacology & Disease Control," grant number 031A307. V.S. acknowledges financial support through the BMBF funded research consortium PrevOP-OVERLOAD, grant number 01EC1408. The funders had no role in study design, data collection, or analysis, decision to publish, or preparation of the article.

Conflict of Interest. No conflicts of interest to declare.

Author Contributions. S.D. and M.v.K. wrote the article and designed the research. S.D., V.S., and M.v.K. performed the research and analyzed the data.

1. Chun, T.W, Moir, S. & Fauci, A.S HIV reservoirs as obstacles and opportunities for an HIV cure. *Nat. Immunol.* **16**, 584–589 (2015).
2. UNAIDS. AIDS by the Numbers 2015. <http://www.unaids.org/en/resources/documents/2015/AIDS_by_the_numbers_2015>. Accessed 31 Mar 2016. Technical report, 2015.
3. Mouquet, H. & Nussenzweig, M.C. HIV: Roadmaps to a vaccine. *Nature* **496**, 441–442 (2013).
4. Boffito, M., Jackson, A. & Asboe, D. Pharmacology lessons from chemoprophylaxis studies. *Clin. Infect. Dis.* **59**(supp. 1), S52–S54 (2014).
5. Cohen, M.S. *et al.* Prevention of HIV-1 infection with early antiretroviral therapy. *N. Engl. J. Med.* **365**, 493–505 (2011).
6. Attia, S., Egger, M., Müller, M., Zwahlen, M. & Low, N. Sexual transmission of HIV according to viral load and antiretroviral therapy: systematic review and meta-analysis. *AIDS* **23**, 1397–1404 (2009).
7. Duwal, S., Winkelmann, S., Schütte, C. & von Kleist, M. Optimal treatment strategies in the context of 'treatment for prevention' against HIV-1 in resource-poor settings. *PLoS Comput. Biol.* **11**, e1004200 (2015).
8. Yousef, K.P. *et al.* Inferring HIV-1 transmission dynamics in Germany from recently transmitted viruses. *J. Acquir. Immune. Defic. Syndr.*, accepted, 2016.
9. Grant, R.M. *et al.* Preexposure chemoprophylaxis for HIV prevention in men who have sex with men. *N. Engl. J. Med.* **363**, 2587–2599 (2010).
10. Plosker, G.L. Emtricitabine/tenofovir disoproxil fumarate: a review of its use in HIV-1 pre-exposure prophylaxis. *Drugs* **73**, 279–291 (2013).
11. Cottrell, M.L. *et al.* A translational pharmacology approach to predicting HIV pre-exposure prophylaxis outcomes in men and women using tenofovir disoproxil fumarate +/- emtricitabine. *J. Infect. Dis.* **214**, 55–64 (2016).
12. Painter, G.R., Almond, M.R., Mao, S. & Liotta, D.C. Biochemical and mechanistic basis for the activity of nucleoside analogue inhibitors of HIV reverse transcriptase. *Curr. Top. Med. Chem.* **4**, 1035–1044 (2004).
13. Bazzoli, C. *et al.* Intracellular pharmacokinetics of antiretroviral drugs in HIV-infected patients, and their correlation with drug action. *Clin. Pharmacokinet.* **49**, 17–45, 2010.
14. García-Lerma, J.G. *et al.* Natural substrate concentrations can modulate the prophylactic efficacy of nucleotide HIV reverse transcriptase inhibitors. *J. Virol.* **85**, 6610–6617 (2011).
15. von Kleist, M., Metzner, P., Marquet, R. & Schütte, C. HIV-1 polymerase inhibition by nucleoside analogs: cellular- and kinetic parameters of efficacy, susceptibility and resistance selection. *PLoS Comput. Biol.* **8**, e40382 (2012).
16. Madrasi, K., Burns, R.N., Hendrix, C.W., Fossler, M.J. & Chaturvedula, A. Linking the population pharmacokinetics of tenofovir and its metabolites with its cellular uptake and metabolism. *CPT Pharmacometrics Syst. Pharmacol.* **3**, e147 (2014).
17. Duwal, S. & von Kleist, M. Top-down and bottom-up modeling in system pharmacology to understand clinical efficacy: An example with NRTIs of HIV-1. *Eur. J. Pharmaceut. Sci.* 2016; e-pub ahead of print 2016. doi: 10.1016/j.ejps.2016.01.016.
18. Duwal, S., Schütte, C. & von Kleist, M. Pharmacokinetics and pharmacodynamics of the reverse transcriptase inhibitor tenofovir and prophylactic efficacy against HIV-1 infection. *PLoS One* **7**, e40382 (2012).
19. Borroto-Esoda, K. *et al.* In vitro evaluation of the anti-HIV activity and metabolic interactions of tenofovir and emtricitabine. *Antivir. Ther.* **11**, 377–384 (2006).
20. von Kleist, M. & Huisinga, W. Pharmacokinetic-pharmacodynamic relationship of NRTIs and its connection to viral escape: an example based on zidovudine. *Eur. J. Pharm. Sci.* **36**, 532–543 (2009).
21. Keele, B.F. *et al.* Identification and characterization of transmitted and early founder virus envelopes in primary HIV-1 infection. *Proc. Natl. Acad. Sci. U. S. A.* **105**, 7552–7557 (2008).
22. Baeten, J.M. *et al.* Antiretroviral prophylaxis for HIV prevention in heterosexual men and women. *N. Engl. J. Med.* **367**, 399–410 (2012).
23. Molina, J.M. *et al.* On-demand preexposure prophylaxis in men at high risk for HIV-1 infection. *N. Engl. J. Med.* **373**, 2237–2246 (2015).
24. McCormack, S. *et al.* Pre-exposure prophylaxis to prevent the acquisition of HIV-1 infection (PROUD): effectiveness results from the pilot phase of a pragmatic open-label randomised trial. *Lancet* **387**, 53–60 (2016).
25. von Kleist, M., Menz, S. & Huisinga, W. Drug-class specific impact of antivirals on the reproductive capacity of HIV. *PLoS Comput. Biol.* **6**, e1000720 (2010).
26. Frank, M. *et al.* Quantifying the impact of nevirapine-based prophylaxis strategies to prevent mother-to-child transmission of HIV-1: a combined pharmacokinetic, pharmacodynamic, and viral dynamic analysis to predict clinical outcomes. *Antimicrob. Agents Chemother.* **55**, 5529–5540 (2011).
27. Duwe, S. *et al.* Frequency of genotypic and phenotypic drug-resistant HIV-1 among therapy-naive patients of the german seroconverter study. *J. Acquir. Immune Defic. Syndr.* **26**, 266–273 (2001).
28. Quinn, T.C. *et al.* Viral load and heterosexual transmission of human immunodeficiency virus type 1. Rakai Project Study Group. *N. Engl. J. Med.* **342**, 921–929 (2000).
29. Bartmeyer, B. *et al.* Prevalence of transmitted drug resistance and impact of transmitted resistance on treatment success in the german HIV-1 seroconverter cohort. *PLoS One* **5**, e12718 (2010).
30. Menéndez-Arias, L. Mechanisms of resistance to nucleoside analogue inhibitors of HIV-1 reverse transcriptase. *Virus Res.* **134**, 124–146 (2008).
31. Menéndez-Arias, L. Molecular basis of human immunodeficiency virus drug resistance: an update. *Antiviral Res.* **85**, 210–231 (2010).
32. Rath, B.A. *et al.* In vitro HIV-1 evolution in response to triple reverse transcriptase inhibitors & in silico phenotypic analysis. *PLoS One* **8**, e61102 (2013).
33. Weber, J. *et al.* Diminished replicative fitness of primary human immunodeficiency virus type 1 isolates harboring the K65R mutation. *J. Clin. Microbiol.* **43**, 1395–1400 (2005).
34. Nicol, M.R. *et al.* Models for predicting effective HIV chemoprevention in women. *J. Acquir. Immune Defic. Syndr.* **68**, 369–376 (2015).
35. Grant, R.N. *et al.* Results of the iPrEx open-label extension (iPrEx OLE) in men and transgender women who have sex with men: PrEP uptake, sexual practices, and HIV incidence. *AIDS* 20–25 (2014).
36. Royce, R.A., Seña, A., Vates, Jr, M. & Cohen, M.S. Sexual transmission of HIV. *N. Engl. J. Med.* **336**, 1072–1078 (1997).
37. Boily, M.C. *et al.* Heterosexual risk of HIV-1 infection per sexual act: systematic review and meta-analysis of observational studies. *Lancet Infect. Dis.* **9**, 118–129 (2009).
38. Sagaon-Teyssier, L. *et al.* Uptake of PrEP and condom and sexual risk behavior among MSM during the anrs IPERGAY trial. *AIDS Care.* **28**, 48–55 (2016).
39. Velter, A. *et al.* HIV prevalence and sexual risk behaviors associated with awareness of HIV status among men who have sex with men in Paris, France. *AIDS Behav.* **17**, 1266–1278 (2012).
40. Louissaint, N.A. *et al.* Single dose pharmacokinetics of oral tenofovir in plasma, peripheral blood mononuclear cells, colonic tissue, and vaginal tissue. *AIDS Res. Hum. Retroviruses* **29**, 1443–1450 (2013).
41. Baeten, J.M. *et al.* Single-agent tenofovir versus combination emtricitabine plus tenofovir for pre-exposure prophylaxis for HIV-1 acquisition: an update of data from a randomised, double-blind, phase 3 trial. *Lancet Infect. Dis.* **14**, 1055–1064 (2014).
42. Anderson, P.L. *et al.* Emtricitabine-tenofovir concentrations and pre-exposure prophylaxis efficacy in men who have sex with men. *Sci. Transl. Med.* **4**, 151ra125 (2012).
43. Hendrix, C.W. Exploring concentration response in HIV pre-exposure prophylaxis to optimize clinical care and trial design. *Cell* **155**, 515–518 (2013).
44. Abraham, B.K. & Gulick, R. Next-generation oral preexposure prophylaxis. *Curr. Opin. HIV AIDS* **7**, 600–606 (2012).
45. Lewis, W., Day, B.J. & Copeland, W.C. Mitochondrial toxicity of NRTI antiviral drugs: an integrated cellular perspective. *Nat. Rev. Drug Discov.* **2**, 812–822 (2003).
46. Anderson, P.L., Kakuda, T.N. & Lichtenstein, K.A. The cellular pharmacology of nucleoside- and nucleotide-analogue reverse-transcriptase inhibitors and its relationship to clinical toxicities. *Clin. Infect. Dis.* **38**, 743–753 (2004).
47. Smith, A.J. & Scott, W.A. The influence of natural substrates and inhibitors on the nucleotide-dependent excision activity of HIV-1 reverse transcriptase in the infected cell. *Curr. Pharm. Des.* **12**, 1827–1841 2006.
48. Trezza, C.R. & Kashuba, A.D.M. Pharmacokinetics of antiretrovirals in genital secretions and anatomic sites of HIV transmission: Implications for HIV prevention. *Clin. Pharmacokinet.* **53**, 611–624 (2014).
49. Bisset, L.R. *et al.* Reference values for peripheral blood lymphocyte phenotypes applicable to the healthy adult population in Switzerland. *Eur. J. Haematol.* **72**, 203–212 (2004).
50. Durand-Gasselin, L. *et al.* Evidence and possible consequences of the phosphorylation of nucleoside reverse transcriptase inhibitors in human red blood cells. *Antimicrob. Agents Chemother.* **51**, 2105–2111 (2007).

Supplementary information accompanies this paper on the *CPT: Pharmacometrics & Systems Pharmacology* website (http://www.wileyonlinelibrary.com/psp4)

S. Duwal, M. von Kleist
Top-down and bottom-up modeling in system pharmacology to understand clinical efficacy: An example with NRTIs of HIV-1
European Journal of Pharmaceutical Sciences 94 (2016): 72-83
available online: https://doi.org/10.1016/j.ejps.2016.01.016

PLOS | COMPUTATIONAL BIOLOGY

RESEARCH ARTICLE

Optimal Treatment Strategies in the Context of 'Treatment for Prevention' against HIV-1 in Resource-Poor Settings

Sulav Duwal[1,2], Stefanie Winkelmann[1], Christof Schütte[1,3], Max von Kleist[1,2]*

1 Department of Mathematics and Computer Science, Freie Universität Berlin, Germany, **2** Junior Research Group "Systems Pharmacology & Disease Control", **3** Zuse Institute Berlin, Germany

* vkleist@zedat.fu-berlin.de

OPEN ACCESS

Citation: Duwal S, Winkelmann S, Schütte C, von Kleist M (2015) Optimal Treatment Strategies in the Context of 'Treatment for Prevention' against HIV-1 in Resource-Poor Settings. PLoS Comput Biol 11(4): e1004200. doi:10.1371/journal.pcbi.1004200

Editor: Victor De Gruttola, Harvard School of Public Health, UNITED STATES

Received: June 17, 2014

Accepted: February 18, 2015

Published: April 30, 2015

Data Availability Statement: All relevant data are within the paper and its Supporting Information files.

Funding: MvK and SD receive funding through the BMBF e:Bio junior research group "Systems Pharmacology & Disease Control", grant number 031A307 and through the DFG-research center MATHEON, project A21 "Modeling, Simulation and Therapy Optimization for Infectious Diseases". MvK receives funding through the Einstein Center for Mathematics Berlin, project CH4: "Optimal control of chemical reaction systems and application to drug resistance mitigating therapy". The funders had no

Abstract

An estimated 2.7 million new HIV-1 infections occurred in 2010. `Treatment-for-prevention' may strongly prevent HIV-1 transmission. The basic idea is that immediate treatment initiation rapidly decreases virus burden, which reduces the number of transmittable viruses and thereby the probability of infection. However, HIV inevitably develops drug resistance, which leads to virus rebound and nullifies the effect of `treatment-for-prevention' for the time it remains unrecognized. While timely conducted treatment changes may avert periods of viral rebound, necessary treatment options and diagnostics may be lacking in resource-constrained settings. Within this work, we provide a mathematical platform for comparing different treatment paradigms that can be applied to many medical phenomena. We use this platform to optimize two distinct approaches for the treatment of HIV-1: (i) a diagnostic-guided treatment strategy, based on infrequent and patient-specific diagnostic schedules and (ii) a pro-active strategy that allows treatment adaptation prior to diagnostic ascertainment. Both strategies are compared to current clinical protocols (standard of care and the HPTN052 protocol) in terms of patient health, economic means and reduction in HIV-1 onward transmission exemplarily for South Africa. All therapeutic strategies are assessed using a coarse-grained stochastic model of within-host HIV dynamics and pseudo-codes for solving the respective optimal control problems are provided. Our mathematical model suggests that both optimal strategies (i)-(ii) perform better than the current clinical protocols and no treatment in terms of economic means, life prolongation and reduction of HIV-transmission. The optimal diagnostic-guided strategy suggests rare diagnostics and performs similar to the optimal pro-active strategy. Our results suggest that 'treatment-for-prevention' may be further improved using either of the two analyzed treatment paradigms.

role in study design, data collection and analysis, decision to publish, or preparation of the manuscript.

Competing Interests: The authors have declared that no competing interests exist.

Author Summary

HIV-1 continues to spread globally. Antiviral treatment cannot cure patients, but it slows disease progression and may prevent HIV transmission by decreasing the amount of transmittable viruses in treated individuals. 'Treatment-for-prevention' argues for immediate treatment initiation and may reduce transmission by 96% (CI: 73–99%), according to the results of a large clinical study (HPTN052). In order to ensure long-lasting treatment success, early therapy initiation demands more sophisticated treatment strategies & exceeding funds. However, countries facing the highest HIV burden are among the poorest. Within this work, we provide a mathematical framework that allows assessing different treatment paradigms using optimal control theory together with stochastic modelling of within-host viral dynamics and drug resistance development. We use this framework to compute and evaluate two distinct *optimal* long-term treatment strategies for resource-constrained settings: (i) a **diagnostic-guided** and (ii) a **pro-active** treatment **strategy**. The cost of a strategy is evaluated from a national economic perspective, valuating a severe patient health status in terms of an economic loss. The *optimal* strategies are compared with current clinical treatment protocols and **no treatment** in terms of costs, life expectation and reduction of secondary cases. Our simulations indicate that the **pro-active** treatment **strategy** performs comparably to the **diagnostic-guided** treatment **strategy**. Both strategies perform better than current clinical protocols, suggesting directions for improvement.

Introduction

HIV-1 infection remains one of the major global health challenges with an estimated 33 million infected and a continuing spread [1]. Currently, an efficient vaccine remains to be developed, while at the same time the complete elimination of replication-competent virus within the host can not be achieved due to the persistence of the virus in inducible, latent cellular reservoirs [2, 3], as well as insufficient pharmacological suppression of actively replicating virus in some anatomical/cellular reservoirs [4, 5]. However, the current situation urges for methods that could bring the epidemic to a halt, or possibly end it. Currently, the most promising strategies are based on the use of antiviral drugs:

i. Pre-exposure prophylaxis (PrEP) [6–9] aims to protect uninfected individuals 'at risk' by decreasing the probability of infection upon virus exposure, e.g. [10]. PrEP may however be too costly to be broadly implemented in resource-poor countries [11].

ii. Currently, the decision to initiate treatment against HIV is largely guided by CD4+ cell levels [12, 13]. However, the viral load, which is the primary determinant of infectiousness [14, 15], may be very high within the time-window between HIV infection and initiation of treatment. 'Treatment for prevention' [16] aims to put infected individuals on therapy as early as possible. This can reduce the infectiousness of a patient by decreasing within-host virus levels, which reduces the amount of transmitted viruses per contact and the probability of infection upon exposure. Analysis of the only completed clinical study to date, HPTN052 [16], estimated that 'treatment for prevention' may reduce the number of *linked* HIV-1 transmissions by 96% and the number of *total* HIV-1 transmissions by 89% relative to delayed treatment initiation and subsequently it was nominated as the "breakthrough of the year 2011" by the *Science* magazine [17].

In the aftermath of the HPTN052 trial, the cost-efficacy of 'treatment for prevention' was analyzed by many mathematical modeling approaches (reviewed in [18]). One problem is that most of these approaches focused solely on the epidemic level and did not model drug resistance development within the hosts, which indirectly assumes that the efficacy of 'treatment for prevention' is constant over time. However, because viral transmission is strongly correlated with viral levels in the transmitting individual [14, 15, 19–21], it is reasonable to assume that also the efficacy of 'treatment for prevention' is intimately connected with viral suppression. One major challenge during HIV treatment lies in the virus' tendency to develop drug resistance [22], which in turn can lead to virus rebound and promote HIV transmission for the time it remains unrecognized. An earlier treatment initiation may thus demand an improved therapeutic strategy, that allows long-term control of virus replication (beyond the typical duration of a clinical trial). While sophisticated patient monitoring and timely treatment changes may allow to minimize windows of unrecognized viral breakthrough, they require significant monetary funds, good infrastructure, diagnostic facilities and the availability of alternative treatment options. Only few of these may be available in resource-constrained countries, where the requirement of resources may strongly dominate the possibility to implement a reasonable 'treatment for prevention' strategy. Obviously, scaling 'treatment for prevention' requires careful examination of various aspects and a policy maker should strike a proper balance between societal and individual perspectives [23].

This work addresses the scaling of 'treatment for prevention' by suggesting *optimal* treatment strategies for the long-term control of HIV within its host (as recommended by [24]). *Optimality* will be defined from a *national economic perspective*, taking into account that a diseased individual implies an economic loss. By considering the national economic perspective, we do not evaluate what *should* be done, but rather what is *already worthwhile*. However, we also evaluate the derived *optimal* strategies from an individual perspective and in terms of their utility in prevention, i.e. whether a strategy prolongs the life of an infected person and whether the risk of HIV onward transmission is reduced.

We hereby focus on two distinct approaches to handle treatment decisions: The first assumes that treatment decisions (i.e. when to change therapy) are made on an *individual* basis, guided by infrequent diagnostics (referred to as **diagnostic-guided strategy**). This represents a medical scenario in which a treating physician decides based on the diagnosed status of the patient that he encounters. The second approach suggests pro-active treatment decisions (referred to as **pro-active strategy**), i.e. does not require diagnostic ascertainment of the patients' disease status. The two approaches are modeled and solved by two distinct mathematical frameworks. The former is addressed using the recently developed framework of 'Markov Decision Processes with Rare State Observations' [25]: For each disease state, it computes the optimal treatment and the next time of medical diagnostics, minimizing viral burden as well as treatment- and diagnostic costs. The latter approach (the **pro-active strategy**) is modeled as an open-loop switched system, where the decision to change the treatment depends on the initial disease state of the patient and the anticipated, (treatment-)induced stochastic dynamics up to some time t. The later strategy allows to switch treatment *before* drug resistance is detectable in the individual (pro-active) and may be easier to implement in resource-constrained settings, where poor infrastructure and the costs of diagnostics limit their applicability. By assessing these two distinct frameworks side-by-side, we can rigorously evaluate the different treatment paradigms in terms of their optimality. Algorithms to solve these problems were developed and are stated in the supplementary materials.

Several other groups have suggested *optimal* [26–28] or *sub-optimal* [29, 30] treatment strategies to mitigate drug resistance in HIV-1. All authors treated the underlying system deterministically, which fails to capture the intrinsic stochastic nature of HIV drug resistance

development [31] and the time-scales on which drug resistance develops. None of the previous work focused on HIV prevention, and neither work questioned the analyzed treatment philosophy, either focusing on pro-active treatment switching strategies [26–28, 30], *or* diagnostic-driven strategies [29]. In contrast, we used a stochastic model of HIV long-term dynamics after drug application [25] to more realistically capture the underlying dynamics. Also, we evaluate different assumptions for the controllability of the disease dynamics, by evaluating the two different optimal control frameworks, which allows for an objective assessment of alternative treatment philosophies.

The manuscript will be organized as follows: We will extend- and parameterize the model introduced in [25] for our needs. After recapitulating essential theory for the **diagnostic-guided strategy**, we introduce the mathematical concepts behind the **pro-active strategy**, solve both optimal control problems and evaluate them with respect to monetary costs, patient survival and reduction of onward transmission. All algorithms that we developed to solve the optimal control problems will be provided in the S1 and S2 Text for the interested reader.

Materials and Methods

Within this work, we investigate optimal treatment strategies *in silico* by formulating- and solving two optimal control problems referred to as the optimal **diagnostic-guided strategy** and the optimal **pro-active strategy**. In general, an optimal control problem requires a mathematical model of the controlled process and a performance- or cost criterion. Likewise, our problem will be broken down into these ingredients.

Model of Controlled HIV Dynamics

The two addressed optimal control approaches share an identical model (Fig 1) that reflects the short-term dynamics of viral decay- and rebound (Fig 2), as well as the stochastic HIV long-term dynamics after drug application, see Fig 3. Within this work, we put a focus on viral kinetics and will only indirectly relate to the patient's health. This is because we are interested in 'treatment for prevention' and particularly its efficacy in decreasing onward transmission, which is correlated with the viral load [19–21] and not necessarily with the immune status of the HIV infected patient.

State space. HIV can be successfully suppressed if drug resistance does not develop. Thus, any model that aims to represent the long-term HIV dynamics upon treatment should include drug resistance development. The process of drug resistance development denotes an intrinsically stochastic process, which is determined by random mutation events (point mutations, recombinations). Long term HIV-dynamics in the context of drug treatment may therefore be dominated by these intrinsically stochastic events [31], necessitating stochastic modeling approaches [32–34]. The fundamental evolution equation for intrinsically stochastic kinetics is the chemical master equation (CME). Each state described by the CME comprises a combination of discrete numbers of individuals of the respective species (e.g. viral strains), resulting in state space dimensions $\mathbb{N}_0 \times \mathbb{N}_0 \times \ldots \times \mathbb{N}_0$, i.e. [35, 36]. A major mathematical drawback is the fact that the CME cannot be solved directly due to this complexity. Therefore, a modeler can either approximate the solution of the CME by Monte-Carlo schemes [37], aim at hybrid approaches [38–40], which can yield particular characteristics of the CME, or perform a state space reduction (lumping). In this manuscript, we adapt a model [25] that relates to the latter approach. For this model we can solve the coarse-grained CME directly when computing optimal control strategies.

In brief, the HIV model contains four lumped viral copy number states for each of the four virus strains. The set of states $\mathcal{S}$ thus has dimension $4^4 = 256$ states + 1 [patient death]: If the

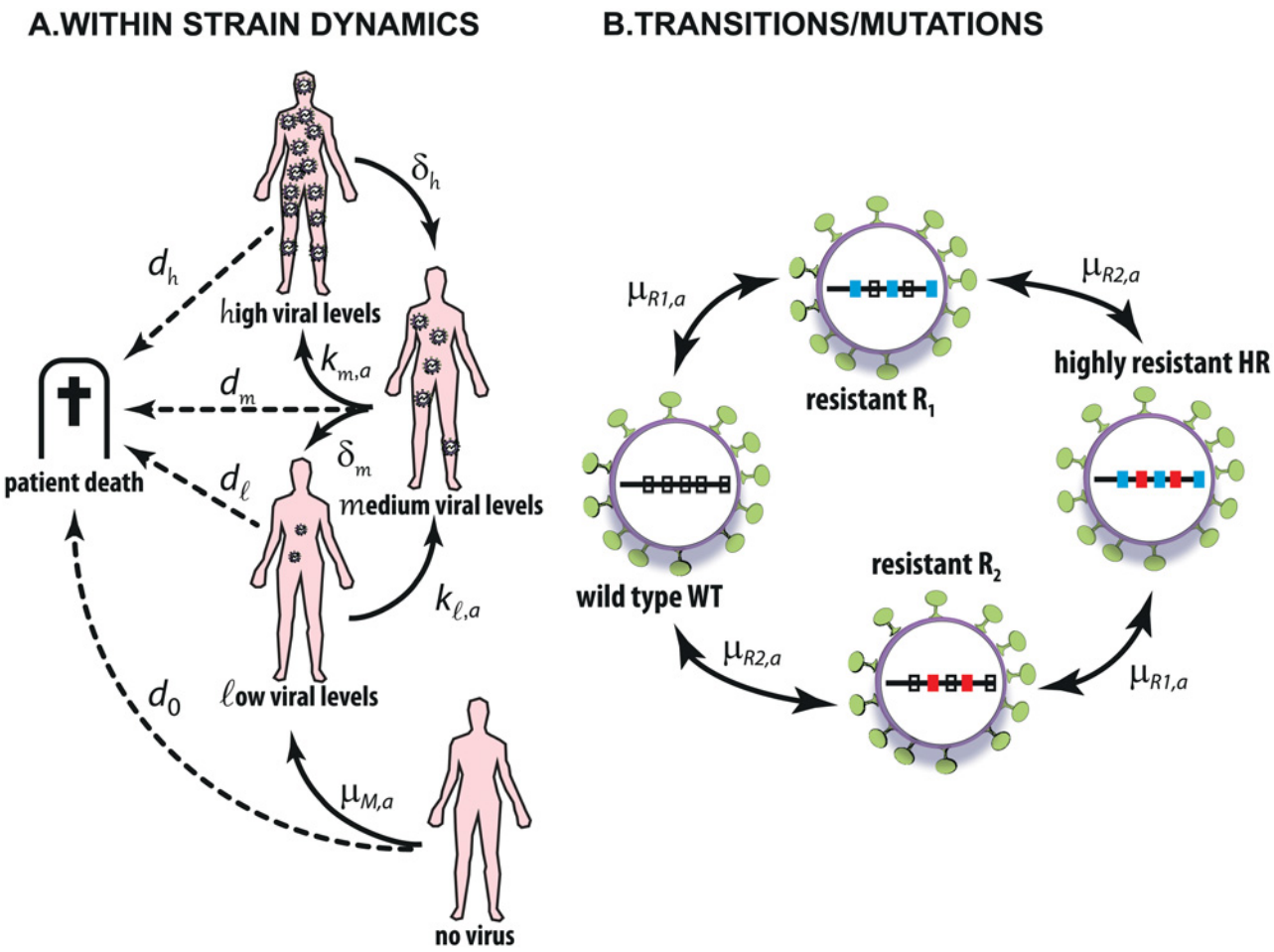

Fig 1. Simplified HIV Model. A: Transitions between copy number states n_C. B: Transitions in between viral strains M.

doi:10.1371/journal.pcbi.1004200.g001

respective virus type is absent, we denote the respective state by 0, if it is present in low copy numbers, i.e., for $<$ 50 virus copies/mL blood (detection limit of assays used in the clinic), the respective state is denoted by ℓ, for medium copy numbers between 50 and 4000 virus copies/mL blood we denote the lumped states by m and for high copy numbers with more than 4000 virus copies/mL blood, it is h. This coarse graining is in line with the levels of virus produced in the distinct cellular reservoirs of HIV, see e.g. [34]. The following four viral strains M are considered: a strain WT (wild type) that is susceptible to all treatment lines, a strain R1 which is susceptible to a second treatment line, but unaffected by (resistant to) the first treatment line, a strain R2 that is susceptible to the first treatment line, but unaffected by the second, and a highly resistant strain HR, which is resistant to all treatments. In order to describe a virologic state x we choose a compact vector notation of the form

$$x = [n_C(WT),\ n_C(\mathrm{R1}),\ n_C(\mathrm{R2}),\ n_C(HR)],$$

where $n_C \in \{0, \ell, m, h\}$ denotes the viral copy number of each viral strain WT, R1, R2 or HR. For example, the state $x = [\ell,\ m,\ 0,\ \ell]$ describes the situation of a ℓow number of wild type strains, a $m$edium number of R1-mutants, the absence of R2-mutants, and a ℓow number of

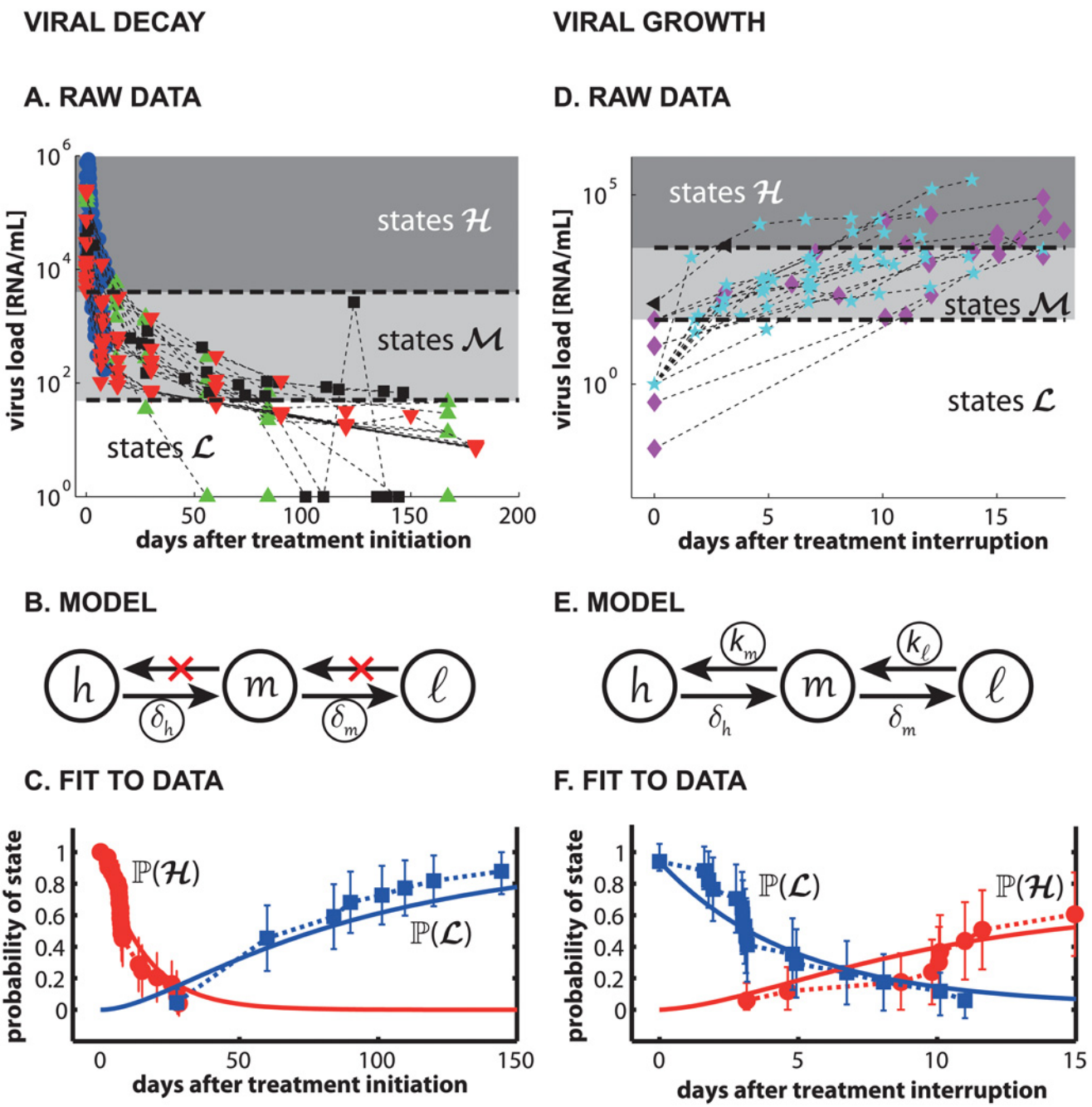

Fig 2. (Short-term) viral dynamics. Left panels (A-C): Viral decay. Right panels (D-F): Viral growth. **A:** Data used for estimating viral decay parameters δ_h, δ_m. Blue circles indicate viral decay profiles from [41], green upward pointing triangles denote data from [42], black squares denote data from [43] and red downward pointing triangles denote data from [4]. Horizontal dashed lines and background shading indicates the assignment of the depicted data to the sets $\mathcal{H}$ (> 4000 viral RNA/mL)), $\mathcal{M}$ and $\mathcal{L}$ ($\leq$ 50 viral RNA/mL) of our model. **B:** When assuming 100% effective treatment ($\eta = 1$), the model shown in panel B is derived. This model is used to identify decay parameters δ_h and δ_m (circled parameters in panel B). **C:** Data-derived (error bars, dashed lines) and predicted (solid lines) probabilities of states $\mathcal{H}$ and $\mathcal{L}$ using the model in panel B with estimated parameters δ_h and δ_m. **D:** Data from treatment interruption trials [43–45] used for estimating viral growth parameters $k_{\ell,\emptyset}$, $k_{m,\emptyset}$. Magenta diamonds indicate viral rebound profiles from [44], cyan pentagrams indicate data from [45] and black left-pointing triangles indicate data from [43]. Horizontal dashed lines and background shading indicates the assignment of the depicted viral growth data to the sets $\mathcal{H}$, $\mathcal{M}$ and $\mathcal{L}$. **E:** We assumed the absence of treatment ($\eta = 0$), such that the model shown in panel E is sufficient to decribe the data and allows identifying growth parameters $k_{\ell,\emptyset}$ and $k_{m,\emptyset}$ (circled parameters in panel E). **F:** Data-derived (error bars, dashed lines) and predicted (solid lines) probabilities of states $\mathcal{H}$ and $\mathcal{L}$ using the model in panel E with δ_h and δ_m and estimated parameters $k_{\ell,\emptyset}$ and $k_{m,\emptyset}$. The parameter estimation procedure is exemplified in the *Material and Methods* section.

doi:10.1371/journal.pcbi.1004200.g002

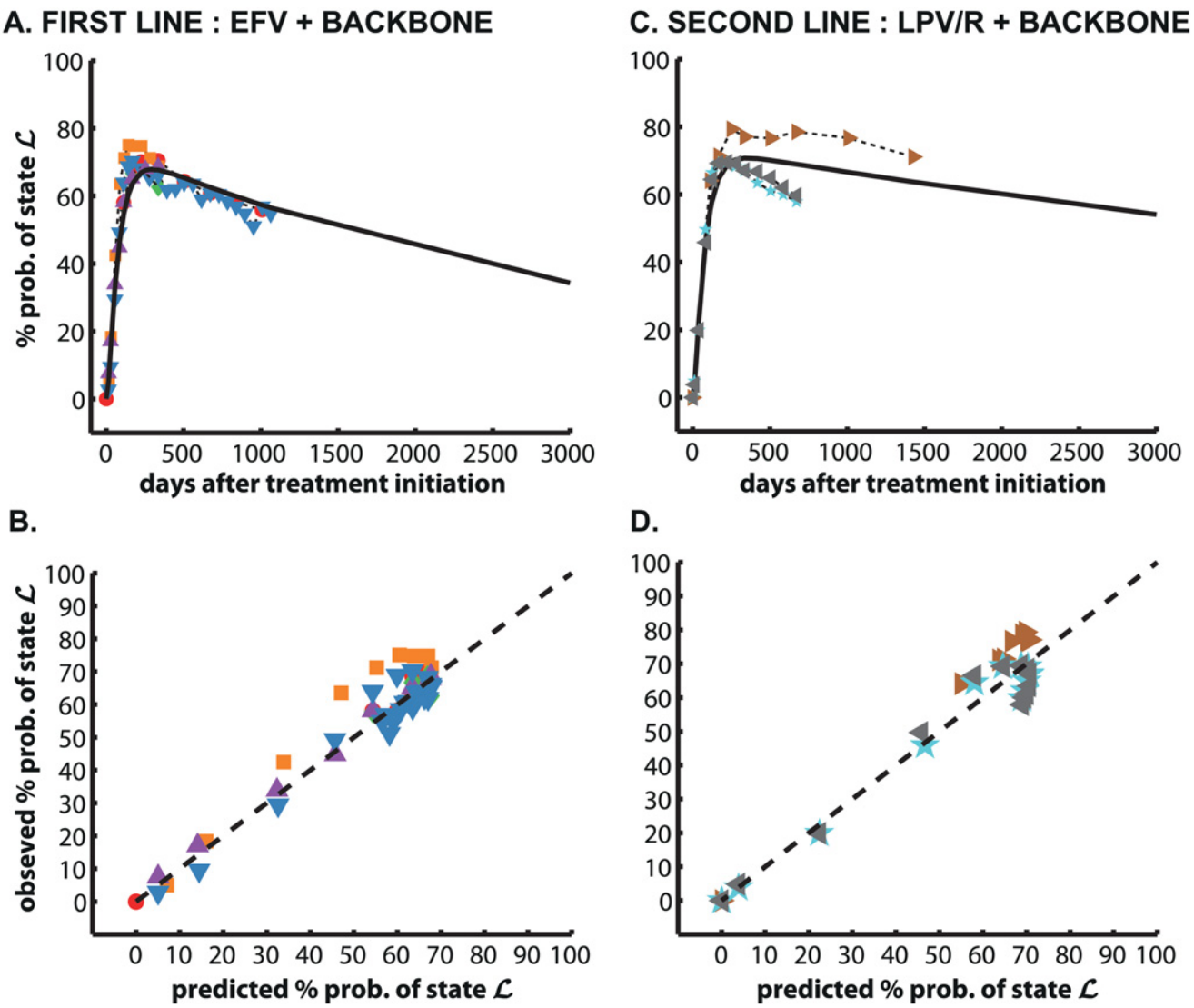

Fig 3. Long-term viral suppression. Long-term data was used to estimate clinical drug efficacy $\eta(a_1, \{WT, R2\})$, $\eta(a_2, \{WT, R1\})$ and rates of drug resistance emergence $\mu_{R1,\emptyset}$, $\mu_{R2,\emptyset}$, using the model depicted in Fig 1, after parameters for viral growth and decay were estimated from data in Fig 2. **A:** Predicted (solid black line) and clinically observed probability of viral suppression (states $\mathcal{L}$; $\leq$ 50 viral RNA/mL) after treatment with efavirenz (EFV) based HAART (first line therapy). Clinical data was derived from [46] (red dots), [47] (orange squares), [48] (green diamonds), [49] (magenta upward pointing triangles) and [50] (blue downward pointing triangles). In all studies, the NRTI backbone consisted of 3TC + AZT. **B:** Goodness-of-fit plot for first line therapy. **C:** Predicted (solid black line) and clinically observed probability of viral suppression (states $\mathcal{L}$; $\leq$ 50 viral RNA/mL) after treatment with ritonavir boosted lopinavir (LPV/r) based HAART (second line therapy). Clinical data was derived from [51] (brown right-pointing triangles), [52] (cyan pentagrams) and [52] (grey left-pointing triangles). In all studies, the NRTI backbone consisted of a deoxycytidine analog + abacavir or tenofovir or stavudine, reflecting clinical practice (the exact choice of the backbone may depend on prior exposure [13]). **D:** Goodness-of-fit plot for second line therapy.

doi:10.1371/journal.pcbi.1004200.g003

highly resistant viruses. Mutations from one strain to another can give rise to novel viral populations, as shown in Fig 1.

Control actions. The actions describe 'what the controller can do to influence the system'. In terms of HIV therapy, a physician can e.g. choose what treatment(-line) to apply and when to change it. In resource-constrained settings, only few treatment lines are available. In the case of South Africa these may include a first- and a second-line therapy [13]. Taking these considerations in account, we consider two distinct treatment lines (actions) a_1,$a_2 \in \mathcal{A}$. Each action a

$\in \mathcal{A}$ induces unique disease dynamics, related to a unique *Markov Jump Process* that is entirely determined by its infinitesimal generator L_a. The entry $L_a[x,y] \geq 0$ represents the rate of transition from state $y \in \mathcal{S}$ to state $x \in \mathcal{S}$, $y \neq x$, given an action a and it holds that $L_a[y,y] = -\Sigma_{x \neq y} L_a[x,y]$. We define a probability space Ω and let $p \in \Omega$ denote a probability distribution vector on the state space $\mathcal{S}$ with the entry $p[x](t)$ referring to the probability of being in the state $x \in \mathcal{S}$ at time t, i.e.

$$p[x](t) := \mathbb{P}(X_t = x), \tag{1}$$

where $\mathbb{P}$ is the probability measure. Obviously, the number of components of a probability vector p is equal to $|\mathcal{S}|$. For a given action $a \in \mathcal{A}$, the dynamics of the probability vector are given by

$$\frac{dp(t)}{dt} = L_a \cdot p(t) \tag{2}$$

The above equation is known as the *Master Equation*. We introduce the transpose of the transition matrix on $\mathcal{S}$ for some time lag τ and action a

$$T_{a,\tau} : \mathbb{R}^{|\mathcal{S}|} \mapsto \mathbb{R}^{|\mathcal{S}|}, \quad T_{a,\tau} p := \mathbf{e}^{L_a \cdot \tau} p, \tag{3}$$

where **e** denotes the matrix exponential. The component $T_{a,\tau}[x,y]$ refers to the transition probability from state y to state x for a time lapse τ under the application of action a and will be used later in the cost functionals of the closed-loop optimal control problem (**diagnostic-guided strategy**) and the open-loop optimal control problem (**pro-active strategy**).

Generator entries. The distinct treatments $a \in \mathcal{A}$ are related to distinct generators L_a of our HIV-model. The basic transitions between copy number states for each viral strain M, $n_C(M)$, are shown in Fig 1 and exemplified for the highly resistant strain HR below.

$$[*, *, *, \ell] \underset{\delta_m}{\overset{k_{\ell,a}}{\rightleftarrows}} [*, *, *, m], \quad [*, *, *, m] \underset{\delta_h}{\overset{k_{m,a}}{\rightleftarrows}} [*, *, *, h] \tag{4}$$

$$[*, *, *, h] \xrightarrow{d_h} \maltese, [*, *, *, m] \xrightarrow{d_m} \maltese, [*, *, *, \ell] \xrightarrow{d_\ell} \maltese, \tag{5}$$

where * indicates an arbitrary number of the respective virus strain (WT, R1 and R2 in the example above). The parameters $k_{\ell,a}$ and $k_{m,a}$ denote the reaction propensities of going from copy number ℓ to copy number m and from copy number m to copy number h respectively (viral growth), which are decreased depending on the treatment $a \in \{a_1, a_2\}$ because treatment essentially suppresses viral growth. The parameters δ_m and δ_h denote the reaction propensities for going from copy number m to copy number ℓ and from copy number h to copy number m respectively (virus elimination). The parameters $d_h > d_m > d_\ell$ denote the propensity for the death of the patient. We assume that high viral burden (states h and m respectively) increases the risk of death, whereas d_ℓ equals the propensity for "natural death". The propensity for death was computed according to $d = 1/(\text{residual life expectancy})$, and is exemplified in [25].

The considered transitions between viral strains M are depicted in Fig 1. Specifically, transitions between viral strains generate a *l*ow number of viral particles from either a *m*edium or *h*igh number of viruses belonging to a distinct strain. Note, that transitions between viral strains may involve several distinct point mutations (indicated by blue and red bars in Fig 1B).

Exemplified for the wild type strain WT those are:

$$[h,\,0,\,*,\,*\,]\xrightarrow{\mu_{\mathrm{R1},a}}[h,\,\ell,\,*,\,*\,],\qquad[m,\,0,\,*,\,*\,]\xrightarrow{\mu_{\mathrm{R1},a}}[m,\,\ell,\,*,\,*\,] \tag{6}$$

$$[h,\,*,\,0,\,*\,]\xrightarrow{\mu_{\mathrm{R2},a}}[h,\,*,\,\ell,\,*\,],\quad[m,\,*,\,0,\,*\,]\xrightarrow{\mu_{\mathrm{R2},a}}[m,\,*,\,\ell,\,*\,] \tag{7}$$

$$[0,\,h,\,*,\,*\,]\xrightarrow{\mu_{\mathrm{R1},a}}[\ell,\,h,\,*,\,*\,],\quad[0,\,m,\,*,\,*\,]\xrightarrow{\mu_{\mathrm{R1},a}}[\ell,\,m,\,*,\,*\,] \tag{8}$$

$$[0,\,*,\,h,\,*\,]\xrightarrow{\mu_{\mathrm{R2},a}}[\ell,\,*,\,h,\,*\,],\quad[0,\,*,\,m,\,*\,]\xrightarrow{\mu_{\mathrm{R2},a}}[\ell,\,*,\,m,\,*\,] \tag{9}$$

where the first two lines indicate drug resistance *arising* from the wild type strain and the remaining two lines indicate transitions from resistant strains *yielding* the wild type strain. The parameters $\mu_{\mathrm{R1},a}$ and $\mu_{\mathrm{R2},a}$ denote the propensity for the emergence- and disappearance of drug resistance to treatment 1 or 2 (a_1,a_2), respectively, emanating from copy number state h or m. Note, that we consider only the following transitions: WT ↔ R1, WT ↔ R2, R1 ↔ HR and R2 ↔ HR, which is motivated by the fact that a direct transition from WT ↔ HR is very unlikely, because the genetic distance between the two viral strains is too large to be overcome at once.

The effect of treatments a_1 and a_2 on the viral growth & transition rates is considered in the following way:

$$k_{\ell,a} = (1-\eta(a,M))k_{\ell,\emptyset} \tag{10}$$

$$k_{m,a} = (1-\eta(a,M))k_{m,\emptyset} \tag{11}$$

$$\mu_{\tilde{M},a} = (1-\eta(a,M))\mu_{\tilde{M},\emptyset} \tag{12}$$

where $M \in \{\mathrm{WT, R1, R2, HR}\}$ denotes the strain of the reactant virus. $\tilde{M} \in \{\mathrm{WT, R1, R2, HR}\}$ denotes the event related to a particular drug resistance emergence/disappearance, see Fig 1B. The parameter $\eta(a,M)$ denotes the efficacy of treatment a on the reactant viral strain M; i.e. if strain M is susceptible to treatment $a \in \{a_1, a_2\}$, then $0 < \eta(a,M) \leq 1$, and if the viral strain M is insusceptible to treatment $a \in \{a_1, a_2\}$ then $\eta(a,M) = 0$. In the absence of medical intervention $a = a_\emptyset$, $\eta(a,M) = 0$. Therefore, the parameters $k_{\ell,\emptyset}$, $k_{m,\emptyset}$ and $\mu_{\tilde{M},\emptyset}$ denote the growth rates and respective transition rates in copy number states m and h in the absence of intervention, as shown in Table 1.

Parameter estimation. In order to estimate model parameters, we proceeded in a stepwise approach: We first estimated parameters related to viral decay (δ_h, δ_m) and then used these estimates in order to estimate parameters related to viral growth in the absence of treatment ($k_{\ell,\emptyset}$, $k_{m,\emptyset}$), using data from [4, 41–45]. Finally, we used the estimated decay- and growth parameters along with data on the long-term (> 2 years) suppression of HIV-1 in order to estimate parameters related to the drug efficacy ($\eta(a_1, \{\mathrm{WT, R2}\})$, $\eta(a_2, \{\mathrm{WT, R1}\})$) and to drug resistance development ($\mu_{\mathrm{R1},\emptyset}$, $\mu_{\mathrm{R2},\emptyset}$) [46–52].

Parameters were estimated in MATLAB using *lsqcurvefit* by minimizing the following weighted least squares criteria, with θ denoting the set of estimable parameters.

$$\theta^* = \underset{\theta}{\operatorname{argmin}} \sum_i \left(\frac{\pi[x](t_i) - p[x](t_i,\theta)}{\omega_i}\right)^2 \tag{13}$$

where $\pi[x](t_i)$ denotes the data-derived probability distribution on the model-defined state-

Table 1. Parameters of the HIV-model.

parameter	value	parameter	value
$k_{\ell,\emptyset}$	0.2027	$k_{m,\emptyset}$	0.1308
δ_m	$1.13{\cdot}10^{-2}$	δ_h	$6.62{\cdot}10^{-2}$
d_ℓ	$9.4{\cdot}10^{-5}$	$\mathbb{IR}(n_C = \ell)$	0.2
d_m	$2.7{\cdot}10^{-4}$	$\mathbb{IR}(n_C = m)$	1.85
d_h	$5.5{\cdot}10^{-4}$	$\mathbb{IR}(n_C = h)$	13.18
$\mu_{R1,\emptyset}$	$1.739{\cdot}10^{-1}$	$\mu_{R2,\emptyset}$	$2.54{\cdot}10^{-2}$
$\eta(a_1, \{WT, R2\})$	0.9894	$\eta(a_1, \{R1, HR\})$	0
$\eta(a_2, \{WT, R1\})$	0.9825	$\eta(a_2, \{R2, HR\})$	0

Infection risks $\mathbb{IR}$ were derived from data, as explained in S5 Text. Parameters d_ℓ, d_m and d_h were estimated from life-expectation data as explained in [25]. All other parameters were estimated from data shown in Figs 2 and 3 and exemplified in the *Material & Methods* section. All values are given in units [1/day] except η [unit less] and $\mathbb{IR}$ [per 100 person-years].

doi:10.1371/journal.pcbi.1004200.t001

space (computed using the *ecdf* function in MATLAB), $p[x](t_i,\theta)$ defines the solution of Eq (2) for time t_i with parameter set θ and ω_i denotes the weight parameter. Parameter estimation was performed 50 times respectively with random start parameters to verify the convergence to globally optimal parameter estimates θ^*.

Viral decay. A total of 311 data points from 31 patients and 4 independent clinical studies were available from [4, 41–43], which accurately assess the dynamics of viral decay after initiation of treatment (see Fig 2A). For the data analyzed, we assumed 100% effective treatment ($\eta = 1$), as proposed by others who estimated viral decay parameters [41, 53]. The lumped viral model (see Fig 1) then further reduces to the model shown in Fig 2B, which allows to identify decay parameters δ_h and δ_m. The data-derived probabilities $\pi[x](t_i)$ were computed as 1− the cumulative probability to leave set $\mathcal{H}$ ($>$ 4000 viral RNA/mL) and the cumulative probability to enter set $\mathcal{L}$ ($\leq$ 50 viral RNA/mL). Error bars were computed using Green's formula. In line with the data, we assumed that the initial HIV virologic status is represented by high copy numbers of susceptible virus.

Viral growth. A total of 89 data points from 17 patients and 3 treatment interruption trials [43–45], was used to estimate viral growth parameters $k_{\ell,\emptyset}$ and $k_{m,\emptyset}$. In line with the data, we assumed the absence of treatment ($\eta = 0$), such that the model shown in Fig 2E is sufficient to describe the data. Data-derived probabilities were computed as 1− the cumulative probability to leave set $\mathcal{L}$ and the cumulative probability to enter set $\mathcal{H}$, respectively, and error bars were computed using Green's formula.

Drug efficacy and -resistance. Using the full model (Fig 1), we estimated parameters relating to the clinical drug efficacy of both treatment lines $\eta(a_1, \{WT, R2\})$ & $\eta(a_2, \{WT, R1\})$ and rates of drug resistance emergence $\mu_{R1,\emptyset}$ and $\mu_{R2,\emptyset}$.

In analogy with the South African treatment guidelines, we assumed that the first-line therapy consists of efavirenz (EFV) + zidovudine (AZT) + lamivudine (3TC). Long-term studies usually evaluate the probability of viral suppression, which is defined in terms of undetectable virus loads ($\leq$ 50 viral RNA/mL). Translated to our model, this refers to the condition in which all viral mutants are in state ℓ or absent; i.e. $[\leq \ell,\ \leq \ell,\ \leq \ell,\ \leq \ell]$, which we denote by the set of states by $\mathcal{L}$. Probabilities of viral suppression from 5 clinical studies [46–50] were used for parameter estimation. As a second-line treatment we assumed a ritonavir-boosted lopinavir (LPV/r) based HAART, see [13]. Since the exact choice of the NRTI backbone may

depend on the prior exposure of the individual patient, we used data evaluating the long-term efficacy of LPV/r + an NRTI backbone consisting of a deoxycytidine analog + stavudine [51] or abacavir [52] or tenofovir [52].

All model parameters are shown in the Table 1. The original data and model predicted dynamics of viral decay and -rebound are shown in Fig 2 (A: raw viral decay data; B: model to evaluate viral decay; C: model-predicted vs. clinical decay profiles; D: raw viral growth data; E: model to evaluate viral growth; F: model-predicted vs. clinical growth profiles). Data for the long-term control of HIV-1, predicted dynamics and goodness-of-fit are shown in Fig 3A–3D for the two treatment lines (a_1 and a_2). As can be seen in Figs 2 and 3, the model appropriately captures both the short-term viral dynamics, as well as long-term dynamics of viral suppression.

Cost assignment. Public health initiatives are often constrained by available funds. The countries with the highest HIV burdened are also among the poorest and financial commitments from donors have stagnated or decreased [54] in recent years. Thus, the requirement of resources may strongly dominate the policy making process in a resource-constrained context. Because of these conditions, we designed the performance criterion from a national economic perspective.

The performance criterion valuates the induced system dynamics and controls, i.e. the viral status of the patient and the costs of treatment. We will consider both the direct costs due to the applied treatments $c_{\mathcal{A}}$ and indirect costs due to the virologic/health status of a patient $c_{\mathcal{S}}$. Our analysis will be conducted from a country's public health-care/monetary perspective. Therefore, the costs related to the different states c_S will be computed based on the average productivity loss $\mathrm{pL}(n_C)$ times the average daily monetary contribution of one individual (assessed in terms of the daily per capita GDP), i.e. $c_S(x) = \mathrm{pL}(x)\cdot\mathrm{GDP}$, with $\mathrm{pL}(x) = \max_{n_C} \mathrm{pL}(n_C)$, which implies that the total virus load reflects the cost of the individual infection status at any point in time. Death is interpreted in terms of a complete loss in productivity. Furthermore, we take diagnostic costs into account, which applies only in the **diagnostic-guided strategy**, the **standard of care** and the **HPTN052 protocol** (the latter two are modeled for comparison). The cost of diagnostics will be set to a fixed value and closely reflect the cost of a drug resistance test for the **diagnostic-guided strategy** and the cost of a virus load determination in the case of the **standard of care** and the **HPTN052 protocol**.

The integration of momentary/running costs yields the objective function (performance criterion) for the optimal control problem. While performance criteria generally depend on the particular application at hand, we decided to consider expected discounted costs on an infinite time horizon. We chose an infinite time horizon, because HIV treatment does not have a previously known endpoint (i.e. time of death). At the same time, a differentiated weighting of immediate and later costs is reasonable due to an upper limitation of life expectancy and aspects of inflation. Costs arising at time $t > 0$ are thus weighted by a discount factor $0 < e^{-\lambda t} < 1$. In this regard, the concrete choice of a discount factor λ will depend on the presumed annual inflation in the considered setting. For all calculations, we consider the inflation rate in South Africa as a representative of a resource-constrained country with a large HIV burden, see Table 2. The discount factor also guarantees convergence of the cost functional and therefore allows the numerical solution of the optimal control problem.

The costs per unit time comprise both the direct costs due to the applied treatments and indirect costs due to the virologic/health status of a patient. Thus, we can write

$$c(x, a) = c_S(x) + c_{\mathcal{A}}(a) \tag{14}$$

Table 2. Cost parameters for South Africa.

parameter	value	unit	reference
$c_{\mathcal{A}}(a_1)$	0.3	US$/d	[65]
$c_{\mathcal{A}}(a_2)$	1.08	US$/d	[65]
k_{dia}	200	US$	[57, 59]
GDP	6,620	US$/p.p./y	[75]
pL($n_C = \ell$)	0	-	[76]
pL($n_C = m$)	0.1	-	[76]
pL($n_C = h$)	0.4	-	[76]
pL(✠)	1	-	-
λ	$1.47 \cdot 10^{-4}$	1/d	[a]

k_{dia} refers to the price for a drug resistance test. The GDP refers to the estimation for the year 2013 by the International Monetary Fund [75]. The state costs are defined by $c_{\mathcal{S}}(x) = \max_{n_C} pL(n_C) \cdot GDP$.

[a] Assuming an annual inflation of 5.4% for South Africa [75].

doi:10.1371/journal.pcbi.1004200.t002

where $c_{\mathcal{A}}: \mathcal{A} \mapsto [0, \infty)$ is the direct cost of action per unit time and $c_{\mathcal{S}}: \mathcal{S} \mapsto [0, \infty)$ is the indirect cost produced by the state per unit time with parameters given in Table 2.

We define a cost function

$$C(x, a, \tau) := \mathbb{E}_x^a \left(\int_0^\tau e^{-\lambda s} c(X_s, a)\, ds \right), \tag{15}$$

which denotes **the expected discounted costs for the time interval $(0,\tau]$** when starting in state x and choosing an action $a \in \mathcal{A}$ for propagation of the stochastic process for the entire interval τ. Further, we define the cost vector $\mathcal{K}_a \in \mathbb{R}^{|\mathcal{S}|}$, where its x$^{\text{th}}$ component denotes the direct and indirect cost per unit time for the state $x \in \mathcal{S}$ as shown below

$$\mathcal{K}_a[x] := c(x, a), \tag{16}$$

so that it holds that

$$C(x, a, \tau) := \mathcal{K}_a' \left(\int_0^\tau e^{-\lambda s} \cdot \mathbf{e}^{L_a \cdot s}\, ds \right) \varphi_x, \tag{17}$$

where the vector φ_x denotes a point-distribution, i.e. a single realization X_t of the Markov Jump Process. If the initial state is described by an arbitrary distribution p on the state space $\mathcal{S}$, we get

$$C(p, a, \tau) = \sum_{x \in \mathcal{S}} C(x, a, \tau) \cdot p[x], \tag{18}$$

where $p[x]$ denotes the probability of the x$^{\text{th}}$ state.

Performance Criterion and Bellman Equation

The two optimal control problems that we solve, i.e. the **diagnostic-guided strategy** and the **pro-active strategy**, differ slightly in the underlying assumption on the controllability of the disease dynamics. Both control strategies will be described in the following, defining in each case a control policy, a performance criterion and an optimality equation.

Diagnostic-guided strategy (closed-loop optimal control). In the **diagnostic-guided strategy**, treatment can only be changed after a (costly) diagnostic test has been made to

determine the virologic state of the patient (i.e. the drug resistance profile). This would correspond to the typical scenario in which a treating physician makes a *patient-specific* decision. However, instead of considering regular diagnostic intervals, we consider *patient-specific* diagnostic intervals. That is, upon assessing the virologic status of the patient, the physician decides both on a treatment a and on a time-lag τ until the next diagnosis. This implies that patients, whose viral status is "critical" may be monitored more closely than those whose status is "uncritical". More precisely, a *policy* for the diagnostic-guided strategy is a function

$$u : \mathcal{S} \to \mathcal{A} \times [0, \infty), \quad x \mapsto u(x) = (a(x), \tau(x)) \tag{19}$$

which prescribes for each disease state $x \in \mathcal{S}$ both a treatment/action $a(x) \in \mathcal{A}$ and an *examination lag time* $\tau(x) > 0$ that denotes the time until the next diagnostic. Each determination of the patient's virologic status incurs a *diagnostic cost* k_{dia}.

Within this framework, controlling the disease process proceeds as follows: Assuming the patient is in state $X_0 = x \in \mathcal{S}$ at the initial time $t_0 = 0$, a treatment/action $a(X_0) \in \mathcal{A}$ and an examination lag time $\tau(X_0) > 0$ are recommended. The stochastic process proceeds unobserved until time $t_1 = t_0 + \tau(X_0)$ when the next diagnostics are performed, revealing disease state X_{t_1} and incurring a diagnostic cost k_{dia}. Based on the state X_{t_1}, a (possibly) new treatment/action $a(X_{t_1})$ and a time lapse for next examination $\tau(X_{t_1})$ are recommended, etc. . . The resulting *examination times* $(t_0, t_1, t_2, \ldots)$ depend on the stochastic dynamics of the process and the applied policy. A switch of actions can only happen at examination times t_j, when the physician changes treatment due to the diagnosed disease status X_{t_j}.

The performance criterion for the corresponding control problem is given by:

$$J(x, u) = \mathbb{E}_x^u \left(\sum_{j=0}^{\infty} e^{-\lambda t_j} \left(C\left(X_{t_j}, a(X_{t_j}), \tau(X_{t_j})\right) + e^{-\lambda \tau(X_{t_j})} k_{\text{dia}} \right) \right), \tag{20}$$

see [25], where $\mathbb{E}_x^u$ stands for the expectation value with respect to the measure determined by the initial state x and the control u. The value function for this problem is given by

$$V(x) := \inf_{u \in \mathcal{U}} J(x, u) \tag{21}$$

with corresponding *Bellman Equation*:

$$V(x) = \min_{a \in \mathcal{A}, \tau \in [0, \infty)} \Big(\quad C(x, a, \tau) + e^{-\lambda \tau} \left(k_{\text{dia}} + (V^{tr} \cdot T_{a,\tau})(x) \right) \Big), \tag{22}$$

see [25] for the proof. The *Bellman Equation* can be used in order to numerically solve this optimal control problem, which requires to find an optimal treatment and an optimal *examination lag time* for each possible disease state, see S1 Text for a detailed description of the algorithm.

Pro-active strategy (open-loop optimal control). In the **pro-active strategy**, no diagnostics are taken. Instead, all possible disease trajectories are anticipated in a probabilistic sense and decisions depend on the actual *probability state* $p \in \Omega$ of a patient; –i.e. the probabilities of being in either of each possible disease states $x \in S$. Given a treatment, this *probability state* of a patient evolves in a deterministic way, see Eq (2). By omitting diagnostics, the **pro-active strategy** may have the advantage of being more easily implementable in settings where resources and infrastructure would not allow for patient-specific diagnosis and treatment.

In this context, an optimal policy prescribes an action to each possible probability measure $p \in \Omega$ on the (infection) state space S:

$$u : \Omega \to \mathcal{A}, \quad p \mapsto u(p) = (a(p))$$

with $p[x] := \mathbb{P}(X = x)$.

We discretize the considered time index and allow treatment changes only for certain times $t_j = j \cdot \bar{\tau}, j \in \mathbb{N}$, where $\bar{\tau}$ is a fixed time lag. Within such a time interval of length $\bar{\tau}$ the action remains fixed, i.e. switching a treatment is possible only after a minimum time interval $\bar{\tau}$. We denote by $p_j = p(j \cdot \bar{\tau})$ the probability state at these time points and set $T_a := T_{a,\bar{\tau}}$ for simplicity. The state equation is then given by

$$p_{j+1} = T_a \cdot p_j, \tag{23}$$

where $a \in \mathcal{A}$ is the action applied in the j$^{\text{th}}$ interval and p_0 is a fixed initial state probability vector. The transition matrix $T_{a,\bar{\tau}}$ related to the action a and time lag $\bar{\tau}$ is defined in Eq (3). Unlike the **diagnostic-guided strategy** where the switching times are also the observation times, for the **pro-active strategy**, the disease process is unobserved.

For the **pro-active strategy** the performance criterion entails only *state* and *action* costs but no diagnostic costs. In analogy to (20), the performance criterion is given by

$$J(p_0, u) = \mathbb{E}^u_{p_0}\left(\sum_{j=0}^{\infty} e^{-\lambda t_j} C(p_j, u_j, \bar{\tau})\right) \tag{24}$$

with $u_j = u(p_j)$. The minimization of the performance criterion $J(p_0,u)$ for a given initial distribution p_0 requires to find a control u of infinite length (an infinite switching signal). In order to allow for a numerical solution of the above stated equation, we assume that the process is controlled for a large, but finite time horizon $(0, N_{\mathcal{I}} \cdot \bar{\tau}]$ after which a constant control $u_\infty \in \mathcal{A}$ is applied. In the current work, we used $\bar{\tau} = 2$ days and $N_{\mathcal{I}} \cdot \bar{\tau} = 5000$ days for a numerical solution. Thus, for the **pro-active strategy** we seek a sequence of $N_{\mathcal{I}}$+1 actions $(u_0,u_1,\ldots u_{N_{\mathcal{I}}-1},u_\infty)$ for a given initial probability distribution p_0. We denote the set of all admissible controls by $\mathcal{U}$. Obviously, the size of control space is $|\mathcal{U}| = |\mathcal{A}|^{N_{\mathcal{I}}+1}$.

Assuming that actions can only be changed for the finite time horizon $[0, N_{\mathcal{I}} \cdot \bar{\tau}]$ and an action is maintained afterwards, we derive a *Bolza Type* of performance criterion from the general formulation in Eq (24):

$$J(p_0, u) = \mathbb{E}^u_{p_0}\left(\sum_{j=0}^{N_{\mathcal{I}}-1} e^{-\lambda t_j} C(p_j, u_j, \bar{\tau}) + e^{-\lambda t_{N_{\mathcal{I}}}} C(p_{N_{\mathcal{I}}}, u_\infty, \infty)\right) \tag{25}$$

denoting the expected costs for the infinite time horizon, given an initial distribution $p_0 \in \Omega$ and a control u. The performance criterion Eq (25) for the **pro-active strategy** contains a terminal cost and a running cost, see S2 Text. Given an initial state vector p_0, a control $u \in \mathcal{U}$ and fixed action u_∞ after the interval $N_{\mathcal{I}}$, the expression can be simplified to

$$J(p_0, u) = \sum_{j=0}^{N_{\mathcal{I}}-1} q'_{u_j,j} \cdot p_j + q'_{u_\infty} \cdot p_{N_{\mathcal{I}}} \tag{26}$$

where $q_{u_\infty} \in \mathbb{R}^{|S|}_+$ and $q_{u_j,j} \in \mathbb{R}^{|S|}_+$ are the terminal and the running cost vectors respectively.

Now, the optimal control problem can be defined as:

$$\begin{aligned} J^*(p_0, u^*) &= \min_{u \in \mathcal{U}} \sum_{j=0}^{N_{\mathcal{I}}-1} q'_{u_j,j} \cdot p_j + q'_{u_\infty} \cdot p_{N_{\mathcal{I}}} \\ \text{w.r.t } p_{j+1} &= T_{u_j} \cdot p_j \\ p_0 &= p(0) \cdot \end{aligned} \tag{27}$$

The *Hamiltonian function* for the j[th] interval is given by the following equation

$$H_j = \xi'_{j+1} \cdot T_{u_j} \cdot p_j + q'_{u_j,j} \cdot p_j \tag{28}$$

where ξ is the *adjoint vector*. The adjoint equation and transversal condition are given by

$$\begin{aligned} \xi'_j &= \xi'_{j+1} \cdot T_{u_j} + q'_{u_j,j} \\ \xi'_{N_{\mathcal{I}}} &= q'_{u_\infty} \cdot \end{aligned} \tag{29}$$

The *Bellman Equation* for the discrete-case [27, 55] is given by

$$\begin{aligned} V(p_j, j) &= \min_{a \in \mathcal{A}} \left(q'_{a,j} \cdot p_j + V(p_{j+1}, j+1) \right) \\ &= \min_{a \in \mathcal{A}} \left(e^{-\lambda \cdot t_j} C(p_j, a, \bar{\tau}) + V(p_{j+1}, j+1) \right) \cdot \end{aligned} \tag{30}$$

Eq (29) allows to redefine the optimal control problem Eq (27) for any $m \in \{0 \cdots N_{\mathcal{I}}\}$ as shown below

$$\begin{aligned} J^*(p_0, u^*) &= \min_{u \in \mathcal{U}} \left(\xi'_m \cdot p_m + \sum_{j=0}^{m-1} q'_{u_j,j} \cdot p_j \right) \\ \text{w.r.t } p_{i+1} &= T_{u_i} \cdot p_i && ; p_0 = p(0) \\ \xi'_l &= \xi'_{l+1} \cdot T_{u_l} + q'_{u_l,l} && ; \xi'_{N_{\mathcal{I}}} = q'_{u_\infty} \end{aligned} \tag{31}$$

where $i = 0 \ldots (m-1)$ and $l = (N_{\mathcal{I}} - 1) \ldots m$. This formulation shows the similarity of the optimal control problem to a two point boundary value problem for a continuous case. The boundary conditions are $p_0 = p(0)$ and $\xi_{N_{\mathcal{I}}} = q_{u_\infty}$. Note that the optimal control problem needs to be solved for all possible boundary conditions for the adjoint vectors, i.e. by iterating over all possible actions for u_∞.

Numerical Solution

Solving optimal control problems is generally computation intense and may not always be achievable. Our two optimal control scenarios require different algorithms for their solution.

For computing the optimal **diagnostic-guided strategy**, we used an adapted policy iteration algorithm, see S1 Text for details.

In order to numerically compute the optimal **pro-active strategy**, we introduce a dynamic programming technique in S2 Text, which was developed for the considered performance criterion (expected discounted costs over an infinite time horizon). It has some similarity with the algorithm introduced by Hernandez-Vargas [27], which, however, considers a different performance criterion (only terminal cost).

Both algorithms were implemented in MATLAB Version 8 and parallelized, where applicable. For the dynamic programming technique in S2 Text we used the state of art solver cplex from the IBM ILOG CPLEX [56] Optimization Studio to solve embedded linear programs.

Results

Optimal Treatment Strategy

The optimal **diagnostic-guided strategy** is given in S1 Table. In brief, for the considered parameters (Tables 1 and 2), it is suggested to use the first-line treatment a_1 in all states, except those where the virus is resistant against treatment a_1, but susceptible to a_2. In the later case treatment line a_2 is suggested. In line with this treatment recommendation, patient monitoring is only suggested as long as the patient is infected with drug-susceptible ("wild-type") virus. If the patient has a *h*igh or *m*edium virus load, the next diagnostic test should be within 25 days, if the patient has a ℓow/non-detectable virus load, after 152 days.

These results may indicate that the cost for diagnostics is too high in relation to the economic benefit resulting from more close monitoring and informed treatment adaptation (this will be discussed later in the *Discussion*). An exemplary trajectory that highlights the treatment strategy is shown in Fig 4A. The blue line indicates a *patient-specific* trajectory. The filled black marks indicate the times when a diagnostic test is performed and the background shading indicates the applied treatment (white: a_1, gray shading: a_2). In the example, the patient initially has a high copy number *h* of wild type (WT) virus, while none of the drug resistant viruses are present. This state is represented by the vector notation $X_{t_0} = [h,\ 0,\ 0,\ 0]$. For this state, the optimal treatment policy (see S1 Table) suggests to use treatment a_1 and to perform the next

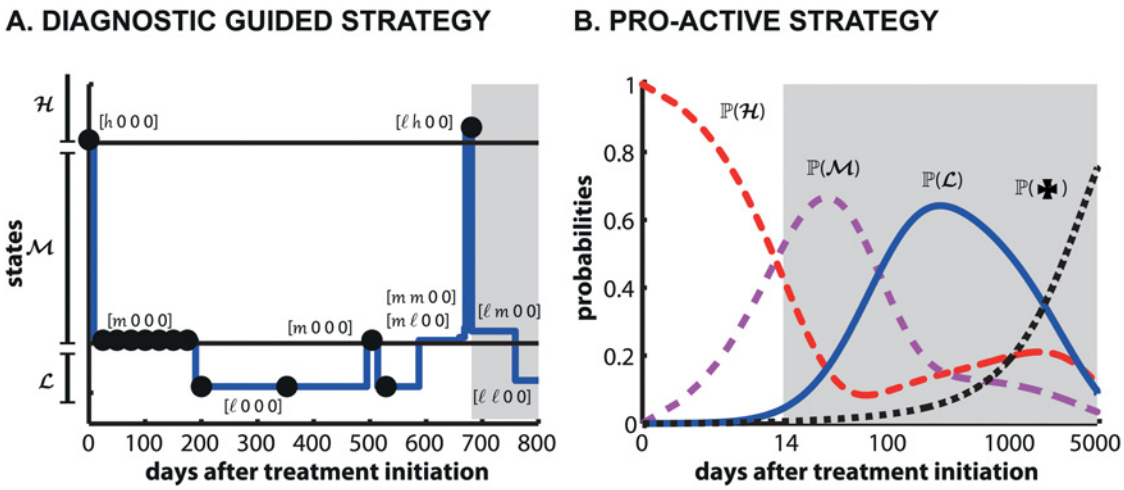

Fig 4. Disease progression for the diagnostic-guided strategy (individual trajectory, panel A) and pro-active strategy (probabilistic measure, panel B). The white region denotes application of treatment a_1 and the gray region denotes the application of treatment a_2. We assumed that the initial HIV virologic status is represented by a treatment-naive patient with high copy number of wild type virus [n_C(WT) = *h*,n_C(R1) = 0,n_C(R2) = 0,n_C(HR) = 0]. In panel **A**, the blue line represents a stochastic realization of HIV dynamics in a single individual treated with the **diagnostic-guided strategy** and black dots indicate diagnostic assessments. In the y-axis, all states belonging to the set of viral states $\mathcal{H}$, $\mathcal{M}$ and $\mathcal{L}$ are indicated. $\mathcal{L}$ denotes an undetectable total viral load, i.e. this is the set of states for which condition $n_C(M) \leq \ell$ for all possible virus mutants *M* holds ($[\leq \ell,\ \leq \ell,\ \leq \ell,\ \leq \ell]$). Likewise, $\mathcal{H}$ denotes a high total viral load, i.e. refers to all states for which for at least one viral strain *M*, $n_C(M) > m$. The remaining viral states belong to $\mathcal{M}$. Only the initial part of the trajectory is presented (day 0–800 after treatment initiation) and details of transitions to each state are labeled for clarity. In panel **B**, the black, red, magenta and blue lines represent the probabilities of states ✠ (patient death), $\mathcal{H}$, $\mathcal{M}$ and $\mathcal{L}$ after application of the **pro-active strategy**. Note, that for the **pro-active strategy**, the x-axis is logarithmically scaled.

doi:10.1371/journal.pcbi.1004200.g004

diagnostic test in 25 days (the second black marking in panel Fig 4A). At the next diagnostic test, the patient is in state $[m,\ 0,\ 0,\ 0]$ for which continuation of treatment a_1 is recommended and the next diagnostic test is scheduled after 25 days (the 3rd–9th black marking in panel Fig 4A). In the following, the virus remains suppressed, with a small detected 'blip' after about 500 days. After about 600 days of treatment, during the time lapse between diagnostic tests, the a_1 resistant strain R1 emerges. Notice transitions from the state $[m,\ 0,\ 0,\ 0] \rightarrow [m,\ \ell,\ 0,\ 0] \rightarrow [m,\ m,\ 0,\ 0]$, then $[\ell,\ m,\ 0,\ 0]$ and finally $[\ell,\ h,\ 0,\ 0]$ in the Fig 4A, where the copy number of a_1 resistant strain R1 increases from a ℓow copy number to a *h*igh copy number (virus rebound after resistance development). At the time point of the next diagnostic (at around 700 days), the emergence of resistance is identified $[\ell,\ h,\ 0,\ 0]$ and a switch to treatment a_2 is suggested (marked by gray region in Fig 4A). After the initiation of treatment a_2, a transition to state $[\ell,\ \ell,\ 0,\ 0]$ can be observed in the trajectory, which implies a decrease in the a_1 resistant strain (viral suppression).

The optimal **pro-active strategy** depends on the initial *probability state* of the patient p_0. We assumed that the patient is treatment naive and has *h*igh virus copy numbers, i.e. $p[h,\ 0,\ 0,\ 0](t_0) = 1$ and $p[x](t_0) = 0$ for $x \in \mathcal{S}\backslash[h, 0, 0, 0]$. For this scenario, it is suggested to start with treatment line a_1 and to switch to a_2 after 14 days, which is then maintained. The trajectories of the patient *probability states* are depicted in Fig 4B. For the ease of interpretation, we illustrate only the sets of viral states $\mathcal{L}$, $\mathcal{M}$, $\mathcal{H}$ and patient death ✠. $\mathcal{L}$ denotes an undetectable total viral load. Translated to our model, this is the set of states for which condition $n_C(M) \leq \ell$ for all possible virus mutants M holds, i.e. the current state has to fulfill $[\leq \ell,\ \leq \ell,\ \leq \ell,\ \leq \ell]$ to belong to this set. Likewise $\mathcal{H}$ denotes a high total viral load, i.e. refers to all states for which for at least one viral strain M, $n_C(M) > m$ is fulfilled. The remaining viral states belong to $\mathcal{M}$. One can nicely see that after approximately 260 days, maximum viral suppression may be achieved in the sense that the probability to have undetectable virus load ($\mathcal{L}$) is maximal (64.19%), while the patient may have intermediate viral loads $\mathcal{M}$ with 15.57% probability and high viral loads $\mathcal{H}$ with only 14.40% probability (the probability of death is 5.84%). After this time, it becomes more likely to fail treatment, as indicated by an increase in states $\mathcal{M}$ and $\mathcal{H}$ relative to $\mathcal{L}$. We also assessed the sensitivity of the optimal **pro-active strategy** to variations in parameter values and found it to be fairly insensitive to parameter perturbations, see S3 Text. For comparison, we also show the dynamics for the case when no treatment switches were conducted in S4 Text in relation to the optimal **pro-active strategy**.

Cost of Strategy

In our model, the cost incurred by a treatment strategy can be divided into two types: The direct costs, which include treatment- and diagnostic costs, and indirect costs incurred by the virologic/health status of a patient (state costs). The **pro-active strategy** does not comprise diagnostic tests, whereas the protocol for the current **standard of care** (S.O.C.), as well as the protocol used in the **HPTN052** [16], which we simulate for comparison, require viral load measurements. Currently, the expensive resistance tests are not part of the protocol for the **standard of care**, nor were they used for treatment decisions in **HPTN052**. The protocol for S.O.C. recommends changing treatment, if viral load (which is measured at month 6 and then every 12 months) is detectable and confirmed in a follow up testing after 2 months. The protocol for the **HPTN052** trial recommends changing treatment, if two consecutive viral load measurements were greater than 1000 copies/mL, 16 weeks after treatment initiation. Viral load was measured at week 2, at month 1, 2, 3 after treatment initiation and then every 3 month. The cost of virologic testing is roughly 30 US$ per test [57, 58]. In contrast to S.O.C. and **HPTN052**, the **diagnostic-guided strategy** requires drug resistance testing. We set the cost of

Table 3. Expected discounted costs for an infinite time horizon.

Type of cost	Standard of care protocol [US$]	HPTN052 protocol [US$]	Pro-active strategy [US$]	Diagnostic-guided strategy [US$]
Treatment costs	1,725	1,974	2,772	1,307
Diagnostic costs	146	416	–	4,232
Total handling cost	1,871	2,390	2,772	5,539
State costs	83,770	82,210	81,047	78,319
Total cost	85,641	84,600	83,819	83,858

For each treatment strategy, the total expected discounted cost for an infinite time horizon are shown. Further, the total cost is splitted into direct cost (treatment cost and diagnostic cost) and indirect cost (state costs).

doi:10.1371/journal.pcbi.1004200.t003

the diagnostics for the **diagnostic-guided strategy** to 200 US$ per test, in line with the recent literature [57, 59].

Table 3 displays the expected discounted costs for an infinite time horizon for different strategies and highlights the direct- and indirect costs of each strategy, respectively. This comparison shows that the **pro-active strategy** performs best (83,819 US$), followed closely by the **diagnostic-guided strategy** (83,858 US$), the **HPTN052 protocol** (84,600 US$) and then by the **standard of care** (85,641 US$). The total expected discounted costs for the **pro-active**- and the **diagnostic-guided strategy** are 2% less than that of the **standard of care**. The state costs (indirect cost related to patient-well being) are the major determinant of the total cost, making up roughly 98%, 97%, 97% and 93% of total cost for the S.O.C., the **HPTN052 protocol**, the **pro-active**—and the **diagnostic-guided strategy** respectively. In terms of state costs, the **diagnostic-guided strategy** performs best.

The direct costs (treatment and diagnostic costs) are highest for the **diagnostic-guided strategy** (5,539 US$) followed by the **pro-active strategy** (2,772 US$), the **HPTN052 protocol** (2,390 US$) and the **standard of care** (1,871 US$). The direct costs make up only 2%, 3%, 3% and 7% of the total costs for S.O.C., the **HPTN052 protocol**, the **pro-active** and the **diagnostic-guided strategy** respectively. The direct costs of the **pro-active** and the **diagnostic-guided strategy** are roughly 48% and 196% more than that of S.O.C.

Patient Survival

Clearly, the primary goal of any treatment strategy is to improve and prolong the life expectancy of the treated individual. We therefore compare the distinct treatment strategies in terms of patient survival. For that purpose, we define the following term:

$$\mathbb{P}(X_s = ✠ | \mathrm{stg})$$

which denotes the probability of death ✠ at time s given that the patient was treated according to treatment strategy stg. Given two distinct strategies; stg and a reference treatment strategy $\mathrm{stg}_{\mathrm{ref}}$, the term $T^{+}_{0\to t}(\mathrm{stg}, \mathrm{stg}_{\mathrm{ref}})$ refers to the expected years of life gained (life prolongation) when the treatment strategy stg is used, relative to the reference treatment $\mathrm{stg}_{\mathrm{ref}}$ at time t after initiation of treatment:

$$T^{+}_{0\to t}(\mathrm{stg}, \mathrm{stg}_{\mathrm{ref}}) = \int_{s=0}^{t} \mathbb{P}(X_s = ✠ | \mathrm{stg}_{\mathrm{ref}}) - \mathbb{P}(X_s = ✠ | \mathrm{stg}) \quad ds \cdot \tag{32}$$

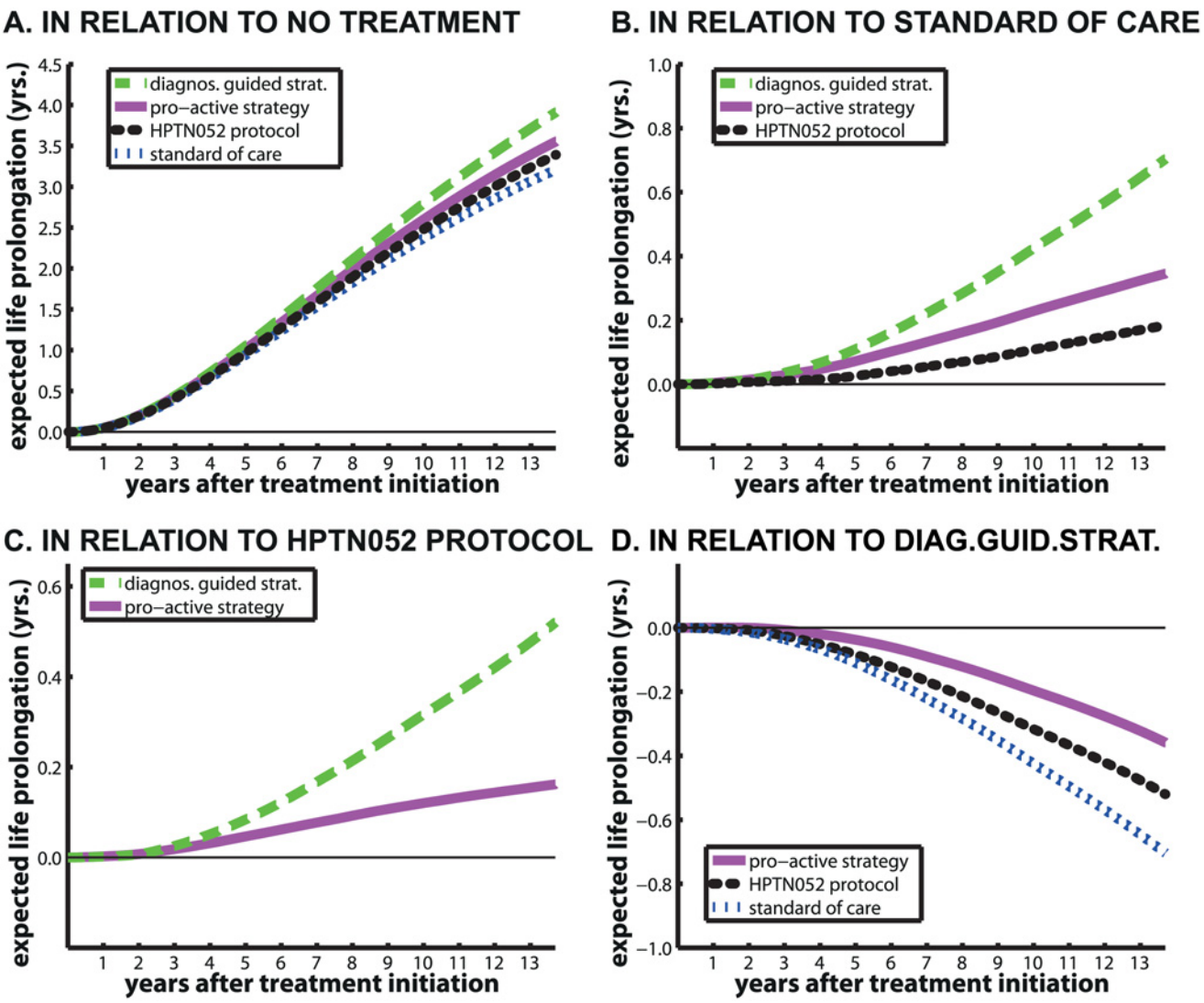

Fig 5. Relative expected life prolongation [years] for different treatment strategies. The purple solid lines, green dashed lines, blue dash-dotted lines and black dots represent the **pro-active strategy**-, the **diagnostic-guided strategy**, the current **standard of care** and the **HPTN052 protocol** respectively. The thin black line denotes the line of unity (no improvement/worsening). Panels A-D show the expected life-time prolongation for the distinct treatment strategies in relation to the **no treatment**, **standard of care**, the **HPTN052 protocol** and the optimal **diagnostic-guided strategy** respectively.

doi:10.1371/journal.pcbi.1004200.g005

In other words, given a patient is treated with stg and another patient is treated with $\mathrm{stg}_{\mathrm{ref}}$ for time t, the terms $T^{+}_{0\to t}(\mathrm{stg}, \mathrm{stg}_{\mathrm{ref}})$ refers to the expected time that a patient treated with stg will live longer than the patient treated with $\mathrm{stg}_{\mathrm{ref}}$.

We compared all strategies with the following reference strategies $\mathrm{stg}_{\mathrm{ref}}$: i) no medical intervention, ii) the **standard of care** treatment, iii) treatment according to the **HPTN052 protocol** and iv) the **diagnostic-guided strategy**. Fig 5A and 5D show the trajectories of expected life prolongation by different strategies in relation to i)-iv). Table 4 displays the expected life-years gained after 1 -, 2 -, 5 -, 8 -, 12—and 13.7 years of treatment respectively, where we additionally show the expected life prolongation in relation to the uninfected state.

The first five rows of Table 4 show the expected loss-of-life-time of an HIV infected person treated with distinct strategies in relation to an HIV uninfected person. After 13.7 years, an

Table 4. Expected relative life-time gained using different strategies.

		Expected life prolongation [years] after					
Ref. Strategy	**Test Strategy**	**1 yr**	**2 yrs**	**5 yrs**	**8 yrs**	**12 yrs**	**13.7 yrs**
No disease	Diag-guided strategy	-0.020	-0.070	-0.360	-0.870	-1.830	-2.300
No disease	Pro-active strategy	-0.020	-0.070	-0.400	-0.990	-2.110	-2.660
No disease	HPTN052 protocol	-0.030	-0.080	-0.450	-1.080	-2.250	-2.820
No disease	Standard of care	-0.030	-0.090	-0.470	-1.150	-2.400	-3.010
No disease	No treatment	-0.070	-0.280	-1.420	-2.980	-5.260	-6.220
No treatment	Diag-guided strategy	0.051	0.206	1.058	2.115	3.427	3.912
No treatment	Pro-active strategy	0.051	0.206	1.020	1.993	3.150	3.554
No treatment	HPTN052 protocol	0.050	0.200	0.970	1.900	3.000	3.390
No treatment	Standard of care	0.050	0.190	0.940	1.830	2.850	3.210
Standard of care	Diag-guided strategy	0.003	0.014	0.110	0.284	0.569	0.704
Standard of care	Pro-active strategy	0.004	0.014	0.072	0.163	0.292	0.345
Standard of care	HPTN052 protocol	0.002	0.007	0.026	0.070	0.149	0.184
HPTN052 protocol	Diag-guided strategy	0.002	0.007	0.084	0.214	0.420	0.520
HPTN052 protocol	Pro-active strategy	0.002	0.007	0.047	0.092	0.144	0.162

The table shows the relative expected gain in life-time for the distinct treatment strategies in comparison to a reference strategy. The reference strategies are i) no infection ii) **no treatment** iii) **standard of care** and iv) the **HPTN052 protocol**. Values were computed using Eq (32).

doi:10.1371/journal.pcbi.1004200.t004

HIV patient receiving **no treatment** lives on average 6.2 years less than a healthy person. An HIV patient receiving treatment according to S.O.C., the **pro-active strategy**, the **diagnostic-guided strategy** or according to the **HPTN052 protocol** lives on average 3, 2.66, 2.3 and 2.82 years less than a healthy person. Fig 5A shows that all treatment strategies are better than receiving **no treatment** at all and prolong the life of an HIV patient by at least 3.2 years in relation. Fig 5B shows that the **diagnostic-guided**, **pro-active strategy** and the **HPTN052 protocol** are better at increasing patient survival than the **standard of care**. Further, Fig 5C shows that the *optimal* strategies are slightly better than the **HPTN052 protocol** and Fig 5D shows that the **pro-active strategy** and the **HPTN052 protocol** are slightly worse than the **diagnostic-guided strategy**. Table 4 shows that during the initial 2–3 years of treatment, there is almost no difference between the **diagnostic-guided** and the **pro-active strategy** with regard to patient survival. After 13.7 years of treatment, the difference between the two *optimal* strategies is less than 5 month (0.358 years).

Expected Reduction in Secondary Cases

Besides the primary goal of improving the life of the HIV patient, 'treatment for prevention' has gained interest in recent years. 'Treatment for prevention' strategies reduce onward transmission of the virus by reducing the infectiousness of HIV positive individuals. In order to measure the efficacy of the treatment strategies in preventing HIV-1 transmission, we estimated the incidence rate per 100 person-years associated with each HIV lumped state (ℓ, m, h) from a meta-analysis by Attia et al [14] (see S5 Text). The meta-analysis summarizes the outcome of 11 clinical studies on HIV-1 transmission in heterosexual sero-discordant couples, primarily from Africa.

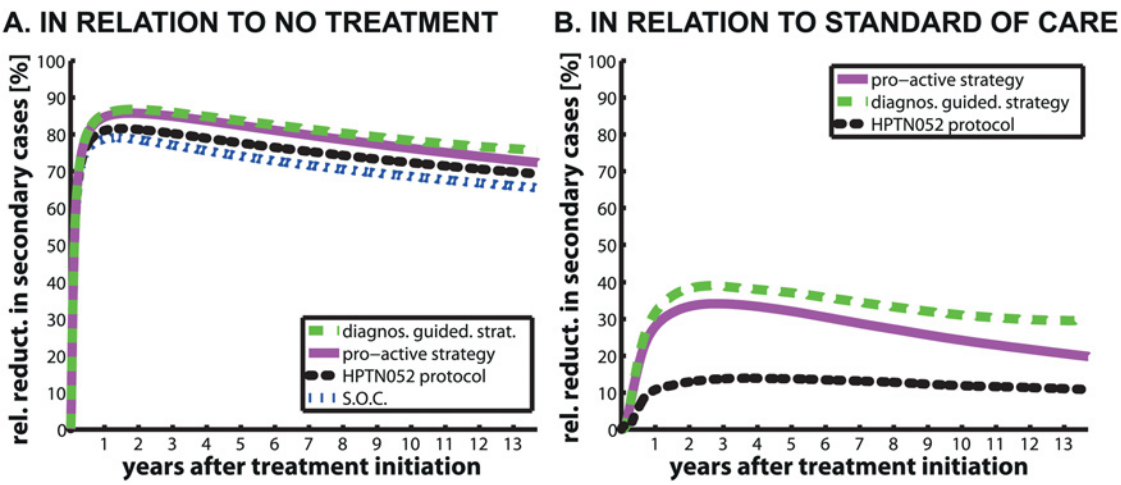

Fig 6. Comparison of the relative reduction of secondary cases per survivor. The purple solid, green dashed, blue dash-dotted lines and black dots represent the expected relative reduction of secondary cases per survivor by the **pro-active-**, the **diagnostic-guided strategy**, S.O.C. and in the **HPTN052 protocol**. In panel A, the reference strategy is **no treatment** and in panel B it is S.O.C.

doi:10.1371/journal.pcbi.1004200.g006

For a strategy stg applied for a time t, the following equation gives a measure of the expected number of secondary cases/transmissions per survivor

$$\mathbb{E}_{0\to t}(\text{transm.}|\text{stg} \wedge \neg\text{✠}) = \int_{s=0}^{t} \frac{\sum_x \mathbb{P}(X_s = x|\text{stg}) \cdot \mathbb{IR}(x)}{1 - \mathbb{P}(X_s = \text{✠})} ds \tag{33}$$

where $\mathbb{IR}(x)$ is the incidence rate per 100 person-years for a state x in our virus dynamics model, as explained in S5 Text and given in Table 1. Given two strategies, stg_1 and stg_{ref}, the percentage of potential infections prevented by strategy stg_1 in comparison to the reference strategy stg_{ref} is given by the quotient:

$$\%\text{transmissions prevented until } t = 100 \cdot \left(1 - \frac{\mathbb{E}_{0\to t}(\text{transm} \cdot |\text{stg}_1 \wedge \neg\text{✠})}{\mathbb{E}_{0\to t}(\text{transm} \cdot |\text{stg}_{\text{ref}} \wedge \neg\text{✠})}\right) \tag{34}$$

We computed the expected reduction of secondary cases for different strategies taking either **no treatment** or the current **standard of care** as the reference strategy. In comparison to **no treatment**, the maximal reduction of secondary cases for the **pro-active** -, the **diagnostic-guided strategy**, the **HPTN052 protocol** and S.O.C. are achieved roughly 1.5–3 years after treatment initiation with values of 86%, 87%, 82% and 79% respectively, see Fig 6A. The relative reduction of secondary cases per survivor for the **diagnostic-guided** and the **pro-active strategy** are very similar, with an increase for the first 2 years, followed by a slow decline (see Fig 6A and Table 5). The relative reduction of secondary cases per survivor for the **HPTN052 protocol** is slightly better than that of S.O.C, with a tendency to decline over time, see Table 5. Note, that the computed relative reduction of secondary cases with the **HPTN052 protocol** was 82% (Table 5), which is slightly lower than the reported relative reduction of transmission events in the actual HPTN052 study [16] (reduction of 96% of linked and 89% of total transmission events). We have discussed reasons for this apparent under-prediction later in the manuscript. The difference between the optimal strategies (**diagnostic-guided** and the **pro-active strategy**) and S.O.C. becomes evident, when looking at the relative risk reduction by the optimal treatment strategies in relation to S.O.C. in Fig 6B. The reduction in secondary cases per survivor

Table 5. Expected relative reduction of secondary cases per survivor using different treatment strategies after different treatment durations.

		relative reduction in secondary cases [%]					
Ref. strategy	**Test strategy**	**1 yr**	**2 yrs**	**3.5 yrs**	**5 yrs**	**8 yrs**	**13.7 yrs**
No treatment	Diagnostic-guided strategy	85.52	86.76	85.42	83.71	80.33	75.72
No treatment	Pro-active strategy	84.72	85.72	84.34	82.41	78.54	72.35
No treatment	HPTN052 protocol	81.01	81.32	79.61	77.66	74.29	69.25
No treatment	Standard of care	78.77	78.55	76.31	74.08	70.50	65.50
Standard of care	Diagnostic-guided strategy	31.79	38.29	37.45	37.15	33.31	29.61
Standard of care	Pro-active strategy	28.04	33.45	33.88	32.11	27.25	19.85
Standard of care	HPTN052 protocol	10.83	12.94	13.93	13.79	12.83	10.85

The table shows the expected relative reduction in secondary cases for different strategies in comparison to **no treatment** and S.O.C. after different treatment durations. Values were computed using Eq (34).

doi:10.1371/journal.pcbi.1004200.t005

by the optimal strategies in comparison to S.O.C. is highest at the beginning and then slowly decreases over time.

Discussion

The main aim of this work was to develop a rigorous mathematical framework that allows to compare different treatment paradigms in terms of monetary costs, treatment benefit and efficacy for 'treatment for prevention'. It was previously stated [60], that the durability of 'treatment for prevention' should be assessed. Our simulations over a long time horizon (up to 5000 days/13.7 years) indicate that the effect of 'treatment for prevention' is significant and remains relatively stable beyond the time horizon typically assessed in clinical studies, see Fig 6A and Table 5, and that it may even be improved. We estimated that a **standard of care** therapy in e.g. South Africa can achieve a 66–79% reduction of HIV-1 onward transmission, in comparison to delivering **no treatment**. We also implemented the **HPTN052 protocol**, as stated in [16] and predicted that it would achieve up to 82% reduction of HIV-1 transmission, being more effective than the current **standard of care**, as shown in Fig 6B.

Statistical assessment of the actual HPTN052 trial [16] yielded estimates for the relative reduction of transmission of 96% for linked transmission and 89% for any transmission. Our simulated **HPTN052 protocol** yielded a 82% reduction of onwards transmission, which is within the confidence range of the reported estimates (CI: 73–99% for linked transmission and CI: 68–96% for any transmission) [16]. Note, that only one linked transmission event (1/1585 person-years) was observed in the early therapy arm of HPTN052 [16], giving rise to the statistical uncertainty in the reported estimate. Nevertheless, our simulations may under-predict the efficacy of HPTN052 due to several factors:

i. The reported treatment efficacy in the HPTN052 study was higher than predicted by our model: Virologic failure was only observed in 5% of participants in the early-therapy group of HPTN052, possibly explaining the difference between the outcome of the simulation vs. the clinical trial.

ii. Despite only 5% failing to suppress the virus in the HPTN052 study, 66% initiated a second line therapy [16], meaning that a significant proportion of patients switched treatment *before/without* virologic failure. In our simulations of the **HPTN052 protocol**, patients only

switched treatment when they showed signs of virologic failure. However, one may speculate that these treatment switches *before/without* virologic failure may have an impact on the long-term viral suppression that could be similar to a pro-active treatment switch.

iii. The primary measurable endpoint of the HPTN052 study was the infection of the sero-discordant partner. Onward transmissions to other individuals could not be quantified for obvious reasons.

While a number of trials are now underway to confirm the results of HPTN052, see e.g. [61, 62], our *in silico* approach specifically addresses the need for an improved treatment strategy, particularly taking affordability into account, which suggests strategies that are suitable for scaling up.

Our work may indicate that if 'treatment for prevention' is scaled up and implemented using the current **standard of care** treatment strategy, its efficacy may not be as high as expected from HPTN052. Unlike in HPTN052, where monitoring of treatment success (viral suppression) and timely execution of treatment changes were realized, in resource-constrained countries close patient monitoring is currently not implemented in a routine setting and may be difficult to realize due to infrastructural and economic requirements.

Two alternative strategies for the immediate initiation of therapy were assessed in our work that take into account the mentioned limitations. Both suggested strategies (the **diagnostic-guided strategy** and the **pro-active strategy**) yielded better results in our simulations in terms of the reduction of onward transmission (see Table 5) at a lower price (Table 3). Both *optimal* strategies could yield a 72–87% reduction in HIV onward transmission in comparison to **no treatment**, see Fig 6A and Table 5. In comparison to the **standard of care**, we estimated that the **diagnostic-guided strategy** and the **pro-active strategy** could yield another 33–38% reduction of onward transmission after 2 years of treatment, but the advantages of the **diagnostic-guided strategy** and the **pro-active strategy** over the **standard of care** slowly declined over time, see Fig 6B. This indicates that both *optimal* strategies have a particular strength in reducing early transmissions (shortly after treatment initiation) in comparison to the current **standard of care**. This may be of particular utility, if transmission occurred primarily during early infection [63, 64]. In our work, we did not take behavioral factors into account, which would lead to a time-dependency of the infection rate. Rather, we assumed that the infection rate $\mathbb{IR}(x)$ is constant over time, but dependent on the total virus load as reported earlier [14, 15, 19–21]. If transmission would primarily take place during an early infection, the advantages of the **diagnostic-guided strategy** and the **pro-active strategy** over the **standard of care** would be even more pronounced than indicated in Fig 6B.

The *optimal* **diagnostic-guided strategy** suggested *patient-specific* diagnostics, i.e. dependent on the patient's virologic status (see S1 Table), unlike fixed intervals as in S.O.C, or the protocol stated in [16]. In summary, the *optimal* **diagnostic-guided strategy** suggests to take frequent diagnostics (≈ every month) if the patient is infected with a *h*igh or *m*edium number of treatment-susceptible virus and less frequent (≈ every 5 month) diagnostics if the patient is infected with a ℓow/undetectable number of virus. No diagnostics are recommended for the remaining virologic states. Altogether, a very sparse diagnostic schedule for individual patients is suggested. Previous work [25] indicated that price reductions for the diagnostic tests would yield a better patient-outcome, which indicates that available drugs may not be utilized optimally in resource-poor settings, because diagnostics are currently too expensive. Of note is the fact that albeit treatment being available at very low expense (due to negotiations by the Clinton Foundation [65]), diagnostics may not be.

Furthermore, we suspected that allowing treatment change only *after* diagnostic confirmation of treatment failure (i.e. some time after drug resistance has occurred) may limit future

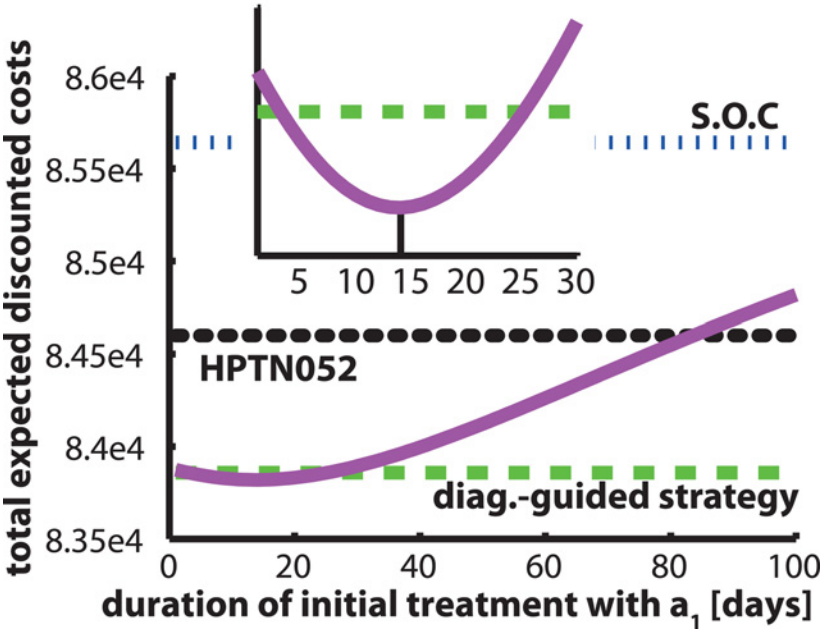

Fig 7. Sensitivity of the pro-active strategy with respect to timing of the treatment switch. The purple solid line represents the total expected discounted costs for the **pro-active strategy** with respect to the switching time (shown on the x-axis). The horizontal green dashed, blue dash-dotted lines and black dots represent the total expected discounted costs for the optimal **diagnostic-guided strategy**, S.O.C. and in the **HPTN052 protocol**. The inset shows a zoom into the first 30 days after treatment initiation.

doi:10.1371/journal.pcbi.1004200.g007

treatment options [34]. Since the *optimal* **diagnostic-guided strategy** suggested rare diagnostics, and because it only allows to change treatment *after* resistance is detectable, we evaluated **pro-active switching strategies**. Note, that pro-active treatment switching strategies tested in the clinic increased virologic suppression and lowered rates of drug resistance emergence in HIV-1, when compared to conventional strategies [66, 67]. Similar strategies are also used against bacterial infections and cancers.

The computed **pro-active strategy** suggests a single treatment change *without* prior ascertainment of the viral status within a treated patient. Surprisingly, this strategy could yield comparable outcomes in terms of monetary costs, patient health and reduction of onward transmission, see Tables 3–5 and Figs 5 and 6. Our work thus indicates that **pro-active strategies**, may be as effective as diagnostically-driven ones, when diagnostics are expensive or inaccessible. Note, that unlike other *optimal* control approaches, i.e. [28] that suggest infinitely fast switching between regimens to mitigate drug resistance emergence, our predicted **pro-active strategy** actually only recommends a single treatment change, which is clinically more realistic. We also analyzed the sensitivity of the **pro-active strategies** with respect to the timing of this switch (see Fig 7). The graphic illustrates, that the switch is optimal after 14 days, however the difference in the performance measure is marginal, as long as the treatment switch is performed before $\approx$ 30 days (1 month) after treatment initiation.

Obviously, pragmatic and clinical considerations need to be taken into account to translate our results into practice. Also, several assumptions have been made, which require careful evaluation. For example, we used a very coarse-grained model of HIV within-host dynamics, which was required to enable the numerical computation of optimal controls, particularly for

the closed-loop system employed in the **diagnostic-guided strategy**. Most models of viral dynamics, e.g. [33, 68, 69], were developed to accurately predict short-term viral dynamics after drug application and are unable to predict virologic failure after long time intervals, in contrast to our coarse-grained model, which was developed and parameterized in order to predict short-term viral dynamics as well as virologic failure after very long time-intervals, see e.g. Figs 2 and 3. It is therefore more suitable than existing models in estimating the long-term response to antiviral treatment. However, in the future we will focus on developing more elaborated HIV-models and on algorithms to solve the control problem for the chemical master equation directly, without state-space lumping. Note, that other computationally efficient numerical approaches, such as model predictive control [30], could be used to approximate the optimal treatment strategies. However, there is no guarantee that the computed control using these approaches will be *optimal*.

In our approach, we modeled treatment change as a switched system, which neglects the pharmacokinetics of the distinct drugs [10, 70–72] and may only indirectly reflect drug adherence in an average population (drug efficacy η is a constant term in our model). Neglecting pharmacokinetics may, however, be a justifiable step in this modeling exercise, because of the considered time-scales (on the order of years), and also because optimizing e.g. drug adherence was not an objective of this study. However, if the main interest is for example in optimizing the switch between two treatment lines by optimal dosing in order to prevent time frames of insufficient viral suppression or drug over-exposure, or to include *patient-specific* or time-dependent drug adherence, we advise to consider a different control system, for example [73]. Within such a framework, monitoring (e.g. viral load assessment) may also be incorporated as a tool to assess individual drug adherence and to allocate resources to improve it.

We did not explicitly consider costs related to contraindications caused by the treatment. For example, the second treatment line a_2 may be less tolerable. Mathematically, this can be modeled in terms of increased treatment costs for a_2, in comparison to the first treatment line a_1. In order to test the sensitivity of the optimal **pro-active strategy** to this parameter, we conducted the necessary computations in S3 Text and found that the computed strategy was fairly insensitive to changes in treatment costs. This may indicate that the benefits of the treatment switch outweigh these potential shortcomings.

Also, we did not include screening costs or the costs of the initial virologic assessment, thus our calculations refer to the public health costs that accrue *from the start* of HIV treatment. These costs will, however, only enter as a constant to each of the tested strategies and will not change the results beyond the addition of this constant to the values stated in Table 3. Additional costs (personnel, infrastructure, transportation) may come along with diagnostic assessments. It is likely that hidden costs for diagnostics are substantial. With a higher cost of diagnosis, the **pro-active strategy** may outperform the **diagnostic-guided strategy**, which may suggest an even less frequent diagnostic schedule, supporting our claim that current diagnostics may be too expensive to be appropriately used.

We used the price of a drug resistance test ($k_{\mathrm{dia}} \approx 200$ US$ [57, 59]) to account for diagnostics in the **diagnostic-guided strategy**. This had the following reason: Current guidelines recommend to measure the total virus load [13] and to switch treatment, if, based on this partial information, virologic failure is anticipated. As reported by others [57], this may lead to unnecessary treatment switches. In contrast, a resistance test directly informs the physician about the necessity of treatment change. Mathematically, partial information, i.e. the *total virus load*, would lead to a distinct control framework, namely Partially Observable Markov Decision Processes (POMDP) [74], which are extremely challenging to solve, particularly for larger models like the one used herein (Fig 1). In POMDPs, partial information may be mapped into a '*believed*' full virologic status, for example *observing* a *h*igh total virus load *may* be due to some

resistance development, e.g. the viral state $[\ell,\ h,\ 0,\ 0]$ with some probability. However, it is hard for us formalize the physicians intuition (i.e. the relation between observation, belief and truth) regarding this 'mapping' of partial measurements to viral states x.

As a primary outcome of our modeling exercise, we estimated the expected *relative* number of secondary infections prevented (Table 5 and Fig 6); -unlike many other approaches (summarized in [18]), which take the *absolute* number of secondary cases into account. Estimating *absolute* numbers of secondary cases would require to model complex behaviors, i.e. sexual relationships, etc. over time, for which we do not have data for validation, nor was it the main focus of the current work. This also prevents us from predicting the course of the epidemic or deriving its reproductive number R_0 in relation to distinct treatment strategies. However, the primary aim of this study was to compare the efficacy of different treatment strategies, which is nicely quantified in terms of the expected *relative* number of secondary infections prevented. Note, that this relative estimate requires no assumptions on the underlying transmission dynamics, except that it assumes that these dynamics are similar for a tested strategy versus its comparator.

In addition to insights in HIV 'treatment for prevention' strategies, the developed mathematical/control theoretic framework may already be applicable to many medical phenomena. Further developments may improve its applicability to even more complex processes, which can be accurately described by intrinsically stochastic dynamics. For example, the open-loop optimal control approach (used to determine the optimal **pro-active** strategy) may be turned into a closed-loop system, if diagnostics are taken from time-to-time to determine the viral state of a patient, i.e. $p[x](t_j)$. Also, the closed-loop system that requires state determination (the **diagnostic-guided strategy**) may be combined with the open-loop system in order to allow for pro-active treatment changes in between diagnostic assessments.

Supporting Information

S1 Text. The supplementary text contains details of the algorithm for solving the closed-loop control system, as well as the pseudo-code.
(PDF)

S2 Text. The supplementary text contains details on the algorithm for solving the open-loop control system, as well as the pseudo-code.
(PDF)

S3 Text. The supplementary text contains an analysis of the sensitivity of the optimal pro-active strategy with respect to parameter variations.
(PDF)

S4 Text. The supplementary text contains the viral dynamics for constant treatment (no switches) in relation to the optimal pro-active strategy.
(PDF)

S5 Text. The supplementary text contains details on the calculation of the incidence rate $\mathbb{IR}(x)$ from the lumped states of our HIV-dynamics model, including a comparison with experimental data.
(PDF)

S1 Table. The supplementary table contains the optimal policy for the diagnostic-guided strategy. The first entry corresponds to the dead patient ✠.
(TXT)

Acknowledgments

We thank Maureen Smith for proof-reading the manuscript.

Author Contributions

Conceived and designed the experiments: SD SW MvK. Performed the experiments: SD SW MvK. Analyzed the data: SD SW CS MvK. Wrote the paper: SD MvK.

References

1. Global report: UNAIDS report on the global AIDS epidemic 2013 (available at http://www.unaids.org/en/media/unaids/contentassets/documents/epidemiology/2013/gr2013/ accessed on 15-may-2014).
2. Buzon MJ, Sun H, Li C, Shaw A, Seiss K, et al. (2014) HIV-1 persistence in CD4+ T cells with stem cell-like properties. Nat Med 20: 139–142. doi: 10.1038/nm.3445 PMID: 24412925
3. Blankson JN, Persaud D, Siliciano RF (2002) The challenge of viral reservoirs in HIV-1 infection. Annu Rev Med 53: 557–593. doi: 10.1146/annurev.med.53.082901.104024 PMID: 11818490
4. Fletcher CV, Staskus K, Wietgrefe SW, Rothenberger M, Reilly C, et al. (2014) Persistent HIV-1 replication is associated with lower antiretroviral drug concentrations in lymphatic tissues. Proc Natl Acad Sci USA 111: 2307–2312. doi: 10.1073/pnas.1318249111 PMID: 24469825
5. von Kleist M, Metzner P, Marquet R, Schütte C (2012) HIV-1 polymerase inhibition by nucleoside analogs: cellular- and kinetic parameters of efficacy, susceptibility and resistance selection. PLoS Comput Biol 8: e1002359. doi: 10.1371/journal.pcbi.1002359 PMID: 22275860
6. Grant RM, Lama JR, Anderson PL, McMahan V, Liu AY, et al. (2010) Preexposure chemoprophylaxis for HIV prevention in men who have sex with men. N Engl J Med 363: 2587–2599. doi: 10.1056/NEJMoa1011205 PMID: 21091279
7. Thigpen MC, Kebaabetswe PM, Paxton LA, Smith DK, Rose CE, et al. (2012) Antiretroviral preexposure prophylaxis for heterosexual HIV transmission in Botswana. N Engl J Med 367: 423–434. doi: 10.1056/NEJMoa1110711 PMID: 22784038
8. Baeten JM, Donnell D, Ndase P, Mugo NR, Campbell JD, et al. (2012) Antiretroviral prophylaxis for HIV prevention in heterosexual men and women. N Engl J Med 367: 399–410. doi: 10.1056/NEJMoa1108524 PMID: 22784037
9. Choopanya K, Martin M, Suntharasamai P, Sangkum U, Mock PA, et al. (2013) Antiretroviral prophylaxis for HIV infection in injecting drug users in Bangkok, Thailand (the Bangkok Tenofovir Study): a randomised, double-blind, placebo-controlled phase 3 trial. Lancet 381: 2083–2090. doi: 10.1016/S0140-6736(13)61127-7 PMID: 23769234
10. Duwal S, Schütte C, von Kleist M (2012) Pharmacokinetics and pharmacodynamics of the reverse transcriptase inhibitor tenofovir and prophylactic efficacy against HIV-1 infection. PLoS One 7: e40382. doi: 10.1371/journal.pone.0040382 PMID: 22808148
11. Nichols BE, Baltussen R, van Dijk JH, Thuma PE, Nouwen JL, et al. (2014) Cost-Effectiveness of PrEP in HIV/AIDS Control in Zambia: A Stochastic League Approach. J Acquir Immune Defic Syndr 66: 221–228. PMID: 24694930
12. World Health Organization (WHO). Global update on HIV treatment 2013: Results, Impact and Opportunities (available at http://www.who.int/hiv/pub/progressreports/update2013/en/ accessed on 02-june-2014).
13. The South African Anti Retroviral Treatment Guidelines 2013, Version 14 (available at http://www.sahivsoc.org/practise-guidelines/national-dept-of-health-guidelines accessed 15-may-2014).
14. Attia S, Egger M, Müller M, Zwahlen M, Low N (2009) Sexual transmission of HIV according to viral load and antiretroviral therapy: systematic review and meta-analysis. AIDS 23: 1397–1404. doi: 10.1097/QAD.0b013e32832b7dca PMID: 19381076
15. Hughes JP, Baeten JM, Lingappa JR, Magaret AS, Wald A, et al. (2012) Determinants of percoital-act HIV-1 infectivity among african HIV-1-serodiscordant couples. J Infect Dis 205: 358–365. doi: 10.1093/infdis/jir747 PMID: 22241800
16. Cohen MS, Chen YQ, McCauley M, Gamble T, Hosseinipour MC, et al. (2011) Prevention of HIV-1 infection with early antiretroviral therapy. N Engl J Med 365: 493–505. doi: 10.1056/NEJMoa1105243 PMID: 21767103
17. Cohen J (2011) Breakthrough of the year. HIV treatment as prevention. Science 334: 1628.

18. Eaton JW, Johnson LF, Salomon JA, Bärnighausen T, Bendavid E, et al. (2012) HIV treatment as prevention: systematic comparison of mathematical models of the potential impact of antiretroviral therapy on HIV incidence in South Africa. PLoS Med 9: e1001245. doi: 10.1371/journal.pmed.1001245 PMID: 22802730

19. Fideli US, Allen SA, Musonda R, Trask S, Hahn BH, et al. (2001) Virologic and immunologic determinants of heterosexual transmission of human immunodeficiency virus type 1 in Africa. AIDS Res Hum Retroviruses 17: 901–910. doi: 10.1089/088922201750290023 PMID: 11461676

20. Quinn TC, Wawer MJ, Sewankambo N, Serwadda D, Li C, et al. (2000) Viral load and heterosexual transmission of human immunodeficiency virus type 1. Rakai Project Study Group. N Engl J Med 342: 921–929. doi: 10.1056/NEJM200003303421303 PMID: 10738050

21. Lingappa JR, Hughes JP, Wang RS, Baeten JM, Celum C, et al. (2010) Estimating the impact of plasma HIV-1 RNA reductions on heterosexual HIV-1 transmission risk. PLoS One 5: e12598. doi: 10.1371/journal.pone.0012598 PMID: 20856886

22. Hosseinipour MC, Gupta RK, Zyl GV, Eron JJ, Nachega JB (2013) Emergence of HIV drug resistance during first- and second-line antiretroviral therapy in resource-limited settings. J Infect Dis 207 Suppl 2: S49–S56. doi: 10.1093/infdis/jit107 PMID: 23687289

23. Hecht R, Bollinger L, Stover J, McGreevey W, Muhib F, et al. (2009) Critical choices in financing the response to the global HIV/AIDS pandemic. Health Aff (Millwood) 28: 1591–1605. doi: 10.1377/hlthaff.28.6.1591

24. Bärnighausen T, Salomon JA, Sangrujee N (2012) HIV treatment as prevention: issues in economic evaluation. PLoS Med 9: e1001263. doi: 10.1371/journal.pmed.1001263 PMID: 22802743

25. Winkelmann S, Schütte C, von Kleist M (2014) Markov control processes with rare state observation: Theory and application to treatment scheduling in HIV-1. Communications in Mathematical Sciences 12: 859–77. doi: 10.4310/CMS.2014.v12.n5.a4

26. Luo R, Piovoso MJ, Martinez-Picado J, Zurakowski R (2011) Optimal antiviral switching to minimize resistance risk in HIV therapy. PloS one 6: e27047. doi: 10.1371/journal.pone.0027047 PMID: 22073250

27. Hernandez-Vargas E, Colaneri P, Middleton R, Blanchini F (2011) Discrete-time control for switched positive systems with application to mitigating viral escape. International Journal of Robust and Nonlinear Control 21: 1093–1111. doi: 10.1002/rnc.1628

28. Hernandez-Vargas EA, Colaneri P, Middleton RH (2013) Optimal therapy scheduling for a simplified HIV infection model. Automatica 49: 2874–2880. doi: 10.1016/j.automatica.2013.06.001

29. Cardozo EF, Zurakowski R (2012) Robust closed-loop minimal sampling method for HIV therapy switching strategies. IEEE Transactions on Bio-Medical Engineering 59: 2227–2234. doi: 10.1109/TBME.2012.2201479 PMID: 22652153

30. Hernandez-Vargas EA, Colaneri P, Middleton RH (2014) Switching strategies to mitigate HIV mutation. IEEE Transactions on Control Systems Technology 22: 1623–1628. doi: 10.1109/TCST.2013.2280920

31. Rouzine IM, Rodrigo A, Coffin JM (2001) Transition between stochastic evolution and deterministic evolution in the presence of selection: general theory and application to virology. Microbiol Mol Biol Rev 65: 151–185. doi: 10.1128/MMBR.65.1.151-185.2001 PMID: 11238990

32. Althaus CL, Boer RJD (2008) Dynamics of immune escape during HIV/SIV infection. PLoS Comput Biol 4: e1000103. doi: 10.1371/journal.pcbi.1000103 PMID: 18636096

33. von Kleist M, Menz S, Huisinga W (2010) Drug-class specific impact of antivirals on the reproductive capacity of HIV. PLoS computational biology 6: e1000720. doi: 10.1371/journal.pcbi.1000720 PMID: 20361047

34. von Kleist M, Menz S, Stocker H, Arasteh K, Schütte C, et al. (2011) HIV quasispecies dynamics during pro-active treatment switching: Impact on multi-drug resistance and resistance archiving in latent reservoirs. PLoS One 6: e18204. doi: 10.1371/journal.pone.0018204 PMID: 21455303

35. Wilkinson DJ (2006) Stochastic Modelling for Systems Biology. Chapman & Hall/CRC.

36. Allen LJS (2011) An Introduction to Stochastic Processes with Applications to Biology. Chapman & Hall/CR.

37. Gillespie DT (1977) Exact stochastic simulation of coupled chemical reactions. J Phys Chem 81: 2340–61. doi: 10.1021/j100540a008

38. Pahle J (2009) Biochemical simulations: stochastic, approximate stochastic and hybrid approaches. Brief Bioinform 10: 53–64. doi: 10.1093/bib/bbn050 PMID: 19151097

39. Menz S, Latorre J, Schütte C, Huisinga W (2012) Hybrid stochastic-deterministic solution of the chemical master equation. SIAM Multiscale Modelling and Simulation 10: 1232–62. doi: 10.1137/110825716

40. Hasenauer J, Wolf V, Kazeroonian A, Theis FJ (2013) Method of conditional moments (MCM) for the Chemical Master Equation: A unified framework for the method of moments and hybrid stochastic-deterministic models. J Math Biol. PMID: 23918091

41. Markowitz M, Louie M, Hurley A, Sun E, Mascio MD, et al. (2003) A novel antiviral intervention results in more accurate assessment of human immunodeficiency virus type 1 replication dynamics and T-cell decay in vivo. J Virol 77: 5037–5038. doi: 10.1128/JVI.77.8.5037-5038.2003 PMID: 12663814

42. Fischer M, Joos B, Niederst B, Kaiser P, Hafner R, et al. (2008) Biphasic decay kinetics suggest progressive slowing in turnover of latently HIV-1 infected cells during antiretroviral therapy. Retrovirology 5: 107. doi: 10.1186/1742-4690-5-107 PMID: 19036147

43. Paci P, Carello R, Bernaschi M, D'Offizi G, Castiglione F (2009) Immune control of HIV-1 infection after therapy interruption: immediate versus deferred antiretroviral therapy. BMC Infect Dis 9: 172. doi: 10.1186/1471-2334-9-172 PMID: 19840392

44. Harrigan PR, Whaley M, Montaner JS (1999) Rate of HIV-1 RNA rebound upon stopping antiretroviral therapy. AIDS 13: F59–F62. doi: 10.1097/00002030-199905280-00001 PMID: 10371167

45. Ruiz L, Martinez-Picado J, Romeu J, Paredes R, Zayat MK, et al. (2000) Structured treatment interruption in chronically HIV-1 infected patients after long-term viral suppression. AIDS 14: 397–403. doi: 10.1097/00002030-200003100-00013 PMID: 10770542

46. Arribas JR, Pozniak AL, Gallant JE, DeJesus E, Gazzard B, et al. (2008) Tenofovir disoproxil fumarate, emtricitabine, and efavirenz compared with zidovudine/lamivudine and efavirenz in treatment-naive patients: 144-week analysis. J Acquir Immune Defic Syndr 47: 74–78. doi: 10.1097/QAI.0b013e31815acab8 PMID: 17971715

47. Cooper DA, Heera J, Goodrich J, Tawadrous M, Saag M, et al. (2010) Maraviroc versus efavirenz, both in combination with zidovudine-lamivudine, for the treatment of antiretroviral-naive subjects with CCR5-tropic HIV-1 infection. J Infect Dis 201: 803–813. doi: 10.1086/650697 PMID: 20151839

48. DeJesus E, McCarty D, Farthing CF, Shortino DD, Grinsztejn B, et al. (2004) Once-daily versus twice-daily lamivudine, in combination with zidovudine and efavirenz, for the treatment of antiretroviral-naive adults with HIV infection: a randomized equivalence trial. Clin Infect Dis 39: 411–418. doi: 10.1086/424009 PMID: 15307010

49. DeJesus E, Herrera G, Teofilo E, Gerstoft J, Buendia CB, et al. (2004) Abacavir versus zidovudine combined with lamivudine and efavirenz, for the treatment of antiretroviral-naive HIV-infected adults. Clin Infect Dis 39: 1038–1046. doi: 10.1086/424009 PMID: 15472858

50. Gulick RM, Ribaudo HJ, Shikuma CM, Lalama C, Schackman BR, et al. (2006) Three- vs four-drug antiretroviral regimens for the initial treatment of HIV-1 infection: a randomized controlled trial. JAMA 296: 769–781. doi: 10.1001/jama.296.7.769 PMID: 16905783

51. Hicks C, King MS, Gulick RM, White AC, Eron JJ, et al. (2004) Long-term safety and durable antiretroviral activity of lopinavir/ritonavir in treatment-naive patients: 4 year follow-up study. AIDS 18: 775–779. doi: 10.1097/00002030-200403260-00008 PMID: 15075512

52. Smith KY, Patel P, Fine D, Bellos N, Sloan L, et al. (2009) Randomized, double-blind, placebo-matched, multicenter trial of abacavir/lamivudine or tenofovir/emtricitabine with lopinavir/ritonavir for initial HIV treatment. AIDS 23: 1547–1556. doi: 10.1097/QAD.0b013e32832cbcc2 PMID: 19542866

53. Perelson AS, Essunger P, Cao Y, Vesanen M, Hurley A, et al. (1997) Decay characteristics of HIV-1-infected compartments during combination therapy. Nature 387: 188–191. doi: 10.1038/387188a0 PMID: 9144290

54. Kates J, Boortz K, Lief E, Avila C, Gobet B (2012) Financing the Response to AIDS in Lowand Middle-Income Countries: International Assistance from the G8, European Commission and Other Donor Governments in 2009. Technical report, UNAIDS.

55. Lenhart S, Workman JT (2007) Optimal control applied to biological models. CRC Press.

56. IBM ILOG CPLEX (available at http://www-01.ibm.com/software/ accessed 15-may-2014).

57. Rosen S, Long L, Sanne I, Stevens WS, Fox MP (2011) The net cost of incorporating resistance testing into HIV/AIDS treatment in South Africa: a Markov model with primary data. J Int AIDS Soc 14: 24. doi: 10.1186/1758-2652-14-24 PMID: 21575155

58. Steegen K, Luchters S, Cabooter ND, Reynaerts J, Mandaliya K, et al. (2007) Evaluation of two commercially available alternatives for HIV-1 viral load testing in resource-limited settings. J Virol Methods 146: 178–187. doi: 10.1016/j.jviromet.2007.06.019 PMID: 17686534

59. Elliott JH, Lynen L, Calmy A, Luca AD, Shafer RW, et al. (2008) Rational use of antiretroviral therapy in low-income and middle-income countries: optimizing regimen sequencing and switching. AIDS 22: 2053–2067. doi: 10.1097/QAD.0b013e328309520d PMID: 18753937

60. Chen YQ, Masse B, Wang L, Ou SS, Li X, et al. (2012) Statistical considerations for the HPTN 052 study to evaluate the effectiveness of early versus delayed antiretroviral strategies to prevent the sexual transmission of HIV-1 in serodiscordant couples. Contemp Clin Trials 33: 1280–1286. doi: 10.1016/j.cct.2012.07.007 PMID: 22813645

61. Hayes R, Ayles H, Beyers N, Sabapathy K, Floyd S, et al. (2014) HPTN 071 (PopART): rationale and design of a cluster-randomised trial of the population impact of an HIV combination prevention intervention including universal testing and treatment - a study protocol for a cluster randomised trial. Trials 15: 57. doi: 10.1186/1745-6215-15-57 PMID: 24524229

62. Iwuji CC, Orne-Gliemann J, Tanser F, Boyer S, Lessells RJ, et al. (2013) Evaluation of the impact of immediate versus WHO recommendations-guided antiretroviral therapy initiation on HIV incidence: the ANRS 12249 TasP (Treatment as Prevention) trial in Hlabisa sub-district, KwaZulu-Natal, South Africa: study protocol for a cluster randomised controlled trial. Trials 14: 230. doi: 10.1186/1745-6215-14-230 PMID: 23880306

63. Brenner BG, Roger M, Routy JP, Moisi D, Ntemgwa M, et al. (2007) High rates of forward transmission events after acute/early HIV-1 infection. J Infect Dis 195: 951–959. doi: 10.1086/512088 PMID: 17330784

64. Recordon-Pinson P, Anies G, Bruyand M, Neau D, Morlat P, et al. (2009) HIV type-1 transmission dynamics in recent seroconverters: relationship with transmission of drug resistance and viral diversity. Antivir Ther 14: 551–556. PMID: 19578240

65. The Clinton Health Access Initiative (2011). Antiretroviral (ARV) ceiling price list (available at http://www.clintonfoundation.org, accessed 22-sept-2014).

66. Martinez-Picado J, Negredo E, Ruiz L, Shintani A, Fumaz CR, et al. (2003) Alternation of antiretroviral drug regimens for HIV infection. A randomized, controlled trial. Ann Intern Med 139: 81–89. doi: 10.7326/0003-4819-139-2-200307150-00007 PMID: 12859157

67. Negredo E, Paredes R, Peraire J, Pedrol E, Côté H, et al. (2004) Alternation of antiretroviral drug regimens for HIV infection. efficacy, safety and tolerability at week 96 of the Swatch study. Antivir Ther 9: 889–893. PMID: 15651747

68. Perelson AS, Nelson PW (1999) Mathematical analysis of HIV-1 dynamics in vivo. SIAM Review 41: 3–44. doi: 10.1137/S0036144598335107

69. Sedaghat AR, Dinoso JB, Shen L, Wilke CO, Siliciano RF (2008) Decay dynamics of HIV-1 depend on the inhibited stages of the viral life cycle. Proc Natl Acad Sci U S A 105: 4832–4837. doi: 10.1073/pnas.0711372105 PMID: 18362342

70. Frank M, von Kleist M, Kunz A, Harms G, Schütte C, et al. (2011) Quantifying the impact of nevirapine-based prophylaxis strategies to prevent mother-to-child transmission of HIV-1: a combined pharmacokinetic, pharmacodynamic, and viral dynamic analysis to predict clinical outcomes. Antimicrob Agents Chemother 55: 5529–5540. doi: 10.1128/AAC.00741-11 PMID: 21947390

71. von Kleist M, Huisinga W (2009) Pharmacokinetic-pharmacodynamic relationship of NRTIs and its connection to viral escape: an example based on zidovudine. Eur J Pharm Sci 36: 532–543. doi: 10.1016/j.ejps.2008.12.010 PMID: 19150497

72. Dixit NM, Perelson AS (2004) Complex patterns of viral load decay under antiretroviral therapy: influence of pharmacokinetics and intracellular delay. J Theor Biol 226: 95–109. doi: 10.1016/j.jtbi.2003.09.002 PMID: 14637059

73. Imran M, Smith HL (2014) A model of optimal dosing of antibiotic treatment in biofilm. Math Biosci Eng 11: 547–571. doi: 10.3934/mbe.2014.11.547 PMID: 24506551

74. Bäuerle N, Rieder U (2011) Markov Decision Processes with Applications to Finance, Springer, chapter Partially Observable Markov Decision Processes. pp. 147–174.

75. The International Monetary Fund. World economic outlook database (available at http://www.imf.org/external/pubs/ft/weo/2013/01/weodata/index.aspx, accessed 22-sept-2014)).

76. Sendi P, Günthard HF, Simcock M, Ledergerber B, Schüpbach J, et al. (2007) Cost-effectiveness of genotypic antiretroviral resistance testing in HIV-infected patients with treatment failure. PLoS One 2: e173. doi: 10.1371/journal.pone.0000173 PMID: 17245449

M.Frank*, M. Von Kleist*+, A. Kunz, G. Harms, C. Schütte and C. Kloft
Quantifying the Impact of Nevirapine-Based Prophylaxis Strategies To Prevent Mother-to-Child Transmission of HIV-1: a Combined Pharmacokinetic, Pharmacodynamic, and Viral Dynamic Analysis To Predict Clinical Outcomes
Antimicrobial Agents and Chemotherapy 55 (2011), 5529–5540
available online: https://doi.org/10.1128/AAC.00741-11

R P Smyth+, L Despons, G Huili, S Bernacchi, M Hijnen, J Mak,
F Jossinet, L Weixi, J-C Paillart, M von Kleist+ and R Marquet+
Mutational interference mapping experiment (MIME) for studying
RNA structure and function
Nature Methods 12 (2015), 866-876
available online: https://doi.org/10.1038/nmeth.3490

Published online 5 March 2018 *Nucleic Acids Research, 2018, Vol. 46, No. 9* ***e57***
doi: 10.1093/nar/gky152
https://doi.org/10.1093/nar/gky152

In cell mutational interference mapping experiment (in cell MIME) identifies the 5′ polyadenylation signal as a dual regulator of HIV-1 genomic RNA production and packaging

Redmond P. Smyth[1,*,†], Maureen R. Smith[2,†], Anne-Caroline Jousset[1], Laurence Despons[1], Géraldine Laumond[3], Thomas Decoville[3], Pierre Cattenoz[1], Christiane Moog[3], Fabrice Jossinet[1], Marylène Mougel[4], Jean-Christophe Paillart[1], Max von Kleist[2,*] and Roland Marquet[1,*]

[1]Université de Strasbourg, CNRS, Architecture et Réactivité de l'ARN, UPR 9002, IBMC, 15 rue René Descartes, 67000 Strasbourg, France, [2]Freie Universität Berlin, Department of Mathematics and Computer Science, Arnimallee 6, 14195 Berlin, Germany, [3]INSERM U1109, Fédération de Médecine Translationnelle de Strasbourg (FMTS), Université de Strasbourg, Strasbourg, France and [4]IRIM CNRS UMR9004, Université de Montpellier, Montpellier, France

Received January 09, 2018; Revised February 02, 2018; Editorial Decision February 15, 2018; Accepted March 01, 2018

ABSTRACT

Non-coding RNA regulatory elements are important for viral replication, making them promising targets for therapeutic intervention. However, regulatory RNA is challenging to detect and characterise using classical structure-function assays. Here, we present in cell Mutational Interference Mapping Experiment (in cell MIME) as a way to define RNA regulatory landscapes at single nucleotide resolution under native conditions. In cell MIME is based on (i) random mutation of an RNA target, (ii) expression of mutated RNA in cells, (iii) physical separation of RNA into functional and non-functional populations, and (iv) high-throughput sequencing to identify mutations affecting function. We used in cell MIME to define RNA elements within the 5′ region of the HIV-1 genomic RNA (gRNA) that are important for viral replication in cells. We identified three distinct RNA motifs controlling intracellular gRNA production, and two distinct motifs required for gRNA packaging into virions. Our analysis reveals the ^{73}AAUAAA^{78} polyadenylation motif within the 5′ PolyA domain as a dual regulator of gRNA production and gRNA packaging, and demonstrates that a functional polyadenylation signal is required for viral packaging even though it negatively affects gRNA production.

INTRODUCTION

Once thought to be a passive carrier of genetic information between the DNA and the protein world, RNA is now appreciated to play a central role in the regulation of almost all cellular activity (1). RNA is unique in that it encodes information in both its sequence and its structure. Like its counterpart DNA, the order of nucleotides in RNA represents the sequence of amino acids during protein synthesis. However, unlike the regular double stranded DNA helix, RNA molecules can fold into complex and elaborate three-dimensional structures that impart functionality by serving as recognition sites for proteins, small molecules, and other nucleic acids.

RNA viruses, with their compact and efficiently encoded genomes, are perfect models of complex RNA function. The genomic RNA (gRNA) of HIV-1 encodes nine proteins: the major structural proteins, Gag, Pol and Env; the regulatory proteins Tat and Rev; and the accessory proteins Vpu, Vpr, Vif and Nef. In addition to its coding capacity, the HIV-1 gRNA is replete with *cis*-acting regulatory sequences that interact in complex ways to modulate gene expression through effects on RNA processing, stability, export and translation. These regulatory sequences are espe-

*To whom correspondence should be addressed. Tel: +33 3 88 41 70 40; Fax: +33 3 88 60 22 18; Email: r.smyth@ibmc-cnrs.unistra.fr
Correspondence may also be addressed to Roland Marquet. Email: r.marquet@ibmc-cnrs.unistra.fr
Correspondence may also be addressed to Max von Kleist. Email: vkleist@zedat.fu-berlin.de
†These authors contributed equally to this work as first authors.
Present address: Pierre Cattenoz, Université de Strasbourg, CNRS UMR7104, IGMBC, 1 rue Laurent Fries, 67404, Illkirch, France.

cially concentrated within the 5′ untranslated region (UTR) and the beginning of the Gag coding sequence (2–7). This region of the gRNA is highly structured, and folds into a series of relatively independent functional domains (Figure 1A): the Trans-Activating Response (TAR) for transcription; PolyA for polyadenylation; the primer binding site (PBS) for reverse transcription; SL1 or the dimerization initiation site (DIS) for gRNA dimerization; SL2 contains the major splice donor (SD) site; and SL3 is historically considered the major packaging signal (Psi). Together, these functional domains regulate key steps of the HIV-1 life cycle (8–11), and serve to highlight the fact that the gRNA sustains not only protein synthesis, but is an active participant in the viral infection process.

Because regulatory elements are essential for viral replication, they represent promising, yet still underexplored antiviral targets (12). Indeed, pioneering work in Hepatitis C virus (HCV) demonstrates that non-coding RNA can be targeted therapeutically with high barriers to resistance, providing impetus for the systematic discovery of functional RNA motifs in viral genomes (13). To date, regulatory RNA is most often identified using truncation or deletion mutants in individual assays to define regions of functionality. However, regulatory regions often overlap in complex RNAs, making these laborious experiments difficult to interpret. Indeed, attempts to define the minimal HIV-1 packaging signal have led to largely conflicting results, and evidence can be found in the literature that almost all regions of the 5′UTR are required for packaging (14), including TAR (15,16), the poly-A stem loop (17,18), PBS (14,18), SL1 (14,19–21), SL2 (22), SL3 (23–25), as well as the first nucleotides of *gag* (6,26,27). Many of these studies used large and imprecise deletions that likely compromised the global folding of the RNA, and some of these studies may not be correctly interpreted. For example, TAR was once considered part of the HIV-1 packaging signal, until work by the Berkhout lab revealed that packaging defects were caused by TAR mutation induced misfolding of the HIV-1 leader RNA (28–30). Finally, truncation and deletion mutagenesis experiments are rarely able to define regions of functionality at single nucleotide resolution, nor do they provide enough information to mechanistically understand RNA function. Thus, there is an urgent need for new high-resolution and quantitative methods to analyse RNA function, especially within the native cellular environment.

We have recently developed Mutational Interference Mapping Experiment (MIME) as a powerful and high resolution method to identify functional regions within long RNA molecules *in vitro* (31). We previously used MIME to precisely map the binding site of the HIV-1 $Pr55^{Gag}$ protein on the viral gRNA *in vitro*, finding that $Pr55^{Gag}$ recognises the region encompassing nucleotides 227 to 337 (31). Whilst $Pr55^{Gag}$ binding to the gRNA is presumed to be the major determinant of gRNA packaging into viral particles, it is currently unclear whether $Pr55^{Gag}$ recognises this same site within cells (32), nor whether there are additional regulatory or packaging signals that may define binding sites for cellular (33) and viral proteins, or even nucleic acids (34). Additionally, the minimal signal required to direct HIV-1 gRNA into viral particles has yet to be precisely determined, with the packaging signal possibly comprising the entire 5′UTR and up to half of the Gag coding sequence (35,36). How such an extended packaging signal interconnects with other regulatory motifs situated in the same region is an open question, whose answer would undoubtedly help with the engineering of safe HIV-1 lentiviral vectors for gene therapy purposes.

Here, we have adapted MIME to identify RNA regulatory sequences within the HIV-1 genome during its replication in cells (in cell MIME) (Figure 1B). By varying the functional selection criteria, we obtained two distinct and high-resolution maps of regulatory RNA controlling intracellular gRNA production and gRNA packaging, respectively. We found three RNA motifs regulating intracellular gRNA production and two motifs regulating genome packaging. Strikingly, a ^{73}AAUAAA^{78} hexamer sequence within 5′ PolyA regulated both gRNA production and packaging, revealing the cellular polyadenylation machinery as a dual regulator of HIV-1 replication.

MATERIALS AND METHODS

Molecular clones

Mutant libraries were cloned into pDRNL43 NotI ATGaag Tat(–) ΔEnv which is a derivative of pDRNL43ΔEnv (37) modified to contain (i) NotI ^{431}GCgGCcGC^{439} and NgoMIV ^{958}GccGgC^{964} restriction sites for the cloning of the mutant library (positions based on pNL43 proviral DNA), (ii) a substitution in the initiation codon of *gag* to prevent Gag expression (27), (iii) a stop codon preventing Tat protein expression, (iv) a deletion in *env* (for biosafety). Gag and GagPol, and accessory proteins Tat and Rev, were expressed from the packaging vector pCMVΔR8.9 (38). PolyA and SL2 mutants were introduced into pDRNL43ΔEnv. Site directed mutagenesis was carried out utilising standard molecular biology techniques using the oligonucleotides listed in Supplementary Table S1.

Cell culture

Human embryonic kidney 293 (HEK 293T) cells were maintained at 37°C in Dulbecco's modified Eagle's medium (DMEM) supplemented with glutamine, penicillin, streptomycin and 10% (v/v) heat-inactivated fetal calf serum.

In cell mutational interference mapping experiment (MIME)

Mutagenesis. RNA expression vector (pDRNL43 NotI ATGaag NgoMIV Tat(–) ΔEnv) was mutated by error-prone PCR using the Mutazyme II DNA polymerase (Agilent) and the primers NL43_NotI_Fw and NgoMIV_Rv (Supplementary Table S1). We chose Mutazyme II as it is reported to produce a more uniform mutational spectrum than traditional error-prone PCR. The PCR reaction volume was 50 μl and consisted of 100 ng of template DNA, 1× buffer, 200 μM dNTPs, 0.5 μM of each primer, 2.5 U of Mutazyme II DNA polymerase. PCR cycling conditions were 95°C for 2 min followed by 35 cycles of 95°C for 30 s, 55°C for 30 s and 72°C for 1 min. We performed two or three rounds of PCR mutagenesis in duplicate. Mutated amplicon libraries were further amplified with the same primers used

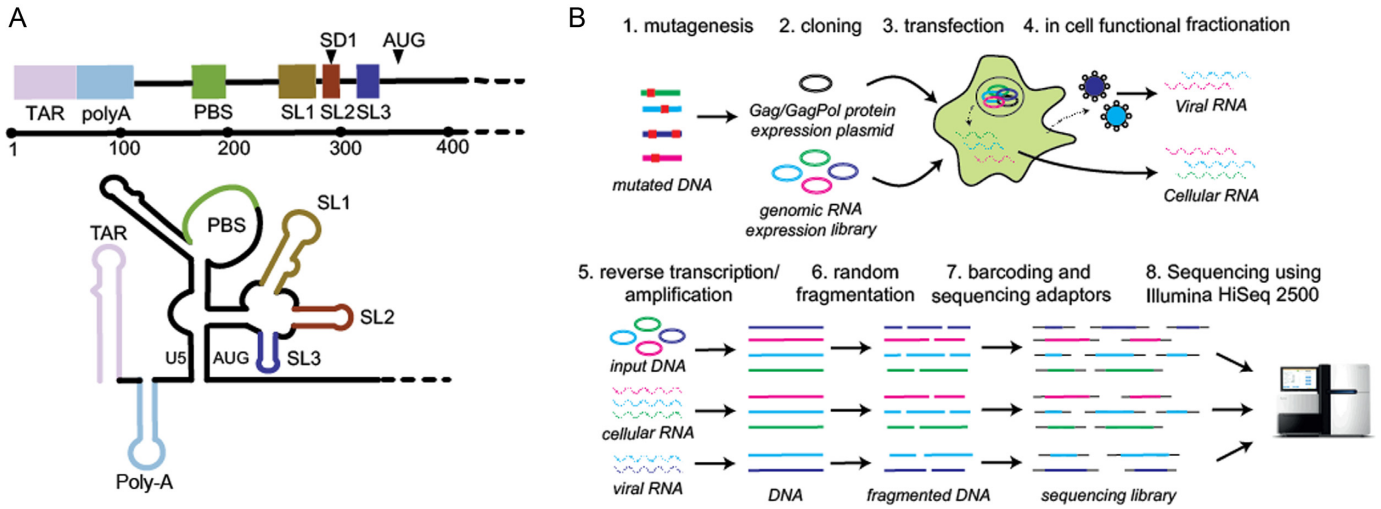

Figure 1. (**A**) The HIV-1 5′UTR folds into a series of structural domains that control key steps of the HIV-1 life cycle including transcription, translation, export, packaging and reverse transcription. From 5′ to 3′ these structural domains are: transactivation response (TAR) for transcription; PolyA stem loop for polyadenylation; the primer binding site (PBS) for reverse transcription; SL1 promotes gRNA dimerization; SL2 contains the major splice donor (SD) site; SL3 has historically been considered the major packaging signal (Psi); the sequences surrounding the AUG start codon are thought to be involved in a base-pairing interaction with the upstream U5 region. (**B**) In cell Mutational Interference Mapping Experiment (in cell MIME). The proviral genome is randomly mutated using error prone PCR, and subsequently cloned into a gRNA expression vector. The structural and enzymatic proteins, Gag and Gag-Pol are expressed from a separate expression plasmid. Co-transfection of the mutant library and Gag/Gag-Pol expression plasmid into 293T cells leads to the transcription of mutant RNAs and subsequent sorting of functional and non-functional RNA populations by the viral and cellular machinery. Viral RNA present in cells and virus is reverse transcribed. Viral cDNA and the input DNA plasmid is amplified, fragmented, barcoded, sequenced on an Illumina HiSeq2500, and analysed using the MIMEAnTo software.

for mutagenesis using Phusion polymerase (NEB). PCR reaction volume was 50 μl and consisted of ∼50 ng of mutated DNA, 1× HF buffer, 200 μM dNTPs, 0.5 μM of each primer, 1 U of Phusion polymerase. Eight PCR amplifications were performed using the PCR cycling conditions 98°C for 30 s, followed by 30 cycles of 98°C for 10 s and 72°C for 1 min. Amplified libraries were column purified (Macherey-Nagel) and stored at –20°C until further use.

Cloning of library. Column purified amplicon libraries and the RNA expression vector pDRNL43 NotI NgoMIV Tat(–) ΔEnv were digested with NotI and NgoMIV. Vector and inserts were gel purified on a 1% agarose gel, and ligated overnight at an approximate molar ratio of 1 (vector):5 (insert) using a temperature cycling protocol of 30 s at 10°C followed by 30 s at 30°C. Overnight ligations were column purified using Nucleospin Gel and PCR Clean-up columns (Macherey-Nagel) and stored at –20°C until further use.

Transfection. Transfections of HEK 293T cells were carried out using the X-tremeGENE-9 DNA Transfection Reagent (Roche) according to the manufacturer's instructions. Briefly, cells were seeded at 70% confluence in 100 mm cell culture dishes and co-transfected with 2.5 μg mutant library, 2.5 μg of pCMVΔR8.9 packaging vector, 1 μg of pCMV RFP with 1 μl of X-tremeGENE-9 per μg DNA. 36 h post-transfection, virus containing media was harvested for storage at 4°C and cells were replenished with fresh media to allow for a second virus harvest 24 h later. Virus containing supernatant was pooled and clarified by centrifugation at 1462 *g* for 30 min, then passed through a 0.22 μm filter to remove cellular debris. Purified virus was concentrated by ultracentrifugation at 100 000 *g* through a 20% sucrose cushion.

RNA extraction. RNA was extracted from viral or cellular pellets using TriReagent (MRC) according to the manufacturer's instructions. Briefly, cells or virions were lysed in 1 ml of TriReagent and incubated at room temperature for 5 min. 0.2 ml of chloroform was added, followed by vigorous mixing, and a further incubation at room temperature for 15 min. After centrifugation at 12 000 *g* for 15 min at 4°C, the upper aqueous phase was transferred into a new tube. RNA was precipitated by the addition of 0.5 ml of isopropanol and 1 μg of glycogen followed by centrifugation at 12 000 *g* for 15 min at 4°C. RNA pellets were washed once in 500 μl of 70% EtOH, air dried, and resuspended in 200 μl of RNase free H_2O. Viral and cellular RNA was then treated to remove contaminating plasmid DNA with 5 μl of RNase free DNase I (Roche), 5 μl RNasin (Promega) in 1× buffer (40 mM Tris–HCl, 10 mM NaCl, 6 mM $MgCl_2$, 1 mM $CaCl_2$, pH 7.9) for 2 h at 37°C. RNA was then extracted with phenol–chloroform, chloroform and precipitated with EtOH, washed with 70% EtOH and dissolved in ultra-pure water. Cellular and viral RNA pellets were dissolved in 200 μl and 20 μl of RNase free H_2O, respectively.

Reverse transcription. Four microliter of RNA was mixed with 1 μl of a 10 μM stock of primer NL43_544_Rv (Supplementary Table S1), denatured at 90°C for 2 min and then chilled on ice. Reverse transcription was carried out in a total volume of 10 μl by adding 1× buffer (50 mM Tris–HCl pH 8.3, 6 mM $MgCl_2$, 40 mM KCl), 200 nM dNTPs and 2 U of RNasin (Promega) and 2 U of AMV RT (MP Biomedicals). Samples were incubated for 5 min at 42°C,

30 min at 50°C and 10 min at 60°C and diluted 1/10 with 90 μl H_2O before use. Negative reverse transcription controls were carried out in the absence of AMV RT to check for the absence of contaminating plasmid DNA. cDNA was quantified by qPCR using primers NL43_C1_seq and NL43_NgoMIV_seq (Supplementary Table S1) and Brilliant II SYBR master mix (Agilent). cDNA was normalized and amplified with primers NL43_C1_seq and NL43_NgoMIV_Seq (Supplementary Table S1) using Phusion polymerase. PCR reaction volume was 50 μl and consisted of 10^5 copies of DNA, 1× HF buffer, 200 μM dNTPs, 0.5 μM of each primer, 1 U of Phusion polymerase. PCR amplifications were performed in duplicate using the PCR cycling conditions 98°C for 10 s, followed by 30 cycles of 98°C for 10 s, 55°C for 15 s and 72°C for 1 min. Pooled PCR products were isolated on a 1% agarose gel and purified using Nucleospin Gel and PCR Clean-up columns (Macherey-Nagel).

Fragmentation. As 2 × 100 nt Illumina sequencing does not completely cover the ∼500 bp fragment analysed in this study, we randomly fragmented 500 ng of gel purified dsDNA with 2.5 μl 10× buffer, 2.5 μl of 10× BSA and 2.5 μl of NEBNext dsDNA fragmentase in a total volume of 25 μl for 45 min at 37°C. Samples were verified on a 1% agarose gel, and digestion was confirmed as a smear on the gel. Fragmented samples were purified using Nucleospin Gel and PCR Clean-up columns, according to the manufacturer's instructions (Macherey-Nagel).

Library preparation. Fragmented DNA was first repaired using 1× T4 DNA ligase buffer (NEB), 0.4 mM each dNTPs, 1 mM ATP, 0.5 μl of *E*scherichia *coli* DNA ligase (from NEB NEBNext dsDNA fragmentase kit), 4.5 U of T4 DNA polymerase (NEB) and 25 U of T4 polynucleotide kinase (NEB) in 50 μl total volume for 1 h at 20°C. Enzymes were then heat inactivated by incubating samples for 30 min at 75°C. DNA was A-tailed by adding 12.5 U of Klenow fragment (3′-5′ Exo-) and 1.25 μl of 100 μM dATP and incubating for 45 min at 37°C. Following a second round of enzyme heat inactivation for 30 min at 75°C, adaptor ligation was performed by adding 9 μl of fresh 10× T4 DNA ligase buffer (NEB), 28 μl of 24% PEG 600 (NEB), 1 μl of 12.5 μM pre-annealed adaptors, and 2.5 μl of T4 DNA ligase (NEB) followed by incubation at 20°C for 1 h. Adaptor sequences IlluminaMAs and IlluminaMAa (Supplementary Table S1) were annealed by mixing in 1× ligase buffer (NEB), heating to 95°C for 1 min and slow cooling to room temperature. Samples were purified using Nucleospin Gel and PCR Clean-up columns. Y-shaped Illumina adaptors were converted into dsDNA using the PCR cycling conditions 98°C for 30 s followed by 5 cycles of 98°C for 15 s, 63°C for 30 s and 72°C for 30 s using the Illumina_1.0 and Illumina Index (Supplementary Table S1) with Phusion polymerase. PCR reaction volume was 50 μl and consisted of adaptor ligated DNA, 1× HF buffer, 200 μM dNTPs, 0.5 μM of each primer, 1 U of Phusion polymerase. Samples were then run on a 1% agarose gel and the range corresponding to 200–600 bp range was isolated, and purified using Nucleospin Gel and PCR Clean-up columns. DNA libraries were quantified by qPCR using Illumina PE PCR primer 1.0 and one of the Illumina Index primers (for multiplexing) with Brilliant II SYBR master mix. Samples were normalized and then re-amplified by PCR Illumina PE PCR primer 1.0 and one of the Illumina Index primers using the PCR cycling conditions 98°C for 30 s; followed by 6 cycles of 98°C for 15 s, 63°C for 30 s and 72°C for 30 s with Phusion polymerase. Samples were then pooled, and a final size selection was performed on a 1% agarose gel to re-isolate the range 200–600 bp ensuring the removal of Illumina adaptor dimers. Samples were sequenced on a single lane of a HiSeq 2500 instrument in 100 bp paired end mode, according to established procedures (IGBMC sequencing platform, Strasbourg, France).

RT-qPCR

Packaging efficiency of wild-type and mutant HIV-1 were carried out by transfecting 10^6 293T cells with 250 ng of plasmid using 4.5 μl of polyethylenimine per μg of DNA (1 mg/ml; Polysciences). Thirty six hours post-transfection, viral supernatant was clarified by centrifugation, syringe filtered through 0.22 μm pores, and pelleted through a 20% sucrose cushion, as outlined above. 293T cells were washed once in PBS. Viral and cellular RNA was then extracted using TriReagent (MRC), treated with DNase I, phenol/chloroform extracted, chloroform extracted, and EtOH precipitated as outlined above. Cellular and viral RNA pellets were dissolved in 200 μl and 20 μl of RNase free H_2O, respectively. Three microliters of RNA were mixed with 2 μl of a 5× mix of random hexamer and anchored oligodT (5× mix; 12.5 μM $dT_{20}VN$; 17.5 μM N_6) denatured at 90°C for 2 min and then chilled on ice. Reverse transcription was carried out in a total volume of 10 μl by adding 1× buffer (50 mM Tris–HCl pH 8.3, 6 mM $MgCl_2$, 40 mM KCl), 200 nM dNTPs and 2 U of RNasin and 2 U of AMV RT (MP Biomedicals). Samples were incubated for 5 min at 42°C, 30 min at 50°C and 10 min at 60°C and diluted 1/10 with 90 μl H_2O before use. Negative reverse transcription controls were carried out in the absence of AMV RT to check for the absence of contaminating plasmid DNA. gRNA, spliced viral RNA, and GAPDH mRNA were quantified by TaqMan qPCR assay using the primers listed in Supplementary Table S1. A standard curve was generated from 10^9 to 10^3 copies of plasmid containing the relevant target. Negative controls demonstrated the DNA contamination levels were present at <1% in all samples. Packaging efficiency was determined by calculating the ratio of the total amount of each RNA present in the supernatant by the amount present in the cells.

Analysis of in cell MIME data

Relation between nucleotide frequencies and the effect on intracellular gRNA production. Employing the derivation outlined in the Supplementary Text Equations (S1)–(S12), we can deduce the effect of a mutation m at position i in the RNA from the frequency of that mutation in the DNA library relative to the frequency in the cells c, i.e.

$$K^m_{\text{prod}}(i) = \frac{k^w_{\text{prod}} \cdot \delta^m_u}{k^m_{\text{prod}} \cdot \delta^w_u}(i) \approx \frac{S^m_{DNA}}{S^w_{DNA}} \cdot \frac{S^w_c(t)}{S^m_c(t)}(i), \quad (1)$$

where $k^w_{\text{prod}}(i)$, $k^m_{\text{prod}}(i)$ denote the rate of intracellular production of the wild type viral RNA and the viral RNA that carries a particular mutation (i.e. A→C, A→G, A→U, if the wild type base is adenosine) at position i and δ^w_u, δ^m_u are the corresponding rates of RNA degradation. The ratios $\frac{S^m_{DNA}}{S^w_{DNA}}(i)$ and $\frac{S^w_c(t)}{S^m_c(t)}(i)$ denote the frequency of mutations in the DNA library and in the pool of viral RNA located in the cell. Whenever the measure above is larger than 1, mutations decrease HIV-1 RNA levels. In order to identify regions that are important for gRNA production, one may also depict the impact of the mutation $m_{\max}(i)$ that has a maximal impact at position i only, as shown in Figure 2A; where $m_{\max}(i) = \underset{m}{\text{argmax}} \, |\log_2(K^m_{\text{prod}}(i))|$ and where m denotes all those mutations that have a significant impact on binding at nucleotide position i (if any), or all possible mutations otherwise.

Relation between nucleotide frequencies and the effect on packaging. Similarly, using derivations (S1–S6) and (S13–S19) in the Supplementary Text, we can deduce the effect of any mutation m at position i in the RNA on packaging from the frequency of mutation m in the cell c relative to the frequency in the virions v, i.e.

$$K^m_{\text{pack}}(i) = \frac{k^w_{on}}{k^w_{off}+k_{rel}} \cdot \frac{k^m_{off}+k_{rel}}{k^m_{on}}(i) \approx \frac{S^m_c(t)}{S^w_c(t)} \cdot \frac{S^w_v(t)}{S^m_v(t)}(i), \quad (2)$$

where k^w_{on}, k^m_{on}, k^w_{off}, k^m_{off} denote the binding- and dissociation rate of the RNA to/from the packaging complex and the rate k_{rel} denotes the rate at which RNA bound to the packaging complex is released from the cell after packing into nascent virions. In order to identify regions that are important for packaging, one may also depict the impact of the mutation $m_{\max}(i)$ that has a maximal impact at position i only, as shown in Figure 3A.

Error correction. The mutation frequencies S^m/S^w needed to evaluate Equations (1) and (2) are not known exactly, however, next generation sequencing (NGS) of the distinct RNA pools (DNA library, cellular RNA and RNA in virions) gives their frequencies in the NGS reads R^m/R^w. These reads however contain substantial sequencing errors, which we have to correct for, akin to the method presented in the Supplementary Notes of (31,39). Error correction allows us then to directly estimate the effects of each mutation m for all position i from the nucleotide frequencies observed in the NGS reads, provided we have a sufficient signal-to-noise ratio (see Supplementary Text):

$$K^m_{\text{prod}}(i) \approx \frac{\frac{R^m_{DNA}}{R^w_{DNA}} - \kappa^{w\to m}_{DNA}}{\frac{R^m_c}{R^w_c} - \kappa^{w\to m}_c}(i), \quad (3)$$

where $\kappa^{w\to m}(i)$ denotes the probability to falsely detect a wild type nucleotide w as some mutant m at position i. $\kappa^{w\to m}(i)$ is computed from experiments with wild type libraries for each type of mutation m and for each position i, akin to (31,39) and as exemplified in the Supplementary Text.

Similarly, for packaging, we derive

$$K^m_{\text{pack}}(i) \approx \frac{\frac{R^m_c}{R^w_c} - \kappa^{w\to m}_c}{\frac{R^m_v}{R^w_v} - \kappa^{w\to m}_v}(i), \quad (4)$$

Statistical assessment of effects. The above described method provides a single estimate of the relative effect for each nucleotide position and for each possible mutation, but it does not assess the confidence range of this estimate, or whether a mutation at position i has a significant impact on binding. In the following, we make use of a jacknife-like resampling procedure to estimate the confidence of each relative effect estimate, analogous to the methods in (31,39): In brief, if we are interested in the effect of a mutation m at position i, then for each pair of nucleotide positions (i,j), we can re-compute $K^{m,w}_{\text{prod}}(i,j)$, respectively $K^{m,w}_{\text{pack}}(i,j)$, N times (i.e. for each $j \neq i$). Each of these estimates can be computed according to:

$$K^{m,w}_{\text{prod}}(i,j) \approx \frac{\frac{R^{m,w}_{DNA}}{R^{w,w}_{DNA}} - \kappa^{w\to m,w}_{DNA}}{\frac{R^{m,w}_c}{R^{w,w}_c} - \kappa^{w\to m,w}_c}(i,j), \quad (5)$$

and analogously,

$$K^{m,w}_{\text{pack}}(i,j) \approx \frac{\frac{R^{m,w}_c}{R^{w,w}_c} - \kappa^{w\to m,w}_c}{\frac{R^{m,w}_v}{R^{w,w}_v} - \kappa^{w\to m,w}_v}(i,j), \quad (6)$$

where $\kappa^{w\to m,w}(i,j)$ denotes the probability to falsely detect a wild type nucleotide w at position i as some mutant m and to correctly detect the wild type at position $j \neq i$ as wild type, with derivations provided in the Supplementary Text. To test whether a mutation at position i significantly increases/decreases gRNA production, i.e. $H_0 : \log_2(K^m_{\text{prod}}(i)) \leq c$, $H_1 : \log_2(K^m_{\text{prod}}(i)) > c$, the raw P-value can be computed according to

$$P^{\text{m}}_{-}(i) = \frac{\#\log_2\left(K^{m,w}_{\text{prod}}(i,j)\right) \leq c}{\#K^{m,w}_{\text{prod}}(i,*)}, \quad (7)$$

where '#' denotes the 'number of estimates' and * indicates that all positions j are evaluated. To test whether a mutation at position i significantly decreases K_{prod},

$$P^{\text{m}}_{+}(i) = \frac{\#\log_2\left(K^{m,w}_{\text{prod}}(i,j)\right) \geq -c}{\#K^{m,w}_{\text{prod}}(i,*)} \quad (8)$$

We used $P < 0.05$ to detect significance. Note, that one can test any threshold $c \geq 0$ (e.g. 2-fold increase/decrease, etc.). Throughout the manuscript we chose $c = |N^{-1}\sum_i \log_2(\widetilde{K^m_{\text{prod}}(i)})|$ i.e. the average over all positions i, i.e. $c = 0.42$. An analogous scheme can be used to assess the effects on packaging, where we determined threshold $c = 0.41$. All reported P-values were corrected by the false discovery rate (FDR)-based method of Benjamini-Hochberg.

Quality criteria. For each pair of reads $R^{\text{m,w}}(i,j)$ / $R^{\text{w,w}}(i,j)$, we assessed its respective signal-to-noise ratio in the corre-

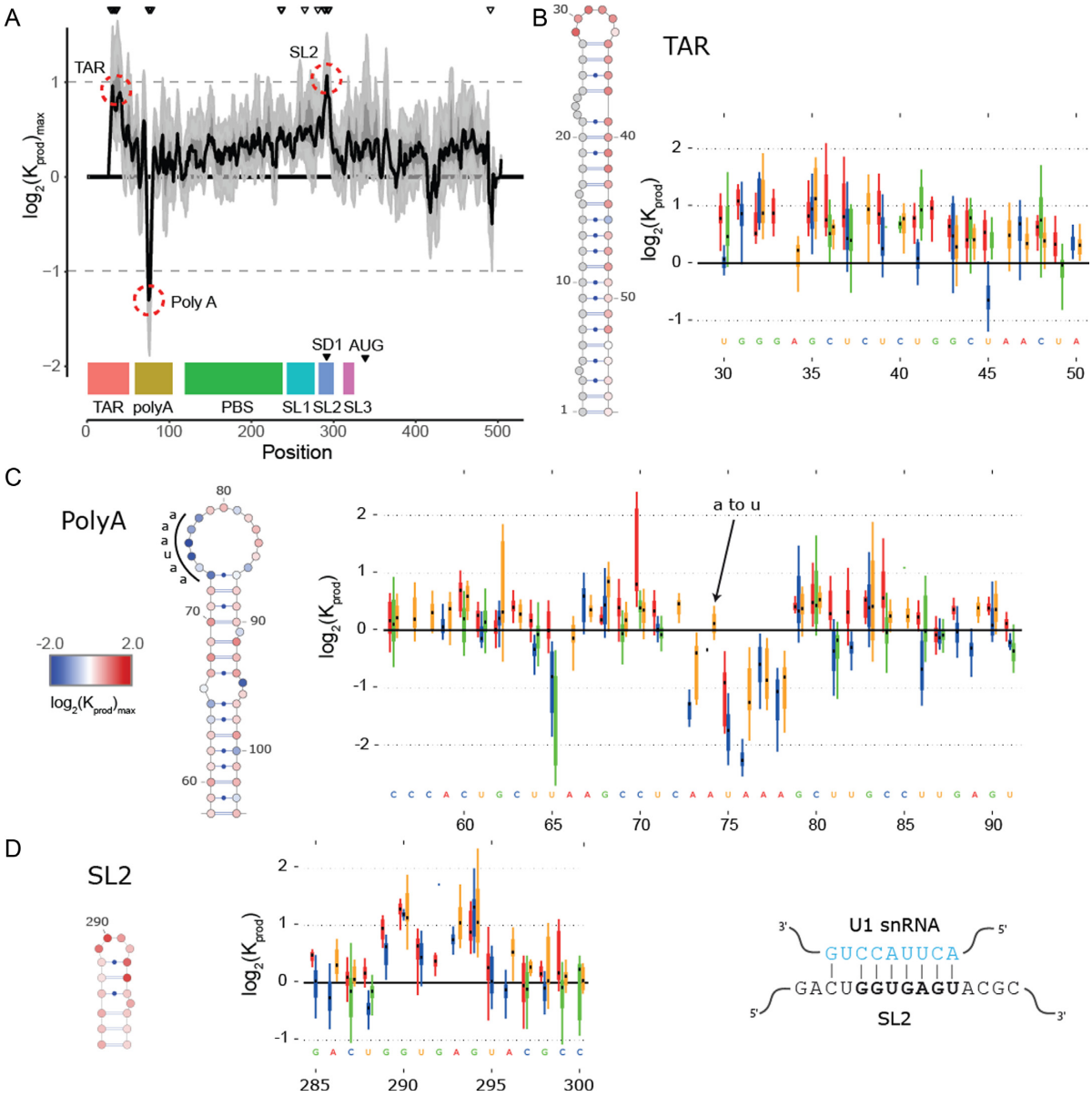

Figure 2. In cell Mutational Interference Mapping Experiment (in cell MIME) discovery of RNA motifs regulating HIV-1 gRNA production (**A**) Log2 K_{prod} showing the maximal effect of mutations on RNA production in cells with the HIV-1 5′ UTR and Gag coding region (smoothed with a linear, two-sided convolution filter of width 2). Functional domains are indicated with coloured boxes below the graph. Positions with significant effects on RNA production are indicated by black triangles above the graph. Three regions with significant ($P < 0.05$) and strong (log2 $K_{prod} \geq 1$ or ≤ -1; gray dotted line) effects on gRNA production are highlighted with red circles. (**B** to **D**) Mutations with maximal effect on log2 K_{prod} mapped on RNA structure. Positions impairing RNA production are shown in red. Positions improving RNA production shown in blue. Box and whisker plots show effect of each class of mutation on log2 K_{prod}. Black dot shows median, box shows quartiles (25% and 75%) and whiskers show extremes (excluding outliers beyond 1.5× IQR). Mutation classes are colour coded: red mutated to A; green mutated to C; blue mutated to G; yellow mutated to U. (**B**) Effect of mutations on gRNA production (log2 K_{prod}) mapped to TAR. (**C**) Effect of mutations on gRNA production (log2 K_{prod}) mapped to 5′ PolyA. All mutations to AAUAAA sequence improve gRNA production except for a single A to U mutation. (**D**) Effect of mutations on gRNA production (log2 K_{prod}) mapped to SL2. Mutations impairing gRNA production cluster to the U1 snRNA binding site.

sponding RNA pool (DNA, cell and virion) according to:

$$D_{m,w}(i,j) \approx \frac{R^{m,w}(i,j)}{R^{w,w}(i,j) \cdot \kappa^{w \to m,w}(i,j)}. \quad (9)$$

If the ratio was below the user-supplied threshold of 2 in both samples (DNA library versus cell and cell versus virion), the corresponding estimates in Equations (5) and (6) were discarded. If the signal was below the threshold in only one of the samples, the respective estimate was tagged as either being a lower- or upper estimate of the mutations' effect and assigned the value of the median effect estimate on RNA production or packaging respectively. This has the following reason: if a mutation strongly decreases RNA production, the frequency of that mutation in the cellular RNA may fall below the required signal-to-noise ratio (a multiple of the sequencing error) and the (negative) effect

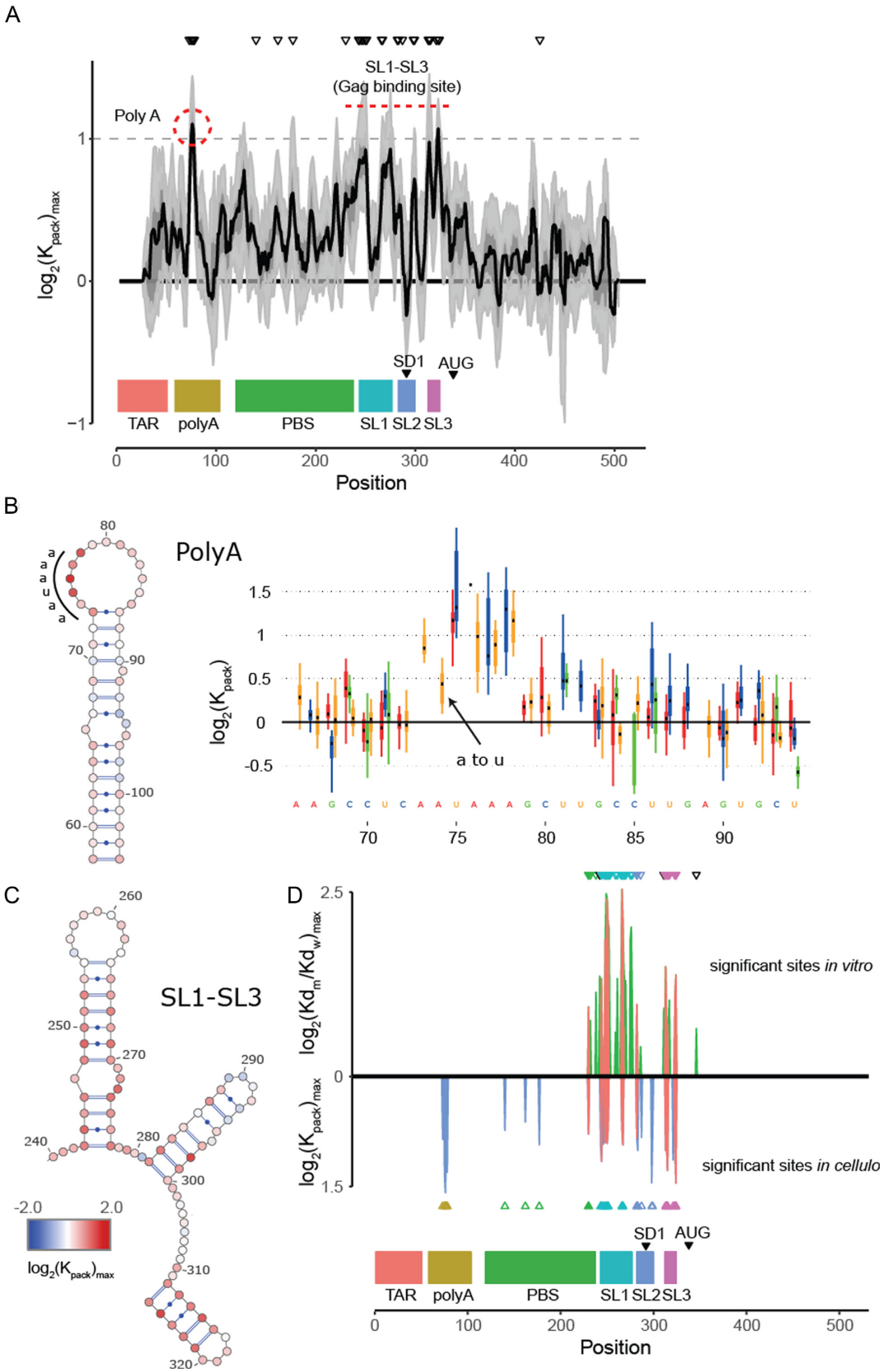

Figure 3. In cell Mutational Interference Mapping Experiment (in cell MIME) discovery of RNA motifs regulating HIV-1 gRNA packaging. (**A**) Log2 K_{pack} showing the maximal effect of mutations on RNA packaging with the HIV-1 5′ UTR and Gag coding region (smoothed with a linear, two-sided convolution filter of width 2). Functional domains are indicated with coloured boxes. Positions with significant effects on gRNA packaging are indicated

on RNA production may actually be higher than estimable. Conversely, if the frequency of that mutation was below the minimum signal-to-noise ratio in the DNA library, but HIV-1 RNA levels increase in the cellular RNA above the threshold, the (positive) effect on RNA production may actually be higher than estimable. Likewise, if a mutation strongly decreases packaging, the frequency of that mutation in the virions may also fall below the sequencing error, while the signal within the cells is sufficient. Again, the actual (negative) effect on packaging may be larger than estimable. We only evaluated Equations (5) and (6) for positions *j* where the total number of sequence fragments covering both *i* and *j* was at least 50% of the maximum coverage. For determining *P*-values, at least 300 estimates had to fulfil the quality criteria.

RESULTS

Mutational interference mapping experiment (MIME) in cells

The 5′UTR folds into a series of functional domains that regulate almost every stage of the HIV-1 life cycle (2,3,5), including intracellular gRNA production and packaging into viral particles. For the most part, the RNA sequences regulating these processes have been mapped to individual stem loops, but a complete nucleotide level understanding of their function is largely lacking. We recently developed Mutational Interference Mapping Experiment (MIME) for dissecting RNA structure and function at single nucleotide resolution (31). This technique is based on (i) the random mutation of the RNA of interest (ii) the physical separation of RNA into functional and non-functional populations and (iii) high-throughput sequencing to identify mutations affecting function. In theory, MIME can be applied to any process where functional and non-functional RNAs can be physically separated, including within cells during a native viral replication cycle. We reasoned that during replication, mutated viral RNA would be naturally segregated into functional and non-functional populations. That is, correctly transcribed and processed viral RNAs will accumulate in the cytoplasm over RNAs that are poorly transcribed or degraded due to defective processing. Similarly, viral RNAs that are efficiently selected for packaging will be more abundant in virions compared to packaging defective RNAs. By physically isolating and sequencing these mutant populations, regulatory RNA controlling two different stages of viral replication can be dissected in cells at unprecedented detail.

The entire 5′UTR and the beginning of the Gag coding region (6,26,27) is thought to contain RNA sequences regulating HIV-1 replication, therefore we targeted the first ∼500 nucleotides of the gRNA for functional analysis. Because mutating the Gag coding region could complicate the identification of non-coding regulatory RNA i.e. by introducing mutations that interfere with viral assembly, we first designed a conditional co-transfection system to separate the production of mutated gRNA from the expression of the viral structural proteins. gRNA was expressed from the lab adapted pNL4.3 HIV-1 vector modified to include (i) restriction sites for cloning of the mutant library, (ii) a substitution in the *gag* ATG start codon preventing Gag/Gag-Pol expression, (iii) a stop codon preventing Tat expression and (iv) a deletion in *env* for biosafety purposes. Unaltered viral proteins $Pr55^{Gag}$, $Pr160^{GagPol}$ and the accessory proteins Tat and Rev were expressed from a separate packaging vector. In this experimental setup, only co-transfected cells produce gRNA, ensuring that all gRNA is produced in the presence of the viral assembly machinery. The inclusion of restriction sites did not affect viral replication in single round assays (Supplementary Figure S1), and the ATG start codon mutation prevents Gag expression without significantly affecting encapsidation (27).

We performed in cell MIME (Figure 1B) using six mutant libraries tested in three independent experiments (two mutant libraries per experiment). Mutations were introduced using commercial PCR based mutagenesis technology. These libraries were then cloned into the gRNA expression vector and co-transfected into 293T cells together with the packaging vector. Viral and cellular gRNA were harvested, reverse transcribed, randomly fragmented, and sequenced using the Illumina HiSeq 2500 platform in 100 nt paired end mode. We also sequenced DNA derived from both the wild-type and mutant DNA libraries, with the non-mutated WT sequences used to control for errors introduced during library preparation and sequencing.

Altogether, we aligned 180 million sequences to the reference genome, finding 1.08×10^8 mutations from 2.15×10^{10} base pairs (Supplementary Table S2). Raw substitution rates were found to be significantly higher in the mutant library compared to the WT controls (Supplementary Figure S2), demonstrating that biologically relevant mutations could be clearly distinguished from the background errors introduced during library preparation and sequencing (*P*-value < 0.01). Importantly, we were able to use the substitution frequencies in the wild-type control to obtain error-corrected mutation frequencies, thus eliminating any biases from errors introduced during library preparation and sequencing (Materials and Methods section and Supplementary Text) (31,39). Error-corrected mutation rates were similar across all six independent libraries from the

←

by black triangles. Two regions with significant ($P < 0.05$) and strong ($\log2\ K_{pack} \geq 1$; gray dotted line) effects on gRNA packaging are highlighted with dot red line/circle. (**B** and **C**) Mutations with maximal effect on $\log2\ K_{pack}$ represented on RNA structure. Positions impairing gRNA packaging are shown in red. Positions improving gRNA packaging are shown in blue. Box and whisker plots show effect of each class of mutation on $\log2\ K_{pack}$. Black dot shows median, box shows quartiles and whiskers show extremes (excluding outliers beyond 1.5× IQR). Mutation classes are colour coded: red mutated to A; green mutated to C; blue mutated to G; yellow mutated to U. (**B**) Effect of mutations on gRNA packaging expressed as $\log2\ K_{pack}$ mapped to 5' PolyA. All mutations to AAUAAA sequence impair gRNA packaging except for a single A to U mutation. (**C**) Effect of mutations on gRNA packaging expressed as $\log2\ K_{pack}$ mapped to RNA structure in the region SL1–SL3. (**D**) Qualitative comparison between the significant effects of mutations on $Pr55^{Gag}$ binding determined by in vitro MIME (upper portion, green) and the effects of mutations on gRNA packaging by in cell MIME (lower portion, blue). Sites significantly affecting both are pictured red. Color-coded arrows below (for in cell) and above (for in vitro) indicate the affected functional domain (colored boxes on the bottom). Filled arrows show significant effects at sites in both in vitro and in cell.

three independent experiments (Supplementary Figure S3) and were highly reproducible for all classes of mutations (Supplementary Figures S4 and S5). Importantly, error corrected mutation rates steadily decreased from DNA (median = 4.8×10^{-3}), cellular gRNA (median = 4.2×10^{-3}) to virion gRNA (median = 3.3×10^{-3}) providing evidence for purifying selection as the viral life-cycle proceeds (Supplementary Figure S3). Interestingly, A–G mutations were found to be consistently more abundant in cellular gRNA (Supplementary Figure S6) compared to the input DNA (*P*-value < 0.01). These cellular A–G mutations were enriched at 5′A<u>A</u>3′ and 5′U<u>A</u>3′ dinucleotides and seemed to cluster at unpaired adenines near regions of double stranded RNA structure (Supplementary Figure S7). Although the biological basis for these abundant A-G mutations is unclear, their nature is suggestive of an editing activity by the dsRNA adenosine deaminases, ADAR1 or ADAR2 (40,41) (Supplementary Figure S7). Whilst intriguing, this phenomenon is likely unrelated to the processes of gRNA production and packaging investigated here, so we ignored this class of mutation in the following analysis.

Regulation of intracellular gRNA production

We first focused on identifying RNA sequences regulating gRNA production in infected cells by comparing the mutation rate in the DNA library with mutations found in the gRNA in cells. Intuitively, mutations impairing gRNA production should be depleted in cells compared to the input DNA. Conversely, mutations improving RNA production should be enriched in the cellular gRNA compared to the input DNA library. Indeed, formal modelling of this biological process revealed a direct relation between mutation frequency and effect on gRNA production (Supplementary Text). In other words, the frequency of a mutation m at position i in the DNA library $S^m_{DNA}/S^w_{DNA}\,(i)$, divided by the mutation frequency in the cellular RNA $S^m_c/S^w_c(i)$ is directly proportional to the decrease/increase of intracellular viral RNA production caused by that mutation. By adapting a previously developed analytical framework (31,39), we were able to infer the mechanistic effects of all mutations m at all positions i on gRNA production and stability simultaneously, summarized as $K^m_{\text{prod}}(i)$ (see Equation (1) in Materials and Methods and Supplementary text). Moreover, we were also able to statistically ascertain mutation effects at each position. $K^m_{\text{prod}}(i) > 1$ means that the mutation (m) at position (i) decreases gRNA production and stability. Conversely, $K^m_{\text{prod}}(i) < 1$ identifies mutations (m) at position (i) that increase gRNA production and stability. Upon performing this analysis, we found three distinct regulatory regions that strongly and significantly affected gRNA production, both positively and negatively (Figure 2A, Supplementary Data Files). These regions mapped to the domains TAR, PolyA and SL2, respectively.

Unsurprisingly, TAR was identified as a positive regulator of gRNA production, consistent with its crucial role in enhancing viral transcription (42,43). This was seen as a strong depletion of mutations in TAR in the cellular gRNA when compared to the input DNA library (Figure 2A, 2B). Although we were not able to analyse the extreme 5′ part of the TAR (due to the binding of a specific primer to this region during sequencing library preparation), it was notable that mutations to the apical portion were more strongly depleted in cells compared to the distal portion of the stem-loop (Figure 2B). This apical region is known to be important for gRNA production by assembling with the HIV-1 Trans-Activator of Transcription (Tat) protein and the cellular factor P-TEFb (42–47). Furthermore, these results are in agreement with detailed mutant-revertant and phylogenetic studies showing that the distal portion of TAR is less important for gene expression compared to the apical portion (48,49). Altogether, these data evidence the ability of in cell MIME to discover regulatory RNA in an unbiased fashion.

The second regulatory motif was found to reside within the 5′ PolyA. Unexpectedly, mutations in the 5′ PolyA were enriched in cells compared to the input DNA, indicating that this motif plays a negative role in gRNA production. Strikingly, mutations improving gRNA production mapped precisely to the ^{73}AAUAAA^{78} hexamer within the 5′ PolyA apical loop (Figure 2A, 2C). All mutations to this hexamer were enriched in cellular gRNA compared to DNA, except for a single ^{73}A<u>A</u>UAAA^{78} to ^{73}A<u>U</u>UAAA^{78} substitution (Figure 2C). As AAUAAA and AUUAAA are the most abundant cellular polyadenylation signals (50), these data imply a role for the cellular polyadenylation machinery in regulating intracellular gRNA levels.

The third regulatory motif mapped to the splice donor site within SL2. Here, mutations were strongly depleted in cellular gRNA compared to DNA (Figure 2A, D) demonstrating that sequences within SL2 are required for gRNA production. Interestingly, mutations disrupting gRNA production mapped precisely to the U1snRNA binding site ^{289}GGUGAGU^{295} (Figure 2D), and all classes of mutation to this region disrupted gRNA production. This was somewhat surprising, as one might expect that disrupting the splice donor site would increase unspliced gRNA production by eliminating the splicing of viral RNAs. Nevertheless, the opposite effect is observed here, and our data argue that an interaction between U1snRNA and the splice donor site is required for gRNA production.

Regulation of gRNA packaging

We next searched for RNA motifs regulating gRNA packaging into virions by comparing the mutation rate in the cellular RNA with that found in RNA extracted from viral particles. In cells, gRNA packaging comprises multiple molecular events, including the formation of a protein : RNA packaging complex, its transport to the cell surface, and its assembly into viral particles. Modelling of this process demonstrates that the frequency of a mutation m at position i in the cells $S^m_c/S^w_c\,(i)$ divided by the mutation frequency in the virion RNA $S^m_v/S^w_v(i)$ is proportional to the mutation's effect on packaging (see Equation (2) in *Methods* and Supplementary Text). We derived the term $K^m_{\text{pack}}(i)$ that summarizes the underlying processes (Equation 2). When $K^m_{\text{pack}}(i) > 1$, the mutation m at position i decreases gRNA packaging, when $K^m_{\text{pack}}(i) < 1$, it increases packaging. Analogous to the analysis of in cell

MIME data for RNA production, we adopted the previously developed analytical framework for error correction and statistical analysis (31,39) (Materials and Methods section and Supplementary Text). Upon analysis, we identified two distinct regions that strongly and significantly affected gRNA packaging (Figure 3 A, Supplementary Data Files). These regulatory sequences mapped to the 5′ PolyA and the region SL1-SL3, respectively.

Strikingly, the packaging signal within 5′ PolyA mapped precisely to the same 5′ PolyA sequence ^{73}AAUAAA^{78} that we identified as a strong regulator of gRNA production (Figure 3A and 3B). Indeed, mutations to this sequence have similar effects on gRNA packaging as mutations to the Psi region (Figure 3A). Like their effect on gRNA production, all mutations to this hexamer sequence impaired gRNA packaging into virions, except for a single ^{73}AAUAAA^{78} to ^{73}AUUAAA^{78} substitution (Figure 3B). Again, because ^{73}AAUAAA^{78} and ^{73}AUUAAA^{78} sequences function as canonical polyadenylation signals, our data provide evidence that the cellular polyadenylation machinery plays an important role in regulating not only gRNA production, but also its incorporation into viral particles (50).

The second packaging signal overlapped the domains SL1 to SL3 (Figure 3C) that we have previously identified as the Pr55^{Gag} binding site *in vitro* (31). These data therefore confirm the idea that Pr55^{Gag} is a central player in the selection of the gRNA (Figure 3D). However, we did find some differences between the sequences required for Pr55^{Gag} binding *in vitro* and those directing gRNA packaging into virions. First, and most remarkably, the ^{257}GCGCGC^{262} palindromic sequence within the SL1 apical loop seen as crucial for Pr55^{Gag} binding to gRNA *in vitro*, was not required for gRNA packaging in cells (Figure 3C and 3D, Supplementary Figure S8). Second, SL2 was slightly more important for gRNA packaging in cells compared to Pr55^{Gag} binding *in vitro*. However, it remained relatively minor when compared to SL1 and SL3 (Figure 3D). Finally, mutations to the stem of SL1 had comparable effects on packaging in cells as mutations to the stem of SL3, in contrast to the situation *in vitro* where SL1 stem mutations were much more deleterious than mutations to the SL3 stem (Supplementary Figure S8) (4,31). Altogether, the region SL1-SL3 is a major gRNA packaging determinant, with SL1 shown to be the most important stem-loop given that is over 2.5 times larger than SL3 (2,3).

Role of the AAUAAA PolyA motif in gRNA production and packaging

To confirm the role of the 5′ PolyA and the U1snRNA binding site on gRNA production, we introduced mutants into these two regions and tested their impact on viral replication in transfected cells by reverse transcription quantitative PCR (RT-qPCR). We inhibited the 5′ polyadenylation signal either by its complete deletion (^{73}ΔAAUAAA^{78}) or its mutation to ^{73}AAUGAA^{78} (Figure 4A). We also included a ^{73}AUUAAA^{78} mutation to serve as a canonical polyadenylation control (Figure 4A). Whilst disruption of 5′ polyadenylation did not lead to a detectible increase in the quantity of gRNA in the cell compared to wild-type (99.0% ^{73}ΔAAUAAA^{78}; 100.2% ^{73}AAUGAA^{78}), we did observe a significant increase in the quantity of spliced RNA produced in the 5′polyadenylation defective mutants compared to wild-type (266.4% ^{73}ΔAAUAAA^{78} $P<0.05$; 292.8% ^{73}AAUGAA^{78} $P < 0.01$) (Figure 4B). On the other hand, the ^{73}AUUAAA^{78} mutant produced both gRNA and spliced RNA at levels comparable to wild-type (107.6% gRNA; 131.7% spliced RNA) (Figure 4B). Together, these data confirm that the 5′PolyA canonical polyadenylation signal regulates gRNA production.

We next assessed the role of the ^{289}GGUGAGU^{295} U1snRNA binding site by designing a mutation predicted to disrupt ^{289}UACGAGU^{295} U1snRNA binding (Figure 4A). Disruption of this binding site led to a thousand-fold reduction in cellular levels of gRNA and spliced RNA (0.3% genomic; 0.15% spliced) (Figure 4B) whereas combining the U1snRNA binding site mutant ^{289}UACGAGU^{295} with a deletion of the 5′ PolyA ^{73}ΔAAUAAA^{78} signal caused levels of gRNA to return to wild-type (110.9%). These data demonstrate a functional interaction between the 5′PolyA and the U1snRNA binding site in gRNA production in agreement with a model that U1snRNA binding is required to inhibit 5′ premature polyadenylation (51,52). To our surprise, spliced viral RNA could also be detected at nearly wild-type levels in this double mutant (118.3%) despite disruption of the U1snRNA binding site. Sequencing of the PCR products revealed that splicing still occurred within SL2, even in the absence of a canonical splice donor sequence, but the splice site was shifted by four nucleotides in the 3′ direction (Supplementary Figure S9). Activation of cryptic splice donor sites has been observed upon mutation of the HIV-1 gRNA (52,53). This highlights that splice site selection is extremely complex, and likely balanced by RNA structure (54,55) as well as interactions between positive and negative splicing elements (53).

To further assess the role of the PolyA sequence on gRNA packaging, we next quantified by RT-qPCR the relative packaging efficiency of gRNA and spliced viral RNAs into viral particles expressed as the ratio of RNA found in cells compared to virus (56). We found a significant reduction ($P<0.05$) in packaging efficiency to 43% and 48% of wild-type, for the ^{73}ΔAAUAAA^{78} and ^{73}AAUGAA^{78} mutants respectively, whereas the packaging efficiency of the ^{78}AUUAAA^{78} mutant remained at 92% of wild-type (Figure 4C). Conversely, we found that spliced viral RNA was incorporated with much greater efficiency in the ^{73}ΔAAUAAA^{78} and ^{73}AAUGAA^{78} mutant, at 266% and 293% of wild-type, respectively (Figure 4C). This compared to a non-significant 131% of wild-type spliced gRNA incorporation for the ^{73}AUUAAA^{78} mutant (Figure 4C). Altogether our results demonstrate that a canonical polyadenylation motif in the 5′ PolyA is required for efficient gRNA packaging, even though it is ordinarily repressed during HIV-1 replication.

DISCUSSION

RNA molecules are important regulators of biological activity (1). They play key roles in bacterial (57) or viral infection processes (58,59), and defects in RNA regulation have been implicated in human disease (60). Although this makes

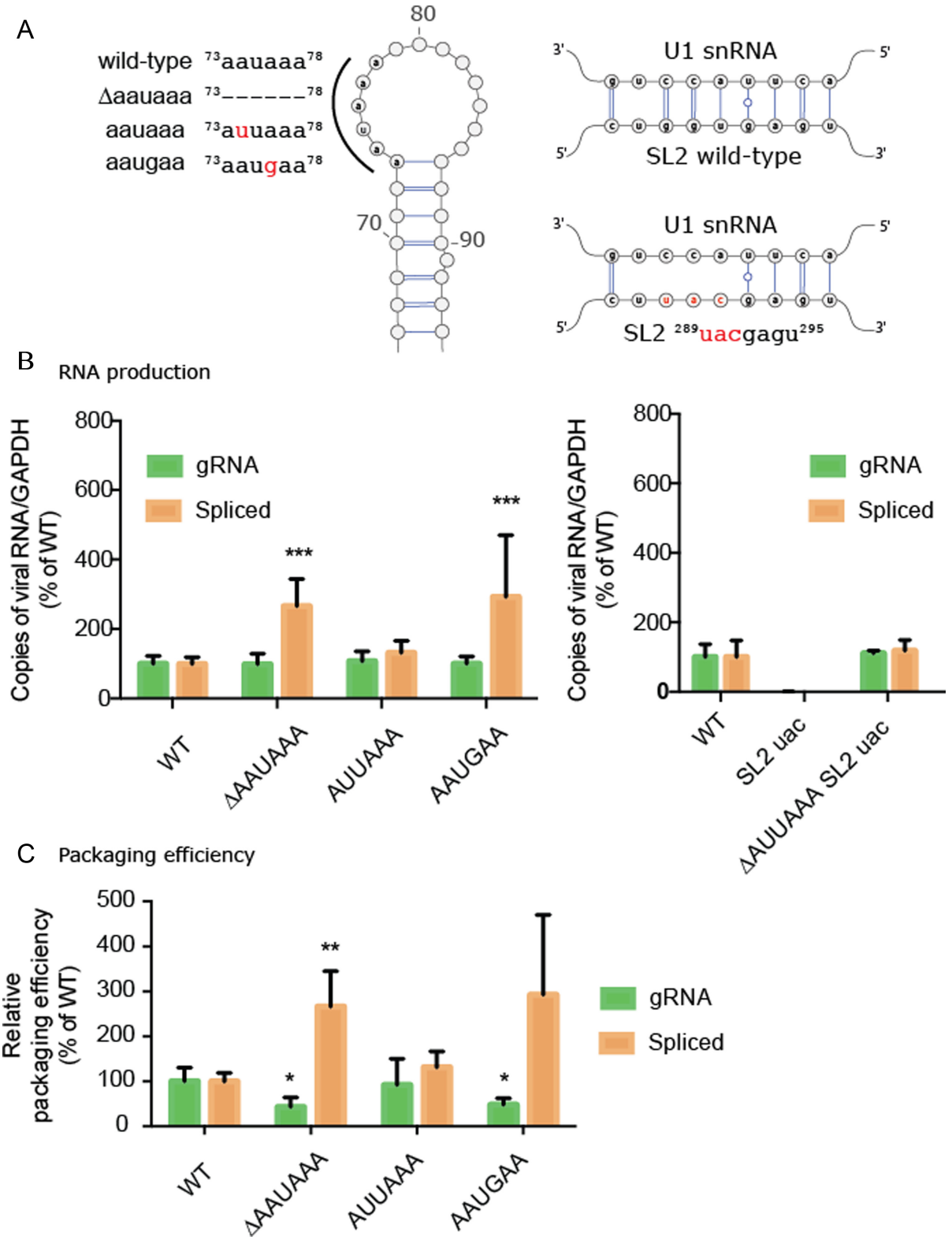

Figure 4. Role of the AAUAAA polyA motif in gRNA production and packaging. (**A**) 5′PolyA mutants contain point mutations or deletions to the AAUAAA sequence. SL2 mutant containing substitutions within the U1snRNA binding site. (**B**) Production of gRNA and spliced viral RNA (mRNA Tat) for 5′ polyA and SL2 mutants. Bar charts represent six independent experiments. (**C**) Relative packaging efficiency of gRNA and spliced viral RNA into viral particles, expressed as a virus/cellular RNA (36). Bar charts represent 3 independent experiments. Statistical tests were carried out using ANOVA corrected for multiple comparisons.

RNA an extremely attractive medical target, RNA-based treatments have so far been challenging to develop.

The first step in exploiting RNA as a drug target is to identify RNA motifs with the most potential for therapeutic intervention. Unfortunately, the functional flexibility of RNA means that the same stretches of RNA often perform multiple roles, which greatly complicates the identification of regulatory RNA by traditional truncation and deletion mutagenesis. This problem is especially evident within RNA viral genomes, where fierce evolutionary pressure for 'data compression' means that regulatory and coding regions overlap in complex ways that impede the understanding of their function. Here, we have implemented in cell MIME to pinpoint regulatory RNA in an unbiased fashion at single nucleotide resolution (31,39). Using different methods of functional selection, we could dissect a complex regulatory network controlling gRNA production and packaging into virions (Figure 5). Surprisingly, a common sequence within 5′ PolyA both negatively and positively regulated these respective processes.

With regards to gRNA production, we were able to identify three distinct RNA motifs (Figure 2). Reassuringly, mutations to TAR impaired gRNA production, with the apical portion proving to be more important for gRNA production than the distal portion. These results are in agreement with the deletion and mutagenesis studies pointing to the minimal sequences required for transactivation as spanning residues 19 to 43 (61,62). Although we were not able to analyse the U-rich bulge (nucleotides 23–25) constituting the binding site for the viral Tat protein (63,64), we could see the importance of the loop sequence (nucleotides 29–34) serving as the binding site for P-TEFb (65,66). Interestingly, TAR is assumed to be the most important motif for gRNA production, but we were able to identify several point mutations that were more detrimental to viral RNA levels in cells than those mapping to TAR. These mutations clustered within the U1 snRNA binding site within SL2 suggesting a crucial role for the splicing factor U1snRNA in gRNA production. Indeed, binding of U1 snRNP, and in particular the U1 snRNP protein 70K, to the HIV-1 gRNA is important for the repression of polyadenylation at the 5′ PolyA site (51,52,67). Without this repression, only short prematurely polyadenylated transcripts would be generated, preventing production of the full-length gRNA. In agreement, our mutations designed to impair U1 snRNA binding strongly repress gRNA production, and that this phenotype could be counteracted by deletion of the ^{73}AAUAAA^{78} (Figure 4). We also observed that individual mutants to ^{73}AAUAAA^{78} were enriched in cells compared to the wild-type sequence. Presumably, disruption of the 5′ canonical polyadenylation signal enhances viral RNA production by eliminating low levels of premature cleavage and polyadenylation. The general assumption is that 5′ PolyA is efficiently repressed in wild-type HIV-1 through inhibitory RNA structure (68–71), proximity to the 5′ cap (72,73), the presence of downstream inhibitory sequences (51,52), and the absence of upstream activating sequences that are only present at the 3′ end of the gRNA (72,73). Our data argue that some level of cleavage and polyadenylation still occurs within the wild-type 5′ PolyA despite these inhibitory mechanisms (71).

With regards to gRNA packaging, we identified two distinct regions required for incorporation of gRNA into viral particles (Figure 3). The central packaging signal spanned SL1 to SL3 and closely corresponds to the Pr55^{Gag} binding site previously defined *in vitro* (4,31) and a region found to bind Pr55^{Gag} in PAR-CLIP crosslinking experiments in cells (32). Mutations to the ^{257}GCGCGC^{262} sequence within the apical loop of SL1 did not impair gRNA packaging in cells. This palindromic sequence initiates gRNA dimerization via a kissing loop interaction – a conserved phenomenon within the *retroviridae* family (10,74,75). gRNA dimerization is required for viral replication (19,20,76–78) and presumed to be mechanistically linked to gRNA packaging (20,21,79). Given that identical mutations severely compromised Pr55^{Gag} binding in a similar MIME assay conducted *in vitro* (31), it was surprising to see that mutations to this sequence did not impair gRNA packaging. Nevertheless, our in cell data is consistent with modest effects on gRNA packaging seen with SL1 apical loop mutants in a variety of studies (19,21,76,80,81). For example, in one study a single G to U mutation ^{257}GCGC<u>U</u>C^{262} lead to a roughly two fold reduction in gRNA packaging (82), whereas our in cell MIME data shows that this same mutation packages 76% of wild-type (68–86% are the 5 and 95 percent confidence intervals) (Supplementary Data Files). SL1 apical loop mutants may also have less impact in cells compared to Pr55^{Gag} binding assays conducted *in vitro* (76) due to the presence of yet unidentified redundant dimerization sites within the full length HIV-1 genome that were not present on the short RNA fragment tested *in vitro*. Alternatively, primary T-lymphocytes can partially rescue defects in reverse transcription induced by deletion or mutation of SL1, implying that cellular factors can also compensate for SL1 defects (76). Regardless of the role of the SL1 apical loop sequence, the SL1 stem and internal loop itself is a bona fide packaging signal, consistent with the fact that its deletion leads to severe packaging defects (18,56,80).

Finally, we make the discovery that ^{73}AAUAAA^{78} within the 5′PolyA is an exceptionally strong packaging signal in cells. Previous studies have shown that destabilizing the PolyA hairpin decreases gRNA packaging (83,84) and that complete deletion of PolyA reduces gRNA packaging by 70% (18,84), similar to a combined deletion of SL1 and SL3 (56). Until now, the best explanation for why PolyA acts as a packaging determinant is that it binds to Pr55^{Gag} directly during viral assembly (56). Although a truncated version of the Gag protein bound 5′ PolyA in an *in vitro* footprinting assay (85), this binding site was not seen by *in vitro* MIME using full length Pr55^{Gag} protein (31). Furthermore, PAR-CLIP experiments conducted in cells also did not identify 5′ PolyA as a Pr55^{Gag} binding site (32). We therefore find a mechanism involving the direct binding of Pr55^{Gag} to the 5′ PolyA unlikely. Instead, our data suggests that the cellular polyadenylation machinery and gRNA packaging are mechanistically linked. Our evidence is two-fold: first, we localized the 5′ PolyA packaging signal, at single nucleotide resolution, to the ^{73}AAUAAA^{78} canonical polyadenylation signal; second, we showed that all mutations to this sequence impair gRNA packaging except for a single A to U mutation (^{73}A<u>U</u>UAAA^{78}) forming the second most frequent polyadenylation signal found

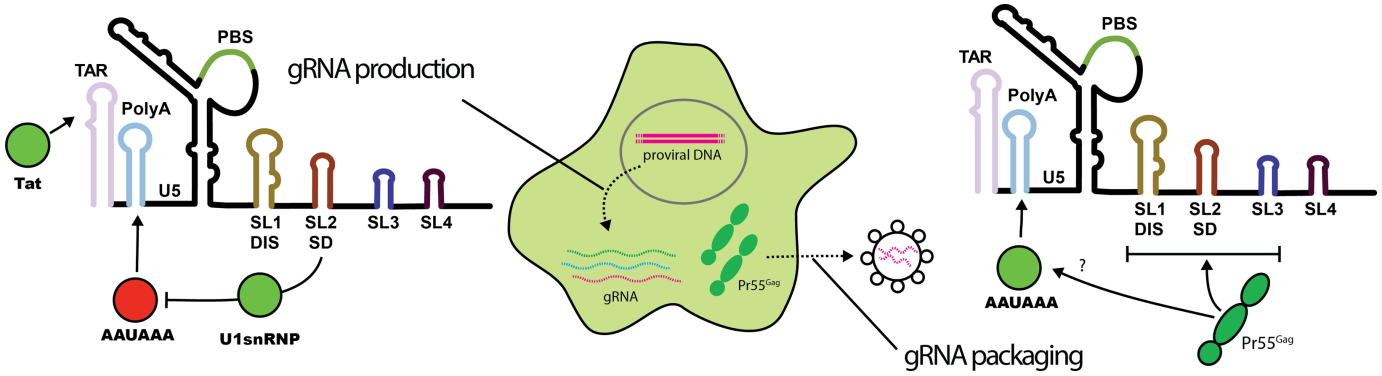

Figure 5. Five regulatory elements controlling HIV-1 replication. gRNA production is positively regulated by sequences within TAR and by the U1snRNP binding site within SL2. gRNA production is negatively regulated by the AAUAAA motif in 5′ polyA. The U1snRNP binding site is required for repression of 5′ polyadenylation. gRNA packaging into virions requires both the $Pr55^{Gag}$ binding site (SL1-SL3), and the AAUAAA motif in 5′ PolyA. Positive regulatory elements are highlighted in green. Negative regulatory elements are highlighted in red.

in mammalian cells (86). Together, these facts argue that a functional polyadenylation signal is required for gRNA packaging into virions. This would explain why HIV-1 conserves the 5′ polyadenylation signal, even though its presence is detrimental for gRNA production. Other retroviruses, such as mouse mammary tumor virus (MMTV) and avian leukosis-sarcoma virus (ALSV), encode a single copy of the AAUAAA polyadenylation signal in the 3′ end of the gRNA, demonstrating that different (seemingly more logical) gRNA organisations are possible.

How might polyadenylation facilitate gRNA packaging? Given that the gRNA packaging is thought to be mainly determined by $Pr55^{Gag}$, one simple explanation could be that there exists a direct or indirect interaction between $Pr55^{Gag}$ and the cellular polyadenylation machinery. This interaction could help recruit or stabilize $Pr55^{Gag}$ on the gRNA to ensure that viral assembly occurs preferentially on the gRNA, rather than cellular RNAs. Interestingly, cellular RNAs that are preferentially packaged into viral particles exhibit particularly long 3′UTRs (87), possibly because these mRNAs are more likely to contain inhibited upstream polyadenylation sequences than the equivalent cellular RNAs with short UTRs. Which component(s) of the polyadenylation machinery are involved in gRNA packaging? The polyadenylation machinery comprises cleavage polyadenylation specificity factor (CPSF), cleavage factors Im and IIm (CFIm and CFIIm), cleavage stimulatory factor (CstF), poly(A) polymerase (PAP), and poly(A) binding protein II (88). At least some of these cellular polyadenylation factors bind to the 5′ polyadenylation signal even when cleavage and polyadenylation is repressed (51,52,68). Amongst these factors, CPSF6—a subunit of CFIm—stands out. Although it does not directly recognize the AAUAAA sequence (88,89), it is a key player in mRNA 3′ end processing and is involved in the repression of 5′ proximal polyadenylation sites (90,91). It also interacts with the CA domain of $Pr55^{Gag}$ providing a possible link between polyadenylation and HIV-1 biology (92–96). Delineating the mechanistic contributions of the cellular polyadenylation machinery to gRNA packaging could provide a new window of therapeutic opportunity not currently exploited by antiretroviral therapy. However, further work will be required to define its potential role in HIV-1 gRNA packaging.

In summary, we have used in cell MIME to identify at single nucleotide resolution RNA motifs regulating gRNA production and packaging into HIV-1 virions. One of the major advantages of the in cell MIME method is that low level random mutagenesis can pinpoint functional RNA motifs whilst reducing the risk of RNA misfolding that often occurs when large and imprecise deletion mutants are used. Although we have not done so here, in principle, in cell MIME data can also be used to identify RNA secondary structure important for regulatory function through the identification of compatible co-varying nucleotide positions. Thus, in cell MIME is a flexible and powerful methodology should help to identify novel regulatory RNA motifs in a wide range of pathogens, as well as lead to a better understanding of non-coding RNA molecules in eukaryotic cells.

DATA AVAILABILITY

Software for analysing MIME data is available from GitHub https://github.com/maureensmith/MIMEAnTo/. Processed data can be found in Supplementary Data Files. Raw sequencing reads are available through NCBI Gene Expression Omnibus number GSE109386.

SUPPLEMENTARY DATA

Supplementary Data are available at NAR Online.

FUNDING

Sidaction and ANRS (Agence Nationale de Recherches sur le SIDA et les Hépatites Virales) to R.M.; ANRS [ECTZ35556 to R.P.S.] and IDEX: Par delà les frontières, l'Université de Strasbourg to R.P.S.; German Ministry for Education & Science (BMBF) [031A307 to M.S. and M.v.K.]; Partenariat Hubert Curien (PHC) programme franco-allemand PROCOPE [37709NJ to R.P.S. and M.v.K.]; IGBMC Microarray and Sequencing platform, a member of the 'France Génomique' consortium

[ANR-10-INBS-0009]. Funding for open access charge: CNRS.

Author contributions: R.P.S. designed the study. R.P.S. performed the MIME experiments including libraries for sequencing. R.P.S., M.R.S., L.D, F.J., P.C. and M.v.K. developed bioinformatic tools. M.v.K. and M.R.S. developed binding models and statistical tools. G.L., T.D. and C.M. performed replication studies of modified HIV-1. R.P.S., A-C.J. and M.M. tested PolyA and SL2 mutants. R.P.S., M.R.S., M.M., J.-C.P., M.v.K. and R.M. analyzed the data. R.P.S. and M.v.K. wrote the paper with contributions from the other authors.

Conflict of interest statement. None declared.

REFERENCES

1. Morris,K.V. and Mattick,J.S. (2014) The rise of regulatory RNA. *Nat. Rev. Genet.*, **15**, 423–437.
2. Wilkinson,K.A, Gorelick,R.J., Vasa,S.M., Guex,N., Rein,A., Mathews,D.H., Giddings,M.C. and Weeks,K.M. (2008) High-throughput SHAPE analysis reveals structures in HIV-1 genomic RNA strongly conserved across distinct biological states. *PLoS Biol.*, **6**, e96.
3. Paillart,J.C., Dettenhofer,M., Yu,X.F., Ehresmann,C., Ehresmann,B. and Marquet,R. (2004) First snapshots of the HIV-1 RNA structure in infected cells and in virions. *J. Biol. Chem.*, **279**, 48397–48403.
4. Abd El-Wahab,E.W., Smyth,R.P., Mailler,E., Bernacchi,S., Vivet-Boudou,V., Hijnen,M., Jossinet,F., Mak,J., Paillart,J.-C. and Marquet,R. (2014) Specific recognition of the HIV-1 genomic RNA by the Gag precursor. *Nat. Commun.*, **5**, 4304.
5. Watts,J.M., Dang,K.K., Gorelick,R.J., Leonard,C.W., Bess,J.W., Swanstrom,R., Burch,C.L. and Weeks,K.M. (2009) Architecture and secondary structure of an entire HIV-1 RNA genome. *Nature*, **460**, 711–716.
6. Lu,K., Heng,X., Garyu,L., Monti,S., Garcia,E.L., Kharytonchyk,S., Dorjsuren,B., Kulandaivel,G., Jones,S., Hiremath,A. *et al.* (2011) NMR detection of structures in the HIV-1 5′-leader RNA that regulate genome packaging. *Science*, **334**, 242–245.
7. Baudin,F., Marquet,R., Isel,C., Darlix,J.L., Ehresmann,B. and Ehresmann,C. (1993) Functional sites in the 5′ region of human immunodeficiency virus type 1 RNA form defined structural domains. *J. Mol. Biol.*, **229**, 382–397.
8. Mailler,E., Bernacchi,S., Marquet,R., Paillart,J.-C., Vivet-Boudou,V. and Smyth,R. (2016) The life-cycle of the HIV-1 Gag–RNA complex. *Viruses*, **8**, 248.
9. Karn,J. and Stoltzfus,C.M. (2012) Transcriptional and posttranscriptional regulation of HIV-1 gene expression. *Cold Spring Harb. Perspect. Med.*, **2**, a006916.
10. Paillart,J.-C., Shehu-Xhilaga,M., Marquet,R. and Mak,J. (2004) Dimerization of retroviral RNA genomes: an inseparable pair. *Nat. Rev. Microbiol.*, **2**, 461–472.
11. Isel,C., Ehresmann,C. and Marquet,R. (2010) Initiation of HIV reverse transcription. *Viruses*, **2**, 213–243.
12. Le Grice,S.F.J. (2015) Targeting the HIV RNA genome: high-hanging fruit only needs a longer ladder. *Curr. Top. Microbiol. Immunol.*, **389**, 147–169.
13. Janssen,H.L.A., Reesink,H.W., Lawitz,E.J., Zeuzem,S., Rodriguez-Torres,M., Patel,K., van der Meer,A.J., Patick,A.K., Chen,A., Zhou,Y. *et al.* (2013) Treatment of HCV Infection by Targeting MicroRNA. *N. Engl. J. Med.*, **368**, 1685–1694.
14. Clever,J.L., Miranda,D., Parslow,T.G., Miranda,D. Jr and Parslow,T.G. (2002) RNA structure and packaging signals in the 5′ leader region of the human immunodeficiency virus type 1 genome. *J. Virol.*, **76**, 12381–12387.
15. Helga-Maria,C., Hammarskjöld,M.-L.L. and Rekosh,D. (1999) An intact TAR element and cytoplasmic localization are necessary for efficient packaging of human immunodeficiency virus type 1 genomic RNA. *J. Virol.*, **73**, 4127–4135.
16. Harrich,D., Hooker,C.W. and Parry,E. (2000) The human immunodeficiency virus type 1 TAR RNA upper stem-loop plays distinct roles in reverse transcription and RNA packaging. *J. Virol.*, **74**, 5639–5646.
17. Russell,R.S., Hu,J., Laughrea,M., Wainberg,M.A. and Liang,C. (2002) Deficient dimerization of human immunodeficiency virus type 1 RNA caused by mutations of the u5 RNA sequences. *Virology*, **303**, 152–163.
18. Didierlaurent,L., Racine,P.J., Houzet,L., Chamontin,C., Berkhout,B. and Mougel,M. (2011) Role of HIV-1 RNA and protein determinants for the selective packaging of spliced and unspliced viral RNA and host U6 and 7SL RNA in virus particles. *Nucleic Acids Res.*, **39**, 8915–8927.
19. Berkhout,B. and van Wamel,J.L. (1996) Role of the DIS hairpin in replication of human immunodeficiency virus type 1. *J. Virol.*, **70**, 6723–6732.
20. Laughrea,M., Jetté,L., Mak,J., Kleiman,L., Liang,C. and Wainberg,M.A. (1997) Mutations in the kissing-loop hairpin of human immunodeficiency virus type 1 reduce viral infectivity as well as genomic RNA packaging and dimerization. *J. Virol.*, **71**, 3397–3406.
21. Paillart,J.C., Berthoux,L., Ottmann,M., Darlix,J.L., Marquet,R., Ehresmann,B. and Ehresmann,C. (1996) A dual role of the putative RNA dimerization initiation site of human immunodeficiency virus type 1 in genomic RNA packaging and proviral DNA synthesis. *J. Virol.*, **70**, 8348–8354.
22. Keane,S.C., Heng,X., Lu,K., Kharytonchyk,S., Ramakrishnan,V., Carter,G., Barton,S., Hosic,A., Florwick,A., Santos,J. *et al.* (2015) RNA structure. Structure of the HIV-1 RNA packaging signal. *Science*, **348**, 917–921.
23. Aldovini,A. and Young,R.A. (1990) Mutations of RNA and protein sequences involved in human immunodeficiency virus type 1 packaging result in production of noninfectious virus. *J. Virol.*, **64**, 1920–1926.
24. Clavel,F. and Orenstein,J.M. (1990) A mutant of human immunodeficiency virus with reduced RNA packaging and abnormal particle morphology. *J. Virol.*, **64**, 5230–5234.
25. Lever,A., Gottlinger,H., Haseltine,W. and Sodroski,J. (1989) Identification of a sequence required for efficient packaging of human immunodeficiency virus type 1 RNA into virions. *J. Virol.*, **63**, 4085–4087.
26. Luban,J. and Goff,S.P. (1994) Mutational analysis of cis-acting packaging signals in human immunodeficiency virus type 1 RNA. *J. Virol.*, **68**, 3784–3793.
27. Nikolaitchik,O.A., Rhodes,T.D., Ott,D. and Hu,W.-S. (2006) Effects of mutations in the human immunodeficiency virus type 1 Gag gene on RNA packaging and recombination. *J. Virol.*, **80**, 4691–4697.
28. Vrolijk,M.M., Ooms,M., Harwig,A., Das,A.T. and Berkhout,B. (2008) Destabilization of the TAR hairpin affects the structure and function of the HIV-1 leader RNA. *Nucleic Acids Res.*, **36**, 4352–4363.
29. Das,A.T., Vrolijk,M.M., Harwig,A. and Berkhout,B. (2012) Opening of the TAR hairpin in the HIV-1 genome causes aberrant RNA dimerization and packaging. *Retrovirology*, **9**, 59.
30. Das,A.T., Harwig,A., Vrolijk,M.M. and Berkhout,B. (2007) The TAR hairpin of human immunodeficiency virus type 1 can be deleted when not required for Tat-mediated activation of transcription. *J. Virol.*, **81**, 7742–7748.
31. Smyth,R.P., Despons,L., Huili,G., Bernacchi,S., Hijnen,M., Mak,J., Jossinet,F., Weixi,L., Paillart,J., von Kleist,M. *et al.* (2015) Mutational interference mapping experiment (MIME) for studying RNA structure and function. *Nat. Methods*, **12**, 866–872.
32. Kutluay,S.B., Zang,T., Blanco-Melo,D., Powell,C., Jannain,D., Errando,M. and Bieniasz,P.D. (2014) Global changes in the RNA binding specificity of HIV-1 gag regulate virion genesis. *Cell*, **159**, 1096–1109.
33. Mouland,A.J., Mercier,J., Luo,M., Bernier,L., DesGroseillers,L. and Cohen,E.A. (2000) The double-stranded RNA-binding protein Staufen is incorporated in human immunodeficiency virus type 1: evidence for a role in genomic RNA encapsidation. *J. Virol.*, **74**, 5441–5451.
34. Eckwahl,M.J., Arnion,H., Kharytonchyk,S., Zang,T., Bieniasz,P.D., Telesnitsky,A. and Wolin,S.L. (2016) Analysis of the human immunodeficiency virus-1 RNA packageome. *RNA*, **22**, 1228–1238.
35. Liu,Y., Nikolaitchik,O.A., Rahman,S.A., Chen,J., Pathak,V.K. and Hu,W.S. (2017) HIV-1 sequence necessary and sufficient to package non-viral RNAs into HIV-1 particles. *J. Mol. Biol.*, **429**, 2542–2555.

36. McBride,M.S., Schwartz,M.D. and Panganiban,A.T. (1997) Efficient encapsidation of human immunodeficiency virus type 1 vectors and further characterization of cis elements required for encapsidation. *J. Virol.*, **71**, 4544–4554.
37. Gibbs,J.S., Regier,D.A. and Desrosiers,R.C. (1994) Construction and In Vitro Properties of HIV-1 Mutants with Deletions in 'Nonessential' Genes. *AIDS Res. Hum. Retroviruses*, **10**, 343–350.
38. Zufferey,R., Nagy,D., Mandel,R.J., Naldini,L. and Trono,D. (1997) Multiply attenuated lentiviral vector achieves efficient gene delivery in vivo. *Nat. Biotechnol.*, **15**, 871–875.
39. Smith,M.R., Smyth,R.P., Marquet,R. and von Kleist,M. (2016) MIMEAnTo—profiling functional RNA in mutational interference mapping experiments. *Bioinformatics*, **32**, 3369–3370.
40. Lehmann,K.A. and Bass,B.L. (2000) Double-stranded RNA adenosine deaminases ADAR1 and ADAR2 have overlapping specificities. *Biochemistry*, **39**, 12875–12884.
41. Suspène,R., Petit,V., Puyraimond-Zemmour,D., Aynaud,M.-M., Henry,M., Guétard,D., Rusniok,C., Wain-Hobson,S. and Vartanian,J.-P. (2011) Double-stranded RNA adenosine deaminase ADAR-1-induced hypermutated genomes among inactivated seasonal influenza and live attenuated measles virus vaccines. *J. Virol.*, **85**, 2458–2462.
42. Sodroski,J., Rosen,C., Wong-Staal,F., Salahuddin,S.Z., Popovic,M., Arya,S., Gallo,R.C. and Haseltine,W.A. (1985) Trans-acting transcriptional regulation of human T-cell leukemia virus type III long terminal repeat. *Science*, **227**, 171–173.
43. Sodroski,J., Patarca,R., Rosen,C., Wong-Staal,F. and Haseltine,W. (1985) Location of the trans-activating region on the genome of human T-cell lymphotropic virus type III. *Science*, **229**, 74–77.
44. Herrmann,C.H. and Rice,A.P. (1995) Lentivirus Tat proteins specifically associate with a cellular protein kinase, TAK, that hyperphosphorylates the carboxyl-terminal domain of the large subunit of RNA polymerase II: candidate for a Tat cofactor. *J. Virol.*, **69**, 1612–1620.
45. Herrmann,C.H., Gold,M.O. and Rice,A.P. (1996) Viral transactivators specifically target distinct cellular protein kinases that phosphorylate the RNA polymerase II C-terminal domain. *Nucleic Acids Res.*, **24**, 501–508.
46. Bardaro,M.F., Shajani,Z., Patora-Komisarska,K., Robinson,J.A. and Varani,G. (2009) How binding of small molecule and peptide ligands to HIV-1 TAR alters the RNA motional landscape. *Nucleic Acids Res.*, **37**, 1529–1540.
47. Richter,S., Cao,H. and Rana,T.M. (2002) Specific HIV-1 TAR RNA loop sequence and functional groups are required for human cyclin T1-Tat-TAR ternary complex formation. *Biochemistry*, **41**, 6391–6397.
48. Klaver,B. and Berkhout,B. (1994) Evolution of a disrupted TAR RNA hairpin structure in the HIV-1 virus. *EMBO J.*, **13**, 2650–2659.
49. Harrich,D., Hsu,C., Race,E. and Gaynor,R.B. (1994) Differential growth kinetics are exhibited by human immunodeficiency virus type 1 TAR mutants. *J. Virol.*, **68**, 5899–5910.
50. Tian,B., Hu,J., Zhang,H. and Lutz,C.S. (2005) A large-scale analysis of mRNA polyadenylation of human and mouse genes. *Nucleic Acids Res.*, **33**, 201–212.
51. Ashe,M.P., Griffin,P., James,W. and Proudfoot,N.J. (1995) Poly(A) site selection in the HIV-1 provirus: inhibition of promoter-proximal polyadenylation by the downstream major splice donor site. *Genes Dev.*, **9**, 3008–3025.
52. Ashe,M.P., Pearson,L.H. and Proudfoot,N.J. (1997) The HIV-1 5′ LTR poly (A) site is inactivated by U1 snRNP interaction with the downstream major splice donor site. *EMBO J.*, **16**, 5752–5763.
53. Takata,M., Soll,S.J., Emery,A., Blanco-Melo,D., Swanstrom,R. and Bieniasz,P.D. (2018) Global synonymous mutagenesis identifies cis-acting RNA elements that regulate HIV-1 splicing and replication. *PLoS Pathog.*, **14**, e1006824.
54. Mueller,N., van Bel,N., Berkhout,B. and Das,A.T. (2014) HIV-1 splicing at the major splice donor site is restricted by RNA structure. *Virology*, **468**, 609–620.
55. Mueller,N., Berkhout,B. and Das,A.T. (2015) HIV-1 splicing is controlled by local RNA structure and binding of splicing regulatory proteins at the major 5′ splice site. *J. Gen. Virol.*, **96**, 1906–1917.
56. Houzet,L., Paillart,J.C., Smagulova,F., Maurel,S., Morichaud,Z., Marquet,R. and Mougel,M. (2007) HIV controls the selective packaging of genomic, spliced viral and cellular RNAs into virions through different mechanisms. *Nucleic Acids Res.*, **35**, 2695–2704.
57. Duval,M., Cossart,P. and Lebreton,A. (2017) Mammalian microRNAs and long noncoding RNAs in the host-bacterial pathogen crosstalk. *Semin. Cell Dev. Biol.*, **65**, 11–19.
58. Wang,Z., Zhao,Y. and Zhang,Y. (2017) Viral lncRNA: A regulatory molecule for controlling virus life cycle. *Non-coding RNA Res.*, **2**, 38–44.
59. Tycowski,K.T., Guo,Y.E., Lee,N., Moss,W.N., Vallery,T.K., Xie,M. and Steitz,J.A. (2015) Viral noncoding RNAs: more surprises. *Genes Dev.*, **29**, 567–584.
60. Cooper,T.A., Wan,L. and Dreyfuss,G. (2009) RNA and disease. *Cell*, **136**, 777–793.
61. Jakobovits,A., Smith,D.H., Jakobovits,E.B. and Capon,D.J. (1988) A discrete element 3′ of human immunodeficiency virus 1 (HIV-1) and HIV- 2 mRNA initiation sites mediates transcriptional activation by an HIV trans activator. *Mol. Cell. Biol.*, **8**, 2555–2561.
62. Berkhout,B., Silverman,R.H. and Jeang,K.T. (1989) Tat trans-activates the human immunodeficiency virus through a nascent RNA target. *Cell*, **59**, 273–282.
63. Dingwall,C., Ernberg,I., Gait,M.J., Green,S.M., Heaphy,S., Karn,J., Lowe,A.D., Singh,M., Skinner,M.A. and Valerio,R. (1989) Human immunodeficiency virus 1 tat protein binds trans-activation-responsive region (TAR) RNA in vitro. *Proc. Natl. Acad. Sci. U.S.A.*, **86**, 6925–6929.
64. Dingwall,C., Ernberg,I., Gait,M.J., Green,S.M., Heaphy,S., Karn,J., Lowe,A.D., Singh,M. and Skinner,M.A. (1990) HIV-1 tat protein stimulates transcription by binding to a U-rich bulge in the stem of the TAR RNA structure. *EMBO J.*, **9**, 4145–4153.
65. Feng,S. and Holland,E.C. (1988) HIV-1 tat trans-activation requires the loop sequence within tar. *Nature*, **334**, 165–167.
66. Wei,P., Garber,M.E., Fang,S.M., Fischer,W.H. and Jones,K.A. (1998) A novel CDK9-associated C-type cyclin interacts directly with HIV-1 Tat and mediates its high-affinity, loop-specific binding to TAR RNA. *Cell*, **92**, 451–462.
67. Ashe,M.P., Furger,A. and Proudfoot,N.J. (2000) Stem-loop 1 of the U1 snRNP plays a critical role in the suppression of HIV-1 polyadenylation. *RNA*, **6**, 170–177.
68. Klasens,B.I., Thiesen,M., Virtanen,A. and Berkhout,B. (1999) The ability of the HIV-1 AAUAAA signal to bind polyadenylation factors is controlled by local RNA structure. *Nucleic Acids Res.*, **27**, 446–454.
69. Gee,A.H., Kasprzak,W. and Shapiro,B.A. (2006) Structural differentiation of the HIV-1 polyA signals. *J. Biomol. Struct. Dyn.*, **23**, 417–428.
70. Graveley,B.R., Fleming,E.S. and Gilmartin,G.M. (1996) RNA structure is a critical determinant of poly(A) site recognition by cleavage and polyadenylation specificity factor. *Mol. Cell. Biol.*, **16**, 4942–4951.
71. Das,A.T., Klaver,B. and Berkhout,B. (1999) A hairpin structure in the R region of the human immunodeficiency virus type 1 RNA genome is instrumental in polyadenylation site selection. *J. Virol.*, **73**, 81–91.
72. Cherrington,J. and Ganem,D. (1992) Regulation of polyadenylation in human immunodeficiency virus (HIV): contributions of promoter proximity and upstream sequences. *EMBO J.*, **11**, 1513–1524.
73. Valsamakis,A., Schek,N. and Alwine,J.C. (1992) Elements upstream of the AAUAAA within the human immunodeficiency virus polyadenylation signal are required for efficient polyadenylation in vitro. *Mol. Cell. Biol.*, **12**, 3699–3705.
74. Paillart,J.C., Marquet,R., Skripkin,E., Ehresmann,B. and Ehresmann,C. (1994) Mutational analysis of the bipartite dimer linkage structure of human immunodeficiency virus type 1 genomic RNA. *J. Biol. Chem.*, **269**, 27486–27493.
75. Paillart,J.C., Skripkin,E., Ehresmann,B., Ehresmann,C. and Marquet,R. (1996) A loop-loop 'kissing' complex is the essential part of the dimer linkage of genomic HIV-1 RNA. *Proc. Natl. Acad. Sci. U.S.A.*, **93**, 5572–5577.
76. Jones,K.L., Sonza,S. and Mak,J. (2008) Primary T-lymphocytes rescue the replication of HIV-1 DIS RNA mutants in part by facilitating reverse transcription. *Nucleic Acids Res.*, **36**, 1578–1588.
77. Hill,M.K., Shehu-Xhilaga,M., Campbell,S.M., Poumbourios,P., Crowe,S.M. and Mak,J. (2003) The dimer initiation sequence stem-loop of human immunodeficiency virus type 1 is dispensable for viral replication in peripheral blood mononuclear cells. *J. Virol.*, **77**, 8329–8335.

78. Sakuragi,J.-I., Sakuragi,S. and Shioda,T. (2007) Minimal region sufficient for genome dimerization in the human immunodeficiency virus type 1 virion and its potential roles in the early stages of viral replication. *J. Virol.*, **81**, 7985–7992.
79. Russell,R.S., Liang,C. and Wainberg,M.A. (2004) Is HIV-1 RNA dimerization a prerequisite for packaging? Yes, no, probably? *Retrovirology*, **1**, 23.
80. Clever,J.L. and Parslow,T.G. (1997) Mutant human immunodeficiency virus type 1 genomes with defects in RNA dimerization or encapsidation. *J. Virol.*, **71**, 3407–3414.
81. St Louis,D.C., Gotte,D., Sanders-Buell,E., Ritchey,D.W., Salminen,M.O., Carr,J.K. and McCutchan,F.E. (1998) Infectious molecular clones with the nonhomologous dimer initiation sequences found in different subtypes of human immunodeficiency virus type 1 can recombine and initiate a spreading infection in vitro. *J. Virol.*, **72**, 3991–3998.
82. Clever,J., Sassetti,C. and Parslow,T.G. (1995) RNA secondary structure and binding sites for gag gene products in the 5′ packaging signal of human immunodeficiency virus type 1. *J. Virol.*, **69**, 2101–2109.
83. Das,A.T., Klaver,B., Klasens,B.I., van Wamel,J.L. and Berkhout,B. (1997) A conserved hairpin motif in the R-U5 region of the human immunodeficiency virus type 1 RNA genome is essential for replication. *J. Virol.*, **71**, 2346–2356.
84. Clever,J.L., Eckstein,D.A. and Parslow,T.G. (1999) Genetic dissociation of the encapsidation and reverse transcription functions in the 5′ R region of human immunodeficiency virus type 1. *J. Virol.*, **73**, 101–109.
85. Kenyon,J.C., Prestwood,L.J. and Lever,A.M.L. (2015) A novel combined RNA-protein interaction analysis distinguishes HIV-1 Gag protein binding sites from structural change in the viral RNA leader. *Sci. Rep.*, **5**, 14369.
86. Beaudoing,E., Freier,S., Wyatt,J.R., Claverie,J.M. and Gautheret,D. (2000) Patterns of variant polyadenylation signal usage in human genes. *Genome Res.*, **10**, 1001–1010.
87. Comas-Garcia,M., Davis,S.R. and Rein,A. (2016) On the Selective Packaging of Genomic RNA by HIV-1. *Viruses*, **8**, E246.
88. Sun,Y., Zhang,Y., Hamilton,K., Manley,J.L., Shi,Y., Walz,T. and Tong,L. (2017) Molecular basis for the recognition of the human AAUAAA polyadenylation signal. *Proc. Natl. Acad. Sci. U.S.A.*, **115**, E1419–E1428.
89. Clerici,M., Faini,M., Aebersold,R. and Jinek,M. (2017) Structural insights into the assembly and polyA signal recognition mechanism of the human CPSF complex. *Elife*, **6**, e33111.
90. Martin,G., Gruber,A.R., Keller,W. and Zavolan,M. (2012) Genome-wide analysis of pre-mRNA 3′ end processing reveals a decisive role of human cleavage factor I in the regulation of 3′ UTR length. *Cell Rep.*, **1**, 753–763.
91. Shi,Y., Di Giammartino,D.C., Taylor,D., Sarkeshik,A., Rice,W.J., Yates,J.R., Frank,J. and Manley,J.L. (2009) Molecular architecture of the human pre-mRNA 3′ processing complex. *Mol. Cell*, **33**, 365–376.
92. Engeland,C.E., Brown,N.P., Börner,K., Schümann,M., Krause,E., Kaderali,L., Müller,G.A. and Kräusslich,H.-G. (2014) Proteome analysis of the HIV-1 Gag interactome. *Virology*, **460–461C**, 194–206.
93. Saito,A., Henning,M.S., Serrao,E., Dubose,B.N., Teng,S., Huang,J., Li,X., Saito,N., Roy,S.P., Siddiqui,M.A. *et al.* (2016) Capsid-CPSF6 interaction is dispensable for HIV-1 replication in primary cells but is selected during virus passage in vivo. *J. Virol.*, **90**, 6918–6935.
94. Lee,K., Ambrose,Z., Martin,T.D., Oztop,I., Mulky,A., Julias,J.G., Vandegraaff,N., Baumann,J.G., Wang,R., Yuen,W. *et al.* (2010) Flexible use of nuclear import pathways by HIV-1. *Cell Host Microbe*, **7**, 221–233.
95. Rasheedi,S., Shun,M.-C., Serrao,E., Sowd,G.A., Qian,J., Hao,C., Dasgupta,T., Engelman,A.N. and Skowronski,J. (2016) The cleavage and polyadenylation specificity factor 6 (CPSF6) subunit of the capsid-recruited pre-messenger RNA cleavage factor I (CFIm) complex mediates HIV-1 integration into genes. *J. Biol. Chem.*, **291**, 11809–11819.
96. Price,A.J., Fletcher,A.J., Schaller,T., Elliott,T., Lee,K., KewalRamani,V.N., Chin,J.W., Towers,G.J. and James,L.C. (2012) CPSF6 defines a conserved capsid interface that modulates HIV-1 replication. *PLoS Pathog.*, **8**, e1002896.

Drug-Class Specific Impact of Antivirals on the Reproductive Capacity of HIV

Max von Kleist[1,2]*, Stephan Menz[2], Wilhelm Huisinga[1]

1 Hamilton Institute, Computational Physiology Group, National University of Ireland Maynooth, Kildare, Ireland, **2** Department of Mathematics and Computer Science, Freie Universität Berlin, Berlin, Germany

Abstract

Predictive markers linking drug efficacy to clinical outcome are a key component in the drug discovery and development process. In HIV infection, two different measures, viral load decay and phenotypic assays, are used to assess drug efficacy *in vivo* and *in vitro*. For the newly introduced class of integrase inhibitors, a huge discrepancy between these two measures of efficacy was observed. Hence, a thorough understanding of the relation between these two measures of drug efficacy is imperative for guiding future drug discovery and development activities in HIV. In this article, we developed a novel viral dynamics model, which allows for a mechanistic integration of the mode of action of all approved drugs and drugs in late clinical trials. Subsequently, we established a link between *in vivo* and *in vitro* measures of drug efficacy, and extract important determinants of drug efficacy *in vivo*. The analysis is based on a new quantity—the reproductive capacity—that represents in mathematical terms the *in vivo* analog of the read-out of a phenotypic assay. Our results suggest a drug-class specific impact of antivirals on the total amount of viral replication. Moreover, we showed that the (drug-)target half life, dominated by immune-system related clearance processes, is a key characteristic that affects both the emergence of resistance as well as the *in vitro–in vivo* correlation of efficacy measures in HIV treatment. We found that protease- and maturation inhibitors, due to their target half-life, decrease the total amount of viral replication and the emergence of resistance most efficiently.

Citation: von Kleist M, Menz S, Huisinga W (2010) Drug-Class Specific Impact of Antivirals on the Reproductive Capacity of HIV. PLoS Comput Biol 6(3): e1000720. doi:10.1371/journal.pcbi.1000720

Editor: Niko Beerenwinkel, ETH Zurich, Switzerland

Received September 2, 2009; **Accepted** February 23, 2010; **Published** March 26, 2010

Funding: MvK and WH acknowledge funding from National University of Ireland and the DFG Research Center Matheon. SM acknowledges financial support by DFG funding, provided through the Dahlem Research School of Freie Universität Berlin. The funders had no role in study design, data collection and analysis, decision to publish, or preparation of the manuscript.

Competing Interests: The authors have declared that no competing interests exist.

* E-mail: vkleist@zedat.fu-berlin.de

Introduction

Since 1996, human immunodeficiency virus (HIV) infection is treated with a combination therapy, known as highly active anti-retroviral therapy (HAART) [1,2], which has substantially improved the clinical management of HIV [3]. Despite the success of HAART, eradication of HIV can currently not be achieved [4,5], most likely due to the persistence of virus in very long lived, latently infected cells [6,7]. For HIV-infected individuals, life-long therapy is therefore required to prevent progression to the acquired immunodeficiency syndrome (AIDS) and death.

During therapy, plasma viral load (HIV RNA per mL blood plasma) is recommended by the National Institute of Health as a marker of therapy success [8], whereas measurement of the CD4 cell count is the most important clinical marker of disease progression [9]. The *in vivo* potency of novel antivirals is usually assessed by viral load decline in small clinical trials of monotherapy, e.g., [10,11], and later evaluated utilizing the novel agent in combination with an optimized background therapy, e.g., [12]. The *in vitro* potency of antivirals is typically assessed by using phenotypic/single-round infectivity assays [13–16], which measure the number of offspring after one round of virus replication.

Investigation of novel drug targets for the treatment of HIV infection resulted in the development of new drug classes. In 2003 and 2007, the fusion inhibitor (FI) enfuvirtide [17], the CCR5-antagonist maraviroc [18] and the integrase inhibitor raltegravir [19] were approved for the treatment of HIV infection. Many more drugs are in late clinical development [20]. With the introduction of new drug classes, in particular integrase inhibitors, a huge discrepancy between the efficacy measured *in vitro*, using phenotypic/single-round infectivity assays, and *in vivo*, using viral load decline, was observed [14,21]. Although integrase inhibitors cause a steep initial decline of plasma viral load [21–26], the *in vitro* efficacy is amongst the lowest [14].

Mathematical modelling of viral dynamics has lead to many insights into the pathogenesis and treatment of HIV. It is a valuable tool to interpret the time course of virological markers (e.g. viral load) during HIV treatment [27–31] and contributes much to our current understanding of the *in vivo* dynamics of HIV. Sedaghat et al. [32,33] used a mathematical modelling approach to analyze the rapid decay of plasma viral load after application of integrase inhibitors. They infer that this characteristic viral decay is a result of the inhibited stage within the viral life cycle rather than superior *in vivo* potency.

Consequently, viral load decay may be misleading for assessing the potency of integrase inhibitors (and other novel inhibitors) in comparison to existing drug classes. However, an alternative, more appropriate measure of drug efficacy, which allows to directly compare drugs from different drug classes is still missing.

Author Summary

To guide drug discovery and development, measures of drug efficacy that are linked to clinical outcome are of key importance. In HIV treatment, decay of plasma viral load is typically used as an *in vivo* measure of drug efficacy, whereas phenotypic assays are used to assess drug efficacy *in vitro*. The recent development of novel HIV drugs resulted in a huge discrepancy between viral load decay and *in vitro* predictions of drug efficacy. We used a mathematical modelling approach to resolve this discrepancy by introducing a new quantity, the reproductive capacity, that allows a transfer of the *in vitro* drug efficacy measure into the *in vivo* context, enabling a direct comparison. We developed a novel model of viral dynamics that incorporates the mechanism of action of all established and novel antivirals. Based on the model, we analyzed the ability of the viral infection to replicate under different drug treatments, and estimated class-specific times until virological failure. We conclude that the half life of the targeted viral stage is an important class-specific attribute that impacts on the overall success of a drug *in vivo*. Our findings have direct implication for the drug discovery and development process.

The objectives of this article are (i) to develop a novel, generic measure of drug potency that facilitates comparison across different drug classes; (ii) to develop a novel mathematical model of the viral replication cycle that incorporates the action of established and novel drugs in a *mechanistic* way; and (iii) to analyze determinants of drug efficacy critical for drug discovery and development. The proposed measure of drug efficacy, termed reproductive capacity, extends the established *in vivo* marker, plasma viral load, by incorporating additional infectious viral stages, and the *in vitro* phenotypic/single-round infectivity assays by taking into account host specific defense mechanisms. This enables us to understand the observed discrepancies between *in vitro* and *in vivo* efficacy for integrase inhibitors, and to elucidate and quantify the role of immune-system related clearance mechanisms in drug action. The results presented herein are of particular value to categorize different molecular targets in the HIV life cycle and are expected to be of significance for guiding future HIV drug discovery and development.

Results

Development of a detailed model of viral life cycle and action of anti-retroviral drugs

We derived a detailed virus-target cell interaction model as depicted in Fig. 1. The model incorporates the mechanisms of action of all currently approved drugs and some drugs in late clinical development.

Target cells are produced by the immune system with some constant rate λ_T. An infectious virus V_I reversibly binds (with effective rate constants k_{on} and k_{off}) to a target cell TU, forming a complex $V_I : TU$. After binding, the virus irreversibly fuses (with rate constant k_{fus}) with the target cell and the viral capsid containing the viral genomic RNA is released; this state is denoted by T_{RNA}. During reverse transcription (with effective rate constant k_{rev}), genomic viral RNA is irreversibly transformed into a more stable DNA. Viral DNA and viral proteins form the pre-integration complex (PIC), denoted by T_1. In the next step, viral DNA of the PIC is irreversibly integrated into the DNA of the target cell (with rate constant k_T), forming the provirus T_2. After integration, the infected cell cannot return to an uninfected stage. From the proviral DNA, viral proteins are amplified and new viruses are released (with effective rate constant $\widehat{N}_T[1/(\text{cells}\cdot\text{day})]$). Only a given percentage $p>0$ of the released viruses are correctly assembled immature viruses V_{IM}, while the remaining percentage $(1-p)$ are defective virions V_D that might e.g. lack the (*gag-pol*-polyprotein contained) enzymes. During the final step, the viral protease, which is packed into the correctly assembled, immature virions V_{IM}, is responsible for the maturation of the virus.

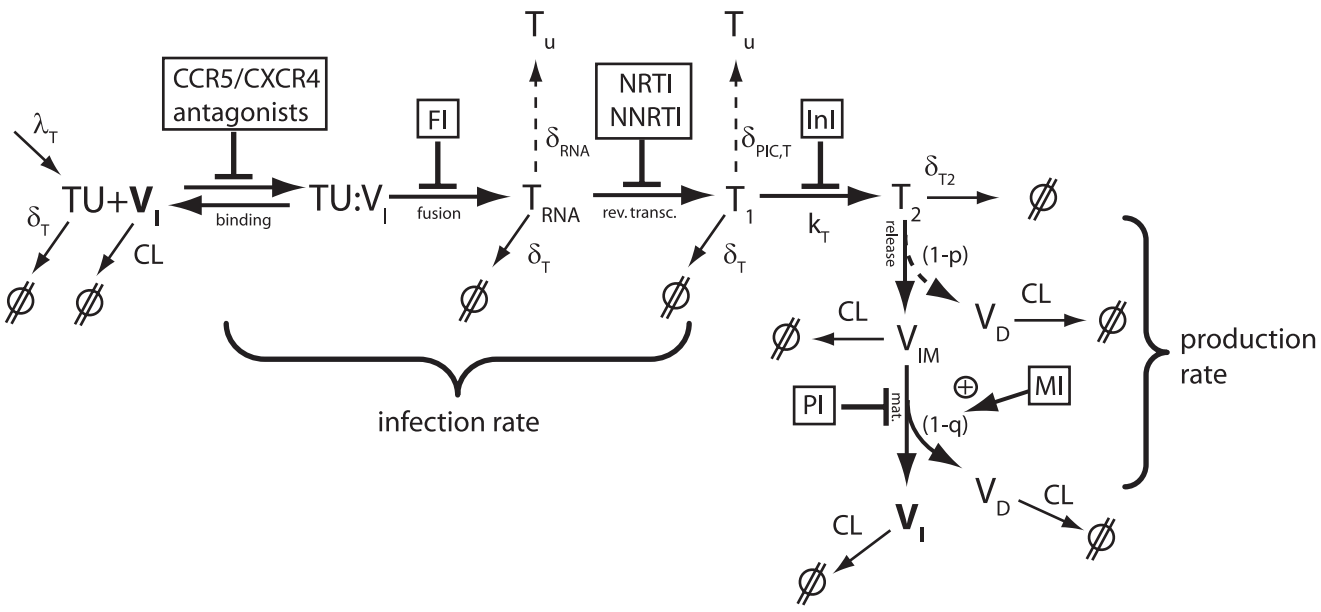

Figure 1. Detailed structural model of the viral life cycle and the mechanisms of action of different anti-retroviral drug classes.
doi:10.1371/journal.pcbi.1000720.g001

The maturation of HIV virions has been shown to be dependent on the highly ordered cascade of cleavages, governed by differences in the inherent processing rates at each cleavage site [34,35]. We assume that a fraction $(1-q)$ of the released virus matures abnormally, contributing to the pool of defective virions V_D. Successful maturation eventually leads to new infectious virus particles V_I (with rate constant k_{mat} and probability q).

Depending on the stage of the life cycle, the host organism has different abilities to clear the virus. It was assumed that infectious, immature and defective virions V_I, V_{IM}, and V_D, respectively, are cleared with rate constant CL by the host. The uninfected target cells TU, the T_{RNA} stage and the early infected stage T_1 are assumed to be cleared with rate constant δ_T, since none of these stages express viral proteins, while the virus-producing late infected cell T_2 is assumed to be cleared with rate constant $\delta_{T2} \gg \delta_T$. In addition to cell death, the target cell may fend-off the viral infection by degrading the viral RNA or parts of the PIC, rendering the cell uninfected. RNA is very unstable with a half life ranging from seconds to a maximum of two hours [36,37]. Therefore, through degradation or, e.g., by hypermutation through APOBEC3G [38], the viral RNA can be cleared with rate constant δ_{RNA}. The cell might also destroy essential components of the PIC (with rate constant $\delta_{PIC,T}$) to clear the virus.

The system of ordinary differential equations (ODEs) describing the rate of change of the different viral species and target cells in the detailed model (depicted in Fig. 1) is given in Supplementary Text S1, Eqs. (S1)–(S8). As typically done in kinetic studies, complex aspects of the viral dynamics are subsumed by 'lumped' parameters in the model. For instance, the rate constant of the reverse transcription k_{rev} contains all the steps necessary to transform the viral RNA into a double stranded DNA. The mechanisms of action of the seven drug classes are based on interfering with the viral life cycle at different stages. We assumed that the effect of a drug on the targeted process is specified by some parameter $\varepsilon(t) \in [0,1]$, i.e.,

$$(1-\varepsilon) = \left(\frac{1}{1+\left(\frac{C}{IC_{50}}\right)^n} \right) \qquad \text{(conc. dependent efficacy)}, \quad (1)$$

assuming some underlying averaged drug concentration $C = \widehat{C}$, see [39], some fifty percent inhibitory concentration IC_{50}, and some drug specific Hill coefficient n, see [14]. For the purpose of the study, this rough approximation is sufficient, however, it is possible to also use time-varying drug concentration $C = C(t)$ resulting from some pharmacokinetic model, or to use more mechanistic effects models [40,41].

The actions of the different drug classes within the viral life cycle are shown in Fig. 1. CCR5 antagonists inhibit the association of HIV with the CCR5 receptor in CCR5-tropic virus. They thus affect the association constant k_{on}. Fusion inhibitors (FI) inhibit the process of HIV fusion, affecting k_{fus}. Activated nucleoside reverse transcriptase inhibitors (NRTI) compete with endogenous deoxynucleoside triphosphates for prolongation of the growing DNA chain, while non-nucleoside reverse transcriptase inhibitors (NNRTI) allosterically inhibit the function of the reverse transcriptase. The effects of both drug classes result in a reduced rate at which the RNA is reversely transcribed into DNA. Integration inhibitors affect the integration of viral DNA into the host genome catalytically [42–45]. In the proposed model, this alters the transition rate constant k_T from early infected cells T_1 to the late infected cells T_2. Protease inhibitors (PI) bind to the catalytic pocket of the viral protease enzyme, which is responsible for the processing of the viral precursor polyproteins and thus the maturation of viral particles. In the proposed model (Fig. 1), PIs therefore inhibit maturation by decreasing the maturation constant k_{mat}. Maturation inhibitors (MI) bind to the substrate of the viral protease (*Gag*-polyprotein) [46] at a specific site. This binding perturbs the ordered sequence of cleavages that is necessary for proper maturation [47,48], resulting in defective virus morphology [49]. In the proposed model (Fig. 1), MIs therefore decrease the probability q that immature virus matures normally, increasing the proportion of abnormally matured, defective viruses V_D.

Impact of antiviral drugs on relative abundance of infectious viral stages

We used the detailed virus-target cell interaction model to predict the effect of the different drug classes on the distinct stages of the viral life cycle. In order to enable a direct comparison between the different drug classes, we artificially eliminated the feedback by keeping the uninfected target cell TU and the infective virions V_I that 'enter' the infection cycle constant (the two leftmost species in Fig. 1), resulting in 'downstream' quasi-steady state numbers $T_{1,ss}$, $T_{2,ss}$, $V_{IM,ss}$, $V_{I,ss}$, and $V_{D,ss}$. For a given drug class and inhibition of the targeted molecular process ε, the effect of the drug on the life cycle was quantified by the four ratios

$$\frac{T_{1,ss}}{TU_0}, \quad \frac{T_{2,ss}}{T_{1ss}}, \quad \frac{V_{I,ss}}{V_{IM,ss}}, \quad \frac{V_{I,ss}}{V_{D,ss}} \qquad (2)$$

as shown in Fig. 2. As expected, the drugs perturb the ratios of viral states that encompass their site of action within the viral life cycle. In the present example, all states that lie downstream of the drugs' target site are affected, while the states that lie upstream are usually not affected. The exception are InIs, which increase the abundance of the preceding stage T_1 (Fig. 2A), while decreasing the number of the subsequent infectious stage T_2 (Fig. 2B). Interestingly, the effect on the ratios is not always a linear function of drug efficacy. PIs and MIs also show a different behavior (Fig. 2D): PIs affect the ratio of infectious-to-defective virions by decreasing the maturation rate k_{mat}, which lowers the number of infective virions V_I, but also lowers the number of virions that mature abnormally (contributing to V_D). MIs increase the proportion of virus that matures abnormally and decrease the proportion of virus that matures normally, thus decreasing V_I and increasing V_D, without affecting k_{mat}.

Development of a simplified two stage virus dynamics model

The detailed model (Fig. 1) contains parameters that are difficult to measure and currently not available. We therefore reduced the detailed model based on reasonable quasi-steady state assumptions to obtain a simplified model of virus-target cell interaction dynamics that is parameterizable in terms of established and validated parameter values (see Supplementary Text S1). In particular, we have eliminated the intermediate stages of the cell-virus complex $TU:V_I$, the infected cells prior to reverse transcription T_{RNA} and the immature virus V_{IM} in the original model (Fig. 1). As a consequence, we derived a lumped infection rate constant β, which describes the infection of a susceptible cell towards the stage, where the viral RNA has been successfully transformed into DNA. We also derived a virus clearance CL_T that is associated with the loss of virus during the intermediate stages before reverse transcription and the release rate constant of infectious virus N.

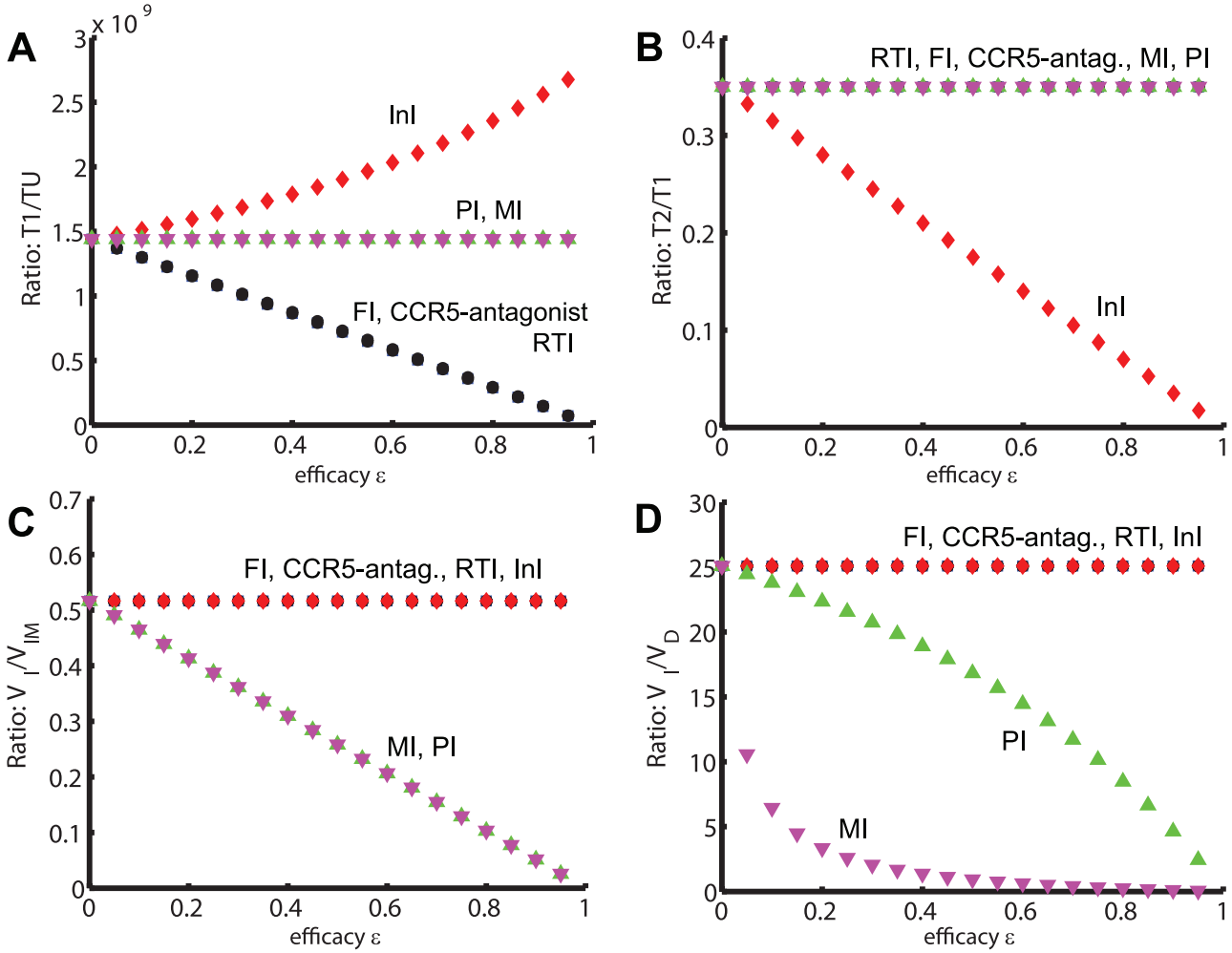

Figure 2. Mechanistic effects of drug classes on viral infective compartments. Ratios are affected through treatment with different drug classes. Predictions are based on the detailed model (see Fig. 1) and mechanistic effect ε varying from 0–1. Chosen parameter values: $CL=23$, $\delta_T=0.02$, $\delta_{T_2}=1$, $k_T=0.35$, $\delta_{PIC,T}=0.35$, $\delta_{RNA}=1440$, $k_{off}=10^6$, $r_{fusion}=1440$, $r_{RT}=48$, $r_{mat}=12$ in [1/day]; $N=1000$ in [1/(cells·day)]; $\lambda=2\cdot10^9$ in [cells/day]; $K_D=1000$ in [cells] and $q=p=0.99$ (unit less).
doi:10.1371/journal.pcbi.1000720.g002

The infection rate constant is given by

$$\beta=\frac{k_{fus}}{K_D}\cdot\rho_{rev,\phi}, \tag{3}$$

where k_{fus} denotes the fusion rate constant, K_D the dissociation constant of the virus-target cell complex, and $\rho_{rev,\phi}$ denotes the probability that reverse transcription is successfully completed (see Supplementary Text S1). The lumped virus clearance (loss of virus by, e.g., genome destruction) in the intermediate stages is given by the parameter

$$CL_T=\left(\frac{1}{\rho_{rev,\phi}}-1\right)\cdot\beta. \tag{4}$$

The number of released, infectious viruses is given by

$$N=q\cdot p\cdot\rho_{PR,\phi}\cdot\widehat{N}, \tag{5}$$

where p and q are the probabilities that the released virus is correctly assembled and matures normally, and $\rho_{PR,\phi}$ is the probability that the released virus matures before being cleared by the immune system (see Supplementary Text S1). The lumped model can be parameterized in terms of six unknown parameters ($\beta,\widehat{N},\lambda_T,\delta_T,\delta_{T_2},CL$), which equals the number of estimated parameters using standard models [28]. For the remaining parameters, we have provided values from the literature (see Supplementary Text S1).

In the following, we considered two types of target cells (T-Cells and a longer lived cell population, which we refer to as macrophages) and finally incorporated the viral mutation process (resulting from erroneous reverse transcription) into the overall model. Whether the longer lived cell population consists solely of macrophages *in vivo* remains unknown. There is, however, some evidence that the kinetic characteristics of the longer lived cell population are similar to those of the macrophage population [33]. The proposed simplified two-stage virus dynamics model is shown in Fig. 3. It comprises T-cells, macrophages, free non-infectious virus (TU,MU,V_{NI}, respectively), free infectious virus of mutant strain i,$V_I(i)$, and four types of infected cells belonging to mutant strain i: infected T-cells and macrophages *prior* to proviral genomic integration ($T_1(i)$ and $M_1(i)$, respectively) and infected T-cells and macrophages *after* proviral genomic integration ($T_2(i)$ and $M_2(i)$, respectively). The rates of

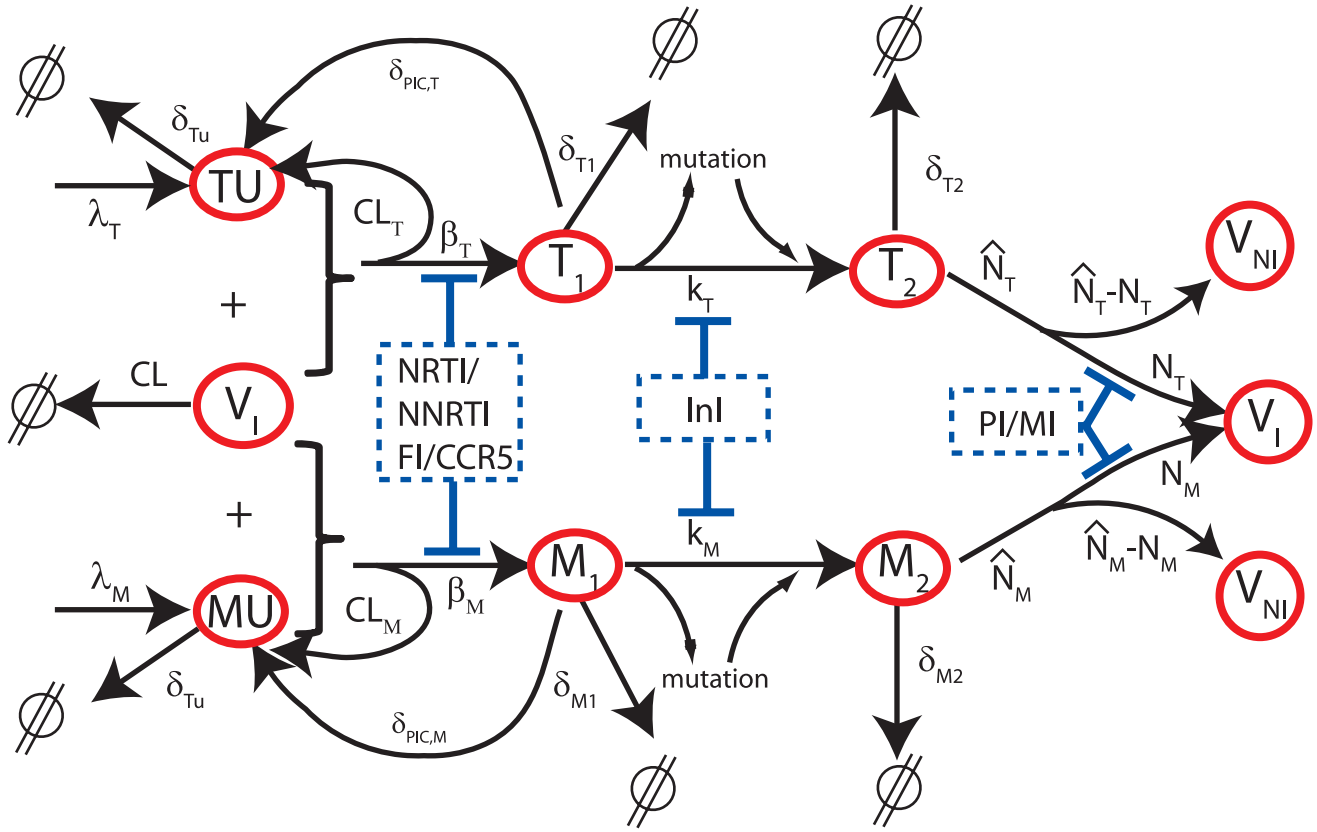

Figure 3. Simplified two stage virus dynamics model. Species (red cycles), reactions (black arrows), drugs and their interference in the life cycle of HIV (blue dashed box). Target cells (TU,MU) can become successfully infected by infective virus V_I with lumped infection rate constants β_T and β_M, respectively, creating early infected cells T_1 and M_1. Infection can also be unsuccessful after the irreversible step of fusion (rate constant CL_T and CL_M), eliminating the virus and rendering the cell uninfected. Early infected cells T_1 and M_1 can destroy essential viral proteins or DNA prior to integration with rate constants $\delta_{PIC,T}$ and $\delta_{PIC,M}$ returning the cell to an uninfected stage. The genomic viral DNA can become integrated with rate constants k_T and k_M creating late infected cells T_2 and M_2, which can release new infectious- and non infectious virus V_I and V_{NI} with rate constants $N_T, \left(\widehat{N_T} - N_T\right)$ and $N_M, \left(\widehat{N_M} - N_M\right)$, respectively. Phenotypic mutation occurs at the stage of viral genomic integration k_T,k_M (see section 'Development of a simplified two stage virus dynamics model'). All cellular compartments x can get destroyed by the immune system with respective rate constants δ_x and the free virus gets cleared with rate constant CL.
doi:10.1371/journal.pcbi.1000720.g003

change of the different species in the reduced two-stage HIV model are given by the following system of ODEs:

$$\begin{aligned}
\frac{d}{dt}\mathrm{TU} &= \lambda_T + \delta_{PIC,T}\cdot \mathrm{T_1}(i) - \delta_T \cdot \mathrm{TU} - \sum_i \beta_T(i)\cdot \mathrm{V}(i)\cdot \mathrm{TU} \\
\frac{d}{dt}\mathrm{MU} &= \lambda_M + \delta_{PIC,M}\cdot \mathrm{M_1}(i) - \delta_M \cdot \mathrm{MU} - \sum_i \beta_M(i)\cdot \mathrm{V}(i)\cdot \mathrm{MU} \\
\frac{d}{dt}\mathrm{T_1}(i) &= \beta_T(i)\cdot \mathrm{V}(i)\cdot \mathrm{TU} - (\delta_{T_1} + \delta_{PIC,T} + k_T(i))\cdot \mathrm{T_1}(i) \\
\frac{d}{dt}\mathrm{M_1}(i) &= \beta_M(i)\cdot \mathrm{V}(i)\cdot \mathrm{MU} - (\delta_{M_1} + \delta_{PIC,M} + k_M(i))\cdot \mathrm{M_1}(i) \\
\frac{d}{dt}\mathrm{T_2}(i) &= \sum_k k_T(k)\mathrm{T_1}(k)\cdot p_{k\to i} - \delta_{T_2}\cdot \mathrm{T_2}(i) \\
\frac{d}{dt}\mathrm{M_2}(i) &= \sum_k k_M(k)\mathrm{M_1}(k)\cdot p_{k\to i} - \delta_{M_2}\cdot \mathrm{M_2}(i) \\
\frac{d}{dt}\mathrm{V_I}(i) &= \mathrm{N_M}(i)\cdot \mathrm{M_2}(i) + \mathrm{N_T}(i)\cdot \mathrm{T_2}(i) \\
&\quad - [\mathrm{CL} + (\mathrm{CL_T}(i) + \beta_T(i))\mathrm{TU} + (\mathrm{CL_M}(i) + \beta_M(i))\mathrm{MU}]\cdot \mathrm{V}(i) \\
\frac{d}{dt}\mathrm{V_{NI}} &= \sum_i [(\widehat{\mathrm{N}}_\mathrm{T}(i) - \mathrm{N_T}(i))\mathrm{T_2}(i) + (\widehat{\mathrm{N}}_\mathrm{M}(i) - \mathrm{N_M}(i))\mathrm{M_2}(i)] - \mathrm{CL}\cdot \mathrm{V_{NI}},
\end{aligned} \tag{6}$$

where λ_T and λ_M are the birth rates of uninfected T-cells and macrophages, and δ_T and δ_M are their death rate constants. The parameters $k_T(k)$ and $k_M(k)$ are the integration rate constants of mutant strain k. The parameters δ_{T_1},δ_{T_2},δ_{M_1} and δ_{M_2} are the death rate constants of T_1,T_2,M_1 and M_2 cells. The parameters $\delta_{PIC,T}$ and $\delta_{PIC,M}$ refer to the intracellular degradation of essential components of the pre-integration complex, e.g., by the host cell proteasome within early infected T-cells and macrophages respectively. $\widehat{N}_T(i)$ and $\widehat{N}_M(i)$ denote the total number of released infectious and non-infectious virus from late infected T-cells and macrophages of mutant strain i and $N_T(i)$ and $N_M(i)$ are the rates of release of infective virus (see Eq (5)). The parameters $CL_T(i)$ and $CL_M(i)$ denote the clearance of mutant virus i through unsuccessful infection of T-cells and macrophages respectively (see Eq. (4)) and the parameters $\beta_T(i)$ and $\beta_M(i)$ denote the successful infection rate constants of mutant virus i for T-cells and macrophages respectively. The parameter $p_{k\to i}$ denotes the probability to mutate from strain k to strain i (to be defined below).

The model enabled us to mechanistically incorporate the action of all drugs that are approved or in late clinical trial. The impact of a compound on a corresponding (lumped) parameter in the model is specified by η:

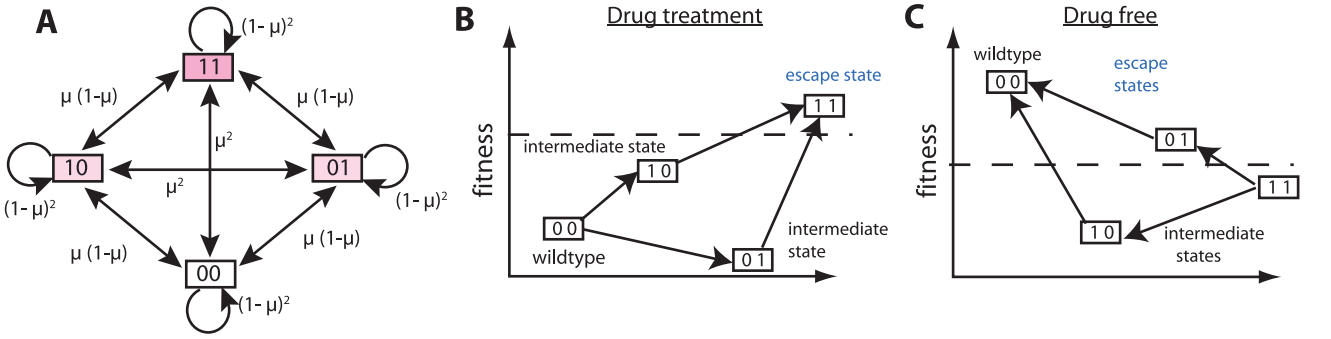

Figure 4. Fitness and possible mutational pathways. A: General transition pathways between wild type (00) and a fully drug resistant strain (11) that involves two partly-resistant intermediates (10,01). B: Fitness in the presence of a drug. C: Fitness in the absence of drugs. Dashed line: critical fitness that allows the strain to survive, i.e, $R_0(i)>1$.
doi:10.1371/journal.pcbi.1000720.g004

$$\beta_{T,(CCR5,FI,RTI)}=(1-\eta_{CCR5})\cdot(1-\eta_{FI})\cdot(1-\eta_{RTI}(\rho_{rev,\phi}))\cdot\beta_T \quad (7)$$

$$CL_{T,(CCR5,FI,RTI)}=(1-\eta_{CCR5})\cdot(1-\eta_{FI})\cdot\left(\frac{1}{\rho_{rev,\phi}}-(1-\eta_{RTI})\right)\cdot\beta_T \quad (8)$$

$$k_{T,(InI)}=(1-\eta_{InI})\cdot k_T \quad (9)$$

$$N_{T,(PI,MI)}=(1-\eta_{MI})\cdot(1-\eta_{PI}(\rho_{PR,\phi}))\cdot N_T. \quad (10)$$

The same quantities are defined for macrophages by replacing the subscript T by M; see Supplementary Text S1 for details. The overall viral dynamics model comprises a complete mutagenic graph. In HIV infection, genomic mutation occurs during the reverse transcription process [50]. The reverse transcriptase of HIV lacks a proof reading mechanism in contrast to host polymerase enzymatic reactions. However, viral proteins from newly mutated viral genomes are only produced after integration of the viral genome into the host cell DNA. The proteins required for the stable integration of the newly mutated viral genome originate from the founder virus. Therefore, phenotypically, drug resistance of new mutants will only be observed after integration, i.e., in the infectious stages T_2 and M_2. In total, the model includes 2^L different viral strains i that contain point mutations in any pattern of the modelled L possible mutations. For two distinct mutations $L=2$, the mutagenic graph is shown in Fig. 4A. Each mutant i can mutate into every other mutant k in one step. The probability $p_{k\to i}$ to mutate from a strain k into another strain i can be directly derived from the mutagenic pathways in Fig. 4A, i.e.,

$$p_{k\to i}=\mu^{h(i,k)}\cdot(1-\mu)^{L-h(i,k)}, \quad (11)$$

where μ denotes the mutation probability per base and reverse transcription process ($\mu\approx 2.16\cdot10^{-5}$ [50]), $h(i,k)$ denotes the hamming distance between strain k and strain i, and L is the total number of different positions that are considered in our model. The phenotype of each mutant strain i is modelled by introducing a selective disadvantage $s(i)$, which denotes the loss of functionality (e.g., in the activity of some viral enzyme that is affected by the mutation) relative to the wild type, and a strain specific inhibitory activity ($\eta(i,j)$) of treatment j against the mutant strain i. For example, the strain specific infection rate i under a certain treatment j is given by $\beta(i,j)=(1-\eta(i,j))\cdot(1-s(i))\cdot\beta(wt,\phi)$, where $\beta(wt,\phi)$ denotes the infection rate constant of the wild type wt in the absence of drug ϕ (given in Table 1). Since some viral strains are present only in very low copy numbers, we used a hybrid stochastic deterministic approach [51] to model the overall virus dynamics model (see *Materials and Methods* section for details).

Reproductive capacity for predicting drug–specific impact on viral replication

The production of infectious offspring is crucial for the survival of a viral population. The phenotypic single-round infectivity assay measures the amount of infectious offspring after one round of replication. For a given drug, the assay quantifies the drug's efficacy by measuring the reduction in viral offspring relative to the drug-free situation. We defined a new quantity—termed the reproductive capacity R_{cap}—, which transfers the principle of the phenotypic single-round infectivity assay into a mathematical term. Its definition involves the quasi-species distribution and the basic reproductive numbers of all pathogenic sub-stages. The reproductive capacity characterizes the fitness of a given state of the infection from the perspective of a potential treatment j by quantifying the expected total number of offspring under the treatment j.

The basic reproductive number R_0 is a well characterized quantity in epidemiology that denotes the expected number of

Table 1. Model parameters generally used in simulations.

Parameter	Value	Reference	Parameter	Value	Reference
λ_T	$2\cdot10^9$	[57]	λ_M	$6.9\cdot10^7$	[33]
β_T	$8\cdot10^{-12}$	[32]	β_M	$1\cdot10^{-14}$	§
$\widehat{N}_T$	1000	[33]	$\widehat{N}_M$	100	[33]
δ_T,δ_{T_1}	0.02	[33]	δ_M,δ_{M_1}	0.0069	[33]
δ_{T_2}	1	[73]	δ_{M_2}	0.09	§
CL	23	[73]	$p\cdot q\cdot\rho_{PR,\phi}$	0.67	†
$\rho_{rev,\phi}$	0.33	[74,75]	μ	$2.16\cdot10^{-5}$	[50]
k_T	0.35	[75]	k_M	0.07	§
$\delta_{PIC,T}$	0.35	[75,76]	$\delta_{PIC,M}$	0.0035	§
k_{mat}	12	[34]	-	-	-

All parameters in units [1/day], except $p\cdot q\cdot\rho_{PR,\phi}$ (unit less) and μ in [1/(rev.trans.·base)]. § parameters chosen to reproduce clinical data. † chosen according to the assumption that $p=q=1$ and utilizing parameters k_{mat} and CL to determine $\rho_{PR,\phi}=k_{mat}/(k_{mat}+CL)=0.67$.
doi:10.1371/journal.pcbi.1000720.t001

secondary infections caused by a single infected cell/virus [52]. If $R_0 > 1$ then the infection will spread, while for $R_0 < 1$ the infection will die out. The strain associated reproductive number $R_0(i,j)$ characterizes the fitness of a viral strain i in a pharmacologically modified environment, specified by a drug treatment j. We used the 'survival function' approach [53] to calculate the reproductive numbers for mutant strains i under treatment j. In our context, the survival function is of particular value, since it captures the possible event of mutation for all infective classes.

Based on the two-stage virus dynamics model, the basic reproductive number $R_V(i,j)$ of a single virus of strain i under treatment j is given by

$$R_V(i,j) = \frac{\beta_T(i,j)\mathrm{TU}\cdot k_T(i,j)\cdot \mathrm{N_T}(i,j)}{r_u(i,j)\cdot r_T(i,j)\cdot \delta_{T_2}} + \frac{\beta_M(i,j)\mathrm{MU}\cdot k_M(i,j)\cdot \mathrm{N_M}(i,j)}{r_u(i,j)\cdot r_M(i,j)\cdot \delta_{M_2}} \quad (12)$$

with constants

$$r_u(i,j) = \mathrm{CL} + [\mathrm{CL_T}(i,j) + \beta_T(i,j)]\mathrm{TU} + [\mathrm{CL_M}(i,j) + \beta_M(i,j)]\mathrm{MU} \quad (13)$$

$$r_T(i,j) = \delta_T + \delta_{PIC,T} + k_T(i,j) \quad (14)$$

$$r_M(i,j) = \delta_M + \delta_{PIC,M} + k_M(i,j). \quad (15)$$

Since infected cells are also pathogens, which can lead to a rebound of the disease even in the absence of any virus, we also determined their basic reproductive numbers under a given treatment j. The basic reproductive numbers $R_{T_1}(i,j)$ and $R_{M_1}(i,j)$ of the infectious stages T_1 and M_1, associated with the viral strain i, are given by

$$R_{T_1}(i,j) = \frac{k_T(i,j)\cdot \mathrm{N_T}(i,j)}{r_T(i,j)\cdot \delta_{T_2}} \cdot \frac{\beta_T(i,j)\mathrm{TU} + \beta_M(i,j)\mathrm{MU}}{r_u(i,j)} \quad (16)$$

$$R_{M_1}(i,j) = \frac{k_M(i,j)\cdot \mathrm{N_M}(i,j)}{r_M(i,j)\cdot \delta_{M_2}} \cdot \frac{\beta_T(i,j)\mathrm{TU} + \beta_M(i,j)\mathrm{MU}}{r_u(i,j)}. \quad (17)$$

Finally, the reproductive numbers $R_{T_2}(i,j)$ and $R_{M_2}(i,j)$ of the infectious stages T_2 and M_2, associated with the viral strain i, are given by

$$R_{T_2}(i,j) = \frac{\mathrm{N_T}(i,j)}{\delta_{T_2}} \cdot \left[\frac{k_T(i,j)\mathrm{TU}\cdot \beta_T(i,j)}{r_u(i,j)\cdot r_T(i,j)} + \frac{k_M(i,j)\mathrm{MU}\cdot \beta_M(i,j)}{r_u(i,j)\cdot r_M(i,j)} \right] \quad (18)$$

$$R_{M_2}(i,j) = \frac{\mathrm{N_M}(i,j)}{\delta_{M_2}} \cdot \left[\frac{k_T(i,j)\mathrm{TU}\cdot \beta_T(i,j)}{r_u(i,j)\cdot r_T(i,j)} + \frac{k_M(i,j)\mathrm{MU}\cdot \beta_M(i,j)}{r_u(i,j)\cdot r_M(i,j)} \right] \quad (19)$$

We defined the reproductive capacity $R_{cap}(j)$ of the entire quasi-species ensemble under treatment j as the weighted sum of the basic reproductive numbers of all pathogenic stages of mutant strain i, i.e., free virus, infected T-cells and infected macrophages, where the weights are the abundance of the corresponding pathogenic stage:

$$R_{cap}(j) = \sum_i [\mathrm{V_I}(i)R_V(i,j) + \mathrm{T_1}(i)R_{T_1}(i,j) + \mathrm{M_1}(i)R_{M_1}(i,j) + \mathrm{T_2}(i)R_{T_2}(i,j) + \mathrm{M_2}(i)R_{M_2}(i,j)]. \quad (20)$$

The reproductive capacity $R_{cap}(j)$ can be interpreted as the expected total number of infectious offspring that the infection produces in one round of replication under a certain treatment j, given the current state of the infection.

Relation to viral load and phenotypic/single-round infectivity assay. The viral load considers the total concentration of free virus, consisting of non-infectious virus $\mathrm{V_{NI}}$ and infectious virus $\mathrm{V_I}(i)$, belonging to all mutant strains i. In contrast to the reproductive capacity, viral load does not assess the ability of distinct viral strains i to replicate (in terms of R_V). In mathematical terms, the viral load is given by

$$\mathrm{V_{load}} = \sum_i \mathrm{V_I}(i) + \mathrm{V_{NI}}. \quad (21)$$

The *in vitro* reproductive capacity, corresponding to the read-out of the phenotypic assay $R_{pA}(j)$ (under treatment j) is conceptionally similar to Eq. (20). However, in comparison to the above defined *in vivo* measure, the *in vitro* measure would not take into account: (i) the clearance of any infective stage by the immune system (relating to the parameters $\mathrm{CL}, \mathrm{CL_T}(i,j), \mathrm{CL_M}(i,j), \delta_T, \delta_M, \delta_{T_2}$, and δ_{M_2}), and (ii) the abundance of the different infected cell types (e.g., T-cells and macrophages). The assay measures one round of replication, denoted by $\hat{R}_{T_2}$, starting from a late stage infected cell $\hat{\mathrm{T}}_2$. Mathematically expressed, the primary output is given by

$$R_{pA}(j) = \sum_i \hat{\mathrm{T}}_2(i)\cdot \hat{R}_{\hat{T}_2}(i,j). \quad (22)$$

Drug-class specific decay of viral load and reproductive capacity

Application of drugs/drug classes changes the total size and the composition of the viral population. The impact of this change is typically evaluated in terms of the decay of the viral load over time. We used the reproductive capacity $R_{cap}(j)$ to also evaluate viral replication under various hypothetical treatments j. In Fig. 5, we predicted the impact of the different drug classes on the decay of the plasma viral load and the reproductive capacity $R_{cap}(\phi)$, i.e., the fitness of the whole virus population, evaluated in the absence of drugs. As typically done, we assumed 100% drug efficacy η.

In terms of the plasma viral load decay (Fig. 5A), we observe a faster initial decay for InIs in comparison to all other compound classes, in agreement with clinical data [21] and theoretical analysis [32,33]. The onset of viral load decay is delayed for all other compound classes as observed clinically [12,27], see also Figure S1. In agreement with clinical data [21], in the case of InI treatment, the second phase of viral decay starts earlier after treatment initiation and exhibits $\approx$70% less viremia in comparison to other drug classes, but shows the same decay. Notably, the change of the ratio of infective virus-to-total virus (see Fig. 5, inset) upon PI or MI administration is not reflected by the total viral decay in the blood plasma.

Most noticeable, the reproductive capacity (Fig. 5B) discriminates between RTIs, FIs and CCR5-antagonists vs. InI vs. PIs and MIs. It can be seen, that protease and maturation inhibitors reduce R_{cap} most efficiently initially and shift it to an overall lower level. Integrase inhibitors cause a slightly faster initial decay in R_{cap}, in comparison to RTIs, FIs and CCR5-antagonists, which consistent with the rapid decay in viral load (Fig. 5A). However, in contrast to viral load decay, the initial fast decay of R_{cap} levels off and the second phase decay is flatter for InIs in comparison to

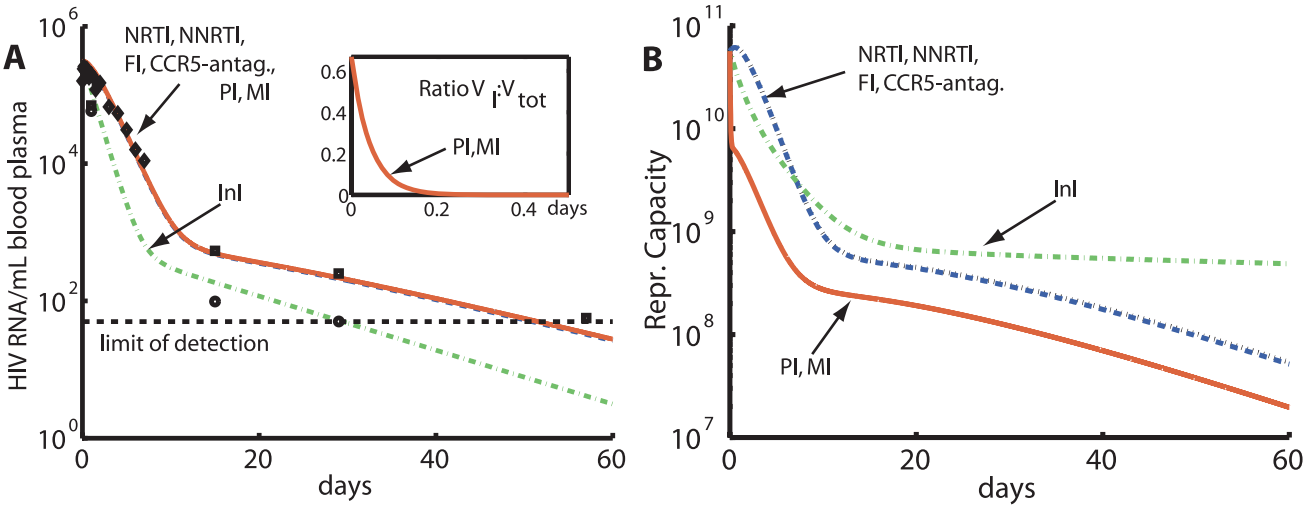

Figure 5. Decay of viral load and reproductive capacity after treatment initiation. A: Plasma virus load decay after treatment initiation. Integrase inhibitors (InI) produce a faster decay of virus load than all other compound classes. Red solid-, black dotted-, green dash-dotted- and blue dashed lines indicate simulation results with different inhibitor classes and parameters from Table 1. Black diamonds indicate median viral load data from [27] (PI monotherapy), numerically available in [70]. Black squares and black bullets indicate median viral load data from [21] (NRTI + background therapy and InI+background therapy, respectively). The horizontal dashed black line indicates the limit of detection of current assays (50 copies of HIV RNA per mL). Inset: Protease- and maturation inhibitors (PI and MI) change the ratio of infectious to total virus ($V_I : V_{tot}$). B: The evolution of the reproductive capacity (evaluated at the drug free state $R_{cap}(\phi)$) after treatment with different drug classes. Model parameters are as indicated in Table 1. The initial infection was assumed to consist of wild type only. Drug efficacy η was assumed to be 100%. Total body virus has been converted to plasma viral load by assuming that the virus distributes into the plasma ($V_{plas.} = 3.1$ liters, which surrounds 2% of infected cells) and the interstitial space ($V_{int.} = 9.6$ liters [71], which surrounds 98% of infected cells). The volume of distribution with reference to the plasma concentration has been calculated using the well-known formula vol. distr $= K_{int.:plas.} \cdot V_{int.} + V_{plas.}$, see e.g. [72], where $K_{int.:plas.} = 98\%/2\% = 50$. Finally, we assume that on average each virus contains 2 viral RNAs (which are measured [viral RNA/mL] plasma).
doi:10.1371/journal.pcbi.1000720.g005

RTIs, FIs, CCR5-antagonists, PIs and MIs. The effect of NRTIs, NNRTIs, CCR5 inhibitors and FIs on R_{cap} is comparable (Fig. 5B). Remarkably, these inhibitors induce an initial increase in R_{cap} (see next section for details), followed by a slow first phase decay, followed by a second phase decay that is parallel to the decay of R_{cap} in the case of PI- and MI-treatment, sustaining overall higher levels of R_{cap} in comparison to PIs and MIs. In the next section, we further elucidate the reasons for these class-specific differences.

Immune-system related clearance is critical determinant of drug-class specific decay

In view of the analysis performed in Fig. 5B, R_{cap} is directly correlated to the overall abundance of viral infectives (V_I,T_1,T_2,M_1,M_2).

PIs and MIs primarily act on infectious virus V_I (see Fig. 5, inset), by reducing the proportionality factor (N_T/CL and N_M/CL) that determines the abundance of infectious virus in the first- and second phase decay (see Eq. (10)). The infectious virus V_I is rapidly cleared by the immune system [54]. Therefore, application of highly efficient PIs and MIs leads to a rapid reduction of infectious virus V_I, as illustrated in Fig. 6D and Fig. 5 (inset). This reduction is also reflected by the initial drop of R_{cap} in Fig. 5B. In the case of PI and MI treatment, infected T-cells are quickly becoming the most abundant infectious compartment (Fig. 6D) and subsequently dominate the decay characteristics of R_{cap} in Fig. 5B. In the final phase, late infected macrophages (M_2) are becoming the most abundant compartment and thus dominate the decay of R_{cap} in the final phase.

Integrase inhibitors prevent the integration of the viral genome and thus prevent the transition of early infected cells (pre-integration, T_1 and M_1) to late infected cells (post-integration, T_2 and M_2), see Fig. 3. By inhibiting the transition from early to late infectious cells, integrase inhibitors increase the decay of late infected T_2-cells (see Fig. 6C). In the case of InI treatment, infectious virus V_I is initially proportional to T_2, explaining the observed more rapid first-phase decline in R_{cap} in Fig. 5B. However, blocking the transition from T_1 to T_2 can also slow the decay of the T_1-compartment, which might become more abundant than V_I after the initial decay. In the final phase both T_1 and V_I become proportional to- and remain more abundant than M_2, which explains the overall higher levels of R_{cap} in the final phase (see Fig. 5B).

The effects of NRTIs, NNRTIs, CCR5 inhibitors and FIs on R_{cap} are comparable (Fig. 5B), as they primarily act on pre-integrative early infected cells (T_1 and M_1). The difference between entry inhibitors and reverse transcriptase inhibitors is marginal, because the clearance of virus by infection is negligible compared to the clearance by the immune system ($CL_T < CL$ and $CL_M < CL$). A positive result of entry inhibitors (FI/CCR5) and RTIs (NRTIs/NNRTIs) is an increased number of uninfected cells, which also results in an initial increase in the reproductive capacity R_{cap} (see Fig. 5B). During treatment with NRTIs, NNRTIs, CCR5 inhibitors and FIs, infective virus V_I is the most abundant compartment. The decay in the first phase is proportional to the decay of the late infected cells, T_2. Once the abundance of T_2 falls below M_2, the decay of V_I and thus R_{cap} in Fig. 5B is proportional to the decay of late infected macrophages M_2.

The pattern of virological removal influences the time to virological rebound after treatment application

In the following, we predict how the distinct viral dynamics after drug application affect drug efficacy *in vivo*. The long-term *in vivo* efficacy of an antiviral drug depends on many different factors,

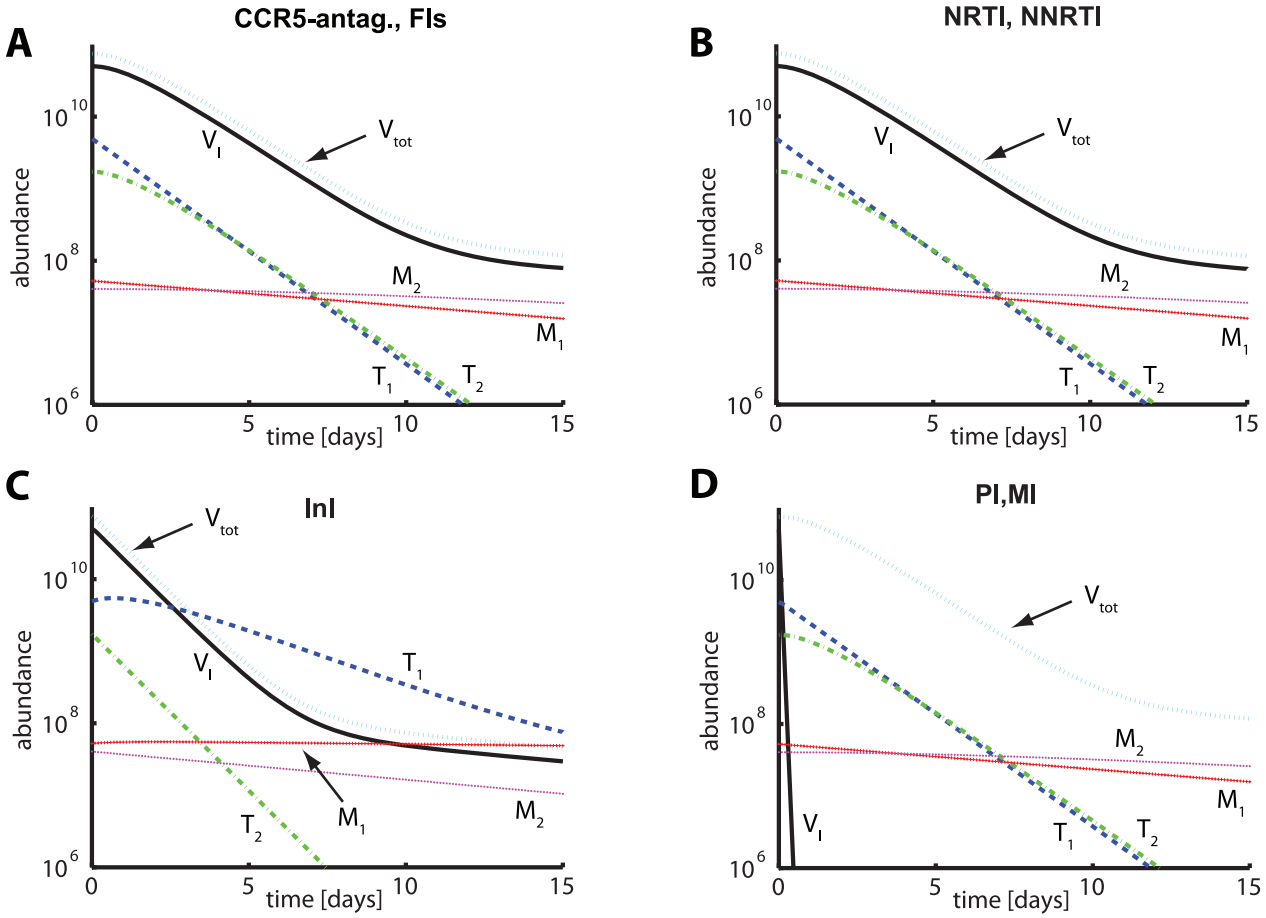

Figure 6. Decay of infective compartments after initiation of drug treatment. A: Decay of infective compartments after treatment with FI and CCR5-antagonists. B: Decay of infective compartments after treatment with NRTIs and NNRTIs. C: Decay of infective compartments after treatment with InIs. D: Decay of infective compartments after treatment with PIs.
doi:10.1371/journal.pcbi.1000720.g006

including the ability of the virus to adapt to the pharmacological challenge by developing resistance mutations. The ability to develop drug resistance is strongly dependent on the induced pattern of resistance mutations against a particular drug, but also on the velocity at which replication competent compartments (V_I,T_1,T_2,M_1,M_2) are removed from the body. Since anti-retroviral drug classes target different stages in the viral life cycle, they are likely to induce different patterns by which viral compartments are removed from the body (see Fig. 6) and might therefore exhibit different long-term *in vivo* efficacies.

To illustrate the sole impact of virological removal (V_I,T_1,T_2,M_1,M_2) on resistance development and therefore on drug efficacy, we have intentionally chosen a simplistic, unified mutational landscape and considered the time to viral rebound as a long-term measure of efficacy. We denoted virological rebound, if the viral load reaches 90% of the pre-treatment viral load. We assumed that the drugs inhibited their targeted (lumped) parameter (see Eqs. (7)–(10)) by 90% in the wild type ($\eta = 0.9$), by 45% in a one-mutation strain ($\eta = 0.45$) and are entirely inefficient in the double-mutant ($\eta = 0$). Drug-specific and more realistic mutational landscapes are possible, but in view of the current analysis (elucidating the impact of class-specific virological removal), they would blur the results.

In Table 2, the time to virological rebound for the different drug classes based on the above simplistic mutation model is reported. The virus generally rebounds to 90% of pre-treatment levels after 1–2 month of monotherapy, which is in the same order of magnitude as clinically observed rebound times [55–57]. Although inhibition η was assumed to be identical across all drug classes, the

Table 2. Virological rebound times resulting from distinct virological removal.

Drug/Selec. Disadvantage	30%	25%	20%	15%	10%	5%	1%
InI	48.13	44.44	41.33	38.70	36.43	34.65	33.25
FI/CCR5-antag.	53.71	47.81	43.09	39.57	36.47	33.77	32.06
NRTI/NNRTI	55.51	48.76	43.86	39.99	36.61	33.94	32.11
PI/MI	55.28	49.03	43.74	39.84	36.66	33.95	32.15

The time to virological rebound depends on both the cost of resistance ('selective disadvantage', s) and the choice of drugs. Each table entry shows the time to virological rebound in [days] in an ensemble of 1000 hybrid stochastic deterministic simulations, where we assumed that the efficacy of the drugs against the wild type was 90%. The drug was 45% effective against an one-mutation strain and completely inefficient against the double-mutant. The fraction of non-infectious viruses ($1-p\cdot q\cdot \rho_{PR,\emptyset}$) was set to one-third and the initial population was assumed to be all wild type. The viral load was said to be rebounded, if the viral load reached 90% of the pre-treatment viral load.
doi:10.1371/journal.pcbi.1000720.t002

times to virological rebound differed. In particular, when resistance confers a marked loss in fitness (i.e. selective disadvantage = 30%), PIs show the longest time to virologically rebound, and the InIs the shortest.

For integrase inhibitors, the difference between the decay of plasma viral load and their predicted long-term efficacy is quite pronounced. Their comparably shorter times to virological rebound are in strong contrast to their steep initial decrease of plasma viral load (see Fig. 5A), but consistent with the decay pattern of the reproductive capacity (Fig. 5B). For the EIs, RTIs, PIs and MIs, the predicted time to virological rebound is also much more consistent with the decay characteristics of the reproductive capacity (Fig. 5B) than with the decay pattern of total viral load (see Fig. 5A).

Discussion

In clinical studies, the first approved integrase inhibitor, raltegravir, induced an extremely rapid decline in viral load when applied both as monotherapy [10] and in combination with an optimized NRTI background therapy [21–24]. While it was initially speculated that the observed decline might be a result of superior potency of raltegravir, it is now emerging that the viral decline in InI-based therapy could be a class-specific phenomenon [25,26]. Moreover, superior potency of InIs (in terms of η) was not confirmed by single-round infectivity assays [14]. The mechanisms underlying the decay dynamics are still not clear [58] and controversially discussed [21,32].

In [32], a two stage model of the viral replication cycle is presented, which explains the differences between the decay of viral load between RTIs and InIs based on the stage at which the drugs affect the dynamics of viral replication. The model explicitly distinguishes two viral stages, early-stage infected cells and late-stage infected target cells, which are specifically defined for a pair of drugs under examination. The authors further conclude that the viral dynamics produced by drugs from different anti-retroviral classes should not be directly compared to infer drug potency [33]. An alternative measure, as it is imperative for guiding drug discovery and prioritizing drug candidates in later development stages, is still lacking.

All currently approved antivirals exert their effect by inhibiting the replication of HIV. The extent at which replication is inhibited, is therefore a unifying indicator for drug efficacy across all drug classes. Replication assays, e.g., phenotypic assays [15] or replication capacity assays [59], analyze drug efficacy in terms of viral replication *in vitro*. The replicative fitness of HIV *in vivo*, however, depends on the interaction of a multitude of viral and host factors. Replication assays represent the dynamics of HIV under the assay conditions, which lack many host factors, in particular the immune responses to the infection. However, since it is particularly useful to compare compounds in terms of replication inhibition, we adopt the dynamic approach of replication assays to define the reproductive capacity R_{cap}. *In silico*, we are able to consider the host response to the viral infection and can thus extrapolate the replication approach from *in vitro* to *in vivo*. In [60], the authors used a similar approach to compare the effect of distinct antiviral classes utilizing age-structured models.

We derived a single detailed model of the viral replication cycle and deduced a reduced two stage model, which incorporates the action of *all* approved HIV drugs. Our two-stage model allows to predict the action of *any number* of drugs simultaneously, including common HAART cocktails, potentially belonging to different drug classes. In contrast, in [32], the stages of the two-stage model of viral replication are not specified *a priori* and have to be determined by the *two* drugs that are analyzed and compared.

Based on the proposed detailed and reduced model, we identify the following effects of currently approved drugs: EI and RTIs decrease the infection rate and thus the number of new infections. The impact on the release of new virus (and virus decline) is therefore delayed by the viral life cycle. MIs and PIs do not interfere with the total amount of virus that is being released, but rather shift the ratio of infective to total virus, $V_I : V_{tot}$ (see Fig. 5, inset), which is not directly reflected by total plasma viral load. Since the kinetics of the free virus are rapid [54], this has an immediate impact on the number of new infections. Subsequently, this impact on the number of new infections affects the total viral release (and thus total plasma virus load) in a similar manner as EIs and RTIs, creating a 'shoulder' phase. Hence, we obtain

$$\text{new infections} = \overbrace{\beta}^{\text{EI,RTI}} \cdot \text{TU} \cdot \underbrace{V_I}_{\text{PI,MI}} \xrightarrow{life-cycle} \text{total virus release}. \quad (23)$$

In our model, EIs, RTIs, PIs and MIs produce an identical decay of plasma viral load (see Fig. 5A), when assuming 100% inhibition, respectively. In particular, the onset of viral load decay is similarly delayed ('shoulder phase') with these inhibitors (see Figure S1), in agreement with clinical observations [12,27]. Previously discussed theoretical differences in the viral response between RTIs and PIs (see Eq. (5.7) vs. Eq. (5.16) in [61]) yield similar dynamics when more recent (higher) estimates of viral clearance are used [54].

In contrast to other inhibitor classes, InIs decrease the amount of late infected cells (T_2,M_2) (see Fig. 2), which has an immediate impact on total virus release, i.e.,

$$\text{total virus release} = \widehat{N} \cdot \underbrace{T_2}_{\text{InI}}. \quad (24)$$

The impact of InIs on viral load decay is immediate and not delayed by the viral replication cycle as in the case of all other compounds [12,27]. Thus, the onset of observed total viral decay is faster for InIs than for other compounds, irrespective of their potency (which was set equal for all compounds in Fig. 5A). Furthermore, the decay of viral load in the first phase is steeper for InIs in comparison to other inhibitor classes (see Fig. 5A). The viral load decline in the first phase is proportional to the decay of the late infected T-cells T_2 (see Fig. 6). Sedaghat et al. [32] derived analytical solutions for the viral decay dynamics after InI and RTI treatment (see Eqs. (9) and (10) in [32]), which demonstrate that the viral decay after InI treatment is determined by the death rate of late infected cells (δ_{T_2}), while in the case of RTI treatment, the decay is determined by the "flushing-out" of the early infected cells (T_1) and the death rate of the late infected cells δ_{T_2}, leading to overall faster viral declines in the case of InI treatment in the first phase.

The long-term *in vivo* efficacy of an antiviral drug depends on many different factors, particularly the ability of the virus to adapt to the pharmacological challenge by developing resistance mutations. The ability to develop drug resistance is strongly dependent on the induced pattern of resistance mutations against a particular drug, but might also be influenced by the velocity at which replication competent compartments are removed from the body. However, viral load decay focusses on only one single variable, namely the total output of virus, whereas other infectious stages (e.g. T_1,T_2,M_1,M_2) remain 'hidden'. Furthermore, the ratio of infective virus-to-total virus (V_I/V_{tot}) is not resolved, which might underestimate the long-term efficacy of PIs and MIs that target this ratio (see Table 2 in relation to Fig. 5A). In the section

'The pattern of virological removal influences the time to virological rebound after treatment application', we have compared the impact of drug-class specific removal patterns on the long-term efficacy of antivirals (in terms of resistance development). We showed that although inhibition η was assumed to be identical across all drug classes, the times to virological rebound (used as a measure of long-term efficacy) differed, with PIs showing the longest time to virologically rebound, and InIs the shortest.

The reproductive capacity has been monitored over time in Fig. 5B to depict class-specific long-term efficacy of antivirals based on the hosts' ability to clear the targeted infectant in the viral life cycle. The main conclusion is that the long-term efficacy is larger for compounds that target viral life-stages that are cleared at a fast rate. It is generally assumed that the free virus is cleared at the fastest rate [27,54]. Since MIs and PIs reduce the production of infective virus V_I (see Fig. 2), they reduce the virus' ability to produce offspring faster than all other drug classes. Furthermore, since resistance development is correlated with the extent of replication, we infer that PIs and MIs, based on their viral target, are the most efficient drug classes in terms of reducing the probability of resistance development. This assumption correlates well with the observed rebound times in Table 2 and is also supported by the fact that the introduction of PIs marked the success of HAART [1].

During drug discovery, the pre-clinical- and the clinical development process, *in vitro* surrogate measures or *in vivo* drug efficacy measures are important to prioritize drug candidates.

The mechanistic mode of action of a compound at its target site can be elucidated by cell free assays that use purified viral protein, e.g. reverse transcriptase for RTIs. The influence of viral mutation, the immune system and pharmacokinetics are absent in this type of assay. However, it is possible to deduce the pharmacodynamic mode (e.g. Eq. (1), see also [41]) and thus the parameter ε from these types of assays, which denotes the extent of inhibition of the molecular process by the compound. Mathematical models of HIV dynamics use a minimal number of parameters, making them suitable for parameter fitting and comparison with clinical data. The parameters used in the models are often lumped, summarizing many viral processes. For example, binding, fusion and reverse transcription are part of the infection rate β (see Eq. (3)). Inhibition of lumped model parameters (denoted by η) might therefore differ from inhibition of the molecular process ε, which is measured by cell-free *in vitro* assays. We have provided equations (Eqs. (S24) and (S31), Supplementary Text S1) that enable the use of pharmacodynamic information ε, derived from cell free assays (inhibition of the targeted molecular process), in a (lumped) mathematical model of HIV dynamics (utilizing η).

The presented model can be extended to incorporate drug-specific escape pathways [62,63] or realistic time-varying drug pharmacokinetics [41]. If *in vivo* pharmacokinetic data is available (in terms of time-varying concentrations $C(t)$ in Eq. (1)), then extrapolation from *in vitro* to *in vivo* is possible and the mechanistic understanding of drug effects, its parametrization and extrapolation is facilitated. For RTIs and PIs, we found a nonlinear relationship between ε and η (see Eqs. (S24) and (S31), Supplementary Text S1). Utilization of Eqs. (S24) and (S31) allows to simulate drug effects based on their mechanistic understanding in a lumped model, that can be compared with clinical data.

The model can also be extended to include latently infected cells (very long lived infected cells). We did not consider them in this study, since they are expected to contribute little to the dynamics analyzed herein (the first and the second decay phase).

The reproductive capacity is a useful concept to analyze and monitor drug efficacy *in silico*. In its current form, the reproductive capacity requires detailed knowledge about (i) the composition of the viral population, and (ii) the fitness of the different viral strains under a given treatment (reproductive numbers, Eqs. (12) and (16)–(19)).

The fitness of certain viral strains can be assessed *in vitro*, e.g., by phenotypic assays. We model strain specific fitness i under treatment j, in terms of two parameters: the selective disadvantage $s(i)$, which denotes the loss in replication of mutant i, relative to the wild type; and the efficacy of treatment j against mutant i in terms of the parameter $\eta(i,j)$. The selective disadvantage can, e.g., be estimated by performing a phenotypic assay with a certain mutant virus i in the absence of drug and then comparing it to the assay with the wild type. The parameter $\eta(i,j)$ is already being assessed in practice (e.g., [15]), usually in terms of a fold increase in IC_{50}.

Acquisition of detailed knowledge about the composition of the viral population might, due to recent advances in sequencing technology [64–67], become feasible in the future. However, novel sequencing technology requires large amounts of viral RNA, which cannot be derived when the viral load is below the limits of detection.

Materials and Methods

Realization of hybrid simulations

The overall virus dynamics in our model comprise different viral strains with copy numbers that can vary over several orders of magnitude. For this reason we have chosen a hybrid (stochastic deterministic) setting for numerical simulation. This approach (i) takes stochastic fluctuations in the slow reaction processes into account; and (ii) reduces the computational costs for the simulation of the fast (deterministic) system dynamics. We used the direct hybrid method proposed in [51]. Elementary reactions were treated stochastically whenever their propensity function or the quantity of at least one of their reactants was below a certain threshold (for all numerical simulations this threshold was set to 5). For the numerical integration of the deterministic part of the system, we implemented a solver in C++ that is based on numerical differentiation formulas [68] and uses strategies for error control and step size control comparable to ode15s in Matlab [69]. To generate the data for Table 2, we performed 1000 hybrid simulations for each condition. With realization start ($t = 0$), the effects of the drug treatment were simulated until the viral population size reached 90% of its pre-treatment value, i.e., virological rebound occurred. During a simulation, the stochastic partitioning of the reaction system was dynamically updated and stochastic reaction events were realized accordingly. Every numerical calculation was computed with a relative error tolerance of 10^{-6} and an absolute error tolerance of 10^{-9}. The hybrid simulations for Table 2 were performed on two Intel Quad-Core Xeon E5345 processors with 2.33 GHz and 32 GB RAM, which took nearly 46 hours in total or approximately 6 seconds per simulation, respectively.

Supporting Information

Text S1 This file contains the derivation of the simplified model (Fig. 3) from the detailed model (Fig. 1).
Found at: doi:10.1371/journal.pcbi.1000720.s001 (0.30 MB PDF)

Figure S1 Delay in the onset of viral load decay, exemplified for PI treatment. Simulation results (red line) using the novel two stage virus dynamics model and simulating 100% effective PI treatment

are shown together with median clinical data (black diamonds) from PI (RTV) monotherapy.
Found at: doi:10.1371/journal.pcbi.1000720.s002 (0.91 MB EPS)

Acknowledgments

Insightful discussions with Prof. Rick Middleton (NUIM) are kindly acknowledged. We are very grateful to the National University of Ireland in Maynooth and the Free University of Berlin for providing computing time on their high-performance clusters. Special thanks to Vanush Misha Paturyan for assistance in scheduling jobs on the computing cluster at NUIM.

Author Contributions

Conceived and designed the experiments: MvK. Performed the experiments: MvK SM. Analyzed the data: MvK SM WH. Wrote the paper: MvK SM WH. Provided guidance and supervision: WH.

References

1. Hammer SM, Squires KE, Hughes MD, Grimes JM, Demeter LM, et al. (1997) A controlled trial of two nucleoside analogues plus indinavir in persons with human immunodeficiency virus infection and CD4 cell counts of 200 per cubic millimeter or less. AIDS clinical trials group 320 study team. N Engl J Med 337: 725–733.
2. Hirsch M, Steigbigel R, Staszewski S, Mellors J, Scerpella E, et al. (1999) A randomized, controlled trial of indinavir, zidovudine, and lamivudine in adults with advanced human immunodeficiency virus type 1 infection and prior antiretroviral therapy. J Infect Dis 180: 659–665.
3. Richman DD (2001) HIV chemotherapy. Nature 410: 995–1001.
4. Kulkosky J, Pomerantz RJ (2002) Approaching eradication of highly active antiretroviral therapy-persistent human immunodeficiency virus type 1 reservoirs with immune activation therapy. Clin Infect Dis 35: 1520–1526.
5. Kulkosky J, Nunnari G, Otero M, Calarota S, Dornadula G, et al. (2002) Intensification and stimulation therapy for human immunodeficiency virus type 1 reservoirs in infected persons receiving virally suppressive highly active antiretroviral therapy. J Infect Dis 186: 1403–1411.
6. Finzi D, Hermankova M, Pierson T, Carruth LM, Buck C, et al. (1997) Identification of a reservoir for HIV-1 in patients on highly active antiretroviral therapy. Science 278: 1295–1300.
7. Wong JK, Hezareh M, Günthard HF, Havlir DV, Ignacio CC, et al. (1997) Recovery of replication-competent HIV despite prolonged suppression of plasma viremia. Science 278: 1291–1295.
8. Current HIV treatment guidelines: (http://www.aidsinfo.nih.gov/guidelines/). Technical report, National Institute of Health (accessed 15-Feb-2010).
9. Langford SE, Ananworanich J, Cooper DA (2007) Predictors of disease progression in HIV infection: a review. AIDS Res Ther 4: 11.
10. Markowitz M, Morales-Ramirez JO, Nguyen BY, Kovacs CM, Steigbigel RT, et al. (2006) Antiretroviral activity, pharmacokinetics, and tolerability of mk-0518, a novel inhibitor of HIV-1 integrase, dosed as monotherapy for 10 days in treatment-naive HIV-1-infected individuals. J Acquir Immune Defic Syndr 43: 509–515.
11. Fätkenheuer G, Pozniak AL, Johnson MA, Plettenberg A, Staszewski S, et al. (2005) Efficacy of short-term monotherapy with maraviroc, a new CCR5 antagonist, in patients infected with HIV-1. Nat Med 11: 1170–1172.
12. Louie M, Hogan C, Mascio MD, Hurley A, Simon V, et al. (2003) Determining the relative efficacy of highly active antiretroviral therapy. J Infect Dis 187: 896–900.
13. Zhang H, Zhou Y, Alcock C, Kiefer T, Monie D, et al. (2004) Novel single-cell-level phenotypic assay for residual drug susceptibility and reduced replication capacity of drug-resistant human immunodeficiency virus type 1. J Virol 78: 1718–1729.
14. Shen L, Peterson S, Sedaghat AR, McMahon MA, Callender M, et al. (2008) Dose-response curve slope sets class-specific limits on inhibitory potential of anti-HIV drugs. Nat Med 14: 762–766.
15. Petropoulos CJ, Parkin NT, Limoli KL, Lie YS, Wrin T, et al. (2000) A novel phenotypic drug susceptibility assay for human immunodeficiency virus type 1. Antimicrob Agents Chemother 44: 920–928.
16. Hachiya A, Aizawa-Matsuoka S, Tanaka M, Takahashi Y, Ida S, et al. (2001) Rapid and simple phenotypic assay for drug susceptibility of human immunodeficiency virus type 1 using CCR5-expressing HeLa/CD4(+) cell clone 1–10 (magic-5). Antimicrob Agents Chemother 45: 495–501.
17. Dando TM, Perry CM (2003) Enfuvirtide. Drugs 63: 2755–66.
18. Carter NJ, Keating GM (2007) Maraviroc. Drugs 67: 2277–88.
19. Croxtall JD, Lyseng-Williamson KA, Perry CM (2008) Raltegravir. Drugs 68: 131–138.
20. Investigational drugs: (http://www.aidsinfo.nih.gov/). Technical report, National Institute of Health (accessed 15-Feb-2010).
21. Murray JM, Emery S, Kelleher AD, Law M, Chen J, et al. (2007) Antiretroviral therapy with the integrase inhibitor raltegravir alters decay kinetics of HIV, significantly reducing the second phase. AIDS 21: 2315–2321.
22. Grinsztejn B, Nguyen BY, Katlama C, Gatell JM, Lazzarin A, et al. (2007) Safety and efficacy of the HIV-1 integrase inhibitor raltegravir (mk-0518) in treatment-experienced patients with multidrug-resistant virus: a phase II randomised controlled trial. Lancet 369: 1261–1269.
23. Markowitz M, Nguyen BY, Gotuzzo E, Mendo F, Ratanasuwan W, et al. (2007) Rapid and durable antiretroviral effect of the HIV-1 integrase inhibitor raltegravir as part of combination therapy in treatment-naive patients with HIV-1 infection: results of a 48-week controlled study. J Acquir Immune Defic Syndr 46: 125–133.
24. Steigbigel RT, Cooper DA, Kumar PN, Eron JE, Schechter M, et al. (2008) Raltegravir with optimized background therapy for resistant HIV-1 infection. N Engl J Med 359: 339–354.
25. Dayam R, Al-Mawsawi LQ, Neamati N (2007) HIV-1 integrase inhibitors: an emerging clinical reality. Drugs R D 8: 155–168.
26. DeJesus E, Berger D, Markowitz M, Cohen C, Hawkins T, et al. (2006) Antiviral activity, pharmacokinetics, and dose response of the HIV-1 integrase inhibitor gs-9137 (jtk-303) in treatment-naive and treatment-experienced patients. J Acquir Immune Defic Syndr 43: 1–5.
27. Perelson AS, Neumann AU, Markowitz M, Leonard JM, Ho DD (1996) HIV-1 dynamics in vivo: virion clearance rate, infected cell life-span, and viral generation time. Science 271: 1582–1586.
28. Perelson AS, Essunger P, Cao Y, Vesanen M, Hurley A, et al. (1997) Decay characteristics of HIV-1-infected compartments during combination therapy. Nature 387: 188–191.
29. Ho DD, Neumann AU, Perelson AS, Chen W, Leonard JM, et al. (1995) Rapid turnover of plasma virions and CD4 lymphocytes in HIV-1 infection. Nature 373: 123–126.
30. Bonhoeffer S, May RM, Shaw GM, Nowak MA (1997) Virus dynamics and drug therapy. Proc Natl Acad Sci U S A 94: 6971–6976.
31. Nowak MA, Bangham CR (1996) Population dynamics of immune responses to persistent viruses. Science 272: 74–79.
32. Sedaghat AR, Dinoso JB, Shen L, Wilke CO, Siliciano RF (2008) Decay dynamics of HIV-1 depend on the inhibited stages of the viral life cycle. Proc Natl Acad Sci U S A 105: 4832–4837.
33. Sedaghat AR, Siliciano RF, Wilke CO (2009) Constraints on the dominant mechanism for HIV viral dynamics in patients on raltegravir. Antivir Ther 14: 263–271.
34. Pettit SC, Lindquist JN, Kaplan AH, Swanstrom R (2005) Processing sites in the human immunodeficiency virus type 1 (HIV-1) Gag-Pro-Pol precursor are cleaved by the viral protease at different rates. Retrovirology 2: 66.
35. Wiegers K, Rutter G, Kottler H, Tessmer U, Hohenberg H, et al. (1998) Sequential steps in human immunodeficiency virus particle maturation revealed by alterations of individual Gag polyprotein cleavage sites. J Virol 72: 2846–2854.
36. Ross J (1995) mRNA stability in mammalian cells. Microbiol Rev 59: 423–450.
37. Houseley J, Tollervey D (2009) The many pathways of RNA degradation. Cell 136: 763–776.
38. Mangeat B, Turelli P, Caron G, Friedli M, Perrin L, et al. (2003) Broad antiretroviral defence by human APOBEC3G through lethal editing of nascent reverse transcripts. Nature 424: 99–103.
39. Rosario MC, Poland B, Sullivan J, Westby M, van der Ryst E (2006) A pharmacokinetic-pharmacodynamic model to optimize the phase IIa development program of maraviroc. J Acquir Immune Defic Syndr 42: 183–191.
40. Jacqmin P, McFadyen L, Wade JR (2008) A receptor theory-based semimechanistic PD model for the CCR5 noncompetitive antagonist maraviroc. Br J Clin Pharmacol 65 Suppl 1: 95–106.
41. von Kleist M, Huisinga W (2009) Pharmacokinetic-pharmacodynamic relationship of NRTIs and its connection to viral escape: an example based on zidovudine. Eur J Pharm Sci 36: 532–543.
42. Hazuda DJ, Felock P, Witmer M, Wolfe A, Stillmock K, et al. (2000) Inhibitors of strand transfer that prevent integration and inhibit HIV-1 replication in cells. Science 287: 646–650.
43. Neamati N, Hong H, Owen JM, Sunder S, Winslow HE, et al. (1998) Salicylhydrazine-containing inhibitors of HIV-1 integrase: implication for a selective chelation in the integrase active site. J Med Chem 41: 3202–3209.
44. Grobler JA, Stillmock K, Hu B, Witmer M, Felock P, et al. (2002) Diketo acid inhibitor mechanism and HIV-1 integrase: implications for metal binding in the active site of phosphotransferase enzymes. Proc Natl Acad Sci U S A 99: 6661–6666.
45. Marchand C, Johnson AA, Karki RG, Pais GCG, Zhang X, et al. (2003) Metal-dependent inhibition of HIV-1 integrase by beta-diketo acids and resistance of the soluble double-mutant (f185k/c280s). Mol Pharmacol 64: 600–609.
46. Salzwedel K, Martin DE, Sakalian M (2007) Maturation inhibitors: a new therapeutic class targets the virus structure. AIDS Rev 9: 162–172.
47. Kräusslich HG, Fäcke M, Heuser AM, Konvalinka J, Zentgraf H (1995) The spacer peptide between human immunodeficiency virus capsid and nucleocapsid proteins is essential for ordered assembly and viral infectivity. J Virol 69: 3407–3419.

48. Pettit SC, Moody MD, Wehbie RS, Kaplan AH, Nantermet PV, et al. (1994) The p2 domain of human immunodeficiency virus type 1 Gag regulates sequential proteolytic processing and is required to produce fully infectious virions. J Virol 68: 8017–8027.
49. Li F, Goila-Gaur R, Salzwedel K, Kilgore NR, Reddick M, et al. (2003) PA-457: a potent HIV inhibitor that disrupts core condensation by targeting a late step in gag processing. Proc Natl Acad Sci U S A 100: 13555–13560.
50. Mansky LM, Temin HM (1995) Lower in vivo mutation rate of human immunodeficiency virus type 1 than that predicted from the fidelity of purified reverse transcriptase. J Virol 69: 5087–5094.
51. Alfonsi A, Cancès E, Turinici G, Ventura B, Huisinga W (2005) Exact simulation of hybrid stochastic and deterministic models for biochemical systems. ESAIM Proc 14: 1–23.
52. Heesterbeek JAP (2002) A brief history of R0 and a recipe for its calculation. Acta Biotheor 50: 189–204.
53. Heffernan JM, Smith RJ, Wahl LM (2005) Perspectives on the basic reproductive ratio. J R Soc Interface 2: 281–293.
54. Ramratnam B, Bonhoeffer S, Binley J, Hurley A, Zhang L, et al. (1999) Rapid production and clearance of HIV-1 and hepatitis C virus assessed by large volume plasma apheresis. Lancet 354: 1782–1785.
55. Nijhuis M, Schuurman R, de Jong D, Erickson J, Gustchina E, et al. (1999) Increased fitness of drug resistant HIV-1 protease as a result of acquisition of compensatory mutations during suboptimal therapy. AIDS 13: 2349–2359.
56. Havlir DV, Eastman S, Gamst A, Richman DD (1996) Nevirapine-resistant human immunodeficiency virus: kinetics of replication and estimated prevalence in untreated patients. J Virol 70: 7894–7899.
57. Wei X, Ghosh SK, Taylor ME, Johnson VA, Emini EA, et al. (1995) Viral dynamics in human immunodeficiency virus type 1 infection. Nature 373: 117–122.
58. Goffinet C, Allespach I, Oberbremer L, Golden PL, Foster SA, et al. (2009) Pharmacovirological impact of an integrase inhibitor on human immunodeficiency virus type 1 cDNA species in vivo. J Virol 83: 7706–7717.
59. Nicastri E, Sarmati L, d'Ettorre G, Palmisano L, Parisi SG, et al. (2003) Replication capacity, biological phenotype, and drug resistance of hiv strains isolated from patients failing antiretroviral therapy. J Med Virol 69: 1–6.
60. Rong L, Feng Z, Perelson AS (2007) Mathematical analysis of age-structured hiv-1 dynamics with combination antiretroviral therapy. Siam J Appl Math 67: 731–756.
61. Perelson AS, Nelson PW (1999) Mathematical analysis of HIV-1 dynamics in vivo. SIAM Review 41: 3–44.
62. Beerenwinkel N, Rahnenführer J, Däumer M, Hoffmann D, Kaiser R, et al. (2005) Learning multiple evolutionary pathways from cross-sectional data. J Comput Biol 12: 584–598.
63. Beerenwinkel N, Däumer M, Sing T, Rahnenführer J, Lengauer T, et al. (2005) Estimating HIV evolutionary pathways and the genetic barrier to drug resistance. J Infect Dis 191: 1953–1960.
64. Eriksson N, Pachter L, Mitsuya Y, Rhee SY, Wang C, et al. (2008) Viral population estimation using pyrosequencing. PLoS Comput Biol 4: e1000074.
65. Bushman FD, Hoffmann C, Ronen K, Malani N, Minkah N, et al. (2008) Massively parallel pyrosequencing in HIV research. AIDS 22: 1411–1415.
66. Rozera G, Abbate I, Bruselles A, Vlassi C, D'Offizi G, et al. (2009) Massively parallel pyrosequencing highlights minority variants in the HIV-1 Env quasispecies deriving from lymphomonocyte sub-populations. Retrovirology 6: 15.
67. Le T, Chiarella J, Simen BB, Hanczaruk B, Egholm M, et al. (2009) Low-abundance HIV drug-resistant viral variants in treatment-experienced persons correlate with historical antiretroviral use. PLoS One 4: e6079.
68. Klopfenstein R (1971) Numerical differentiation formulas for stiff systems of ordinary differential equations. RCA Review 32: 447–462.
69. Shampine L, Reichelt M (1997) The matlab ode suite. SIAM Journal on Scientific Computing 18: 1–22.
70. Rong L, Perelson AS (2009) Modeling HIV persistence, the latent reservoir, and viral blips. J Theor Biol 260: 308–331.
71. Kawai R, Mathew D, Tanaka C, Rowland M (1998) Physiologically based pharmacokinetics of cyclosporine a: extension to tissue distribution kinetics in rats and scale-up to human. J Pharmacol Exp Ther 287: 457–468.
72. von Kleist M, Huisinga W (2007) Physiologically based pharmacokinetic modelling: a sub-compartmentalized model of tissue distribution. J Pharmacokinet Pharmacodyn 34: 789–806.
73. Markowitz M, Louie M, Hurley A, Sun E, Mascio MD, et al. (2003) A novel antiviral intervention results in more accurate assessment of human immunodeficiency virus type 1 replication dynamics and T-cell decay in vivo. J Virol 77: 5037–5038.
74. Pierson TC, Zhou Y, Kieffer TL, Ruff CT, Buck C, et al. (2002) Molecular characterization of preintegration latency in human immunodeficiency virus type 1 infection. J Virol 76: 8518–8531.
75. Zhou Y, Zhang H, Siliciano JD, Siliciano RF (2005) Kinetics of human immunodeficiency virus type 1 decay following entry into resting CD4+ T cells. J Virol 79: 2199–2210.
76. Koelsch KK, Liu L, Haubrich R, May S, Havlir D, et al. (2008) Dynamics of total, linear nonintegrated, and integrated HIV-1 DNA in vivo and in vitro. J Infect Dis 197: 411–419.

HIV-1 Polymerase Inhibition by Nucleoside Analogs: Cellular- and Kinetic Parameters of Efficacy, Susceptibility and Resistance Selection

Max von Kleist[1]*, Philipp Metzner[2], Roland Marquet[3], Christof Schütte[1]

1 Department of Mathematics and Computer Science, Free University Berlin, Berlin, Germany, **2** Institute of Computational Science, University of Lugano, Lugano, Switzerland, **3** Architecture et Réactivité de l'ARN, Université de Strasbourg, CNRS, IBMC, Strasbourg, France

Abstract

Nucleoside analogs (**NA**s) are used to treat numerous viral infections and cancer. They compete with endogenous nucleotides (dNTP/NTP) for incorporation into nascent DNA/RNA and inhibit replication by preventing subsequent primer extension. To date, an integrated mathematical model that could allow the analysis of their mechanism of action, of the various resistance mechanisms, and their effect on viral fitness is still lacking. We present the first mechanistic mathematical model of polymerase inhibition by **NA**s that takes into account the reversibility of polymerase inhibition. Analytical solutions for the model point out the cellular- and kinetic aspects of inhibition. Our model correctly predicts for HIV-1 that resistance against nucleoside analog reverse transcriptase inhibitors (NRTIs) can be conferred by decreasing their incorporation rate, increasing their excision rate, or decreasing their affinity for the polymerase enzyme. For all analyzed NRTIs and their combinations, model-predicted macroscopic parameters (efficacy, fitness and toxicity) were consistent with observations. NRTI efficacy was found to greatly vary between distinct target cells. Surprisingly, target cells with low dNTP/NTP levels may not confer hyper-susceptibility to inhibition, whereas cells with high dNTP/NTP contents are likely to confer natural resistance. Our model also allows quantification of the selective advantage of mutations by integrating their effects on viral fitness and drug susceptibility. For zidovudine triphosphate (AZT-TP), we predict that this selective advantage, as well as the minimal concentration required to select thymidine-associated mutations (TAMs) are highly cell-dependent. The developed model allows studying various resistance mechanisms, inherent fitness effects, selection forces and epistasis based on microscopic kinetic data. It can readily be embedded in extended models of the complete HIV-1 reverse transcription process, or analogous processes in other viruses and help to guide drug development and improve our understanding of the mechanisms of resistance development during treatment.

Citation: von Kleist M, Metzner P, Marquet R, Schütte C (2012) HIV-1 Polymerase Inhibition by Nucleoside Analogs: Cellular- and Kinetic Parameters of Efficacy, Susceptibility and Resistance Selection. PLoS Comput Biol 8(1): e1002359. doi:10.1371/journal.pcbi.1002359

Editor: Thomas Lengauer, Max-Planck-Institut für Informatik, Germany

Received August 1, 2011; **Accepted** December 5, 2011; **Published** January 19, 2012

Funding: MvK acknowledges acknowledges financial support by the German Ministry of Education and Sciences (BMBF) and from the DFG research center MATHEON. PM acknowledges funding from the DFG research center MATHEON and DFG SPP 1276 (MetStröm). RM was supported by grants from Sidaction and ANRS (Agence Nationale de Recherches sur le SIDA et les Hépatites). The funders had no role in study design, data collection and analysis, decision to publish, or preparation of the manuscript.

Competing Interests: The authors have declared that no competing interests exist.

* E-mail: vkleist@zedat.fu-berlin.de

Introduction

Viral encoded polymerases perform essential enzymatic steps through amplification- or transformation of the viral genome during the viral life cycle [1]. As such, viral encoded polymerases constitute an attractive drug target for the treatment of many viral infections [2]. Nucleoside analogs (**NA**s) were among the first polymerase inhibitors that showed *clinical* efficacy [3–5] and are nowadays broadly used to treat hepatitis B-, herpes simplex- and HIV-1 infection [2], where they constitute the typical backbone components of modern highly active antiretroviral treatment (HAART). Nucleoside analogs are typically formulated as pro-drugs, which require intracellular phosphorylation to form an analog of (deoxy-) nucleoside-triphosphate (NA-TP; mimicking either adenosine, thymidine, guanine, cytosine or uracil), which can be incorporated into nascent viral DNA by the viral polymerase. After incorporation, nucleoside analogs bring the polymerization machinery to a halt, as they lack the chemical group that is necessary to attach the next incoming nucleotide [6]. Incorporated **NA**s can, however, be selectively excised by some viral polymerases, rescuing the nascent viral DNA and inducing a transient-, rather than permanent mode of inhibition. Inhibition of the crucial step of viral DNA polymerization can lower the probability by which circulating virus can successfully infect host cells [7] and the number of viral progeny produced per unit time, shifting the balance between viral clearance by the immune system and viral replication in favor of the immune system. For the ease of notation, we will subsequently only refer to the active (tri-phosphorylated) nucleoside analog moiety.

Inhibition of DNA polymerization by **NA**s is not restricted to viral polymerase, but can also affect cellular polymerases, leading to unwanted side-effects [8,9]. The therapeutic window of **NA**s largely depends on molecular kinetic properties of the respective enzymes with regard to a particular inhibitor [10,11]. **NA**s therefore require high specificity for the targeted viral enzyme to allow for a clinical benefit. Viral resistance development can revert

Author Summary

Nucleoside analogs (**NA**s) represent an important drug class for the treatment of viral infections and cancer. They inhibit DNA/RNA polymerization after being incorporated into nascent DNA/RNA, which prevents primer extension. Viruses are particularly versatile and frequently develop mutations enabling them to avert the effects of **NA**s. The mechanisms of resistance development are, however, still poorly understood. Through mathematical modeling, we assess the mechanisms by which HIV-1 can develop resistance against nucleoside analog reverse transcriptase inhibitors (NRTI). We quantify the effects of treatment and estimate the fitness of drug resistant mutants. We correctly predict that HIV-1 can develop resistance by decreasing NRTI incorporation rate, increasing its excision rate, or decreasing its affinity for the viral polymerase enzyme. Our model also allows quantification of the cell specific factors affecting NRTI efficacy. Resistance development also changes drug susceptibility distinctly and we show, for the first time, that selection of drug resistance can occur in particular target cells. This finding could provide an explanation of how *clinically* observed resistant viral mutants may arise. It also pin-points important parameters that may impact clinical efficacy of **NA**s used to treat other viruses.

this specificity by changing the kinetic properties of the viral enzyme [12,13]. While a number of enzymatic studies have revealed crucial insights into the mechanisms of polymerase inhibition by **NA**s and the kinetic consequences of resistance development, an integrated mathematical insight into these mechanisms has rarely been achieved. In this study, we aim to mathematically formulate a model of polymerase inhibition by **NA**s, by integrating available enzymatic knowledge. The derived mathematical model should subsequently allow us to assess the impact of distinct cellular- and molecular determinants of **NA** inhibition and to achieve a greater understanding of viral resistance development and epistatic interactions. Results will be exemplified for inhibition of DNA polymerization during reverse transcription (RT) of HIV-1 by nucleoside analog reverse transcriptase inhibitors (NRTIs).

Initial mathematical modelling efforts in the context of RT inhibition by NRTIs of HIV-1 were based on the assumption that incorporation of chain-terminating nucleoside analogs is permanent [14]. The effect of NRTIs was therefore solely explained by their incorporation probability. In subsequent years after the introduction of ziduvudine (AZT; the first NRTI against HIV-1), resistant strains were detected which displayed increased removal kinetics of AZT from terminated primers [15–17], rather than discriminating between the natural nucleotide and AZT [18]. This indicated that nucleoside analog removal is very significant and constitutes a major resistance pathway against thymidine analogs (like AZT) and many other NRTIs [13]. The particular mechanism of resistance to AZT indicated that chain termination by nucleoside analogs may not be permanent. Hence, a distinct view on polymerase inhibition by NRTIs is necessary, which departs from the assumption of permanent chain termination. Subsequent modeling work [19] used lumped kinetic expressions and Monte-Carlo simulations instead of deriving analytical expressions, which precludes the identification of key molecular determinants of efficacy and drug resistance. Both previous mathematical modeling efforts were not able to compute the fitness loss associated with mutations in the RT enzyme, an important determinant in clinical settings and for studying epistatic interactions [20–23].

In this work, we present a distinct view of viral polymerase inhibition by NRTIs, which departs from the assumption of permanent chain termination. We propose that NRTIs delay the process of DNA polymerization, rather than permanently terminating it, simultaneously keeping in mind that any delay of the process decreases the number of viral progeny and the likelihood of target cell infection by the virus. The developed mathematical formulation allows us to study viral polymerase inhibition by NRTIs as well as fitness effects related to drug resistance development. By integrating fitness effects and drug susceptibility, it is further possible to quantify the selective pressure exerted by NRTIs and to study epistasis. The derived analytical expressions can be used to study the effects of single- and multiple NRTIs on DNA polymerization in the absence and presence of resistance mutations and can be useful for drug design. Chain termination by **NA**s may also be reversible in other viruses [24–26], against which **NA**s are being developed. Hence, the model may also be applicable to study **NA** inhibition of these viruses.

Results

Mechanism of action of nucleoside analogs on DNA polymerization

A schematic view of the process of viral DNA polymerization in the presence of **NA**s is illustrated in Fig. 1. We interpret the process of DNA polymerization as a Markov jump process with $2{\cdot}N-1$ states (Fig. 1A), where each state in the model corresponds to the number of incorporated nucleosides: state '0' corresponds to the initiation of polymerization, states $i=1...N$ in the model correspond to the condition in which i nucleosides have been attached and state $'N'$ corresponds to the final polymerization product. States $\tilde{i}$ correspond to the condition, in which the DNA-chain consists of $i-1$ natural nucleosides, but where the last (ith) molecule in the chain is a chain-terminating nucleoside analog.

At each state i, the nascent DNA-chain can either be shortened (pyrophosphorolysis reaction r_{pyro}), -prolonged with a nucleoside (polymerase reaction r_{pol}) or -terminated by a nucleoside analog (reaction r_{term}). If the chain has been terminated (state $\widetilde{i+1}$), it can get released with rate r_{exc} (excision reaction) to produce a chain of length i. The kinetics of these reactions will be detailed later.

Taking into account the mode of action of chain terminating nucleoside analogs, we conclude that polymerization will be decelerated in the presence of these inhibitors, because the overall time required to go from state '0' (initiation of polymerization) to state $'N'$ (final polymerization product) in Fig. 1 will be prolonged in their presence by introducing 'waiting states' $\tilde{i}$. The residual polymerase activity of the wildtype enzyme in the presence of activated (tri-phosphorylated) nucleoside analogs $(1-\varepsilon(\text{NA},\text{wt}))$ can thus be expressed as:

$$1-\varepsilon(\text{NA},\text{wt})=\frac{T_{0\to N}(\phi,\text{wt})}{T_{0\to N}(\text{NA},\text{wt})} \qquad \text{(inhibition of wildtype)}, \quad (1)$$

where $T_{0\to N}(\phi,\text{wt})$ and $T_{0\to N}(\text{NA},\text{wt})$ denote the expected time to finalize DNA polymerization in the wildtype $'\text{wt}'$ in the absence of drugs $'\phi'$ and in the presence of active nucleoside analogs **NA** respectively.

Analogously, we can define the effect of chain terminating nucleoside analogs on some viral mutant, $1-\varepsilon(\text{NA},\text{mut})$ and the fitness loss associated with some mutant in the absence of treatment ϕ, $f(\text{mut})$:

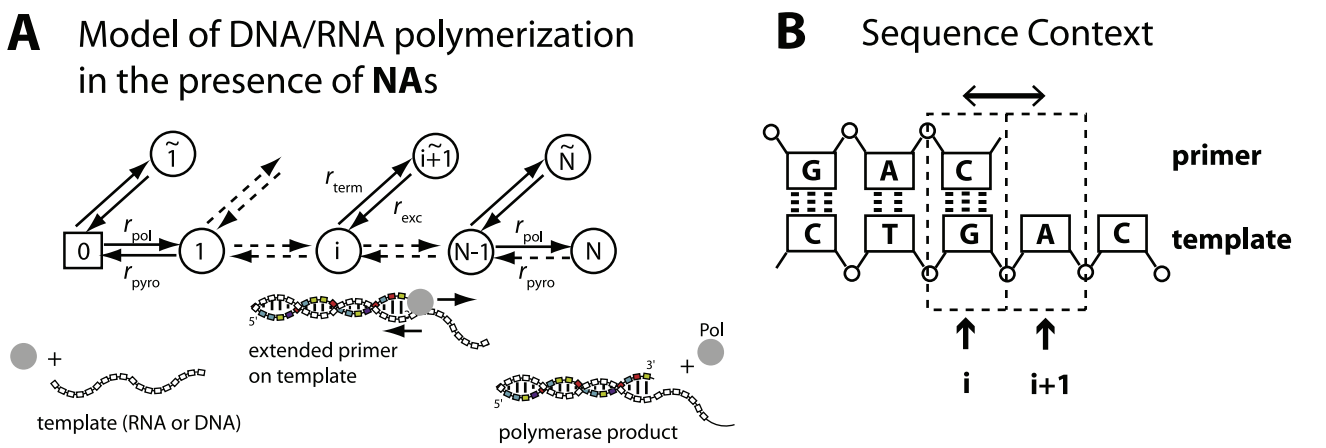

Figure 1. DNA-polymerization in the presence of chain terminating nucleoside analogs. A: The mathematical model defines a Markov jump process: Each state in the model corresponds to the number of incorporated nucleotides: state '0' corresponds to the polymerase enzyme binding to the template, prior to polymerization, states $i=1...N$ in the model correspond to the condition in which i nucleosides have been attached and state $'N'$ corresponds to full-length product, after which the enzyme dissociates from the template/primer. States $\widetilde{i+1}$ correspond to the condition, in which a DNA-chain consisting of i natural nucleosides has been produced, but where the last $(i+1\text{th})$ nucleoside in the chain is a chain-terminating **NA**. At each state i, the nascent DNA-chain can either be shortened (pyrophosphorolysis r_{pyro}), -prolonged with a nucleoside (polymerase reaction r_{pol}) or -terminated by a nucleoside analog (reaction r_{term}). If the chain has been terminated (state $\widetilde{i+1}$), it can get released with rate r_{exc} (excision reaction) to produce a chain of length i. B: Sequence context. The reaction rates r_{pol}, r_{pyro}, r_{term} and r_{exc} depend on the nucleoside sequence of the template. In the illustration, the next incoming nucleoside could be either a thymidine or a thymidine-analog (corresponding to position $i+1$ in the template sequence). Therefore, $r_{\text{pol}}(i+1)$ and $r_{\text{term}}(i+1)$ would refer to thymidine- and thymidine-analog incorporation. The pyrophosphorolysis reaction, on the other hand, would refer to cytosine removal (position i in the primer sequence).
doi:10.1371/journal.pcbi.1002359.g001

$$1-\varepsilon(\text{NA},\text{mut})=\frac{T_{0\to N}(\phi,\text{mut})}{T_{0\to N}(\text{NA},\text{mut})}\qquad(\text{inhibition of mutant})\quad(2)$$

$$f(\text{mut})=\frac{T_{0\to N}(\phi,\text{wt})}{T_{0\to N}(\phi,\text{mut})}\qquad(\text{fitness of mutant}).\qquad(3)$$

These constituents can be seen as building blocks for describing the fitness landscape of any arbitrary viral mutant 'mut' in the absence- and presence of inhibitors, see e.g. [7,27].

Based on the definitions above, we can also assess the combined effects of selection and drug pressure for any viral strain, i.e. $f(\text{mut})\cdot(1-\varepsilon(\text{NA},\text{mut}))$. This allows us to assess the selective advantage $S_{\text{mut/wt}}(\text{NA})$ of a mutant viral strain over the wild type in an environment that is pharmacologically modified by **NA**s.

$$\begin{aligned}S_{\text{mut/wt}}(\text{NA})&=\frac{f(\text{mut})\cdot(1-\varepsilon(\text{NA},\text{mut}))}{(1-\varepsilon(\text{NA},\text{wt}))}\\&=\frac{T_{0\to N}(\text{NA},\text{wt})}{T_{0\to N}(\text{NA},\text{mut})}\qquad(\text{selective advantage})\end{aligned}\qquad(4)$$

This parameter integrates the (usually opposed) effects of mutations on resistance and viral fitness. If $S_{\text{mut/wt}}(\text{NA})<1$, the wild type virus is selected over the mutant strain, whereas $S_{\text{mut/wt}}(\text{NA})>1$ indicates selection of a mutant virus over the wild type. Since $S_{\text{mut/wt}}(\text{NA})$ depends on the concentration of **NA**s, a critical concentration of nucleoside analog $\text{NA}^*(\text{mut})$ can exist, above which the selection of a particular viral strain over the wild type is favored. $S_{\text{mut1/mut2}}(\text{NA})=\frac{T_{0\to N}(\text{NA},\text{mut2})}{T_{0\to N}(\text{NA},\text{mut1})}$ can also be used to assess selection between two arbitrary mutant strains mut1 and mut1 in a pharmacologically modified environment.

Finally, we can assess epistatic interactions for combinations of mutations with regard to viral replication. Briefly, in a two-locus-two-allele model, epistasis is positive if some double mutant m12 replicates better than expected from the single mutants m1 and m2, normalized by the replication of the wild type wt (background). Epistasis is negative if the replication of the double mutant is less than expected from the single mutants. Along the same lines, epistasis has been used to study interactions of mutations in the absence of drugs [22] and for escalating drug concentrations [23]. Using the definitions above, in the presence of **NA**s, we derive:

$$\begin{aligned}E_{\text{Rep.}}(\text{NA})&=\log((1-\varepsilon(\text{NA},\text{mut12})\cdot f(\text{mut12})\cdot(1-\varepsilon(\text{NA},\text{wt}))\cdot f(\text{wt}))\\&-\log((1-\varepsilon(\text{NA},\text{mut1}))\cdot f(\text{mut1})\cdot(1-\varepsilon(\text{NA},\text{mut2}))\cdot f(\text{mut2})).\end{aligned}\qquad(5)$$

The equation above becomes positive if the first term is greater that the second, i.e. the double mutant replicates better than expected from the single mutants, in agreement with the definition of epistasis [22,23]. The epistasis term $E_{\text{Rep.}}(\text{NA})$ defined above regards both fitness effects and drug resistance. In the absence of drugs, $(1-\varepsilon)=1$, see eqs. (1)–(2) above, we get the fitness epistasis:

$$\begin{aligned}E_f(\phi)&=\log(f(\text{mut12})\cdot f(\text{wt}))-\log(\cdot f(\text{mut1})\\&\cdot f(\text{mut2}))\qquad(\text{fitness epistasis})\end{aligned}\qquad(6)$$

It is also possible to only analyze epistatic effects on resistance:

$$\begin{aligned}E_{\text{Res.}}(\text{NA})&=\log((1-\varepsilon(\text{NA},\text{mut12})\cdot(1-\varepsilon(\text{NA},\text{wt})))\\&-\log((1-\varepsilon(\text{NA},\text{mut1}))\cdot(1-\varepsilon(\text{NA},\text{mut2})))\\&(\text{resistance epistasis}).\end{aligned}\qquad(7)$$

Note, that the defined terms are additive, i.e. $E_{\text{Rep.}}(\text{NA})=E_f(\phi)+E_{\text{Res.}}(\text{NA})$.

Polymerization of Hetero-Polymeric sequences

The process of DNA polymerization (Fig. 1) defines a birth-death process. We are interested in the derivation of an explicit formula for the *mean first passage time* $T_{0\to N}$ (the average time required to finalize DNA polymerization). Let $T_{i\to i+1}$ denote the expected time required to extend the DNA-chain by one nucleoside (going from state i to state $i+1$, derivation see eq (22)–(28); Methods section)

$$T_{i\to i+1}=(\tau_{\widetilde{i+1}}\cdot\rho_{i\to\widetilde{i+1}}+\tau_i+\rho_{i\to i-1}T_{i-1\to i})\frac{1}{\rho_{i\to i+1}}. \quad (8)$$

where $\tau_i,\tau_{\widetilde{i+1}}$ are the waiting times in states i and $\widetilde{i+1}$ respectively and $\rho_{i\to i+1},\rho_{i\to i-1}$ are the probabilities to jump from state i to state $i+1$ and to state $i-1$ respectively. The parameter $\rho_{i\to\widetilde{i+1}}$ denotes the probability that the chain of length i gets terminated by incorporation of a nucleoside analog (state $\widetilde{i+1}$). The waiting times τ and jump-probabilities ρ are defined as follows:

$$\tau_i=\frac{1}{r_{\mathrm{pol}}(i+1)+r_{\mathrm{pyro}}(i)+r_{\mathrm{term}}(i+1)},\quad \tau_{\widetilde{i+1}}=\frac{1}{r_{\mathrm{exc}}(i+1)},$$
$$\rho_{i\to i+1}=r_{\mathrm{pol}}(i+1)\cdot\tau_i,\quad \rho_{i\to i-1}=r_{\mathrm{pyro}}(i)\cdot\tau_i,\quad \rho_{i\to\widetilde{i+1}}=r_{\mathrm{term}}(i+1)\cdot\tau_i, \quad (9)$$

where $r_{\mathrm{pol}}(i+1)$ and $r_{\mathrm{term}}(i+1)$ denote the polymerase- and chain terminating reactions (attachment of the next incoming nucleoside or its analog), which depend on the efficacy of incorporation of the respective types of nucleosides (deoxyadenosine, -thymidine, -guanine or -cytosine triphosphate) or their respective analogs at position $i+1$ in the primer, see Fig. 1B. The parameter $r_{\mathrm{exc}}(i+1)$ denotes the rate of release (excision reaction) of a primer that has been terminated at position $i+1$ by **NA**. The parameter $r_{\mathrm{pyro}}(i)$ denotes the pyrophosphorolysis reaction, i.e. the rate at which a nucleoside is removed from the end of the primer. Note, that τ and ρ depend on the sequence context because the rates of nucleoside attachment and -removal depend on the types of nucleosides (and -analogs) to be incorporated and -removed respectively (see e.g. Fig. 1B). Eq. (8) allows us to calculate the time to finalize polymerization recursively, using the relation:

$$T_{0\to N}=\sum_{i=0}^{N-1}T_{i\to i+1}. \quad (10)$$

If $i=0$ corresponds to the unextended primer, we have $r_{\mathrm{pyro}}(0)=0$ in eq. (9) and therefore eq. (8) simplifies to

$$T_{0\to 1}=(\tau_{\widetilde{1}}\cdot\rho_{0\to\widetilde{1}}+\tau_0)\frac{1}{\rho_{0\to 1}}, \quad (11)$$

with $\tau_0=\frac{1}{r_{\mathrm{pol}}(1)+r_{\mathrm{term}}(1)},\tau_{\widetilde{1}}=\frac{1}{r_{\mathrm{exc}}(1)}$ and $\rho_{0\to 1}=r_{\mathrm{pol}}(1)\cdot\tau_0$, $\rho_{0\to\widetilde{1}}=r_{\mathrm{term}}(1)\cdot\tau_0$, which can be used as a recursion start to compute the polymerization time.

In the case where no chain-terminating inhibitor is applied, we have $r_{\mathrm{term}}(i)=0$ for all i in eq. (9) and therefore eq. (8), and eqs. (10)–(11) simplify accordingly.

Eq. (8)–(10) can subsequently be used to estimate the residual polymerase activity in the presence of **NAs** in the wild type and any mutant enzyme, using eq. (1) and eq. (2) respectively, to estimate the fitness of some mutant with regard to polymerization, using eq. (3), or to estimate the selective advantage of a viral strain against a competitor, using eq. (4). This will be exemplified in the next section.

Sequence dependent DNA-polymerization in the presence of NAs. Using eq. (10), it is possible to compute the average polymerization time ($T_{0\to i}$) in the absence- and presence of **NAs** for any arbitrary sequence to be polymerized. In this section, we motivate the use of this approach and show how key phenotypic characteristics can be derived from this simple mathematical model.

NAs compete with the natural nucleoside substrates for the same binding site on the polymerase enzyme. We therefore take into account competitive inhibition for the kinetics of nucleoside- and nucleoside analog incorporation.

$$r_{\mathrm{term}}=\frac{k_{\mathrm{term}}\cdot[\mathrm{NA}]}{K_{\mathrm{D,NA}}\left(1+\frac{[\mathrm{dNTP}]}{K_{\mathrm{D,dNTP}}}\right)+[\mathrm{NA}]} \quad (12)$$

$$r_{\mathrm{pol}}=\frac{k_{\mathrm{pol}}\cdot[\mathrm{dNTP}]}{K_{\mathrm{D,dNTP}}\left(1+\frac{[\mathrm{NA}]}{K_{\mathrm{D,NA}}}\right)+[\mathrm{dNTP}]} \quad (13)$$

where [dNTP] is the concentration of the deoxynucleoside triphosphates (adenosine-, thymidine-, cytidine- and guanosine-) of which the **NA** is an analog of. The variable [NA] denotes the concentrations of activated (tri-phosphorylated) nucleoside analog that competes with its natural nucleoside counterpart for incorporation into the nascent viral DNA. The parameters k_{term} and k_{pol} denote the catalytic rate constants for incorporation of the **NA** and the dNTP respectively. $K_{\mathrm{D,NA}}$ and $K_{\mathrm{D,dNTP}}$ denote the dissociation constants for **NA** and **dNTP** binding to the polymerase respectively. In the absence of inhibitors ϕ, we have [NA] = 0 and therefore eq. (13) and eq. (12) simplify accordingly:

$$r_{\mathrm{pol}}(\phi)=\frac{k_{\mathrm{pol}}\cdot[\mathrm{dNTP}]}{K_{\mathrm{D,dNTP}}+[\mathrm{dNTP}]}, \quad (14)$$

$$r_{\mathrm{term}}(\phi)=0. \quad (15)$$

Physiological dNTP concentrations for the most important target cell types of HIV-1 are indicated in Table 1. Parameters for natural nucleoside DNA- and RNA- dependent polymerization by wild type HIV-1 reverse transcriptase (RT) are indicated in Table S1 (supplementary material). In the forthcoming example, we will analyze the effect of a chain-terminating adenosine analog (ddATP, the active metabolite of didanosine, ddI) at a fixed concentration on both single nucleotide incorporation $T_{i\to i+1}$ (see eq. (8)) and on cumulative nucleoside polymerization $T_{0\to i}$ (see eq. (10)) for physiological dNTP concentrations in resting $CD4^+$ T-cells (Table 1). Furthermore, we will assess how polymerization is impaired by the (clinically relevant) 'K65R' mutation in reverse transcriptase in the absence- and presence of ddATP.

In Fig. 2 we have computed the average polymerization time for a short sequence (indicated on the x-axis in Fig. 2) and typical parameters for DNA-dependent polymerization for HIV-1 RT, see Table 1 and Table S1 (supplementary material). In this example, we have assumed that $r_{\mathrm{pyro}}=r_{\mathrm{exc}}=0.0016s^{-1}$ [17] for all dNTP and for ddATP respectively. We examine polymerization in the absence- or the presence of $1.45\mu\mathrm{M}$ intracellular ddATP. The solid black line denotes the polymerization time in

Table 1. Physiological dNTP levels in different cell types.

	activated $CD4^+$ -cells	resting $CD4^+$ -cells	macrophages	ref.
dATP	5.1	1.7	0.023	[34]
dTTP	7.9	1.5	0.019	[34]
dCTP	5.9	1.9	0.03	[34]
dGTP	4.5	1.7	0.032	[34]
PPi	79	8	7	[35]
ATP	1400	2200	1600	[35]

All values are expressed in μM.
doi:10.1371/journal.pcbi.1002359.t001

the wild type RT in the absence of ddATP, whereas the blue dashed- and the red dotted lines indicate the polymerization time in the presence of ddATP in the wild type and drug-resistant mutant enzyme (bearing the 'K65R' mutation) respectively. The fold changes in the kinetic parameters, induced by the 'K65R' mutation, are stated in Table S2 (supplementary material). In the wild type enzyme the predicted incorporation probability $\rho_{i\to i+1}$ for ddATP over dATP is 9.4% in the presence of 1.45μM ddATP. For the 'K65R' mutant $\rho_{i\to i+1}$ it is 3.2%. In Fig. 2A one can see the cumulative time to form the polymerization product $T_{0\to i}$. In the presence of ddATP, the cumulative polymerization time is substantially increased (dashed blue line), which is partly compensated in the drug resistant enzyme bearing the 'K65R' mutation (dotted red line). In Fig. 2B we show the single nucleoside polymerization time $T_{i\to i+1}$. It can be seen, that in the presence of ddATP the single nucleoside polymerization time $T_{i\to i+1}$ is substantially elevated, in relation to the wild type, whenever the respective natural nucleoside (here adenosine) needs to be incorporated (the solid black line vs. the dashed blue line). In the 'K65R' mutant (red dotted line), this is partially compensated for. However, in the mutant, the single nucleoside polymerization time $T_{i\to i+1}$ for incorporation of other nucleosides is also increased, which indicates, that the 'K65R' mutant might decrease the fitness of the enzyme. We have calculated the fitness of the mutant enzyme, the residual polymerase activity in the wild type enzyme -and the 'K65R' mutant and the selective advantage of the 'K65R' mutant over the wild type for the presented example, using eqs (1)–(4). The derived values are stated in Table 2. It can be seen that the 'K65R' mutant decreases ddATP inhibition of DNA dependent polymerization substantially (the residual polymerization is increased from 3.3% to 22.3%). However, the predicted fitness of the enzyme (in terms of DNA-dependent polymerization) is reduced to 37.9%. The predicted selective advantage of the 'K65R' mutant is 2.55, indicating that the 'K65R' resistance would be selected over the wild type in the presence of 1.45μM ddATP.

Note, that in this section, we have exemplified the effects of a particular **NA** on polymerization, given a specific concentration of the respective **NA** and certain kinetic attributes of the polymerase enzyme (wild type RT vs. 'K65R' mutant RT). In the next sections, we will assess the general impact of certain resistance mechanisms, by analyzing a range of kinetic parameters and we will also study the efficacy of **NA**s for different concentration ranges.

Molecular determinants of inhibition

While in a hetero-polymeric sequence context, polymerase inhibition by **NA**s depends on the *particular* succession of the

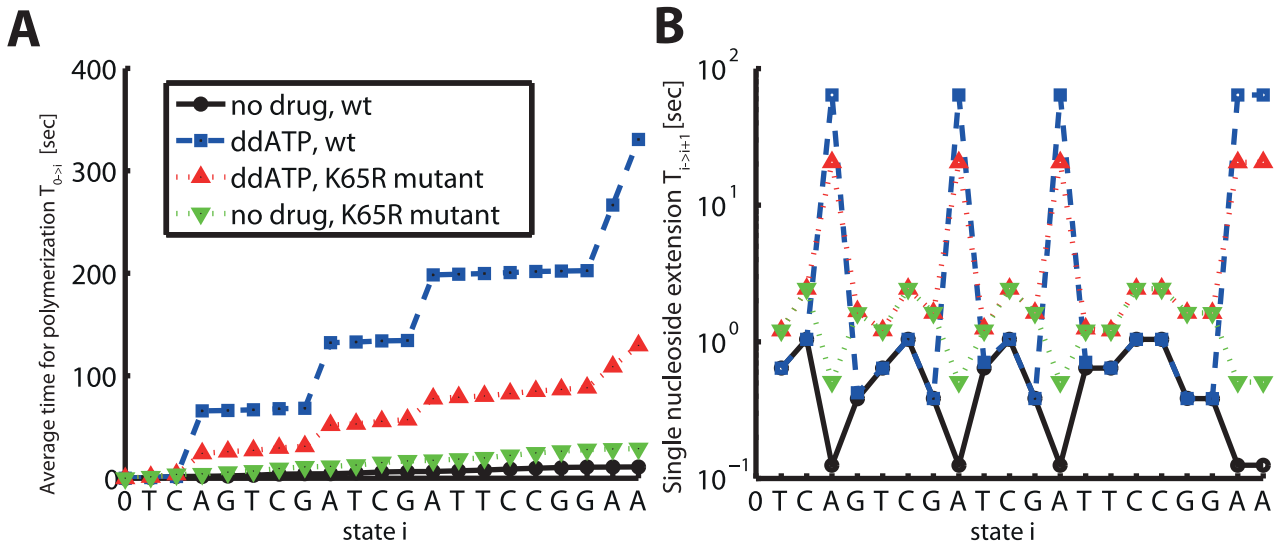

Figure 2. DNA-dependent polymerization of a hetero-polymeric sequence by HIV-1 RT in the presence- and absence of a chain terminating adenosine analog (ddATP). A: Cumulative time for polymerization of a hetero-polymeric sequence in the presence of a chain-terminating nucleoside analog (ddATP). The solid black line (filled dots) indicates the cumulative polymerization time up to sequence position i (the sequence position is indicated at the x-axis) in the absence of inhibitors in the wild type enzyme (calculated using eq. (10)). The dashed blue line (open squares) indicates the time required for polymerization in the presence of 1.45μM ddATP. The dotted red- and green lines (upward and downward pointing triangles) show the time required for polymerization in the 'K65R' mutant RT enzyme in the presence- and absence of 1.45μM ddATP. Kinetic parameters are presented in Table 1 and Table S1, S2 (supplementary material) for the wild type and the 'K65R' mutant. B: Single nucleoside incorporation time $T_{i\to i+1}$ in the absence of ddATP in the wildtype and the 'K65R' mutant (solid black and dashed green lines respectively) and in the presence of ddATP in the wild type enzyme (dashed blue line) and in the mutant enzyme (dotted red line), calculated using equation eq. (8).
doi:10.1371/journal.pcbi.1002359.g002

Table 2. Efficacy & fitness.

$1-\varepsilon$(ddATP,wt)	3.31%
$1-\varepsilon$(ddATP,'K65R')	22.3%
f('K65R')	37.9%
$S_{\mathrm{K65R/wt}}$(ddATP)	2.55

Residual DNA-dependent polymerase activity ($1-\varepsilon$) of HIV's RT in resting $CD4^+$ T-cells in the presence of 1.45μM ddATP and fitness (f) and selective advantage $S_{\mathrm{K65R/wt}}$ with regard to DNA polymerization for the 'K65R' mutant. Calculations are based on formulas (1)–(4).

doi:10.1371/journal.pcbi.1002359.t002

nucleosides, see e.g. Fig. 2B, this is not the case for homo-polymeric sequences, which consist of only one type of nucleoside, e.g. poly-adenosine; 'Poly-A'. This allows us to derive a general, analytical expression for polymerase inhibition by **NA**s, which is valid for *any* homo-polymeric sequence. We will make use of this fact to highlight key determinants of inhibition. For assessing the impact of nucleoside analogs in a *particular* hetero-polymeric sequence context, we advice to use eqs. (8)–(11). In a homo-polymeric sequence, we have $r_{\mathrm{pol}}(i)\equiv r_{\mathrm{pol}}, r_{\mathrm{pyro}}(i)\equiv r_{\mathrm{pyro}}$, $r_{\mathrm{term}}(i)\equiv r_{\mathrm{term}}$ and $r_{\mathrm{exc}}(i)\equiv r_{\mathrm{exc}}$ for all i. In this particular case, the explicit solution for the *mean first passage time* $T_{0\to N}$ reads (see eq. (31)–(32); Methods section)

$$T_{0\to N}(\mathrm{NA})=\left(\frac{r_{\mathrm{term}}+r_{\mathrm{exc}}}{r_{\mathrm{exc}}}\right)\frac{(r_{\mathrm{pol}}+r_{\mathrm{pyro}})^{N-1}+r_{\mathrm{pol}}^{N-1}\cdot(N-1)}{r_{\mathrm{pol}}^{N}}. \quad (16)$$

When no inhibitor is present (ϕ), we have $r_{\mathrm{term}}=0$ and thus eq. (16) simplifies accordingly:

$$T_{0\to N}(\phi)=\frac{(r_{\mathrm{pol}}(\phi)+r_{\mathrm{pyro}})^{N-1}+r_{\mathrm{pol}}(\phi)^{N-1}\cdot(N-1)}{r_{\mathrm{pol}}(\phi)^{N}}, \quad (17)$$

where r_{pol} and $r_{\mathrm{pol}}(\phi)$ are the polymerization rates in the presence- and absence (ϕ) of a competing **NA**, given in eq. (13) and eq. (14). Recalling the effect of **NA**s on polymerization, see eq. (1), we can derive the **residual polymerase activity** during **NA** treatment on a **homo-polymeric sequence**, $(1-\eta)=\dfrac{T_{0\to N}(\phi)}{T_{0\to N}(\mathrm{NA})}$:

$$(1-\eta)=\frac{r_{\mathrm{exc}}}{r_{\mathrm{term}}+r_{\mathrm{exc}}}\frac{r_{\mathrm{pol}}^{N}}{r_{\mathrm{pol}}(\phi)^{N}}\left(\frac{(r_{\mathrm{pol}}(\phi)+r_{\mathrm{pyro}})^{N-1}+r_{\mathrm{pol}}(\phi)^{N-1}\cdot(N-1)}{(r_{\mathrm{pol}}+r_{\mathrm{pyro}})^{N-1}+r_{\mathrm{pol}}^{N-1}\cdot(N-1)}\right) \quad (18)$$

The above expression simplifies further, if the pyrophosphorolysis reaction is very inefficient relative to polymerization, which is the case for most viral polymerase enzymes; e.g. $r_{\mathrm{pyro}}\ll r_{\mathrm{pol}}\le r_{\mathrm{pol}}(\phi)$.

$$(1-\eta)\approx\frac{r_{\mathrm{exc}}}{\underbrace{r_{\mathrm{term}}+r_{\mathrm{exc}}}_{\text{incorporation \& termination}}}\cdot\frac{r_{\mathrm{pol}}}{\underbrace{r_{\mathrm{pol}}(\phi)}_{\text{binding competition}}} \quad (19)$$

Eq. (19) highlights the two distinct mechanisms by which inhibition can be conferred, namely a) inhibitor incorporation (and subsequent quasi-termination of the polymerization reaction) and b) competition for binding with natural nucleoside substrates. The efficacy of quasi-termination of the nascent DNA chain depends on the efficacy of inhibitor incorporation r_{term} and the duration of the chain termination, determined by r_{exc}. Binding competition is solely determined by the fractional decrease of the natural polymerization reaction (relative to the absence of inhibitor), see eq. (13).

After substituting the enzymatic rate expressions eqs. (12)–(14) into equation (19), we can solve for the fifty percent inhibitory concentration $\mathbf{IC_{50}}$ (see eqs. (33)–(35); Methods section), which refers to polymerase inhibition in a homo-polymeric sequence (e.g. 'Poly-A') and to the intracellular concentration of activated (triphosphorylated) **NA**.

$$\mathrm{IC}_{50}\approx\frac{r_{\mathrm{exc}}}{k_{\mathrm{term}}+r_{\mathrm{exc}}}\cdot K_{\mathrm{D,NA}}\left(1+\frac{[\mathrm{dNTP}]}{K_{\mathrm{D,dNTP}}}\right) \quad (20)$$

The above equation highlights the processes, which determine the efficacy of a chain-terminating nucleoside analog, namely the kinetic constants k_{term},$K_{\mathrm{D,NA}}$ and $K_{\mathrm{D,dNTP}}$, the concentration of natural nucleoside [dNTP] and the excision rate of the inhibitor r_{exc}.

Cell-specific susceptibility to chain-terminating nucleoside analogs. Viruses can infect numerous activated- and resting cells. HIV-1, for example, has been shown to infect activated- and resting $CD4^+$ T-cells, macrophages, dendric cells, natural killer cells and microglial cells [28–32], and possibly many more. It is important to understand- and take into account heterogeneous- or cell specific drug efficacy, as it may be a primary source of residual viral replication and subsequent resistance development during treatment [33].

In the context of nucleoside analog efficacy, the major cell-specific factors (apart from pharmacokinetics), are cell type-, or cell stage specific dNTP pools (see Table 1) and possibly cell specific rates of excision r_{exc}. In Fig. 3A, we predicted the impact of cell-specific [dNTP] contents on DNA-dependent polymerization during HIV-1 reverse transcription in the presence of ddATP, using typical kinetic parameters (see Table S1, supplementary material).

Under the parameters used, a 100 fold increase in dNTP concentrations would result in a 19 fold increase in the $\mathbf{IC_{50}}$ value ($2.8\cdot10^{-3}$ vs. $5.3\cdot10^{-2}$μM), whereas a 100-fold decrease in the dNTP concentrations would only result in a 1.2 fold reduction in the $\mathbf{IC_{50}}$ value. This is an important observation, because it indicates that cells that contain high concentrations of dNTP can confer natural resistance against NRTIs, whereas cells with low dNTP content, like macrophages [34], do not necessarily confer hypersusceptibility to NRTIs. This phenomenon can be explained from eq. (20): The $\mathbf{IC_{50}}$ value does not decrease, if $[\mathrm{dNTP}]\ll K_{\mathrm{D,dNTP}}$.

Resting cells on the other hand might insufficiently phosphorylate NRTIs and subsequently contain lower levels of activated compound. However, these cells do not simultaneously require smaller NRTI concentrations for inhibition ($\mathbf{IC_{50}}$ value in Fig. 3A does not decrease with decreasing dNTP levels). Therefore, resting cells could constitute reservoirs for residual replication during antiviral treatment, if NRTI phosphorylation/activation is affected.

Excision of nucleoside reverse transcriptase inhibitors (NRTIs) of HIV-1 from terminated primers has been shown to be mediated by pyrophosphate (PPi) and ATP dependent mechanisms [35]. Whereas ATP concentrations are fairly similar in activated- and resting lymphocytes, as well as macrophages and monocytes [34–38] (1 to 5 mM), PPi levels have been shown to vary substantially

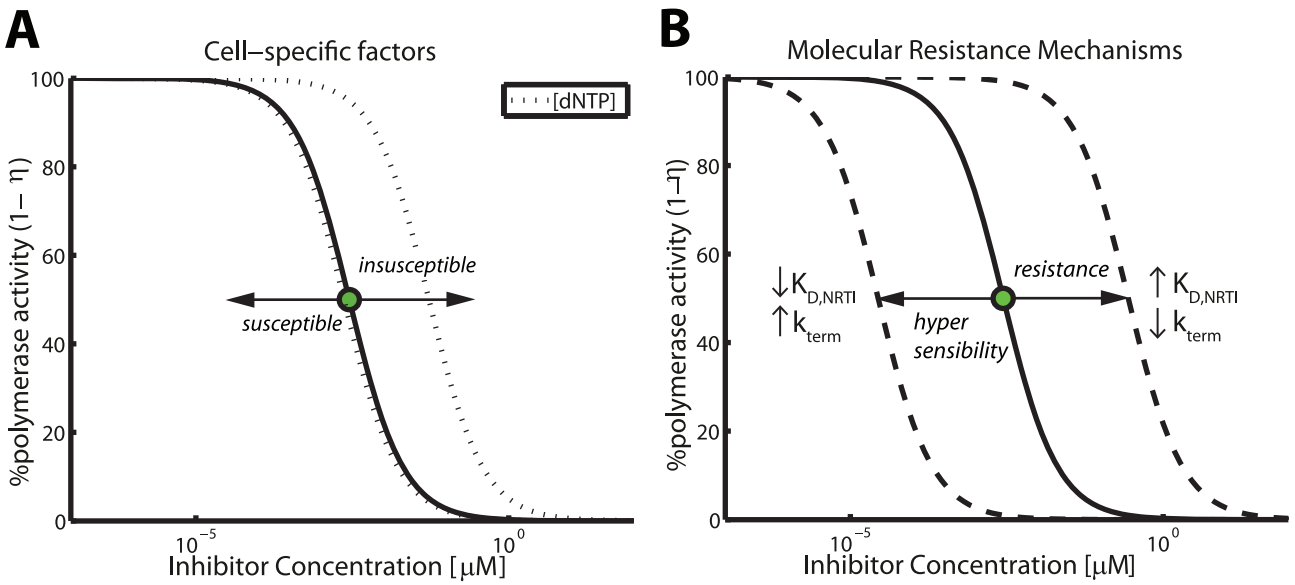

Figure 3. Factors that modify inhibition of DNA polymerization by nucleoside analogs. A: Cell-specific factors: Concentration response curve of ddATP for wild type RT during DNA-dependent polymerization (homo-polymeric sequence) in unstimulated $CD4^+$ T-cells (solid line) and the impact of a 100-fold variation of the the intracellular nucleoside concentrations (dotted line). The illustration was generated by evaluating eq. (19) and typical parameters for DNA-dependent polymerization during HIV-1 reverse transcription and its inhibition by ddATP (all parameters are indicated in Table 1 and Table S1, supplementary material). The corresponding IC_{50} is depicted by a green filled circle. B: Molecular mechanisms of drug resistance and hyper-susceptibility (dashed lines). Impact of (i) selective attrition of inhibitor incorporation ($\downarrow k_{term}$) and (ii) selective attrition of inhibitor binding to the primer-template ($\uparrow K_{D,NA}$) on drug susceptibility. Hypersusceptibility is conferred by the opposite change in the indicated parameters. In order to generate the dashed lines, the respective parameters have been increased/decreased by a factor of 100.
doi:10.1371/journal.pcbi.1002359.g003

[35] $(8-80\mu M)$, see also Table 1. This indicates that IC_{50} values for polymerase inhibition by **NAs** might be cell-specific and may in some cells lead to incomplete suppression. Here, we did not analyze the effect of cell-specific PPi and ATP contents, as the kinetic parameters were not readily available for ddATP. We however discuss their impact on polymerase inhibition by zidovudine (AZT) in a subsequent section.

Molecular mechanisms of viral drug resistance against chain-terminating nucleoside analogs. The enzymatic properties of a viral polymerase can be adapted in an evolutionary process to counteract inhibition by **NAs**. Eq. (20) indicates that the following three distinct molecular mechanisms are likely to induce selective resistance against chain-terminating **NAs**, and indeed these three mechanisms of resistance have been described for HIV-1 RT [13].

- selective attrition of inhibitor incorporation ($\downarrow k_{term}$)
- selective attrition of inhibitor binding to the primer-template ($\uparrow K_{D,NA}$)
- enhanced excision of the **NA** from the terminated primer ($\uparrow r_{exc}$, by e.g. increasing the catalytic efficacy of removal or by increasing phosphate-donor, e.g. PPi- or ATP- binding).

The consequences of mutational modification of inhibitor incorporation (k_{term}) and -binding ($K_{D,NA}$) with regard to the predicted efficacy of ddATP are illustrated in Fig. 3B, where we have used typical parameters for DNA-dependent polymerization during HIV-1 reverse transcription (see Table S1, supplementary material). Under the utilized parameters a 100-fold change in the respective parameter k_{term} or $K_{D,NRTI}$ leads to a 100-fold change in the compounds IC_{50} value. We did not analyze the effect of enhanced **NA** excision in Fig. 3B, as the kinetic parameters were not readily available for ddATP. These effects will be discussed in the context of polymerase inhibition by zidovudine (AZT) in the next section.

Mechanism of zidovudine (AZT) resistance by thymidine analog mutations (TAMs)

It has been argued [17], that the main mechanism of AZT resistance is due to increased excision of AZT-MP from the terminated primer. In particular, this process has been shown to be both pyrophosphate- (PPi) and ATP- dependent *in vivo* [35]. For the rate of excision r_{exc} we can therefore write

$$r_{exc} = \frac{k_{ATP}\cdot[ATP]}{K_{D,ATP}+[ATP]} + \frac{k_{PPi}\cdot[PPi]}{K_{D,PPi}+[PPi]}. \qquad (21)$$

The variables [ATP] and [PPi] in the above equation refer to the concentration of adenosine triphosphate and pyrophosphate and the parameters k_{ATP} and k_{PPi} denote the catalytic rate constants for (ATP- and PPi dependent) excision. Parameters $K_{D,ATP}$ and $K_{D,PPi}$ denote the corresponding dissociation constants. The respective concentrations of PPi and ATP in various cell types are shown in Table 1 and kinetic parameters for AZT-MP excision during DNA- and RNA dependent polymerization by HIV-1 RT (wild type and AZT-resistant mutant) are indicated in Table S3 (supplementary material).

Residual polymerization in the presence of AZT. In Fig. 4, we have illustrated the predicted concentration-response relationship for intracellular AZT triphosphate and RNA- and DNA dependent polymerization of homo-polymeric- (panels A & B) and hetero-polymeric sequences in unstimulated $CD4^+$ T-cells for the wild type enzyme (solid blue lines) and an AZT-resistant quadruple mutant ('D67N/K70R/T215Y/K219Q'; dashed lines), respectively. From Fig. 4, several conclusions can be drawn: First,

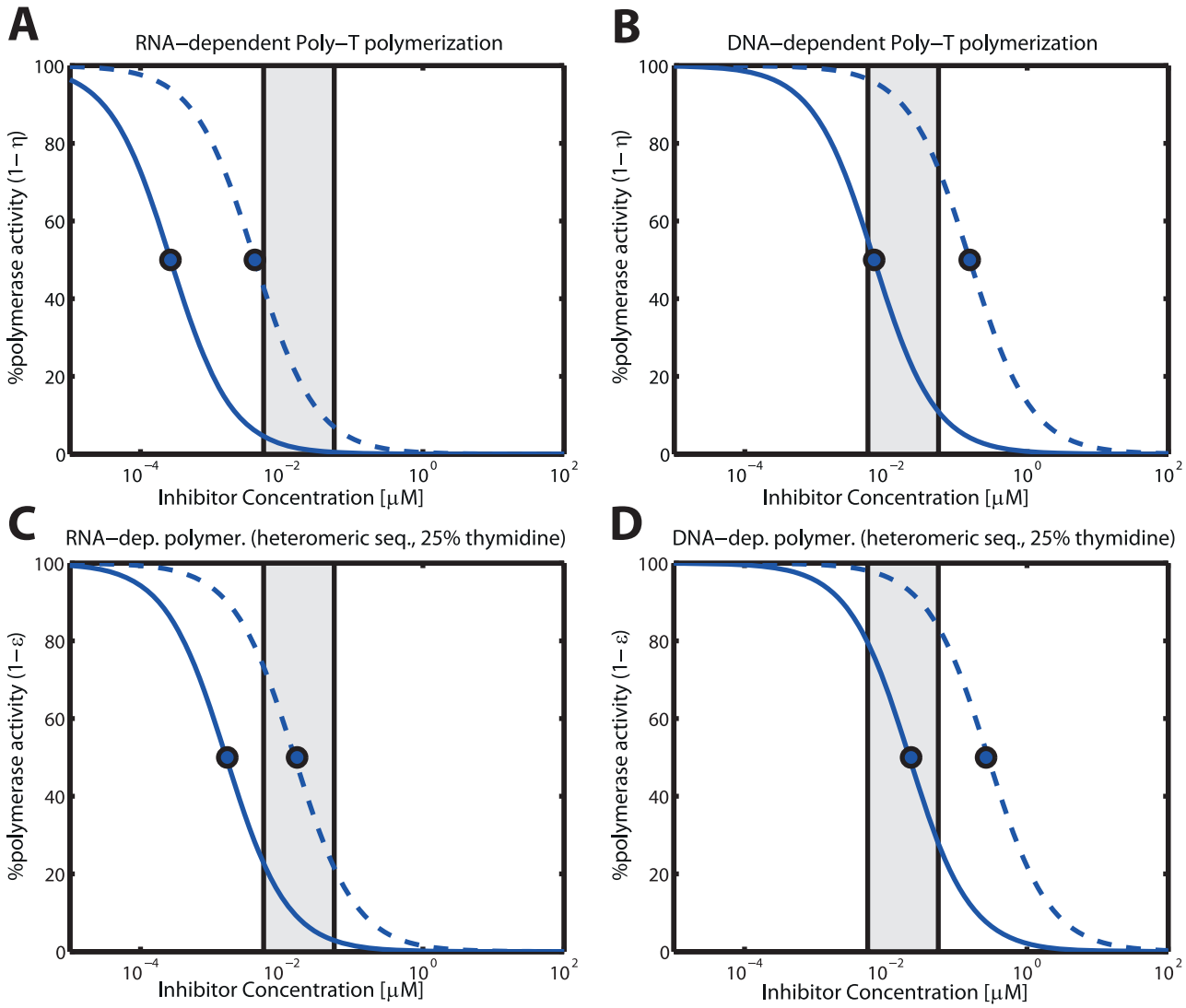

Figure 4. RNA- and DNA-dependent polymerization in the presence of intracellular AZT triphosphate in unstimulated $CD4^+$ T-cells. The solid blue curves indicate the level of residual polymerization with the wild type enzyme, whereas the dashed lines indicate the residual polymerization with the 'D67N/K70R/T215Y/K219Q' mutant. Panels A & B: Residual RNA- and DNA dependent polymerization of a homo-polymeric thymidine sequence (Poly-'T'). Calculations were obtained by solving eq. (19). Panels C & D: RNA- and DNA polymerization of a hetero-polymeric random sequence of length 500 with 25% respective dNTP content. The illustration was generated using eq. (10). The light grey area indicates the *in vivo* concentrations range of AZT in purified circulating $CD4^+$ T-cells from [71], converted to units μM by assuming a cell volume of $180\mu m^3$ for resting $CD4^+$ T-cells [72]. All utilized parameters are indicated in Tables 1, S1, S2, S3 (supplementary material).
doi:10.1371/journal.pcbi.1002359.g004

as expected, polymerase inhibition by intracellular AZT is more efficient in homo-polymeric sequences that contain only thymidine versus hetero-polymeric sequences that contain a mixture of all four nucleosides (panel A & B vs. C & D). Second, AZT inhibition of RNA-dependent polymerization is more efficient than inhibition of DNA-dependent polymerization (panels A & C vs. panels B & D). Predicted inhibition of RNA-dependent polymerization of hetero-polymeric sequences is nearly complete for the wild type and under *in vivo* intracellular AZT-TP concentrations (residual activity is $\leq$20%, solid blue line and grey area in Fig. 4C). For DNA-dependent polymerization, we predict residual activity under *in vivo* AZT-TP concentrations ($\geq$20%, solid blue line and grey shaded area in Fig. 4D). Third, the resistance mutations 'D67N/K70R/T215Y/K219Q' (dotted lines) increase the fifty percent inhibitory AZT-TP concentrations. For DNA-dependent polymerization, the IC_{50} is shifted to concentrations that lie beyond clinically achieved concentrations (see Fig. 4B & Fig. 4D), almost completely diminishing inhibition by AZT (Fig. 4D). RNA-dependent polymerization is still partially inhibited in the 'D67N/K70R/T215Y/K219Q' mutant in unstimulated $CD4^+$ T-cells ($\geq$20% residual polymerization, Fig. 4A & Fig. 4C).

Cell type specific susceptibility to AZT and impact of resistance. In Table 3, we have calculated the cell-specific IC_{50} values for RNA- and DNA dependent polymerization of homo-polymeric (Poly-'T') sequences. Our results indicate that AZT is much more potent in resting cells (unstimulated $CD4^+$ T-cells and macrophages), as suggested by the smaller IC_{50} values for the wildtype in Table 3 (second- and fifth column). This cell-specific property is mainly due to lower PPi concentrations in resting cells

(see Table 1) and subsequently lesser pyrophosphorolysis of AZT-MP terminated primers in resting cells (see eqs. (20)–(21)) as discussed previously (section *Cell-specific susceptibility to chain-terminating nucleoside analogs*), and is only marginally affected by lower dNTP levels in resting cells, as decreasing dNTP levels may not induce hyper-susceptibility as shown in Fig. 3A. The greatest kinetic change induced by the 'D67N/K70R/T215Y/K219Q' affects the catalytic rate of ATP-mediated excision of AZT-MP from the terminated primer k_{ATP} (see Table S3, supplementary material). This change increases the predicted IC_{50} of AZT in unstimulated $CD4^+$ cells and macrophages in a much more pronounced way than in activated $CD4^+$ T-cells (fold resistance >15 in unstimulated $CD4^+$ T-cells and macrophages vs. <5 in activated $CD4^+$ T-cells; fourth and seventh columns in Table 3). In activated T-cells PPi-mediated excision of AZT-MP from the terminated primer is likely the dominant mechanism, as a consequence of the much higher PPi concentrations in these cells (see Table 1). Therefore, increasing k_{ATP} will only have a strong effect once ATP-mediated excision becomes the dominant mechanism of AZT-removal. Therefore, further increase of k_{ATP} might turn ATP-mediated excision into the main removal pathway and subsequently impact on resistance in a more pronounced way in activated $CD4^+$ cells as well. Overall, the IC_{50} for polymerase inhibition in the 'D67N/K70R/T215Y/K219Q' mutant is probably shifted into concentration ranges which are rarely achieved *in vivo*.

Molecular mechanism of AZT-resistance by ATP-mediated excision. Excision of AZT-MP from the terminated primer is the major mechanism by which AZT resistance is thought to be mediated [17]. In particular, ATP-mediated excision has been discussed as the major *in vivo* mechanism of AZT resistance [15,16]. However, at the molecular level, it is unclear, if the mechanism by which enhanced excision is achieved is due to an increased removal rate (parameter k_{ATP} in eq. (21)) or increased binding affinity of ATP to the primer-template (affected parameter: $K_{D,ATP}$ in eq. (21)). In particular, in a recent paper [39], it was argued, based on crystal structures of resistant RT, that the main mechanism of AZT-resistance could be conferred by increasing ATP's binding affinity to the resistant RT enzyme. In Fig. 5, we analyze the impact of the two potential AZT-resistance mechanisms (increased removal rate k_{ATP} vs. decreased $K_{D,ATP}$). Our predictions show that increasing the affinity for ATP binding $K_{D,ATP}$ (dashed red line) does not lead to resistance development under the parameters used, because ATP binding to the wild type enzyme is already saturated ($K_{D,ATP} < [ATP]$) at physiological conditions and further decrease of $K_{D,ATP}$ enhances the saturation effect. However, increasing the removal rate k_{ATP} (dashed blue line) desensitizes reverse transcriptase-mediated polymerization to AZT inhibition since $r_{exc} \approx k_{ATP}$, in cells with low PPi contents and under saturation conditions (see Table 1 and eq. (21)).

Table 3. Cell-specific IC_{50} values of AZT-TP for 'poly-thymidine' polymerization and susceptibility change by resistance development.

	RNA/DNA			DNA/DNA		
cell type	**'wt'**	**'res'***	**fold res.**	**'wt'**	**'res'***	**fold res.**
act. $CD4^+$	$2.4{\cdot}10^{-3}$	$1{\cdot}10^{-2}$	4.5	$6.6{\cdot}10^{-2}$	$2.7{\cdot}10^{-1}$	4.1
rest. $CD4^+$	$2.7{\cdot}10^{-4}$	$4.2{\cdot}10^{-3}$	15.7	$6.8{\cdot}10^{-3}$	$1.5{\cdot}10^{-1}$	22.6
macr.	$2.3{\cdot}10^{-4}$	$3.9{\cdot}10^{-3}$	17.2	$5.4{\cdot}10^{-3}$	$1.2{\cdot}10^{-1}$	22.5

IC_{50} values, expressed in μM, were calculated using eqs. (20)–(21). Cell-specific parameters were taken from Table 1. All kinetic parameters were taken from Table 1 and Tables S1, S2, S3 (supplementary material).
*'res' = D67N/K70R/T215Y/K219Q mutant.
doi:10.1371/journal.pcbi.1002359.t003

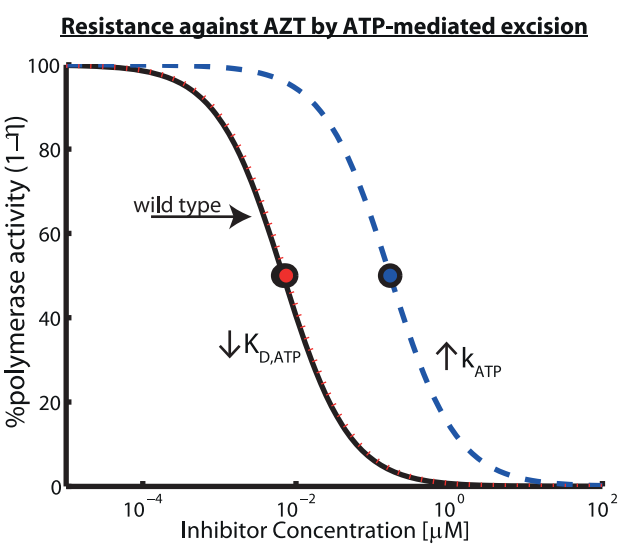

Figure 5. Molecular mechanisms of HIV-1 resistance development against AZT by ATP-mediated excision. Potential mechanisms for resistance development against AZT through increasing its excision rate r_{exc} via an ATP-mediated mechanism (see eq. (21)). We calculated residual DNA-dependent polymerization of a Poly-T sequence in unstimulated $CD4^+$ T-cells using eq. (19) with parameters from Tables 1, S1 and S3 (supplementary material). The solid black line shows residual DNA polymerization $(1-\eta)$ in the wild type virus, whereas the dotted red line and the dashed blue line refer to residual polymerization if $K_{D,ATP}$ and k_{ATP} were decreased- and increased 100-fold respectively.
doi:10.1371/journal.pcbi.1002359.g005

Selection of resistance

Selection of drug resistance depends on the competitive advantage of some resistant mutant over its competitors (either the wild type or some competing viral mutant) in a particular environment. In order to quantify whether drug resistant mutants become selected in an environment that is modified by **NA**s, we have previously defined the selective advantage S in eq. (4) (and paragraph below).

Selection of thymidine associated mutations (TAMs) by AZT in different cell-types. In Fig. 6A and Fig. 6B, the selective advantage of TAMs over the wild type $S_{TAM/wt}$(AZT-TP) is shown for RNA-dependent polymerization (panel A) and DNA-dependent polymerization (panel B) respectively in distinct cell-types relevant to HIV-1 infection (solid green-, blue and red lines indicate $S_{TAM/wt}$(AZT-TP) for activated $CD4^+$ T-cells, resting $CD4^+$ T-cells and macrophages, respectively). The respective threshold concentrations AZT* (TAM) above which resistance becomes selected, $S_{TAM/wt}$ (AZT-TP)>1, are $5.4{\cdot}10^{-4}$μM (resting $CD4^+$ cells) $<6.3{\cdot}10^{-4}$μM (macrophages) $<7.3{\cdot}10^{-3}$μM (activated $CD4^+$ cells) for RNA-dependent polymerization. For DNA-dependent polymerization, the corresponding thresholds are $6.2{\cdot}10^{-3}$μM (macrophages) <0.01μM (resting $CD4^+$ cells) <0.36μM (activated $CD4^+$ cells).

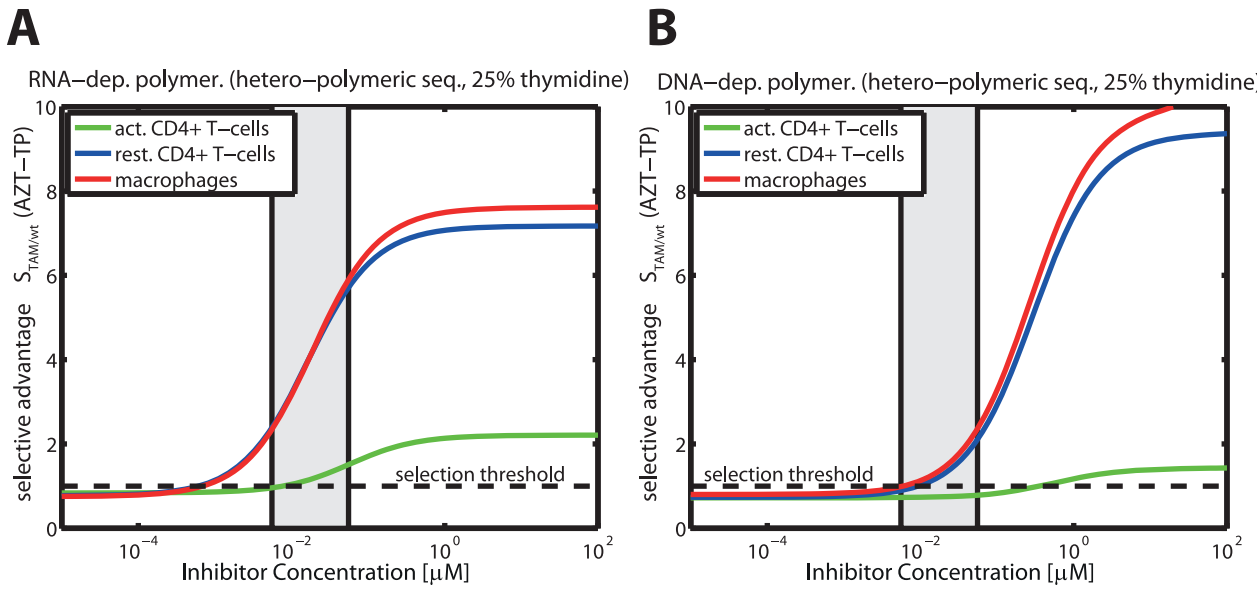

Figure 6. Selective advantage of the 'D67N/K70R/T215Y/K219Q' mutant against the wild type during RNA- and DNA-dependent polymerization in the presence of AZT-TP. The solid lines (green = activated $CD4^+$ cells, blue = unstimulated $CD4^+$ cells, red = macrophages) indicate the selection parameter $S_{\mathrm{TAM/wt}}(\mathrm{AZT\text{-}TP})$, defined in eq. (4), for different levels of intracellular ATZ-TP during RNA- and DNA dependent polymerization (Panels A & B) of a random sequence of length 500 with 25% respective dNTP content. The light grey area indicates the *in vivo* concentrations range of AZT in purified circulating $CD4^+$ T-cells from [71], converted to units μM by assuming a cell volume of $180\mu m^3$ for resting $CD4^+$ T-cells [72]. The dashed horizontal line indicates the threshold for resistance selection, i.e. $S=1$. All utilized parameters are indicated in Table 1 and Tables S1, S2, S3 (supplementary material).
doi:10.1371/journal.pcbi.1002359.g006

Two major findings can be derived from Fig. 6: Firstly, it can be seen that in the case of RNA-dependent polymerization, the 'D67N/K70R/T215Y/K219Q' mutation becomes selected ($S_{\mathrm{TAM/wt}}(\mathrm{AZT\text{-}TP}\geq 1$; dashed horizontal black line) at lower intracellular AZT-TP concentrations (below clinically achieved concentrations in resting $CD4^+$ T-cells and macrophages; light grey area) compared to DNA-dependent polymerization. During DNA-dependent polymerization, 'D67N/K70R/T215Y/K219Q' is only selected at clinically relevant levels of AZT-TP (resting $CD4^+$ T-cells and macrophages) or far above (activated $CD4^+$ T-cells). We have shown previously in Fig. 4C & D that inhibition of RNA-dependent polymerization by AZT-TP is much more efficient compared with inhibition of DNA-dependent polymerization (see also Table 3), explaining the higher selective pressure exerted at lower AZT-TP concentrations during RNA-dependent polymerization. Therefore, we would expect that resistance is favored at lower concentrations during RNA-dependent polymerization, when compared to DNA-dependent polymerization.

Secondly, and quite surprisingly, Fig. 6A & B indicate that resistance to AZT may not become selected over the wildtype in activated $CD4^+$ cells as it only confers a very small selective advantage in these cell types during RNA-dependent polymerization and at clinically relevant concentrations of AZT-TP (solid green line and grey area in Fig. 6A). For DNA-dependent polymerization the selection parameter indicates a disadvantage ($S_{\mathrm{TAM/wt}}(\mathrm{AZT\text{-}TP})<1$) of the 'D67N/K70R/T215Y/K219Q' mutant at clinically relevant AZT-TP concentrations. In resting $CD4^+$ T-cells and macrophages on the other hand, resistance selection is favored at clinically relevant AZT-TP concentrations (DNA-dependent polymerization) and below (RNA-dependent polymerization). These results indicate, that selection of the 'D67N/K70R/T215Y/K219Q' mutation by AZT is cell-specific and may preferably occur within resting $CD4^+$ T-cells and macrophages, whereas resistance selection in activated $CD4^+$ T-cells is less likely. This finding, however, warrants further investigation of the intermediate strains in the TAM resistance pathway, once kinetic data becomes available.

Subsequent selection of Q151M-complex mutations by TDF. The selective advantages of intermediate viral strains of the Q151M-complex (multi-drug) resistance pathway (Q151M, A62V/V75I/F77L/F116Y/Q151M (Q151Mc) and Q151Mc/K70Q) with respect to increasing tenofovir diphosphate (TFV-DP) concentrations are shown in Fig. 7 for DNA-dependent polymerization in resting $CD4^+$ T-cells. Panel A shows the selective advantage of the respective mutant in relation to the wild type, i.e. $S_{\mathrm{Q151M/wt}}(\mathrm{TFV\text{-}DP})$ (dashed blue line), $S_{\mathrm{Q151Mc/wt}}(\mathrm{TFV\text{-}DP})$ (solid green line) and $S_{\mathrm{Q151Mc+K70Q/wt}}(\mathrm{TFV\text{-}DP})$ (dotted magenta line). At *in vivo* concentrations ranges of TFV-DP (light grey area) the selective pressure towards the Q151M and the Q151Mc strains is relatively weak ($1<S_{\mathrm{Q151M/wt}}(\mathrm{TFV\text{-}DP})\leq S_{\mathrm{Q151Mc/wt}}(\mathrm{TFV\text{-}DP})<3$), whereas it is strong for the Q151Mc/K70Q mutant ($4<S_{\mathrm{Q151Mc+K70Q/wt}}(\mathrm{TFV\text{-}DP})<10$). It can be seen that the selective advantage is of the order $S_{\mathrm{Q151M/wt}}(\mathrm{TFV\text{-}DP})\leq S_{\mathrm{Q151Mc/wt}}(\mathrm{TFV\text{-}DP})<S_{\mathrm{Q151Mc+K70Q/wt}}(\mathrm{TFV\text{-}DP})$, indicating a distinctly graded 'selection landscape' from the wild type towards the Q151Mc/K70Q mutant. A graded landscape would imply that the presence of TFV-DP favors subsequent resistance mutations in the resistance pathway. We therefore further analyzed the form of the 'selection landscape' in panel B, where we have plotted the selective advantage of the respective mutants in relation to their progenitors in the resistance pathway, i.e. $S_{\mathrm{Q151M/wt}}(\mathrm{TFV\text{-}DP})$, $S_{\mathrm{Q151Mc/Q151M}}(\mathrm{TFV\text{-}DP})$, $S_{\mathrm{Q151Mc+K70Q/Q151Mc}}(\mathrm{TFV\text{-}DP})$. It can be seen that the Q151M single mutation has a weak selective advantage over the wild type ($S\approx 2$ dashed blue line). The Q151M-complex (Q151Mc) has an even weaker selective advantage over the Q151M single mutation in the presence TFV-DP ($S<1.5$, solid green line). However, the subsequent mutation, Q151Mc→Q151Mc/K70Q has a strong

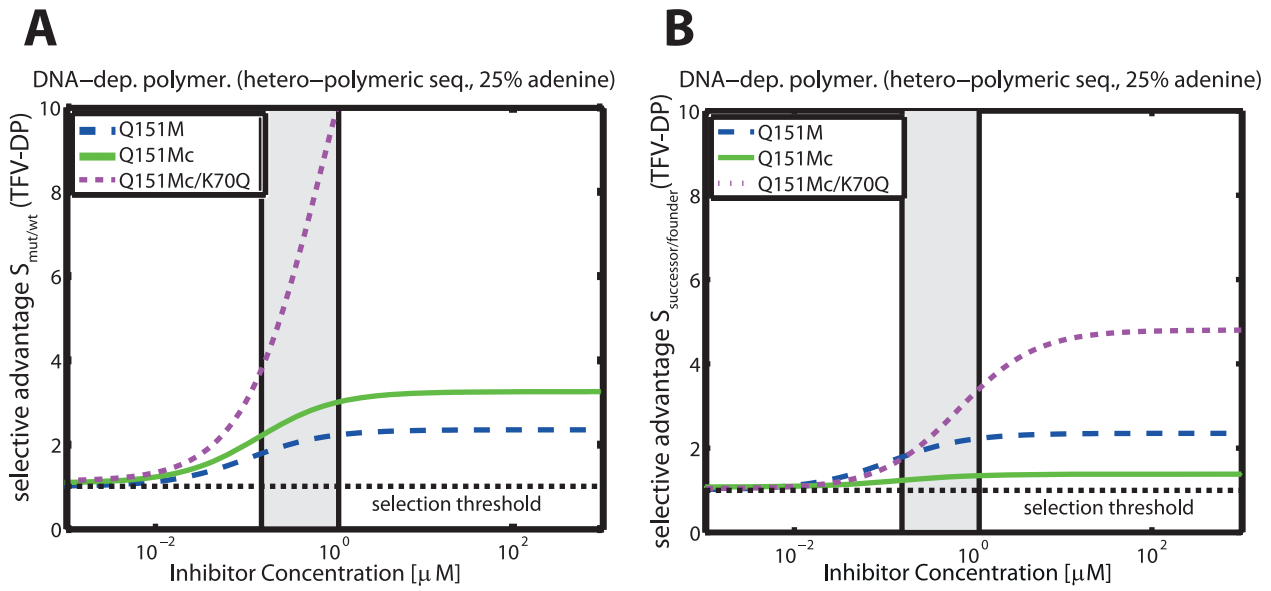

Figure 7. Selective advantage S of intermediate viral mutants of the Q151M-complex during DNA-dependent polymerization in the presence of TFV-DP. Dashed blue-, solid green- and dotted magenta line indicate the selective advantage of the Q151M, the multi-drug resistant Q151M-complex (Q151Mc: A62V/V75I/F77L/F116Y/Q151M) and the Q151Mc+K70Q mutation during DNA-dependent polymerization of a random sequence of length 500 with 25% respective dNTP content in unstimulated $CD4^+$ cells. The light grey area indicates the *in vivo* concentrations range of TFV-DP from [56,71,73], converted to units μM by assuming a cell volume of $180\mu m^3$ for resting $CD4^+$ T-cells [72]. The dashed horizontal line indicates the threshold for resistance selection, i.e. $S=1$. Panel A: Selective advantage of the respective mutants with regard to wild type $S_{mut/wt}$(TFV-DP). B: Selective advantage of a succeeding mutants with regard to progenitor in Q151M complex formation $S_{mut1/mut2}$(TFV-DP). All utilized parameters are indicated in Table 1 and Tables S1, S2 (supplementary material).
doi:10.1371/journal.pcbi.1002359.g007

selective advantage in the presence of TFV-DP ($S>2$). The selection landscape therefore exhibits a slight increase (wt→Q151M), followed by a plateau (Q151M→Q151Mc), followed by a steep increase (Q151Mc→Q151Mc/K70Q). Our analysis indicates that TDF treatment slightly favors Q151M over the wild type, it, however, does not favor the Q151M-complex $S_{Q151Mc/Q151M}(\text{TFV-DP})\approx 1$. Once the Q151M-complex has arisen (due to co-administered drugs), TDF could select for the K70Q mutation.

Epistasis

Epistasis has been used to describe the phenomenon where the phenotype of one mutation is modified by one or several other mutations [22,23]. In a two-locus-two allele model, epistasis is said to be positive when the combined effects of a double mutant result in greater replication than expected if the effects on replication coming from the two single mutations were independent. Conversely, epistasis is said to be negative, when the combined effects of a double mutant result in lesser than expected replication. Resistance mutations against NRTIs of HIV-1 are located within the same gene (the *Pol* gene). It is therefore likely, that the combination of mutations produce a phenotype that has unexpected/novel properties. The intention of this analysis is to elucidate how epistasis depends on the environment in which the virus replicates (and which is altered by **NA**s), analogously to [23]. In Fig. 8, we assessed epistasis with regard to replication (solid blue line), fitness (solid red line) and resistance (solid green line), based on eqs. (5)–(7) for the K65R/M184V mutant and varying TFV-DP concentrations for DNA-dependent polymerization in resting $CD4^+$ T-cells.

It can be seen that epistasis in the absence of drugs $E_f(\phi)$ (fitness epistasis) is positive (solid red line). This result is based on the fact that the predicted fitness of the double mutant $f_{M184V/K65R}=30\%$ is larger than expected if the fitness effects coming from the respective single mutants $f_{M184V}=46\%$ and $f_{K65R}=38\%$ were independent. Resistance epistasis $E_{Res.}(NA)$ (green line) on the other hand is negative at clinically relevant TFV-DP concentrations (light grey area). Whereas the M184V mutation is slightly hypersusceptible (predicted fold resistance relative to the wild type: 0.76 see also [40]), the K65R mutation confers $\approx$5.3-fold resistance in relation to the wild type, mainly by decreasing TFV-DP's incorporation rate k_{term}, see Table S2 (supplementary information). We predicted that the double mutant 'M184V/K65R' is $\approx$2-fold resistant in relation to the wildtype. Resistance epistasis $E_{Res.}(NA)$ thus reduces replication of the double mutant in the presence of TFV-DP and is negative. The combined effects of fitness and drug resistance are indicated by the blue line in Fig. 8. Our predictions indicate that epistasis is positive at clinically relevant TFV-DP concentrations (light grey area), because the (positive) fitness epistasis overweighs the negative resistance epistasis in the clinically relevant range of TFV-DP concentrations. At higher TFV-DP concentrations, however, the negative resistance epistasis overweighs.

Residual DNA-dependent polymerization of mutant reverse transcriptase (RT) of HIV-1 in the presence of distinct nucleoside reverse transcriptase inhibitors (NRTIs)

Viral fitness is an important determinant for the pre-treatment abundance of drug resistant mutants and their persistence in circulating virus after withdrawal of drugs. Moreover, it has also important implications for the therapeutic strategy and on disease progression [20,21]. For these reasons, we assessed viral fitness of the distinct mutants in the absence of drugs. We estimated viral

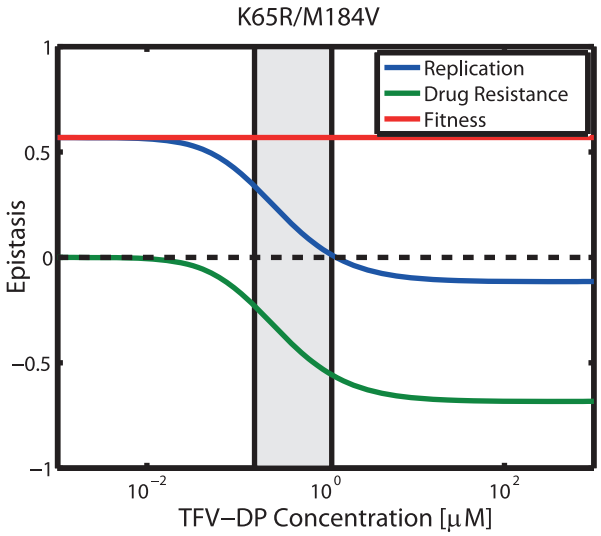

Figure 8. Epistatic interactions for DNA-dependent polymerization in the presence of TFV-DP. Solid blue-, green- and red line indicate epistasis with regard to replication $E_{\mathrm{Rep.}}(\mathrm{NA})$, resistance $E_{\mathrm{Res.}}(\mathrm{NA})$ and fitness $E_f(\phi)$ as defined in eqs. (5)–(7) for the double mutant 'K65R/M184V'. The black dashed horizontal line indicates the value, where no epistatic interactions occur. The light grey area indicates the *in vivo* concentrations range of TFV-DP from [56,71,73], converted to units μM by assuming a cell volume of $180\mu m^3$ for unstimulated $CD4^+$ T-cells [72]. All utilized parameters are indicated in Table 1 and Tables S1, S2 (supplementary material).
doi:10.1371/journal.pcbi.1002359.g008

Table 4. Estimated *in vivo* % residual DNA-dependent polymerization $(1-\varepsilon)$ for distinct mutants and drug combinations.

	wt	Q151M	M184V	K65R	M184V/ K65R
TFV-DP	4.16–24.11	9.20–42.55	3.32–20.05	19.11–63.34	8.72–41.14
AZT-TP	29.47–80.69	-	-	-	-
d4T-TP	2.08–25.95	-	7.44–56.97	-	-
FTC-TP	2.07–21.45	1.24–14.00	-	21.28–77.76	47.37–92.09
3TC-TP	1.54–4.95	0.86–2.81	51.22–77.71	12.29–31.77	86.19–95.40
CBV-TP	7.63–14.18	82.27–90.27	45.49–62.53	-	-
FTC-TP	1.39–12.69	1.11–11.75	-	11.02–53.12	7.80–39.22
+TFV-DP					
d4T-TP	0.91–4.40	-	7.01–49.20	-	
+3TC-TP					
CBV-TP	1.33–3.89	0.87–2.84	32.20–53.53	-	-
+3TC-TP					
CBV-TP	1.27–3.81	-	-	-	-
+3TC-TP					
+AZT-TP					
fitness	100	100	46	38	30

In vivo concentration ranges were 3TC-TP = 12.2–40.5; FTC-TP = 1.5–19.4; TFV-DP = 0.16–1.17; CBV-TP = 0.44–0.88; d4T-TP = 0.034–0.56; and AZT-TP = 0.0056–0.056 μM respectively [56,71,73–75], assuming an average cell volume of $180\mu m^3$ for resting $CD4^+$ T-cells [72].
doi:10.1371/journal.pcbi.1002359.t004

fitness on the basis of the relative decrease in polymerization time, see eq. (3), for a hetero-polymeric sequence context and based on DNA-dependent polymerization during reverse transcription. The results are presented in Table 4 (bottom row). The fitness of the viral mutants was of the order $\mathrm{K65R/M184V} < \mathrm{K65R} \leq \mathrm{M184V} < \mathrm{Q151M} \approx \mathrm{wildtype}$ and is in general agreement with published data on viral fitness [21,41]. Notably, the K65R and M184V mutants conferred substantial fitness losses, which explains the low prevalence of K65R even in treatment experienced patients [21], and M184V reversion to wild type when 3TC, ABC or FTC are eliminated from second or third-line anti-retroviral regimens [42].

Estimated residual DNA-dependent polymerization for mutant and wild type RT under *in vivo* concentration ranges of triphosphorylated NRTIs in resting $CD4^+$ T-cells and on a hetero-polymeric sequence context (using eqs. (1)–(2)) are presented in Table 4. Utilized kinetic parameters for nucleoside incorporation are provided in Table S2 (supplementary material). We predicted that most inhibitors decreased DNA-dependent polymerization to values of 2–25% in the wildtype enzyme. However, 3TC displayed superior efficacy (only 1.5–5% residual polymerization) and AZT only poorly inhibited DNA-dependent polymerization. However, as discussed in section *Residual polymerization in the presence of AZT*, AZT is likely to exert its main effect through inhibition of RNA-dependent polymerization. The Q151M mutation decreased the efficacy of carbovir triphosphate (CBV-TP) markedly (8 fold) and had only marginal impact on tenofovir diphosphate (TFV-DP), whereas lamivudine triphosphate (3TC-TP) and emtricitabine triphosphate (FTC-TP) were unaffected (see also [40,43]). Combination treatment with 3TC-TP+CBV-TP could, however, restore inhibition of polymerization and combination treatment FTC-TP+TFV-DP was very efficient, however not markedly different from FTC-TP alone. The M184V mutation decreased susceptibility to 3TC-TP ($\approx$20 fold) and CBV-TP (8 fold), having marginal impact on stavudine triphosphate (d4T-TP) and no effect on TFV-DP, which is consistent with phenotypic measurements [40,43]. Susceptibility to the combination of d4T-TP+3TC-TP was comparable to d4T-TP alone. The efficacy of 3TC-TP+CBV-TP was strongly reduced. We predicted that the K65R mutation reduced the impact of 3TC-TP, FTC-TP and TFV-DP (7-, 4 and 3-fold respectively) and also reduced the susceptibility to the combination FTC-TP+TFV-DP (5-fold), consistent with phenotypic measurements [40,43]. The double mutation K65R/M184V conferred complete resistance to 3TC-TP and near complete resistance to FTC-TP and partly restored susceptibility to TFV-DP or TFV-DP+FTC-TP, compared to K65R alone, in agreement with phenotypic measurements [40,43].

Inhibition of human mitochondrial polymerase $-\gamma$ by various NRTIs

Despite their antiviral activity, NRTIs have been reported to cause severe mitochondrial toxicity [9,44], limiting their therapeutic use. A dominant hypothesis for the manifestation of mitochondrial toxicity by NRTIs is that NRTIs inhibit polymerase-γ (pol $-\gamma$) function, which is necessary to duplicate the mitochondrial genome, thereby leading to mtDNA depletion and subsequent mitochondrial abnormalities. The anticipated mechanism of pol $-\gamma$ inhibition is highly similar to inhibition of polymerization during reverse transcription: tri-phosphorylated NRTIs compete with endogenous dNTPs for incorporation into the nascent mtDNA, and, once incorporated, lead to quasi-chain

termination [9]. Polymerase-γ can perform two crucial catalytic functions, namely DNA polymerization and exonuclease activity; the later enabling the removal of incorporated NRTIs. The mechanism of action of NRTIs on $\mathrm{pol}-\gamma$ leads us to believe that our mathematical model of polymerase inhibition by **NA**s can be useful in predicting NRTI-induced inhibition of $\mathrm{pol}-\gamma$.

Utilizing pre-steady state kinetic data for the incorporation of dNTPs and various NRTIs (see Table S4, supplementary material), we estimated the residual $\mathrm{pol}-\gamma$ function in a hetero-polymeric sequence context and under concentration ranges of NRTI-TPs typically observed *in vivo*. The results are stated in Table 5. For simulation purposes we utilized eqs. (1) and assumed dNTP levels typically observed in unstimulated $\mathrm{CD4}^+$ cells (see Table 1). Under the parameters used, we found that mtDNA polymerization is substantially inhibited in the presence of d4T-TP and moderately inhibited by 3TC-TP for *in vivo* -triphosphate concentration ranges. Similarly, combinations 3TC-TP+D4T-TP reduced $\mathrm{pol}-\gamma$ activity substantially and 3TC-TP+CBV-TP or 3TC-TP+AZT-TP+CBV-TP reduced $\mathrm{pol}-\gamma$ activity moderately. We found the following order of inhibition of polymerase-γ : $\mathrm{d4T-TP} > \mathrm{3TC-TP} > \mathrm{TFV-DP} \geq \mathrm{FTC-TP} \geq \mathrm{AZT-TP} \geq \mathrm{CBV-TP}$, which agrees with experimental findings [9]. The mitochondrial toxicity of AZT is likely not due to $\mathrm{pol}-\gamma$ inhibition. Instead, it has been explained in terms of various other mechanisms, which are exemplified in the *Discussion* section.

We subsequently defined a therapeutic index as the ratio of the mean inhibition of $\mathrm{pol}-\gamma$ and wild type RT respectively. The therapeutic index indicated the following order for the inhibitors and their combinations: $\mathrm{d4T-TP} < \mathrm{d4T-TP+3TC-TP} < \mathrm{TFV-DP} < \mathrm{FTC-TP} \leq \mathrm{CBV-TP} < \mathrm{FTC-TP+TFV-DP} < \mathrm{3TC-TP} < \mathrm{CBV-TP+3TC-TP}$. Note, that AZT has been excluded from this assessment, because its mitochondrial toxicity has been contributed to mechanisms other than $\mathrm{pol}-\gamma$ inhibition (see *Discussion* section).

Table 5. Estimated *in vivo* % residual human mitochondrial polymerase-γ activity in resting $\mathrm{CD4}^+$ cells.

	$(1-\varepsilon_{\mathrm{tox}})$	ther. Index*
TFV-DP	63.54–92.72%	5.5
AZT-TP	98.74–99.87%	†
d4T-TP	0.15–2.40%	0.1
FTC-TP	94.05–99.51%	8.2
3TC-TP	25.69–53.43%	12.2
CBV-TP	98.78–99.38%	9.1
FTC-TP/TFV-DP	61.96–92.55%	11
3TC-TP/d4T-TP	0.16–2.48%	0.5
CBV-TP/3TC-TP	25.18–52.70	14.9
CBV-TP/3TC-TP/AZT-TP	26.22–54.13%	†

In vivo concentration ranges were 3TC-TP = 12.2–40.5; FTC-TP = 1.5–19.4; TFV-DP = 0.16–1.17; CBV-TP = 0.44–0.88; d4T-TP = 0.034–0.56; and AZT-TP = 0.0056–0.056 μM, respectively [56,71,73–75], assuming an average cell volume of $180\mu m^3$ for resting $\mathrm{CD4}^+$ T-cells [72].

*calculated as the ratio of average effect on polymerase-γ and wildtype reverse transcriptase of HIV-1: $\overline{(1-\varepsilon_{\mathrm{tox}})}/\overline{(1-\varepsilon_{\mathrm{RT-wt}})}$.

†mitochondrial toxicity of AZT has been attributed to mechanisms other than $\mathrm{pol}-\gamma$ inhibition (see *Discussion* section).

doi:10.1371/journal.pcbi.1002359.t005

Discussion

We presented a novel mechanistic mathematical model of HIV-1 polymerase inhibition by **NA**s that, for the first time, focussed on the transient aspect of this inhibition. This is an important characteristic, as HIV-1 can exploit the transient nature of inhibition by reducing the residence time of the apparent chain terminator (the incorporated **NA**) in the nascent viral DNA to achieve drug resistance (summarized in [13]). **NA** removal from quasi-terminated RNA/DNA chains has also been described for hepatitis B & C viruses [24–26]. Hence, the developed model may also be applicable to study polymerase inhibition by **NA**s in these viruses. In contrast to previous mathematical approaches [14,19], we therefore describe the effects of nucleoside analogs on DNA-polymerization in terms of an increase in the average polymerization time, which is analogous to a reduction of the overall polymerization rate, i.e. $\bar{v}_{\mathrm{poly}}(\phi) = 1/T_{0\to N}(\phi)$. This mathematical approach not only allows to study various resistance mechanisms, but also allows for the first time to estimate the inherent fitness of drug resistant mutants, resulting from microscopic changes in the polymerization rate constants (e.g. k_{pol}, $K_{\mathrm{D,dNTP}}$) of the mutant viral enzyme (see eqs. (1)–(3)). The derived model can readily be used to assess the probability to successfully finish polymerization. In supplementary Text S1 we have given an example for HIV-1 reverse transcription. It is also explained therein how the model can be integrated in larger (systems biology) models of the viral life cycle in order to study the effects of **NA**s.

The developed model can be parameterized in terms of physiological parameters (such as dNTP concentrations) and microscopic kinetic rates (e.g. k_{pol}, k_{term}, K_{D}), typically derived from cell-free *in vitro* assays. These parameters can usually be precisely determined with standard errors $<20\%$. We demonstrated the applicability of the model for various distinct polymerization processes, in particular for polymerase inhibition during HIV-1 RT and mitochondrial $\mathrm{pol}-\gamma$ by NRTIs, respectively. Adaptation to distinct polymerization processes was achieved by utilizing the kinetic constants for the respective processes, while the model remained unchanged. Notably, model-predicted macroscopic predictions (viral fitness, drug efficacy and toxicity) were consistent with various experimental macroscopic findings and thus underline the usefulness of the proposed model.

Based on the developed model of polymerization and its inhibition by **NA**s, we derived two sets of mathematical solutions: Eqs. (1)–(11) can be used to compute the average effect of **NA**s and combinations of **NA**s on polymerization of arbitrary (hetero-polymeric) DNA sequences. Analogously, these equations can be used to determine the deceleration of polymerization resulting from resistance mutations in the absence of any **NA**, as an indicator of their inherent fitness cost. On the other hand, eqs. (16)–(20) represent analytical solutions for polymerase inhibition by **NA**s in a simplified homo-polymeric sequence context. The resulting equations (19)–(20) immediately highlight key determinants of **NA** inhibition and resistance development in this context. These equations can also be used to determine the model's sensitivity for different combinations of kinetic- and physiological parameters, see Fig. 3 and Fig. 5. Based on eqs. (19)–(20), we found that factors impacting on **NA** inhibition can generally be divided into two categories: (i) kinetic- and (ii) cellular factors.

Eq. (20) revealed that the rate of **NA** incorporation k_{term}, its binding affinity $K_{\mathrm{D,NA}}$ and the catalytic rate of **NA** removal r_{exc} are key molecular kinetic determinants for the efficacy of **NA**s. All indicated molecular kinetic determinants (k_{term}, $K_{\mathrm{D,NA}}$ and r_{exc}) depend on the viral polymerase enzyme and are thus prone to resistance development. The impact of alterations in these

parameters is illustrated in Fig. 3B for ddATP and in Fig. 4 & 5 for AZT-TP.

Various reports indicate cell-specific differences in **NA** efficacy against HIV-1 [45–47]. Differences in efficacy were often brought in association with intracellular NA-TP:dNTP ratios [48,49]. Utilizing the derived model, we elucidated the impact of cellular factors on HIV-1 RT polymerase inhibition by NRTIs. Quite surprisingly, we found that cells that contain low dNTP content do not necessarily confer hypersusceptibility to NRTIs if $[\mathrm{dNTP}] \ll K_{\mathrm{D,dNTP}}$ (see Fig 3A). For AZT, we predicted that alteration of PPi and ATP levels can have a strong impact on its efficacy (see Table 3). In summary, we demonstrated that the concurrence of multiple kinetic- and physiological factors, rather than a single parameter, can determine the susceptibility of an infected cell towards **NAs**, see eq. (20)–(21). In addition to cells that contain an unfavorable NA-TP:dNTP ratio [48,49], cells that contain high levels of PPi or ATP and low levels of **NA** (regardless of their dNTP content) could be resistant to NRTI treatment and residual viral replication despite treatment could persist in these cells as well. This finding can have important consequences for HIV-1 treatment with NRTIs, as HIV-1 exhibits a broad cell tropism [28–32]: While some evidence for low-level ongoing replication in the context of apparently suppressive antiviral therapy has been reported [50], the cellular source remains to be determined [51]. Whereas it has been shown previously [33], that heterogeneous viral inhibition facilitates drug resistance development, we show evidence for cell-specific (thus heterogeneous) inhibition by NRTIs. Thus, a possible mechanism for the emergence of drug resistance against could be explained on the basis of the mechanism of action of these compounds. However, further evidence is required to confirm this hypothesis.

We analyzed the specific mechanisms of AZT resistance through TAMs. It is well known, that TAMs induce resistance through increasing the excision of incorporated **NAs** from nascent viral DNA. However, the precise mechanism that increases excision is controversial. A recent crystal structure of resistant RT [39], showed that the orientation of ATP is altered in the mutant enzyme. Based on this structure [39], the authors argued that ATP, which serves as an excision substrate for incorporated AZT, would bind with higher affinity to the quasi-terminated nascent viral DNA, accelerating the removal of incorporated AZT. To the contrary, our kinetic model indicated that increasing the affinity for ATP binding $K_{\mathrm{D,ATP}}$ does not lead to resistance development (see Fig. 5), because ATP binding to the wild type enzyme is already saturated ($K_{\mathrm{D,ATP}} < [\mathrm{ATP}]$) at physiological conditions, and further decrease of $K_{\mathrm{D,ATP}}$ enhances the saturation effect. Increasing the removal rate k_{ATP} desensitizes reverse transcriptase-mediated polymerization to AZT inhibition since $r_{\mathrm{exc}} \approx k_{\mathrm{ATP}}$, in cells with low PPi contents and under saturation conditions (see Table 1 and eq. (21)). We therefore propose that the main kinetic resistance effect of the altered orientation of ATP in mutant RT is mediated by an increased removal rate k_{ATP}, in agreement with a pre-steady state kinetic analysis [17], although binding could be affected. In particular, the crystal structure showed that the resistance mutations affect the positioning of ATP in the RT catalytic site [39], which must translate into an effect on k_{ATP}.

We quantified the inhibitory effects of AZT during RNA- and DNA dependent polymerization and we analyzed how TAMs ('D67N/K70R/T215Y/K219Q') induce susceptibility changes. We found that AZT inhibition during HIV-1 reverse transcription is more efficient during RNA-dependent polymerization than during DNA-dependent polymerization, see Fig. 4. Moreover, inhibition, as well as susceptibility changes induced by TAMs were found to be cell-specific (see Table 3).

While the emergence of a particular viral strains depends on a) the probability that the mutant is generated (related to residual replication and genetic distance), it also critically depends on the likelihood that the generated mutant becomes selected subsequently. However, if inhibition- and selection forces are different in distinct target cells (see Table 3 and Fig. 6), then the processes of mutant strain generation and subsequent selection might also we divided among target cells. We therefore further looked at the selective advantage $S_{\mathrm{TAM/wt}}$ of the 'D67N/K70R/T215Y/K219Q' mutant in distinct cell types. Specifically, we predicted that the selective advantage of the 'D67N/K70R/T215Y/K219Q' mutation in the presence of AZT at clinically relevant concentrations is quite distinct in activated $\mathrm{CD4}^+$ cells, resting $\mathrm{CD4}^+$ cells and macrophages (see Fig. 6). We found that the 'D67N/K70R/T215Y/K219Q' mutation is less likely selected over the wild type in activated $\mathrm{CD4}^+$ cells, whereas this mutation is preferred in resting $\mathrm{CD4}^+$ cells and macrophages (see Fig. 6) at clinically relevant concentrations. While these results indicate, for the first time, that selection forces against **NA** treatment can be quite distinct for diverse target cells, a detailed analysis of the various intermediate mutants in the TAM resistance pathway is required, in particular a construction of the 'selection landscape' for particular mutants in the resistance pathway and for different cell types infected with HIV-1 in the presence of combinations of drugs to fully understand resistance dynamics *in vivo*. The developed model can be used to facilitate such an analysis: In Fig. 7, we started to reconstruction the 'selection landscape' for intermediate mutants of the Q151M-complex during TDF treatment in unstimulated $\mathrm{CD4}^+$ cells. We found for this cell type, that TDF alone is unlikely to select the Q151M-complex over the Q151M single mutation. Once the Q151M-complex has arisen, however, TDF would select for the additional K70Q mutation. An extended analysis of the resistance pathways in the case where particularly large genetic barriers are involved may in the future help to understand and influence the dynamics of resistance emergence for e.g. TAMs and the Q151M complex.

Epistasis has been suggested as a method to study evolutionary dynamics of virus populations [52]. It describes the phenomenon where the replicative fitness of one mutation is modified by one or several other mutations [22,23]. Epistasis is said to be positive when the combined effects of two-or-more mutations result in greater replication than expected if the effects coming from the two single mutations were independent. Since resistance mutations against NRTIs of HIV-1 are located within the same enzyme (RT), several mutations could modify the enzyme in unexpected ways, i.e. result in epistatic interactions with regard to fitness and resistance. We have shown in Fig. 8 that our model can be used to analyze different aspects of epistasis (fitness, resistance and replication). In the presented example, we detected positive fitness epistasis E_f of the 'M184V/K65R' double mutant and negative resistance epistasis $E_{\mathrm{Res}}(\mathrm{NA})$ with increasing TFV-DP concentrations in comparison with the single mutations. The combined effects of fitness- and resistance were positive at relevant concentration ranges of TFV-DP. The major conclusion from this analysis is that the combination of mutations can alter the RT enzyme in unexpected ways. The phenotypic attributes of a multiple mutated strain may not be intuitively related to the attributes of the single mutants. It is thus required to view each multiple mutated strain as an independent entity with regard to resistance and fitness. For deriving information about intermediate viral mutants in a resistance pathway (e.g. the Q151M-complex, or TAMs), it is therefore necessary to measure the attributes of each

intermediate strain independently. Related experimental work [23] indicated that replication ranking, rather than epistasis predicts dynamics of resistance emergence, in line with our analysis in section *"Selection of Resistance"*.

Based on the developed model, we predicted that the 'D67N/K70R/T215Y/K219Q' mutation induces a 4.1 to 22.6 fold increase in the IC_{50} value for poly-thymidine polymerization, depending on the cell type and the template (RNA or DNA). In cellular assays, the 'D67N/K70R/T215Y/K219Q' mutant can induce a 120–150 fold increase in the fifty percent inhibitory (extracellular) concentration when measured in $CD4^+$ HeLa-cells [46] and a 8000 fold increase in MT-4 human T-lymphoid cells [47], respectively, while at the same time resistance at the enzymatic level was observed to be far more moderate [47]. This indicates that a direct quantitative comparison of susceptibility changes observed in different cell-based assays and changes computed at the enzymatic level, e.g. on the basis of DNA-dependent polymerization in resting $CD4^+$ cells (see Table 3) might not be possible. Here, we summarize a few mechanisms, which could contribute to this difference: (i) Firstly, the cell types utilized in distinct cell-based assays differ, which can results in distinct susceptibility changes to NRTIs. We discussed- and illustrated the impact of these cell-specific differences in *Cell type specific susceptibility to AZT and impact of resistance* and in Table 3 for AZT. For AZT, these cell-specific differences were attributed to different contents of PPi and dTTP. (ii) Secondly, two different outputs are measured by the two methods: In contrast to RT activity, phenotypic assays measure the production of viral proteins, which denotes a step in the viral life cycle following polymerization and reverse transcription of the viral genome. (iii) Thirdly, and most importantly, the IC_{50} values based on enzymatic activity (as computed in this work) refer to intracellular concentrations of AZT-triphosphate, while the fold change derived by cell-based assays refers to the concentrations of extracellular pro-drug (AZT) added to the medium surrounding the cells. This has important consequences: AZT phosphorylation is known to be non-linear and might be saturated at the bottlenecking step of thymidilate kinase (monophosphate$\rightarrow$diphosphate) [53,54]. We have shown previously that the *in vivo* maximally achievable AZT-TP concentration is close to the clinically achieved AZT-TP concentration in peripheral blood mononuclear cells (PBMCs), when 300 mg AZT is given twice daily, see [53]. In order to disproportionately increase the IC_{50}(AZT) value several hundred-fold, as observed with some mutants e.g. 'M41L/D67N/K70R/T210W/Y215F', at the enzymatic level all that is required is a minor fold change in the IC_{50} (for AZT-TP), that shifts the fifty percent inhibitory concentration of intracellular AZT-TP beyond the maximally achievable levels. Thus, by adding more extracellular AZT, sufficient concentrations of AZT-TP may never be reached. In the case of saturating intracellular AZT monophosphate (AZT-MP) concentrations, the cell-specific levels of thymidilate kinase enzyme will ultimately determine the maximally achievable AZT-TP concentration, which are therefore also cell-specific [55].

In Table 4 we analyzed, based on the developed model, how different mutations can specifically alter the efficacy of distinct NRTIs and their combinations on DNA-directed polymerization and at physiological concentrations. Estimated susceptibility changes resulting from distinct mutations were *qualitatively* in good agreement with results from cell culture assays (see [40]), although, as mentioned earlier, it should be noted that a direct *quantitative* comparison of our estimations with results from cell-culture assays may not be possible. While estimating the effect of combinations of **NA**s on DNA polymerization is straightforward using eq. (1)–(11), we did not assess clinically relevant pharmacokinetic interactions between different **NA**s. Pharmacokinetic interactions between NRTIs of HIV-1 have mainly been attributed to interactions during the cellular activation cascade [56]. For our estimations in Table 4 we therefore assessed only drug combinations that use distinct enzymes in their phosphorylation cascade and which therefore bear lesser potential for pharmacokinetic interaction than drugs which utilize the same intracellular phosphorylation pathway.

Inhibition of mitochondrial polymerase-γ by NRTIs has been proposed as a central process for their clinical toxicity [9]. We therefore studied inhibition of polymerase-γ by distinct NRTIs at physiologically relevant triphosphate concentrations. The ranking of polymerase-γ inhibition by the analyzed NRTIs was in good agreement with published results [9], indicating a strong inhibition of pol$-\gamma$ by d4T and moderate inhibition by 3TC at physiological intracellular triphosphate concentrations. However, it should also be noted, that mitochondria in different tissues might contain different levels of dNTP and NRTI-TPs and might therefore be differentially prone to pol$-\gamma$ inhibition, potentially contributing to site-specific toxicities of some NRTIs [9]. Mitochondrial toxicity of AZT has been explained by other mechanisms than pol$-\gamma$ inhibition. In particular, AZT might deplete dNTP pools in the mitochondria, rather than quasi-terminate nascent mtDNA by its incorporation [57,58].

Although we demonstrated the use of the developed model on nucleoside reverse transcriptase inhibitors of HIV-1 throughout the article, we did not construct a mathematical model of the complete reverse transcription process, but rather focussed on the sub-process of polymerization, which is primarily targeted by NRTIs and other **NA**s. The aim was to point out general principles of inhibition and resistance development, rather than establishing customized models for the respective targeted viral processes. Therefore, the presented model can be used to also assess effects on distinct polymerase enzymes, or as demonstrated in Table 5 to assess off-target effects of **NA**s. Furthermore, the model can readily be used to assess inhibition of polymerization by NcRTIs, a novel class of pre-marketed nucleoside inhibitors which compete with natural dNTPs for binding to the polymerase enzyme, without becoming incorporated [59–61].

In the future, the developed model could be extended for the "dead-end complex"-mechanism observed during inhibition of HIV-1 RT [13], if respective kinetic parameters become available. Extension of the model is straightforward, as it only requires the introduction of an additional state in the mathematical model ($\tilde{I} \rightleftarrows \dagger$ in Fig. 1) and the subsequent derivation of the corresponding equations, analogously to the derivations in this article.

Recent *in vitro* experiments with single-molecules of HIV-1 RT indicated that additional complexities might occur during the reverse transcription process, such as enzyme-template dissociation and association and reversal of orientation to perform distinct tasks, such as RNAse H cleavage of the viral RNA template [62,63]. While these results warrant further investigation, it has been shown that *in vivo* an excess of RT (50–200 enzymes/virion) in comparison to RNA template may be present [64], such that different enzymes could perform different tasks (polymerization/RNAse H) at the same time *in vivo*. The cooperativity of multiple RT enzymes can also explain the distinct shape of the dose-response curve observed in primary human cells with inhibitors that directly target the enzyme, such as non-nucleoside reverse transcriptase inhibitors (NNRTIs), in contrast to inhibitors that target the RNA/DNA template (NRTIs) [65,66]. The development of models of reverse transcription that also incorporate the effects of non-nucleoside reverse transcriptase inhibitors (NNRTIs) [67,68] warrants further mechanistic understanding of the

complex overall process of reverse transcription and will be left for future research. The developed model can however be readily be used to model the effects of NAs and will be further extended to model e.g. the complete reverse transcription process of HIV-1 genomic RNA, or analogous processes in other viruses (see also supplementary Text S1).

Methods

Derivation of a recursive solution for the polymerization times on arbitrary hetero-polymeric sequences

In this section we will derive the analytical solution for the polymerization time given in eq. (10), which is based on ideas given in [69]. Recall that the proposed model is a Markov jump process and that the polymerization time $T_{0\to N}$ is given by the *mean first passage time* (MFPT) to go from state '0' (initiation of polymerization) to the state $'N'$ (final polymerization product).

Starting point for the derivation are the MFPT-equations ($i=0,\ldots,N-1$) [70],

$$\begin{aligned}-1 &= -(r_{\text{pol}}(i+1)+r_{\text{pyro}}(i)+r_{\text{term}}(i+1))T_{i\to N}\\ &+r_{\text{pol}}(i+1)\cdot T_{i+1\to N}+r_{\text{pyro}}(i)\cdot T_{i-1\to N}+r_{\text{term}}(i+1)\cdot T_{\widetilde{i+1\to N}},\end{aligned} \tag{22}$$

$$-1 = -r_{\text{exc}}(i+1)\cdot T_{\widetilde{i+1\to N}}+r_{\text{exc}}(i+1)\cdot T_{i\to N}. \tag{23}$$

Eq. (23) yields

$$T_{\widetilde{i+1\to N}} = \frac{1}{r_{\text{exc}}(i+1)}+T_{i\to N}$$

such that eq. (22) simplifies to

$$\begin{aligned}-1 &= -T_{i\to N}(r_{\text{pol}}(i+1)+r_{\text{pyro}}(i)+r_{\text{term}}(i+1))+r_{\text{pol}}(i+1)\cdot T_{i+1\to N}\\ &+r_{\text{pyro}}(i)\cdot T_{i-1\to N}+\frac{r_{\text{term}}(i+1)}{r_{\text{exc}}(i+1)}+r_{\text{term}}(i+1)\cdot T_{i\to N}.\end{aligned}$$

Further algebraic rearrangements yield

$$\begin{aligned}-1 &= -T_{i\to N}(r_{\text{pol}}(i+1)+r_{\text{pyro}}(i))+r_{\text{pol}}(i+1)\cdot T_{i+1\to N}\\ &+r_{\text{pyro}}(i)\cdot T_{i-1\to N}+\frac{r_{\text{term}}(i+1)}{r_{\text{exc}}(i+1)},\end{aligned}$$

and finally

$$\begin{aligned}T_{i\to N} &= \frac{1}{r_{\text{pol}}(i+1)+r_{\text{pyro}}(i)}\\ &\left[1+\frac{r_{\text{term}}(i+1)}{r_{\text{exc}}(i+1)}+r_{\text{pol}}(i+1)\cdot T_{i+1\to N}+r_{\text{pyro}}(i)\cdot T_{i-1\to N}\right].\end{aligned} \tag{24}$$

We define the general relation

$$T_{i\to i+1} = T_{i\to N}-T_{i+1\to N}, \tag{25}$$

which allows us to express $T_{0\to N}$ as a telescope sum ($T_{N\to N}=0$), i.e.,

$$T_{0\to N} = \sum_{i=0}^{N-1} T_{i\to i+1}. \tag{26}$$

From the general relation (25), we can derive $T_{i+1\to N}=T_{i\to N}-T_{i\to i+1}$ and $T_{i-1\to N}=T_{i\to N}+T_{i-1\to i}$, which were substituted into equation (24). Rearrangement produces the recursion

$$T_{i\to i+1} = \frac{1}{r_{\text{pol}}(i+1)}\left(1+\frac{r_{\text{term}}(i+1)}{r_{\text{exc}}(i+1)}+r_{\text{pyro}}(i)\cdot T_{i-1\to i}\right), \tag{27}$$

which equals

$$T_{i\to i+1} = (\tau_{\widetilde{i+1}}\cdot\rho_{\widetilde{i\to i+1}}+\tau_i+\rho_{i\to i-1}T_{i-1\to i})\frac{1}{\rho_{i\to i+1}}, \tag{28}$$

with parameter definitions given in eq. (9) of the main text.

Equation (27) is satisfied by

$$T_{i\to i+1} = \sum_{k=1}^{i+1}\frac{r_{\text{term}}(k)+r_{\text{exc}}(k)}{r_{\text{pol}}(k)\cdot r_{\text{exc}}(k)}\left(\prod_{j=k}^{i}\frac{r_{\text{pyro}}(j)}{r_{\text{pol}}(j+1)}\right) \tag{29}$$

such that the initial condition holds, i.e.,

$$T_{0\to 1} = \frac{1}{r_{\text{pol}}(1)}\left(\frac{r_{\text{term}}(1)+r_{\text{exc}}(1)}{r_{\text{exc}}(1)}\right).$$

Finally, inserting (29) into (26) results in the analytical expression for $T_{0\to N}$,

$$T_{0\to N} = \sum_{i=0}^{N-1}\left[\sum_{k=1}^{i+1}\frac{r_{\text{term}}(k)+r_{\text{exc}}(k)}{r_{\text{pol}}(k)\cdot r_{\text{exc}}(k)}\left(\prod_{j=k}^{i}\frac{r_{\text{pyro}}(j)}{r_{\text{pol}}(j+1)}\right)\right]. \tag{30}$$

Derivation of an analytic solution for polymerization times of homo-polymeric sequences

In case where the sequence to be polymerized is homo-polymeric, e.g. 'Poly-A', all rates are uniform, i.e., $r_{\text{pol}}(i)\equiv r_{\text{pol}}, r_{\text{pyro}}(i)\equiv r_{\text{pyro}}, r_{\text{term}}(i)\equiv r_{\text{term}}$ and $r_{\text{exc}}(i)\equiv r_{\text{exc}}$ for any i. Then by exploiting twice the identity

$$\sum_{k=0}^{i}\left(\frac{r_{\text{pol}}}{r_{\text{pyro}}}\right)^k = \frac{r_{\text{pyro}}^{i+1}-r_{\text{pol}}^{i+1}}{(r_{\text{pyro}}-r_{\text{pol}})\cdot r_{\text{pyro}}^i} \tag{31}$$

the polymerization time from eq. (30) simplifies to

$$\begin{aligned}T_{0\to N} &= \left(\frac{r_{\text{term}}+r_{\text{exc}}}{r_{\text{pol}}\cdot r_{\text{exc}}}\right)\sum_{i=0}^{N-1}\left(\frac{r_{\text{pyro}}}{r_{\text{pol}}}\right)^i\sum_{k=0}^{i}\left(\frac{r_{\text{pol}}}{r_{\text{pyro}}}\right)^k\\ &= \left(\frac{r_{\text{term}}+r_{\text{exc}}}{r_{\text{pol}}\cdot r_{\text{exc}}}\right)\left(\frac{1}{r_{\text{pol}}-r_{\text{pyro}}}\right)\sum_{i=0}^{N-1}\left(r_{\text{pol}}-\left(\frac{r_{\text{pyro}}}{r_{\text{pol}}}\right)^i r_{\text{pyro}}\right)\\ &= \left(\frac{r_{\text{term}}+r_{\text{exc}}}{r_{\text{exc}}\cdot(r_{\text{pol}}-r_{\text{pyro}})^2}\right)\left(r_{\text{pyro}}\left(\left(\frac{r_{\text{pyro}}}{r_{\text{pol}}}\right)^N-N-1\right)+r_{\text{pol}}\cdot N\right)\\ T_{0\to N} &= \left(\frac{r_{\text{term}}+r_{\text{exc}}}{r_{\text{exc}}}\right)\frac{(r_{\text{pol}}+r_{\text{pyro}})^{N-1}+r_{\text{pol}}^{N-1}\cdot(N-1)}{r_{\text{pol}}^N},\end{aligned} \tag{32}$$

which is displayed in eq. (16) of the main article.

Determination of the fifty percent inhibitory concentration (IC_{50})

Starting point for calculating the fifty percent inhibitory concentration (for polymerization of uniform sequences) is equation (19). We set

$$0.5=\frac{r_{\mathrm{exc}}}{r_{\mathrm{term}}+r_{\mathrm{exc}}}\cdot\frac{r_{\mathrm{pol}}}{r_{\mathrm{pol}}(\phi)}\quad\Leftrightarrow\quad\frac{2}{r_{\mathrm{pol}}(\phi)}=\frac{r_{\mathrm{term}}+r_{\mathrm{exc}}}{r_{\mathrm{exc}}\cdot r_{\mathrm{pol}}},\qquad(33)$$

substitute eqs. (12)–(14) and solve for the **NA** concentration (that yields 50% inhibition, the IC_{50} value). After rearranging, we get the quadratic formula

$$a\cdot\mathrm{IC}_{50}{}^2+b\cdot\mathrm{IC}_{50}+c\cdot=0\qquad(34)$$

with

$$a=\frac{K_{\mathrm{D,dNTP}}}{K_{\mathrm{D,NA}}}(r_{\mathrm{exc}}+k_{\mathrm{term}}),\quad b=k_{\mathrm{term}}(K_{\mathrm{D,dNTP}}+\mathrm{dNTP})$$

$$c=-r_{\mathrm{exc}}\frac{K_{\mathrm{D,NA}}}{K_{\mathrm{D,dNTP}}}(K_{\mathrm{D,dNTP}}+\mathrm{dNTP})^2,$$

which yields

$$\mathrm{IC}_{50}=\frac{r_{\mathrm{exc}}}{k_{\mathrm{term}}+r_{\mathrm{exc}}}\frac{K_{\mathrm{D,NA}}(K_{\mathrm{D,dNTP}}+[\mathrm{dNTP}])}{K_{\mathrm{D,dNTP}}}\qquad(35)$$

Supporting Information

Table S1 Pre-steady state kinetic constants for nucleoside incorporation by wild type HIV-1 reverse transcriptase. Indicated parameters are average values from the respective literature sources.
(PDF)

Table S2 Fold change of kinetic parameters for DNA-dependent polymerization in various HIV-1 reverse transcriptase mutants, relative to wildtype RT. r_{exc}(wt) was set to the value of 0.0016 [1/s] in resting $CD4^+$ T-cells for thymidine- and adenosine analogs respectively, see Table S3 (supplementary material) and eq. (18) (main article) and to the value of 0.00053 [1/s] for guanine- and cytosine analogs, see [76]. [b] excision of TFV-TP from terminated templates was assumed to be 100%, 50%, 100% and 40% of the wild type excision rate for the M184V, the K65R, the Q151M and the K65R/M184V mutant, see [77]. [§] CBV-TP excision in the Q151M mutant was set to 5300% of wild type excision, see [76]. D4T-TP excision in the M184V mutant was set to 83% of the wild type excision, assuming a similar effect of M184V on D4T-TP and AZT-TP [77]. If no other information was available, excisions of nucleoside analogs in the mutant enzymes were assumed to be equal to the wild type excision rate. [*] Q151Mc denotes the 'A62V/V75I/F77L/F116Y/Q151M' mutant. [**] 4-TAM denotes the 'D67N/K70R/T215Y/K219Q' mutant. [†] set to the value of 1, because of insufficient information. [‡] set equal to the rate in Q151Mc.
(PDF)

Table S3 Pre-steady state kinetic constants for AZT excision by HIV-1 reverse transcriptase wildtype and 'D67N/K70R/T215Y/K219Q' mutant. [*] Parameter could not be accurately determined in the respective study [17].
(PDF)

Table S4 Pre-steady state kinetic constants for nucleoside incorporation by human mitochondrial polymerase-γ. $^*r_{\mathrm{pyro}}$ was set to value zero because of insufficient information.
(PDF)

Text S1 The supplementary text contains the modelling required to compute the probability to successfully complete reverse transcription (RT) in HIV-1, based on the parameters presented in the main manuscript.
(PDF)

Acknowledgments

Mvk and CS acknowledge fruitful discussions with Dr. Michael Wulkow, CiT (Rastede, Germany).

Author Contributions

Conceived and designed the experiments: MvK PM RM CS. Performed the experiments: MvK. Analyzed the data: MvK RM PM CS. Wrote the paper: MvK RM.

References

1. Clercq ED (2002) Strategies in the design of antiviral drugs. Nat Rev Drug Discov 1: 925 13–25.
2. Tsai CH, Lee PY, Stollar V, Li ML (2006) Antiviral therapy targeting viral polymerase. Curr Pharm Des 12: 1339–1355.
3. Straus SE, Takiff HE, Seidlin M, Bachrach S, Lininger L, et al. (1984) Suppression of frequently recurring genital herpes. A placebo-controlled double-blind trial of oral acyclovir. N Engl J Med 310: 1545–1550.
4. Douglas JM, Critchlow C, Benedetti J, Mertz GJ, Connor JD, et al. (1984) A double blind study of oral acyclovir for suppression of recurrences of genital herpes simplex 3 virus infection. N Engl J Med 310: 1551–1556.
5. Fischl MA, Richman DD, Grieco MH, Gottlieb MS, Volberding PA, et al. (1987) The efficacy of azidothymidine (AZT) in the treatment of patients with AIDS and AIDS-related complex. A double-blind, placebo-controlled trial. N Engl J Med 317: 185–191.
6. Painter GR, Almond MR, Mao S, Liotta DC (2004) Biochemical and mechanistic basis for the activity of nucleoside analogue inhibitors of HIV reverse transcriptase. Curr Top Med Chem 4: 1035–1044.
7. von Kleist M, Menz S, Huisinga W (2010) Drug-class specific impact of antivirals on the reproductive capacity of HIV. PloS Comput Biol 6: e1000720.
8. Johnson AA, Ray AS, Hanes J, Suo Z, Colacino JM, et al. (2001) Toxicity of antiviral nucleoside analogs and the human mitochondrial DNA polymerase. J Biol Chem 276: 40847–40857.
9. Lewis W, Day BJ, Copeland WC (2003) Mitochondrial toxicity of NRTI antiviral drugs: an integrated cellular perspective. Nat Rev Drug Discov 2: 812–822.
10. Brown JA, Pack LR, Fowler JD, Suo Z (2011) Pre-steady-state kinetic analysis of the incorporation of anti-HIV nucleotide analogs catalyzed by human x- and y-family DNA polymerases. Antimicrob Agents Chemother 55: 276–283.
11. Hanes JW, Zhu Y, Parris DS, Johnson KA (2007) Enzymatic therapeutic index of acyclovir. Viral versus human polymerase gamma specificity. J Biol Chem 282: 25159–25167.
12. Menndez-Arias L (2008) Mechanisms of resistance to nucleoside analogue inhibitors of HIV-1 reverse transcriptase. Virus Res 134: 124–146.
13. Goldschmidt V, Marquet R (2004) Primer unblocking by HIV-1 reverse transcriptase and resistance to nucleoside RT inhibitors (NRTIs). Int J Biochem Cell Biol 36: 1687–1705.
14. Goody RS, Mller B, Restle T (1991) Factors contributing to the inhibition of HIV reverse transcriptase by chain-terminating nucleotides in vitro and in vivo. FEBS Lett 291: 1–5.
15. Meyer PR, Matsuura SE, Mian AM, So AG, Scott WA (1999) A mechanism of AZT resistance: an increase in nucleotide-dependent primer unblocking by mutant HIV-1 reverse transcriptase. Mol Cell 4: 35–43.
16. Boyer PL, Sarafianos SG, Arnold E, Hughes SH (2001) Selective excision of AZTMP by drug-resistant human immunodeficiency virus reverse transcriptase. J Virol 75: 4832–4842.
17. Ray AS, Murakami E, Basavapathruni A, Vaccaro JA, Ulrich D, et al. (2003) Prob-ing the molecular mechanisms of AZT drug resistance mediated by HIV-1 reverse transcriptase using a transient kinetic analysis. Biochemistry 42: 8831–8841.

18. Krebs R, Immendrfer U, Thrall SH, Whrl BM, Goody RS (1997) Single-step kinetics of HIV-1 reverse transcriptase mutants responsible for virus resistance to nucleoside inhibitors zidovudine and 3-TC. Biochemistry 36: 10292–10300.
19. Khalili S, Monaco JM, Armaou A (2010) Development of a stochastic model for the efficacy of NRTIs using known mechanisms of action. J Theor Biol 265: 704–717.
20. Buckheit RW (2004) Understanding HIV resistance, fitness, replication capacity and compensation: targeting viral fitness as a therapeutic strategy. Expert Opin Investig Drugs 13: 933–958.
21. Martinez-Picado J, Martnez MA (2008) HIV-1 reverse transcriptase inhibitor resis-tance mutations and fitness: a view from the clinic and ex vivo. Virus Res 134: 104–123.
22. Bonhoeffer S, Chappey C, Parkin NT, Whitcomb JM, Petropoulos CJ (2004) Evidence for positive epistasis in hiv-1. Science 306: 1547–1550.
23. Martnez JP, Bocharov G, Ignatovich A, Reiter J, Dittmar MT, et al. (2011) Fitness ranking of individual mutants drives patterns of epistatic interactions in hiv-1. PLoS One 6: e18375.
24. D'Abramo CM, Cellai L, Gtte M (2004) Excision of incorporated nucleotide analogue chain-terminators can diminish their inhibitory effects on viral RNA-dependent RNA polymerases. J Mol Biol 337: 1–14.
25. Deval J, Powdrill MH, D'Abramo CM, Cellai L, Gtte M (2007) Pyrophosphorolytic excision of nonobligate chain terminators by hepatitis C virus NS5B polymerase. Antimicrob Agents Chemother 51: 2920–2928.
26. Urban S, Urban S, Fischer KP, Tyrrell DL (2001) Efficient pyrophosphorolysis by a hepatitis b virus polymerase may be a primer-unblocking mechanism. Proc Natl Acad Sci U S A 98: 4984–4989.
27. von Kleist M, Menz S, Stocker H, Arasteh K, Schütte C, et al. (2011) HIV quasispecies dynamics during pro-active treatment switching: Impact on multi-drug resistance and resistance archiving in latent reservoirs. PloS One 6: e18204.
28. Klatzmann D, Barr-Sinoussi F, Nugeyre MT, Danquet C, Vilmer E, et al. (1984) Selective tropism of lymphadenopathy associated virus (LAV) for helper-inducer T lymphocytes. Science 225: 59–63.
29. Koenig S, Gendelman HE, Orenstein JM, Canto MCD, Pezeshkpour GH, et al. (1986) Detection of AIDS virus in macrophages in brain tissue from AIDS patients with encephalopathy. Science 233: 1089–1093.
30. Patterson S, Rae A, Hockey N, Gilmour J, Gotch F (2001) Plasmacytoid dendritic cells are highly susceptible to human immunodeficiency virus type 1 infection and release infectious virus. J Virol 75: 6710–6713.
31. Valentin A, Rosati M, Patenaude DJ, Hatzakis A, Kostrikis LG, et al. (2002) Persistent HIV-1 infection of natural killer cells in patients receiving highly active antiretroviral therapy. Proc Natl Acad Sci U S A 99: 7015–7020.
32. Takahashi K, Wesselingh SL, Griffin DE, McArthur JC, Johnson RT, et al. (1996) Localization of HIV-1 in human brain using polymerase chain reaction/in situ hybridization and immunocytochemistry. Ann Neurol 39: 705–711.
33. Kepler TB, Perelson AS (1998) Drug concentration heterogeneity facilitates the evolution of drug resistance. Proc Natl Acad Sci U S A 95: 11514–11519.
34. Smith AJ, Scott WA (2006) The influence of natural substrates and inhibitors on the nucleotide-dependent excision activity of HIV-1 reverse transcriptase in the infected cell. Curr Pharm Des 12: 1827–1841.
35. Smith AJ, Meyer PR, Asthana D, Ashman MR, Scott WA (2005) Intracellular substrates for the primer-unblocking reaction by human immunodeficiency virus type 1 reverse transcriptase: detection and quantitation in extracts from quiescent- and activated-lymphocyte subpopulations. Antimicrob Agents Chemother 49: 1761–1769.
36. Traut TW (1994) Physiological concentrations of purines and pyrimidines. Mol Cell Biochem 140: 1–22.
37. Goday A, Simmonds HA, Webster DR, Levinsky RJ, Watson AR, et al. (1983) Importance of platelet-free preparations for evaluating lymphocyte nucleotide levels in inherited or acquired immunodeficiency syndromes. Clin Sci (Lond) 65: 635–643.
38. Goday A, Webster DR, Simmonds HA, Levinsky RJ, Perrett D, et al. (1984) Nu1-cleotide levels in peripheral blood mononuclear cells of immunodeficient children: problems of measurement. Adv Exp Med Biol 165 Pt B: 179–182.
39. Tu X, Das K, Han Q, Bauman JD, Clark AD, et al. (2010) Structural basis of HIV-1 resistance to AZT by excision. Nat Struct Mol Biol 17: 1202–1209.
40. Stanford University (2011) HIV drug resistance database. URL http://hivdb.stanford.edu/pages/phenoSummary/Pheno.NRTI.Simple.html.
41. Frankel FA, Invernizzi CF, Oliveira M, Wainberg MA (2007) Diminished efficiency of HIV-1 reverse transcriptase containing the K65R and M184V drug resistance muta-tions. AIDS 21: 665–675.
42. Svedhem V, Lindkvist A, Lidman K, Snnerborg A (2002) Persistence of earlier HIV-1 drug resistance mutations at new treatment failure. J Med Virol 68: 473–478.
43. Petropoulos CJ, Parkin NT, Limoli KL, Lie YS, Wrin T, et al. (2000) A novel pheno- typic drug susceptibility assay for human immunodeficiency virus type 1. Antimicrob Agents Chemother 44: 920–928.
44. Kakuda TN (2000) Pharmacology of nucleoside and nucleotide reverse transcriptase inhibitor-induced mitochondrial toxicity. Clin Ther 22: 685–708.
45. Aquaro S, Perno CF, Balestra E, Balzarini J, Cenci A, et al. (1997) Inhibition of replication of HIV in primary monocyte/macrophages by different antiviral drugs and comparative efficacy in lymphocytes. J Leukoc Biol 62: 138–143.
46. Kellam P, Boucher CA, Larder BA (1992) Fifth mutation in human immunodefi-ciency virus type 1 reverse transcriptase contributes to the development of high-level resistance to zidovudine. Proc Natl Acad Sci U S A 89: 1934–1938.
47. Byrnes VW, Emini EA, Schleif WA, Condra JH, Schneider CL, et al. (1994) Suscepti- bilities of human immunodeficiency virus type 1 enzyme and viral variants expressing multiple resistance-engendering amino acid substitutions to reserve transcriptase in- hibitors. Antimicrob Agents Chemother 38: 1404–1407.
48. Garca-Lerma JG, Aung W, er Cong M, Zheng Q, Youngpairoj AS, et al. (2011) Natural substrate concentrations can modulate the prophylactic efficacy of nucleotide hiv reverse transcriptase inhibitors. J Virol 85: 6610–6617.
49. Perez-Bercoff D, Wurtzer S, Compain S, Benech H, Clavel F (2007) Human immun- odeficiency virus type 1: resistance to nucleoside analogues and replicative capacity in primary human macrophages. J Virol 81: 4540–4550.
50. Buzon MJ, Massanella M, Llibre JM, Esteve A, Dahl V, et al. (2010) HIV-1 replication and immune dynamics are affected by raltegravir intensification of HAART-suppressed subjects. Nat Med 16: 460–465.
51. Brennan TP, Woods JO, Sedaghat AR, Siliciano JD, Siliciano RF, et al. (2009) Anal- ysis of human immunodeficiency virus type 1 viremia and provirus in resting CD4+ T cells reveals a novel source of residual viremia in patients on antiretroviral therapy. J Virol 83: 8470–8481.
52. Elena SF, Sol RV, Sardanys J (2010) Simple genomes, complex interactions: epistasis in rna virus. Chaos 20: 026106.
53. von Kleist M, Huisinga W (2009) Pharmacokinetic-pharmacodynamic relationship of NRTIs and its connection to viral escape: an example based on zidovudine. Eur J Pharm Sci 36: 532–543.
54. Lavie A, Schlichting I, Vetter IR, Konrad M, Reinstein J, et al. (1997) The bottleneck in AZT activation. Nat Med 3: 922–924.
55. Lavie A, Su Y, Ghassemi M, Novak RM, Caffrey M, et al. (2008) Restoration of the antiviral activity of 3′-azido-3′-deoxythymidine (AZT) against AZT-resistant human immunodeficiency virus by delivery of engineered thymidylate kinase to T cells. J Gen Virol 89: 1672–1679.
56. Ray AS (2005) Intracellular interactions between nucleos(t)ide inhibitors of HIV re-verse transcriptase. AIDS Rev 7: 113–125.
57. McKee EE, Bentley AT, Hatch M, Gingerich J, Susan-Resiga D (2004) Phosphoryla- tion of thymidine and AZT in heart mitochondria: elucidation of a novel mechanism of AZT cardiotoxicity. Cardiovasc Toxicol 4: 155–167.
58. Bradshaw PC, Li J, Samuels DC (2005) A computational model of mitochondrial AZT metabolism. Biochem J 392: 363–373.
59. Freisz S, Bec G, Radi M, Wolff P, Crespan E, et al. (2010) Crystal structure of HIV-1 reverse transcriptase bound to a non-nucleoside inhibitor with a novel mechanism of action. Angew Chem Int Ed Engl 49: 1805–1808.
60. Radi M, Maga G, Alongi M, Angeli L, Samuele A, et al. (2009) Discovery of chiral cyclopropyl dihydro-alkylthio-benzyl-oxopyrimidine (S-DABO) derivatives as potent HIV-1 reverse transcriptase inhibitors with high activity against clinically relevant mutants. J Med Chem 52: 840–851.
61. Jochmans D, Deval J, Kesteleyn B, Marck HV, Bettens E, et al. (2006) Indolopyri- dones inhibit human immunodeficiency virus reverse transcriptase with a novel mech- anism of action. J Virol 80: 12283–12292.
62. Liu S, Harada BT, Miller JT, Grice SFJL, Zhuang X (2010) Initiation complex dy- namics direct the transitions between distinct phases of early hiv reverse transcription. Nat Struct Mol Biol 17: 1453–1460.
63. Liu S, Abbondanzieri EA, Rausch JW, Grice SFJL, Zhuang X (2008) Slide into action: dynamic shuttling of hiv reverse transcriptase on nucleic acid substrates. Science 322: 1092–1097.
64. Thomas DC, Voronin YA, Nikolenko GN, Chen J, Hu WS, et al. (2007) Determination of the ex vivo rates of human immunodeficiency virus type 1 reverse transcription by using novel strand-specific amplification analysis. J Virol 81: 4798–4807.
65. Shen L, Peterson S, Sedaghat AR, McMahon MA, Callender M, et al. (2008) Dose- response curve slope sets class-specific limits on inhibitory potential of anti-HIV drugs. Nat Med 14: 762–766.
66. Shen L, Rabi SA, Sedaghat AR, Shan L, Lai J, et al. (2011) A critical subset model provides a conceptual basis for the high antiviral activity of major hiv drugs. Sci Transl Med 3: 91ra63.
67. Xia Q, Radzio J, Anderson KS, Sluis-Cremer N (2007) Probing nonnucleoside inhibitor-induced active-site distortion in HIV-1 reverse transcriptase by transient kinetic analyses. Protein Sci 16: 1728–1737.
68. Sluis-Cremer N, Tachedjian G (2008) Mechanisms of inhibition of HIV replication by non-nucleoside reverse transcriptase inhibitors. Virus Res 134: 147–156.
69. Karlin S, Taylor HM (1975) A first course in stochastic processes. London: Academic Press.
70. Norris JR (1998) Markov chains. Cambridge, UK: Cambridge University Press.
71. Anderson PL, Zheng JH, King T, Bushman LR, Predhomme J, et al. (2007) Concen- trations of zidovudine- and lamivudine-triphosphate according to cell type in HIV-seronegative adults. AIDS 21: 1849–1854.
72. Chapman EH, Kurec AS, Davey FR (1981) Cell volumes of normal and malignant mononuclear cells. J Clin Pathol 34: 1083–1090.
73. Kiser JJ, Aquilante CL, Anderson PL, King TM, Carten ML, et al. (2008) Clinical and genetic determinants of intracellular tenofovir diphosphate concentrations in HIV- infected patients. J Acquir Immune Defic Syndr 47: 298–303.
74. Anderson PL, Kiser JJ, Gardner EM, Rower JE, Meditz A, et al. (2011) Pharmacological considerations for tenofovir and emtricitabine to prevent HIV infection. J Antimicrob Chemother 66: 240–250.

75. Becher F, Landman R, Mboup S, Kane CNT, Canestri A, et al. (2004) Monitoring of didanosine and stavudine intracellular trisphosphorylated anabolite concentrations in HIV-infected patients. AIDS 18: 181–187.
76. Ray AS, Basavapathruni A, Anderson KS (2002) Mechanistic studies to understand the progressive development of resistance in human immunodeficiency virus type 1 reverse transcriptase to abacavir. J Biol Chem 277: 40479–40490.
77. Ly JK, Margot NA, MacArthur HL, Hung M, Miller MD, et al. (2007) The balance between NRTI discrimination and excision drives the susceptibility of HIV-1 RT mu- tants K65R, M184V and K65R+M184V. Antivir Chem Chemother 18: 307–316.

OPEN ACCESS Freely available online

PLoS one

HIV Quasispecies Dynamics during Pro-Active Treatment Switching: Impact on Multi-Drug Resistance and Resistance Archiving in Latent Reservoirs

Max von Kleist[1]*, Stephan Menz[1], Hartmut Stocker[2], Keikawus Arasteh[2], Christof Schütte[1], Wilhelm Huisinga[3,4]

1 Department of Mathematics and Computer Science, Freie Universität, Berlin, Germany, **2** Department of Gastroenterology and Infectious Diseases, Vivantes-Auguste-Viktoria-Klinikum, Berlin, Germany, **3** Hamilton Institute, National University of Ireland, Maynooth, Republic of Ireland, **4** Institute of Mathematics, University of Potsdam, Potsdam, Germany

Abstract

The human immunodeficiency virus (HIV) can be suppressed by highly active anti-retroviral therapy (HAART) in the majority of infected patients. Nevertheless, treatment interruptions inevitably result in viral rebounds from persistent, latently infected cells, necessitating lifelong treatment. Virological failure due to resistance development is a frequent event and the major threat to treatment success. Currently, it is recommended to change treatment after the confirmation of virological failure. However, at the moment virological failure is detected, drug resistant mutants already replicate in great numbers. They infect numerous cells, many of which will turn into latently infected cells. This pool of cells represents an archive of resistance, which has the potential of limiting future treatment options. The objective of this study was to design a treatment strategy for treatment-naive patients that decreases the likelihood of early treatment failure and preserves future treatment options. We propose to apply a single, pro-active treatment switch, following a period of treatment with an induction regimen. The main goal of the *induction regimen* is to decrease the abundance of randomly generated mutants that confer resistance to the *maintenance regimen*, thereby increasing subsequent treatment success. Treatment is switched before the overgrowth and archiving of mutant strains that carry resistance against the *induction regimen* and would limit its future re-use. *In silico* modelling shows that an optimal trade-off is achieved by switching treatment at ≈ 80 days after the initiation of antiviral therapy. Evaluation of the proposed treatment strategy demonstrated significant improvements in terms of resistance archiving and virological response, as compared to conventional HAART. While continuous pro-active treatment alternation improved the clinical outcome in a randomized trial, our results indicate that a similar improvement might also be reached after a single pro-active treatment switch. The clinical validity of this finding, however, remains to be shown by a corresponding trial.

Citation: von Kleist M, Menz S, Stocker H, Arasteh K, Schütte C, et al. (2011) HIV Quasispecies Dynamics during Pro-Active Treatment Switching: Impact on Multi-Drug Resistance and Resistance Archiving in Latent Reservoirs. PLoS ONE 6(3): e18204. doi:10.1371/journal.pone.0018204

Editor: Art Poon, British Columbia Centre for Excellence in HIV/AIDS, Canada

Received November 4, 2010; **Accepted** February 27, 2011; **Published** March 24, 2011

Funding: MvK acknowledges financial support by BMBF funding. SM acknowledges financial support by DFG funding, provided through the Dahlem Research School of Freie Universität Berlin. The funders had no role in study design, data collection and analysis, decision to publish, or preparation of the manuscript.

Competing Interests: The authors have declared that no competing interests exist.

* E-mail: vkleist@zedat.fu-berlin.de

Introduction

In 1996, the tremendous clinical success of highly active antiretroviral therapy had led many researchers to believe that the eradication of HIV would be feasible. However, it was soon realized that inducible pro-virus persists in latently infected cells despite ongoing therapy and that the latent reservoir prevents HIV eradication within the patients lifetime [1]–[6].

Latent infection is established when $CD4^+$ T-lymphoblasts containing integrated provirus [5,7] escape both immune effector mechanisms and the cytopathic effects of the virus and revert to a resting memory state [8]. Besides preventing eradication of HIV, the latent reservoir also serves as a memory of any virus species replicating during the course of HIV infection [9,10], including drug resistant variants. The contents of this archive of resistance are strong predictors of future treatment failure [9,11].

Despite the impressive improvement of antiviral therapy, many patients still experience virological failure caused by the selection of drug resistant virus populations. Current guidelines recommend changing treatment after the confirmation of virological failure. However, in the face of the rapid viral turnover this approach could be sub-optimal [12]. Changing therapy after the appearance of drug resistant mutants will (i) allow the resistant viral population size to expand and evolve and (ii) lead to an archivation of resistant viral strains. An optimal treatment strategy should therefore prevent viral relapse with drug resistant strains and, more importantly, prevent drug resistant mutants from establishing latent infection.

Induction-maintenance (IM) approaches are used for the treatment of a growing number of infectious- and neoplastic diseases [13–15]. Typically, patients start with an intensified induction regimen (composed of a number of potent and potentially toxic drugs), which will subsequently be replaced by a maintenance regimen (composed of a smaller number of less toxic drugs) [16]. However, patients treated with a large number of drugs are particularly vulnerable to drug interactions [17] and

adverse side effects that complicate HIV therapy and seriously undermine the success of clinical management [18].

Another approach to overcome the development of resistance is to alternate antiretroviral therapy [19]. This strategy has been shown to significantly delay virological failure [20,21], yet it is flawed by its high psychological and physical burden [22].

We propose an approach that combines the advantages of conventional IM- and treatment alternation strategies, but minimizes their inherent disadvantages. We suggest a single, pro-active treatment switch from an inducer drug combination to a maintenance combination. The inducer drug combination should rapidly lower the viral population size and eliminate resistant mutants. Subsequently, it will be replaced by a maintenance drug regimen with a completely different resistance profile, before drug resistant strains are archived.

We have previously introduced a novel model of virus dynamics and adaptation [23], which allows us to consider the distinct molecular effects of all novel (and some developmental) HIV drugs. In this article, we present a novel mathematical concept, which prevents the emergence of drug resistance in each individual realization (virtual patient) of the model by switching between therapies. Utilizing this concept, we deduce a distribution of (individual) switching-times, which we use to determine a single fixed duration for the induction therapy, which increases the treatment success probability in the whole virtual patient population and which minimizes the risk for resistance to become archived in the latent reservoir. Finally, the performance of this novel induction-maintenance-strategy is evaluated against conventional HAART therapy.

Results

Virus dynamics model

We have extended the existing viral dynamics model, described in [23], for the compartment of very long lived, latently infected T-cells T_L (Fig. 1 and *Materials and Methods* section), which are believed to prevent eradication of HIV [24] and to lead to the archiving of drug resistance [9,10].

Briefly, the virus dynamics model (Fig. 1) comprises T-cells, macrophages, free non-infectious virus (T_U,M_U,V_{NI}, respectively), free infectious virus of mutant strain i,$V_I(i)$, and five types of infected cells belonging to mutant strain i: infected T-cells and macrophages *prior* to proviral genomic integration ($T_1(i)$ and $M_1(i)$, respectively) and infected T-cells and macrophages *after* proviral genomic integration ($T_2(i)$,$T_L(i)$ and $M_2(i)$, respectively). The latently infected cell type T_L does not express viral genes, but can become activated with rate α, transforming this cell into a virus producing post-integration infected T-cell T_2. The average rates of change of the different species are displayed in the *Materials and Methods* section. All parameter values have been chosen

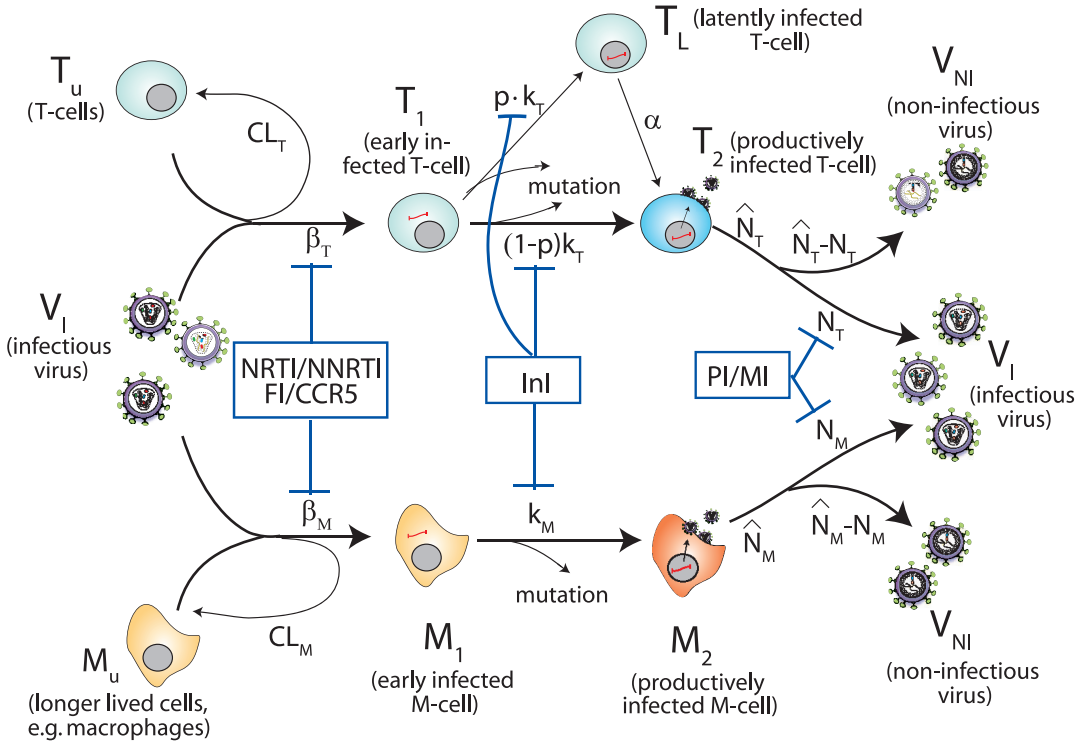

Figure 1. Extended virus dynamics-, mutation- and drug interference model. Target cells (T_U,M_U) can become successfully infected by infective virus V_I with infection rate constants β_T and β_M, respectively, creating early infected cells T_1 and M_1. Infection can also be unsuccessful after the step of viral fusion (rate constant CL_T and CL_M), eliminating the virus and rendering the cell uninfected. Early infected cells T_1 and M_1 can also destroy essential viral proteins or DNA prior to integration, returning the cell to an uninfected stage. The genomic viral DNA can become integrated with rate constants k_T and k_M creating post-integration, infected cells T_2,T_L and M_2. The latently infected cell type T_L does not express viral genes, but can become activated with rate α, transforming this cell into a productively infected T-cell T_2. Virus producing cells T_2,M_2 release new infectious- and non infectious virus V_I and V_{NI} with rate constants N_T,$\left(\widehat{N_T}-N_T\right)$ and N_M,$\left(\widehat{N_M}-N_M\right)$, respectively. Phenotypic mutation occurs at the stage of viral genomic integration k_T,k_M (see [23]). All cellular compartments x can get destroyed by the immune system with respective rate constants δ_x and the free virus (infectious and non-infectious) gets cleared with rate constant CL (not shown in the illustration). The site of drug interference with the replicative cycle of HIV is indicated by blue bars for the respective drug classes (NRTIs, NNRTIs, FIs, CCR5-inhibitors, INIs, PIs, and maturation inhibitors).
doi:10.1371/journal.pone.0018204.g001

according to previous studies and are displayed in Table 1. Since some viral strains are present only in very low copy numbers, we used a hybrid stochastic-deterministic approach [25] to perform simulations (see *Materials and Methods* section for details).

Treatment change before virological failure

Currently, changes of antiretroviral treatment regimes are largely triggered by virological failure or toxicity. In Fig. 2A, we show the simulated viral load in the case of first line treatment failure. The corresponding population dynamics of HIV are shown in Fig. 2B. During first line treatment failure, resistant mutants (green- and cyan colored lines in Fig. 2B) are selected from the quasi-species population and quickly evolve into the dominant virus population, leading to viral rebound. While the total virus population is temporarily shrinking, mutants that confer resistance against a potential follow-up treatment (red line, dark grey shaded area in Fig. 2B) are depleted (possibly eradicated). However, during viral rebound the total viral population re-expands and consequently erroneous reverse transcription generates novel mutants that can confer resistance against a second line therapy. Once the viral population size has been restored, the second line therapy, although composed of entirely different drugs, is as likely to fail as before the initiation of first line therapy. Furthermore, it is likely that drug resistant viral strains become archived while they dominate the viral population (light grey shaded area in Fig. 2B).

In Fig. 2C, we show the viral load dynamics during the proposed induction-maintenance therapy. The corresponding population dynamics of HIV are shown in Fig. 2D. The inducer combination reduces the viral load (see Fig. 2C). However, treatment is changed (vertical dashed black line) to the maintenance combination, before resistant strains (green and cyan line in Fig. 2D) can become more abundant than the wildtype (magenta line in Fig. 2D). Therefore, at the time of treatment change (vertical dashed black line in Fig. 2D), total virus has been decreased and mutants that confer resistance to the maintenance therapy (red line, dark grey shaded area in Fig. 2D) are likely to be eradicated, which improves the probability to achieve durable virological suppression with the maintenance therapy. With this strategy, the abundance of the wildtype is larger than the abundance of drug-resistant mutants, which lowers the probability that drug resistance enters the latent reservoir (light grey shaded area is absent in Fig. 2D).

Table 1. Model parameters generally used in simulations.

Param.	Value	Ref.	Param.	Value	Ref.
λ_T	$2\cdot10^9$	[64]	λ_M	$6.9\cdot10^7$	[65]
δ_T,δ_{T_1}	0.02	[65]	δ_M,δ_{M_1}	0.0069	[65]
δ_{T_2}	1	[36]	δ_{M_2}	0.09	[23]
CL	23	[36]	δ_L	10^{-4}	[16,66]
$\delta_{PIC,T}$	0.35	[67,68]	$\delta_{PIC,M}$	0.0035	[23]
α	10^{-3}	[66]	p	$8\cdot10^{-6}$	[66]
μ	$2.2\cdot10^{-5}$	[42]	ρ_{rev}	0.33	[68,69]
$k_T(wt,\phi)$	0.35	[68]	$k_M(wt,\phi)$	0.07	[23]
$\beta_T(wt,\phi)$	$8\cdot10^{-12}$	[49]	$\beta_M(wt,\phi)$	10^{-14}	[23]
$\widehat{N}_T$	1000	[65]	$\widehat{N}_M$	100	[65]
$b\cdot q\cdot\rho_{PR}$	0.67	[23]	-	-	-

All parameters refer to the wildtype 'wt' in the absence of drug treatment ϕ. All parameters in units [1/day], except p, ρ_{rev}, $b\cdot q\cdot\rho_{PR}$ (unit less) and μ in [1/(rev.trans.·base)]. $CL_{T/M}(wt,\phi)=\left(\frac{1}{\rho_{rev}}-1\right)\cdot\beta_{T/M}(wt,\phi)$, $N_{T/M}(wt,\phi)=b\cdot q\cdot\rho_{PR}\cdot\widehat{N}_{T/M}$ [23].

doi:10.1371/journal.pone.0018204.t001

In order to determine the optimal time point for switching from inducer- to maintenance- drug combinations, t_{switch}, we first determined relevant sets of parameters for (i) the *in vivo* efficacy $\eta(wt,j)$ of each utilized drug j against the wildtype wt and (ii) the *in vivo* fitness loss that is associated with resistance development $s(i)$ (shown in Table S1), since the corresponding *in vivo* parameters are known to vary substantially between different patients, e.g. [26]. For simulation purposes, we assumed that a single point mutation is sufficient to create high-level resistance (99%) to a single drug. This is somewhat a worst-case assumption, but is justified for a number of drugs, see e.g. [27,28]. Relevant clinical failure rates after one year in previously treatment-naive patients, who receive HAART in a clinical trial setting, are $\approx 15-25\%$ [29], (see Table S1).

We then use an algorithm that automatically switches from inducer- to maintenance drug combination, minimizing virological failure for each realization (virtual patient), respectively. A histogram of the derived (individual) switching times from a total of 6000 simulations is shown in Fig. 3. Based on the histogram, we finally chose a fixed time t_{switch} for changing from induction- to maintenance therapy. In the sequel, we evaluate, if the chosen time t_{switch} to change from inducer- to maintenance combination leads to a general improvement compared to conventional HAART therapy, in terms of treatment success and drug resistance archiving.

Determination of treatment changing time

In [23] we introduced the 'reproductive capacity' $R_{cap}(j)$. For the extended model used herein, we have provided the derivation of $R_{cap}(j)$ in the *Materials and Methods* section. The reproductive capacity $R_{cap}(j)$ can be envisaged as the amount of offspring that the whole viral population is expected to produce under some treatment j during one round of replication. It can be calculated from any model simulation and enables to evaluate each state of the infection from the perspective of any potential treatment j. As the viral population adapts to some currently applied treatment, $R_{cap}(j)$ changes accordingly: $R_{cap}(j)$ is large initially and decreases subsequently until drug resistant strains develop and render the treatment j inefficient. We want to assess the point in time, when some inducer- drug combination stops to provide any benefits (in terms of the viral population) for the *next* drug combination (maintenance combination). We therefore evaluate $R_{cap}(j)$ for $j=$*maintenance combination* while the induction combination is applied and change from the induction- to the maintenance therapy when $R_{cap}(j)$ reaches its minimum;

$$\text{switch if :}\quad \frac{d}{dt}R_{cap}(j)=0. \tag{1}$$

The derived switch-times are displayed in Fig. 3. We chose the 0.5th percentile at $t_{switch}=80$ days as a fixed time for treatment change in the forthcoming evaluation of the proposed induction-maintenance-strategy.

Implementation of conventional vs. proposed induction-maintenance-strategy

In order to reflect the clinical practice of HIV care, we have implemented the following routine for assessing the efficacy of the applied treatment combinations.

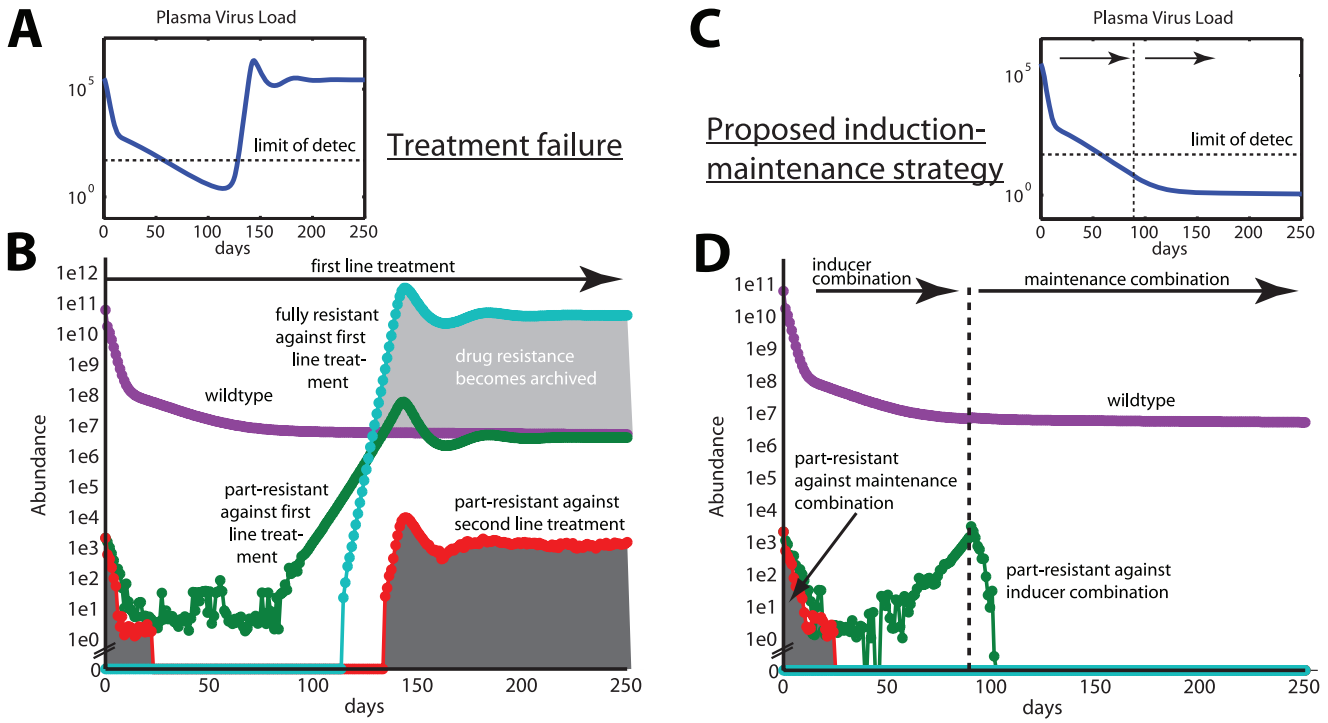

Figure 2. Abundance of viral mutants during first-line treatment failure and during proposed induction-maintenance strategy. A: Plasma virus load during first line treatment failure (blue line). B: Total abundance of distinct viral mutants during first-line treatment failure. C: Plasma virus load (blue line) during proposed induction-maintenance strategy with switch between induction- and maintenance treatment at 80 days (vertical dashed line). D: Total abundance of distinct viral mutants during proposed induction-maintenance strategy. The magenta line denotes the abundance of wildtype virus. Green- and cyan lines denote the abundance of mutants that are part-resistant against the first line regimen (resistant against two out of three drugs) and mutants that are fully resistant against the first line regimen, respectively. The red lines denote the abundance of all mutants, which are part-resistant against a second line treatment. The area under the red line is highlighted by the dark grey shaded area, to stress the negative impact of these mutants on the success of a second line regimen. The light shaded area in panel B indicates that resistant mutants are more abundant than the wildtype and therefore highlights when drug resistance archiving in latently infected cells takes place. The simulations were performed by assuming 70% drug efficacy $\eta(wt,j)$ and a fitness loss s of 20% per drug resistance mutation. Furthermore, it was assumed that a single point mutation can confer absolute resistance to a single drug.
doi:10.1371/journal.pone.0018204.g002

Our virtual patients are monitored every month for efficacy assessment until virus levels fall below the limit of detection (50 HIV RNA/mL plasma). Thereafter, they are monitored every other month. Virological failure has been defined according to treatment guidelines [24]: At the first efficacy assessment (one month after treatment initiation), viral load should have fallen by at least 2 logs [HIV RNA/mL plasma]. Each consecutive measurement should be below the previous assessment. By month 4, viral load should be below the level of detection (50 HIV RNA/mL plasma). After that, detectable virus is defined as virological failure.

We implemented conventional HAART in the following way: The virtual patients are initially treated with a drug combination consisting of two nucleoside reverse transcriptase inhibitors (NRTIs) and one non-nucleoside reverse transcriptase inhibitor (NNRTI) (e.g. tenofovir (TDF) + emtricitabine (FTC) + efavirenz (EFV)), until virological failure is detected, in which case treatment is changed to a second line regimen consisting of a protease inhibitor (PI), an integrase inhibitor (InI) and an entry inhibitor (EI) (e.g. ritonavir (RTV) -boosted PI + raltegravir (RLV) + maraviroc (MVR)).

In the proposed induction-maintenance-strategy, patients are initially treated with a combination consisting of a PI, an InI and an EI, until $t_{\text{switch}} = 80$ days. After that, a treatment consisting of two NRTIs and one NNRTI is applied. If failure is detected at any efficacy assessment time point, treatment change is applied.

In the following, we performed 1000 hybrid stochastic-deterministic simulations for each relevant parameter set (deduced from Table S1) and counted the number of realizations, in which virological failure occurred. Furthermore, we assessed, if the number of drug resistant mutants in the very long-lived infected cells T_L was higher at the end of the simulation than upon initiation of treatment. In this case we recorded "archiving" of drug resistance. The results of our simulations are discussed in the next section.

Proposed induction-maintenance-strategy improves success rate and minimizes archiving of drug-resistance

Fig. 4A shows that the proposed induction-maintenance-strategy (blue line) with a fixed treatment switch time of $t_{\text{switch}} = 80$ days leads to a significant reduction in the probability to experience virological failure compared to the conventional treatment strategy (red line). This observation holds true for a wide range of parameters (see Table 2, second column). In only two cases, where failure rarely occurs during conventional therapy, we do not get significant differences at the $p = 0.05$ level.

Fig. 4B shows that virological failure and the average number of archived drug resistance mutations are strongly correlated (spearman's correlation coefficient $r_S > 0.99$, $p < 0.001$). This indicates that virological failure is a strong predictor for drug resistance archiving.

Tables 2 (third–fifth column) show the number of cases in which archiving of multi-drug resistant viral strains (with ≥ 2, ≥ 3 and

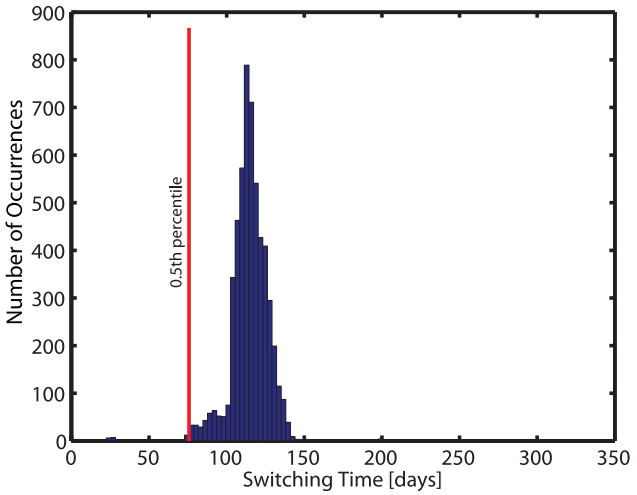

Figure 3. Histogram of optimal, individual treatment switching times. Switching times for changing from inducer- to maintenance therapy were automatically determined and carried out (using eq. (1)). The 0.5th percentile, marked by the red line, was determined and the corresponding time $t_{\text{switch}} = 80$ days was used as a fixed value in the suggested strategy to switch from inducer- to maintenance therapy. Hybrid deterministic-stochastic simulations were performed at clinically relevant parameter sets (see Table S1). Drug switches occurred in a total of 5478 out of 6000 simulations.
doi:10.1371/journal.pone.0018204.g003

≥ 5 drug resistance mutations) occurred in the latent reservoir, under the proposed induction-maintenance strategy and conventional HAART, respectively. It can be seen that the proposed treatment strategy leads to a significant reduction in multi-drug resistance archiving for the majority of parameters evaluated. This indicates, that although two treatment lines have been used for the novel therapy, more therapeutic options are on average available in the follow-up period, compared to conventional therapy.

Discussion

We have presented and tested (in terms of a mathematical model) a very simple treatment strategy that can lead to significant reductions in virological failure in comparison to conventional HAART treatment. A unique drug combination (inducer combination) is used for a short time (80 days) and pro-actively switched to a maintenance combination. The purpose of the inducer combination is to decrease viral population size and thereby increase the likelihood that the subsequent therapy (maintenance) will achieve durable suppression. Clinical implementation of this novel treatment strategy requires only one additional clinical visit at 80 days in comparison with the conventional HAART therapy. The important finding of our study is, that although two drug combinations are always utilized during the proposed induction-maintenance strategy, less archiving of drug resistance occurs in comparison with a conventional treatment strategy, where a second treatment line would be applied only in the case of virological failure or toxicity. Less drug resistance archiving implies that more treatment options will be available for the follow-up and long-term management of HIV-infected patients when the proposed induction-maintenance treatment strategy is used (see Table 2, third–fifth column).

Fig. S1 shows that only a few archiving events (≥ 40 fully resistant mutants) are sufficient to eliminate treatment options permanently. The number of circulating latently infected cells is small [2,7,30,31]. Detecting a small subset of mutants within the circulating latently infected cells is experimentally not feasible, because standard sequencing technology will detect the major strains [32], while novel, second generation methods require large samples [33]. Hence, mathematical modelling is a reasonable tool to investigate drug resistance archiving following treatment application.

The time for switching between combinations t_{switch} ($= 80$ days) is the most critical parameter for the success of the proposed strategy. The following two considerations have to be taken into account: (i) The inducer combination should be applied only for a

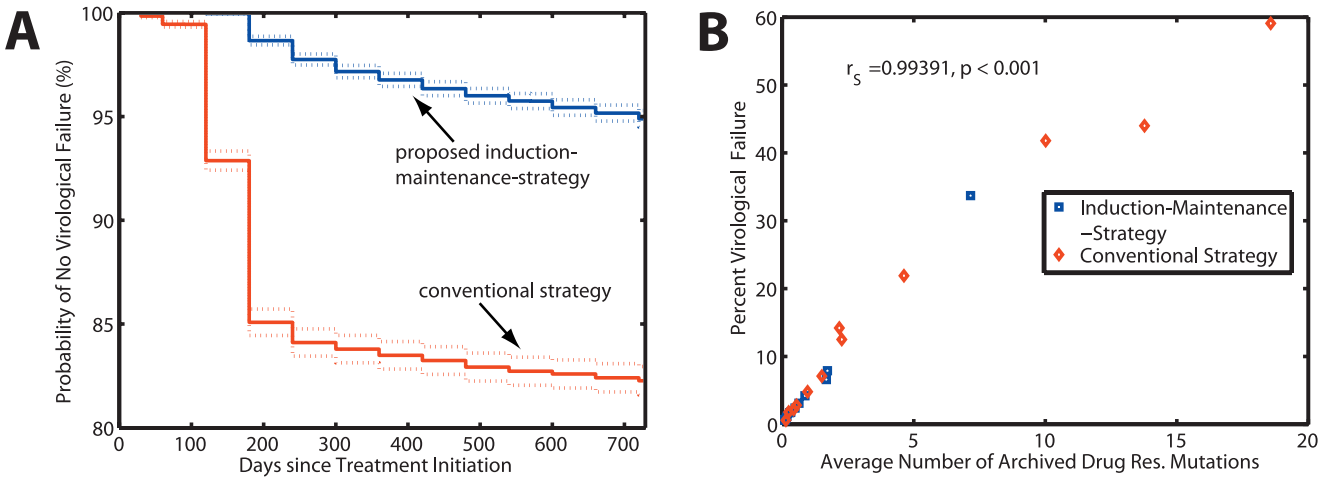

Figure 4. Kaplan-Meier estimates for treatment success, and correlation between virological failure and archiving of drug resistance. The plots summarize the results trough the whole simulated parameter space from Table 2 (12000 simulations in total). A: Probability of no virological failure (%) for the IM-strategy (blue line) and the conventional therapy (red line), respectively. Dashed lines are the 95% confidence ranges, calculated using Greenwood's formula. Virological failure was defined according to [24] and is summarized in section "Implementation of conventional vs. proposed induction-maintenance-strategy". B: The probability to virological failure vs. the average number of drug resistance archiving in the latent reservoir. A strong positive correlation ($p < 0.001$) between virological failure and drug resistance archiving exists, as indicated by spearman's non-parametric rank correlation coefficient $r_S > 0.99$.
doi:10.1371/journal.pone.0018204.g004

Table 2. Probability of virological failure and -archivation of multi-drug resistant virus during suggested induction-maintenance-(IM) vs. conventional HAART strategy.

Parameter set	Failure rate	Probability of multi-drug resistance archivation		
ID $(1-\eta; s)$	IM, HAART	≥2 mutations	≥3 mutations	≥5 mutations
R1 (0.7; 0.3)	1.7, 4.8%**	1.8,4.8%**	1.7,4.8%**	0,0.1%
R2 (0.7; 0.25)	4.2, 14.2%**	4.8,14.2%**	4.2,13.9%**	0.1,0.2%
R3 (0.7; 0.2)	6.6, 41.8%**	18.5,42.2%**	9.6,41.6%**	0.1,2.9%**
R4 (0.75; 0.25)	0.9, 2.8%*	0.9,2.9%*	0.9,2.8%*	0,0%
R5 (0.75; 0.2)	1.8, 12.5%**	2.2,12.6%**	1.8,12.5%**	0,0.4%
R6 (0.8; 0.2)	0.7, 2.2%*	0.8,2.3%*	0.7,2.2%*	0,0.2%
R7 (0.8; 0.15)	3.1, 21.9% **	2.8,22.1% **	3.1,21.9% **	0.2,0.9% *
R8 (0.8; 0.1)	7.9, 44% **	9.3,44% **	8.3,44% **	0.7,14.6% **
R9 (0.85; 0.15)	0.6, 0.6%	0.9,1.3%	0.6,0.6%	0,0%
R10 (0.85; 0.1)	2.4,7.1% **	2.7,8.1% **	2.4,7.2% **	0.3,0.4%
R11 (0.85; 0.05)	33.7, 59.1% **	34.7,59.5% **	34,59.3% **	3.4,17.2% **
R12 (0.9; 0.05)	1.2, 1.8%	2.3,2.5%	1.3,1.8%	0.1,0.1%

Columns 2–5 show the distinct treatment outcome for the suggested induction-maintenance strategy (left entry) and a conventional HAART strategy (right entry) for different parameter sets R1–R12 in terms of mutation-associated reproductive fitness losses s and different levels of drug efficacy $(1-\eta)$ (indicated in column 1), following 1000 simulations respectively. Relevant parameter combinations had been identified beforehand, see Table S1 and section ''Treatment change before virological failure''. Column 2: Percentage of virological failure after 2 years of therapy according to the HIV treatment guidelines (summarized in section ''Implementation of conventional vs. suggested induction-maintenance strategy''). Column 3–5: Probability of multi-drug resistance archiving during the proposed strategy and during conventional HAART strategy. Cross tab χ^2 tests of independence between treatment strategy (suggested vs. conventional strategy) and outcome (virological failure or archivation of multi-drug resistance) are stated. A small p-value indicates that the distinct outcome depends on the treatment strategy and is not due to random effects (** $p<0.001$, * $p<0.05$).

doi:10.1371/journal.pone.0018204.t002

short time, to prevent the selection and archiving of mutants, which are resistant to the *current* drug combination and would limit the further use of this drug combination (risk of the strategy), (ii) while at the same time, it has to be applied long enough to possibly eradicate viral mutants, which are resistant to the *next* drug combination (the benefit of the strategy).

The time required for resistant mutants to emerge, depends on their abundance before the initiation of therapy (if they pre-exist and are selected from the population) and also on their genetic distance to the wildtype (if resistance is *de novo* developed). As discussed above, we determine the abundance of mutants at the time of therapy initiation by utilizing the deterministic fix-point as starting condition for our simulations. We have shown the non-inferiority of our approach in Fig. 5, if drug resistant mutants are more abundant than expected. We have assumed the shortest genetic distance possible between wildtype and fully drug resistant mutants (one mutation is sufficient to create full resistance against a single drug, three distinct mutations are required for full resistance against a triple-drug combination). For some drugs, however, subsequent accumulation of mutations creates fully drug resistant mutants [34]. In our model, drug resistance might therefore develop more rapidly than *in vivo* for drugs with a large genetic barrier [35]. This implies that *in vivo* the inducer combination could possibly be applied for a longer time frame than the 80 days utilized in our model, if the genetic distance between wildtype and fully drug resistant mutant was greater than considered here (greater than one point mutation). However, our results demonstrate that even a very short time (80 days) in which the inducer combination is applied, can improve the clinical outcome significantly (see Fig. 4 and Table 2). This short time already minimizes the probability that drug resistance emerges and can, in that sense, be considered safer than a longer induction phase.

Eradication of viral mutants depends critically on their abundance prior to the initiation of therapy and on the rate at which viral compartments (and therefore resistant mutants) are cleared *in vivo*. The elimination of viral compartments *in vivo* has been quantified and validated in a number of clinical studies [36–38]. We used the expected abundance of viral mutants (the deterministic fix-point of the model) to estimate the abundance of different viral mutants at the time of treatment initiation. In Fig. 5 we show non-inferiority of our approach in the case, where an unexpectedly high abundance of drug resistant mutants is present (1% of the wildtype; detection limit of second generation sequencing technologies [33,39,40]), which would require longer time for eradication.

One limitation of the proposed induction-maintenance strategy is the potential inability to eliminate viral strains, that carry resistance to the maintenance therapy. This is particularly the case, if viral mutants, which carry resistance against all (or at least the majority of) drugs in the maintenance combination, are archived in the latent reservoir prior to treatment initiation. In Fig. S1B, we have quantified that $\geq$ 40 fully resistant viral mutants in the latent reservoir eliminate treatment options permanently. However, the likelihood for fully resistant archival copies (resistant against all drugs in the maintenance regimen) in the treatment naive patient, who was infected with wildtype 'wt' virus, is relatively small. Based on quasi-species theory, Ribero et al. [41] calculated the pre-treatment frequency of viral mutants. According to [41], the frequency of double mutants (part-resistant) relative to the wildtype equals

$$F_{\mathrm{dbl.:wt}} = \frac{\mu^2}{s_{\mathrm{dbl.}}} \cdot \left(\frac{1}{s_1} + \frac{1}{s_2} - 1\right), \qquad (2)$$

where s_1,s_2 and $s_{\mathrm{dbl.}}$ are the selective disadvantages of the strain

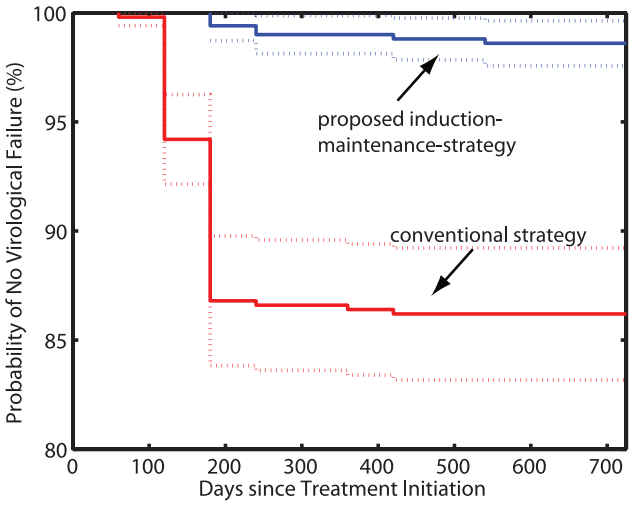

Figure 5. Kaplan-Meier estimates of treatment success (probability of no virological failure) for very high initial abundance of drug resistant mutants. The figure shows the outcome of 500 simulations for the proposed induction-maintenance strategy (blue line) and for the conventional HAART therapy (red line), respectively. Dashed lines indicate the 95% confidence ranges, calculated using Greenwood's formula. The initial abundance of drug resistant mutants was set to 1% of the population. Other parameter values: $(1-\eta)=0.75$, $s=0.8$.
doi:10.1371/journal.pone.0018204.g005

carrying the first-, the second- and the both drug-resistance mutations and $\mu=2.16\cdot10^{-5}$ is the single point mutation rate [42]. It is reasonable to assume that resistant mutants are, at best, as likely to enter the latent reservoir as the wildtype in the absence of any drugs, due to their inherent fitness loss, i.e. $P(\text{dbl.}|T_L) \leq F_{\text{dbl.:wt}}$. Considering a maintenance combination consisting of efavirenz (EFV), tenofovir (TDF) and emtricitabine (FTC), with primary resistance mutations K103N, K65R and M184V and respective selective disadvantages for the single-point mutants $s_{K103N}=0.125, s_{K65R}\geq0.8$ and $s_{M184V}\geq0.9$ [43] and additive fitness losses in the double mutants $s_{K103N/K65R}, s_{K103N/M184V}$, $s_{K65R/M184V}$ (i.e. $s_{\text{dbl.}}=1-(1-s_1)\cdot(1-s_2)$), the probability that mutants, resistant against two out of three maintenance drugs, enter the latent reservoir are $P(K103N/K65R|T_L)\leq5\cdot10^{-9}$, $P(K103N/M184V|T_L)\leq4\cdot10^{-9}$ and $P(K65R/M184V|T_L)\leq 6.5\cdot10^{-10}$ respectively. Using *in vivo* data, Chun et al. [7] estimated the average number of latently infected cells with replication-competent provirus to be $T_L\approx1.4\cdot10^6$ cells, so that the expected number of partly-resistant mutants $E(\text{dbl.},T_L)=T_L\cdot P(\text{dbl.}|T_L)$ that are archived prior to treatment initiation is $E(K103N/K65R,T_L)\leq0.007, E(K103N/M184V,T_L)\leq0.006$ and $E(K65R/M184V,T_L)\leq0.0009$. In other words, it is very unlikely that part-resistant mutants are archived in patients prior to treatment, since $E(\text{dbl.},T_L)\ll1$. Furthermore, part-resistant mutants are still susceptible to one out of the three drugs in the maintenance combination. For triple-drug (fully) resistant strains, the likelihood of archival copies is even smaller.

Infection with drug resistant strains, mainly against established drug classes, is a major, growing health concern [44]. During infection with drug-resistant viral strains, archivation in the latent reservoir is likely, since this reservoir is established early in the infection [45]. If the circulating viral population reverses to a drug-susceptible type, archived resistant mutants from the time of infection might remain undetected and can complicate subsequent treatment (see Fig. S1). This particular circumstance applies equally to the proposed induction-maintenance therapy and conventional HAART.

For our strategy, we have chosen drugs from novel classes (e.g. InI, EI) for the inducer-combination, while we selected drugs from well-established classes for the maintenance combination (NNRTI, NRTI). This has the following rationale: The inducer combination will only be applied for a short time (80 days), while the maintenance combination could possibly be applied for much longer periods of time (until it fails, or toxicological events occur). Second or third generation drugs within the established drug-classes are often more convenient to apply (e.g. once daily dosing) and are less toxic, which has important implications for the long-term management of HIV [46]. Secondly, drugs from the novel drug classes (InI, EI), are currently not available as generic formulations, whereas low-cost alternative drugs exist for established drug classes. Therefore, in order to reduce treatment costs, it is of advantage to select a strategy, in which inexpensive drugs can be used for the majority of time, while cost-intensive ones are only applied for short treatment periods.

Some drug classes can cause a distinct viral load decline. In particular, the only approved InI raltegravir causes a more rapid viral load decay, compared with other HIV inhibitors [47,48]. It might therefore seem logical, based on viral load decay, to use raltegravir in the induction treatment. It has been shown, however, that the faster viral decay with raltegravir could be a consequence of the particular site of action of InIs within the viral life cycle and may not be due to an overall increased removal rate of replication-competent viral compartments by raltegravir [23,49]. Long-term studies of raltegravir- versus efavirenz-based HAART showed equal outcomes with either therapies [50,51], arguing against the superiority of raltegravir-based drug combinations in removing replication-competent virus; however, further analysis is required.

Intuitively, it might be more advantageous to use drug resistance tests to guide treatment switches, instead of using a fixed time for a pro-active switch from inducer- to maintenance combination [19]. However, under the considerations discussed above, a switch from inducer- to maintenance combination should be applied before any resistant strains become abundant. This implies that the most frequent viral strain at the time of switch should be the wildtype. Standard assays fail to detect minority species [32]. Ultra-deep/pyro-sequencing might provide a more holistic picture of the quasi-species composition and can pick up viral mutants that are abundant in $\approx1\%$ of the quasi-species population and if the sample is large enough [33,39,40]. However, even in this case, viral mutants are likely to dominate once the results are available (>1 week), owing to the rapid viral kinetics [52].

In our *in silico* study, we considered time-invariant, as well as anatomically homogeneous *average* drug efficacy $(1-\eta)$, for the ease of modelling. It is also possible to consider drug- and patient-specific time-varying pharmacokinetics and to study the impact of compliance on drug resistance development. However, if compliance is identical between the two study arms, the qualitative difference between the outcome of conventional HAART versus the proposed induction-maintenance strategy is not expected to change. As shown in Table 2, the proposed induction-maintenance therapy performs better than conventional HAART for a wide range of parameter values for $(1-\eta)$. Furthermore, it was shown in a clinical study [20,21] that treatment alternation leads to significantly less virological failure than conventional HAART, when compliance is imperfect but identical between the two study arms. However, since the study in [20,21] is not identical to the

treatment strategy presented herein, a clinical study should be performed to fully investigate the potential of the proposed induction-maintenance strategy. Ideally, this prospective randomized trial could evaluate the time to virological failure in patients taking a single unchanged regimen and patients on induction-maintenance regimens. Importantly, the trial should be designed to evaluate whether the induction maintenance strategy affects the durability of second- and third line regimens. The presence and relative frequency of viral minority populations as well as their mutational patterns could be monitored by analyzing proviral DNA from circulating T-cells using, e.g., next-generation sequencing. This data could serve to validate our mathematical model.

Based on a recent, successful pre-exposure prophylaxis (PrEP) trial, where emtricitabine (FTC) + tenofovir (TDF) were given to high-risk individuals [53], it could be envisioned that PrEP is used more broadly. One risk with such a strategy is the selection of FTC/TDF resistance, which occurred in both subjects with acute HIV infection at enrolment in the PrEP trial [53]. Furthermore, there is a high risk for the selection of drug resistance, if subjects get infected despite PrEP (e.g. due to low adherence; $<50\%$ in the PrEP trial [53]). While FTC/TDF is a core component of first-line HAART, the long-term epidemiological consequences of drug-resistance selection are of utmost importance. One interesting question is whether the proposed induction-maintenance therapy can re-sensitize those subjects towards FTC/TDF treatment, who had become infected with HIV despite PrEP. While a thorough analysis of this question is beyond the scope of the current article, related scenarios are frequently encountered in the context of prevention of mother-to-child transmission (MTCT) programs, when short-course intrapartum nevirapine is used. In the MTCT context, protease-inhibitor-based induction therapy has been used for the re-sensitization of pre-exposed children towards nevirapine [54]. Further analysis, however, is required to elucidate the potential of induction-maintenance strategies for re-sensitization of pre-exposed HIV infected individuals.

Materials and Methods

Model Equations

The virus dynamics model (Fig. 1) comprises T-cells, macrophages, free non-infectious virus (T_U,M_U,V_{NI}, respectively), free infectious virus of mutant strain i,$V_I(i)$, and five types of infected cells belonging to mutant strain i: infected T-cells and macrophages *prior* to proviral genomic integration ($T_1(i)$ and $M_1(i)$, respectively) and infected T-cells and macrophages *after* proviral genomic integration ($T_2(i)$,$T_L(i)$ and $M_2(i)$, respectively). The latently infected cell type T_L does not express viral genes, but can become activated with rate α, transforming this cell into a virus producing post-integration infected T-cell T_2. The average rates of change of the different species are given by the following system of ODEs:

$$\frac{d}{dt}T_U = \lambda_T + \delta_{PIC,T}\cdot T_1(i) - \delta_T\cdot T_U - \sum_i \beta_T(i,j)\cdot V_I(i)\cdot T_U$$

$$\frac{d}{dt}M_U = \lambda_M + \delta_{PIC,M}\cdot M_1(i) - \delta_M\cdot M_U - \sum_i \beta_M(i,j)\cdot V_I(i)\cdot M_U$$

$$\frac{d}{dt}T_1(i) = \beta_T(i,j)\cdot V_I(i)\cdot T_U - (\delta_{T_1} + \delta_{PIC,T} + k_T(i,j))\cdot T_1(i)$$

$$\frac{d}{dt}M_1(i) = \beta_M(i,j)\cdot V_I(i)\cdot M_U - (\delta_{M_1} + \delta_{PIC,M} + k_M(i,j))\cdot M_1(i) \quad (3)$$

$$\frac{d}{dt}T_L(i) = \sum_k p\cdot k_T(k,j)T_1(k)\cdot r_{k\to i} - (\delta_L + \alpha)\cdot T_L(i)$$

$$\frac{d}{dt}T_2(i) = \sum_k (1-p)\cdot k_T(k,j)T_1(k)\cdot r_{k\to i} + \alpha\cdot T_L(i) - \delta_{T_2}\cdot T_2(i)$$

$$\frac{d}{dt}M_2(i) = \sum_k k_M(k,j)M_1(k)\cdot r_{k\to i} - \delta_{M_2}\cdot M_2(i)$$

$$\frac{d}{dt}V_I(i) = N_M(i,j)\cdot M_2(i) + N_T(i,j)\cdot T_2(i) - V_I(i)\cdot[CL + (CL_T(i,j) + \beta_T(i,j))T_U + (CL_M(i,j) + \beta_M(i,j))M_U]$$

$$\frac{d}{dt}V_{NI} = \sum_i [(\widehat{N}_T - N_T(i,j))T_2(i) + (\widehat{N}_M - N_M(i,j))M_2(i)] - CL\cdot V_{NI},$$

where λ_T and λ_M are the birth rates of uninfected T-cells and macrophages, and δ_T and δ_M denote their death rate constants. The parameters $k_T(k,j)$ and $k_M(k,j)$ are the integration rate constants of mutant strain k under treatment j. The parameters δ_{T_1},δ_L,δ_{T_2},δ_{M_1} and δ_{M_2} are the death rate constants of T_1,T_L,T_2,M_1 and M_2 cells, respectively. The free virus (infectious and non-infectious) gets cleared by the immune system with rate constant CL. The parameters $\delta_{PIC,T}$ and $\delta_{PIC,M}$ refer to the intracellular degradation of essential components of the pre-integration complex, e.g., by the host cell proteasome within early infected T-cells and macrophages, respectively. $\widehat{N}_T$ and $\widehat{N}_M$ denote the total number of released infectious and non-infectious virus from late infected T-cells and macrophages of mutant strain i, and $N_T(i,j)$ and $N_M(i,j)$ are the rates of release of infective virus under treatment j. The parameters $CL_T(i,j)$ and $CL_M(i,j)$ denote the clearance of mutant virus i through unsuccessful infection of T-cells and macrophages, respectively [23], and the parameters $\beta_T(i,j)$ and $\beta_M(i,j)$ denote the successful infection rate constants of mutant virus i under treatment j for T-cells and macrophages, respectively. In our model, T-cells can become latently infected T_L with probability p. Latent infected cells can undergo apoptosis with rate δ_L and can become activated with rate α. Activation of latent cells by antigen- or other activating stimuli triggers the production of viral building blocks via positive feedback loops [55,56] in the late replication cycle of HIV, which turns the cell into a virus producing cell T_2 that becomes susceptible to HIV-related cytopathic effects and destruction by the immune system.

The parameter $r_{k\to i}$ denotes the probability to mutate from strain k to strain i and is defined by

$$r_{k\to i} = \mu^{h(i,k)}\cdot(1-\mu)^{L-h(i,k)}, \tag{4}$$

where μ denotes the point mutation probability per base and reverse transcription process ($\mu \approx 2.16\cdot10^{-5}$ [42]), $h(i,k)$ denotes the hamming distance between strain k and strain i, and L is the total number of different positions that are considered in our model (here, $L=6$ point mutations). In total, the model includes 2^L different viral strains i that contain point mutations in any pattern of the modelled L possible mutations. The phenotype of each mutant strain i is modelled by introducing a selective disadvantage $s(i)$, which denotes the loss of functionality (e.g., in the activity of some viral enzyme that is affected by the mutation) relative to the wildtype, and a strain specific inhibitory activity $\eta(i,j)$ of treatment j against the mutant strain i. For example, the strain specific infection rate i under a certain treatment j is given by $\beta(i,j)=(1-\eta(i,j))\cdot(1-s(i))\cdot\beta(wt,\phi)$, where $\beta(wt,\phi)$ denotes the infection rate constant of the wildtype $'wt'$ in the absence of drug ϕ (parameters listed in Table 1). The strain-specific specific inhibitory activity is calculated via $\eta(i,j)=\eta(wt,j)\cdot\mathrm{res}(i,j)$, where the efficacy of the drugs against the wildtype $\eta(wt,j)$ is generally stated in the corresponding tables and figures (Fig. 2, Fig. 5 and Table 2) and the resistance of a particular mutant $\mathrm{res}(i,j)$ was either set to 1 (100% susceptible) or 0.01 (99% resistant), if the particular mutant $i$conferred resistance to the particular drug j.

All parameter values have been chosen according to previous studies (see Table 1). The particular viral decay dynamics after application of distinct drug classes were validated in [23]. The model (Fig. 1) with above described parameters reproduces an average frequency of latently infected cells of $26/10^6$ $\mathrm{CD4}^+$ cells (reference range: $0.82/10^6$ – $205/10^6$ $\mathrm{CD4}^+$ cells [2,7,30,31]), a total of $4.5\cdot10^6$ latently infected cells (reference: $1.4\cdot10^6$ [7]), with a halflife of 20.6 month (average of [2,57–60]: 21 month) and a plasma viremia of $\approx$1 HIV RNA/mL [61] from the latent reservoir.

Realization and Implementation of the Model

The overall virus dynamics in our model comprise different viral strains with copy numbers that can vary over several orders of magnitude. For this reason we have chosen a hybrid (stochastic-deterministic) setting for numerical simulation. This approach (i) takes into account stochastic fluctuations in the slow reaction processes; and (ii) reduces the computational costs for the simulation of the fast (deterministic) system dynamics. We used the direct hybrid method proposed in [25], where we treated elementary reactions r_j as discrete stochastic processes whenever their propensity function a_j or the quantity of at least one of their reactants was below a threshold of 20. All other reactions were approximated as continuous deterministic processes. Elementary reactions r_j with propensity functions a_j and their respective net changes v_j can be deduced from eqs. (3). For example, the term $\beta_T\cdot V_I\cdot T_U$ denotes the infection reaction of T-cells by infectious virus. The propensity function of this reaction is $a_j=\beta_T\cdot V_I\cdot T_U$. This reaction changes the species levels as follows: one T_U cell and one V_I virus get consumed (the term is once subtracted from each corresponding ODE), and one T_1 cell is produced (the term is once added to the ODE of T_1).

In brief, the hybrid method comprises the following algorithmic workflow:

(1) Set initial time $t=t_0$ and initial number of molecules $X(t_0)$.

(2) Generate two uniformly distributed pseudo-random variables ξ_1 and ξ_2 on the open unit interval $(0,1)$ and determine the partitioning of reactions into deterministic and stochastic subsets $\mathcal{D}$ and $\mathcal{S}$, respectively. The latter is realized by comparing the actual propensity and the reactant levels of every reaction with pre-specified thresholds. If one value is below the thresholds, a reaction is included in the stochastic subset $\mathcal{S}$, otherwise it is put in the deterministic subset $\mathcal{D}$.

(3) Set $g(\tau|t)=\ln(\xi_1)$ and solve the ODE system for the deterministic part of the system starting at time $\tau=t$

$$\frac{\mathrm{d}}{\mathrm{d}\tau}X(\tau)=\sum_{j\in\mathcal{D}}v_j a_j(X(\tau)), \tag{5}$$

together with

$$\frac{\mathrm{d}}{\mathrm{d}\tau}g(\tau|t)=\sum_{j\in\mathcal{S}}a_j(X(\tau)), \tag{6}$$

until time $\tau=s$ such that $g(s|t)=0$.

(4) Take the integer m satisfying

$$\sum_{j=1}^{m-1}a_j(X(\tau))<\xi_2\sum_{j\in\mathcal{S}}a_j(X(\tau)) \leq\sum_{j=1}^{m}a_j(X(\tau)) \text{ with } j,m\in\mathcal{S}, \tag{7}$$

in order to determine the stochastic reaction r_m to be performed.

(5) Update $X(s)$ according to reaction r_m, hence set $X(s)\leftarrow X(s)+v_m$.

(6) Set $t\leftarrow s$, and stop the procedure if the final time is reached. Otherwise go to Step (2).

The above algorithmic scheme requires the use of numerical integrators that allow to stop integration in step (3) when a stochastic reaction event is detected at a time τ where $g(s|t)=0$. The utilized integrator is based on numerical differentiation formulas [62], and uses strategies for event detection and error- and step size control comparable to ode15s in MATLAB [63]. To generate the data for Fig. 4, we performed 12000 hybrid simulations in total. With realization start ($t_0=0$) the effects of drug treatment were simulated, until $t=730$ days was reached. Every numerical calculation was computed with a relative error tolerance of 10^{-6} and an absolute error tolerance of 10^{-9}. Our simulation code is provided in Source Code S1–S6.

Reproductive Numbers

For the model above (eq. (3)), the reproductive numbers, which indicate the expected number of offspring in the next generation, are defined as follows: the reproductive number $R_V(i,j)$ of a single virus of strain i under treatment j is given by

$$R_V(i,j)=\frac{\beta_T(i,j)T_U\cdot k_T(i,j)\left(1-p\cdot\frac{\delta_L}{\delta_L+\alpha}\right)\cdot N_T(i,j)}{c_u(i,j)\cdot c_T(i,j)\cdot\delta_{T_2}}+ \frac{\beta_M(i,j)M_U\cdot k_M(i,j)\cdot N_M(i,j)}{c_u(i,j)\cdot c_M(i,j)\cdot\delta_{M_2}},$$

with constants

$$c_u(i,j) = \mathrm{CL} + [\mathrm{CL_T}(i,j) + \beta_\mathrm{T}(i,j)]\mathrm{T_U} + [\mathrm{CL_M}(i,j) + \beta_\mathrm{M}(i,j)]\mathrm{M_U},$$

$$c_T(i,j) = \delta_\mathrm{T} + \delta_\mathrm{PIC,T} + k_\mathrm{T}(i,j),$$

$$c_M(i,j) = \delta_\mathrm{M} + \delta_\mathrm{PIC,M} + k_\mathrm{M}(i,j).$$

Since infected cells are also pathogens, which can lead to a rebound of the disease even in the absence of any virus, we also determined their basic reproductive numbers under a given treatment j. The basic reproductive numbers $R_{\mathrm{T}_1}(i,j)$ and $R_{\mathrm{M}_1}(i,j)$ of the infectious stages T_1 and M_1, associated with the viral strain i, are given by

$$R_{\mathrm{T}_1}(i,j) = \frac{k_\mathrm{T}(i,j)\left(1 - p\cdot\frac{\delta_\mathrm{L}}{\delta_\mathrm{L}+\alpha}\right)\cdot\mathrm{N_T}(i,j)}{c_T(i,j)\cdot\delta_{\mathrm{T}_2}} \cdot \frac{\beta_\mathrm{T}(i,j)\mathrm{T_U} + \beta_\mathrm{M}(i,j)\mathrm{M_U}}{c_u(i,j)},$$

$$R_{\mathrm{M}_1}(i,j) = \frac{k_\mathrm{M}(i,j)\cdot\mathrm{N_M}(i,j)}{c_M(i,j)\cdot\delta_{\mathrm{M}_2}} \cdot \frac{\beta_\mathrm{T}(i,j)\mathrm{T_U} + \beta_\mathrm{M}(i,j)\mathrm{M_U}}{c_u(i,j)}.$$

Finally, the reproductive numbers $R_{\mathrm{T}_2}(i,j), R_{\mathrm{T_L}}(i,j)$ and $R_{\mathrm{M}_2}(i,j)$ of the infectious stages $\mathrm{T}_2, \mathrm{T_L}$ and M_2, associated with the viral strain i, are given by

$$R_{\mathrm{T}_2}(i,j) = \frac{\mathrm{N_T}(i,j)}{\delta_{\mathrm{T}_2}} \cdot \left[\frac{k_\mathrm{T}(i,j)\mathrm{T_U}\cdot\beta_\mathrm{T}(i,j)}{c_u(i,j)\cdot c_T(i,j)} + \frac{k_\mathrm{M}(i,j)\mathrm{M_U}\cdot\beta_\mathrm{M}(i,j)}{c_u(i,j)\cdot c_M(i,j)}\right],$$

$$R_{\mathrm{T_L}}(i,j) = \frac{\alpha}{\delta_\mathrm{L}+\alpha}\frac{\mathrm{N_T}(i,j)}{\delta_{\mathrm{T}_2}} \cdot \left[\frac{k_\mathrm{T}(i,j)\mathrm{T_U}\cdot\beta_\mathrm{T}(i,j)}{c_u(i,j)\cdot c_T(i,j)} + \frac{k_\mathrm{M}(i,j)\mathrm{M_U}\cdot\beta_\mathrm{M}(i,j)}{c_u(i,j)\cdot c_M(i,j)}\right],$$

$$R_{\mathrm{M}_2}(i,j) = \frac{\mathrm{N_M}(i,j)}{\delta_{\mathrm{M}_2}} \cdot \left[\frac{k_\mathrm{T}(i,j)\mathrm{T_U}\cdot\beta_\mathrm{T}(i,j)}{c_u(i,j)\cdot c_T(i,j)} + \frac{k_\mathrm{M}(i,j)\mathrm{M_U}\cdot\beta_\mathrm{M}(i,j)}{c_u(i,j)\cdot c_M(i,j)}\right].$$

Reproductive Capacity

We have previously introduced the reproductive capacity $R_{\mathrm{cap}}(j)$ [23], which can be interpreted as the expected total number of infectious offspring that the infection produces in one round of replication under a certain treatment j, given the current state of the infection. In this article, we utilize the reproductive capacity in order to get individual treatment switching times (see eq. (1), main article), which are displayed in Fig. 3. The reproductive capacity of the entire quasi-species ensemble under treatment j is defined as the weighted sum of the basic reproductive numbers of all pathogenic stages of mutant strain i, i.e., free virus, infected T-cells and infected macrophages, weighted by the abundance of the corresponding pathogenic stage [23]:

$$R_{\mathrm{cap}}(j) = \sum_i [\mathrm{V_I}(i)R_\mathrm{V}(i,j) + \mathrm{T_1}(i)R_{\mathrm{T}_1}(i,j) + \mathrm{M_1}(i)R_{\mathrm{M}_1}(i,j) + \mathrm{T_2}(i)R_{\mathrm{T}_2}(i,j) + \mathrm{T_L}(i)R_{\mathrm{T_L}}(i,j) + \mathrm{M_2}(i)R_{\mathrm{M}_2}(i,j)],$$

where $R_\mathrm{V}(i,j), R_{\mathrm{T}_1}(i,j), R_{\mathrm{M}_1}(i,j), R_{\mathrm{T}_2}(i,j)$ and $R_{\mathrm{M}_2}(i,j)$ are the strain-specific reproductive numbers of the different infective compartments (see previous sections).

Supporting Information

Figure S1 Time and probability of virological failure depends on pool-size of archived drug-resistant virus. A: The median time until virological failure, in relation to the number of fully-resistant archived virus (fully = resistant against all drugs in the triple-drug combination). B: Probability that virological failure occurs within two years after initiation of HAART therapy as a function of the number of fully-resistant archived virus. 500 stochastic-deterministic runs were performed for each pool size of the latently infected drug-resistant reservoir. Parameter values used: $(1-\eta) = 0.75$, $s = 0.8$.
(PDF)

Table S1 Determination of relevant parameter space for further investigation. We assessed virological failure rates after one year of triple drug therapy for varying values of efficacy $(1-\eta(wt,j))$ of drug j against the wildtype 'wt' and selective disadvantage per mutation s. All other parameters have been taken from Table 1. A parameter combination (in terms of $(1-\eta(wt,j))$ and s) was considered relevant, if it produced realistic failure rates after one year of therapy [29]. Confidence ranges are indicated in brackets and were calculated using Greenwood's formula. Each condition has been evaluated by 100 stochastic deterministic simulations.
(PDF)

Source Code S1 The File 'HAART.m' can be used to simulate the kinetics of HIV after application of conventional HAART treatment in MATLAB.
(M)

Source Code S2 The File 'HIVmodel.m' builds the original HIV model used throughout the manuscript for use in MATLAB.
(M)

Source Code S3 The File 'InductionMaintenance.m' can be used to simulate the kinetics of HIV after under the proposed induction-maintenance therapy in MATLAB.
(M)

Source Code S4 The File 'PatientMonitoring.m' contains the MATLAB implementation of routine patient monitoring.
(M)

Source Code S5 The File 'ReadMeFirst.txt' Contains a description of all supplied source code files, contact details, information on runtime and execution and a copy of the GNU public license.
(TXT)

Source Code S6 The File 'SpeciesLevelsIndices.pdf' contains an interpretation of the output generated by executing the provided MATLAB Source Code Files (Source Code S1–S4).
(PDF)

Acknowledgments

The authors would like to thank Prof. Karin Mölling (Head of Virology Dep., University Zürich, Switzerland) for helpful comments regarding the manuscript. We are very grateful to the National University of Ireland in Maynooth for providing the high-performance computing cluster. Special thanks to Vanush Misha Paturyan for assistance in scheduling jobs on the computing cluster.

Author Contributions

Conceived and designed the experiments: MvK. Performed the experiments: MvK SM. Analyzed the data: MvK SM HS KA WH CS. Wrote the paper: MvK HS KA WH CS.

References

1. Finzi D, Hermankova M, Pierson T, Carruth LM, Buck C, et al. (1997) Identification of a reservoir for HIV-1 in patients on highly active antiretroviral therapy. Science 278: 1295–1300.
2. Finzi D, Blankson J, Siliciano JD, Margolick JB, Chadwick K, et al. (1999) Latent infection of CD4+ T cells provides a mechanism for lifelong persistence of HIV-1, even in patients on effective combination therapy. Nat Med 5: 512–517.
3. Wong JK, Hezareh M, Günthard HF, Havlir DV, Ignacio CC, et al. (1997) Recovery of replication-competent HIV despite prolonged suppression of plasma viremia. Science 278: 1291–1295.
4. Carter CC, Onafuwa-Nuga A, McNamara LA, Riddell J, Bixby D, et al. (2010) HIV-1 infects multipotent progenitor cells causing cell death and establishing latent cellular reservoirs. Nat Med 16: 446–451.
5. Chun TW, Finzi D, Margolick J, Chadwick K, Schwartz D, et al. (1995) In vivo fate of HIV-1-infected T cells: quantitative analysis of the transition to stable latency. Nat Med 1: 1284–1290.
6. Chun TW, Stuyver L, Mizell SB, Ehler LA, Mican JA, et al. (1997) Presence of an inducible HIV-1 latent reservoir during highly active antiretroviral therapy. Proc Natl Acad Sci U S A 94: 13193–13197.
7. Chun TW, Carruth L, Finzi D, Shen X, DiGiuseppe JA, et al. (1997) Quantification of latent tissue reservoirs and total body viral load in HIV-1 infection. Nature 387: 183–188.
8. Pierson T, McArthur J, Siliciano RF (2000) Reservoirs for HIV-1: mechanisms for viral persistence in the presence of antiviral immune responses and antiretroviral therapy. Annu Rev Immunol 18: 665–708.
9. Siliciano JD, Siliciano RF (2004) A long-term latent reservoir for HIV-1: discovery and clinical implications. J Antimicrob Chemother 54: 6–9.
10. Lambotte O, Chaix ML, Gubler B, Nasreddine N, Wallon C, et al. (2004) The lymphocyte HIV reservoir in patients on long-term HAART is a memory of virus evolution. AIDS 18: 1147–1158.
11. Reekie J, Mocroft A, Ledergerber B, Beniowski M, Clotet B, et al. (2010) History of viral suppression on combination antiretroviral therapy as a predictor of virological failure after a treatment change. HIV Med 11: 469–478.
12. Ho DD, Neumann AU, Perelson AS, Chen W, Leonard JM, et al. (1995) Rapid turnover of plasma virions and CD4 lymphocytes in HIV-1 infection. Nature 373: 123–126.
13. Blumberg HM, Leonard MK, Jasmer RM (2005) Update on the treatment of tuberculosis and latent tuberculosis infection. JAMA 293: 2776–2784.
14. Horstkotte D, Follath F, Gutschik E, Lengyel M, Oto A, et al. (2004) Guidelines on prevention, diagnosis and treatment of infective endocarditis executive summary; the task force on infective endocarditis of the european society of cardiology. Eur Heart J 25: 267–276.
15. Zimmerli W, Ochsner PE (2003) Management of infection associated with prosthetic joints. Infection 31: 99–108.
16. Curlin ME, Iyer S, Mittler JE (2007) Optimal timing and duration of induction therapy for HIV-1 infection. PLoS Comput Biol 3: e133.
17. Catanzaro LM, Slish JC, DiCenzo R, Morse GD (2004) Drug interactions with antiretrovirals. Curr HIV/AIDS Rep 1: 89–96.
18. Carr A (2003) Toxicity of antiretroviral therapy and implications for drug development. Nat Rev Drug Discov 2: 624–634.
19. D'Amato RM, D'Aquila RT, Wein LM (1998) Management of antiretroviral therapy for HIV infection: modelling when to change therapy. Antivir Ther 3: 147–158.
20. Martinez-Picado J, Negredo E, Ruiz L, Shintani A, Fumaz CR, et al. (2003) Alternation of antiretroviral drug regimens for HIV infection. A randomized, controlled trial. Ann Intern Med 139: 81–89.
21. Negredo E, Paredes R, Peraire J, Pedrol E, Côté H, et al. (2004) Alternation of antiretroviral drug regimens for HIV infection. efficacy, safety and tolerability at week 96 of the Swatch study. Antivir Ther 9: 889–893.
22. Sherr L, Lampe F, Norwood S, Leake-Date H, Fisher M, et al. (2007) Successive switching of antiretroviral therapy is associated with high psychological and physical burden. Int J STD AIDS 18: 700–704.
23. von Kleist M, Menz S, Huisinga W (2010) Drug-class specific impact of antivirals on the reproductive capacity of HIV. PLoS Comput Biol 6: e1000720.
24. Panel on Antiretroviral Guidelines for Adults and Adolescents. Guidelines for the use of antiretroviral agents in HIV-1-infected adults and adolescents Department of Health and Human Services. December 1, 2009. (http://www.aidsinfo.nih.gov/contentfiles/adultandadolescentgl.pdf) (accessed 01-Oct-2010). pp 1–161.
25. Alfonsi A, Cancès E, Turinici G, Ventura B, Huisinga W (2005) Exact simulation of hybrid stochastic and deterministic models for biochemical systems. ESAIM Proc 14: 1–23.
26. Fabbiani M, Giambenedetto SD, Bracciale L, Bacarelli A, Ragazzoni E, et al. (2009) Pharmacokinetic variability of antiretroviral drugs and correlation with virological outcome: 2 years of experience in routine clinical practice. J Antimicrob Chemother 64: 109–117.
27. Clavel F, Hance AJ (2004) HIV drug resistance. N Engl J Med 350: 1023–1035.
28. Clavel F (2009) HIV resistance to raltegravir. Eur J Med Res 14(Suppl 3): 47–54.
29. Riddler SA, Haubrich R, DiRienzo AG, Peeples L, Powderly WG, et al. (2008) Class-sparing regimens for initial treatment of HIV-1 infection. N Engl J Med 358: 2095–2106.
30. Blankson JN, Finzi D, Pierson TC, Sabundayo BP, Chadwick K, et al. (2000) Biphasic decay of latently infected CD4+ T cells in acute human immunodeficiency virus type 1 infection. J Infect Dis 182: 1636–1642.
31. Fondere JM, Planas JF, Huguet MF, Baillat V, Bolos F, et al. (2004) Enumeration of latently infected CD4+ T cells from HIV-1-infected patients using an HIV-1 antigen ELISPOT assay. J Clin Virol 29: 33–38.
32. Richman DD (2000) Principles of HIV resistance testing and overview of assay performance characteristics. Antivir Ther 5: 27–31.
33. Eriksson N, Pachter L, Mitsuya Y, Rhee SY, Wang C, et al. (2008) Viral population estimation using pyrosequencing. PLoS Comput Biol 4: e1000074.
34. Nijhuis M, Schuurman R, de Jong D, Erickson J, Gustchina E, et al. (1999) Increased fitness of drug resistant HIV-1 protease as a result of acquisition of compensatory mutations during suboptimal therapy. AIDS 13: 2349–2359.
35. Arora P, Dixit NM (2009) Timing the emergence of resistance to anti-HIV drugs with large genetic barriers. PLoS Comput Biol 5: e1000305.
36. Markowitz M, Louie M, Hurley A, Sun E, Mascio MD, et al. (2003) A novel antiviral intervention results in more accurate assessment of human immunodeficiency virus type 1 replication dynamics and T-cell decay in vivo. J Virol 77: 5037–5038.
37. Perelson AS, Neumann AU, Markowitz M, Leonard JM, Ho DD (1996) HIV-1 dynamics in vivo: virion clearance rate, infected cell life-span, and viral generation time. Science 271: 1582–1586.
38. Perelson AS, Essunger P, Cao Y, Vesanen M, Hurley A, et al. (1997) Decay characteristics of HIV-1-infected compartments during combination therapy. Nature 387: 188–191.
39. Ji H, Massé N, Tyler S, Liang B, Li Y, et al. (2010) HIV drug resistance surveillance using pooled pyrosequencing. PLoS One 5: e9263.
40. Archer J, Braverman MS, Taillon BE, Desany B, James I, et al. (2009) Detection of low-frequency pretherapy chemokine (CXC motif) receptor 4 (CXCR4)-using HIV-1 with ultra-deep pyrosequencing. AIDS 23: 1209–1218.
41. Ribeiro RM, Bonhoeffer S, Nowak MA (1998) The frequency of resistant mutant virus before antiviral therapy. AIDS 12: 461–465.
42. Mansky LM, Temin HM (1995) Lower in vivo mutation rate of human immunodeficiency virus type 1 than that predicted from the fidelity of purified reverse transcriptase. J Virol 69: 5087–5094.
43. Martinez-Picado J, Martínez MA (2008) HIV-1 reverse transcriptase inhibitor resistance mutations and fitness: a view from the clinic and ex vivo. Virus Res 134: 104–123.
44. Smith RJ, Okano JT, Kahn JS, Bodine EN, Blower S (2010) Evolutionary dynamics of complex networks of HIV drug-resistant strains: the case of San Francisco. Science 327: 697–701.
45. Ghosn J, Pellegrin I, Goujard C, Deveau C, Viard JP, et al. (2006) HIV-1 resistant strains acquired at the time of primary infection massively fuel the cellular reservoir and persist for lengthy periods of time. AIDS 20: 159–170.
46. Bartlett JA (2002) Addressing the challenges of adherence. J Acquir Immune Defic Syndr 29(Suppl 1): S2–10.
47. Murray JM, Emery S, Kelleher AD, Law M, Chen J, et al. (2007) Antiretroviral therapy with the integrase inhibitor raltegravir alters decay kinetics of HIV, significantly reducing the second phase. AIDS 21: 2315–2321.
48. DeJesus E, Berger D, Markowitz M, Cohen C, Hawkins T, et al. (2006) Antiviral activity, pharmacokinetics, and dose response of the HIV-1 integrase inhibitor gs-9137 (jtk-303) in treatment-naive and treatment-experienced patients. J Acquir Immune Defic Syndr 43: 1–5.
49. Sedaghat AR, Dinoso JB, Shen L, Wilke CO, Siliciano RF (2008) Decay dynamics of HIV-1 depend on the inhibited stages of the viral life cycle. Proc Natl Acad Sci U S A 105: 4832–4837.
50. Lennox JL, DeJesus E, Lazzarin A, Pollard RB, Madruga JVR, et al. (2009) Safety and efficacy of raltegravir-based versus efavirenz-based combination therapy in treatment-naive patients with HIV-1 infection: a multicentre, double-blind randomised controlled trial. Lancet 374: 796–806.
51. Lennox JL, Dejesus E, Berger DS, Lazzarin A, Pollard RB, et al. (2010) Raltegravir versus efavirenz regimens in treatment-naive HIV-1-infected patients: 96-week efficacy, durability, subgroup, safety, and metabolic analyses. J Acquir Immune Defic Syndr 55: 39–48.
52. Ramratnam B, Bonhoeffer S, Binley J, Hurley A, Zhang L, et al. (1999) Rapid production and clearance of HIV-1 and hepatitis C virus assessed by large volume plasma apheresis. Lancet 354: 1782–1785.
53. Grant RM, Lama JR, Anderson PL, McMahan V, Liu AY, et al. (2010) Preexposure chemoprophylaxis for HIV prevention in men who have sex with men. N Engl J Med 363: 2587–2599.

54. Coovadia A, Abrams EJ, Stehlau R, Meyers T, Martens L, et al. (2010) Reuse of nevirapine in exposed HIV-infected children after protease inhibitor-based viral suppression: a randomized controlled trial. JAMA 304: 1082–1090.
55. Weinberger LS, Burnett JC, Toettcher JE, Arkin AP, Schaffer DV (2005) Stochastic gene expression in a lentiviral positive-feedback loop: HIV-1 tat fluctuations drive phenotypic diversity. Cell 122: 169–182.
56. Lassen KG, Ramyar KX, Bailey JR, Zhou Y, Siliciano RF (2006) Nuclear retention of multiply spliced HIV-1 RNA in resting CD4+ T cells. PLoS Pathog 2: e68.
57. Zhang L, Ramratnam B, Tenner-Racz K, He Y, Vesanen M, et al. (1999) Quantifying residual HIV-1 replication in patients receiving combination antiretroviral therapy. N Engl J Med 340: 1605–1613.
58. Chun TW, Justement JS, Moir S, Hallahan CW, Maenza J, et al. (2007) Decay of the HIV reservoir in patients receiving antiretroviral therapy for extended periods: implications for eradication of virus. J Infect Dis 195: 1762–1764.
59. Siliciano JD, Kajdas J, Finzi D, Quinn TC, Chadwick K, et al. (2003) Long-term follow-up studies confirm the stability of the latent reservoir for HIV-1 in resting CD4+ T cells. Nat Med 9: 727–728.
60. Ramratnam B, Mittler JE, Zhang L, Boden D, Hurley A, et al. (2000) The decay of the latent reservoir of replication-competent HIV-1 is inversely correlated with the extent of residual viral replication during prolonged anti-retroviral therapy. Nat Med 6: 82–85.
61. Coffin J, Maldarelli F, Palmer S, Weigand A, Brun S, et al. (2006) Long-term persistance of low-level HIV-1 in patients on suppressive antiretroviral therapy. Abstract 169 13th Conference on Retroviruses and Opportunistic Infections; 5–8 February 2006; Denver, Colorado, United States Available at http://wwwretroconferenceorg/2006/Abstracts/28061htm.
62. Klopfenstein R (1971) Numerical differentiation formulas for stiff systems of ordinary differential equations. RCA Review 32: 447–462.
63. Shampine L, Reichelt M (1997) The Matlab ODE Suite. SIAM Journal on Scientific Computing 18: 1–22.
64. Wei X, Ghosh SK, Taylor ME, Johnson VA, Emini EA, et al. (1995) Viral dynamics in human immunodeficiency virus type 1 infection. Nature 373: 117–122.
65. Sedaghat AR, Siliciano RF, Wilke CO (2009) Constraints on the dominant mechanism for HIV viral dynamics in patients on raltegravir. Antivir Ther 14: 263–271.
66. Callaway DS, Perelson AS (2002) HIV-1 infection and low steady state viral loads. Bull Math Biol 64: 29–64.
67. Koelsch KK, Liu L, Haubrich R, May S, Havlir D, et al. (2008) Dynamics of total, linear nonintegrated, and integrated HIV-1DNA in vivo and in vitro. J Infect Dis 197: 411–419.
68. Zhou Y, Zhang H, Siliciano JD, Siliciano RF (2005) Kinetics of human immunodeficiency virus type 1 decay following entry into resting CD4+ T cells. J Virol 79: 2199–2210.
69. Pierson TC, Zhou Y, Kieffer TL, Ruff CT, Buck C, et al. (2002) Molecular characterization of preintegration latency in human immunodeficiency virus type 1 infection. J Virol 76: 8518–8531.